University of Reading

Climate change and socioeconomic transformations in the Late Antique Eastern Mediterranean and Middle East

Doctor of Philosophy

School of Archaeology, Geography, and Environmental Science

Matthew J. Jacobson

October 2021

Declaration of original authorship

Declaration: I confirm that this is my own work and the use of all material from other sources has been properly and fully acknowledged.

Signed

Matthew J Jacobson

Abstract

Predicting the nature and societal impacts of future climate change requires the publication of a dense network of palaeoclimate proxy records and multi-scalar examination of past human-environment-climate relationships. In the study region of this thesis, the Late Antique (3rd-7th centuries CE) Eastern Mediterranean and Middle East, there are deficiencies in both disciplines: spatio-temporal gaps in the network of records, frequent use of records to discuss disparate regions, and a bias towards studying the Byzantine Empire. This interdisciplinary thesis contributes to the fields of palaeoclimatology, archaeology, and history, through three case-studies presented as four stand-alone journal articles.

The main case-study, which is examined as a micro-region, to ensure datasets are proximate and comparable, is SW Anatolia (Turkey). Following the production of a new speleothem-based palaeoclimate record from Kocain Cave (Chapter 3) and a new archaeological dataset of 381 settlements (Chapter 4), evidence from this region is sufficient for analysis of human-climate-environment relationships. Climate change is found to be unimportant for settlement expansion in the Roman Imperial Period. Whilst a shift to drier conditions after 460 CE is initially adapted to, settlement abandonment occured at least a century later, following further drying and a combination of other factors.

Chapters 5 and 6 present two additional case-studies for polities which have previously not been studied in relation to climatic factors – the Kingdom of Himyar and the Sasanian Empire. A new speleothem-based record from Hoti Cave (Oman, Chapter 5) reveals its driest conditions at the start of the 6th century CE, which are argued to have weakened the Kingdom of Himyar leading to cascading socio-political change. Conversely, coincident dry conditions in the Sasanian Empire (Chapter 6) had no impact, with the empire's most significant growth-phase continuing unabated. Mitigation strategies against future climate change can be informed by further study of past societal responses.

Acknowledgements

I am grateful for the support provided to me by my supervisory team. Without the influence of Dominik Fleitmann, I never would have started this project and he has acted as my *Doktorvater* since long before I started my PhD. To Alison Gascoigne, my co-supervisor from UoSouthampton, I owe special thanks as without frequent meetings and assistance from her, this project would have ended a long time ago!

I would like to thank my family for supporting me all the way through this project, enduring my complaining and keeping me company throughout the long lockdown summer (the second one!)

Furthermore, those I lived with throughout my PhD deserve thanks for putting up with me and helping me to relax when the working day was over – Tom Earnshaw, Arica Roberts, Fran Evans and Sascha Valmé

Additional thanks go to colleagues and collaborators, who provided me with excellent ideas during discussions and with incredible opportunities, for which I am eternally grateful - especially Jordan Pickett, Sam Nicholson, Pascal Flohr, Warren Eastwood, John Haldon, Maria Rabbani, and Mark Altaweel!

Special thanks go to Lisa Backhouse for supporting me in so many ways, by reading work, keeping me sane during lockdown, accompanying me on runs and walks, and calming me down during the stresses of doing a PhD!

Table of Contents

CHAPTER 1: INTRODUCTION 1

1.1. PALAEOCLIMATE STUDIES IN THE EASTERN MEDITERRANEAN AND MIDDLE EAST 1

1.2. LATE ANTIQUITY 3

1.2.1. HISTORICAL CONTEXT 3

1.2.2. ARCHAEOLOGICAL CONTEXT 10

1.2.3. HISTORY OF (LATE ANTIQUE) CLIMATE AND SOCIETY 12

1.3. AIMS AND OBJECTIVES 12

1.4. STRUCTURE OF THE THESIS 14

CHAPTER 2: RECREATING EASTERN MEDITERRANEAN AND MIDDLE EASTERN CLIMATE 19

2.1. PREFACE 19

2.2. MODERN CLIMATOLOGY 21

2.3. PALAEOCLIMATE RECONSTRUCTIONS 24

2.3.1. SPELEOTHEMS 24

2.3.2. OTHER PALAEOCLIMATE EVIDENCE 30

2.3.3. AVAILABILITY OF HIGH-RESOLUTION PALAEOCLIMATE RECORDS 33

2.4. LINKING PALAEOCLIMATIC AND SOCIETAL CHANGE 40

2.5. SUMMARY 43

CHAPTER 3: HETEROGENOUS LATE HOLOCENE CLIMATE IN THE EASTERN MEDITERRANEAN – THE KOCAIN CAVE RECORD FROM SW TURKEY 44

3.1. PREFACE 44

3.2. JOURNAL ARTICLE 45

3.2.1. INTRODUCTION 46

3.2.2. CAVE SETTING 48

3.2.3. Materials, Methodology and Chronology 50

3.2.4. Interpretation of the Ko-1 multi-proxy record 51

3.2.5. Ko-1 Record and EM Palaeoclimate 54

3.2.5.1. Heterogeneity of Eastern Mediterranean climate and proxies 57

3.2.6. Conclusion 59

Acknowledgments, Samples, and Data 59

3.3. Supplementary Information 60

3.3.1. Geological Setting of Kocain Cave 60

3.3.2. Detailed Methodology 61

3.3.3. Growth-axis changes and speleoseismology 64

CHAPTER 4: SETTLEMENT, ENVIRONMENT, AND CLIMATE CHANGE IN SW ANATOLIA: DYNAMICS OF REGIONAL VARIATION AND THE END OF ANTIQUITY 72

4.1. Preface 72

4.2. Journal Article 73

4.2.1. Introduction 74

4.2.2. Study area geography 75

4.2.3. Methods 77

4.2.3.1. Data Critique 78

4.2.4. Results 81

4.2.5. History of climate and society in the Eastern Mediterranean 87

4.2.5.1. A Roman Climatic Optimum? 89

4.2.5.2. Late Antique prosperity and adaptation? 93

4.2.5.3. Middle Byzantine abandonment and re-nucleation? 99

4.2.6. Conclusions 104

CHAPTER 5: DROUGHTS AND SOCIETAL CHANGE: THE ENVIRONMENTAL CONTEXT FOR THE EMERGENCE OF ISLAM IN LATE ANTIQUE ARABIA 107

5.1. PREFACE 107

5.2. JOURNAL ARTICLE 108

5.3. SUPPLEMENTARY INFORMATION 119

5.3.1 MATERIALS AND METHODS 119

5.3.2. ANALYSIS OF PRECIPITATION OVER THE ARABIAN PENINSULA 124

5.3.3. AGRICULTURE IN HIMYAR 125

5.3.4. HISTORICAL AND ARCHAEOLOGICAL EVIDENCE FOR DROUGHTS AND RAINFALL FLUCTUATIONS IN THE MIDDLE EAST BETWEEN THE 3RD AND 6TH CENTURY C.E. 130

5.3.5. HISTORICAL CONTEXT 133

CHAPTER 6: CLIMATE CHANGE AND THE SASANIAN EMPIRE (224 - 651 CE): A REVIEW 142

6.1. PREFACE 142

6.2. JOURNAL ARTICLE 142

6.2.1. INTRODUCTION 142

6.2.2. THE SASANIAN EMPIRE 147

6.2.3. HOW RESILIENT WAS THE SASANIAN EMPIRE TO CLIMATIC FLUCTUATIONS? 156

6.2.4. CLIMATE CHANGE IN THE SASANIAN PERIOD 162

6.2.5. SOCIO-ECONOMIC IMPACTS FROM CLIMATE CHANGE? 170

6.2.6. CONCLUSIONS AND FUTURE RESEARCH AGENDAS 175

ACKNOWLEDGEMENTS AND DATA 176

CHAPTER 7: SUMMARY DISCUSSION AND CONCLUSIONS 177

7.1. PALAEOCLIMATOLOGY 178

7.1.1. KOCAIN CAVE 178

7.1.2. HOTI CAVE 181

7.1.3. COMPARISON WITH OTHER RECORDS 181

7.2. HISTORY OF CLIMATE AND SOCIETY **185**

7.2.1. SW ANATOLIA 186

7.2.2. THE KINGDOM OF HIMYAR 188

7.2.3. THE SASANIAN EMPIRE 189

7.2.4. RECURRENT THEMES 190

7.3. CONCLUDING REMARKS 191

BIBLIOGRAPHY **194**

APPENDICES **249**

APPENDIX A - DATA **249**

A.1. CHAPTER 3 DATA: KOCAIN CAVE GEOCHEMISTRY DATASET 249

A.2. CHAPTER 4 DATA: SOUTHWEST TURKEY SETTLEMENT CHANGE DATASET 249

A.3. CHAPTER 5 DATA: HOTI CAVE GEOCHEMISTRY DATASET 249

APPENDIX B – PUBLICATIONS **250**

B.1. SPELEOTHEMS FROM THE MIDDLE EAST: AN EXAMPLE OF WATER LIMITED ENVIRONMENTS IN THE SISAL DATABASE 250

B.2. NEW INSIGHTS INTO THE ROLE OF ENVIRONMENTAL DYNAMICS SHAPING SOUTHERN MESOPOTAMIA: FROM THE PRE-UBAID TO THE EARLY ISLAMIC PERIOD 280

B.3. MAIN CONTROLS ON THE STABLE CARBON ISOTOPE COMPOSITION OF SPELEOTHEMS 309

B.4. THE STALAGMITE RECORD OF SOUTHERN ARABIA: CLIMATIC EXTREMES, HUMAN EVOLUTION, AND SOCIETAL DEVELOPMENT 354

APPENDIX C – LIST OF CONFERENCE PRESENTATIONS **374**

List of Figures

Chapter 1

Figure 1. Region definitions 4

Figure 2. Territorial extent of Late Antique states 5

Chapter 2

Figure 3. Maps of averaged seasonal precipitation and air temperature. 22

Figure 4. Locations of available high-resolution palaeoclimate archives. 34

Figure 5. Temporal coverage and resolution of available high-resolution archives. 36

Chapter 3

Figure 6. Map of Eastern Mediterranean palaeoclimate archives compared with winter precipitation and agricultural droughts. 47

Figure 7. Palaeoclimate and weather station data from SW Turkey. 49

Figure 8. Full palaeoclimate data and age-depth model of speleothem Ko-1. 53

Figure 9. Late Holocene Eastern Mediterranean palaeoclimate data. 56

Figure 10. Geological map of SW Turkey 61

Figure 11. Köppen-Geiger Climate Classification zones of Turkey 61

Figure 12. Scans of speleothem Ko-1 with sampling locations 63

Figure 13. Scan of speleothem Ko-1 with Fe/Ca ratios 64

Figure 14. Growth axes and speleoseismology of speleothem Ko-1 67

Figure 15. Direct comparison of Ko-1 records 68

Figure 16. Trace-element profiles in the common era 69

Figure 17. Statistical relationship of isotopes, precipitation, and temperature in Antalya 70

Figure 18. Direct comparisons between Ko-1 Mg/Ca and other archives 70

Figure 19. Correlation of SPEI and winter precipitation from the Ko-1 0.5° grid square 71

Chapter 4

Figure 20. Maps of the study region (Lycia-Pamphylia), with palaeoclimate archives, pollen records and settlements 76

Figure 21. Settlement data and evidence types by period. 82

Figure 22. Settlement elevation data. 83

Figure 23. Periodised maps of settlement evidence. 84

Figure 24. Comparison of settlement data with regional surveys and pollen OJCV values 86

Figure 25. Palaeoclimate data from Lycia-Pamphylia 90

Figure 26. Settlement change heatmaps 91

Figure 27. Photographs and archaeological plans from Lycia-Pamphylia. 98

Chapter 5

Figure 28. Maps of palaeoclimate records and settlements in southern Arabia. 110

Figure 29. Hoti Cave palaeoclimate data and meteorological records 111

Figure 30. Palaeoclimate records and historic events in the 5th-6th centuries CE 113

Figure 31. Records of summer monsoon wind strength and precipitation 115

Figure 32. Images and plans of Hoti Cave 120

Figure 33. Scan and drawing of cut speleothem H12. 122

Figure 34. Age-depth model for speleothem H12 123

Figure 35. Monthly precipitation at Al Hamra. 124

Figure 36. Spatial correlation of precipitation in the Hoti Cave 0.5° grid square 125

Figure 37. Present-day precipitation isohyets in Yemen 126

Figure 38. Google Earth images of terraces in Yemen. 128

Figure 39. Farming calendar for the most important cereals in Himyar. 129

Figure 40. Paleogeographical development of Khawr Rawri in Southern Oman 132

Chapter 6

Figure 41. Territorial extent of the Sasanian Empire, with palaeoclimate archives, pollen records and settlements 144

Figure 42. Timeline of the Sasanian Empire 146

Figure 43. Map showing case-study regions and survey data 146

Figure 44. Cereal and walnut pollen percentages from lake palaeoenvironmental records 151

Figure 45. Map of modern precipitation and weather station data in Sasanian territories 158

Figure 46. Palaeohydrological data from the Sasanian Empire 164

Figure 47. Z-scores of palaeohydrological data from the Sasanian Empire 166

Figure 48. Temperature and forcing mechanism records 169

Figure 49. Palaeoclimate data and wars with kingdoms from Central Asia and Arabia 173

Chapter 7

Figure 50. Summary of new speleothem-based palaeoclimate data resulting from this thesis 180

Figure 51. Standardised first millennium palaeoclimate archives from the EMME region. 184

Figure 52. The Adaptive Cycle, with stages for the states discussed in this thesis 187

List of Tables

Chapter 1

Table 1. Journal articles produced as part of this thesis. 17

Chapter 2

Table 2. High-resolution EMME palaeoclimate proxies covering the 1st Millennium 37

Chapter 4

Table 3. Measures of resolution 78

Table 4. Settlement metadata by period. 85

Chapter 6

Table 5. List of agricultural produce and animals in Sasanian Mesopotamia 160

Table 6. Palaeohydrological records in Sasanian Persia 163

List of Abbreviations

AHRC	Arts and Humanities Research Council [organisation]
AO	Arctic Oscillation
AP	Arabian Peninsula
BCE	Before the Common Era
CA	Central Asia
CAP	Central Anatolian Plateau
CE	Common Era
CRU TS	Climatic Research Unit Time-Series [climate data]
CYCE	Crisis Years Cold Event
DACP	Dark Ages Cold Period
DVE	Dust Veil Event [536 CE]
EATL/WRUS	East Atlantic – West Russian [pattern]
EM	Eastern Mediterranean
EMME	Eastern Mediterranean-Middle East [region]
ENSO	El Niño – Southern Oscillation
EPD	European Pollen Database
FC	Fertile Crescent
GNIP	Global Network of Isotopes in Precipitation
GRL	Geophysical Research Letters [journal]
GVF	Global Volcanic Forcing
HCS	History of Climate and Society
IPCC	Intergovernmental Panel for Climate Change
JIH	Journal of Interdisciplinary History
LA-ICP-MS	Laser Ablation-Inductively Coupled Plasma-Mass Spectrometry
LALIA	Late Antique Little Ice Age
LIA	Little Ice Age
LWB	Lake Water Balance
MCA	Medieval Climate Anomaly
ME	Middle East

NAO	North Atlantic Oscillation
NCP	North Sea – Caspian Pattern
NEO	Navarino Environmental Observatory
NOAA	National Oceanic and Atmospheric Administration
PAGES	Past Global Changes [organisation]
PCA	Principal Component Analysis
pCO_2	Partial pressure of carbon dioxide
PCP	Prior Calcite Precipitation
PG	Persian Gulf
PLOS	The Public Library of Science
RCO	Roman Climate Optimum
RWP	Roman Warm Period
SCAND	Scandinavian [pattern]
SCE	Short-term Cataclysmic Event
SE	Sasanian Empire
SI	Stable Isotope
SST	Sea Surface Temperature
TAQ	*Terminus Ante Quem* [latest possible date]
TE	Trace Element
TPQ	*Terminus Post Quem* [earliest possible date]
TSI	Total Solar Irradiance
UNESCO	United Nations Educational, Scientific and Cultural Organisation
VPBD	Vienna Pee Dee Belemnite [geochemical standard]

Chapter 1: Introduction

1.1. Palaeoclimate studies in the Eastern Mediterranean and Middle East

In recent years, impacts from climate change in the Eastern Mediterranean - Middle East region (EMME; see Figure 1) have been significant, and will likely get worse (Giorgi, 2006; Lelieveld et al., 2012). Superimposed on a drying trend (Barlow et al., 2016; Karami, 2019), widespread droughts have been occurring with increasing frequency (Kaniewski et al., 2012), as have forest fires that result from the intensifying heat and aridity (Çolak & Sunar, 2020; Ertuğrul et al., 2018; Xanthopoulos & Nikolov, 2019). These changes have impacted humans through effects on agricultural productivity (Gornall et al., 2010), leading to recurrent famines and have been argued to factor into recent geo-political instability (Gleick, 2014; Kelley et al., 2015).

The Intergovernmental Panel for Climate Change (IPCC) states that to predict both the nature and impacts of future climate change accurately, past climatic variability must be constrained (Masson-Delmotte et al., 2013). Modern weather-station data, and observations, reveal climatic conditions in the EMME region to be complex and highly variable, both temporally, on seasonal to multi-decadal (and sometimes centurial) timescales, and spatially (Beck et al., 2018; Ulbrich et al., 2012). However, the meteorological data required to fully understand this spatio-temporal variance are lacking; in many regions data are entirely absent due to political instability and where present, information rarely extends back longer than 100 years (Jürg Luterbacher et al., 2012). The solution to this problem is the collection and analysis of palaeoclimate archives such as speleothems, lake sediment cores, tree rings and corals, which store information about past climate in their chemistry or physical characteristics (Elias, 2021). Palaeoclimate proxy data are also input into, and used to assess, palaeoclimate models. Palaeoclimate modelling intercomparison projects (PMIPs) facilitate understanding of regional responses to climate change, and to external forcing mechanisms such as solar irradiation and volcanic eruptions, where meteorological data are lacking and on longer timescales (Bradley, 2015; Elias, 2021; Masson-Delmotte et al., 2013). Additionally, climate reconstructions, produced from palaeoclimate proxy records or modelling, can be

studied alongside the archaeological and historical record to examine social, cultural, and economic impacts from and human resilience in the face of climate change. Such studies, on historical human-environment-climate interactions, are now termed the "history of climate and society" (HCS: Degroot et al., 2021). When palaeoclimate data are utilised for HCS studies, chronological resolution must be very high and low age uncertainties are required in order to associate climatic and societal change (see Knapp & Manning, 2016).

In the EMME region, defined in this thesis as EM: Greece, Turkey, Cyprus, the Levant, and N Egypt, and ME: the Levant, the Fertile Crescent (FC: Syria, Iraq, and Iran), and the Arabian Peninsula (AP) (see Figure 1), climate change and its impact on societies is of increasing interest. Palaeoclimate proxy data suggests that the high spatial and temporal variability revealed by modern weather-station data and observations extends back throughout the earth's geological history. A dense network of highly-resolved and precisely-dated palaeoclimate records is therefore required to adequately reconstruct this variability. Unfortunately, a scarcity and uneven distribution of records is caused by climatic, environmental, and erosive conditions (Altaweel et al., 2019; Appendix B.2; Finné et al., 2011). One key climatic variable here is the requirement of adequate effective moisture for the formation of most continental records: speleothems, lakes, and trees. In hyper-arid regions, which are especially abundant in the ME, these records will not form. Lake sediment (lacustrine) records can detail past changes in lake-water balance (LWB), the difference between the amount of water entering the lake (through river/surface inflow, subterranean inflow and precipitation) and leaving the lake (through overflow, subsurface outflow and evaporation), which can be influenced by past environmental and climatic conditions (Bengtsson, 2012; Cardille et al., 2004). Lacustrine records are absent from most locations; where present, they often suffer from considerable chronological uncertainties due to radiocarbon dating and are low-resolution records, detailing climate averages over several centuries. Existing tree-ring sequences only cover relatively recent periods in the EMME region, rarely extending back further than 1,000 years. Speleothems (most commonly stalagmites) are increasingly being utilised as archives of past terrestrial climatic variability. They can provide multiple proxies of palaeoclimate variability at a high-resolution that covers long periods and can be accurately dated using uranium-series methods (Burstyn et al., 2019; Appendix B.1). Speleothems in the region reflect winter-spring precipitation or effective

moisture, the main hydrological (and an important agricultural) season (Burstyn et al., 2019; Appendix B.1), whereas lake records and tree rings often reflect annual or seasonal precipitation, or temperature. Further analysis of speleothems can fill the spatial and temporal gaps in palaeoclimatic understanding of the EMME region, providing information useful for constraining, and predicting, future climate change and for understanding past human-environment-climate interactions.

1.2. Late Antiquity

1.2.1. Historical context

The phrase Late Antiquity (3rd-7th centuries CE) refers to a period of political, religious and economic transformations in a region spanning western Europe to Central Asia (Bowersock et al., 1999; Inglebert, 2012). Traditionally, it has been viewed as a transitional phase between the Classical/Antique and Medieval periods where the ancient western world was dissipating and was eventually replaced by three major civilisations: western Europe, the Middle Byzantine Empire, and Islam (Brown, 1971, 1978). In the Late Antique EMME region, there was a large, complex, and shifting, network of interconnected empires, kingdoms, and tribes. In this thesis, I focus on the three largest states: (1) the Byzantine Empire in the EM, (2) the Sasanian Empire in Persia, and (3) the Kingdom of Himyar in the AP (see Figure 2). Smaller kingdoms and tribal confederations, both within and external to the region, also had significant impacts on their histories, located in the Caucasus (Armenia, Avars, Iberia, Lazica), the AP (Ghassanids, Kinda, Madhhij, Lakhmids), Africa (Aksum, Vandals), CA (Göktürks, Hephthalites) and towards India (Kushan).

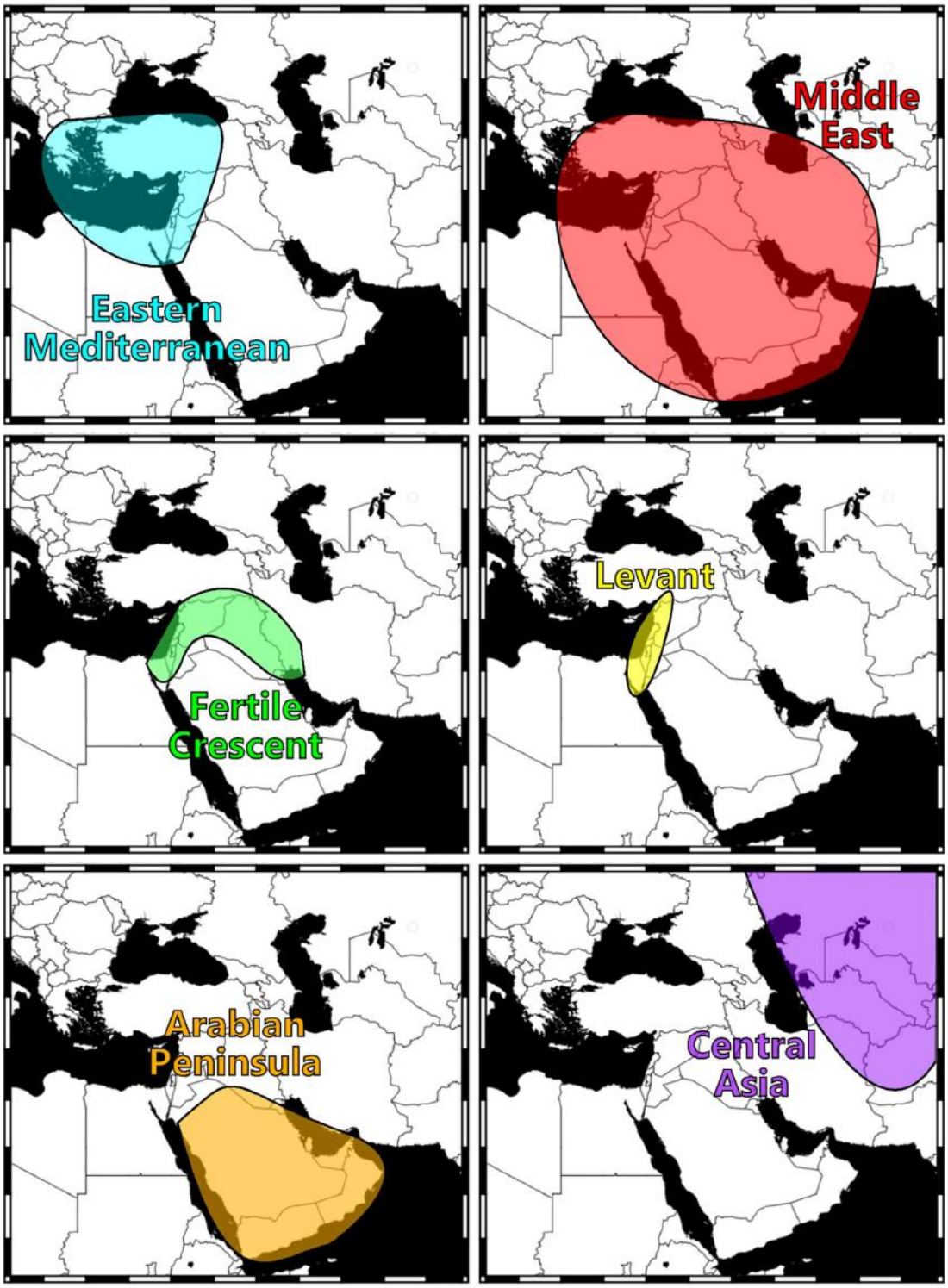

Figure 1. Borders of modern countries with region definitions employed in this thesis overlain. Abbreviations are as follows: Eastern Mediterranean (EM), Middle East (ME), Fertile Crescent (FC), Arabian Peninsula (AP) and Central Asia (CA).

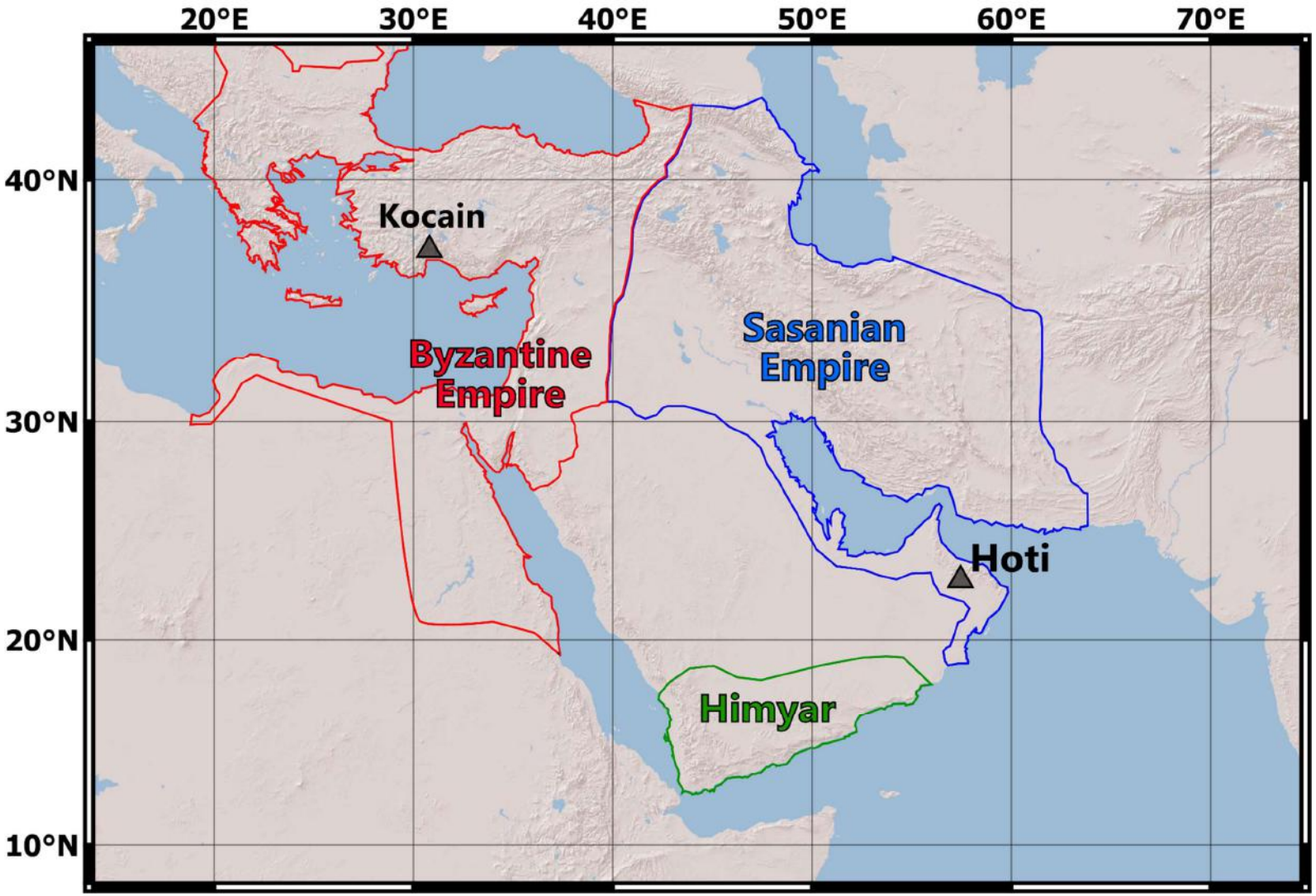

Figure 2. Territorial extent of the Late Antique states discussed in this thesis.

In the Mediterranean, the power of the Roman Empire, previously centred on Rome, slowly shifted to the east. Administrative changes by Diocletian in 286 CE initiated separation of the eastern and western provinces, the Roman capital was moved to Constantinople (modern Istanbul) in 330 CE, and in 395 CE the Eastern and Western Roman Empires were officially divided between Theodosius I's two sons upon his death (Ball, 2016; Cameron, 2012; Rees, 2004). The Western Roman Empire ended formally in 476 CE, following a long-lasting decline (Harper, 2017; Heather, 2005; Marx et al., 2018; Ward-Perkins, 2005), but the more-centralised Eastern Roman (Byzantine) Empire endured, with its capital in Constantinople, for around a millennium (Harris, 2007, 2010). Starting in the 3rd century CE, the traditional Roman religion and associated traditions declined, and were eventually legislated against, following the adoption of Christianity as the state religion (Maxwell, 2012). Economically, substantial sums were collected on a consistent basis due to the introduction of a regular tax period, with rates potentially rising throughout the period (Cameron, 2012). Taxation focused on labour and land used for agricultural activity; however, senatorial wealth and commerce taxes were introduced later in the period (Sarris, 2015, 2018). The primary purpose of these funds was to maintain the military, but it was also reinvested into agricultural infrastructure and developing trade-networks (Laiou, 2002; Morrisson & Sodini, 2002). The Byzantines increasingly traded with other states in the EMME, but also at longer distances to western Europe, Scandinavia, Africa, CA, India and China (Dark, 2007; McCormick, 2012; Pieri, 2012).

In Persia, internal strife and conflict with the Romans weakened the Parthian Empire and they were subsequently overthrown by Ardashir I in 224 CE, leading to the establishment of the Sasanian Empire with its capital at Ctesiphon (Bivar, 1983; R.N. Frye, 2005; Katouzian, 2009; Olbrycht, 2016). The Sasanian core territories were in eastern Mesopotamia and the Iranian Plateau, though eventually they came to control lands from Egypt, Anatolia, and the Levant, to the Indus River (Canepa & Wiesehöfer, 2018; Daryaee & Rezakhani, 2016; E. Sauer, 2017). Compared to the Parthian Empire, the Sasanians had a more centralised system of leadership; they similarly named their state *Eranshahr* ("the Empire of the Iranians"), after their Achaemenid ancestors whom they frequently imitated (Altaweel & Squitieri, 2018; Bosworth, 1999). Zoroastrianism was the state religion, which despite persecution evolved into several successful branches, such as Manichaeism and Mazdakism (Crone, 2012; Hutter, 1993). Kings claimed a divine right to rule; religion and empire were heavily intertwined

(Altaweel & Squitieri, 2018; Canepa & Wiesehöfer, 2018; Daryaee, 2019; Daryaee & Rezakhani, 2016). Zoroastrian fire temples also served as economic institutions, with religious professionals managing regional administration (Payne, 2014). Sasanian society became highly monetised, with soldiers, officials, and taxes, paid in coins (Kennedy, 2002, p. 157). Taxation was primarily agricultural, but was also conducted on internal sales, imports, exports, and Sasanian industry/artisan trades, which reworked raw materials into high-value commodities (Fakhar & Hesari, 2013; Gyselen, 1998; Payne, 2018). Cities were founded by Sasanian kings for this purpose and investment in irrigation infrastructure (primarily qanats and canals) was funded by taxation of the arable lands it provided (Asadi et al., 2013; Canepa & Daryaee, 2018; Hartnell, 2014). The Parthian and Sasanian empires both also acted as facilitators of, and profited from, long-distance trade, due to their important location along the land routes of the Silk Roads (R.N. Frye, 1993; T. Li, 2021; Payne, 2018).

In the south, the Kingdom of Himyar, with its capital in Zafar, increased its dominance over the AP, conquering the Saba'a and Hadhramawt regions ~280 CE and allying with the central Arabian Kinda and Madhhij tribes (Cameron, 2012; Phillipson, 2012; Yule, 2007). The polytheistic worship of a pantheon of south-Arabian gods, that was previously common to the region (Hoyland, 2001; Robin, 2006; Schippmann, 2001), gave way to monotheism influenced by Judaism (Robin, 2015; Schiettecatte, 2018). The Kingdom of Himyar planned the improvement of their land and invested in terraces, dams, and soil-retention walls, which enabled more productive agriculture and a wider diversity of crops (Charbonnier, 2009, 2011; Edwell, 2015; Stathakopoulos, 2004). Both agriculture and long-distance trade were important for the economy, with southern coastal towns trading local products, particularly aromatics and metals, and acting as a conduit for trade between the Mediterranean, Indian Ocean, and East Africa (Brunner, 1997; Schippmann, 2001; Shahîd, 2010).

From the above sections, similar historical patterns are observable in all three of these major Late Antique kingdoms, at least partially resulting from the fact that they developed with ongoing interactions with one another. The loose territorial empires and kingdoms of the previous periods were replaced by greater administrative control and investment in infrastructure for agricultural (e.g. terraces, canals, dams, qanats) and economic (e.g. trade and tax systems, coin minting, production centres) purposes. Whilst agriculture was still the basis of their economies (Canepa & Wiesehöfer, 2018; Hollander, 2019; Schippmann, 2001;

Takaoğlu, 2020; Yule, 2007), local and long-distance trade grew in importance leading to increased interconnectivity between regions (Cameron, 2012; Dark, 2007). The Sasanian Empire and Kingdom of Himyar both acted as conduits for Byzantine trade further east (Haas, 2018; Payne, 2018). Northern Arabian tribal confederations allied with the Byzantine and Sasanian empires to link them to the Indian Ocean and East African trade via the southern coastal towns in Himyar (Brunner, 1997; Schippmann, 2001; Shahîd, 2010). A "religious revolution" was also experienced across the region, with a gradual shift from polytheism to monotheism and increasing importance of religion to individual identities (Bowersock et al., 1999; Gwynn & Bangert, 2010; Stroumsa, 2015, pp. 27–28). Religion and politics were increasingly intertwined, with rulers concerned with the religion of their subjects (Howard-Johnston, 1995; Hoyland, 2012). Despite this, religious ideas were increasingly spread via trade networks and not all individuals adhered to their state religion; diverse religious communities existed across the EMME region (Cameron, 2012; Maxwell, 2012). For example, early Christianisation, which occurred in the Roman-Byzantine Empire, but also in the kingdoms of Aksum (Ethiopia), Iberia (Georgia), and Armenia (Haas, 2008), travelled via trade routes, and there were also large Christian communities in the Sasanian Empire and Kingdom of Himyar (Bowersock, 2013; Bowersock et al., 1999; Brock, 1982; Yule, 2007).

Not all interstate contact was friendly, however; constant and recurring conflicts were characteristic of Late Antiquity. Roman-Persian hostilities, which had begun in 54 BCE and were a continuation of the Greco-Persian wars with their origins in the 5th or 6th century BCE (Green, 1996; Katouzian, 2009), continued, with Roman-Parthian and Roman/Byzantine-Sasanian conflicts (Sicker, 2000). Despite the Byzantines and Sasanians viewing each other as equal rivals, with the terms *Basileús* and *Caesar* reserved exclusively in diplomatic documents for Sasanian kings and Roman emperors (Brockley, 1984, 1992; Canepa, 2009; Chrysos, 1978), they frequently warred over lands in Mesopotamia, the Caucasus, and Arabia, and launched invasions into each other's home territories (Canepa & Wiesehöfer, 2018; Sicker, 2000). In the northern regions of the AP, the tribal confederations that facilitated trade for the empires also fought proxy wars on their behalf, acting as a buffer between their territories and serving as mercenaries in their armies. These were the Tanukhids, Salagids and Ghassanids, for the Byzantines and the Lakhmids for the Sasanians (Cameron, 2012; Robin, 2015; Shahîd, 2010). Himyar was largely protected from these conflicts by their Kinda and Madhhij allies in central

and northern Arabia (Yule, 2007). However, they had a powerful adversary in Africa, the Christian Kingdom of Aksum (Haas, 2008), which attacked them frequently from at least the 3rd century CE (Hoyland, 2001; Seland, 2012). External pressure was also constant for the Byzantines, who fought with the Visigoths, Avars, Slavs, and Carthage, and the Sasanians, who had clashes to their east, with Kushan and Hunnic tribal confederations such as the Hephthalite Khanate (Cameron, 2012; Rezakhani, 2017).

At the end of Late Antiquity, in the 7th century CE, a further period of socio-cultural/-economic and religious change occurred. Islam emerged from Medina and Mecca in 622 CE and, over the next decade, spread rapidly throughout Arabia to the kingdoms and tribal confederations previously allied with the Byzantines and Sasanians (Cameron, 2012; Korotayev et al., 1999). After the Prophet Muhammad's death in 632 CE, the Rashidun Caliphate was established (Robinson, 2011; Whittow, 2011). The Caliphate rapidly conquered most of the Byzantine Empire's key economic territories in the Levant and Egypt, and invaded Persia, eventually leading to the end of the Sasanian Empire in 651 CE (Wiesehöfer, 2010). The coming of Islam to the EMME region was traditionally seen as an external Arabian force that overcame and replaced Antiquity; however, it is now increasingly identified as a distinctly Late Antique phenomenon arriving at the end of a gradual and multifaceted shift in society and culture (Conrad, 2000; Hoyland, 2012; Kennedy, 1999). Furthermore, changes experienced in the EMME region prior to the conception of the Islamic Caliphate are often considered vital for the success of their rapid conquests (e.g. Crone, 1987; Korotayev et al., 1999). A complex web of numerous interconnected natural and societal factors (recurrent plague epidemics, earthquakes, climate change, and invasions) starting in the mid-6th century CE, and continuing through the arrival of Islam, caused a general pattern of reduced long-distance trade, settlement numbers, and population (e.g. Cameron, 2012; Hirschfeld, 2006; Korotayev et al., 1999; Pourshariati, 2008). This thesis relates to the relative influence of climate as a contributory factor in Late Antiquity, with a particular focus on the changes of the 6th-7th centuries CE; socio-economic changes and other factors are therefore introduced and discussed in detail in each of the case-study discussion chapters.

1.2.2. Archaeological context

The political and historical changes described above are reflected in Late Antique archaeology. EMME archaeology provides physical evidence for expansion of settlement, investment in infrastructure and religious architecture, and long-distance trade. An increase in settlement numbers until the 6th century CE is observed in many regions, particularly in rural locations and associated with increased agricultural productivity. In Byzantine territory, peak settlement numbers come in the 5th and 6th centuries CE in almost all archaeological surveys across Anatolia and the Levant (Baird, 2004; Decker, 2018a, 2009; Decker & Cooper, 2012; Doonan, 2004; Izdebski et al., 2016; Meyer, 2013). Similarly, the Sasanian Period had the greatest number of settlements for any period in diverse regions, including the lower Diyala Basin (Adams, 1965, p. 69), Deh Luran (Neely, 2016), the Persian Gulf (Asadi et al., 2013) and Iranian Azerbaijan (Alizadeh et al., 2021; Alizadeh & Ur, 2007). Investment in agricultural infrastructure also peaks during this period in most regions, for example, in all the archaeological surveys mentioned above and in Sasanian Mesopotamia around Nippur (Altaweel et al., 2019; Appendix B.2; Campopiano, 2017; Wilkinson et al., 2012), and in the Himyaritic Yemeni mountains (Charbonnier, 2011). Construction of religious architecture also expanded during Late Antiquity, with the requirement for churches in Byzantine cities or *poleis* (Bowden, 2001; Haldon, 2016; Saradi, 2006) and construction of Zoroastrian fire temples across the Sasanian Empire, which also served as administrative centres (Boucharlat, 2014; Boyce, 1975; Hozhabri & Watson, 2013; Payne, 2014). Churches are also visible in excavations in Sasanian and Himyarite territories (e.g. Simpson, 2005; Zarins et al., 1983) and along the long-distance trade routes described above (Dark, 2007; Gardberg, 2001).

Long-distance trade is evidenced archaeologically for all kingdoms by the presence of characteristic products from other regions, and from finds in those regions of Byzantine, Sasanian, and Himyaritic technologies. Both raw materials and manufactured commodities were transported in large quantities. Across the Mediterranean and further afield, Byzantine Red Slip Wares (RSW) produced mainly in northern Africa increasingly dominate pottery assemblages (Arthur, 2008; Bonifay, 2008; Cameron, 2012), and evidence increased interconnectivity in the Byzantine Empire (Costa, 2015; Hayes, 2000; Mackensen & Scheider, 2006). For the Sasanian Empire, utilising their characteristic silver coinage as an example, these have been found in abundance across the EMME region (Darley & Canepa, 2018;

Schindel, 2013b; Sears & Ariel, 2000), China (Li, 2006; Skaff, 1998), and CA (R.N. Frye, 1993; T. Li, 2021). Other examples are found in diverse places such as Britain (Abdy & Williams, 2006) and Thailand (Tomber, 2007). The archaeology of Himyar includes less evidence for long-distance trade (resulting from a lack of excavation), which we know was well-established and important for the kingdom (Schippmann, 2001; Shahîd, 2010); Byzantine amphorae and other foreign products are identified from excavations at Zafar and coastal towns, such as Aqaba (Raith et al., 2013; Yule, 2013). These are only characteristic archaeological examples; many other products were traded over long-distances but do not survive archaeologically, e.g. incense, aromatics, and agricultural produce. Investment in trade networks is also evidenced by installation of road networks (e.g. Adak & Şahin, 2007) and development of manufacturing zones and storage facilities in port cities in the Mediterranean, Red Sea and Persian Gulf (Daryaee, 2003; Haas, 2018; Pashazanous et al., 2014; Rice, 2020).

Subsequent to the growth observed in the 4th- early 6th centuries in the EMME region, there is widespread evidence for reductions in settlement, population, investment and management, and inter-regional exchange. Settlement-number decline starts in the mid-6th to 8th centuries in many regions (Decker, 2018a; Izdebski, 2013a; Roberts et al., 2018b); however, there are many exceptions (Cassis et al., 2018). Maintenance and construction of agricultural infrastructure ended in the 6th and 7th century CE in many regions, leading to terraces, canals, and dams falling into disrepair. The largest example is the Ma'rib dam in Yemen, which required organised maintenance and fell into disrepair by ~580 CE (Brunner, 2000a; Robin, 2012). Similar occurrences happened, for example, in canals in Iranian Azerbaijan (Alizadeh et al., 2021) and drainage infrastructure in the Konya Plain (Baird, 2004). Contemporary reductions in inter-regional exchange and long-distance trade are evidenced ceramically by declining prominence of external forms, such as RSWs, and an increase in locally produced wares (Armstrong, 2009; Costa, 2015; Jackson et al., 2012).

The main archaeological bias in Late Antiquity comes from an implicit focus on the Byzantine Empire to the detriment of the study of other regions and communities. Until a few decades ago, archaeological interest in the Sasanian Empire and Kingdom of Himyar was extremely limited (Canepa, 2009; Genito, 2016; Whitcomb, 2014; Wilkinson et al., 1997). Byzantine archaeology is comparatively better-developed, with extensive research on many topics. Many reasons are given for this, principally, privileged study of the origins of Europe,

earlier periods, and Islamic history (Payne, 2014; Pourshariati, 2008; Whitcomb, 2014), but also geo-political obstacles to excavations in certain countries (Bernbeck, 2012). However, a recent trend towards field-based and remote-sensing settlement surveys (Decker, 2018b), is improving coverage of relatively unexplored and endangered regions (e.g. the EAMENA Project: Bewley et al., 2016).

1.2.3. History of (Late Antique) climate and society

Climatic factors have been suggested as a major factor in societal changes connected to the decline of the western Roman Empire (Büntgen et al., 2016; Harper, 2017; Marx et al., 2018; McCormick et al., 2012) and are increasingly considered as contributory factors in the Late Antique socio-economic transformations described in the previous sections (e.g. Izdebski et al., 2016b; Labuhn et al., 2018). However, there are several gaps in knowledge and key criticisms of such studies.

Firstly, studies often examine large regions and ignore spatial heterogeneity of climatic conditions and societal change, selecting bodies of evidence that cannot be connected to each other (Finné et al., 2011). This partly results from a general paucity of palaeoclimate archives in the EMME region (Section 1.1), and particularly a lack of regions containing both high-quality palaeoclimatic and archaeological evidence. This has led to a call for micro-regional case-studies (Haldon et al., 2014; Horden & Purcell, 2000).

Secondly, there have been numerous examinations of climatic impacts on the Roman and Byzantine empires, especially in Anatolia (e.g. Haldon et al., 2014; Xoplaki et al., 2018). However, akin to the archaeological bias, but more pronounced, examination of climatic impacts on other EMME communities and regions is almost entirely absent. Work that has been done is fragmentary, being either correlations between the end of an empire with climate changes in discussion of palaeoclimate records (e.g. Büntgen et al., 2020; Sharifi et al., 2015) or historical work that does not utilise palaeoclimate records (e.g. Korotayev et al., 1999).

1.3. Aims and objectives

The overall aim of this thesis is to investigate the influence of palaeoclimate change on humans and societies, in the Late Antique Eastern Mediterranean and Middle East. In order to achieve this, I aim to address the three key research gaps identified in the sections above: (1) Spatio-temporal coverage of palaeoclimate records, (2) micro-regional case-studies examining local impacts of climate change, (3) examination of climatic factors in the Sasanian Empire and Kingdom of Himyar. This can be divided into two main research aims, with associated objectives:

1. To classify climatic conditions during Late Antiquity

    a. Produce new speleothem-based palaeoclimate records, for SW Turkey and N Oman

    b. Synthesise existing palaeoclimate evidence

2. To examine the influence of climate change on social, economic, and political change, at varied scales

    Micro-regional:

    a. Construct a unified picture of settlement and socio-economic development for a micro-regional case study (SW Turkey)

    b. Identify factors contributing to societal and economic change

    c. Assess the relative importance of climatic conditions as a factor in this change

    Large-scale:

    a. Classify broad periods of socio-political change that correlate with significant shifts in palaeoclimate

    b. Evaluate the relative contribution of palaeoclimate change to socio-political transformations by assessing causal links

1.4. Structure of the thesis

To achieve the aims and objectives of the thesis, the climate of the study region, methodological issues relating to (1) climate reconstructions, and (2) their utilisation in historical discussions, are examined (Chapter 2). Work related to Chapter 2 contributed to four published journal articles co-authored by MJJ (Table 1). These can be found in Appendix B.

Three case-study regions are then explored, one micro-regional: SW Anatolia (Chapters 3-4), and two polity-wide: S Arabia (Kingdom of Himyar: Chapter 5), and Iraq/Iran (Sasanian Empire: Chapter 6). Finally, the findings of these chapters are summarised and discussed in relation to the thesis aims (Chapter 7). The thesis case studies (results) are presented as stand-alone papers in four chapters, formatted in the style of the journal to which they were submitted (Table 1). Author contributions are defined at the start of each chapter. Chapters are edited to link with other sections of the thesis and all references are collated at the end of the thesis. Specific research aims for each paper are outlined below.

Chapters 3 & 4 encompass the main case-study of the thesis, SW Anatolia (Turkey). This small sub-region now has high-quality evidence of both climatic and societal change.

- Chapter 3: "Heterogenous late Holocene climate in the Eastern Mediterranean – the Kocain Cave record from SW Turkey"

This chapter was accepted for publication in the journal *Geophysical Research Letters* (*GRL*) on 14th September 2021. It presents a new multi-proxy speleothem record of effective moisture from Kocain Cave, SW Turkey. The specific objectives of this paper are:

1. To constrain late Holocene palaeoclimate variability for SW Turkey, with a new high-resolution speleothem proxy record from Kocain Cave
2. To assess how the climate of this region varies compared to other Eastern Mediterranean regions

- Chapter 4: "Settlement, environment, and climate in SW Anatolia: the Roman to Middle Byzantine periods"

This chapter was submitted for publication in the journal *The Public Library of Science One* (*PLOS One*) on 7th January 2022. It utilises a new dataset of settlements derived from historical toponyms, and the Kocain Cave palaeoclimate data from Chapter 3, to examine established hypotheses around climate-driven socio-economic prosperity and decline for Late Antique SW Anatolia (Turkey). The specific objectives of this paper are:

1. To establish a unified picture of settlement and socio-economic development in SW Turkey
2. To examine the influence of climatic and environmental factors on periods of economic and settlement prosperity and decline during Late Antiquity

Chapters 5 and 6 present two large-scale case-studies for states which have previously received little attention.

- Chapter 5: "Droughts and societal change: the environmental context for the emergence of Islam in late Antique Arabia"

This chapter was submitted for publication in the journal *Science* on 4th January 2021. It presents a new speleothem-based palaeoclimate proxy record from Hoti Cave, Oman, and assesses the potential impact of climate on the disintegration of Arabian polities, including the Kingdom of Himyar, in the 6th and 7th centuries CE. The specific objectives of this paper are:

1. To present a new high-resolution speleothem record from Hoti Cave, Northern Oman
2. To assess the evidence for Arabian droughts in Late Antiquity
3. To determine whether droughts contributed to the socio-political transformations in Arabia in the 6th and 7th centuries CE

- Chapter 6: "Climate change and the Sasanian Empire (224-651 CE): a review"

This chapter was prepared for submission to the *Journal of Interdisciplinary History* (*JIH*). It provides an initial review of the impact of climate change on the Sasanian Empire (224-651 CE), located in modern Iraq and Iran. The specific objectives of this paper are:

1. To evaluate mechanisms through which climatic change could influence the Sasanian Empire
2. To establish a history of 1st millennium CE climate change for Iraq/Iran, the key territories of the Sasanian Empire
3. To determine to what extent climatic conditions contributed to the empires end in 651 CE

Chapter 7 summarises the three case studies to draw final conclusions about the impact of climate change in the Late Antique Eastern Mediterranean/Middle East, and to address four key research questions:

1. How did climatic conditions change in the EMME region during Late Antiquity?
2. To what extent did changing climatic conditions impact societies and their economies?
3. Was climatic change an important factor in the decline of empires and kingdoms in the 6th and 7th centuries CE?
4. Do micro-regional case-studies improve our understanding of socio-economic impacts from climate change?

Table 1. Journal articles produced as part of this thesis.

Paper Title	Chapter	Journal	Status	Estimated contribution by MJJ (%)
Speleothems from the Middle East: An Example of Water Limited Environments in the SISAL Database	2	*Quaternary*	Published	15
New insights on the role of environmental dynamics shaping southern Mesopotamia: From the Pre-Ubaid to the Early Islamic Period	2	*Iraq*	Published	10
Main controls on the stable carbon isotope composition of speleothems	2	*Geochimica et Cosmochimica Acta*	Published	15
The stalagmite record of southern Arabia: climatic extremes, human evolution and societal development	2	*Frontiers in Earth Science*	Published	30
Heterogenous late Holocene climate in the Eastern Mediterranean – the Kocain Cave record from SW Turkey	3	*Geophysical Research Letters*	Published	70
Settlement, environment, and climate change in SW Anatolia: dynamics of regional variation and the end of Antiquity	4	*PLOS ONE*	Submitted	70

Droughts and societal change: the environmental context for the emergence of Islam in late Antique Arabia	5	*Science*	Submitted	15
Climate change and the Sasanian Empire (224 - 651 CE): a review	6	*Journal of Interdisciplinary History*	Not yet submitted	100

Chapter 2: Recreating Eastern Mediterranean and Middle Eastern Climate

2.1. Preface

Work related to the writing of this review chapter contributed to four journal articles co-authored by MJJ. These were published in peer-reviewed, influential journals:

1. Burstyn, Y., Martrat, B., Lopez, Jordi, F., Iriarte, E., **Jacobson, M.J.**, Lone, M. A., Deininger, M. (2019). Speleothems from the Middle East: An Example of Water Limited Environments in the SISAL Database. *Quaternary*, *2*(16). https://doi.org/10.3390/quat2020016

This paper was accepted for publication in the journal *Quaternary* on 4th April 2019 and produced by the Middle East regional division of the SISAL PAGES working group. As of the 14th October 2021, this paper has been cited 15 times. MJJ contributed to the study concept design and by writing sections 1 (Introduction) and 2 (Climate of the Middle East), as well as parts of 4.3 (Holocene Climatic Events and Spatial Heterogeneity across the Middle East), relating to the past 2,000 years, and 5.2 (The Importance of Fertile Crescent Speleothem Data). The estimated percentage contribution of MJJ to this paper is ~15%.

2. Altaweel, M., Marsh, A., Jotheri, J., Hritz, C., Fleitmann, D., Rost, S., Lintner, S.F., Gibson, M., Bosomworth, M., **Jacobson, M.J.**, Garzanti, E., Limonta, M., Radeff, G., 2019. New insights on the role of environmental dynamics shaping southern Mesopotamia: From the Pre-Ubaid to the Early Islamic Period. *Iraq* 81, 23–46. https://doi.org/10.1017/irq.2019.2

This paper was accepted for publication in the journal *Iraq* on 18th July 2019. As of the 14th October 2021, this paper has been cited 12 times. MJJ contributed to the Introduction, Methods: Speleothems, Speleothem Climate Results and the Climate Discussion sections. This work is also associated with Chapter 6. The estimated percentage contribution of MJJ to this paper is ~10%.

3. Fohlmeister, J., Voarintsoa, N.R.G., Lechleitner, F.A., Boyd, M., Brandtstätter, S., **Jacobson, M.J.**, Oster, J.L., 2020. Main controls on the stable carbon isotope composition of

speleothems. *Geochimica et Cosmochimica Acta* 279, 67–87. https://doi.org/10.1016/j.gca.2020.03.042

This paper was accepted for publication in the journal *Geochimica et Cosmochimica Acta* on 29th March 2020 and produced by the carbon stable-isotopes division of the SISAL PAGES working group. As of the 14th October 2021, this paper has been cited 30 times. MJJ contributed to the study concept design and to sections 1 (Introduction), 3.1 (Climate influence on speleothem $\delta^{13}C$), 3.2 (Influence of local processes on speleothem $\delta^{13}C$ values), 5.1 (Controls on modern speleothem $\delta^{13}C$ values) and 5.3 (Governing processes in karst and speleothem $\delta^{13}C$ values). The estimated percentage contribution of MJJ to this paper is ~15%.

4. Nicholson, S.L., **Jacobson, M.J.**, Hosfield, R., Fleitmann, D. 2021. The stalagmite record of southern Arabia: climatic extremes, human evolution and societal development. *Frontiers in Earth Science.*

This paper was accepted for publication in the journal *Frontiers in Earth Science* on the 30th November 2021. The work was requested for a special issue titled "Extreme Events in Human Evolution: From the Pliocene to the Anthropocene". MJJ contributed to the study concept design, and by writing the Holocene sections of the Discussion and Conclusion, and by providing feedback on the manuscript. The estimated percentage contribution of MJJ to this paper is ~30%.

All four articles can be found in Appendix B, with key findings discussed in Chapter 7.

This chapter provides important background information on the modern climatology of the study region, palaeoclimate archives, and their utilisation in historical and archaeological analyses. Chapters 3-6 contain specific literature reviews relevant for their discussions.

2.2. Modern Climatology

The study region of this thesis, comprising the EM and ME, experiences marked heterogeneity of climatic conditions over relatively short distances (Jürg Luterbacher et al., 2012; Ulbrich et al., 2012; Xoplaki et al., 2018). The EMME region is located on the sub-tropical high-pressure belt, the boundary between the Northern Hemisphere tropical (Hadley cell) and the mid-latitude atmospheric circulation (Ferrel cell) (Burstyn et al., 2019; Levine et al., 2015). Broadly speaking, the whole region is characterised by hot and dry summers (Jun-Aug), with milder and wetter winter (Oct-Feb) and spring (Mar-May) seasons (Figure 3). A temperature and precipitation gradient is observed, with wetter and colder climates in the northwest (Aegean) and hot and dry climates in the southeast (AP and south Iran). However, there are large ranges in precipitation and temperature, varied seasonal patterns, and high inter-annual variability (Barlow et al., 2016; Gerlitz et al., 2020). Spatial variations in temperature are primarily determined by distance from the equator and altitude. Precipitation is more complicated, being influenced by proximity to moisture sources, cyclone frequency and trajectories, topography, large-scale atmospheric phenomena, and teleconnections (Xoplaki et al., 2004).

Mediterranean cyclones, which transport moisture to Greece, Turkey, the Levant, the FC, and more rarely, the AP, are the primary source of precipitation, propelled by westerly storm tracks that originate in the North Atlantic or in the Cyprus Lows (Trigo et al., 2002; Ulbrich et al., 2012). Cyclogenesis is amplified in the EM by an eastward gradient of increasing salinity and sea surface temperatures (SSTs) in the Mediterranean, which creates a greater temperature difference between the sea and the surrounding land (Brayshaw et al., 2010). The northern parts of Greece and Turkey also receive cyclones originating to the northwest over Central Europe, the Black Sea and the Gulf of Genoa (Karaca et al., 2000; Trigo et al., 2002). In NE Turkey, the Caucasus, and N Iran, cyclones from the Black Sea and Caspian Sea bring additional precipitation (Maslova et al., 2020; Molanejad et al., 2015). In the AP, as well as Mediterranean frontal systems, the Indian Summer Monsoon (ISM) occasionally brings summer precipitation to the southernmost regions (Beck et al., 2018; Findlater, 1969; Fleitmann & Matter, 2009) and moisture advected from the Red Sea causes precipitation in the west (Almazroui et al., 2012).

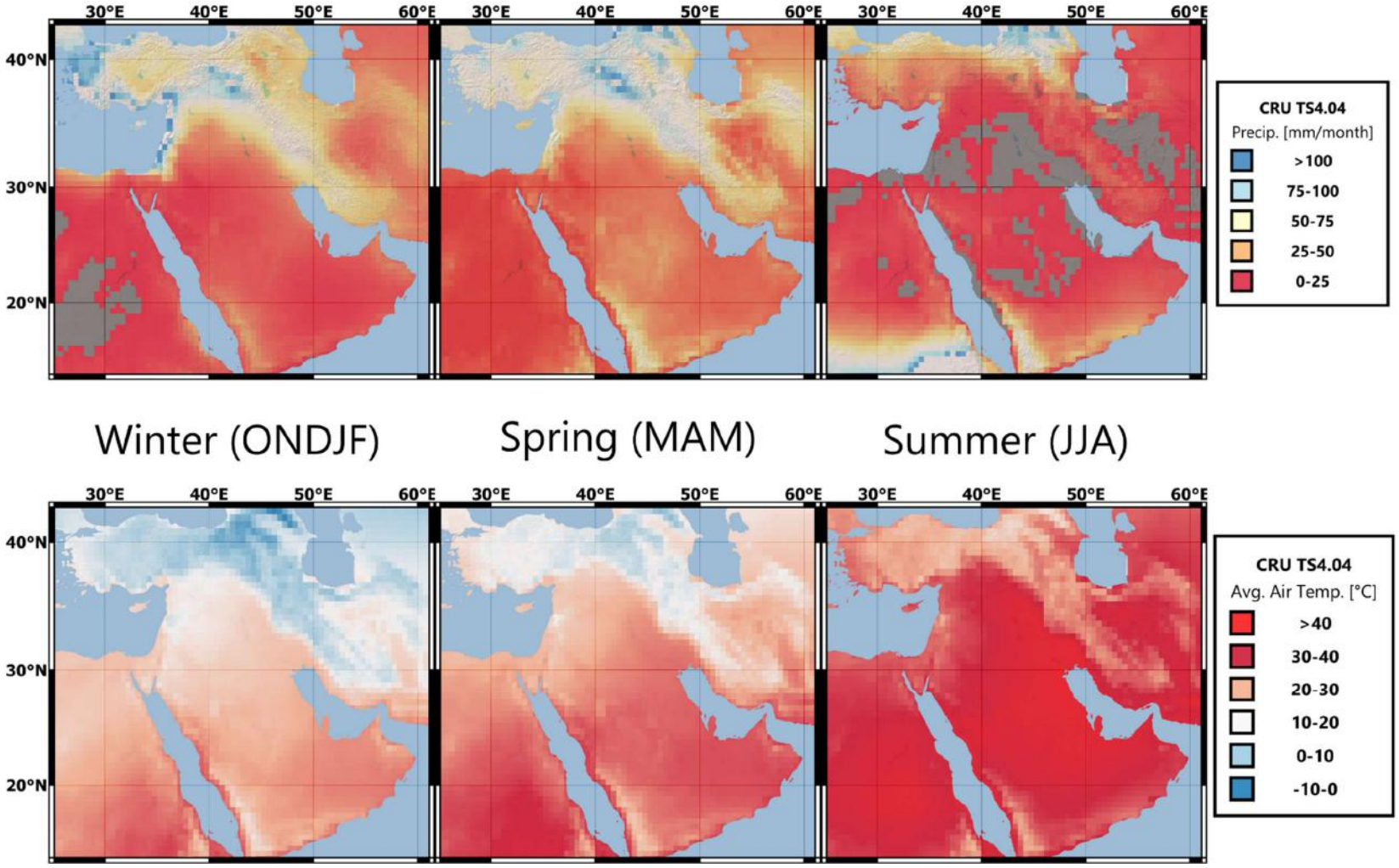

Figure 3. CRU TS4.04 (monthly gridded climate observations calculated from daily data provided by National Meteorological Services: 1901-2019) averaged seasonal precipitation (top) and air temperature (bottom) data for the Middle East collected from the KMNI climate explorer (van Oldenborgh, 2020; University of East Anglia Climatic Research Unit et al., 2020). Grey regions in precipitation data experienced no precipitation.

The physical geography of the region, particularly the coastlines and mountain ranges, significantly influences local precipitation. Orographic precipitation, resulting from humid coastal air being cooled as it rises over mountains, occurs on the coasts of the Mediterranean, Black and Caspian seas (Evans et al., 2004; Maslova et al., 2020; Molavi-Arabshahi et al., 2016). In addition to augmenting precipitation on their windward side, mountains inversely act as orographic barriers which block storm tracks from penetrating further inland and trap hot air (Babaeian & Rezazadeh, 2018). This, combined with their latitude, makes the AP, and the Syrian and South Iranian deserts, some of the hottest and driest locations on earth (Djamali et al., 2011; Edgell, 2006; Mildrexler et al., 2006). This is further enhanced by *rainout*, whereby the intensity and probability of precipitation decreases further inland as air-masses dry up, exaggerated by greater evaporation at the base of clouds in hotter regions (Evans et al., 2004).

Teleconnection patterns also influence the hydroclimate of the ME, with the North Atlantic Oscillation (NAO) being the most impactful, especially during winter. In the positive phase, pressure at the Azores high is elevated and at the Icelandic low is deepened. This is suggested to shift the dominant storm track south, decreasing precipitation in western Turkey and increasing precipitation in the southern Levant (Hurrell, 1995; Türkeş & Erlat, 2003). However, NAO impact was suggested to be negligible by Evans et al. (2004), who found NAO influences were only important for the southern Zagros region and proposed that a more subtle impact than movement of the storm track was likely occurring. Other teleconnection patterns impacting the ME include: North Sea – Caspian Pattern (NCP); East Atlantic – West Russian (EATL/WRUS); Scandinavian (SCAND); and the El Niño – Southern Oscillation (ENSO) (Alizadeh-Choobari, 2017; Kutiel et al., 2002; Yuyun Liu et al., 2014; Mellado-Cano et al., 2019).

The climatology of specific regions is explored in greater detail in their respective chapters: Turkey (Chapter 3), Arabia (Chapter 5), and Iraq/Iran (Chapter 6).

2.3. Palaeoclimate Reconstructions

In this section, methodologies for understanding past climates are introduced, with detailed information on speleothems and their geochemical proxies, other palaeoclimate archives, archaeological data, and historical records. The spatio-temporal availability of high-resolution EMME palaeoclimate proxy records that cover Late Antiquity is then examined.

2.3.1. Speleothems

Speleothems are deposits of calcium carbonate ($CaCO_3$) precipitated from cave drip-waters. In karstic regions, groundwater interacts with carbon dioxide (CO_2) whilst moving through the aquifer, leading to the formation of carbonic acid (H_2CO_3). The carbonate bedrock is dissolved by this acid and the resultant calcium and bicarbonate ions (Ca^{2+} and HCO_3^-) are transported by percolating groundwater into caves below. Once inside the cave, CO_2 is degassed to redeposit $CaCO_3$ (White, 2016). Depending on cave conditions and water movement characteristics, this process will deposit speleothems in various forms. Stalagmites develop upwards from the cave floor or other surfaces, stalactites form downwards from the cave ceiling, flowstones accumulate along surfaces, and a variety of other crystalline or cluster structures, such as anthodites or moonmilk, can be deposited (Fairchild et al., 2007; Ford & Williams, 2007; White, 2012).

Speleothems are employed in palaeoclimate reconstructions as their formation is determined by the input of groundwater to a cave, commonly comprising local precipitation and/or snow-melt. Additionally, their subterranean location protects them from the natural weathering and human interference which often damage or complicate other palaeoclimate archives (McDermott et al., 2006). The most frequently utilised form of speleothem for palaeoclimate reconstructions is stalagmites, composed of minute calcite/aragonite accumulations on a cave floor or surface from cave drip-water. Physically, stalagmites' simple geometry and formation processes mean depth along the growth-axis (the central point of deposition) corresponds to age; their relatively rapid growth-rates allow for analysis at higher resolutions, and they are not limited by weight considerations, unlike stalactites which break

more frequently (Bell & Walker, 2005; White, 1976). Stalagmites also form closer to isotopic equilibrium with their parent cave drip-water, simplifying stable-isotope analysis (Gascoyne, 1992; McDermott et al., 2006).

Stable-isotope analysis, trace-element ratios, organic acid contents, fluid inclusion composition, and physical characteristics such as growth rates, laminae thickness, and colour, are all potentially valuable palaeoclimate proxies held within stalagmites (McDermott, 2004; White, 2012). Shifts identified in these proxies can correspond to changes in precipitation (amount, source and/or seasonality), temperature, or atmospheric CO_2. However, these proxies can be altered by factors unrelated to climate or by multiple influences simultaneously, complicating analysis (see below). This potential for obtaining multiple proxy records from a single speleothem, enables examination of their relationships to one another which informs influences on each proxy. When combined with their long and often continuous formation, precise chronologies from uranium-series dates (see below) and high-resolution analysis (up to sub-annual), speleothems are established as one of the highest quality archives for climate variability (Burstyn et al., 2019; Fairchild & Baker, 2012; Jürg Luterbacher et al., 2012; McDermott et al., 2006).

Stable Isotopes of Oxygen and Carbon

Material excavated from the growth-axis of a speleothem is primarily composed of $CaCO_3$, enabling measurements of stable isotopes of oxygen ($\delta^{18}O$) and carbon ($\delta^{13}C$). These stable-isotope ratios are impacted by climatic variables and are therefore utilised to reconstruct palaeoclimatic change.

Stable isotopes of oxygen (^{16}O and ^{18}O), which are given as a ratio ($\delta^{18}O$), are the most common proxy utilised from speleothems for palaeoclimatic reconstruction. The principal determinant of $\delta^{18}O$ values is the *source effect*, whereby they are strongly influenced by the marine reservoir that contributes its vapor to rain formation. For the EMME region, precipitation is derived from multiple sources (see above), each with their own isotopic signature. The Mediterranean is the primary source and its values are impacted by Nile outflow and the eastward salinity/SST gradient described above. Nile outflow is isotopically

light (more ^{16}O) and salinity/SST impacts evaporation, which preferentially removes ^{16}O (Hennekam et al., 2014; Lachniet, 2009; Wang et al., 2010).

The *source effect* is the principal determinant of $\delta^{18}O$ values on long timescales; however, the impact is negligible on the timescales examined in this thesis. Smaller variations in $\delta^{18}O$ values are related to short-term climatic change. Before precipitation reaches a cave site, the $\delta^{18}O$ is impacted by multiple effects. The *amount effect*, which is a negative correlation between precipitation $\delta^{18}O$ and amount (Dansgaard, 1964), is frequently considered the main determinant of $\delta^{18}O$ variation in EMME speleothems, and speleothems globally. Seasonality is also important for precipitation $\delta^{18}O$ in the EMME, where $\delta^{18}O$ values are lower in winter and higher in summer (Feng et al., 2009; Lachniet, 2009). Increased summer precipitation or less winter precipitation can therefore alter $\delta^{18}O$ to appear 'drier' (Lachniet, 2009). This is caused by the temperature-dependent equilibrium fractionation and higher summer temperatures. Increased evaporation at the base of the cloud preferentially removes ^{16}O, thus increasing $\delta^{18}O$ (Rozanski et al., 1992). Through the same process, average temperature changes will impact $\delta^{18}O$ (*temperature effect*). Increasing altitude (*altitude effect*), due to the impacts of topography discussed above, decreases $\delta^{18}O$ values (Kern et al., 2020). Decreasing temperatures lower evaporation rates and prior orographic precipitation leaves the lighter elements remaining. Generally, precipitation $\delta^{18}O$ decreases as air masses move further from the ocean (*continental effect*) due to rainout (Kern et al., 2020).

Upon precipitating, moisture must reach the cave to form a speleothem. During this process of penetration, a fraction of the precipitation is lost to evaporation and transpiration or diverted away from the cave (Fetter, 1994; Geyh, 2000). Evaporation in the soil or epikarst can increase $\delta^{18}O$ values further, which is especially prevalent in the arid regions of the EMME. Where present, vegetation density and type can impact this evaporation, opening the possibility of anthropogenic impacts on $\delta^{18}O$ (McDermott et al., 2006). Mixing of precipitated water with soil moisture can alter overall $\delta^{18}O$, but the effect is minor when this process is consistent as there is less variation in soil moisture $\delta^{18}O$ values (Geyh, 2000; Lachniet, 2009). In the epikarst, there are further impacts from transit times of water and the amount of recharge, such as evaporation and potential lags between $\delta^{18}O$ in precipitation and calcite. Further evaporation can occur in caves with low relative humidity, long residence times for drip-waters or in well-ventilated caves (e.g. Kocain Cave: Chapter 3).

Whilst $\delta^{18}O$ is often noisy, especially in fast-growing speleothems, stable isotopes of carbon (^{12}C and ^{13}C, given as the ratio: $\delta^{13}C$) are less sensitive to short-term variations (Bar-Matthews & Ayalon, 2011; Burstyn et al., 2019; Appendix B.1). The precision of $\delta^{13}C$ is higher than that of $\delta^{18}O$ when using the Vienna PeeDee Belemnite standard (VPDB); the error for carbon is ±0.02‰, whereas for oxygen it is ±0.05‰ (Miller & Wheeler, 2012). Additionally, carbon is held at the centre of $CO3^-$ groups and therefore requires more energy to be fractionated, resulting in smaller variations between samples (Ford & Williams, 2007). However, climatic controls on $\delta^{13}C$ are discussed less frequently due to the complexity of fractionation effects, which results in challenging analysis (Fairchild et al., 2006; Fohlmeister et al., 2020; Appendix B.3). Soil gas CO_2 is the source of 80-95% of the carbon in cave drip-waters (Genty et al., 2001; Rampelbergh et al., 2013). This CO_2 is derived from respiring vegetation and organic matter. $\delta^{13}C$ in soil gas CO_2 is influenced by the photosynthetic pathway of the vegetation; this pathway can be characterised as C3 (cool-season plants), C4 (water-stressed) or CAM (arid) plants. C4 plants respire CO_2 with elevated $\delta^{13}C$ compared to C3 plants, leading to higher $\delta^{13}C$ under drier conditions; CAM plants complicate this interpretation as they have $\delta^{13}C$ values between those of C3 and C4 plants (Cerling, 1984; Herrera, 2009). The density of vegetation, as well as soil respiration rate, also impact $\delta^{13}C$ in soil gas CO_2. Heavy carbon dissolved from the bedrock will comprise the majority of the rest of the carbon in the drip-water; the contribution ratio between carbon dissolution and soil gas CO_2 is determined by how open or closed the soil system is (Hendy, 1971). In a closed system where waters are isolated from soil gas CO_2, carbonate dissolution will occur leading to changes in $\delta^{13}C$ (McDermott, 2004). In an open system with longer residence times, the $\delta^{13}C$ of the drip-water will reflect $\delta^{13}C$ of the soil gas CO_2. Systems are normally not fully "open" or "closed", and a mix of these two sources will be present (Fohlmeister et al., 2020). Drip-water $\delta^{13}C$ can also be derived from magmatic CO_2, dead organic matter CO_2, or trapped methane, although circumstances required for their input are rare (Geyh, 2000).

Calcite is precipitated when percolating groundwater reaches an area where the partial pressure of CO_2 (pCO_2) is lower. This also occurs prior to speleothem formation when the drip-water enters voids above the cave. Prior calcite precipitation (PCP) elevates $\delta^{13}C$ as isotopically-lighter ^{12}C is preferentially deposited (Fohlmeister et al., 2020). The above factors,

as well as recharge conditions and drip-rate, are driven by hydroclimatic conditions, altering $\delta^{13}C$ in the same direction with respect to EM.

Trace Elements

Trace elements within speleothems, presented as ratios with Ca, are increasingly employed as palaeo-climatic and -environmental proxies. Trace elements can derive from numerous sources, including the above bedrock, sediments, organic matter, and atmospheric deposition. Most commonly, Mg/Ca and Sr/Ca are utilised for palaeoclimate analysis as their elements form divalent cations (Mg^{2+} and Sr^{2+}) which can substitute for Ca^{2+} in the carbonate crystal lattice (Borsato et al., 2007; Fairchild & Treble, 2009). These elements are primarily derived from dolomite and calcite phases in the above bedrock, which remain relatively homogenous through time, especially on shorter time scales. Mg is commonly employed as an effective moisture proxy worldwide: e.g. Ireland (Tooth & Fairchild, 2003), Italy (Regattieri et al., 2014), Australia (Treble et al., 2003), Brazil (Bernal et al., 2016), Morocco (Wassenburg et al., 2013), and Iraq (Flohr et al., 2017). Mg is preferentially used instead of Sr, which has other sources that can alter its abundance, such as input from aeolian dust, sea spray, and silicates (Fairchild & Treble, 2009; Stoll et al., 2012). For these two ratios, the amount of PCP (described above) is important for the climatic interpretation. PCP is enhanced during periods of lower effective moisture due to longer residence times of percolating groundwater, lower drip-rates and the creation of air pockets in soil that has undergone evapotranspiration (Fairchild & Treble, 2009; Tremaine & Froelich, 2013). During PCP, Ca^{2+} is preferentially removed (over Mg^{2+} and Sr^{2+} cations) from the cave drip-water, enhancing the trace-element ratios (Borsato et al., 2007; McDonald et al., 2004; Treble et al., 2003; Wassenburg et al., 2020). Additionally in drier intervals, longer groundwater residence times cause additional dissolution of overlying dolomitic limestones if they are present. This contributes extra Mg^{2+} to the percolating groundwater, enhancing Mg/Ca further (Fairchild & Treble, 2009). P/Ca ratios provide an additional palaeoclimate proxy; however, interpretations are more complicated due to multiple sources and influences (Frisia et al., 2012; Johnson et al., 2006). Increased biological activity, either as vegetation on the surface or from soil microbes, releases bio-available P that is transported during intense soil infiltration (Fairchild et al.,

2001, 2007; Treble et al., 2003). P/Ca can also be influenced by PCP, but inversely to the other records, wherein P accumulates on mineral surfaces during the process (Lewis et al., 2011). Other trace-elements have been utilised as palaeoclimatic indicators, but can also inform impacts from atmospheric input and pollution, mining activities within caves, aeolian transport, and volcanic eruptions (Badertscher et al., 2014; Fairchild & Treble, 2009).

Physical Characteristics

Periods of palaeoclimatic change identified in geochemical analyses of speleothems can be further supported through physical observations and characteristics. Growth-rate, apex-diameter, laminae thickness, and colour intensity and hue, have all been utilised as palaeoclimate proxies. Speleothem formation is dependent on sufficient effective moisture; furthermore, the amount of growth relates directly to the volume of cave drip-waters and the amount of calcium carbonate carried into the cave to be precipitated. Once an age-depth model is established (see below), growth-rate can be calculated (distance/time) and will be linked to water input to the speleothem, which is ultimately dependent on effective moisture (Martín-Chivelet et al., 2017). Laminae (growth-layer) thickness and apex-diameter follow a similar pattern, where higher drip-rates increase their size (Muñoz-García et al., 2016). The colour of layers also indicates past conditions, which can be verified using other proxies. For example, dust layers may be visible and these can derive from exogenous dust carried in with the cave drip-water or from cave dust adhered to the speleothem as it formed (Carolin et al., 2019; Fairchild & Treble, 2009).

Uranium-Series Dating and Age-Depth Modelling

Once speleothem-based proxy records are linked to climatic (or other) changes, their chronology must be established so that specific deviations can be dated. This is achieved first by performing uranium-series dating on speleothem material and then modelling growth from these dates. U-Th dating works by analysing isotope ratios of Uranium (^{238}U and ^{234}U) and Thorium (^{234}Th, ^{232}Th, and ^{230}Th) and calculating the time that has passed since deposition according to decay constants (Cheng et al., 2013). Uranium is highly soluble and

transported in the cave drip-water to be precipitated during speleothem formation. Thorium is insoluble and does not undergo the same process. As such, when ^{238}U is deposited, ^{230}Th will build up from radioactive decay. Where there is incorporation of other materials containing Thorium (detrital contamination), isotope ratios can be corrected by measuring ^{232}Th and assuming an initial $^{230}Th/^{232}Th$ ratio (Spötl & Boch, 2019).

From a set of U-Th dates, and their corresponding depths, age-depth models can be constructed. For the records in this thesis, *StalAge* (Scholz & Hoffmann, 2011) was utilised, an algorithm created for constructing speleothem age models. The system identifies outliers objectively for the user, calculates 95% confidence limits for uncertainty, and uses further information to improve the age model, much like Bayesian chronological testing. *StalAge* performs 300 iterations of a Monte-Carlo simulation where ensembles of straight lines are fit to sub-sets of the given age data and bases the age-model on the simplest possible age-distance relationship (Scholz & Hoffmann, 2011).

2.3.2. Other palaeoclimate evidence

Speleothems are primarily utilised in this thesis for palaeoclimate reconstruction, due to their potential to provide highly resolved and well-dated multi-proxy records (see above). However, other archives provide evidence of climatic change. Whilst high-resolution tree ring data from the EMME region does not yet extend into the first millennium CE (Touchan et al., 2014a, 2014b), lacustrine records often have long durations (Jones et al., 2019; Leng et al., 2006), historical records can be used to describe weather patterns and certain phenomena (McCormick et al., 2012), and archaeological evidence can indirectly inform on climatic conditions (Izdebski et al., 2016b). These methods are discussed further below.

Lakes

Palaeolimnology, the study of past environmental and climatic conditions from lacustrine sediments (Last & Smol, 2001; Leng et al., 2006), has seen extensive use in the EMME region (Jones et al., 2019; Roberts et al., 2008, 2012). Fossil pollen and sedimentation

processes in lakes can provide palaeoclimatic evidence (Chevalier et al., 2020); however, disentangling anthropogenic influence from pollen changes is often impossible, so pollen in occupied regions is used to reconstruct past land-use (Roberts et al., 2019; Woodbridge et al., 2019). Numerous other lacustrine proxies exist that reflect changes in LWB (Bengtsson, 2012; Chapter 1.1). LWB can be influenced by past effective moisture, similarly to some speleothem records, via the impacts of evaporation (dependent on temperature and solar irradiance) and precipitation (Cardille et al., 2004).

$\delta^{18}O$ measurements (from carbonates and diatoms) have been utilised in the EMME region (e.g. Dean et al., 2018; Eastwood et al., 2007; Jones et al., 2006). These reflect changes in LWB and also the $\delta^{18}O$ of precipitation; evaporative enrichment is more important than in speleothems (Jones & Roberts, 2008). Depending on the material that $\delta^{18}O$ measurements are taken from, different seasons are represented. For example, in the Lake Nar record, carbonates form in the summer (Jun/Jul) whilst diatoms grow in the spring (Mar/Apr); $\delta^{18}O$ measurements of these materials therefore evidence LWB during those seasons (Dean et al., 2015, 2018).

Geochemical records of lacustrine sediments have been increasingly utilised in the last decade, with Peloponnese lakes in particular seeing extensive study at high resolutions (Section 2.3.3; Seguin et al., 2020b). Elements are measured which reflect inputs into the lake (e.g. carbonaceous, clastic, exogenous dust, terrestrial) and these are often calculated as a ratio to establish wet and dry phases in the lakes' history (e.g. Seguin et al., 2020a; Sharifi et al., 2015). For example, Ca/Fe ratios at Lake Salda reflect the relative input of carbonate content and detrital input, which reflect drier and wetter conditions, respectively (Danladi & Akçer-Ön, 2018). Alternatively, principal component analyses (PCA) of elements can provide a variable that similarly distinguishes between the various inputs, which are impacted by hydroclimatic variations (e.g. Seguin et al., 2020b).

Lacustrine sediment archives therefore offer multiple proxies that are influenced by climatic conditions and provide long-lasting records. However, they are often lower resolution due to compaction and formation processes and can suffer from considerable dating inaccuracies (Von Gunten et al., 2009; Izdebski et al., 2016a). Age uncertainties within radiocarbon dates from lakes are generally much higher than uranium-series dates from

speleothems, ranging from decades to thousands of years. Furthermore, radiocarbon dates from lakes often utilise 1-σ errors, meaning there is only a 68% probability the date falls within that range; uranium-series dates from speleothems are presented with 2-σ errors, which have a 95.4% probability (Dorale et al., 2004; Spötl & Boch, 2019; Taylor & Bar-Yosef, 2014). In freshwater lakes, radiocarbon ages can also be impacted by the "freshwater reservoir effect", whereby hard water rich in dissolved ancient $CaCO_3$ produces anomalously old radiocarbon ages (Philippsen, 2013). Fast-forming and varved (annually laminated) lakes help to improve resolution, as samples can be taken from individual varves, and reduce age uncertainties, through varve-counting (Zolitschka et al., 2015). Improvements in laboratory methods are increasing the resolution of lake records (Leng & Henderson, 2013), with geochemical elemental records in particular having increasingly high resolutions (e.g. Lake Trichonida; Seguin et al., 2020a; see Table 2).

Archaeological and Historical Evidence

Past climatic changes can also be evidenced by aspects of the archaeological record and referenced either directly or indirectly in historical texts. Archaeological sites can provide important indications of past regional and local climate change (Sandweiss & Kelley, 2012). These indications are especially valuable where no high-resolution terrestrial archives (such as ice-cores, lacustrine sediments and speleothems) are available proximate to the locations in which people were living (see Section 2.4). Palaeoclimatic evidence from archaeological contexts can be divided into three main types: biogeographical, infrastructural, and isotopic.

Biogeographical approaches, such as the Mutual Climatic Range (MCR) method, characterise modern environmental and climatic constraints on individual species, then overlap these to determine conditions conducive to the survival of all species in an assemblage (best-developed for beetles: Elias, 1994; Huppert & Solow, 2004). This can also be achieved with plant fossils, such as pollen and non-pollen palynomorphs (NPPs), in archaeological contexts using the same methodology as in lacustrine deposits; however, with additional caveats (Dimbleby, 1985; Lechterbeck & Jensen, 2020; Mercuri et al., 2010; Sadori et al., 2013). Similarly, certain soils and sediments can only be formed or mobilised under

specific climatic conditions (Gilbertson et al., 1999; Hollesen et al., 2016; Sandweiss & Kelley, 2012).

Archaeological infrastructure and locations can be indicative of past climatic changes. Specific adaptations can hint at climatic change; for example, cutting fountain outlets at a lower level due to reduced water supply (e.g. at Sagalassos: Martens, 2008). Construction of infrastructure in, or movement of settlements to, regions that are currently climatically uninhabitable or inarable also suggests different prevailing conditions in the past (e.g. the Levant: Hirschfeld, 2006).

Isotopic analyses can be performed on materials found in archaeological contexts to provide indications of palaeoclimatic conditions. This includes fossils and remains, such as measuring $\delta^{18}O$ in marine shells or fish otoliths to make inferences about precipitation amounts (Sandweiss & Kelley, 2012), or $\delta^{13}C$ in food products or plant-consuming animals to determine whether environments had predominantly C3 or C4 plants (Cheung et al., 2019; Riehl et al., 2014). Additionally, geochemical evidence from calcites in water infrastructure can retain climatic information similarly to speleothems (e.g. Martens, 2008).

Historical documents can contain both direct references to weather phenomena and to events such as floods, famines, or food shortages (McCormick et al., 2012; Stathakopoulos, 2004). These records can often reference specific changes in given years, which can be linked to overall climatic change. However, they suffer from historical biases towards extreme events, exaggeration, and are not necessarily indicative of climatic changes; thus they should be used with caution (Haldon et al., 2014, 2018, 2020).

2.3.3. Availability of high-resolution palaeoclimate records

The locations and temporal coverage of key palaeoclimate records are introduced in this section, while archives from specific regions are reviewed and discussed in more detail in the discussion chapters. High-resolution records covering the first millennium, here defined as records with >5 samples per 100 years (<20 years between samples), are rare and unevenly distributed in the EMME region (Figures 3 and 4; for references and metadata, see Table 2).

Perhaps the best represented region is southern Greece around the Peloponnese. In the northwest, a sub-annually resolved geochemical lake record is available from Lake Trichonida (Seguin et al., 2020a). In the southwest, on Schiza Island, a stable-isotope record is present from Mavri Trypa Cave, which ends ~650 CE (Finné et al., 2017). A cluster of five palaeoclimate records with decadal resolutions is found in the central Peloponnese: Asea, Phenos, Stymphalia, and Kaisari lakes, and Kapsia Cave (Finné et al., 2014; Seguin et al., 2019, 2020b; Unkel et al., 2014). A speleothem stable-isotope record is available from Skala Marion Cave, Thassos Island in the northern Aegean, ending ~470 CE (Psomiadis et al., 2018).

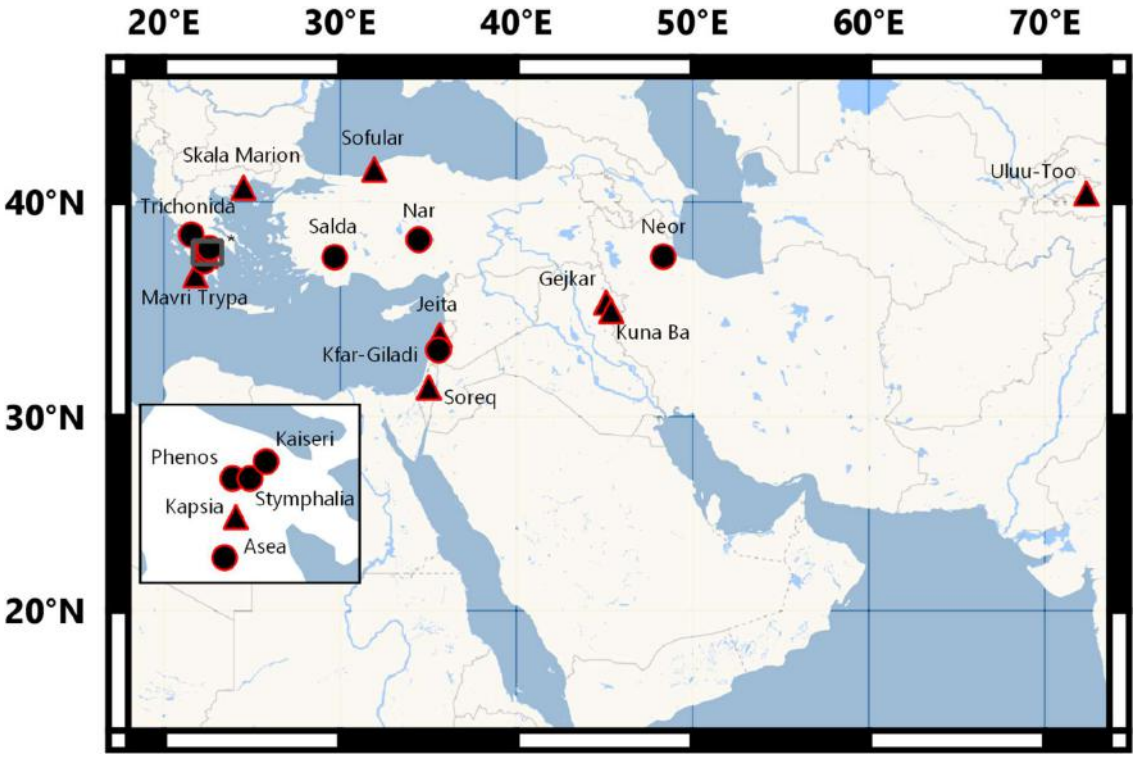

Figure 4. Map showing locations of available high-resolution speleothem (triangles) and lake (circles) palaeoclimate archives covering the 1st Millennium CE in the EMME region and Central Asia. *Grey box indicates coverage of inset map, which shows abundant records in the central Peloponnese. Record metadata and references in Table 2.

In Turkey, three high-resolution records are available. The lake Salda geochemical record, located at high elevation in Burdur province, southwest Turkey, starts ~560 CE (Danladi & Akçer-Ön, 2018). In the Black Sea coastal region, a sub-decadal stable-isotope

record is available from Sofular Cave (Fleitmann et al., 2009; Göktürk et al., 2011). From Lake Nar on the Central Anatolian Plateau, a high-resolution $\delta^{18}O$ (carbonates) record is available, complemented by lower resolution $\delta^{18}O$ (diatoms) dataset (Dean et al., 2018; Jones et al., 2006).

Three high-resolution Levantine records are available. The Jeita (Cheng et al., 2015) and Soreq Cave (Bar-Matthews et al., 2003; Orland et al., 2009) stable-isotope records are located in northern Lebanon and southern Israel, respectively. Also in Israel, an annually-resolved precipitation reconstruction is available from Kfar-Giladi (Morin et al., 2019), based on Dead Sea lake-level data (Bookman et al., 2004; Enzel et al., 2003).

In the ME, records are even more sparsely distributed. Two speleothem-based stable-isotope records are located close to one another in the Zagros foothills in northern Iraq, from Gejkar and Kuna Ba caves (Flohr et al., 2017; Sinha et al., 2019). The Neor Lake geochemistry record is located in northwest Iran, proximate to the Caspian Sea (Sharifi et al., 2015). In Central Asia, one high-resolution stable-isotope record is available, from Uluu-Too Cave in Kyrgyzstan (Wolff et al., 2017).

Overall, there are numerous large spatio-temporal gaps in the network of high-resolution Late Antique records: (1) eastern Aegean, (2) southwestern and southern Turkey (prior to 560 CE), (3) eastern Turkey and the Caucasus, (4) Syria and western Iraq, (5) across the entire AP and everywhere south of 30°N, and (5) eastwards from the FC (no records between 50-70°E).

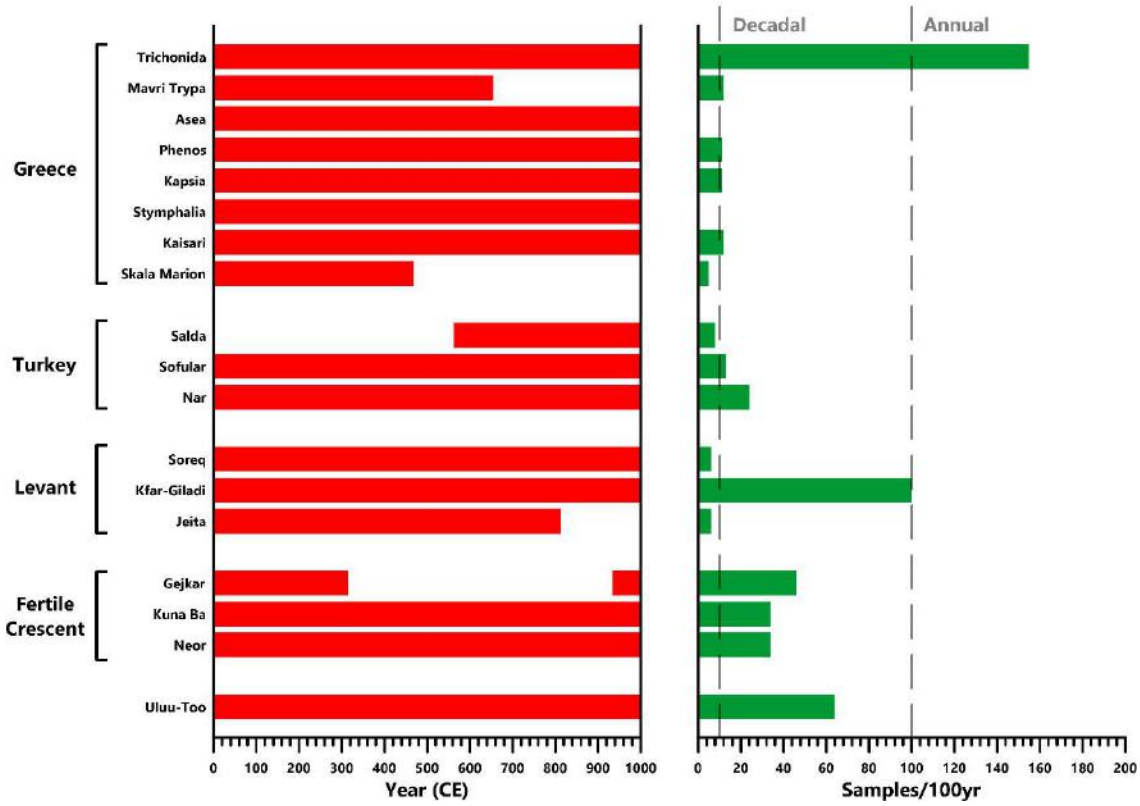

Figure 5. Temporal coverage (left) and resolution (right) of available high-resolution 1st Millennium CE palaeoclimate proxy archives from the EMME region and Central Asia, ordered by longitude. Locations in Figure 4 and metadata in Table 2.

Table 2. High-resolution EMME hydrological palaeoclimate proxy archives covering the 1st Millennium CE, ordered by longitude. Resolution (visually presented in Figure 5) is calculated as samples per 100 years ((no. of 1st Mil. samples/years evidenced)*100). Resolution for Asea and Stymphalia could not be calculated as datasets were unavailable; however, they are visibly high-resolution and comparable to Phenos and Kaiseri lakes (see Seguin et al., 2020b). Locations are in Figure 4.

Record	Type	Proxy	Interpretation	1st Millennium Coverage (CE)	1st Millennium Resolution	Lat.	Lon.	Reference(s)
Greece:								
Trichonida	Lake	Rb/Sr	Effective moisture	0-1000	155	38.56	21.55	(Seguin et al., 2020a)
Mavri Trypa	Cave	$\delta^{18}O$	Precipitation Amount/ Effective moisture	0-654	12	36.74	21.78	(Finné et al., 2017)
Asea	Lake	Ca/Ti	Effective moisture	0-1000	-	37.38	22.27	(Seguin et al., 2020b; Unkel et al., 2014)
Phenos	Lake	Ca/Ti	Effective moisture	0-1000	11	37.85	22.33	(Seguin et al., 2020b)
Kapsia	Cave	$\delta^{18}O$	Precipitation Amount	0-1000	11	37.62	22.35	(Finné et al., 2014)
Stymphalia	Lake	Rb/Sr Ca/Ti	Effective moisture	0-1000	-	37.85	22.46	(Seguin et al., 2019, 2020b)
Kaisari	Lake	Ca/Ti	Effective moisture	0-1000	12	37.95	22.58	(Seguin et al., 2020b)

Skala Marion	Cave	$\delta^{18}O$	Effective moisture	0-469	5	40.64	24.51	(Psomiadis et al., 2018)
Turkey:								
Salda	Lake	Ca/Fe	Effective moisture	563-1000	8	37.55	29.68	(Danladi & Akçer-Ön, 2018)
Sofular	Cave	$\delta^{13}C$	Effective moisture	0-1000	13	41.42	31.93	(Fleitmann et al., 2009; Göktürk et al., 2011)
Nar	Lake	$\delta^{18}O$ (carbonates)	Effective moisture (Summer: Jun-Jul)	0-1000	24	38.34	34.46	(Dean et al., 2018; Jones et al., 2006)
Levant:								
Soreq	Cave	$\delta^{18}O$	Precipitation Amount	0-1000	6	31.45	35.03	(Bar-Matthews et al., 2003; Orland et al., 2009)
Kfar-Giladi	Lake	Dead Sea Lake Level	Reconstructed Precipitation Amount	0-1000	100	33.2425	35.575	(Morin et al., 2019)
Jeita	Cave	$\delta^{18}O$	Precipitation Amount	0-813	6	33.95	35.65	(Cheng et al., 2015)
Fertile Crescent:								

Gejkar	Cave	$\delta^{18}O$	Effective moisture	0-351 933-1000	46	35.48	45.10	(Flohr et al., 2017)
Kuna Ba	Cave	$\delta^{18}O$	Precipitation Amount	0-1000	34	35.09	45.38	(Sinha et al., 2019)
Neor	Lake	Ti	Dust Influx Aridity	0-1000	34	37.57	48.33	(Sharifi et al., 2015)
Central Asia:								
Uluu-Too	Cave	$\delta^{18}O$	Seasonality Precipitation Temperature	0-1000	64	40.38	72.35	(Wolff et al., 2017)

2.4. Linking palaeoclimatic and societal change

In the previous section, the challenges of interpreting palaeoclimate data were highlighted. There are no simple correlations between proxy variables and climatic parameters, which must be disentangled from numerous site-specific and non-climatic influences before inferences can be made. Significant age uncertainties are also present in many records, which further complicates analysis. Large spatio-temporal gaps in the coverage of high-resolution records cause additional problems as the region has spatially heterogenous climatic conditions. These challenges are compounded when palaeoclimate proxy records are utilised in discussions of climatic impacts on societies (History of Climate and Society: HCS; Degroot et al., 2021). As a result, past studies have often tended to be environmentally deterministic, either overlooking the complexities and uncertainties of palaeoclimate records, or simply not utilising them.

Environmental determinism – the concept that the physical environment controls societal development (Martin, 2005; D. Mitchell, 2000) – has its modern origins with Carl Ritter's work *Die Erdkunde im Verhältniss zur Natur und zur Geschichte des Menschen* [Geography in relation to nature and to human history] (Ritter, 1832) and Friedrich Ratzel's *Anthropogeographie* (Ratzel, 1882, 1891). The school of thought was later popularised further by Ellsworth Huntington, who saw all societal change (and human biological variation) rooted in climatic conditions (Huntington, 1913, 1915), including the end of the Western Roman Empire (Huntington, 1917). Environmental determinism was later criticised as oversimplistic and implicated in attempts to rationalise colonisation, imperialism, and white supremacy (Landes, 1998; C. O. Sauer, 1925), leading to an enduring disregard of environmental factors in the humanities during the 20th century CE (Gallaher et al., 2009; Gilmartin, 2009; Martin, 2005).

Climate change entered the political zeitgeist from the late-20th century CE, starting with the conception of global warming (Broecker, 1975), the formation of the Intergovernmental Panel on Climate Change (IPCC : 1988) and the publication of their first report (IPCC & Houghton, 1990). It was later consolidated as a major social issue by the documentary film "An Inconvenient Truth" (Gore et al., 2006). Following this, a new era of (neo-)environmental determinism was introduced (Coombes & Barber, 2005; W. B. Meyer &

Guss, 2017; Sluyter, 2003), with a significant focus on correlations between "negative" climatic change and the collapse of civilisations in both popular-science books (e.g. Diamond, 1997, 2005; Keys, 1999) and academic articles (e.g. Binford et al., 1997; deMenocal, 2001; Staubwasser et al., 2003; Weiss et al., 1993). Despite their flaws, these initial forays into HCS stimulated interest in the subject and subsequently, nuanced perspectives are increasingly coming to the forefront.

In the last decade especially, palaeoenvironmental scientists and historians/ archaeologists have made significant progress in their approaches to HCS. Important contributions were made in the *Journal of Interdisciplinary History* (*JIH*), with papers emphasising the challenges of synthesising environmental records with historical and archaeological datasets (Haldon et al., 2014; McCormick, 2011; McCormick et al., 2012). Following this, institutions such as the "Climate Change and History Research Initiative" (CCHRI) based at Princeton University and the Navarino Environmental Observatory (NEO) have been particularly influential in pushing for interdisciplinary collaboration, consilience, and considerate approaches to HCS (e.g. Haldon et al., 2018; Izdebski et al., 2016a; Weiberg et al., 2016; Weiberg & Finné, 2018). Arguments can be successfully made by individuals with sufficient knowledge of HCS (for an excellent example: Preiser-Kapeller, 2015); however, increased collaboration strengthens projects as subject specialists can more confidently assess evidence from their respective field (Degroot et al., 2021).

In palaeoclimate records, high resolution and accurate dating are required to establish causal links, with resolutions and uncertainties ideally <10 years (Knapp & Manning, 2016). Resolution and chronological precision of records is always increasing due to methdological and instrument improvements, with speleothems and geochemical lake records becoming especially strong in some regions (see above). Low resolution records are now more suitably used to classify broad climatic trends, which are understood to have different impacts on past societies than short-term climatic variability (Mordechai, 2018). Strong regional summaries of palaeoclimate data are now increasingly available, which consider the uncertainties of records and indicate high spatial variability (e.g. Burstyn et al., 2019; Finné et al., 2011; Labuhn et al., 2018; Roberts et al., 2008, 2018; Appendix B.1). Similar robust syntheses of these data alongside archaeological (e.g. Izdebski et al., 2016b; Spate, 2019), historical (e.g. McCormick et al., 2012; Telelis, 2008), palaeoenvironmental (e.g. Roberts

et al., 2018) and climate modelling (e.g. Xoplaki et al., 2018) data are also increasingly abundant.

When palaeoclimate records are suitably resolved with strong chronologies, and a climate shift aligns with societal transformation, temporal correlation alone is not enough; an explanatory framework for causality is required (Coombes & Barber, 2005). It must be demonstrated that the recorded climatic variable is relevant to a society; this is primarily through influence on agriculture and consequent impacts on the economy (Contreras, 2016; Zhang et al., 2011). To link a palaeoclimate proxy to agriculture, it should reflect an important climatic constraint for plant-growth (bio-productivity) in the growing season, which varies per region (Jones et al., 2019; Nemani et al., 2003). For example, it was previously assumed that higher temperatures and increased precipitation will enhance agricultural productivity, which is false in many (semi-arid and arid) regions (Haldon et al., 2014). Once a temporal correlation is observed, robust palaeoenvironmental, archaeological and/or historical evidence is required to illustrate the human impact. Improvement of modelling of land use, agricultural productivity and ecological niches is an important step in the right direction for establishing causal links, as has been done, for example, in France (Contreras et al., 2019), the Tibetan Plateau (Bocinsky & Kohler, 2014), and the US Southwest (Bocinsky & Kohler, 2014).

Perhaps the most critical recent focus has been on the concepts of resilience and vulnerability/fragility. Across numerous HCS case-studies, it has been observed that magnitude of palaeoclimate change does not correspond to the likelihood of societal impacts (Coombes & Barber, 2005). Large shifts in climate often correspond to no societal change and, inversely, small changes can have severe consequent effects (Knapp & Manning, 2016). This has led to the understanding that societal resilience or vulnerability can mitigate or intensify the impacts from climate change (Aldrich, 2012; Mordechai, 2018; Weiberg & Finné, 2018). Resilience is the ability of an organisation to adapt to challenges, with vulnerability as susceptibility to challenges (Brand & Jax, 2007; Cumming & Peterson, 2017; Yoffee, 2019). These aspects are particularly important for providing insights for mitigation of future climate change (Holm & Winiwarter, 2017).

Despite these developments over the past decade, which signify marked improvement in HCS studies, there are still some significant and persistent issues in research.

In academic and popular-science books particularly, there are often still environmentally deterministic arguments and selective use of data (e.g. Bulliet, 2009; Cline, 2014; Ellenblum, 2012; Harper, 2017; Weiss, 2017). Due to a lack of high-quality datasets in certain regions, incomparable evidence is often selected from disparate regions (Finné et al., 2011). Additionally, HCS still mischaracterises human-environment relationships through an overwhelming focus on collapse (Degroot et al., 2021; Haldon et al., 2020).

2.5. Summary

In summary, recreating past climates is challenging in the EMME region, especially so when examining HCS. Spatio-temporal heterogeneity of climatic conditions necessitates a dense network of palaeoclimate records, which is currently lacking in coverage. More high-resolution records with low chronological uncertainties are required. Care is required when utilising palaeoclimate records to discuss societal change and other factors must be eliminated or assessed in conjunction with the palaeoclimate data. In the following four chapters, I will contribute solutions to some of these issues by filling two spatio-temporal gaps in records (Chapters 3 and 5), providing a micro-regional case-study that avoids the use of disparate data (Chapter 4), and assessing HCS for the Kingdom of Himyar and Sasanian Empire which has previously been ignored (Chapters 5 and 6).

Chapter 3: Heterogenous late Holocene climate in the Eastern Mediterranean – the Kocain Cave record from SW Turkey

3.1. Preface

This chapter was submitted as a journal article manuscript to *Geophysical Research Letters* (*GRL*) on 8th June 2021, comments were provided by three reviewers on 27th July 2021, with minor revisions required for publication. The manuscript was re-submitted on 10th August 2021 and accepted for publication on 14th September 2021. The journal article was published online on 29th September 2021 (https://doi.org/10.1029/2021GL094733). The chapter is therefore written in the style of a journal article, according to the regulations of *GRL*. Authorship: Matthew J Jacobson (University of Reading, UK), Pascal Flohr (University of Kiel, Germany), Alison L Gascoigne (University of Southampton, UK), Melanie J Leng (British Geological Survey, UK), Aleksey Sadekov (University of Western Australia), Hai Cheng (Xi'an Jiaotong University, China), R Lawrence Edwards (University of Minnesota, USA), Okan Tüysüz (Istanbul Technical University, Turkey), Dominik Fleitmann (University of Basel, Switzerland).

MJJ and DF designed the project. MJJ drilled samples for laboratory analysis, performed data analysis, produced all figures, and led the interpretation and writing of the paper. PF and AS completed the laser-ablation mass spectrometry of trace-elements. MJL completed the stable-isotopes laboratory analysis. HC and RLE performed uranium-series dating. DF and PF contributed to interpretation. All co-authors provided comments on drafts of the paper. The estimated percentage contribution of MJJ to this paper is >70%.

3.2. Journal Article

Key Points:

- Speleothem Ko-1 record of effective moisture from SW Turkey stresses spatial and temporal heterogeneity of Turkish climate
- Climate changes share more similarities with other Eastern Mediterranean coastal regions, than central or northern Turkey
- Heterogeneity of modern climate and proxy records highlight the complexity of historical comparisons

Abstract:

Palaeoclimate variability must be constrained to predict the nature and impacts of future climate change in the Eastern Mediterranean. Here, we present a late Holocene high-resolution multiproxy dataset from Kocain Cave, the first of its kind from SW Turkey. Regional fluctuations in effective moisture are recorded by variations in magnesium, strontium, phosphorous and carbon isotopes, with oxygen isotopes reacting to changes in precipitation and effective moisture. The new record shows a double-peak of arid conditions at 1150 and 800 BCE, a wet period 330-460 CE followed by a rapid shift to dry conditions 460-830 CE, and a dry/wet Medieval Climate Anomaly/Little Ice Age pattern. Large discrepancies exist between Turkish records and the Kocain record, which shares more similarities with other Eastern Mediterranean coastal records. Heterogeneity of regional climate and palaeoclimate proxy records are emphasised.

Plain Language Summary:

Records of past climate are essential in the Eastern Mediterranean to understand regional impacts of modern climate change. In combination with archaeology, these allow us to examine climatic impacts on people in the past to help us prepare for the future. Here, we

examine a speleothem (Ko-1) from Kocain Cave, southwest Turkey, which contains information about past climate change in its chemistry. Measurements of trace-metals and carbon isotope ratios record the amount of water entering the cave, oxygen isotope ratios record rainfall amount. Measurements of uranium are used to date the climate changes. Earthquakes that damaged nearby cities and caused tsunamis changed the angle of the speleothem, providing more evidence for dating the sample.

The Kocain Cave record shows climatic conditions changed frequently in southwest Turkey. Important are dry conditions 1150 and 800 BCE, wet conditions 330-460 CE followed by a rapid shift to dry conditions 460-830 CE, and a dry/wet Medieval Climate Anomaly/Little Ice Age pattern. These climate changes were different to records from elsewhere in Turkey and matched better with coastal records from Greece and Lebanon/Israel. The complex nature of past climate is emphasised due to varied climatic regions in Turkey and the many impacts on each record.

3.2.1. Introduction

To predict the nature and impacts of future climate change in the Eastern Mediterranean (EM), a "hot-spot" which will experience severe impacts (Giorgi, 2006), past climatic variability must be constrained (Masson-Delmotte et al., 2013). Paucity of meteorological data (<100 years) renders palaeoclimate records vital for understanding spatio-temporal variance. Likewise, an abundance of archaeological data facilitates analysis of human-climate-environment interactions and resilience of past societies to climatic fluctuations (Jürg Luterbacher et al., 2012).

The climate of the EM is heterogenous over short distances (Ulbrich et al., 2012). Figure 6 shows spatial variations in winter precipitation and Old World Drought Atlas (OWDA)-derived Palmer Drought Severity Index (PDSI) for two agricultural drought periods (Cook et al., 2015; University of East Anglia Climatic Research Unit et al., 2020), which are largely determined by effective moisture. Agricultural droughts in (semi-)arid regions have a greater societal impact than individual climatic variables (Dalezios et al., 2017; Jones et al., 2019; Mannocchi et al., 2004). Confidently reconstructing this variability requires a dense

network of precisely-dated and highly-resolved palaeoclimate records. Past spatio-temporal climate variability in the EM is, however, poorly documented due to unevenly distributed records (Burstyn et al., 2019; Appendix B.1; Luterbacher et al., 2012).

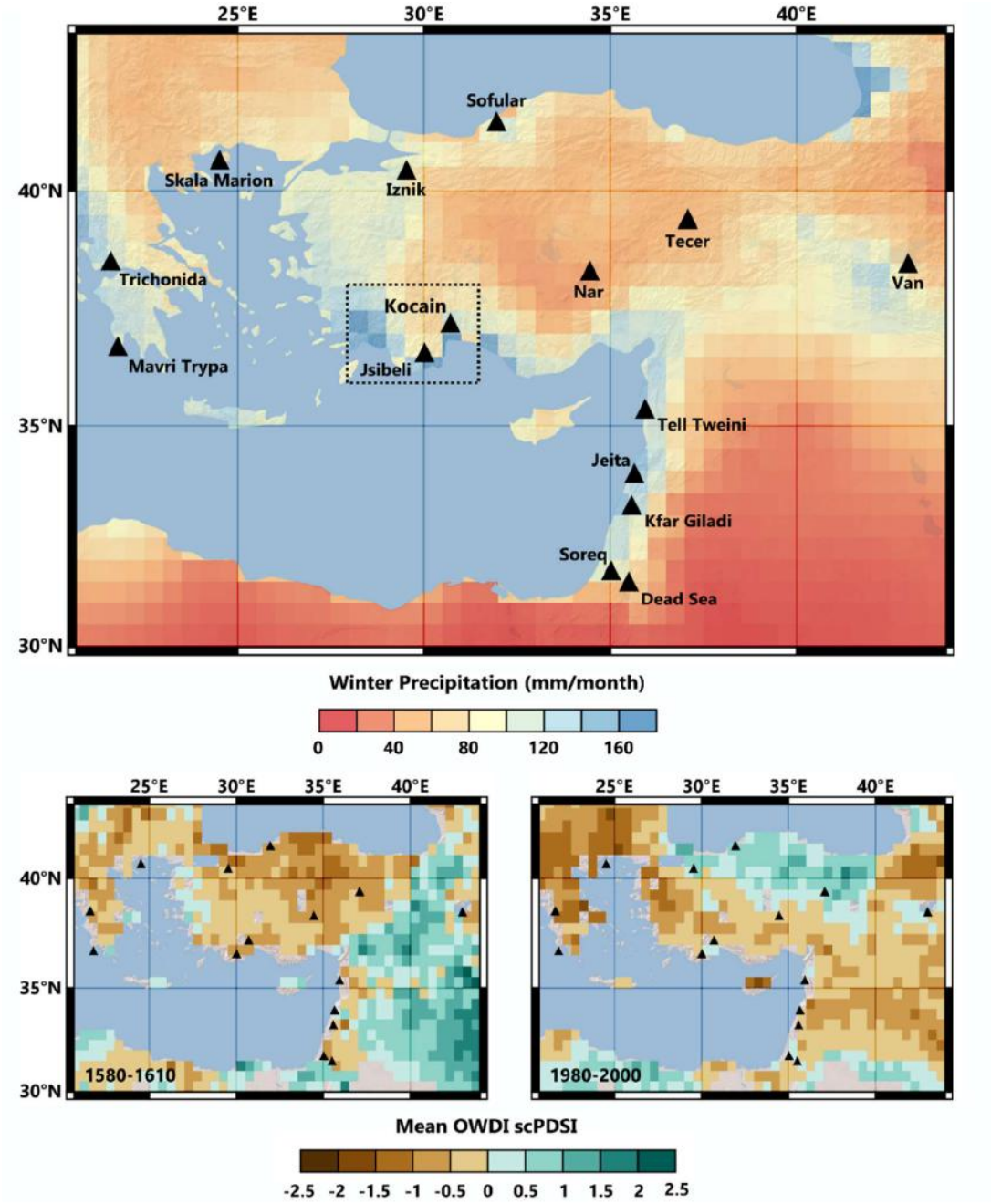

Figure 6. Late Holocene palaeoclimate archives (triangles) compared with CRU TS4.04 (University of East Anglia Climatic Research Unit et al., 2020) winter (Nov-Mar) precipitation and OWDA-derived PDSI (E. R. Cook et al., 2015) during agricultural drought periods (1580-1610 CE and 1980-2000 CE). Dotted square highlights Figure 7c. Data generated in the KNMI Climate Explorer (van Oldenborgh, 2020).

Extensive archaeological and pollen investigations (e.g. Vandam et al., 2019; Woodbridge et al., 2019) make SW Turkey a suitable testbed for examining human-climate-environment interactions. However, high-resolution palaeoclimate datasets from the region only extend back ~1000 (tree-rings) and ~1400 (Lake Salda) years (Danladi & Akçer-Ön, 2018; Heinrich et al., 2013), or do not cover the late Holocene (Dim Cave; Rowe et al., 2020; Ünal-İmer et al., 2016, 2015). Stable-isotopes from Lake Gölhisar (Warren J. Eastwood et al., 2007) reveal low-resolution (~80 years) changes in lake water balance (LWB) throughout the Holocene, albeit with significant dating uncertainties of ±165 years. This record and tree-rings are seasonally biased towards spring/summer, whereas precipitation mainly occurs in winter (Peterson & Vose, 1997). High-resolution palaeoclimate archives are available from other regions of Turkey (Lake Nar, Sofular Cave; Dean et al., 2018; Göktürk et al., 2011); however, these are not local and experience wholly different climatic conditions (Section 3.2.5.1). Here, we provide a new speleothem record (Ko-1) from Kocain Cave, SW Turkey, to fill the late Holocene gap. We present highly-resolved trace-element (T-E) data starting ~950 BCE, and a stable-isotope record that extends from the present to ~1350 BCE. An age-model is constructed from uranium-series dates (^{230}Th), with supporting evidence from the impact of historically-attested earthquakes on Ko-1. This enables us to establish high-resolution climate variability in SW Turkey for >3000 years during the late Holocene.

3.2.2. Cave setting

Kocain Cave (37°13'57'' N, 30°42'42'' E; 730 m asl), western Taurus Mountains, formed within dolomitic Jurassic-Cenomanian shallow-marine limestones (Section 3.3.1; Figure 10; Demer et al., 2019) and is exceptionally large (opening width: 75m; gallery size: 36,000 m^2). Kocain has been utilised by humans since the Neolithic and contains a Roman spring-fed cistern, dated by early-Christian inscriptions (Talloen, 2015). Terrain above the cave is sparsely covered by typical C3-type Mediterranean vegetation, mainly evergreen shrubs (Koç et al., 2020).

Precipitation (1929-2018; Peterson & Vose, 1997) at Antalya exhibits a marked winter-peak, 90% occurring Nov-Mar, and high inter-annual variability, ranging from 207 mm (2008) to 1914 mm (1969). Alike the entire EM (Lionello, 2012; Xoplaki et al., 2018), SW Turkey

experiences spatial heterogeneity of climate across short distances (Figures 5 and 10). Moisture is brought by westerly storm tracks (Ulbrich et al., 2012) and mountains promote orographic precipitation caused by rising moist air and associated rainout effects (Evans et al., 2004). Weather station data (Figure 7b) reveals that despite similar seasonal patterns, coastal stations (e.g. Antalya) are significantly warmer and wetter than inland stations (e.g. Isparta). Precipitation and temperature are enhanced during negative phases of the North-Sea Caspian Pattern (NCP), Arctic Oscillation (AO), and North Atlantic Oscillation (NAO), likely linked to increased cyclonic activity and circulation over the warm Mediterranean; however, these patterns are not the same across Turkey (Sariş et al., 2010; Unal et al., 2012; Section 3.2.5.1).

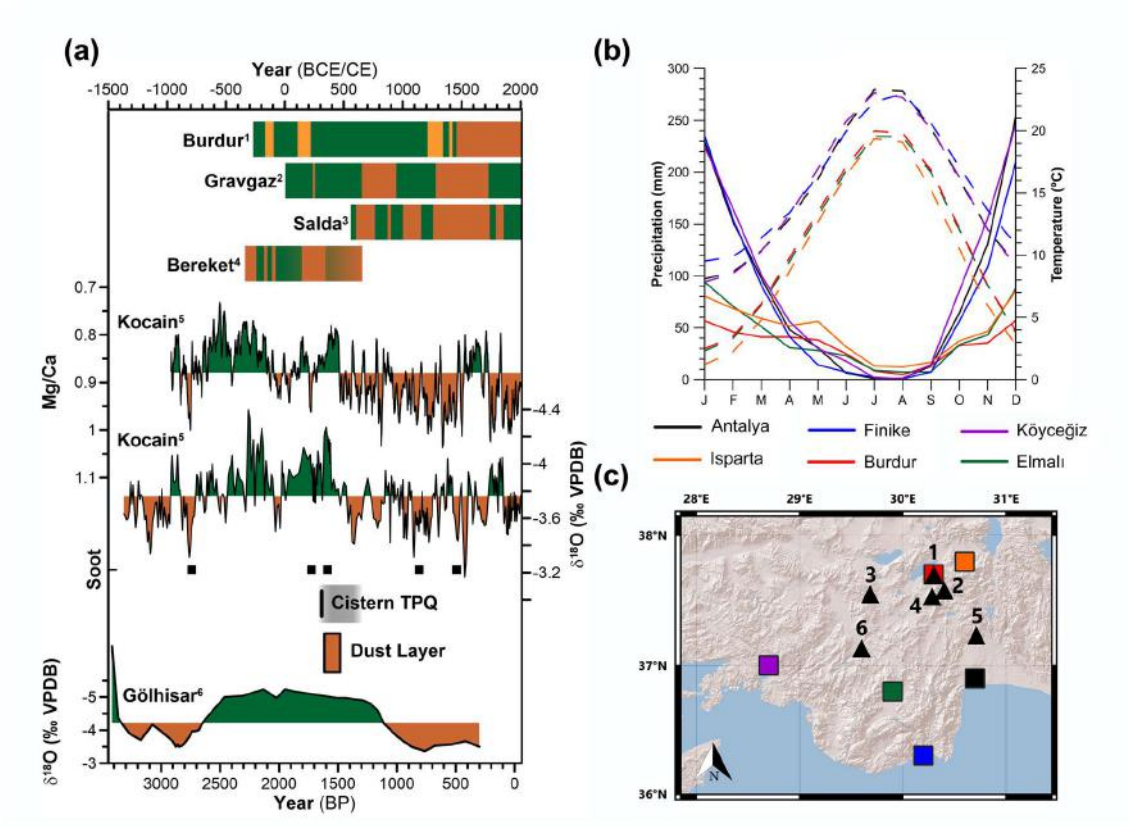

Figure 7. Conditions in the region surrounding Kocain cave. (**a**) Late Holocene palaeohydrological data with periods of high/low effective moisture (green/brown shading), as indicated by original authors (Burdur, Gravgaz, Salda, Bereket) or deviations from the mean (Kocain, Gölhisar). The cistern terminus post quem (312 CE), soot layers (Koç et al., 2020), and dust-layer (335-485 CE) are displayed. (**b**) Average monthly precipitation (solid lines) and temperature (dashed lines) from weather stations in SW Turkey (Peterson & Vose, 1997). (**c**) Map of SW Turkey with late Holocene palaeoenvironmental archives (triangles) and weather stations (squares); colours correspond to stations in 2b.

3.2.3. Materials, Methodology and Chronology

The actively-growing speleothem (Ko-1) from Kocain Cave, was collected ~450 m from the cave entrance in August 2005. Bedrock thickness above Ko-1 is ~80 m. A total of 31,503 measurements of T-Es (Ca, Mg, Sr, and P) were performed on the top 156 mm at a resolution of ~5 µm using Laser Ablation-Inductively Coupled Plasma-Mass Spectrometry (LA-ICP-MS) (Tanner et al., 2002). For oxygen ($\delta^{18}O$) and carbon ($\delta^{13}C$) isotope measurements, the first 174.5 mm was sampled at intervals of 0.5 mm or less, providing a total of 370 measurements. Further methodological description and sample extraction locations can be found in Section 3.3.2 and Figure 12.

For the chronology of Ko-1, 25 ^{230}Th ages were produced (following the analytical protocol of Cheng et al., 2013) ranging from 61±51 to 3387±80 BP (years before 1950 CE). Eight ages affected by significant detrital contamination ($^{230}Th/^{232}Th$ ratios <30) were not included in the age model (Figure 8b). The 17 remaining ^{230}Th ages have uncertainties varying from ±38-133 years (M=±67) and only one, at 43 mm depth, is not in stratigraphic order. Using these dates and the known collection date (August 2005), a *StalAge* age-model (Scholz & Hoffmann, 2011) was calculated.

Lateral shifts in the growth-axis at 457±100 CE (87.8 mm) and 176+30/-139 CE (110.3 mm) associated with historically-attested regional earthquakes provide additional evidence for the reliability of the constructed age-model. Tectonic activity altering the cave floor tilt is often a cause for speleothem growth-axis changes (Becker et al., 2006; Cadorin et al., 2001; Forti & Postpischl, 1984; Gilli, 2004; Gilli, 2005). For the ~457 CE displacement, earthquakes in 500, 518 and 528 CE were responsible for destruction of buildings in SW Turkey (Ergin et al., 1967; Gates, 1997; Malalas, 2017; Pirazzoli et al., 1996; Similox-Tohon et al., 2006; Stiros, 2001; Waelkens et al., 2000). The ~176 CE deviation is closely linked to an earthquake in 142 CE which caused extensive damage locally and a tsunami (Altinok et al., 2011; Ambraseys, 2009; Erel & Adatepe, 2007; Kokkinia, 2000; Papadopoulos et al., 2007; Tan et al., 2008). Further details of growth-axis deviations and speleoseismology can be found in Section 3.3.3 and Figure 14.

3.2.4. Interpretation of the Ko-1 multi-proxy record

$\delta^{13}C$ and $\delta^{18}O$ values from Ko-1 were previously interpreted as reflecting changes in winter temperature and associated snow melt (Göktürk, 2011). New T-E measurements (Figure 8) disprove this interpretation, indicating variations in the multi-proxy record can be used to characterise regional fluctuations in effective moisture (Mg/Ca, Sr/Ca), effective moisture/biological activity (P/Ca, $\delta^{13}C$), and effective moisture/precipitation amount ($\delta^{18}O$).

All Ko-1 proxy records correlate and are visually similar as all are influenced to various extents by changes in effective moisture (Figures 7a, 14 and 15). Prior calcite precipitation (PCP) occurs when cave drip-waters reach a gas phase above the cave with lower partial pressure of carbon dioxide (ρCO_2) than the soil gas CO_2 with which they were previously in equilibrium (McDonald et al., 2004). This enhances Mg/Ca, Sr/Ca, and $\delta^{13}C$ ratios, as Ca^{2+} and ^{12}C are preferentially deposited (Fohlmeister et al., 2020; McDermott et al., 2006; Appendix B.3). Additional PCP occurs in periods of low effective moisture as there are more aerated spaces above the cave and longer aquifer interaction times (Fairchild & Treble, 2009; Treble et al., 2003; Tremaine & Froelich, 2013). A positive correlation between Mg/Ca and Sr/Ca ($r=0.57$, $p<0.0001$) provides evidence for PCP (Wassenburg et al., 2020). During drier intervals, longer groundwater residence times will enhance Mg/Ca further, but not Sr/Ca, due to dissolution of the overlying dolomitic limestones (Fairchild & Treble, 2009).

Increased effective moisture enhances vegetation cover, soil microbial activity and drip-rates, and causes the ratio between C_3 and C_4 plants to increase (Cheng et al., 2015; Genty et al., 2001). C_4 plants are adapted to warm and (semi-)arid climates and have ~14‰ less negative $\delta^{13}C$ than C_3 plants (Farquhar, 1983; Farquhar et al., 1989; Henderson et al., 1992). Increased biological activity depletes speleothem $\delta^{13}C$ values and releases bio-available P that is transported during intense soil infiltration (Fairchild et al., 2001, 2007; Treble et al., 2003). The influence of effective moisture on P/Ca ratios is supported by strong negative correlations with Mg/Ca ($r=-0.60$, $p<0.0001$) and Sr/Ca ($r=-0.87$, $p<0.0001$). A positive correlation between $\delta^{18}O$ and $\delta^{13}C$ ($r=0.47$, $p<0.0001$) provides evidence for kinetic fractionation, likely related to fluctuations in drip-rate (Hendy, 1971). However, the interpretation of $\delta^{18}O$ in Ko-1 is complicated, as with other Turkish speleothems (see Fleitmann et al., 2009; Göktürk, 2011). Global Network of Isotopes in Precipitation (GNIP) data

from Antalya (Figure 17; IAEA/WMO, 2021) show a negative correlation between $\delta^{18}O$ and precipitation ($r=-0.30$, $p<0.0001$; "the amount effect"; Dansgaard, 1964), and a stronger correlation with temperature ($r=0.44$, $p<0.0001$). Precipitation seasonality will also alter $\delta^{18}O$, with isotopically-lighter $\delta^{18}O$ precipitated in winter (Nov-Mar; M=–5.6 ‰, SD=2.1) compared to summer (Jun-Aug; M=–3.4 ‰, SD=2.6). In Ko-1, more negative $\delta^{18}O$ coincides with lower Mg/Ca (Figure 8), this relationship can be explained by the importance of precipitation (and temperature) in determining effective moisture (Sinha et al., 2019).

Furthermore, agreement between high magnitude changes in the Ko-1 proxies, and other regional proxies, suggest they reflect effective moisture (Figures 6, 8 and 17; Section 3.2.5). Most notable is a distinct phase of high effective moisture (330-460 CE), near-contemporaneous with a distinct brown/orange dust-layer on Ko-1 (87.3-98 mm; 335-485 CE), containing a soot layer (Koç et al., 2020), and cistern construction in Kocain Cave (Figure 7). A prominent labarum/*Chi-Rho* symbol (☧) gives this cistern (~250 m^3 capacity) a 312 CE *terminus post quem* (earliest possible construction date), as that is when it was incorporated as a shield emblem by Emperor Constantine (Cameron & Hall, 1999), its use remained extensive until the 6th century CE (Hörandner & Carr, 2005). During numerous visits to the cave by the authors between Aug. 2005 and Apr. 2019, this cistern was 0-10% full (0-25 m^3) and spring flow was occurring but minimal. We suggest it was built during a period of greater spring flow and this, combined with the caves large opening width, made it suitable for use by herders. This assumption is further supported by a regional increase in grazing during the Late Roman Period (300-450 CE), specifically a shift towards goat herding in "marginal" mountainside areas (De Cupere et al., 2017; Fuller et al., 2012; Izdebski, 2012; Poblome, 2015). Animal herds' use of the cistern would have mobilised fine dust from the cave floor, which was then incorporated into the speleothem. High Fe/Ca ratios are detected in this layer, suggesting dust particles were trapped as it was precipitated (Fairchild and Treble, 2009; Figure 13). This mechanism could explain the dust-layer; which would usually suggest drier conditions if corresponding to increases in Mg/Ca (see Carolin et al., 2019).

High effective moisture in the 4th and early 5th centuries CE is also evidenced by wild weeds that require high moisture availability growing in the territory of Sagalassos (Johan Bakker et al., 2012; Kaniewski et al., 2007); wetland conditions and spring reactivation in the Bereket Valley and Gravgaz Marsh (J Bakker et al., 2013; Van Geel et al., 1989; Kaptijn et al.,

2013; Vermoere et al., 2002); and deep-water conditions at Lake Burdur (Tudryn et al., 2013). Similar changes are evidenced in EM proxies, suggesting this wet phase was a regional phenomenon (see below). The above interpretations, and corroborating evidence, strengthen our claim that decreases in Ko-1 Mg/Ca, Sr/Ca, $\delta^{13}C$ and $\delta^{18}O$, with increases in P/Ca, are indicative of wetter climatic conditions in SW Turkey.

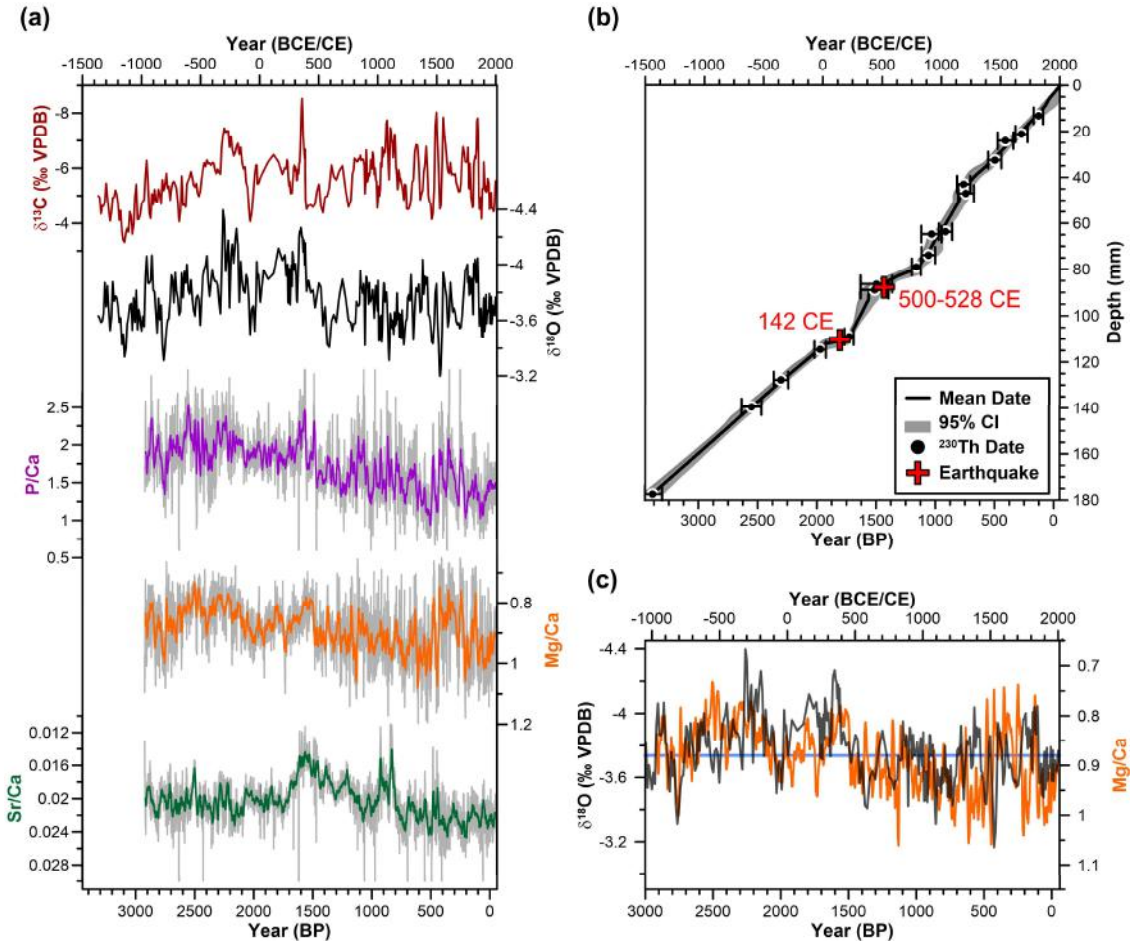

Figure 8. Stable-isotope (‰) and trace-element (mmol/mol^{-1}) palaeoclimate proxy records from Kocain Cave. (**a**) Ko-1 proxies aligned so peaks represent wetter conditions. Trace-elements are displayed as annual (grey) and 15-year (colours) averages. (**b**) *StalAge* model for Ko-1. Earthquakes were not input to the model. (**c**) Comparison between Mg/Ca and $\delta^{18}O$ ratios. Blue line represents the mean value of both records (0.88mmol/mol^{-1} and –3.76‰).

3.2.5. Ko-1 Record and EM Palaeoclimate

Key palaeohydrological changes for SW Turkey are reflected in geochemical proxies in Ko-1 (Figures 7 and 15). First, distinct phases of low effective moisture are centred at ~1150 and ~800 BCE, with intervening wetter conditions between ~1000 and 900 BCE. Secondly, high effective moisture occurred between ~330 and 460 CE, followed by a rapid shift to drier conditions that lasted until ~830 CE. Finally, there was a dry/wet Medieval Climate Anomaly (MCA; 850-1300 CE)/Little Ice Age (LIA; 1400-1700 CE) pattern, with high variability during 1450-1550 CE.

Marked palaeohydrological changes between 1200 and 750 BCE are widespread and often associated with cold phases, such as the 3.2 and 2.8 ka events and Crisis Years Cooling Event (CYCE), and reductions in solar irradiance (Kaniewski et al., 2019; Mayewski et al., 2004; F Steinhilber et al., 2009; Wanner et al., 2015). Links between these changes and socio-political change remain controversial (Drake, 2012; Finné et al., 2017; Kaniewski et al., 2013; Knapp & Manning, 2016; Manning et al., 2020). While similar palaeohydrological changes to those revealed by Ko-1 are observed in records such as Gölhisar, Skala Marion, and Tell Tweini (Warren J. Eastwood et al., 2007; Kaniewski et al., 2019; Psomiadis et al., 2018), others are dissimilar (Figure 9). No aridification is observed at Sofular, Nar, or Tecer (Dean et al., 2018; Fleitmann et al., 2009; Göktürk et al., 2011; Jones et al., 2006; Kuzucuoğlu et al., 2011), whereas a single shift to more arid conditions is evidenced at Iznik, Van, Mavri Trypa, Jeita, Soreq, and in the Middle East in general (Bar-Matthews et al., 2003; Barlas Şimşek & Çağatay, 2018; Cheng et al., 2015; Finné et al., 2017; Sinha et al., 2019; Ülgen et al., 2012).

Wet conditions between ~330 and 460 CE rapidly shift to an arid phase between ~460 and 830 CE in the Ko-1 record, roughly coincident with the Dark Ages Cold Period (DACP: 450-800 CE; Helama et al., 2017; Figure 9). An effective moisture peak in SW Turkey is supported by local palaeoenvironmental evidence and archaeological evidence in Kocain Cave (see above). Similar wet peaks are observed across the EM at ~300-500 CE. Speleothem $\delta^{18}O$ data from Mavri Trypa and Skala Marion caves demonstrate wet conditions at ~300-350 CE (Finné et al., 2017; Psomiadis et al., 2018). Effective moisture proxies from Lake Trichonida show an apparently delayed response, with the records wettest phase between ~420 and 500 CE (Seguin et al., 2020a). Reconstructed precipitation based on Dead Sea data suggests

~350-490 CE may be the wettest interval in the late Holocene for the southern Levant, whereas a depletion of isotopes from Jeita Cave suggests a break from arid conditions between ~320 and 400 CE (Cheng et al., 2015; Morin et al., 2019).

Generally, these wet phases are followed by a rapid shift to drier conditions in the 5th century (Figure 9). This pre-dates the Late Antique Little Ice Age (LALIA)/"536-550 CE climate downturn" (Büntgen et al., 2016; Newfield, 2018), a phasing that is also observed in records from the Middle East (e.g. Sharifi et al., 2015). However, other Turkish records show very different palaeohydrological changes. Locally, wet conditions prevailed longer: high detrital and low carbonate content at the start of the Lake Salda record (~550-600 CE) indicate wet conditions, cluster analysis of pollen and non-pollen palynomorphs from Gravgaz Marsh reveal wet conditions until 640 CE, and $\delta^{18}O$ data from Gölhisar remains depleted until ~800 CE (Bakker et al., 2011; Danladi & Akçer-Ön, 2018; Eastwood et al., 2007). Records from northern (Sofular), central (Nar, Tecer) and eastern (Van) Turkey show the inverse to Ko-1, with a marked dry phase starting ~300-350 CE, followed by a shift to humid conditions at ~500-550 CE that endured for centuries (Barlas Şimşek & Çağatay, 2018; Dean et al., 2018; Fleitmann et al., 2009; Kuzucuoğlu et al., 2011).

Enhanced variation in effective moisture is evidenced in the Ko-1 record from ~800 until 1850 CE (Figures 7 and 8). From ~900 CE until ~1460 CE, drier conditions prevailed, with more-humid intervals every ~120-150 years (~1030, ~1180, ~1300 CE), encompassing the MCA. Hydroclimate was highly variable between ~1450 and 1550 CE, experiencing an extreme dry-wet-dry-wet pattern. The driest conditions in the entire Ko-1 record occur between 1510-1530 CE, indicated by the highest $\delta^{18}O$ value and 15-year Mg/Ca and P/Ca averages. Subsequently, effective moisture was still highly variable but elevated until ~1840 CE, a period roughly coincident with the LIA (1400-1850 CE). Reconstructed winter-spring temperatures from tree-rings in Jsibeli suggest cooling after ~1500 CE, with the coldest conditions at ~1750 CE (Heinrich et al., 2013), when there was a break from high effective moisture at Kocain (Figure 9).

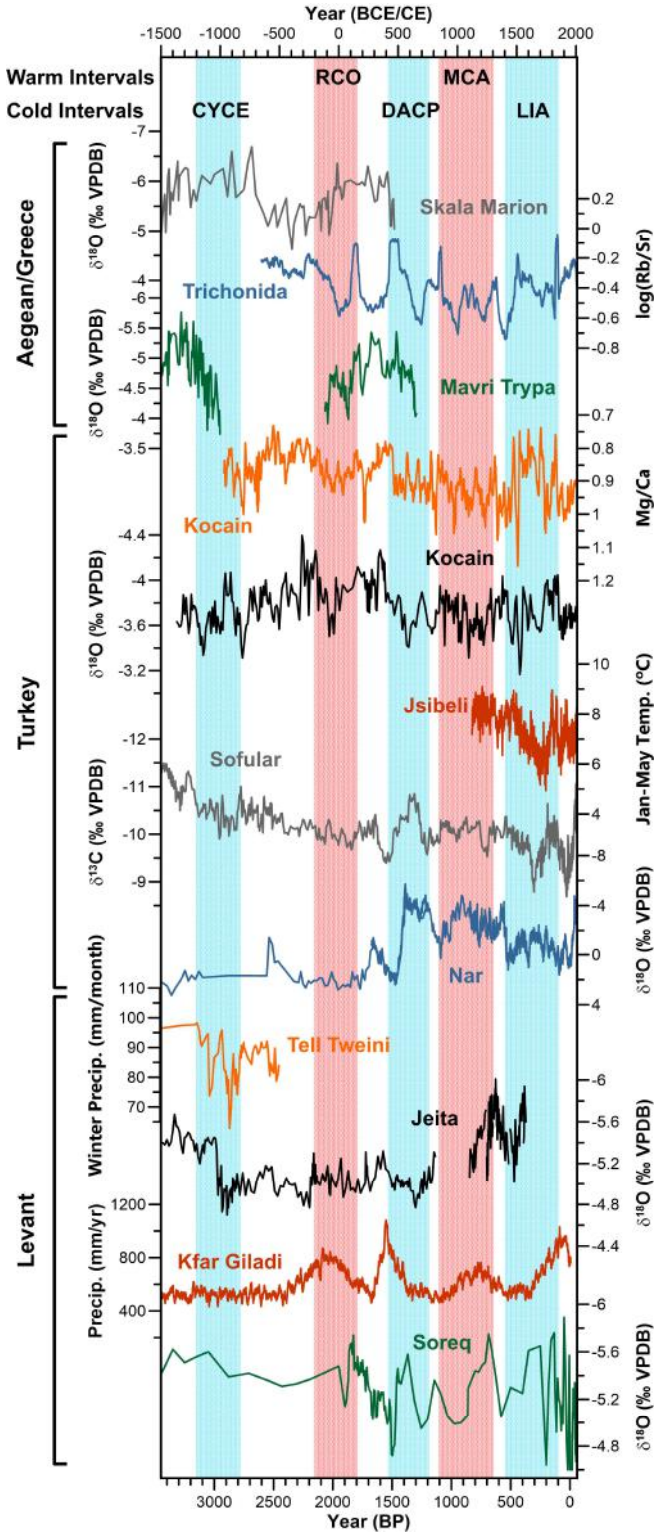

Figure 9. Late Holocene EM palaeoclimate data compared with Ko-1 Mg/Ca (15-year averages) and $\delta^{18}O$ (‰VPDB). Peaks in all records (excl. Jsibeli) indicate wetter conditions. Warm/cold intervals are: Crisis Years Cold Event (CYCE), Roman Climatic Optimum (RCO), Dark Ages Cold Period (DACP), Medieval Climate Anomaly (MCA), and Little Ice Age (LIA). For references, see main text.

The dry/wet MCA/LIA pattern observed at Kocain Cave contrasts with other records from Turkey (Burdur, Salda, Nar, Sofular, Iznik), which show the inverse pattern (Danladi & Akçer-Ön, 2018; Dean et al., 2015; Fleitmann et al., 2009; Tudryn et al., 2013; Ülgen et al., 2012), and from the Fertile Crescent (Jeita, Kfar Giladi, Soreq, Gejkar, Neor), which show no pattern (Bar-Matthews et al., 2003; Cheng et al., 2015; Flohr et al., 2017; Luterbacher et al., 2012; Morin et al., 2019; Sharifi et al., 2015; Figure 9 and 17). Most high-resolution Greek/Aegean records do not cover this more recent time interval. However, Trichonida log(Rb/Sr) exhibits strong similarities to Ko-1 (Figure 9). Dry conditions ~900-1450 CE follow a wetter phase ~850 CE, with breaks at 1050 and 1300 CE. Increased effective moisture is then demonstrated until 1650 CE, before another peak in the early 19th century CE, also evidenced in Nar diatom $\delta^{18}O$ (Dean et al., 2018; Seguin et al., 2020a).

3.2.5.1. Heterogeneity of Eastern Mediterranean climate and proxies

Large discrepancies exist between the Ko-1 record of effective moisture and other hydrological proxies from the EM, most likely caused by: (1) spatial climate variations and challenges in palaeoclimate analysis, related to (2) interpretation of different types of proxies with varied sensitivity to hydroclimatic change and (3) chronological uncertainties. The greatest differences between records discussed here are observed between Ko-1 and other records from Turkey. Climatic heterogeneity in SW Turkey is more extreme across the large country (780,000 km^2), which has complex and diverse topography, and numerous moisture sources (Lionello, 2012; Xoplaki et al., 2018). These factors lead to varied temperatures (Aydın et al., 2019), seasonal patterns (Sariş et al., 2010), and impacts from teleconnections (Ünal-İmer et al., 2015; Unal et al., 2012).

The two other high-resolution Turkish records that contrast with Ko-1, Lake Nar (central Anatolian plateau: CAP) and Sofular Cave (NW Turkey; Black Sea coast), are in completely different climatic regions. The high elevation CAP region experiences low precipitation (m=455 mm/yr^{-1}), with two peaks (Apr.-May/Oct.-Dec.), and cold semi-arid and dry continental climates (Öztürk et al., 2017; Peel et al., 2007). The Black Sea coast is temperate, with precipitation of a similar magnitude to SW Turkey (m=915 mm/yr^{-1}), but there is no dry season and precipitation is high throughout the year (Göktürk et al., 2008,

2011; Karaca et al., 2000). The impact of large-scale atmospheric teleconnections (NCP, AO, NAO) also differs in these regions, compared to SW Turkey which has enhanced precipitation and temperature during negative phases (Kutiel et al., 2002; Sezen & Partal, 2019). Negative phases cause higher temperatures across Turkey, particularly in winter. However, the CAP experiences significantly greater increases (Kutiel & Türkeş, 2005; Türkeş & Erlat, 2009). Impacts on precipitation are more varied. The Black Sea weakens the impacts of teleconnections on precipitation in NW Turkey (Göktürk et al., 2011; Türkeş & Erlat, 2003). AO- and NCP- phases cause their most significant impact on precipitation in SW Turkey (Kutiel & Benaroch, 2002), with CAP only impacted by AO- phases in winter (Sezen & Partal, 2019) and the transition between enhancements/reductions in precipitation from NCP- phases located <50 km from Nar (Kutiel et al., 2002; Kutiel & Türkeş, 2005). NAO influence is weaker and focused on the western and central regions (Unal et al., 2012). These differences lead to spatial variations in droughts, which impact each record differently (Figures 5 and 18; Vicente-Serrano et al., 2010). Lake Nar records LWB, with higher $\delta^{18}O$ corresponding to hydrological droughts (lake-water deficits) (Jones et al., 2019). Speleothems record fluctuations in EM, which are more akin to agricultural droughts (soil-moisture availability) (Fleitmann et al., 2009; Göktürk et al., 2011). However, none of these records are simple, being influenced by multiple climatic and geological/geographical factors, the importance of which changes over time. Additionally, proxies represent different seasons. The carbonate $\delta^{18}O$ record from Lake Nar is primarily deposited in early summer in response to evaporation and aridity (Dean et al., 2015). Speleothem records are winter-season biased due to the lighter-isotopic signature of winter precipitation and seasonality of precipitation (e.g. in SW Turkey).

The impact of temperature change on precipitation and proxy records is also poorly understood and variable. Antalya GNIP data shows a negative correlation between precipitation and temperature ($r=-0.53$, $p<0.0001$; Figure 17). However, proxy records show both increases and decreases in effective moisture during periods with lower temperatures: during the CYCE effective moisture is low, but during the LIA effective moisture is high at Kocain Cave (Figure 9).

Comparison between records is further complicated by chronological uncertainties of decadal-centurial length in lake and speleothem records. Multiple and varied lags are present

between climatic changes in different regions, and between climatic shifts and their signal in records. Different resolutions hinder comparison and the specifics of resolutions, i.e., whether a sample is an average across a large period or a specific point in time, are rarely addressed.

3.2.6. Conclusion

Speleothem Ko-1, from Kocain Cave, provides the first highly-resolved, well-dated palaeohydrological proxy record covering the late Holocene for SW Turkey. Key periods of palaeoclimatic change are revealed, notably: (1) a double-peak of arid conditions (1150 and 800 BCE), (2) a distinct period of high effective moisture in the 4th and 5th centuries CE (~330 to 460 CE), followed by (3) a rapid shift to low effective moisture (460 CE) that persisted until ~830 CE, and finally (4) a dry/wet MCA/LIA pattern. Changes were often in contrast to palaeoclimate records from northern and central Turkey, and sometimes locally, more frequently correlating with changes in coastal records from the Aegean and Levant regions. Considering the heterogeneity of climate and the multitude of impacts on records, palaeoclimatic interpretations are complex and care must be taken especially when they are utilised for discussions of societal impacts.

Acknowledgments, Samples, and Data

The new Kocain speleothem (Ko-1) uranium-series, trace-element and stable-isotope data used in this study are available from the NOAA palaeoclimate archive via https://www.ncdc.noaa.gov/paleo/study/33854 and in Appendix A.1. This work was supported by the AHRC South, West and Wales Doctoral Training Partnership (Grant AH/L503939/1 to MJJ), the Swiss National Science Foundation (Grant PP002-110554/1 to DF), the U.S. National Science Foundation (Grant 1702816 to RLE), the ERC Advanced Grant (2010 NEWLOG ADG-267931 to AS, awarded to Prof. H. Elderfield) and the National Natural Science Foundation of China (Grant NSFC 41888101 to HC). The isotope and trace-element data were provided by the National Environmental Isotope Facility and the Department of Earth Science, University of Cambridge, respectively. We would also like to thank Dr. Mark Lütscher for his support during the 2005 field trip when the Ko-1 sample was collected.

3.3. Supplementary Information

This section contains information that supports the analysis presented in the main manuscript. The geological and geographical setting of Kocain Cave is introduced in more detail, with geology displayed in a figure. Köppen-Geiger zones of Turkey, produced by Öztürk et al. (2017) emphasise regional heterogeneity of climate. We then further discuss the methodology and display sampling locations on Ko-1. Fa/Ce ratios over the sample are displayed. More details of speleothem growth-axis changes and the impact of earthquakes on speleothems (speleoseismology) follow, with the Ko-1 deviations and a schematic of the tectonic process shown in a figure. Statistical results of the geochemical analysis are then introduced, with figures displaying and comparing the Ko-1 proxies to one-another. Global Network of Isotopes in Precipitation (GNIP) data are presented to establish their relationships and the influence of climatic variables on $\delta^{18}O$. Finally, Ko-1 Mg/Ca values are then compared with other Eastern Mediterranean proxy records and spatial correlations of modern climatic variables are displayed to emphasise climatic heterogeneity in the region.

3.3.1. Geological Setting of Kocain Cave

Kocain Cave is located in the Taurides, one of the main tectonic units of southern Turkey, which consists of southward younging thrust sheets that occurred in the Late Cretaceous, Eocene and Early Miocene. These thrusts were placed over the Beydağları autochtonous, which is formed of Precambrian, Cambrian, Carboniferous and Middle Triassic-Danian sedimentary deposits. Kocain Cave is located above, in the Jurassic to Cenomanian part of the stratigraphic sequence in shallow marine limestones (Figure 10). At the base of the limestones, dolomitization is high, the limestones are medium to thickly bedded, lightly coloured and oolitic in places. The Lower Cretaceous limestones are thinly bedded and dark in colour, with bituminous horizons. In the above Cenomanian part, patch reefs are present in the limestones.

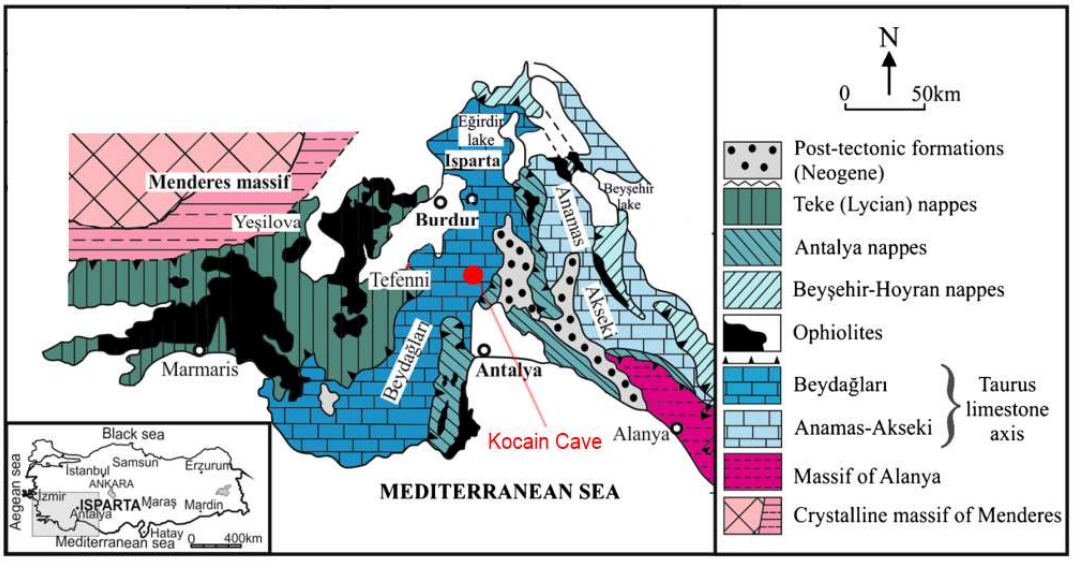

Figure 10. Geological map of SW Turkey, with location of Kocain Cave (adapted from Demer et al., 2019).

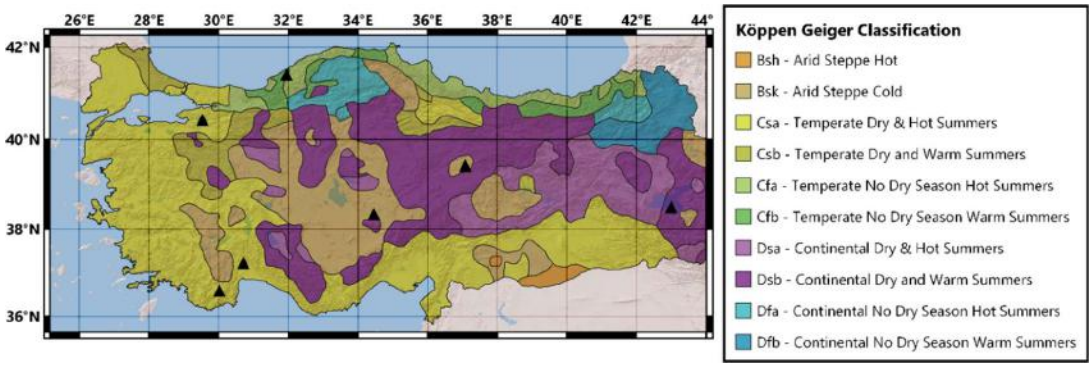

Figure 11. Köppen-Geiger Climate Classification zones of Turkey calculated from 512 meteorological stations (Öztürk et al., 2017). Turkish palaeoclimate records displayed as triangles, for labels see Figure 6.

3.3.2. Detailed Methodology

Trace element analyses were performed on the top 156mm of Ko-1 with a 0.00516mm resolution using Laser Ablation-Inductively Coupled Plasma Mass Spectrometry (LA-ICP-MS) at the Department of Earth Science, University of Cambridge. An Analyte G2 excimer laser (Teledyne Photon Machines Inc.) was coupled with a Thermo® i-CapQ ICPMS to measure trace-element profiles. The ^{43}Ca elemental profile was measured in counts per

second (CPS); all other elements (^{25}Mg, ^{31}P, ^{88}Sr) are presented as a ratio with ^{43}Ca in mmol/mol^{-1}. The trace metal elemental profiles were measured along the laser profile tracks (Figure 12). We used a Thermo® i-CapQ ICPMS collision cell in kinetic energy discrimination (KED) mode to minimize interferences on transitional mass elements (Tanner et al., 2002). The flow in the collision cell was tuned using ^{56}Fe mass to maximised signal-to-noise ratio. The Laser Ablation system was optimised for high spatial resolution using an aperture slit of 120x15 µm aligned to the direction of the speleothem growth and a 10Hz frequency with 1.8J/cm^2 laser fluence. The laser speed scan along the tracks was set up at 5 µm/sec, resulting in similar spatial resolution for Mg/Ca measurements. Approximately the top 1 mm of speleothem calcite was removed using pre-ablation with 150x30 µm laser spot to avoid any potential surface contamination, which significantly improved signal stability. The ICP-MS sensitivity was optimised using NIST610 reference glass material for maximum sensitivity across Mg-U mass range and maintaining ThO/Th <0.5% and Th/U ratio ~1. Data reduction involved initial screening of spectra for outliers, subtraction of the mean background intensities (measured with the laser turned off) from the analysed isotope intensities, internal standardisation to ^{43}Ca, and external standardisation using the NIST-SRM610 glass reference material. In-house eBlue calcite standards and NIST-SRM612 were used to monitor reproducibility, which was Sr/Ca = 0.236 ±0.0047 (1SE), 0.416 ±0.013 (1SE) and Mg/Ca = 1.48 ±0.02 (1SE), 3.12 ±0.12 (1SE) mmol/mol respectively.

Stable-isotope analysis was performed on the top 174.5mm of Ko-1, producing 370 oxygen and carbon isotope measurements at 0.3 mm resolution for the top 15 mm and 0.5 mm for the remainder of the sample. Samples were extracted with a microdrill along two separate tracks (DT1 and DT2, Figure 12), to remain close to the speleothem growth-axis. 60-100 micrograms of carbonate were measured using a glass vial sealed with septa for each sample in an IsoPrime dual inlet mass spectrometer with a Multiprep device at the British Geological Society (Nottingham, UK). The system evacuates vials and delivers anhydrous phosphoric acid to the carbonate at 90°C. The evolved CO_2 is collected for 15 minutes, cryogenically cleaned and delivered to the mass spectrometer. Results are reported as per mil (‰) difference relative to the Vienna-Peedee Belemnite (VPDB) scale. The precision (1σ) is ≤0.2‰ for δ^{18}O and ≤0.1‰ for δ^{13}C. Kinetic effects on δ^{18}O and δ^{13}C are usually identified using the 'Hendy Test', the drilling of isotope samples along a single growth layer (Hendy,

1971); unfortunately, the relatively low growth-rate of Ko-1 makes sampling within a single growth layer virtually impossible.

^{230}Th dating was performed using Thermo-Finnigan Neptune multicollector inductively coupled plasma mass spectrometers (MC-ICP-MS) at Xi'an Jaiotong University, China, and the University of Minnesota, USA (following the analytical protocol of Cheng et al., 2013).

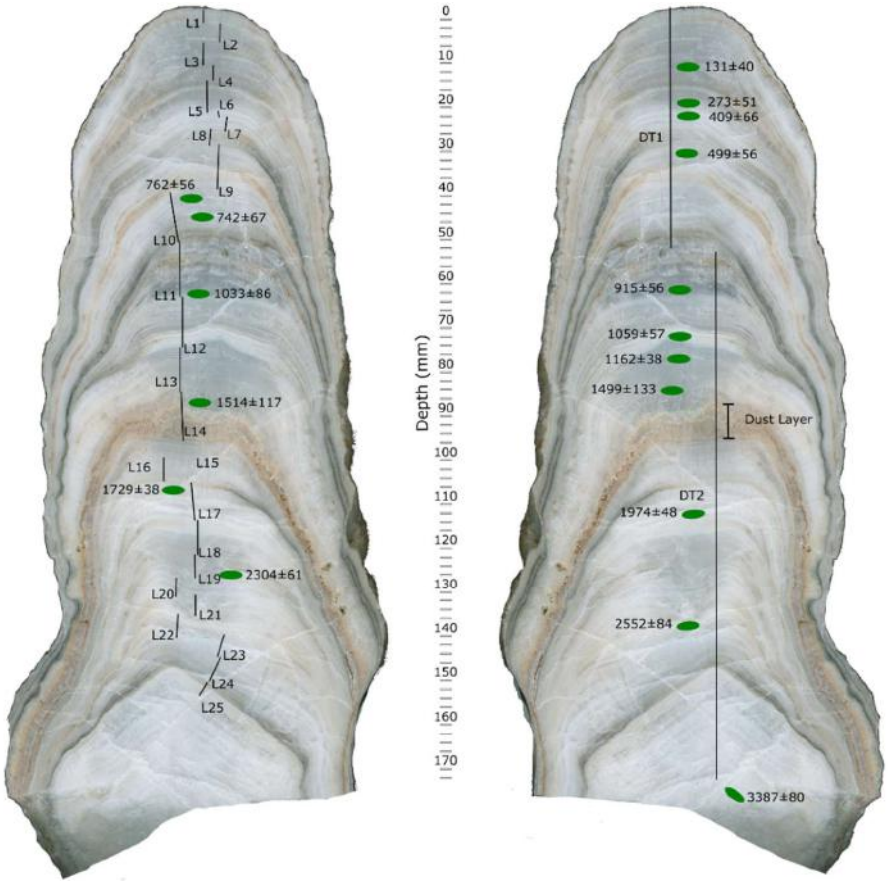

Figure 12. Scans of speleothem Ko-1 with the laser-ablation paths (L1-25), drill-tracks (DT1-2) and accepted ^{230}Th dates (green ovals). NB: Samples for analysis and dating were removed from both sides of the halved speleothem, this is shown in the figure. Dust Layer (335-485 CE) is denoted.

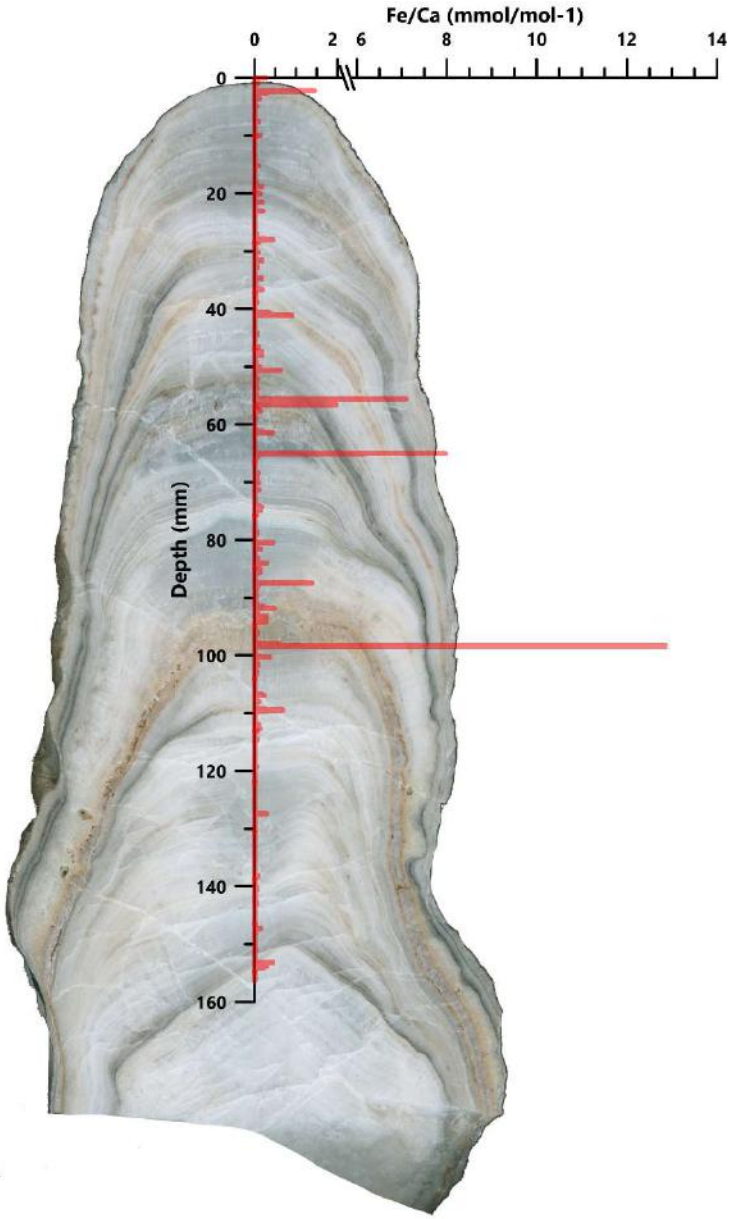

Figure 13. Scan of speleothem Ko-1 with Fe/Ca ratios by depth overlain. Ferrous material at the start of the dust layer (98.37mm) supports the hypothesis that it is formed from dust particles trapped within the calcite as it was precipitated (see Fairchild & Treble, 2009).

3.3.3. Growth-axis changes and speleoseismology

Four deviations in the growth-axis of Ko-1 were identified using digital image analysis of a high-resolution (3,200 dpi) scan. The mean dates for these deviations, extracted from the ^{230}Th *StalAge* model, are 938(±61) CE (68.2 mm), 457(±100) CE (87.8 mm), 176(+30/-139) CE

(110.3 mm), and 811(±45) BCE (149.0 mm) (Figure 14). Deviations in speleothem growth axes are frequently related to cessations in speleothem growth, local perturbations, or movements of the plate on which the speleothem is forming. Local perturbations include air currents that cause drip-water to fall at an angle, gravitational movement of rock within the cave, and intruding ice (Gilli, 2004). Our age model shows Ko-1 grew continuously throughout the period so no cessations to growth occurred. The large cave opening width of Kocain Cave (~75m) would have kept ventilation consistently high, meaning air currents are unlikely to change. As Ko-1 was collected from the wall of the cave, as opposed to on a boulder or other loose material, gravity will not have impacted speleothem growth.

Although earthquakes have previously been signified as the cause of breaks and discontinuities within speleothems, this has largely been dismissed due to the results of laboratory experiments (e.g. Cadorin et al., 2001), the absence of damage following recent earthquakes, and the existence of well-ornamented caves in seismic zones (Gilli, 2005). However, when earthquakes occur, they can instead lead to a permanent change in the tilt of the cave floor, resulting in a change in speleothem growth axes (Becker et al., 2006; Figure 14b). The 87.8 and 110.3 mm deviations are in close coherence to archaeologically and historically attested earthquakes at 500/518/528 CE and 142 CE, respectively, suggesting these growth-axis deviations resulted from tectonic activity. Regarding the former, two earthquakes, with three potential dates, fit within the dating inaccuracy for this deviation in the speleothem growth-axis. The deviation occurred toward the end of a period known as the Early Byzantine Tectonic Paroxysm (EBTP), a clustering of major seismic activity around the Eastern Mediterranean between ~350-550 CE caused by reactivation of the Anatolian-Aegean plate (Pirazzoli et al., 1996; Stiros, 2001). A 528 CE earthquake with its seismic centre in Fethiye-Meis (Erel & Adatepe, 2007) is one possible cause of this deviation. The Chronicle of John Malalas discusses the damage caused by this earthquake in middle Lycia, noting that the city of Myra was the worst affected (Malalas, 2017, p. 262). An earlier earthquake, with no firm date but possibly occurring in either 500 or 518 CE, with its epicentre to the north of Antalya (Ergin et al., 1967), may also have been destructive, and has previously been associated with the collapse of some light buildings and the monumental gates in nearby Sagalassos (Gates, 1997; Waelkens et al., 2000). With no way of ascertaining a clear date for these archaeologically attested destruction events at Sagalassos, they have since been

ascribed to the beginning of the 6th century (Similox-Tohon et al., 2006). The situation regarding the deviation in the growth-axis, originally dated to 176 CE, is clearer. This was likely caused by a strong (MMI=X) earthquake occurring in the Finike-Kumluca plain in 142 CE (Erel & Adatepe, 2007). This earthquake is evidenced by inscriptions pertaining to subsequent repair work in 28 Lycian cities (Kokkinia, 2000) and reports of extensive destruction in areas hit by the resultant tsunami (Altinok et al., 2011; Papadopoulos et al., 2007). The proximity of Kocain Cave to the Gulf of Antalya (<35km), an area known to have been damaged by the earthquake (Ambraseys, 2009), gives weight to this hypothesis. No evidence exists for earthquakes contemporaneous to the youngest growth-axis deviation (983 CE; 68.2mm), or the oldest (856 BCE; 149.0mm). The oldest deviation occurred in a period not covered in currently published earthquake catalogues of Turkey – future research may therefore refine the chronology of Ko-1 further.

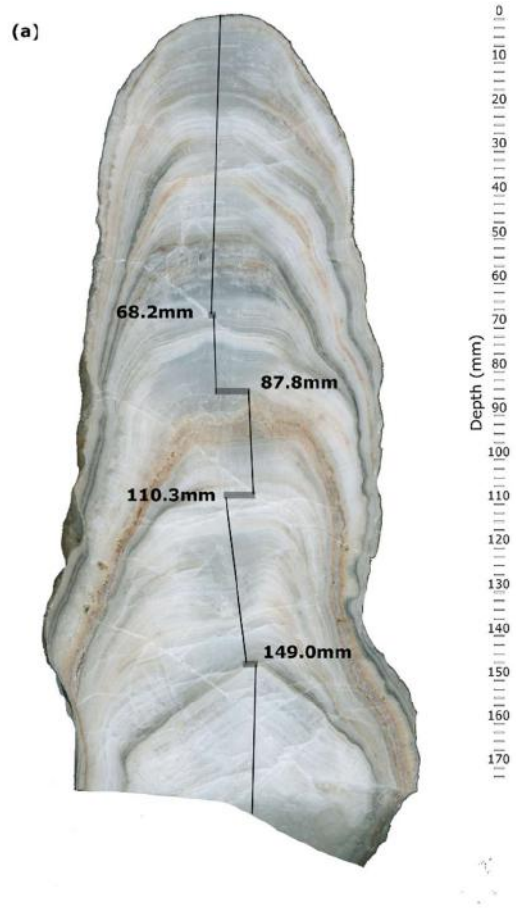

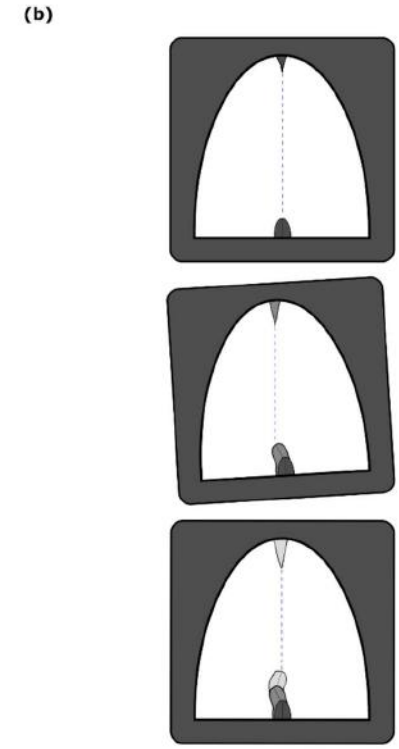

(c)

Depth (mm)	^{230}ThAge	Known Earthquake(s)	Deviation Angle (°)	Deviation Distance (mm)
68.2	938 (±61)CE		8.16	0.55
87.8	457 (±100)CE	500/518/ 528 CE	5.00	7.54
110.3	176 (+30/-139) CE	142 CE	0.27	6.34
149.0	811 (±45)BCE		4.10	2.35

Figure 14. (a) Scan of speleothem Ko-1 with lines representing growth direction and dated growth-axis changes. (b) Schematic diagrams demonstrating the impact of tectonic movements on speleothem growth (Forti and Postpischl, 1984). (c) Growth-axis deviation physical characteristics.

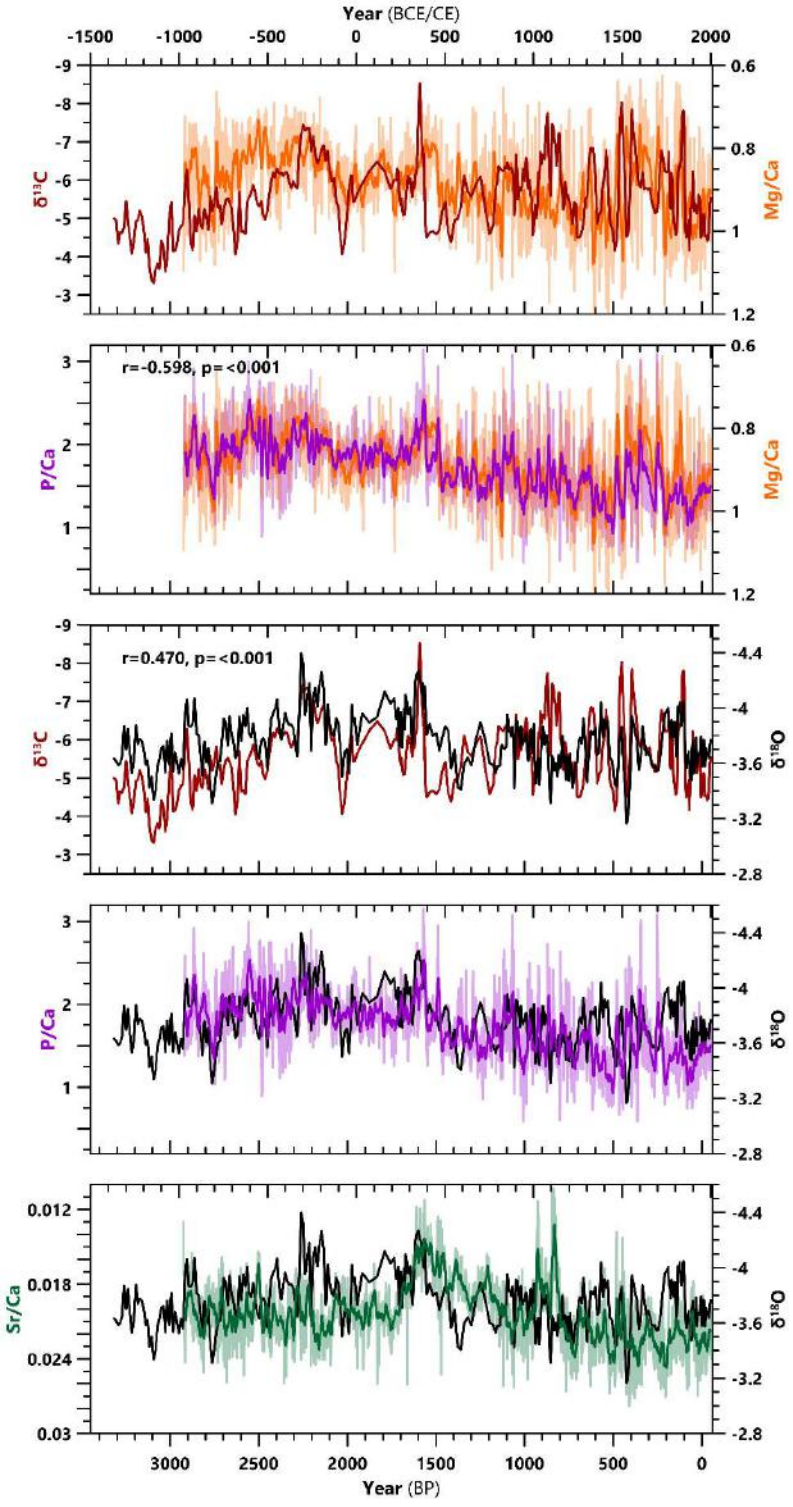

Figure 15. Direct comparison of Ko-1 records. Trace-element profiles are displayed as annual averages and 15-year averages (light and dark lines respectively).

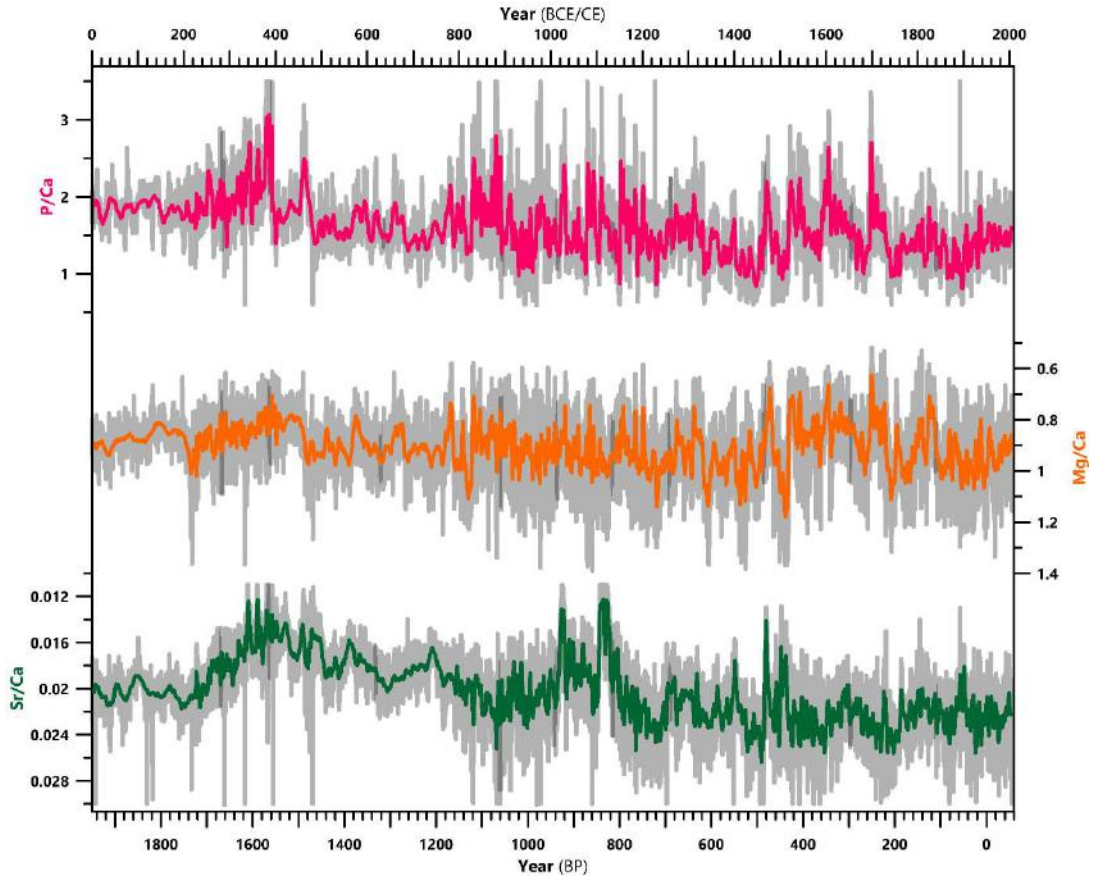

Figure 16. Trace-element profiles in the common era. Data is displayed in full (grey), with 45-point moving averages (colours). Annual averages in other figures remove noise created by the high-resolution analysis.

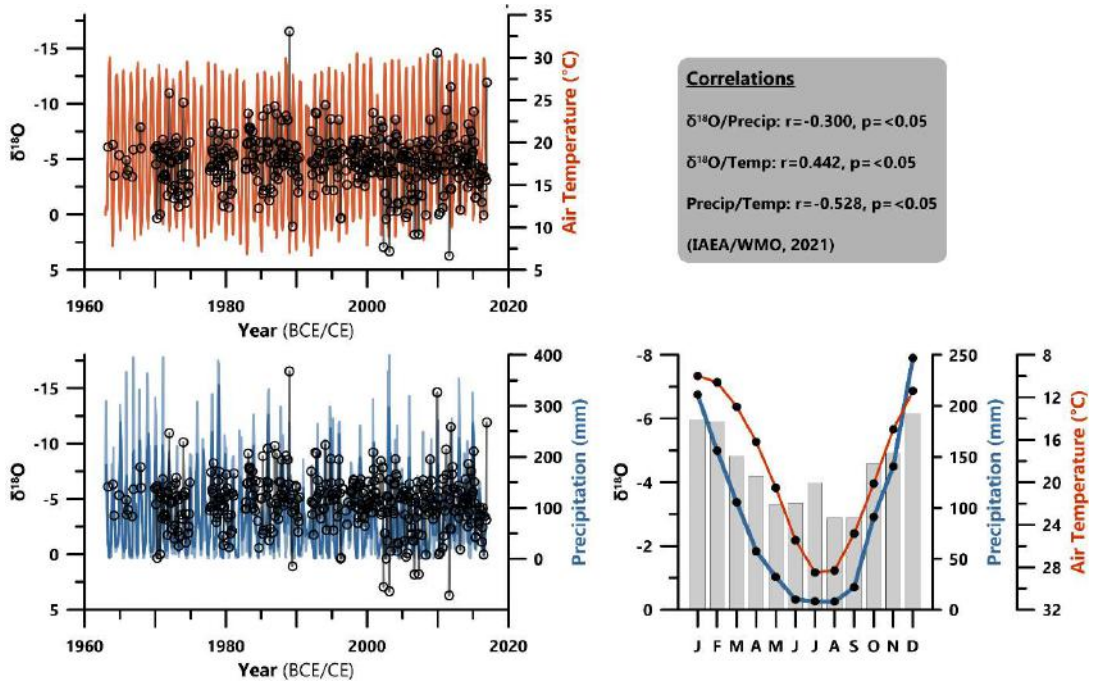

Figure 17. Statistical relationship of isotopes, precipitation, and temperature at Antalya weather station (IAEA/WMO, 2021)

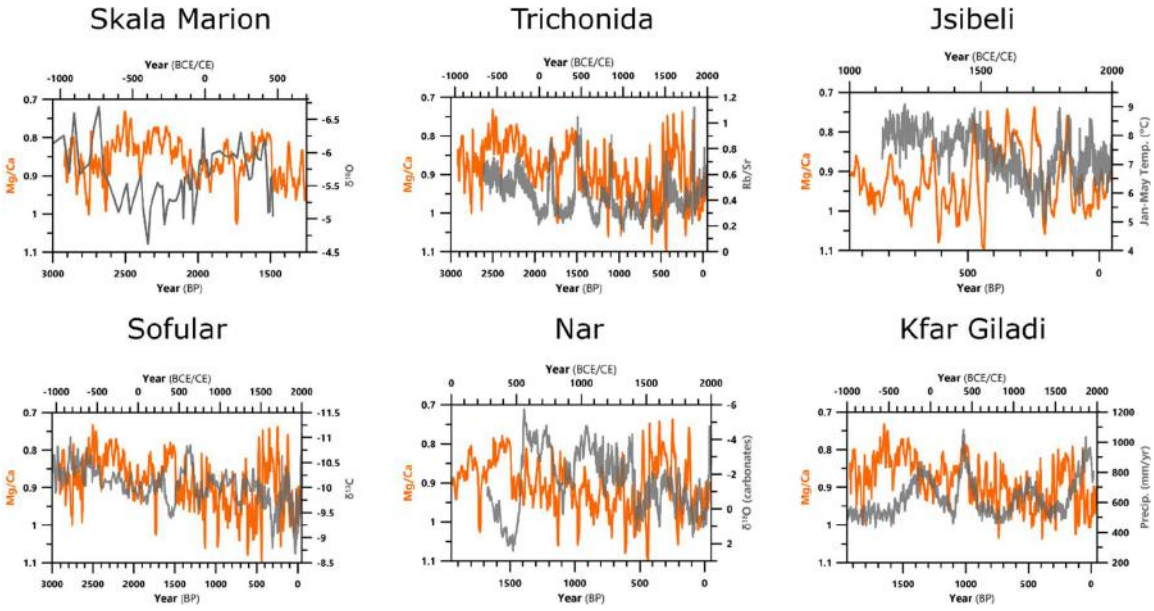

Figure 18. Direct comparisons between Ko-1 Mg/Ca and other proxy records from Figure 9. For references, see main text.

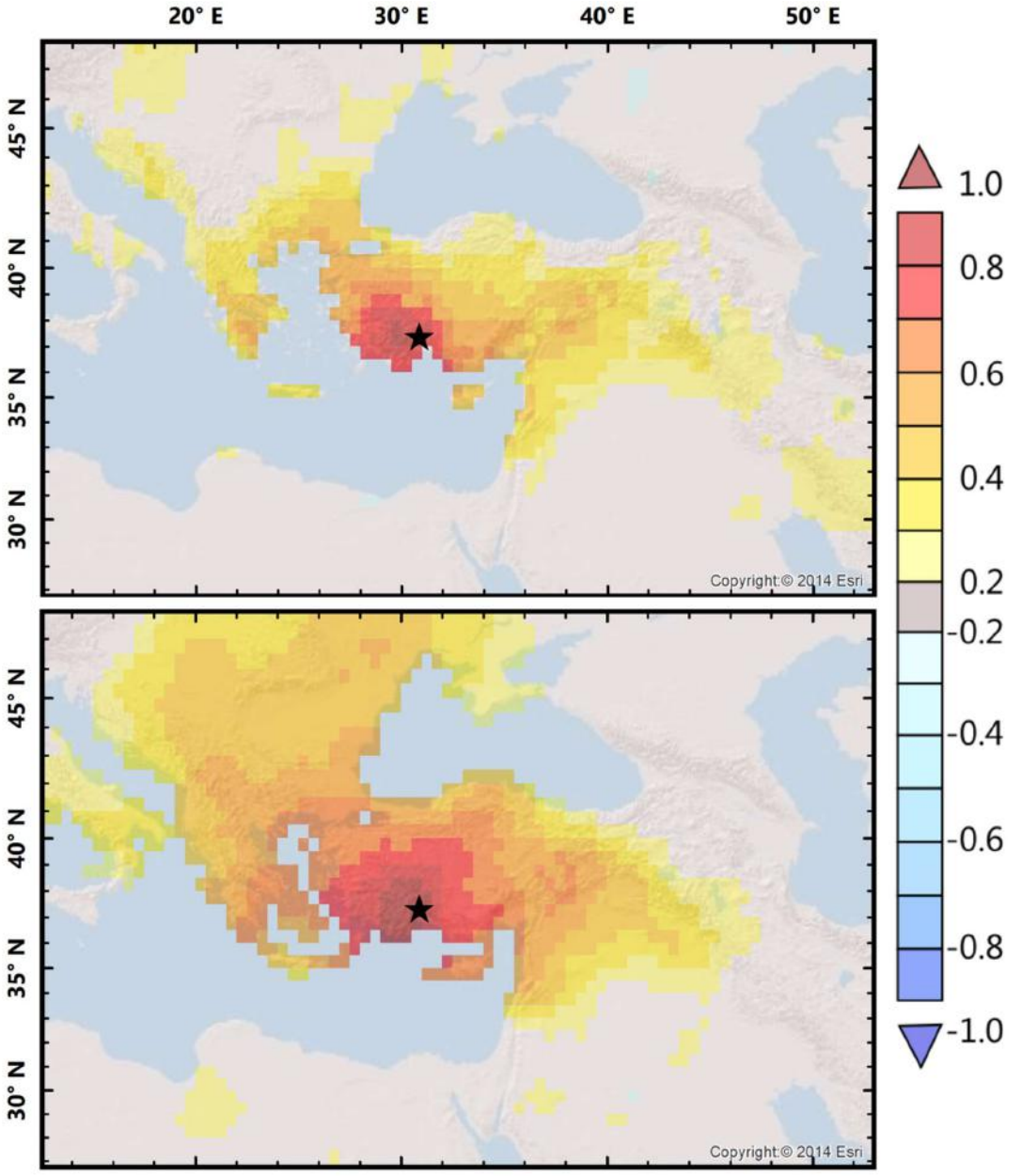

Figure 19. Correlation of SPEI (Vicente-Serrano et al., 2010; top) and winter precipitation (Nov-Mar; bottom) in the Ko-1 0.5° grid square (black star) with the surrounding region, generated in the KNMI Climate Explorer (van Oldenborgh, 2020).

Chapter 4: Settlement, environment, and climate change in SW Anatolia: dynamics of regional variation and the end of Antiquity

4.1. Preface

This chapter was prepared in the style of a journal article and submitted to the journal *The Public Library of Science One* (PLOS One). Authorship: Matthew J Jacobson, Jordan Pickett (University of Georgia, USA), Alison L Gascoigne (University of Southampton, UK).

MJJ and JP designed the project and adapted volume 8 of the TIB into a settlement record. MJJ led the interpretation and writing of the manuscript, with assistance from JP. MJJ performed all data analysis and produced all figures. ALG provided comments on the paper. The estimate percentage contribution of MJJ to this paper is >70%.

4.2. Journal Article

Highlights:

- Lycia-Pamphylia contains rich comparative palaeoenvironmental and archaeological datasets
- *Tabula Imperii Byzantini* adapted into a regional-scale dataset of 381 settlements
- Roman Climatic Optimum (RCO) did not contribute to settlement expansion in the 1st and 2nd centuries CE
- Dry shift occurs after ~460 CE, concurrent with change in settlement and infrastructure character
- Settlement abandonment comes in the mid-6th to mid-7th century CE, suggesting a combination or "perfect storm" of factors was more important

Abstract:

In this paper we develop a micro-regional dataset of change at 381 settlements for Lycia-Pamphylia in southwest Anatolia (Turkey) from volume 8 of the *Tabulae Imperii Byzantini* – a compilation of historical toponyms and archaeological evidence. This region is rich in archaeological remains and high-quality palaeo-climatic and -environmental archives. Our archaeological synthesis enables comparison of these datasets to discuss current hypotheses of climate impacts on historical societies. A Roman Climatic Optimum (warmer and wetter conditions) facilitating Roman expansion cannot be supported here; Early Byzantine settlement did not benefit from enhanced precipitation in the 4th-6th centuries CE as often supposed; widespread settlement decline in an archaeologically difficult period c. 550-650 CE is likely caused by a "perfect storm" of environmental and socio-economic factors (climatic, seismic, pathogenic, defensive, and adaptive), though a shift to drier conditions appears to have come first c. 460 CE.

4.2.1. Introduction

Past climatic and environmental conditions are often considered influential for socio-cultural change in Anatolia and the broad Eastern Mediterranean-Middle East region (e.g. (Haldon et al., 2014; Izdebski et al., 2016b; Roberts et al., 2018b). Large-scale analyses are often necessitated, but also hindered, by low availability of high-quality comparable interdisciplinary datasets proximate to one-another (e.g. the Negev desert: Bar-Oz et al., 2019; Vaiglova et al., 2020). This presents difficulties in analysis as both climatic and socio-economic conditions exhibit high spatial and temporal variability (Horden & Purcell, 2000; Jürg Luterbacher et al., 2012; Ulbrich et al., 2012). Here, we develop a micro-regional settlement change dataset for Lycia and Pamphylia, in SW Turkey (Figure 20), adapted from volume 8 of the *Tabula Imperii Byzantini* (TIB 8: Hellenkemper and Hild, 2004)—a compilation of historical toponyms and associated archaeological research (Külzer, 2020). The region is rich in the archaeological remains of cities, harbours, and rural settlements, in addition to high-quality palaeo-climatic and -environmental datasets.

Previously, the archaeological evidence in Lycia-Pamphylia was disjointed due to a lack of data-synthesis (Terpoy, 2019a). Following the production of our settlement dataset, available evidence in Lycia-Pamphylia meets a sufficient standard to test hypotheses linking climatic and socio-cultural change. Abundant palaeo-environmental datasets (15 pollen records, from 9 sites) located at varied altitudes (Figure 20c), detail past ecological conditions and the intensity of human agricultural activities (J Bakker et al., 2013; Izdebski, 2013a). Pollen in these records detail a period of human-induced land-cover change known as the Beyşehir Occupation Phase (BOP), characterised by reduced presence of forest taxa and increased presence of cultivated trees (Roberts, 2018). For analysis in this paper, we utilise the presence of cultivated trees, represented by OJCV (*Olea* (Olive), *Juglans* (Walnut), *Castanea* (Chestnut) and *Vitis* (Grapevine)) pollen, calculated as an average of standardised percentages for archaeological periods and overlapping 200-year time windows, as a proxy for anthropogenic influence/ intensity of agricultural activities (Mercuri et al., 2013; Woodbridge et al., 2019). The potential agricultural productivity of land is heavily determined by location (including elevation) and climatic factors. In SW Turkey, effective moisture, which is the amount of soil moisture available for utilisation by plants (equivalent to precipitation minus evaporation), is the primary climatic constraint to plant growth and therefore agricultural productivity (see

(Jones et al., 2019; Nemani et al., 2003). The recent publication of a highly-resolved speleothem (stalagmite) proxy record from Kocain Cave, ~38km north of Antalya enables reconstruction of regional effective moisture and precipitation amount for >3,000 years (Chapter 3). Measured ratios of magnesium with calcium (Mg/Ca) record changes in effective moisture at a very high resolution (10.7 samples per year). Variations in oxygen isotope ratios ($\delta^{18}O$) provide information about past precipitation at decadal timescales (average of 9 years between samples). Two other palaeoclimate records are in our study region and cover the period under discussion. The lower resolution Lake Gölhisar $\delta^{18}O$ record (Eastwood et al., 2007), located within the Lycian Taurus mountains at 930m asl, reflects lake-water balance, a variable akin to effective moisture, on a sub-centurial timescale (average of 71 years between samples for 1,000 BCE – 1,050 CE). The multi-proxy Lake Salda record (Danladi & Akçer-Ön, 2018), located in Burdur Province at 1180m asl, extends back to ~560 CE and reflects lake-water balance at decadal timescales (average of 12 years between samples for 560-1050 CE). These records detail high climatic variability during the Late Holocene, with numerous dry and wet phases identified (discussed in Sections 4.2.5.1-4.2.5.3).

Our record of settlement change is compared diachronically to these high-quality palaeo-climatic and -environmental datasets to examine the influence of climate change on settlement patterns. Based on this comparison, we argue that in our study region climate change does impact agricultural productivity, which can lead to changes in settlement density and locations. However, the relative impact is highly variable, and socio-political factors are often more influential.

4.2.2. Study area geography

Our study region, covered by the TIB 8, pertains to the ancient regions of Lycia and Pamphylia, as well as parts of southern Pisidia, which are contained within 28°30'-32°30'E, 36°00'-38°00'N (Figure 20b). The Western Taurus mountains form an orographic barrier to southerly and south-westerly airflows, separating the coastal and interior plateau regions into zones with distinct microclimates, ecological conditions, and high numbers of endemic species (Quézel & Médail, 2003; Sadori et al., 2013; Tekeli & Gokce, 2016). According to the Köppen-Geiger climate classification system, coastal regions are categorised as hot-summer

Mediterranean (Csa) climates, with high levels of precipitation that exhibits a clear winter peak; inland regions are characterised by cold semi-arid (Bsk) and Mediterranean-influenced hot/warm-summer humid continental (Dsa/b) climates (Beck et al., 2018; Öztürk et al., 2017; Yılmaz & Çiçek, 2018). Colder conditions, with reduced precipitation (~33% less) are experienced in regions further inland and at higher elevations (Sariş et al., 2010; Türkeş & Erlat, 2009). Fertile river valleys (e.g. the Dalaman and Köprüçay) that cut through the mountains are ideal for both rain-fed and irrigated agriculture. These run from the elevated Anatolian plateau, which is dotted with lacustrine basins and upland sheep and goat pastures called yaylas, down to indented coastlines that provide convenient natural harbours for maritime trade (Çiner, 2019; Giray, 2012; Kazancı & Roberts, 2019; McNeill, 1992).

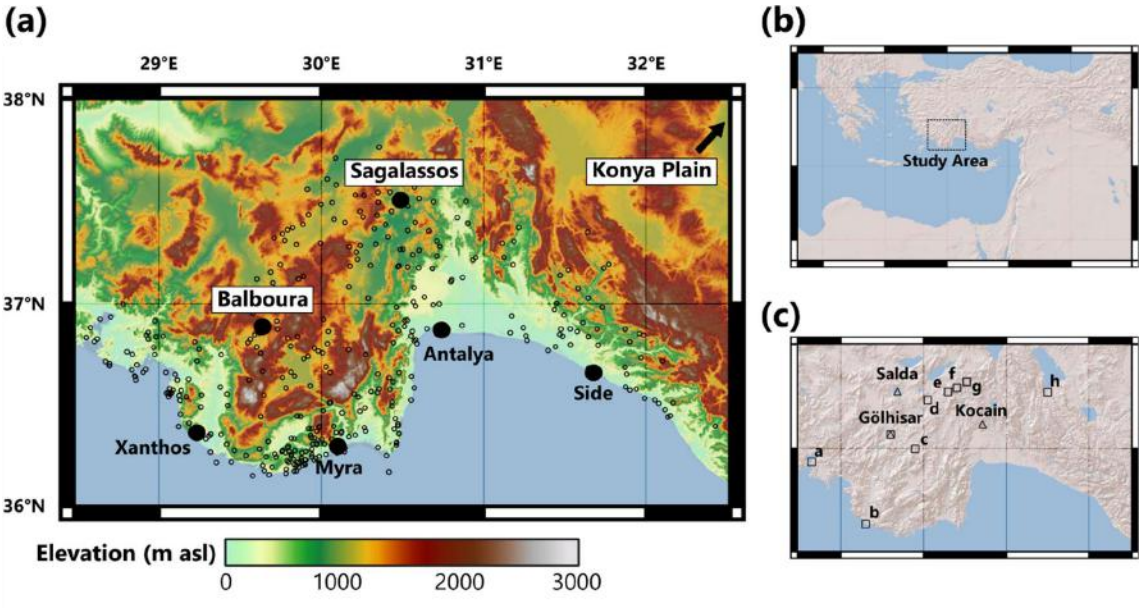

Figure 20. Maps of the study region: (**a**) All TIB 8 settlements compared to elevation. Important locations are named, ancient (modern) names: Xanthos (Letoon), Balboura (Çölkayiği), Myra (Demre), Attaleia (Antalya), Side (Manavgat). (**b**) Location of study region within the Eastern Mediterranean. (**c**) with palaeoclimate records (triangles, named) and pollen records (squares). Pollen records are: Köyceğiz (a), Ova (b), Sögüt (c), Pinarbaşı (d), Bereket Basin (e), Gravgaz Marsh (f), Ağlasun (g) and Beyşehir (h).

4.2.3. Methods

We tabulated entries in Lycia-Pamphylia from the TIB 8 to create a record of settlement change between the Bronze Age and Middle Byzantine period. The TIB is a long-term project organised by the Austrian Academy of Sciences since 1966, which has coordinated historical and modern toponyms for provinces of the Roman-Byzantine Empire with an extensive compilation of primary historical sources for all periods and relevant languages, ancient inscriptions, nineteenth and early twentieth century traveller accounts, and published data from extensive and intensive archaeological surveys and excavations (Külzer, 2020). All toponyms in the TIB 8 that could be accurately located, with archaeological or primary source evidence that could be attributed to at least one of six periods (Table 4) were compiled and their locations and elevations were identified using satellite imagery and GIS. The history and bibliography of each toponym was reviewed, including new publications since the TIB 8 was published (2004), to attribute presence or absence of evidence to each period throughout c. 3000 BCE – 1050 CE. The periodisation of evidence is based on established historical time-periods. The type and nature of evidence from each site was also noted according to 5 categories (in order of spatial and chronological certainty):

1. New/Restored Architecture – including monumental and public or domestic structures, and fortifications.
2. Architectural Contraction – pertaining to church contractions in the Middle Byzantine period only, where communities constructed a smaller chapel within the confines of an older church complex (Section 4.2.5.3; Erdoğan and Ceylan, 2019).
3. Material culture – mainly ceramics, also tombs and graves, coins and inscriptions located within settlements
4. Textual reference – settlements referenced by ancient primary sources, whether in literature, or by inscriptions and mint marks of coins found outside the named settlement (e.g. the tribute lists of the Delian League)
5. Spolia – older construction materials that have been reused in ancient, medieval, or modern settlements. In large quantities from ancient and medieval contexts these portend earlier settlement at a site; settlements with limited quantities of spolia in early modern contexts that may have been transported for some distance have not been included.

Our study ends at the beginning of the Turkish conquests in the 11th century CE, at which point the region fragmented politically and the nature of archaeological and textual evidence changed radically (Foss, 1994; Hellenkemper & Hild, 2004). Measures of spatial and chronological resolution were assigned to each settlement, based on confidence in its location and archaeological history, for the best represented period (Table 3).

Table 3. Measures of resolution

Measure of Resolution	Explanation	Number of Settlements
Spatial		
1	Site location <1km	291
2	Site location 1-3km	76
3	Site location >3km	14
Chronological		
1	Site has been excavated or systematically surveyed and published	56
2	Site has been extensively surveyed by scholars; often reliant on architectural description and broad period indicators	226
3	Site has been summarily visited by scholars; no formal excavation or survey; or, reused architectural elements of a given period noted in medieval-modern settlement	99

4.2.3.1. Data Critique

Significant interpretative challenges are presented when producing a settlement dataset from historical toponyms; these are analogous to those well-understood for archaeological survey data (e.g. Cassis et al., 2018; Contreras et al., 2018; Kowalewski, 2008; Palmisano et al., 2017; references below). Our dataset will reflect part of the original distribution of settlements; however, understanding biases produced by chronological challenges and varied preservation is important to determine the accuracy of the pattern. There are four main issues present:

Firstly, the six periods utilised in this study vary in length from 250 to 1850 years (Table 4), which will lead to overemphasis of settlement numbers during longer periods. Time-adjusted settlement numbers can also help to compensate for this bias, these are calculated (following the methodology of Contreras et al., 2018 and Barton et al., 1994) as follows:

= Total Settlement Number ÷ (Period Length ÷ Shortest Period Length)

The shortest period length in our study is the Early Byzantine Period (250 years). In our discussion, we focus on periods with relatively short and similar durations.

Secondly, categorising settlements into periods by relative dating (periodisation/ "time-averaging") brings inherent bias. This makes settlements appear to exist for the entire period (the "synchronistic paradigm"; Plog, 1973); they are only given a *terminus ante* and *post quem* at the start and end of the archaeological period. For many settlements, particularly rural, it is impossible to tell whether, in a particular period, they were occupied throughout, for a short duration, or abandoned and reoccupied (Dewar, 1991). Settlements can therefore appear contemporaneous though they were not (the "contemporaneity problem"; Premo, 2014; Schacht, 1984). The precise definition of chronological boundaries also obscures the uncertainty associated with archaeological chronologies, which rarely correspond perfectly to one-another: for instance, the Lycian-type tombs and sarcophagi that dot the landscape remain little changed between the Late Iron Age into the Early Roman period. Different strategies and resolutions for periodisation are utilised in different fields (e.g. by ceramicists compared to historians).

Thirdly, destruction of evidence in later periods and time-dependent degradation will lead to an overemphasis of settlement numbers in more recent periods and alter the settlement pattern via "preservation bias" (Garvey, 2018). Evidence in a particular period determines its archaeological visibility. Standing architectural remains, which constitute the bulk of archaeological evidence in our study region since the Iron Age, have an exceptional degree of preservation in Lycia-Pamphylia due to inaccessibility and low population density. This has contributed to a long history of archaeological exploration (e.g. Fellows, 1840) via extensive survey and architectural description, at the expense of excavated ceramics whose publication is more limited. Ceramics are generally robust, but different raw materials and

production processes change the level of survival, and visibility, which can change the number of sherds surviving from each period (Orton & Hughes, 2013, pp. 262–271). In addition to the archaeological taphonomy of settlements, biases impacting the survival of ancient site toponyms may influence our record. Whilst we include some settlements with archaeological remains that can only be identified by a modern Turkish toponym, ancient toponym survival is comparatively strong in our study region, caused by the continued presence of Greek communities until population exchanges after 1923 (Hirschon, 2003). However, the literary and historical record does yield additional ancient toponyms that cannot be securely located on the landscape, and there are likely many smaller settlements whose toponyms did not survive, left no archaeological evidence, or were subsequently destroyed.

Finally, indications of settlement or population size, whose estimates are typically dependent on measurable area within city walls or counts of housing units (Cesaretti et al., 2016), are beyond the scope of this paper. A related problem is the nature of the historical *polis*, commonly translated as "city": the polis was a rank of settlement since ~600 BCE that signalled the presence of municipal government and elite investment in monumental architecture (Hansen, 2006). However, such settlements did not necessarily have high-density populations; Lycian-Pamphylian cities mostly lack substantial domestic architecture, and they never reached the size, density, or population, of Ephesos, Antioch, or even Tarsos (Elton, 2019; Grainger, 2009, pp. 31–41, 234). In the Early Byzantine period the rank of *polis* was extended to more settlements, even as agrarian and artisanal-industrial activities were introduced to within city walls (Saradi, 2006; Section 4.2.5.2). In the Middle Byzantine period, many *poleis* retained their status even in cases where the archaeological evidence suggests they were now small villages (e.g. Pinara or Pednelissos; Section 4.2.5.3). The extent to which Lycian-Pamphylian *poleis* may be classified as low- or high-density urban environments is therefore irresolvable in many cases (Smith, 2010). In our metadata, increasing settlement density across the study region could therefore represent expansion or fragmentation, with associated population increases or decreases. Settlement types, so far as they can be reconstructed, are included in our full data (Appendix A.2).

Our dataset therefore evidences human presence and is a quantitative dataset of settlement movement through time, which provides a novel comparison with other factors.

However, it is unlikely to be an exhaustive record of all settlement change within Lycia and Pamphylia due to the biases described above.

4.2.4. Results

Within our study area, 381 out of the total 1038 toponym entries in TIB 8 could be located and identified as a settlement, with sufficient survival or publication to enable identification of historical presence between the Bronze Age and the Middle Byzantine period (Figure 21 and Table 4). The remaining 658 entries were either duplicates, dated to later periods only, infrastructure not associated with settlement (e.g., bridges), natural phenomena (e.g., rivers, mountains), regional toponyms, or their location was unknown. Toponyms associated with settlements are varied, including cities, farmsteads, peri-urban harbours and temples, hilltop fortifications, island villages and caves. Settlement function, size, and status changed over time. Of 381 settlements, only 8 were occupied in all six periods; ¾ of the total contained evidence for 1-3 periods (283). Elevation of settlements varied overall (0-1835m asl) and by period (Figure 22); however, lower elevation settlements dominate, with 29.4%<200m asl and 70%<1,000m asl. Most settlements (291) could be located to <1km and only a small portion (14) could not be located to <3km (Table 3). Chronological resolution of settlements was weaker, with only 56 excavated or systematically surveyed and published; 226 settlements were extensively surveyed but with reliance on broad (and primarily architectural) indications for chronology. The remaining 99 have weak chronological resolution, being only summarily visited by travellers or scholars since 1800, or dated by re-used building materials, easily recognisable within later buildings (e.g. Classical architectural sculpture or inscriptions recycled in Late Roman fortifications). The character of settlement evidence also varied by period (Figures 20c and 22).

Interpreting changes in the number and locations of settlements for each period presents significant challenges, associated with chronology, interpretive uncertainty, and preservation bias (see Section 4.2.3.1). However, some patterns are still observable that are broadly consistent with the regional history, archaeological evidence, and palaeoenvironmental data. The clearest of these trends is a steady increase of settlement numbers that peaks in the Roman and Early Byzantine periods, followed by a significant

reduction of Middle Byzantine evidence (Section 4.2.5; Figures 20a and 22). These changes are consistent with data from across the Eastern Mediterranean (Alcock and Cherry, 2016; Izdebski et al., 2016b; Roberts et al., 2019; Figure 24) and are frequently hypothesised to result in part from changing climatic and environmental conditions. In Section 4.2.5 below, we discuss these hypotheses, utilising a micro-regional case-study approach that includes comparison of our dataset with pre-existing evidence.

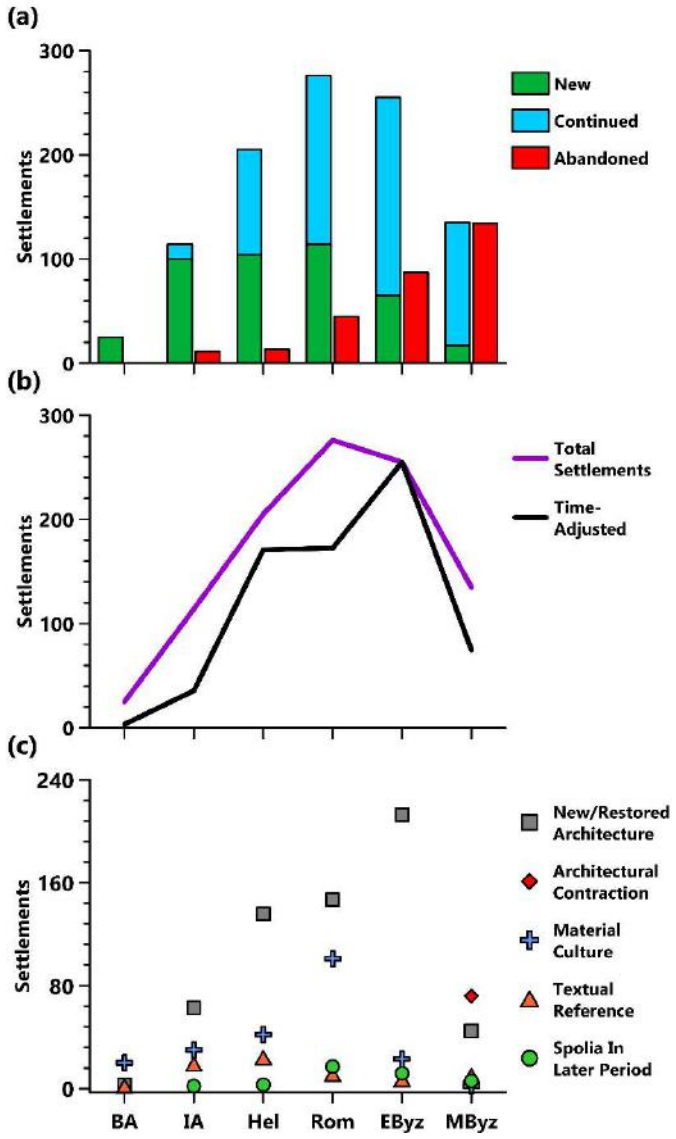

Figure 21. Presentation of the TIB data. (**a**) Total settlement data, (**b**) time-adjusted data, (**c**) settlement numbers by evidence type.

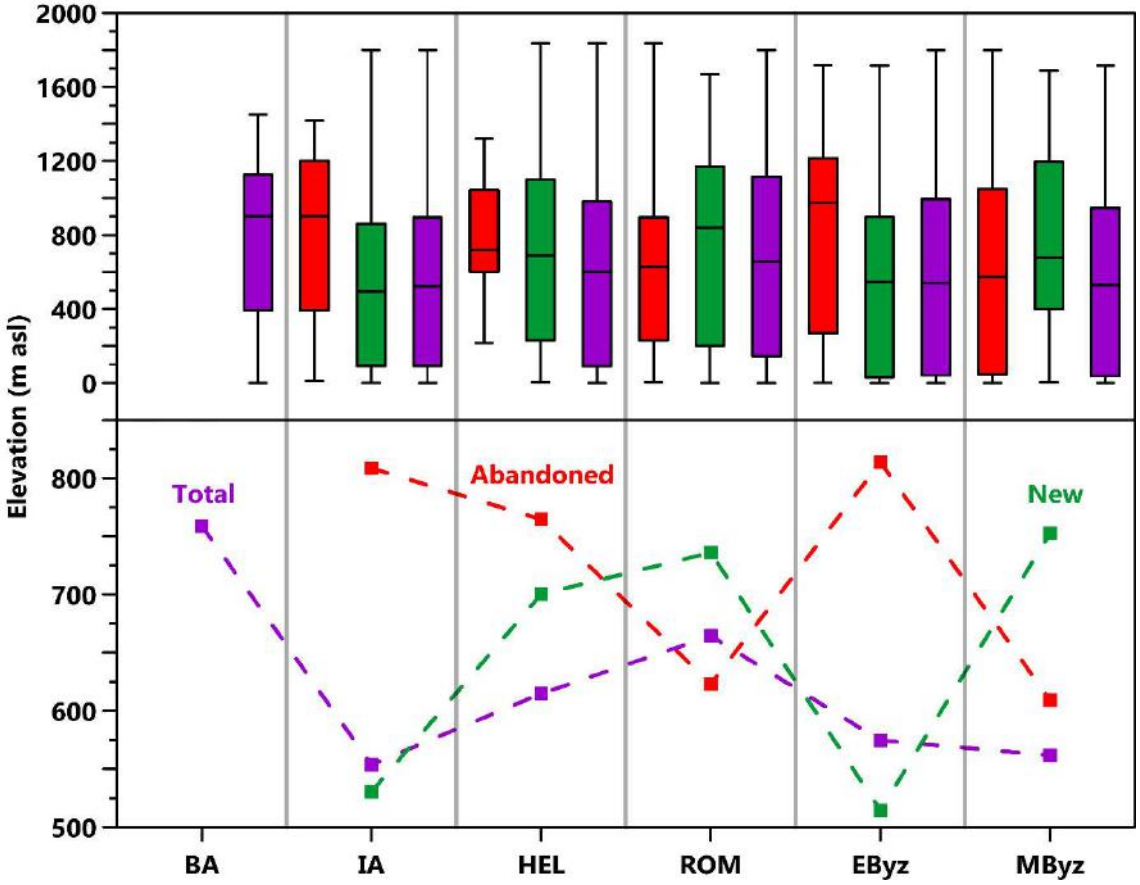

Figure 22. Settlement elevation data by period. Box-plots with inter-quartile ranges and median values (top) and mean elevations (bottom).

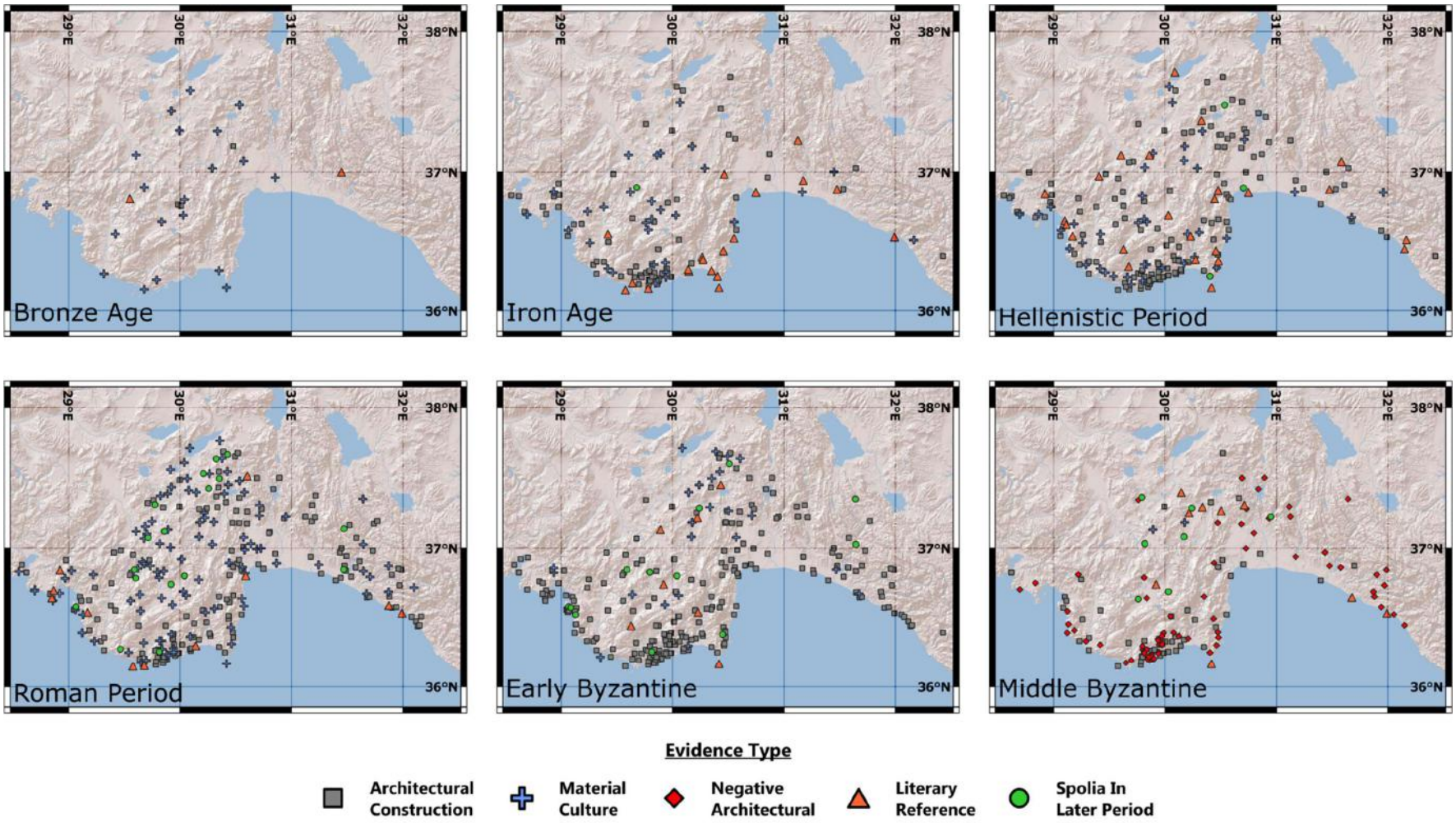

Figure 23. Maps showing settlement evidence by period.

Table 4. Settlement metadata by period. "New" settlements are those with evidence in the period, but no evidence in the preceding period; "Continued" settlements are those with evidence in the period and preceding period; "Abandoned" settlements are those with no evidence in the period, but evidence in the preceding period; time-adjusted settlement numbers are calculated following the methodology of Contreras et al., (2018) and Barton et al. (1999), explained in Section 4.2.3.1.

Period	Length (years)	Total Settlements	New Settlements	Continued Settlements	Abandoned Settlements	Time-Adjusted	Avg. Elevation (m asl)
Bronze Age (3000 – 1150 BCE)	1850	25	25	N/a	N/a	3.38	759
Iron Age (1150 – 350 BCE)	800	114	100	14	11	35.63	554
Hellenistic (350 – 50 BCE)	300	205	104	101	13	170.83	615
Roman (50 BCE – 350 CE)	400	276	116	160	45	172.5	664
Early Byzantine (350 – 600 CE)	250	255	66	190	87	255	575
Middle Byzantine (600 – 1050 CE)	450	135	17	118	137	75	562

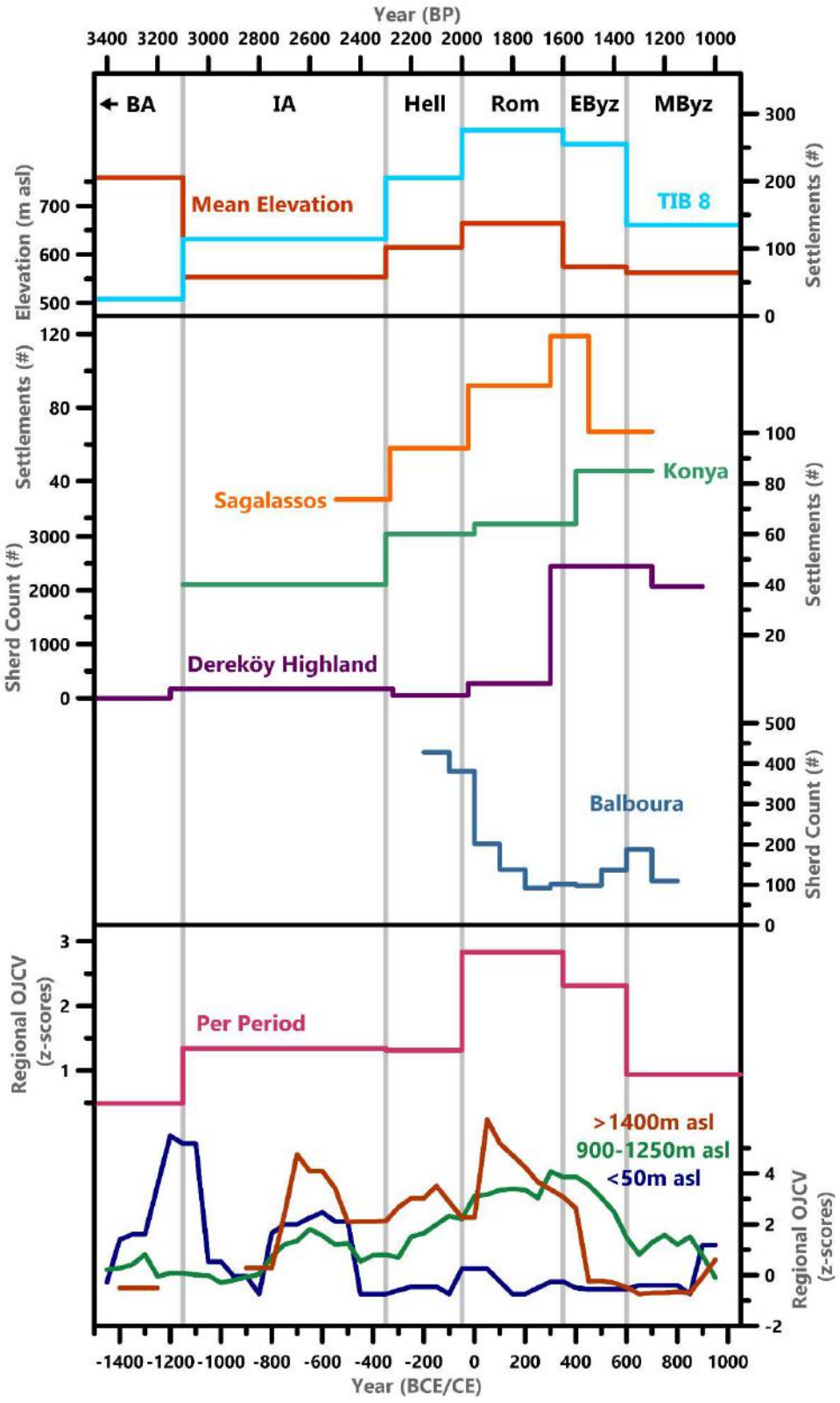

Figure 24. TIB settlement data and mean elevation by period compared to other regional surveys and OJCV value z-scores – per period and as 200-year averages. Datasets references are found within the main text.

4.2.5. History of climate and society in the Eastern Mediterranean

Studying associations between historical climatic and socio-cultural change, now termed the 'history of climate and society' (HCS; Degroot et al., 2021), in the Eastern Mediterranean has been extensive, due to the region's historical significance, and a focus of many popular-science books (e.g. (Cline, 2014; Ellenblum, 2012; Harper, 2017). Generally, such studies produce a history of climate, linked to large-scale climatic events (such as those in Figure 25), from a combination of palaeoclimate proxy records, model simulations, historical records, and archaeological evidence. Assembled climate histories are then compared to historical and archaeological evidence for social, economic, and cultural change, to assess human-climate-environment relationships. These studies intend to provide insight into past societal resilience and fragility, to prepare for potential impacts of future climate change (Knapp & Manning, 2016; Jürg Luterbacher et al., 2012). However, reviews of HCS studies (e.g., (Contreras, 2016; Decker, 2017a, b; Degroot et al., 2021; Haldon et al., 2020) have identified significant and recurring issues, namely (**1**) correlation-based conclusions that lack convincing causal explanations, (**2**) a bias towards periods of "crisis" which mischaracterises human-environment interactions, (**3**) a focus on large regions linked to a lack of high-quality comparative datasets, leading to calls for "micro-regional" case-studies (stressed originally in Horden and Purcell, 2000), and (**4**) the interdisciplinary challenge of comparing archaeological, palaeo-environmental, and -climatic, data of varied resolutions. These challenges are confronted in our presentation of micro-regional data for climate and society in Lycia-Pamphylia.

HCS studies focused on the Eastern Mediterranean are numerous, with climate change frequently presented as an important factor driving prosperity and decline. In the sections below (4.2.5.1-4.2.5.3), we critique this over-simplified and generalised model, by examining three previous hypotheses. Firstly, the Roman Climatic Optimum (RCO; previously Roman Warm Period), is a proposed period of warm and wet conditions controversially referenced as a driving force behind the large-scale success of the Roman Empire. Advantageous climatic conditions are suggested to have contributed to enhanced agricultural productivity, with associated economic, demographic, and settlement growth, between 200 BCE and 150 CE (Harper, 2017). The 1st and 2nd centuries CE have long been suggested as a period of unprecedented prosperity (the "Pax Romana") - a concept recently

critiqued and discussed in Cornwell (2017) and Goldsworthy (2016). Secondly, enhanced precipitation has been designated as an enabling factor for Central and Eastern Mediterranean prosperity in the 4th- early 6th centuries CE (Decker, 2009b; Haldon et al., 2018a; Izdebski, 2013b; Izdebski et al., 2016b). During this period, increased interconnectivity between regions, agricultural productivity, population, and settlement numbers, alongside expansion of rural settlement onto previously unoccupied marginal land, are suggested (Elton, 2019).Thirdly, a period of cooling and/or drying, beginning in the 6th century CE, has been suggested as an important contributing factor for a decline across the Eastern Mediterranean and surrounding regions in the 6th and 7th centuries CE (Büntgen et al., 2016; Helama et al., 2018; Korotayev et al., 1999; Chapter 5). Epidemics and famines are theorised to have been caused by climatic deterioration, leading to demographic contraction and settlement abandonment through deaths and migration.

There are several key criticisms of these types of hypotheses, linked to the above broader criticisms of HCS studies. Most apparent is the generalised and large-scale nature of such hypotheses. Care must be taken when discussing generalised patterns for broad regions or periods, as both climatic and socio-economic conditions have the potential for high variability on both spatial and temporal scales, especially in the Eastern Mediterranean (Horden and Purcell, 2000, pp. 78–79, 179; Luterbacher et al., 2012; Terpoy, 2019a; Ulbrich et al., 2012; Chapter 3). Micro-regional analyses are therefore required where the main climatic constraint on agricultural productivity is identified; additionally, for many regions the assumption that higher temperatures and water availability will facilitate higher agricultural productivity is false (Haldon et al., 2014; Nemani et al., 2003). We provide this for our study region, enabled by our new dataset of settlement character and location, and the existing high quality palaeo-environmental and -climatic records (introduced in Section 4.2.2). Chronological and preservation biases in settlement datasets are limiting factors for this analysis (Section 4.2.3.1). However, the consistency of patterns across varied data-types, particularly for the period under discussion (Roman to Middle Byzantine), suggests they result from regional changes in settlement density and distribution. Comparing datasets of varied chronological resolutions, such as highly-resolved palaeoclimate records and period-averaged settlement data, presents significant challenges. Averaging of palaeoclimate data for archaeological periods or centuries is one methodology frequently utilised in the Eastern Mediterranean (e.g., (Labuhn et al., 2018; Roberts et al., 2018b, 2019), here providing

interesting results (Figures 24a and 24b). A visual relationship between $\delta^{18}O$ and settlement evidence is apparent (Figure 25b). However, this conceals the high variability of climatic conditions within each period (Figure 25c). Additionally, agricultural productivity, the mechanism through which climate change would primarily impact settlement locations, is more reliant on effective moisture, which for the higher resolution Kocain Mg/Ca record shows a weaker relationship (note the Roman Period in Figure 25a). In the sections below, we consider the full picture of climatic variability during the periods under discussion and assess the extent of their impact on regional settlement location and character, in addition to the contribution of other factors.

4.2.5.1. A Roman Climatic Optimum?

Roman settlements in our dataset were largely continuous with the preceding Hellenistic period; 45 Hellenistic settlements were abandoned and the remaining 160 constitute 58% of the 276 Roman period settlements. A shift from low to high elevations is observed, with the highest mean elevation of all considered periods for new (736m asl) and total (664m asl) Roman Period settlements (Figure 22). Abandoned settlements are more frequent at low elevations (37/45<1000m asl; mean=622m asl) in south central and western Lycia, especially in association with older Iron Age and Hellenistic Lycian dynastic centres. For example, within 20km of Myra and Finike (ancient Phoinix), at least 10 settlements contain Hellenistic fortified tower-farmsteads or "turmgehöfte" (Morris, 2005) that show no signs of Roman occupation, though many were reoccupied in the drier Early Byzantine period (e.g. Beymelek, Davazlar, Gelemen or Pharroa; Section 4.2.5.2). Of all new Roman settlements, a significant portion are located at mid-high elevations (68/116>600m asl), with highland concentrations in Pamphylia north of Side and Alanya and in northern Lycia/south Pisidia (Figures 22 and 25). In the latter region, many rural Roman settlements are identified, primarily via inscriptions and ceramics, in surveys conducted by the Sagalassos Archaeological Research Project (Poblome et al., 2017; Waelkens, 2000). Rural settlements overall make up a large proportion of new Roman settlements overall (63 villages and farmsteads). Industrial rural estates based on the Italian *villa rustica* model appear at 10

settlements (e.g. at Çaylakkale, Gedelma, Hamaxia). Conversely, most Roman period urban settlements were continuations from the Hellenistic period (70/81).

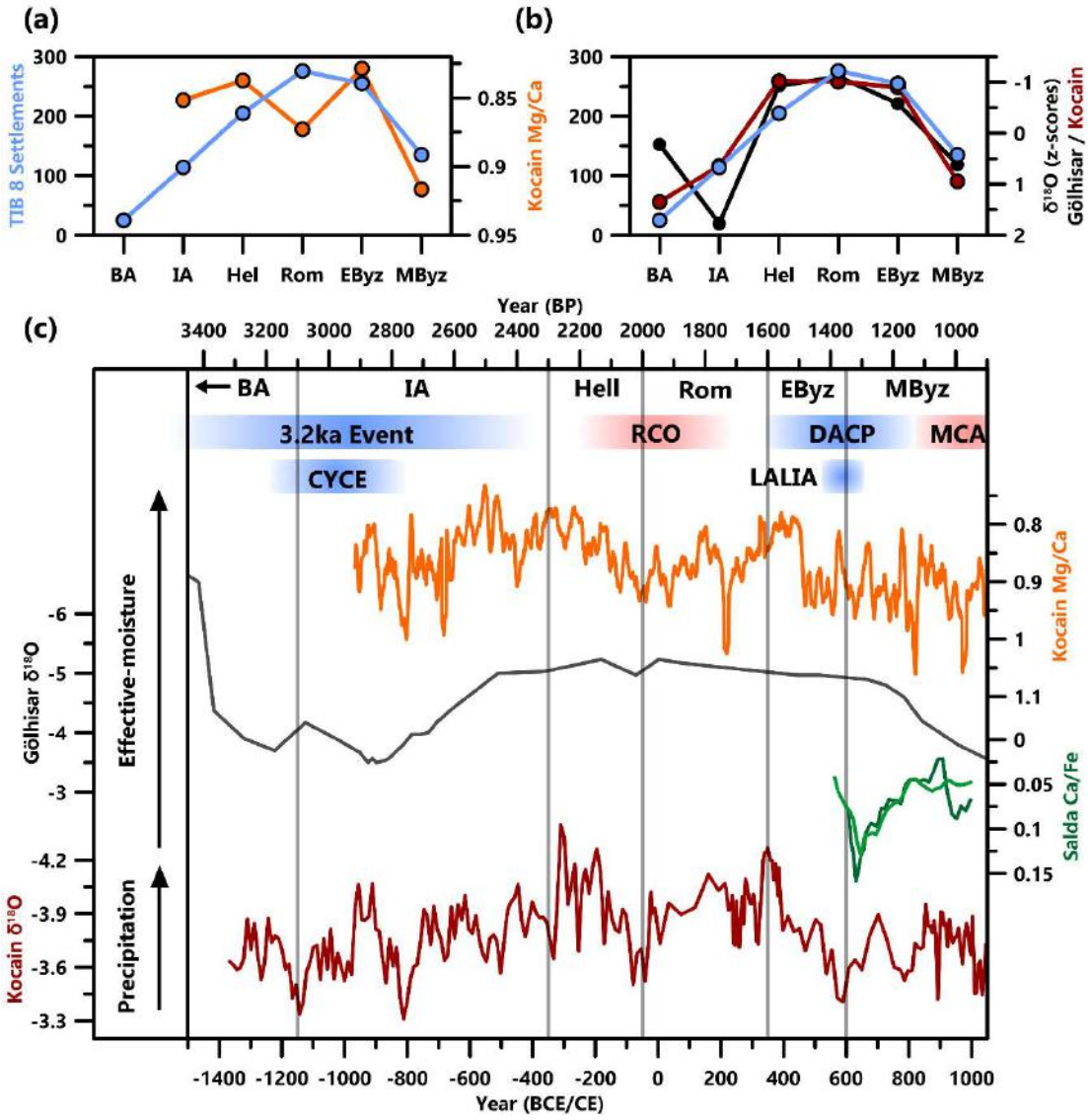

Figure 25. Regional palaeoclimate data compared to (a) Mg/Ca averages from Ko-1 and (b) δ18O from Gölhisar and Ko-1. (c) Full palaeoclimate data with warm/cold intervals: Crisis Years Cold Event (CYCE), Roman Climatic Optimum (RCO), Dark Ages Cold Period (DACP), Late Antique Little Ice Age (LALIA) and Medieval Climate Anomaly (MCA). Kocain Mg/Ca, Gölhisar $\delta^{18}O$, and Salda Ca/Fe, are largely indicative of effective moisture; Kocain $\delta^{18}O$ reflects precipitation, with secondary influences from seasonality and temperature (Danladi and Akçer-Ön, 2018; Eastwood et al., 2007; Chapter 3).

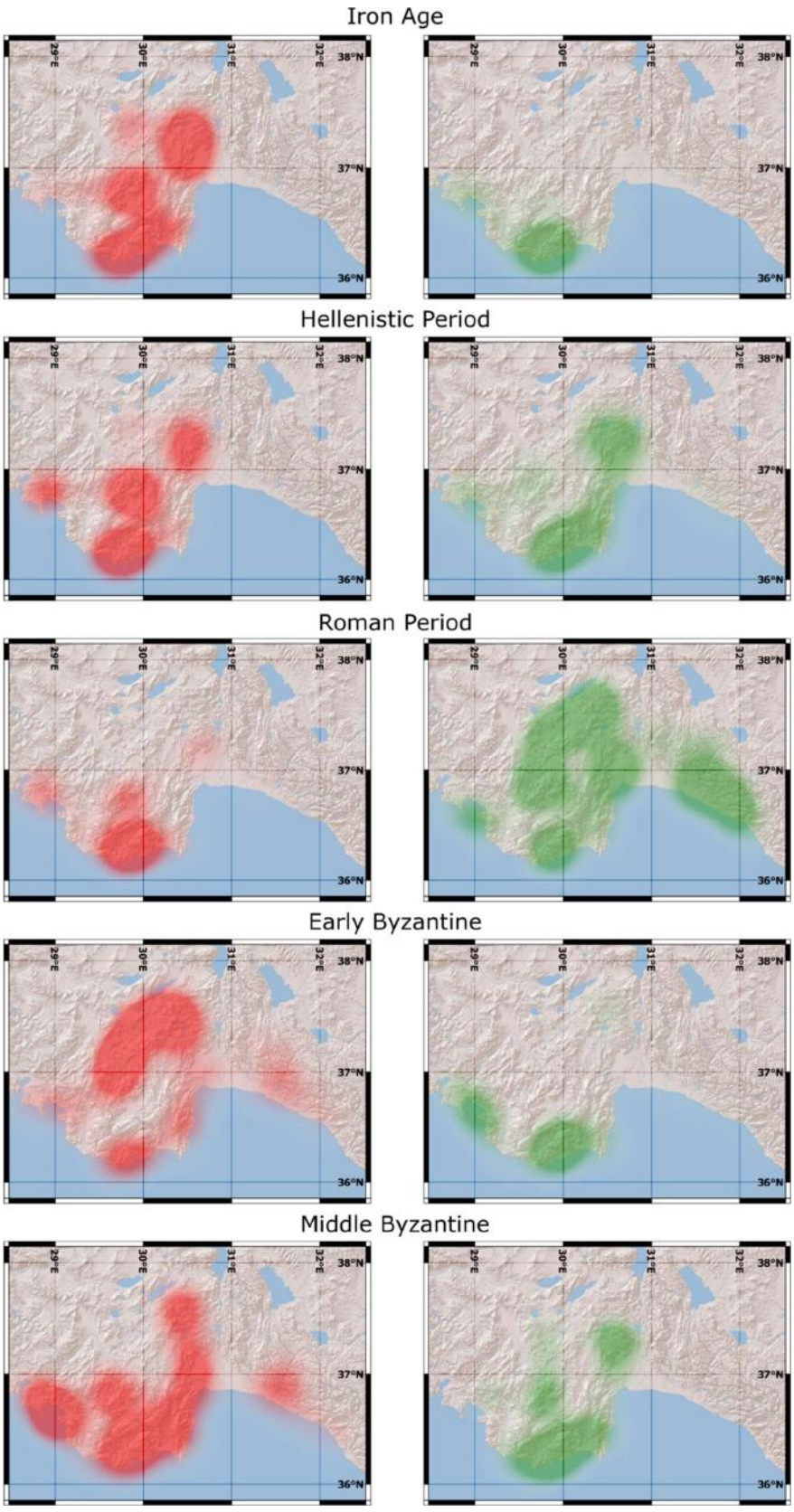

Figure 26. Settlement change heatmaps, red indicates settlements abandoned since the previous period whereas green indicates newly occupied settlements. Full settlement map in Figure 23.

Pollen data from around Sagalassos suggest that interior regions with high Roman period settlement density in our dataset (and in Vandam et al., 2019b; Figure 24) experienced expansion of upland agriculture and arboriculture in the 1st century CE. At the high-elevation Bereket Basin site, OJCV values peak with significant increases also occurring at Ağlasun, Gölhisar, and Gravgaz (De Cupere et al., 2017; Figure 24). Despite proliferation of imperial period architecture and material culture, and expansion of agricultural activity that matches with the RCO hypothesis, these do not appear to have been determined (or enabled) by climatic factors.

During the RCO, Mg/Ca from Kocain Cave indicates that effective moisture was declining from ~100 BCE until ~30 BCE, then remained low until ~100 CE, with a further short-lived dry phase at ~220 CE also evidenced by a soot layer and pollen statistical analysis at Gravgaz Marsh (Bakker et al., 2011; Koç et al., 2020; Chapter 3). Between these dry phases, Mg/Ca ratios were close to their mean values (0.88mmol/mol^{-1}) until ~120 CE and then lower (indicating slightly wetter conditions) until ~200 CE. $\delta^{18}O$ values from both Kocain Cave and Lake Gölhisar suggest slightly wetter conditions from 50-1 BCE; however, this may result from the lower-resolution of these archives which misses out shorter-term climatic variability. Slightly enhanced precipitation is suggested by $\delta^{18}O$ from Kocain Cave during 150-200 CE, matching the wetter conditions suggested by Mg/Ca. This likely reflects conditions wetter than the average for the period under discussion, but not as wet as the start of the preceding Hellenistic Period or the distinct period of high effective moisture in the 4th and 5th centuries CE (~330-460 CE; Chapter 3). In our study region, during the RCO, and Roman Period, there was a high level of variability, with little evidence to suggest an enduring warm and wet phase. In fact, a lack of evidence for the climatic-element of the RCO is observed throughout the Eastern Mediterranean (Haldon et al., 2018b; Labuhn et al., 2018).

At least in our study region, wetter climatic conditions could not have driven expansion of agricultural activity and settlement during the Roman period. Instead, we argue that integration of the region into the Roman imperial system after ~50 BCE was more important. A formal treaty of Lycia with Caesar was signed in 46 BCE (Mitchell, 2005), under Augustus (27 BCE – 14 CE) the first colonies were established (e.g., at Balboura and Olbasa), and final annexation of Lycia occurred under Claudius in 43 CE (Bennett, 2011; Brandt & Kolb, 2005). Over a century of heavy investment followed, financed both by the state and by local

elites choosing to incorporate into the Roman imperial system (Kokkinia, 2000; Waelkens, 2002). Monumental agorai, theatres, baths, aqueducts, and temples, were rapidly constructed in both coastal and upland Roman settlements (Figure 27b; Brandt and Kolb, 2005; Milner, 2016). Interconnectivity increased with infrastructural investment, and agricultural products critical for supply of Roman armies on the Danube and Syrian-Mesopotamian frontiers were more readily exported (Akyürek, 2016). Roads were systematised, as evidenced by milestone inscriptions and the important Stadiasmus Patarensis inscription that details regional road networks (Adak & Şahin, 2007). Lycian harbours became important nodes in regional grain markets and saw significant infrastructure upgrades; for example, granaries were built at Andriake and Patara, with a lighthouse at the latter (Rice, 2020). Tax collection from cities was standardised across Roman territory, and the state now profited from the rich resources of Lycia-Pamphylia, including traditional agricultural produce but also sponges, goat hair for ropes, wild animals for the circus, fish processed as garum, and most importantly, timber (Bennett, 2011; Brandt & Kolb, 2005, pp. 99–101). Agricultural efficiency for the Mediterranean triad (grapes, grains and olives), was enhanced with Roman innovation of the screw press for grapes and olives, and the rotary mill for grain (Curtis, 2008; Greene, 2000). Roman hegemony also brought newfound security from unrest and a regional threat of banditry and looters (Bennett, 2011), and might be reflected by a reduction in both urban fortifications and tower-farmsteads (Çevik & Bulut, 2007; Takaoğlu, 2020). All the above factors increased the importance of Lycia-Pamphylia for trade and enabled intensification of settlement and agriculture in the hinterlands (Dündar, 2018; Rice, 2020).

These developments occurred despite prevailing climatic conditions that likely made agriculture more challenging when compared to the preceding and succeeding periods. The dense settlement detected in the Roman period continues into the Early Byzantine period, however a shift in the character and location of settlement is observed.

4.2.5.2. Late Antique prosperity and adaptation?

Peak settlement numbers in our study region come in the Roman period, with the majority continuing into the Early Byzantine period (189/276: 68%); overall settlement numbers remained high, with a slight decline in absolute numbers, with 255/381 (67%) dated

to the Early Byzantine period. When bias from period length is counteracted by a time-adjustment (Section 4.2.3.1), the Early Byzantine period experiences the settlement evidence peak (Figure 21b). Important however, is the shifting character and location of settlement between these two periods. There is a loss of settlement density in interior Lycia (Figures 22 and 25) caused by the abandonment of Roman Period highland rural settlements, which contributed to the highest mean elevation of abandonments for any period (814m asl). Dense settlement on the coast continues however, with 87 settlements <200m asl, including older Hellenistic and Roman cities (Figure 26). New rural settlements also appear in the hinterlands of these cities, for instance around Fethiye, Olüdeniz, and Myra; the lowest mean elevation of new settlements for any period (514m asl) lowers the overall mean elevation (575m asl; Figure 22).

These findings are largely coherent with regional understanding. Harrison (2001) previously suggested that coastal cities in Lycia declined from the 5th century CE, with population and important settlements migrating inland to the mountainous regions. However, the inverse has since been suggested, and is supported by our dataset, with increased settlement density in coastal regions and a possible decline in the interior regions (Cassis et al., 2018; Foss, 1993, 1994; Terpoy, 2019a, b). The pollen data provides further support for this trend, with an Early Byzantine period decline in OJCV values at the high elevation Sögüt and Bereket Basin sites (Figure 24), coincident with the end of the BOP ended at these sites (Roberts, 2018). A decline in OJCV values is also observed in the other records from around Sagalassos (Ağlasun and Gravgaz Marsh), coincident with a reduction in settlement numbers in the hinterland survey (Figure 24; Vandam et al., 2019b). Similar to the Roman period, long-distance maritime transport of agricultural produce was important, with the state subsidising supply of food staples both to Constantinople and to Byzantine armies campaigning against Sasanian Persia (Commito, 2019; Morrisson & Sodini, 2002). This may have promoted expansion of settlements near to the coastlines and made inaccessible mountainside settlements comparatively less efficient (Izdebski, 2013b; Terpoy, 2019a). Coastal regions are also more productive and allow for greater crop diversity due to their extended growing season (Decker, 2009b) and enhanced precipitation and temperature compared to the interior regions (Section 4.2.2). The idea of a period of "prosperity" in the

4th-6th centuries CE is therefore more complicated, at least in our study region (e.g. Foss, 1994; Terpoy, 2019a).

Izdebski et al. (2016) examined Early Byzantine "prosperity" in relation to climatic conditions, concluding that enhanced precipitation contributed to the expansion of rural settlement and agriculture into environmentally marginal terrain. However, at that time the only available high-resolution palaeoclimate records in Anatolia were those from Nar Gölü (Dean et al., 2015, 2018; Jones et al., 2006) and Sofular Cave (Göktürk et al., 2011), located in the Central Anatolian Plateau and Black Sea coastal regions, respectively. These records, and associated archaeological and historical data, suggest enhanced aridity 350-470 CE, followed by wetter conditions (Izdebski et al., 2016b). However, the climate of Lycia-Pamphylia is now better understood due to the local Kocain Cave record, which stresses spatial heterogeneity of climate in Anatolia. The record demonstrates that the SW region experienced the inverse pattern to that previously suggested, sharing more similarities with the Aegean (Chapter 3; previously theorised in Labuhn et al., 2018). Kocain $\delta^{18}O$ and Mg/Ca ratios indicate very high precipitation and effective moisture between 330 and 400-460 CE, followed by a rapid shift to drier conditions that persisted until ~830 CE (Figure 25; Section 4.2.5.3). This is important as high-resolution variability of climatic conditions in SW Anatolia were previously unknown for most of this period; the Salda record starts 560 CE, and there are no historical references to climatic conditions from the region (Danladi & Akçer-Ön, 2018; Warren J. Eastwood et al., 2007; McCormick et al., 2012).

Reduced effective moisture from the mid-5th century CE may also be reflected in regional archaeological evidence for urban water infrastructure adaptations. Construction and refurbishment of large vaulted reservoirs for water storage escalated from the mid-5th century CE, with large-scale projects at seven of the regions major cities, including the well-excavated sites of Sagalassos, Patara, Rhodiapolis, Side, and Xanthos (Akyürek & Tiryaki, 2010; Işkan, 2013; Martens, 2008; Sodini et al., 1996). Also at Sagalassos, a reduction in the supply output of the older Roman aqueducts is visible in changes made to the city's fountains during the 6th century, with outlets cut at lower basin levels in the Upper Agora, alongside construction of new metal and textile workshops. New public fountains were still constructed in Sagalassos; geochemical evidence from calcites in feeder channels indicates supply via rain-capture and snow-melt (Martens, 2008, p. 257), contrary to traditional Roman

patterns of urban water supply via spring-fed aqueducts (Pickett, 2017, 2020). New settlements entirely reliant on rainwater capture also appear in the Early Byzantine period, for instance at Lyrboton Kome (Hellenkemper & Hild, 2004, p. 696) and Gemiler Adasi (Asano, 2010). These urban water infrastructure adaptations coincide with the demonumentalisation and ruralisation of cities, the appearance of church architecture, and renewal of fortifications described below. These economising adaptations are traditionally associated in scholarship with "decline" but lately are considered indicative of "adaptive reuse" (Commito, 2019, p. 126), here possibly linked to drier climatic conditions revealed by the Kocain Cave record.

Early Byzantine settlement is most clearly evidenced archaeologically by church architecture, which appears almost exclusively after the mid-5th century CE (Hellenkemper & Hild, 2004, p. 217). Intensified investment is suggested by the number of settlements evidenced by architecture (213/255 Early Byzantine settlements; Figure 21c), comprised mostly of church construction and renewal of fortifications. Roman *poleis* were required to have bishops, necessitating construction of churches and episcopal complexes. Church construction was frequently coincident with the demonumentalisation and ruralization of city settlements. Churches were often well-integrated into Roman street plans but incorporated building materials from recently demolished Roman structures: they signalled more than change in religious belief, indicating new political and economic realities in cities (Haldon, 2016; Saradi, 2006). Churches are also found in close proximity to agricultural developments in the countryside such as terracing (as at Asarcik, but unfortunately not dated; e.g as in Turner, 2021), and in cities near artisanal installations (at Patara or Sagalassos), or large scale water storage (at Xanthos or Gemiler Adasi). At Xanthos, for instance, recent excavations in the western agora have revealed two churches, one at the agora's center and one built into its western portico, surrounded by workshops and water installations that facilitated artisanal activity, all dated to the fifth and sixth centuries (Figure 27e; Dönmez, 2018). Whilst new churches are not necessarily indications of communal wealth, they did require significant investment (Bowden, 2001; Izdebski, 2013b). This was especially true in Lycia where churches featured high-quality stone carving, even within village settings (e.g. north of Demre around Asarcık, Figure 27c; Grossmann and Severin (2003)). Lycian churches have long been a focus of scholarly attention (e.g. Fellows, 1840), which, combined with their robustness, increases the archaeological visibility of rural settlements. These factors are perhaps reflected in the

increase of rural settlements in our data between the Roman (43%: 119) and Early Byzantine (51%: 130) periods.

From the mid-5th century CE, older Roman cities throughout our region begin to lose their monumental aspect, with less maintenance of Roman public buildings (including theaters, baths, and agorai). Concurrently, these older Roman spaces had begun to be adopted for artisanal and industrial activities. For instance at Side, glass workshops appeared in the theater and around an abandoned temple in the agora after the 5th century (Alanyalı, 2010, 2011). At Limyra, baths near the theater were abandoned in the later fifth and became home to workshops for textiles, metal and/or glass, and bone-carving (Österreichischen Archäologischen Instituts, 2017, pp. 37–39). At Andriake, a workshop for the extraction of precious murex dye was built in the 6th century using spolia from an older church: remaining were massive piles of murex shells and more than 22,000 amphorae fragments of the sixth and seventh centuries thought to be related to murex production and transport there (Çevik & Bulut, 2011; Yener-Marksteiner, 2009).

Whilst reduced effective moisture (and a range of potentially adaptive responses) appears in southwest Anatolia after ~450 CE, climatic shifts will not be homogenous across the Eastern Mediterranean (Chapter 3). A complex web of interconnected factors is suggested elsewhere to have its origin in the mid-6th century CE. These include natural factors such as cooling and drying associated with volcanic-induced reductions in solar irradiation, earthquakes, and epidemics, and insecurity resulting from conflicts between the Byzantine and Sasanian Empires, the Umayyad Caliphate, and nomadic groups. These are discussed below in Section 4.2.5.3.

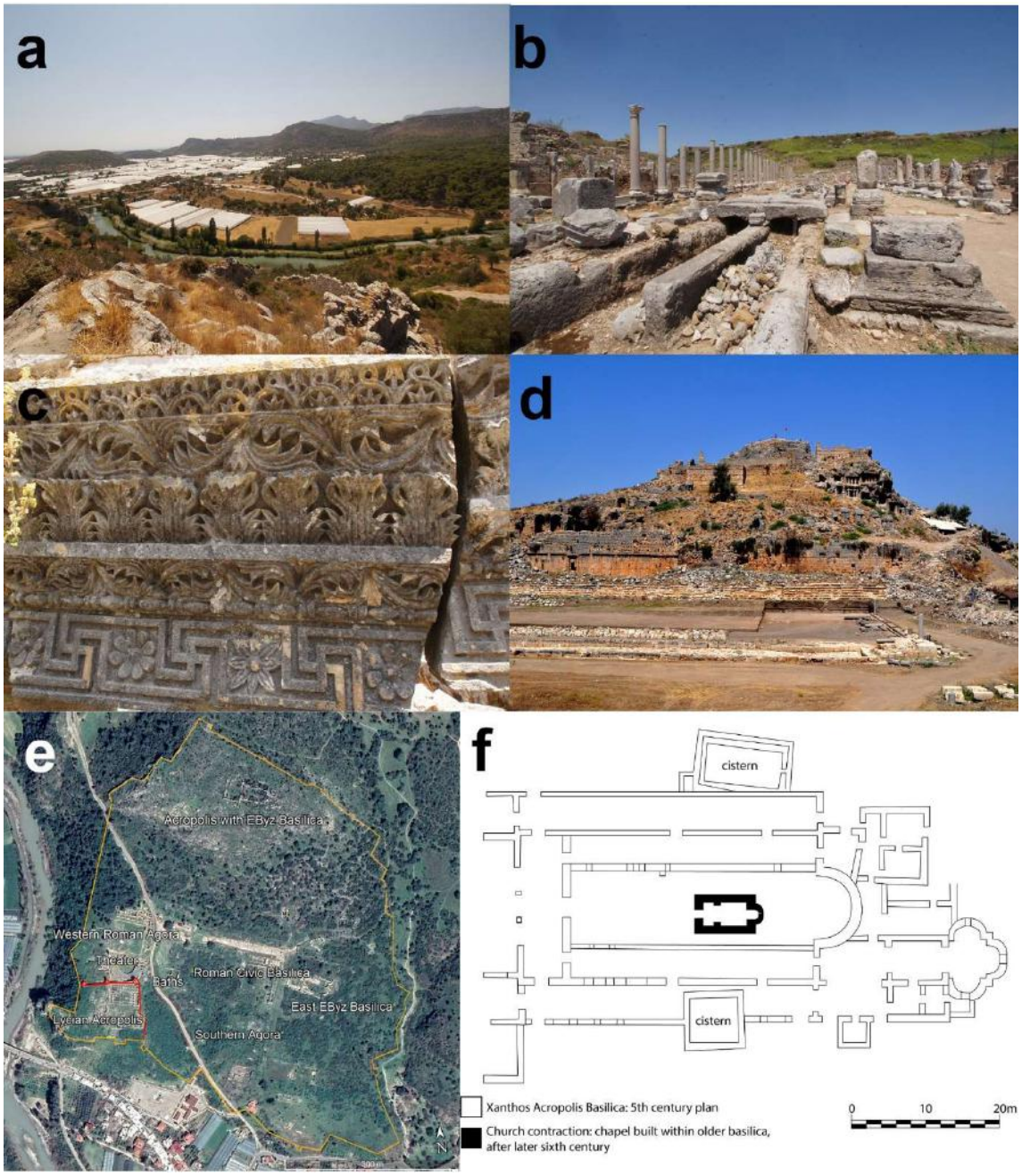

Figure 27. Photographs and plans from our study region by Jordan Pickett. (a) A Lycian alluvial landscape, looking west over the river Eşen Çayı / anc. Xanthos from 7th-9th century Byzantine fortifications on the Lycian Acropolis at city of Xanthos, with modern greenhouses below; (b) the Roman colonnaded street with cascading fountains fed by aqueduct at Perge; (c) Sixth century CE architectural sculpture from church at Asarcık; (d) Tlos, with Roman stadium in foreground, Iron Age-Hellenistic sarcophagi and tombs in mid-ground, and Early-Middle Byzantine fortifications built atop the Iron Age acropolis; (e) annotated satellite image of Xanthos, with Lycian Acropolis (since 8th BC), Iron Age fortifications (in orange), late Classical and Hellenistic city grid with agorai at east, Roman agora and theater at west, Early Byzantine basilicas, and Middle Byzantine refortification of the Iron Age Lycian Acropolis (in red); (f) plan of Middle Byzantine contraction of older church basilica on Xanthos Acropolis (by Jordan Pickett, after Erdoğan and Ceylan 2019).

4.2.5.3. Middle Byzantine abandonment and re-nucleation?

The transition between our Early Byzantine-Middle Byzantine periods shows a significant shift in the intensity and character of settlement. Settlement density was reduced in the Middle Byzantine period, with a total of 135 settlements. Of the settlements with Early Byzantine period evidence, 134/255 (52%) had been abandoned and only 17 new settlements are evidenced. An even more pronounced reduction is settlement density is suggested when the length of the longer period is considered, with time-adjustments (Section 4.2.3.1; Figure 21b).

Additionally, settlements were no longer occupied at the scales of the preceding Roman and Early Byzantine periods: Antalya, which became a centre for the Byzantine navy and administration alongside significant investment in new architecture and fortifications may be one exception, though 20th century development has prevented any archaeological conclusions (Foss, 1991; Oikonomides, 1983). In larger urban settlements elsewhere, a *citte ad isole* [cities to islands] pattern is frequently observed, whereby small clusters of activity or "islands" are visible within the skeleton of older Roman and Early Byzantine cities, which were otherwise abandoned. For example, Myra contained three separate fortified enclosures: at the acropolis (Borchhardt, 1975, p. 46), at the Church of St Nicholas, which was rebuilt as a domed basilica in the 8th century CE (Ousterhout, 2019, p. 251), and at its harbour Andriake (Foss, 1994, p. 24). Furthermore, over half of the Middle Byzantine settlements are only evidenced by church contraction (72). Very small chapels, often <3x5m^2 and sometimes with datable frescoes, are erected inside older derelict structures, mostly much larger church complexes (see Figure 27f; Erdoğan and Ceylan, 2019). Whilst church contractions could be indicative of the persistence of Christian holy spaces, they also suggest insecurity, inability to invest, and demographic decline.

Investment in new construction or restorations is evidenced at 45 settlements, a figure lower even than the Iron Age. This was largely comprised of smaller settlements where older Iron Age or Hellenistic circuits were refurbished (e.g. Idebessos, Tlos), and village settlements with small chapels constructed within older fortifications (e.g. at Asar Dağı, Trysa). Despite indications of both abandonment and reduced settlement intensity throughout our study region, continued investment in some of the larger cities suggests

renucleation. Major church construction (e.g. at Antalya, Myra, Patara) and resettlement of disused urban acropolises (e.g. at Perge, Tlos, Xanthos) was accompanied by increased administrative importance (Peschlow, 2017). Byzantine lead seals, which were used to secure documents and indicate information about the author (Oikonomides, 1983), demonstrate the importance of Antalya, Myra, Perge, and Tlos, as centres of Byzantine naval and fiscal administration in the Kibyrrhaeot theme (Brubaker and Haldon, 2011, pp. 667–670; Hellenkemper and Hild, 2004, p. 119).

Other regional surveys, relying primarily on ceramic evidence, show divergent patterns (Figure 24). In the Sagalassos hinterland survey, settlement numbers had already declined for the period starting 450 CE (Section 4.2.5.2), whereas in the Dereköy Highland sherd counts remained high in their period starting 700 CE (Vandam et al., 2019a, b, c). In the Balboura survey, sherd count increases in the 7th century CE, after re-dating of Cypriot Red Slip Ware (CRSW) by Armstrong (2009) – a local/regional production that satisfies basic household needs (Jackson et al., 2012). In both surveys, the majority of Middle Byzantine sherds are local (Armstrong, 2012; Coulton, 2012b, a; Vionis et al., 2009). This pattern, which suggests a reduction in inter-regional exchange, is observed across the region, at settlements such as Sagalassos, Limyra and Xanthos (Cavalier, 2006; Commito, 2019; Poblome et al., 2017). This reduction in inter-regional exchange was accompanied by a reconfiguration in some contexts, away from Constantinople and towards the southeast: 7th-9th century CE deposits from Sagalassos contained LR7 amphora with fish remains from Egypt, and deposits from Limyra contained wares from Cyprus, Egypt, and the Levant (Vroom, 2011).

The transition from the Early to Middle Byzantine periods also marks a major shift in the agricultural history of our study region and the Eastern Mediterranean more broadly. Intensive crop cultivation ended, pastoralism grew in importance, and re-wilding of the landscape occurred with pine forest recolonisation (De Cupere et al., 2017; W. J. Eastwood et al., 1998; Izdebski, 2011). At the pollen sites where the BOP had not already ended (Gölhisar, Ağlasun, Gravgaz), it did in the 7th-8th CE (summarised in Roberts, 2018). This is reflected in the OJCV values (Figures 23), which are minimal during the Middle Byzantine period.

Climate may have some responsibility for these changes in historical society within our study region. The Kocain Cave Mg/Ca record (Figure 25c; Chapter 3) suggests that in

Lycia-Pamphylia, a rapid shift away from high effective moisture occurred ~460 CE and conditions remained relatively dry until at least 830 CE, except for short-lived breaks from aridity at ~571-578, 672-676 and 778-784 CE. Especially dry conditions occurred around the start of the 7th century CE, with a minimum of precipitation indicated by Kocain $\delta^{18}O$ at ~590 CE and high Salda Ca/Fe ratios between ~620 and 650 CE overlain on a 600-770 CE dry-phase Very dry conditions are suggested again around the start of the 9th century CE, with Kocain Mg/Ca and $\delta^{18}O$ ratios consistently high between 790 and 830 CE and the start of a shift to less negative Gölhisar $\delta^{18}O$ ratios (Warren J. Eastwood et al., 2007). The initial drying precedes the 536 CE eruption that resulted in a 12–18-month dust-veil covering much of the northern hemisphere, chronicled by Byzantine, Syrian and Chinese sources (Arjava, 2005; Houston, 2000; Stothers, 2002). In other regions, climatic deterioration is suggested to have followed cooling resulting from this eruption and two others (540 and 547 CE), reinforced by sea-ice feedbacks: the Late Antique Little Ice Age ("LALIA": 536-660 CE). However, this is now thought to have lasted for a shorter period of time, "the 536-550 CE climate downturn" (Büntgen et al., 2016; Newfield, 2018). The Kocain Cave record, and other Eastern Mediterranean records, perhaps support the suggestion that the 536 CE dust-veil event occurred superimposed over a longer-lasting pattern of cooling/drying climate known as the Dark Ages Cold Period ("DACP": 450-800 CE; Helama et al., 2017; see discussion in Chapter 3). Records from elsewhere in Anatolia, in Lake Nar and Sofular Cave, show either wetter conditions or no indication of a climatic impact from the 536-550 CE downturn (Dean et al., 2015, 2018; Göktürk et al., 2011; Jones et al., 2006), further stressing regional and micro-regional climatic variability.

An extended dry period is suggested for Lycia-Pamphylia (~460-830 CE) that would have lowered potential agricultural productivity, potentially disenabling arboriculture at higher elevations, and may have contributed to socio-economic and settlement decline. However, it is important to consider that there were earlier instances of dry climates where the local population appears to be relatively unafflicted, or even to have prospered. For example, during exceptionally dry conditions in the middle of the Iron Age (800 and 700 BCE), Greek colonisation started in our region and, during the RCO agriculture thrived despite relatively low effective moisture (Section 4.2.5.1). Additionally, the shift to drier conditions occurred at least a century earlier than the reduction in settlement numbers and investment,

with a shift away from agriculture and towards pastoralism, which can be broadly dated to somewhere between 550 and 650 CE. This suggests that either the duration of the climatic change, or its combination with other factors was more important. These are primarily (1) pathogenic, (2) seismic, and (3) defensive.

(1) The appearance of the Plague of Justinian after 541 CE and lasting into the 8th century CE, an early epidemic of the bubonic plague caused by the bacterium *Yersinia pestis*, was traditionally understood as a mass mortality event, especially during the 540s CE (Harper, 2017; Stathakopoulos, 2004). Its presence in Lycia-Pamphylia is securely evidenced, with a detailed and contemporary account of widespread death at Myra, probably in 542 CE, that interrupted agricultural commerce from the Lycian interior to the port-city (McCormick et al., 2012; Ševčenko & Ševčenko, 1984), and aDNA of *Yersinia pestis* identified from human remains at Sagalassos (Van de Vijver, 2018). However, the demographic impact of the pandemic has recently been questioned (Eisenberg & Mordechai, 2019; Mordechai et al., 2019). The historical account of Myra also indicates recovery of the rural landscape thereafter (Ševčenko and Ševčenko, 1984; McCormick et al., 2012) and, with the exception of the single victim at Sagalassos, aDNA is lacking (Van de Vijver, 2018). Late Antique plague may have been a greater stimulus for shifts in religio-cultural beliefs and traditions than demographic or economic problems (Meier, 2004, 2016, 2020). However, regional evidence indicates its presence, and it cannot be excluded as a factor in the widespread settlement abandonment, and possible demographic contraction, visible in the archaeology of Lycia-Pamphylia after the 6th century CE.

(2) Another major factor in 6th century changes elsewhere, and with evidence for in our study region, are earthquakes (Korotayev et al., 1999; Mordechai & Pickett, 2018). The Aegean tectonic plate, a subduction zone, nearly parallel to and offshore from the south Anatolian coast (Bird, 2003), causes frequent earthquakes in Lycia-Pamphylia (Ambraseys, 2009). An early 6th century (possibly 500 or 518 CE) earthquake occurred north of Antalya (Ergin et al., 1967; Similox-Tohon et al., 2006), collapsing numerous light buildings and the monumental gates at Sagalassos (Gates, 1997; Waelkens et al., 2000), with rebuilding activities widely visible in the city's archaeology (Waelkens, 2019). In 528/9 CE, an earthquake centred on Fethiye-Meis (Erel & Adatepe, 2007) caused extensive damage across Lycia, particularly at Myra (Malalas, 2017), with support given from imperial funds for

reconstruction, according to typical protocols (Mordechai & Pickett, 2018). Communities suffering from earthquakes after the 6th century did not receive help or repair, however. Another earthquake around 600 CE "virtually wiped out Sagalassos as an urban settlement" (Waelkens, 2019, p. 24) and further earthquakes in the seventh and eighth centuries have been observed in damaged (and unrepaired) structures at Side and around Myra (Hellenkemper & Hild, 2004, pp. 207, 226).

(3) Regional insecurity also increased from the 7th century. Towards the end of the Byzantine-Sasanian conflicts, the Sasanians captured nearby Tarsus in 613 CE and Rhodes from 622/623 CE. The Umayyad caliphate's capture of Egypt in 642 CE ended the Annona grain supply to Constantinople, whose transport relied on Lycian harbour cities. An Umayyad navy formed in 649 CE that created coastal insecurity for centuries. Byzantine naval hegemony ended with defeat at the Battle of the Masts in 655, and was followed by direct raids on our study region in 666, 671-673, 676-678, 715, 807 and 1034 CE (Mango et al., 1997). As Baird (2004) observes for the Konya Plain, investment in land for agriculture would quickly have become unstable upon the mere threat of seasonal Umayyad raids, which could have disrupted the economy and population without the need for destruction of property. An interesting suggestion, beyond the scope of this paper, is that the complex web of interconnected factors (including climatic deterioration), which impacted varied regions across the northern hemisphere, may have "pushed" or "enabled" invasions by the Rashidun/Umayyad Caliphates (Korotayev et al., 1999; Chapter 5), and nomadic groups (Büntgen et al., 2016, 2020).

Overall, evidence from Lycia-Pamphylia indicates settlement abandonment and contraction suggestive of demographic contraction, a shift from BOP agriculture to pastoralism, and the presence of dry climatic conditions, plague, earthquakes, and insecurity – all present at the transition between our Early and Middle Byzantine periods ("end of Late Antiquity") after the 6th century CE. However, clear causal attribution between archaeologically-visible developments and the aforementioned factors remain difficult to determine throughout Anatolia (Mitchell, 2018). Evidence is overall stronger for the natural hazards, when compared to the evidence for societal response to them. Better chronological precision for archaeological change and site-specific studies of proxies for societal response (e.g. urban trash mounds; Bar-Oz et al., 2019) are required to disentangle the causes of this

change. Additionally, as with climate, there are earlier instances of plagues, earthquakes, and conflicts, where the population of Lycia-Pamphylia appear to have been unafflicted (for earthquakes: Mordechai, 2018; Mordechai and Pickett, 2018). This emphasises these factors as contributory, rather than ultimate, and that it is ultimately socio-political factors that determine regional resilience and ability to adapt.

4.2.6. Conclusions

The micro-regional record of historical settlements provided by the TIB 8, combined with regional climatic and environmental proxies, provides a more complete picture of settlement change for a region with previously disjointed evidence. Settlement numbers peak in the Roman and Early Byzantine periods, followed by a clear decline in absolute numbers alongside evolutions in the character and locations of settlement that begin with demonumentalisation from ~460 CE and continue into the Middle Byzantine period. These shifts occur prior to the well-known LALIA period, the beginning of the Justinianic Plague and increased seismic activity, though they appear to have been intensified by the latter.

We find that, during the "Pax Romana" (1st and 2nd centuries CE), increasing agricultural productivity and settlement numbers, with possible population increases and economic investment, did occur. However, linking this to warmer and wetter climatic conditions (as in the Roman Climatic Optimum; Harper, 2017) is too simple, with evidence suggesting our study region was drier than in the preceding and succeeding periods. During a previously proposed period of enhanced winter precipitation in the 4th-6th centuries CE, Lycia-Pamphylia experienced both enhanced effective moisture (330-460 CE) and dry conditions (from 460 CE). This shift was concurrent with a change in the character of settlement, with urban water infrastructure possibly changing as an adaptation to drier conditions, demonumentalisation and ruralisation of cities, appearance of church architecture, and renewal of fortifications. Dry conditions that continue until at least 830 CE, and other factors with their origins in the mid-6th century, including recurrent plague epidemics, earthquakes, and interstate conflict, may contribute to a significant decline in settlement numbers. Surviving settlements also show contraction, in churches, occupied area, and investment, suggesting population decline; renucleation to some of the large centres

also takes place. However, the individual contribution of each factor is hard to quantify and the combination of many factors into a "perfect storm" appears to be more important.

Overall, we demonstrate that making simplistic correlations between positive or negative climatic conditions and positive or negative socio-economic circumstances has numerous caveats, especially considering the spatial heterogeneity of both climatic and societal change in the Eastern Mediterranean. Utilising proximate palaeoclimate data that details variables demonstrably relevant to agricultural productivity is essential; however, even when this data is available, it must be assessed on a case-by-case basis to produce meaningful conclusions. Furthermore, it is ultimately the situation in which a community or society finds itself and the constraints determining its ability to adapt or respond to challenges that determines a region's resilience.

Future Work

Examining human-climate-environment interactions has been demonstrated as requiring strong archaeological and historical evidence, as well as high-quality palaeo-environmental and -climatic datasets. Further similar work can be done utilising earlier periods in this archaeological dataset. For example, interesting settlement, environmental, and climatic, changes are identified in the Iron Age and Hellenistic period. Additionally, similar archaeological datasets can be produced in other TIB regions, many of which contain highly-resolved speleothem and lake palaeoclimate records suitable for similar analysis – e.g. 2) Cappadocia (Nar Lake: Dean et al., 2018), 3) Nicopolis and Cephalonia (Lake Trichonida: Seguin et al., 2020), 6) Thrace (Uzuntarla Cave: Göktürk, 2011), 9) Bithynia (Sofular Cave: Fleitmann et al., 2009; Göktürk et al., 2011), 10) Northern Aegean (Skala Marion Cave: Psomiadis et al., 2018). Furthermore, the Kocain Cave Mg/Ca record (and other high-resolution effective moisture records) may enable agroecosystem modelling of agricultural productivity for these regions (as in Contreras et al., 2018), which could more confidently establish a causal mechanism for climatic impacts on agriculture.

Acknowledgements

We would like to thank John Haldon (Princeton University, USA), Michael E. Smith (Arizona State University, USA), and Hugh Elton (Trent University, Canada), for constructive comments and feedback. We would also like to thank Ralf Vandam (KU Leuven, Belgium) for providing the Sagalassos settlement and Dereköy Highland sherd count dataset, as well as Jessie Woodbridge (University of Plymouth, UK), Nils Broothaerts (KU Leuven, Belgium), and the European Pollen Database for providing the raw pollen data utilised for Figure 24.

Chapter 5: Droughts and societal change: the environmental context for the emergence of Islam in late Antique Arabia

5.1. Preface

This chapter was submitted for publication in the journal *Science* on 4th January 2021. The paper is therefore written in the style of a journal article, according to the regulations of Science. Authorship: Dominik Fleitmann (University of Basel, Switzerland), John Haldon (Princeton University, USA), Raymond S Bradley (University of Massachusetts, USA), Stephen J Burns (University of Massachusetts, USA), Hai Cheng (Xi'an Jiaotong University, China), R Lawrence Edwards (University of Minnesota, USA), Christoph C Raible (University of Bern, Switzerland), Matthew J Jacobson (University of Reading, UK), Albert Matter (University of Bern, Switzerland).

DF led the project design, interpretation and writing of the paper, as well as performed stable-isotope analyses. DF and SJB collected speleothem H12. MJJ performed diameter measurements. HC and RLE performed uranium-series dating. Meteorological data were analysed by CCR. All authors contributed to interpretation, writing the paper, and provided comments. The estimated percentage contribution of MJJ to this paper is ~15%.

5.2. Journal Article

One Sentence Summary:

Persistent droughts in Arabia were an underlying factor for profound societal changes during the 6th century CE, establishing the environmental conditions in which Islam emerged during the 7th century CE.

Abstract:

In Arabia, the 6th and 7th centuries CE are marked by profound societal changes which promoted the disintegration of the major Arabian polities. The demise of Himyar, the dominant power in Arabia until 525 CE, induced significant socio-economic transformations and political changes, promoted a reassertion of tribal identities across Arabia and raised the influence of pilgrimage centres such as Mecca. Here, we present hydroclimate records from and around Southern Arabia, including a new high-resolution speleothem record from Northern Oman. The records reveal that unprecedented droughts during the 6th century CE amplified such socio-political transformations across Arabia, establishing the environmental context in which Islam emerged.

Main Text:

The Himyarite kingdom was the dominant power in the Arabian Peninsula from the late 3rd until the early 6th century CE (Figure 28a). Its dissolution over the course of the 6th century CE marked the end of a 1400-year long pre-Islamic period of supra-tribal polities in Arabia (Bowersock, 2013; Korotayev et al., 1999; Lecker, 2010; Robin, 2012; Schippmann, 2001; Yule, 2007). Himyar's decline over several decades was characterized by political disorder, socio-economic change, shifts in settlement patterns and demography (Figure 28b, c) and the decline or destruction of major irrigation systems (Brunner, 1997; Korotayev et al., 1999; Robin, 2012; Schiettecatte, 2008; Schippmann, 2001). The annexation of crisis-ridden

Himyar by the Aksumites (today's Ethiopia) in 525 CE and frequent interventions in Arabia from the Byzantine and Sasanian Empires were additional factors contributing to profound social, economic and political transformations during the 6th and first half of the 7th century CE in Arabia (Lecker, 2010; Schippmann, 2001; Yule, 2007). Current explanations for these changes focus almost entirely on socio-political factors (Korotayev et al., 1999; Schippmann, 2001). Climate, however, has been largely ignored (Korotayev et al., 1999; Wilkinson, 2011; Yule, 2007), despite the fact that Himyar and the southern Arabian region more widely were extremely vulnerable to droughts as its economy was based on rain-fed and irrigated agriculture (Schippmann, 2001; Wilkinson, 2011; Yule, 2007). The lack of highly-resolved and precisely dated palaeoclimate records from southern Arabia, has prevented an assessment of whether droughts were a factor contributing to Himyar's decline and the associated major socio-political transformations across Arabia in the 6th century CE, which culminated in the rapid emergence and expansion of the Islam in the early 7th century. Here we combine hydrological, historical and archaeological records from the Middle East and East Africa with a new high-resolution speleothem record of winter/spring precipitation and effective moisture (EM) in Northern Oman to demonstrate that severe and persistent droughts must have been a pivotal contributing factor for the major socio-economic transformations in southern Arabia in the 6th century CE (Hoyland, 2001; Korotayev et al., 1999; Robin, 2012; Schippmann, 2001).

Speleothem H12, collected from Hoti Cave in Northern Oman (57º 21' E, 23º 05' N, 800m above sea level) (Figures 27, 31 and 32), provides a high resolution, well-dated hydroclimatic record that spans this critical period of history. Rainfall in Northern Oman and most of Arabia originates predominantly from Mediterranean frontal systems, whereas summer monsoon (SM) precipitation affects only the southernmost tip of Arabia, i.e. the Yemeni highlands and southern Oman (Fleitmann et al., 2003). Thunderstorms during summer and occasional cyclones are additional sources of rainfall. Regional precipitation varies between 50 and 255 mm yr-1 (Al Hamra; 1978-1997) and occurs in winter and spring (~65 % of total annual rainfall) and summer (Figure 35; Fleitmann et al., 2003). Importantly for this study, changes in rainfall (Figure 36) are consistent across southern Arabia, particularly for extreme droughts which are often supra-regional (Barlow et al., 2016).

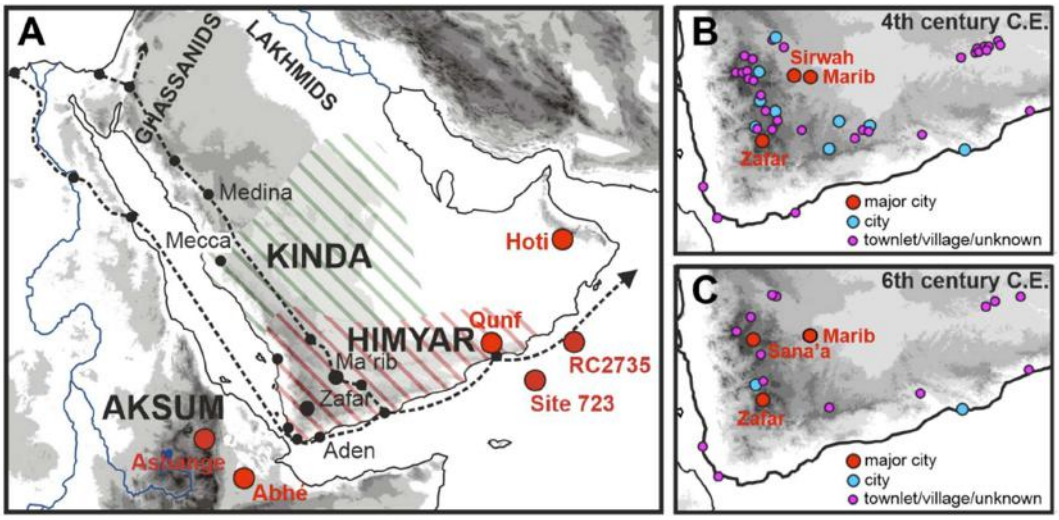

Figure 28. Location and Settlement Maps. (A) Location map showing the location of key-proxy records and suggested extent of Himyar (red line) and Kinda (green line) at the beginning of the 6th century CE (Yule, 2007). Black dashed lines denote the main trading routes (Yule, 2007). (B and C) Settlement patterns in Himyar in the 4th and 6th century C.E. (Schiettecatte, 2008).

The chronology of speleothem H12 is based on 20 U-Th ages, with an average growth rate of ~0.23 mm yr-1 over the last 2650 years (Appendix B.3; Figure 34). The oxygen ($\delta^{18}O$) and carbon ($\delta^{13}C$) isotope records have a ~2.3 year resolution and are related to rainfall amount and effective moisture respectively (Fleitmann et al., 2007), as indicated by several observations. Firstly, H12 $\delta^{18}O$ values are significantly correlated ($r=-0.69$; $p= <0.001$) with mean annual rainfall in Oman and are also consistent with rainfall anomalies for the entire Arabian Peninsula (AlSarmi & Washington, 2011; Kwarteng et al., 2009), with higher rainfall related to more negative calcite $\delta^{18}O$ values (Figure 29a, b). Secondly, more positive H12 $\delta^{18}O$ values correspond to a reduced diameter of the speleothem cap (Figure 29c), indicative of lower drip rates and winter/spring precipitation respectively (Martín-Chivelet et al., 2017). Thirdly, the strong correlation between H12 $\delta^{18}O$ and $\delta^{13}C$ values ($r2 =0.52$) indicates that calcite did not precipitate in isotopic equilibrium with its parent drip water. Because $\delta^{13}C$ values are strongly governed by CO2 degassing, more positive $\delta^{13}C$ values indicate lower drip rates and lower pCO2 of cave air due to enhanced ventilation of Hoti Cave at times of lower precipitation and cave lake levels, respectively (Figure 32). Additionally, vegetation density and soil microbial activity is reduced during drier years, leading to lower biogenic soil pCO2

and therefore more positive calcite $\delta^{13}C$ values (Fleitmann et al., 2004). Thus, H12 $\delta^{18}O$ and $\delta^{13}C$ values are primarily governed by precipitation and effective moisture respectively.

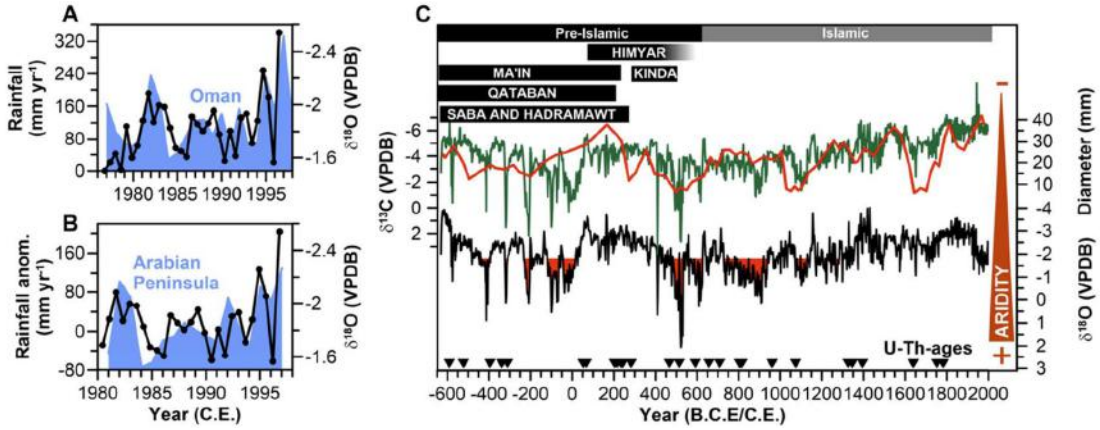

Figure 29. Hoti Cave and Meteorological Records. (A and B) Comparison between H12 $\delta^{18}O$ values and (A) mean annual rainfall for Oman (Kwarteng et al., 2009) and (B) precipitation anomalies (with respect to the 1978-1997 average of -1.8‰) averaged for the Arabian Peninsula (AlSarmi & Washington, 2011). (C) H12 $\delta^{18}O$ (black), $\delta^{13}C$ (green) and speleothem diameter (red line) records. Red shaded area shows effective moisture anomalies with respect to the 1978-1997 mean (-1.8‰). Black triangles denote ^{230}Th dates (Appendix A.3). Black shaded bars denote the estimated lifetime of kingdoms in southern and central Arabia (Hoyland, 2001).

The H12 $\delta^{18}O$ profile displays high variability in effective moisture over the last ~2600 years with two periods of persistently lower EM, from ~250 B.CE to 25 CE and ~480-1400 CE, on which distinct decadal to multi-decadal fluctuations in $\delta^{18}O$ were superimposed (Figure 29c). The most pronounced minimum in effective moisture occurred from ~520 to 532 CE, with the most severe drought conditions of the entire H12 record centred at ~523 CE ± 30 years (Figure 30b). This date is in excellent agreement with other independently-dated winter/spring rainfall records from the Middle East (Figure 30). In the Neor Lake record from northern Iran (Sharifi et al., 2015), a sharp rise in titanium (high dust flux) starts at the beginning of the 6th century CE Dead Sea lake level (Bookman et al., 2004) declined sharply from ~ 490 CE onward, and more positive $\delta^{13}C$ values (reduced EM) are observed in the Jeita Cave $\delta^{13}C$ record from Lebanon at ~510 CE (Cheng et al., 2015). Likewise, the frequency of historical accounts of droughts in the Middle East peaks between 520 and 530 CE (Figure 30f), with the spring of Siloam in Jerusalem reportedly drying up at ~520 CE (McCormick et

al., 2012; Telelis, 2008) (Section 5.3.4). Overall, key hydrological records from the Middle East indicate drought conditions related to a decline in winter/spring precipitation and a substantial decrease in effective moisture from ~480 CE onward. In contrast, the Nar Lake $\delta^{18}O$ record from Turkey (Jones et al., 2006) documents a significant increase in precipitation, which is most likely related to a northward displacement of storm tracks in the Eastern Mediterranean at the beginning of the 6th century CE, with fewer rain-bearing storms reaching the Fertile Crescent and Arabian Peninsula.

Though winter/spring precipitation is the main source of annual rainfall throughout the Middle East, summer monsoon (SM) precipitation is an additional crucial source of rainfall in southern Arabia and Yemen (Himyar) in particular. SM records from Southern Oman (Qunf Cave) (Fleitmann et al., 2003, 2007), Ethiopia (Lake Ashange and Lake Abhé) (Gasse, 2000; Marshall et al., 2009), the Arabian Sea (core sites RC2735 and Site 723) (Anderson et al., 2010; Gupta et al., 2003), India (Sahiya Cave) (Sinha et al., 2015) and China (Dongge Cave) (Wang et al., 2005) indicate that SM wind strength and precipitation reached its absolute minimum during the 6th-century CE as boreal summer insolation, a primary driver of monsoon intensity (Fleitmann et al., 2007) reached its lowest Holocene values (Figure 31). Furthermore, an abrupt decline in precipitation between 450 and 500 CE is evident in the SM records from Ethiopia (Lake Ashange) (Marshall et al., 2009), the Arabian Sea (RC735 and Site 723) (Anderson et al., 2010; Gupta et al., 2003) and India (Core 16A) (Ponton et al., 2012) and, taking age uncertainties of the individual records into account, these are broadly concurrent with decreasing winter/spring precipitation in the H12 $\delta^{18}O$ and other hydroclimate records displayed in Figure 31. In addition, the precisely-dated and highly-resolved Sahiya Cave (India) SM record (Sinha et al., 2015) reveals a decrease in SM rainfall after ~490 CE (Figure 31h). Taken together, total annual precipitation in Arabia and northeastern Africa reached an absolute minimum at the beginning of the 6th century CE, with the most severe drought conditions persisting between ~500 and 530 CE (Figures 29 and 30).

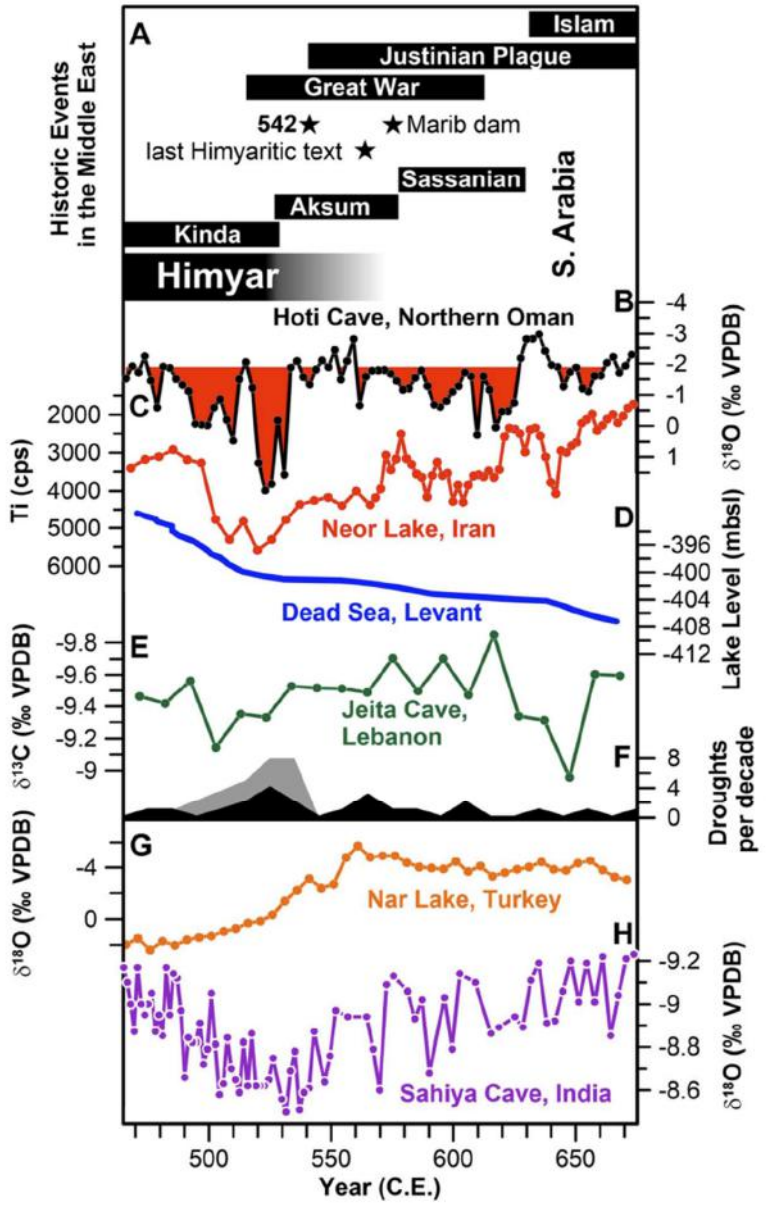

Figure 30. Climate Proxy Records and Historic Events. (A) Key historic and cultural events in southern Arabia. Black bars denote ruling powers in southern Arabia, socio-cultural events (star symbols) such as disappearance of Himyarite inscriptions (Butzer & Endfield, 2012; Piotrovsky, 1994) and destruction of the dam of Marib (Brunner, 1997). (B) H12 $\delta^{18}O$ record from Hoti Cave, red shaded area marks periods of below normal precipitation (with respect to the 1978-1997 average of -1.8‰). (C) Lake Neor titanium record from Iran (Sharifi et al., 2015). (D) Dead Sea level (Bookman et al., 2004). (E) Jeita Cave $\delta^{13}C$ record (Cheng et al., 2015). (F) Historic accounts (plotted as droughts per decade) derived from the Middle East after McCormick et al. (2012) (black shaded curve) and Telelis (2008) (grey shaded curve). (G) Nar Lake $\delta^{18}O$ record from Turkey (Jones et al., 2006). (H) Sahiya Cave $\delta^{18}O$ record from India (Sinha et al., 2015).

The synchronicity between peak aridity in southern Arabia and the sudden decline of Himyar points to a possible causal relationship between both. Himyar with its centralized political system of kingship- and subordinate chiefdoms was the dominant power in southern and central Arabia until the early 6th century CE (Figure 28) (Robin, 2012; Yule, 2007). Though international trade in aromatics and metals had earlier also been a major source of revenue, agricultural production was fundamental to both central and regional economies (Brunner, 1997; Schippmann, 2001). The importance of agriculture to Himyar is evidenced by widespread terraced fields in the highlands, numerous irrigation systems along the desert margin and a considerable expansion of hydraulic structures between the first and fourth centuries CE (Charbonnier, 2009, 2011; Schiettecatte, 2016; Schippmann, 2001) (5.3.3; Figure 37). The dams, for instance, were a symbol and instrument through which Himyarite rulers exerted their authority, as indicated by inscriptions. Dams and terraced fields were designed to harvest rainfall and runoff ("runoff irrigation") as water was the most limited agricultural resource. The structural integrity of the terraced fields depended on the proper maintenance of the whole system of hillside terraces and dams which required constant repairs, which only a well-organized workforce and stable society could provide (Brunner, 1997; Robin, 2012; Yule, 2007). Furthermore, a stable society and a functioning political entity were crucial to manage the proper allocation of water for the irrigated plots, particularly during drier years with more frequent water disputes (Varisco, 1983). Himyar's agricultural productivity was dependent on a consistent rainfall cycle with two rainy seasons in spring (March-May) and summer (July-September) (Section 5.3.3; Figure 39). All these factors combined made Himyar vulnerable to droughts and low agricultural yields would have had a negative impact on Himyar's socio-economic and political stability and thus the proper management of all water-harvesting structures. Thus, the abrupt and persistent decrease in rainfall and effective moisture respectively throughout Arabia at the end of the 5th and beginning of the 6th century CE must have been a substantial stressor, undermining Himyar's resilience to both internal and external socio-economic and geo-political conflicts, particularly Christian Aksumite attempts (later supported by the Byzantine empire) to control the lucrative trading routes along the Red Sea and Arabian Sea coasts. Such stress may well have been further exacerbated by the possible effects of the global cooling that marked the beginning of the so-called Late Antique Little Ice Age that is visible in proxy data from the later 530s CE (Büntgen et al., 2016).

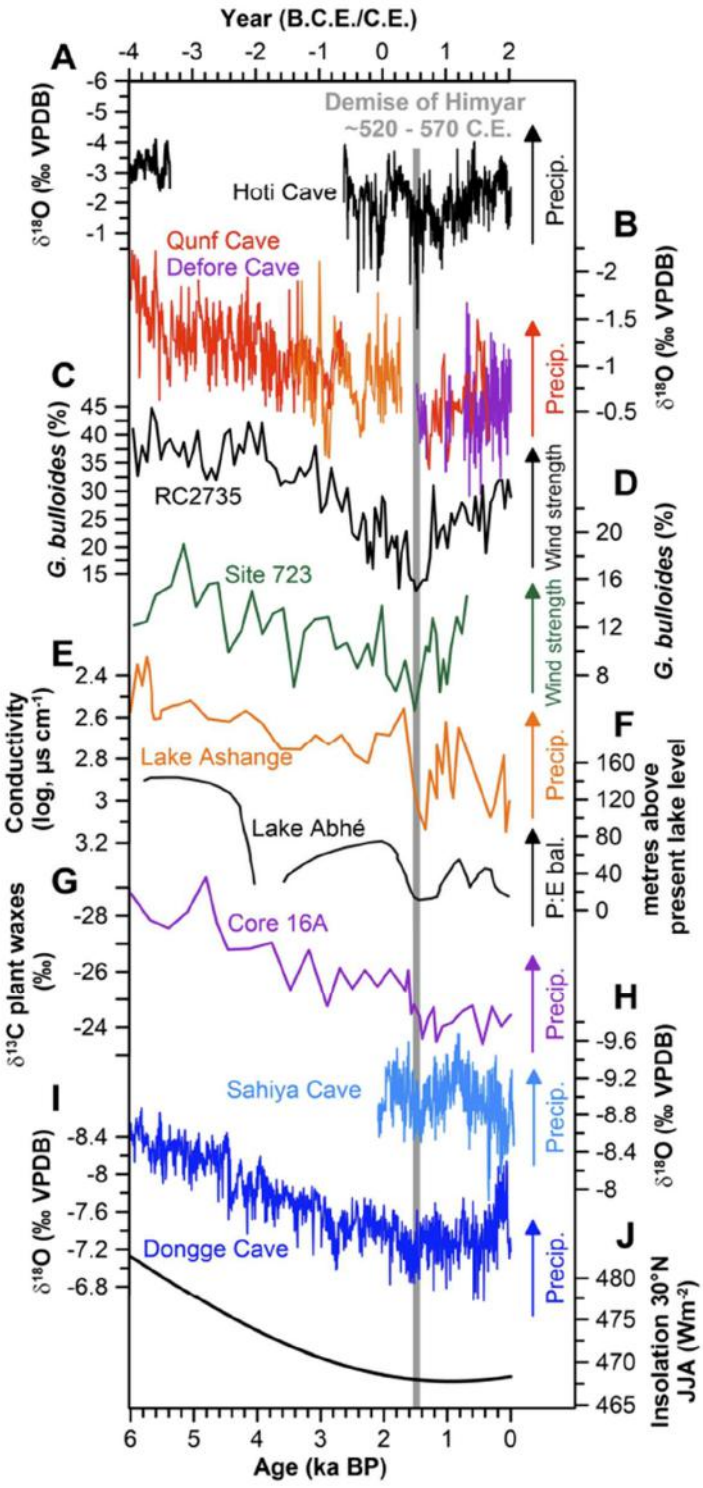

Figure 31. Comparison of the H12 $\delta^{18}O$ record with summer monsoon records (A) Hoti Cave $\delta^{18}O$ record, (B) Salalah Cave (pink) and Qunf Cave (red and orange) $\delta^{18}O$ records from southern Oman (Fleitmann et al., 2003), (C and D) G. bulloides monsoon upwelling records from the Arabian Sea (Anderson et al., 2010; Gupta et al., 2003), (E) Lake Ashange conductivity record from Ethiopia (Marshall et al., 2009), (F) Lake level record from Lake Abhé at the Etiopia-Djibouti border (Gasse, 2000), (G) $\delta^{13}C$ plant wax record from core 16A offshore India (Ponton et al., 2012), (H) Sahiya Cave $\delta^{18}O$ record from India (Sinha et al., 2015) and (I) Dongge Cave $\delta^{18}O$ record from China (Wang et al.,

2005). (J) insolation curve (heavy black line) at 30°N, averaged from June to August (Berger & Loutre, 1991). All records reflect either summer monsoon wind strength or precipitation. The grey shaded bar marks the time interval between ~520 and 570 C.E. which covers the period of Himyar's demise.

From the 480s CE there are clear indications that Himyar faced a number of problems. Internal conflict between rival elite lineages, partly informed by religious affiliations to either Judaism or Christianity, and exacerbated by Aksumite intervention between 518 and 530 CE, reduced Himyar to vassal status (Hatke, 2011; Hoyland, 2001; Piotrovsky, 1994; Robin, 2015; Schippmann, 2001). This was followed by a brief revival of Himyarite power (but under an Aksumite general, Abreha), to which a short-lived increase in winter/spring precipitation between 530-545 CE (Figures 28 and 29) may perhaps have contributed (Schippmann, 2001). Yet, it took this new regime at least four expeditions over more than 15 years to attempt to re-establish Himyarite political hegemony outside the Yemen and Hadramaut, indicating both the weakening of its power and the extent of fragmentation of the traditional order in the region (Hatke, 2011). Further indications of this include evidence for drought-induced migration across the region into Persian and Byzantine-controlled Syria and Iraq, as well as southwards into Yemen and Hadramaut, the failure to maintain the dam of Ma'rib, leading to a collapse of the system in ~580 CE, and its final destruction at ~600 C.E (an event significant enough to find mention in the Koran: sura 34: 15-17) (Brunner, 1997; Robin, 2012; Schippmann, 2001). The disappearance of Himyarite inscriptions after ~559 CE (Schippmann, 2001) may also indicate a breakdown of political authority and the established order. From ca. 570 CE Himyar came under Persian domination and effectively ceased to exist as an independent polity (Bowersock, 2013; Lecker, 2010; Robin, 2012, 2015; Schippmann, 2001; Yule, 2007).

The weakening of Himyar from the 480s CE onward, and its rapid conquest by Aksum in 525 C.E, were thus directly coincident with increasing aridity and declining agricultural yields due to a simultaneous reduction in winter/spring and summer monsoon precipitation, culminating in the most severe drought conditions of the entire Holocene in the early 6th century CE. Himyar's continued weakening through the middle decades of the 6th century CE, in spite of the temporary resurgence under Abreha, and its final dissolution in the 570s CE, should thus be understood in the light of these conditions and the evidence for the persistence of drought conditions during the 6th century CE (Figure 29 and 30). While

correlation is not necessarily causation, the unique magnitude and persistence of 6th century drought, superimposed on a region that was highly dependent on rainfed agriculture, is coincident with a clear turning point in Arabian history (Korotayev et al., 1999; Robin, 2012; Schippmann, 2001; Yule, 2007), when a cascade of regional political and socio-religious transformations took place over the following decades. Himyar's decline as the dominant Arabian polity induced a socio-political vacuum, as former supra-tribal political structures in southern and central Arabia dissolved (Brunner, 1997; Korotayev et al., 1999; Schippmann, 2001; Yule, 2007). One result of this situation throughout Arabia during the 6th and early 7th centuries CE is thought to have been a growth in the importance of regional pilgrimage and economic centers. Of these, Mecca (the birthplace of Muḥammad) gained considerable influence in central and southern Arabia beginning in the first half of the sixth century CE (Crone, 1987). Furthermore, the reduction in the reach of Himyarite power drew the competing Middle Eastern superpowers, the Byzantine and Sasanian empires, into intensified competition for political and religious influence in the region as well as for economic resources, including precious metals, in the region (Heck, 1999; Kennedy, 2004). Such influence was exercised both through their client kingdoms, the Ghassanid and Lakhmid confederacies in north-western and north-eastern Arabia, respectively, as well as through Aksum. Finally, such interventions stimulated a hostile reaction, both to Christian Aksumite proselytizing and to the political maneuvering of the neighbouring empires (Hoyland, 2001), although whether this also promoted a search for a new 'Arab' identity, as some have argued, remains debatable (Crone, 1987; Heck, 1999; Robin, 2012). The decline and dissolution of Himyar and the resultant tribal conflicts in the 6th century CE were thus a critical element in the socio-economic, political and religious-cultural transformations in Arabia that ultimately framed the emergence of a range of new religious leaders or movements, many focused around monotheistic beliefs, including Islam. The challenges faced by the Islamic leadership in unifying the Arabian Peninsula in the 620s CE, in spite of substantial opposition from such competitors as well as from tribes that had converted to Judaism or were hostile to the Quraysh (Muḥammad's tribe) reflected this situation (Bowersock, 2013; Korotayev et al., 1999; Robin, 2012; Yule, 2007) (see Section 5.3.5. for historical details). But with Himyar no longer a regional power, Muḥammad had the field to himself in respect of the ability to mount long-distance military expeditions. We do not suggest that the extreme droughts of the late 5th to early 7th-century CE in Arabia were the direct trigger for these fundamental changes (Heck,

1999), but they nevertheless constituted a crucial, and hitherto largely neglected, factor that must have fatally undermined Himyarite resilience to both longer-term and more immediate internal and external stresses (Korotayev et al., 1999; Robin, 2012) (Section 5.3.5).

Acknowledgements

We thank Michael Cook, Adam Izdebski, Lee Mordechai and Timothy Newfield for their thoughtful comments.

Funding: Support of the Swiss National Science Foundation (grants PP002-110554/1 and grant CRSI22_132646/1 to D. Fleitmann) and National Natural Science Foundation of China (grant NSFC 41888101 to H. Cheng).

Author contributions: D.F. designed this study with input from J.H., R.S.B. and A.M.; D.F. and S.J.B. collected speleothem H12; D.F. performed stable isotope analysis; H.C. and R.L.E. performed Uranium-series dating; D.F. and M.J.J. performed diameter measurements; meteorological data were analyzed by C.C.R.; D.F., J.H. and R.S.B. wrote the paper with contributions from all other authors.

Data availability: The data will be made available on the NOOA palaeoclimatology server (www.ncdc.noaa.gov/dataaccess/paleoclimatology-data/datasets).

Competing interests: The authors declare no competing interests.

5.3. Supplementary Information

5.3.1 Materials and Methods

Hoti Cave

Hoti cave is located in the southern side of the Jabal Akhdar near the village Al Hamra. The cave system is a subterranean wadi with Al Hota Cave its inlet and Al Fallah as its outlet. The cave system lies in the Cretaceous Natih Formation, the lower formation of the Wasia Group of the Hajar Super Group (Figure 32). The total length of Hoti Cave is about 5 km, whereas most of the speleothems were found near the Main Hall, Al Fallah cave system, and in 200 to 300 metres distance from the Al Hota entrance. Cave air temperature in Hoti is variable due to its two entrances and barometric pressure changes there is an almost permanent airflow. Despite the permanent air flow, cave air temperatures (25-27 °C) roughly correspond to mean annual air temperature outside the cave. Relative humidity within the cave varies between 60% (near the entrances) and 100% (further inside) (Scholz & Hoffmann, 2011). Speleothem H12 was collected near Al Hota Cave entrance (Figures 31 and 32).

Radiometric Dating- University of Minnesota

Uranium-series dates (^{230}Th hereinafter) were determined at Minnesota University and University of Bern (Appendix A.3). For analysis between 70 and 100 mg of powder was drilled along discrete growth horizons. ^{230}Th-ages were determined on a multi-collector inductively coupled plasma mass spectrometer (MC-ICP-MS, Thermo-Finnigan Neptune) at the Department of Geology and Geophysics, University of Minnesota. Details of the methods, including standards used for mass fractionation and yield correction can be found in Cheng et al. (2000, 2013).

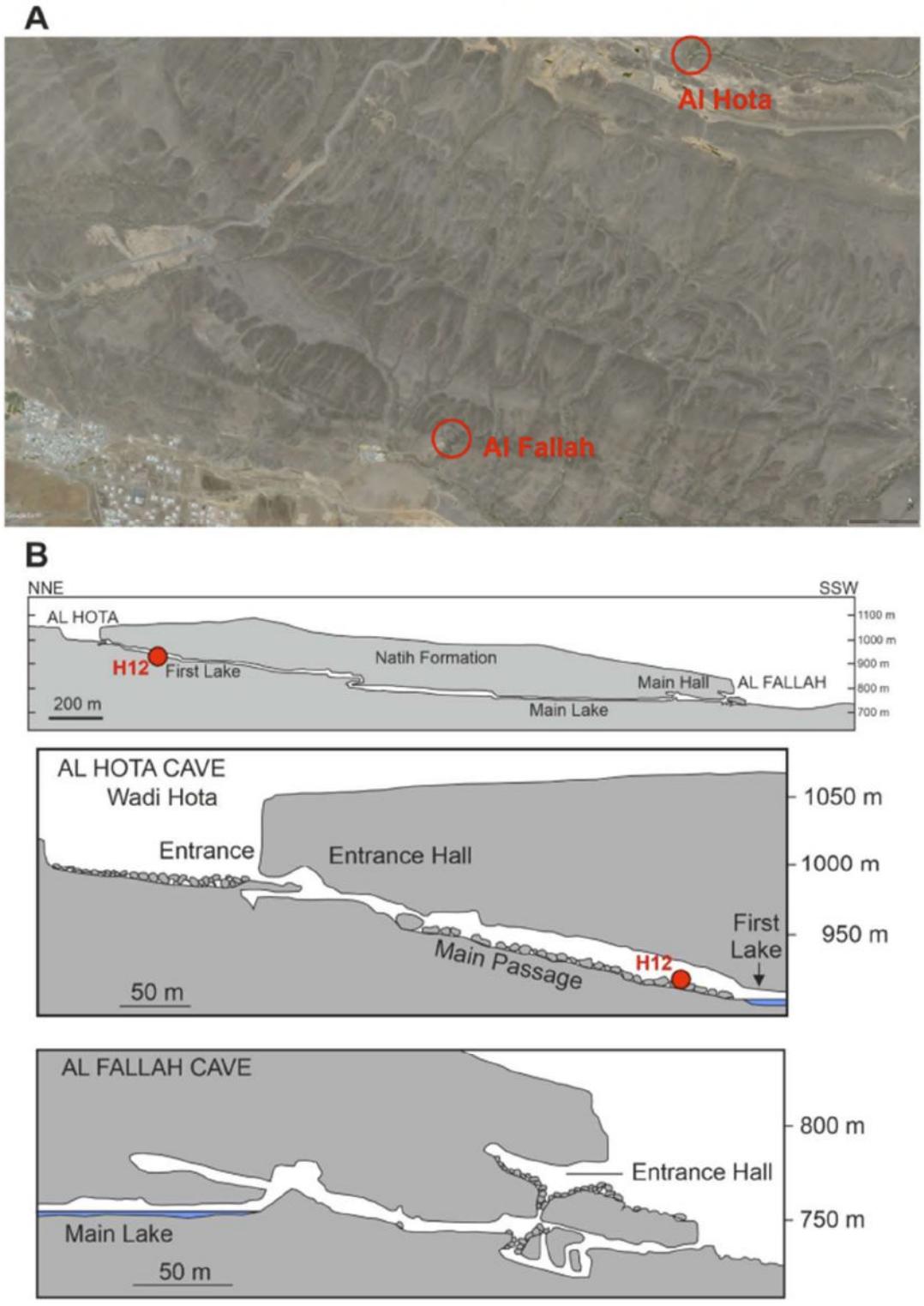

Figure 32. (A) Satellite image of Hoti Cave, location of both entrances is marked by red circles. (B) Cave maps of Hoti Cave and cave entrances Al-Hota and Al Fallah Caves.

Radiometric Dating – University of Bern

For MC ICP-MS analyses, 0.1 – 0.2 g of powdered sample were spiked with a mixed ^{229}Th-^{236}U spike and dissolved in nitric acid and taken to dryness. U and Th were separated on anion columns using a 0.5 ml UTEVA resin bed. A first separation, using ^{7}N nitric acid, produced a pure Th fraction and an impure U fraction, which was purified on the same columns using ^{5}N hydrochloric acid. After evaporation, the fractions were placed in oxygen plasma for a minimum of 30 minutes to also remove organic residues from the plasma. U and Th mass spectrometry was done on a Nu Instruments® multicollector ICP-MS equipped with an ESI Apex® desolvating system without membrane and using a self-aspirating element specific nebuliser and disposable capillaries. With an uptake rate of ca. 50 µl/min the ion yield for U and Th was about 70V/ppm. U measurements were done from 0.5 N nitric acid solutions in static mode, whereby masses 236 and 234 were measured in parallel electron multipliers and 235 and 238 in Faraday cups. Baselines were taken on either side of peaks and interpolated. The electron multiplier yield was calibrated every five samples by running a NIST U050 solution. The ^{238}U/^{235}U ratio was used for instrumental fractionation correction if the ^{238}U signal was greater than 1 V; if smaller, the fractionation factor was input from bracketing standards. Normal washout time for U between samples was 5 minutes with 0.5 N nitric acid (< 1 ‰ memory); longer washout times were used where significant isotope differences between samples were expected. Runs on the NIST U960 standard yielded $\delta(^{234}U/^{238}U)$ -37.2 ± 2.1 ‰ (1SD, N=35), where the equilibrium ratio is after Cheng et al. (2000, 2013). Th measurements were made from 3N hydrochloric solutions in a two cycle multi-collector dynamic mode, whereby one electron multiplier, equipped with a WARP filter, alternately measured masses 229 and 230. U standard was added to Th run solutions for two reasons: first, to correction for instrumental mass fractionation, and second, to provide a reference isotope (238) to eliminate the effects of plasma flicker in obtaining the ^{229}Th/^{230}Th ratios. Variations of U and Th signals during the run are fully correlated if no organic matter is present. Baselines were measured at 229.5 and 230.5 for samples and standards with significant (>10-12A) 232Th. For speleothems, the baseline was quite flat and measured at 230.5. Washout time was 15 min. to 1 ‰ of the Th signal, if the capillary and nebulizer were free of organics.

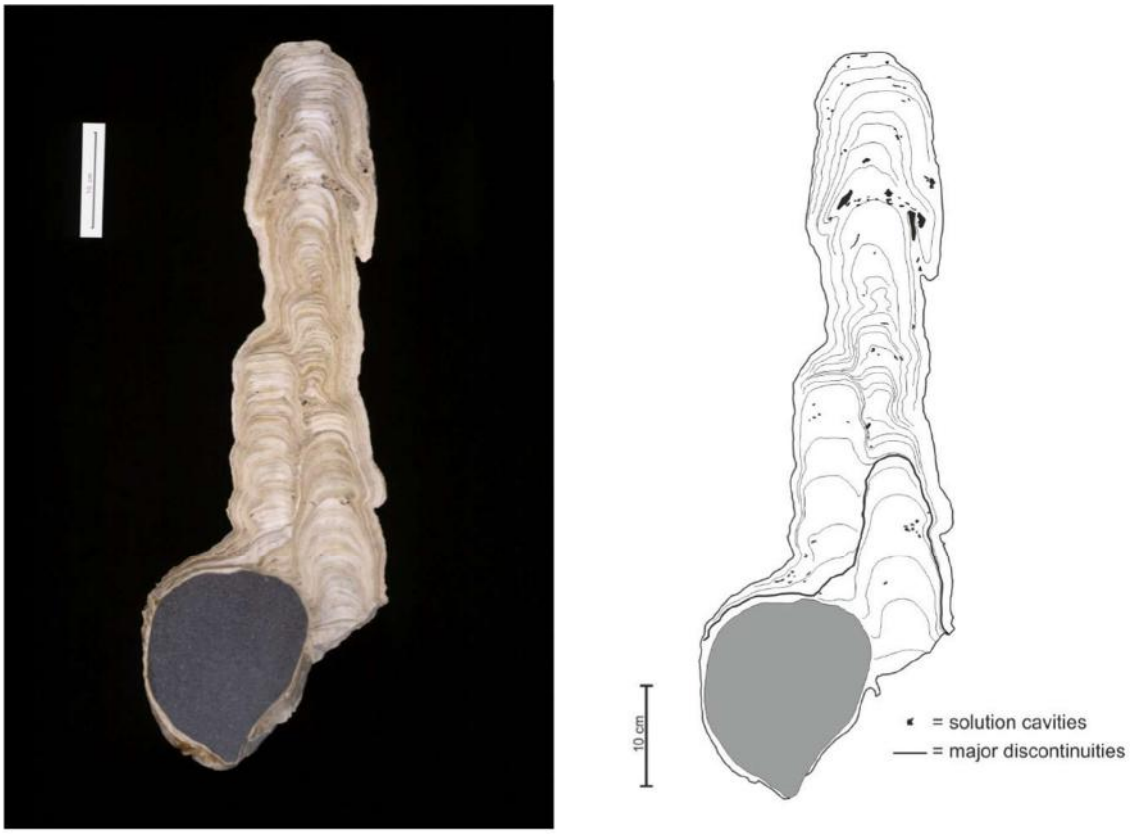

Figure 33. Scan and drawing of cut speleothem H12.

Stable isotope analysis

For stable carbon and oxygen isotope analysis, a total of 1360 samples were micromilled continuously at 0.2 mm and ~0.5 mm increments from 0 to 26.8 mm and 26.8 to 593 mm, respectively. Powdered samples were measured using a Finnigan Delta V Advantage mass spectrometer equipped with an automated carbonate preparation system (Gas Bench II) at the Institute of Geological Sciences, University of Bern, Switzerland. Results are reported relative to the international Vienna Peedee Belemnite (VPDB) standard. Analytical errors for $\delta^{18}O$ and $\delta^{13}C$ are 0.07 and 0.06 ‰ VPDB (1σ-error), respectively.

Age Model

A total of 29 ^{230}Th ages were determined for speleothem H12. Of these only 20 ^{230}Th ages with ^{230}Th /^{232}Th activity ratios >20 (see Appendix A.3 for further details) were used for chronology building using STALAGE (Scholz & Hoffmann, 2011), the other ^{230}Th ages were excluded due to detrital contamination and initial ^{230}Th respectively. The depth versus age plot for speleothem H12 is shown in Figure 34.

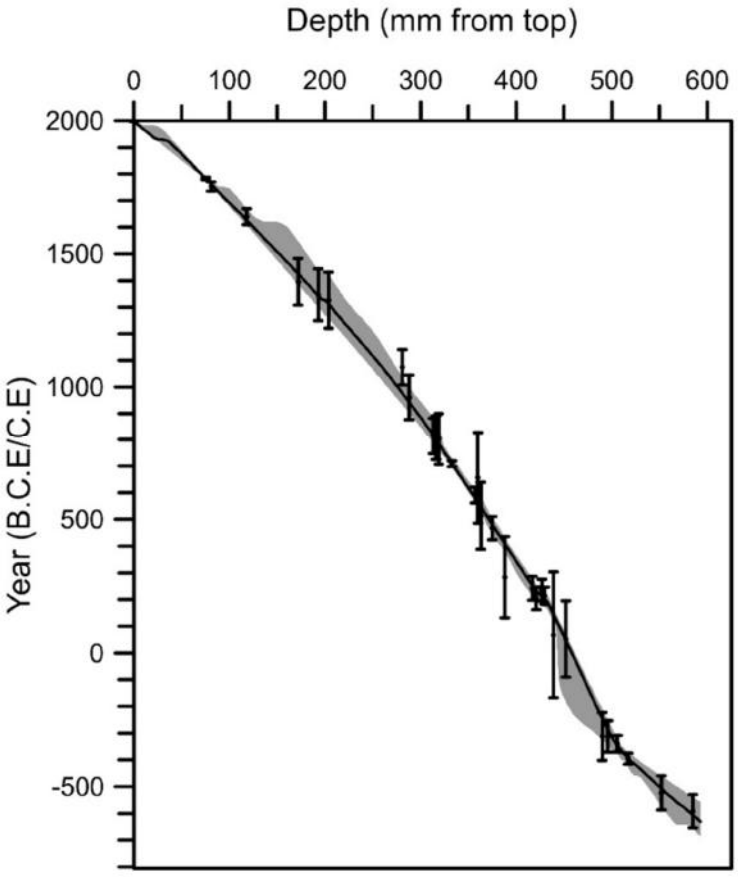

Figure 34. Age/depth plot for speleothem H12. Vertical error bars denote age uncertainties (2-σ). The grey shaded area shows the 95% confidence intervals of the H12 age model as determined with StalAge (Scholz & Hoffmann, 2011).

5.3.2. Analysis of precipitation over the Arabian Peninsula

Major droughts in the Middle East are associated with lower rainfall during the winter half of the year. Droughts are frequent throughout the region, have a great spatial extent and can last for several years or even decades. The spatial extent of rainfall anomalies on the Arabian Peninsula under present day conditions is assessed in the reanalysis product ERA interim. The ERA interim data covers the period from 1979 to 2017, and is used in its highest resolution of 0.75° x 0.75° (Dee et al., 2011). To obtain a hint the spatial representative of the proxy record from Hoti Cave, we selected the closest grid point of ERA interim and use the precipitation at this location as index. This index is then correlated with the precipitation field for each month of the year, separately. During the rainy season from October to April, we find that precipitation at Hoti Cave is positively correlated (around r = 0.5) with precipitation over the Arabian Peninsula, mainly the mid to southern part. This is in excellent agreement with previous analysis of meteorological data from the wider Middle East (Barlow et al., 2016), which show a close correlation of r=0.6 between annual precipitation (1951-2010) sin Yemen and Oman. During the dry months (May to September) the correlation pattern is more localized, thus the Hoti cave speleothem record can only register local signals in the eastern part of the Arabic Peninsula. As the signal of the Hoti Cave proxy record is dominated by the wet (winter-spring) season we conclude that precipitation at this site is to some extent representative for at least the central to southern part of the Arabic Peninsula and thus is a reasonably indicator for dry and wet years in this region.

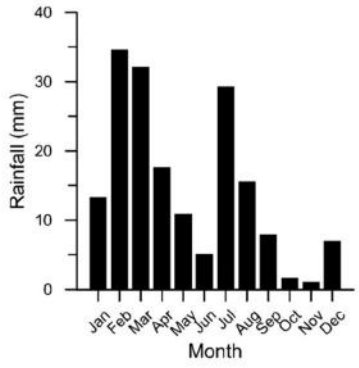

Figure 35. Monthly precipitation (1978-1997) at Al Hamra, approximately 10 km away from Hoti Cave.

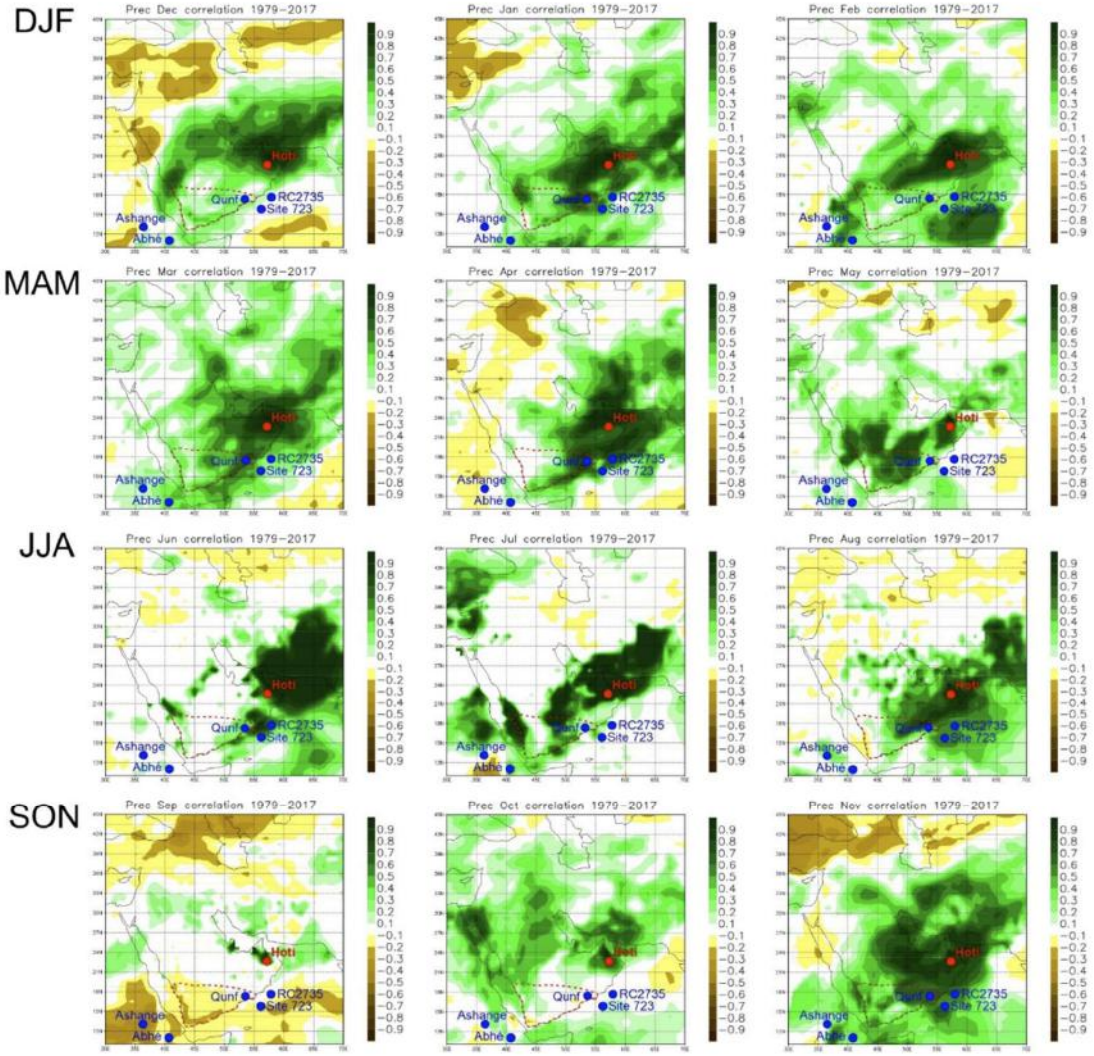

Figure 36. Correlation patterns between the precipitation close to Hoti Cave and the Arabic Peninsula for each month of the year using ERA interim day from 1979 to 2017 (Dee et al., 2011). DJF = December, January, February; MAM = March, April, May; JJA = June, July, August; SON = September, October, November. Red dashed line denotes the approximate extend of the Himyarite Kingdom. Location of palaeoclimate records is also shown (blue and red dots).

5.3.3. Agriculture in Himyar

Yemen has a long and diverse agricultural tradition that developed over several millennia to cope with the harsh climatic conditions, making a careful management of water necessary (Kopp, 1981). In Himyar, sedentary agriculture was the primary source of agricultural production, rather than pastoral nomadism. Almost all arable areas in Yemen were already cultivated 2 millennia ago (Kopp, 1981), and pre-islamic documents provide

evidence for a highly developed agrarian society. Present-day rainfall ranges from 150 to 450 mm yr-1 in most parts of Yemen (Figure 35) but can reach up to ~1000 mm yr-1 in the highlands. Rainfall typically lasts from January to May (termed ṣayf) and July to September (termed kharīf), whereas the summer rainfall period is more intense and accounts for 50-70% of the mean annual rainfall. Himyar utilized ingenious water management strategies to maximize agricultural yields despite low mean annual rainfall (Brunner, 2000b). Harvesting surface water was the basic strategy to maximize agricultural yields. In the highlands, large-scale terraced fields, dams and soil retention walls prevailed, whereas spate irrigation was used along the Ramlat as-Sab'atayn desert margin (Figure 37). Overall, Himyar's agriculture was primarily rainfed, the use of wells and cisterns was only marginal and mainly for household consumption.

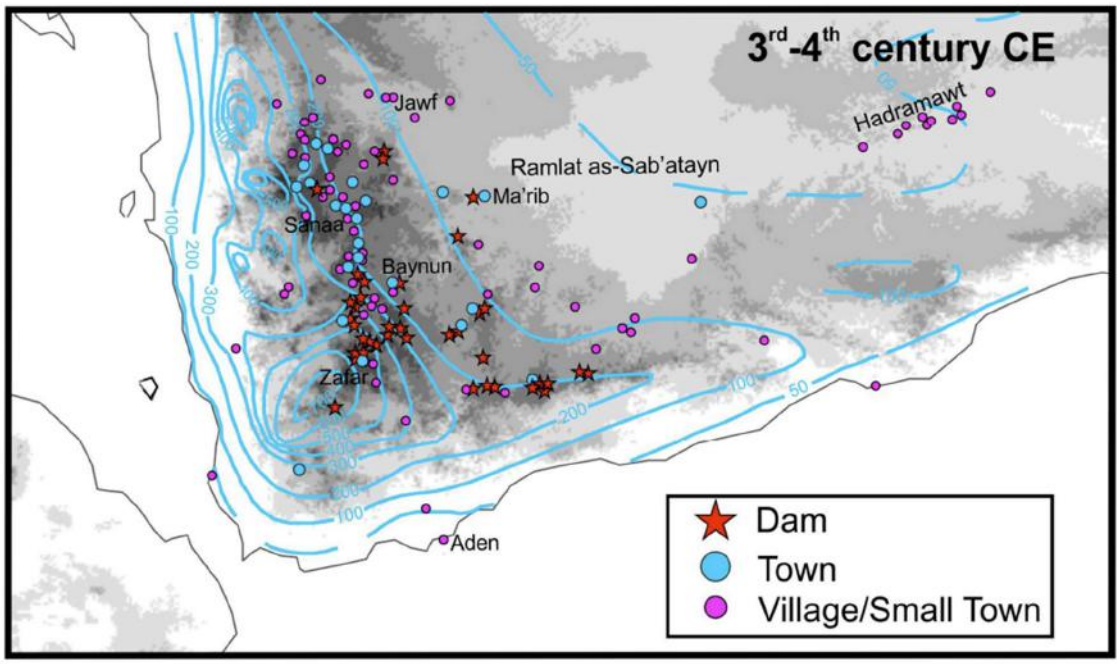

Figure 37. Present-day precipitation isohyets (blue lines) in Yemen. Also shown are settlements and dams during the 3rd and 4th centuries CE.

The importance of agriculture to Himyar is evidenced by the considerable increase in the extent of terraces and erection of numerous dams and soil retention walls between the

first and fourth centuries C.E. (Charbonnier, 2009), much more compared to preceding periods. The terraced fields were designed to collect rainwater, prevent soil erosion and increase the area of cultivated land (Kopp, 1981). Terraces were not designed as individual terraces but rather as part of a wider connected infrastructure covering entire mountains (Figure 38). Furthermore, large dams were built near major Himyarite settlements (Figure 37), some more than 100 meters long and 20 meters high (Charbonnier, 2011). Textual evidence suggests that Zafar, the capital of Himyar, was surrounded by eighty water dams (Charbonnier, 2011). The dams allowed peasants to increase their productivity and grow a wider range of crops. It is noteworthy that the dams fulfilled a political role to demonstrate the influence of the Himyarite ruler and to exert his authority (Brunner, 2000b; Charbonnier, 2011). The erection of terraces and dams clearly indicated a coherent plan of land improvement and required major capital investments. Along the Ramlat as-Sab'atayn desert margin, dams were built and maintained to catch water from episodically floods (termed sayl) and to divert it onto the fields where it can seep into the soil (Brunner, 2000b). The Ma'rib dam was the largest example of such a structure, it supported 9,600 ha of arable land and approx. 60,000 inhabitants.

The farming calendar in Himyar (Figure 39) was governed by the seasonal rainfall pattern and the most important cereals were wheat, barely, sorghum and millet. Sorghum, for instance, was planted at the end of March or early April after the winter/spring rains and harvested in November; wheat and barley would have also been grown during summer to take advantage of both rainy seasons. However, they could also be sown during December and January to be harvested in May and June, when a sufficient amount of winter/spring rainfall would allow crops to mature by harvest. It is therefore evident that agricultural yields depended on a consistent rainfall cycle and both rainy seasons (sayf and kharīf) were important factors for high agricultural productivity.

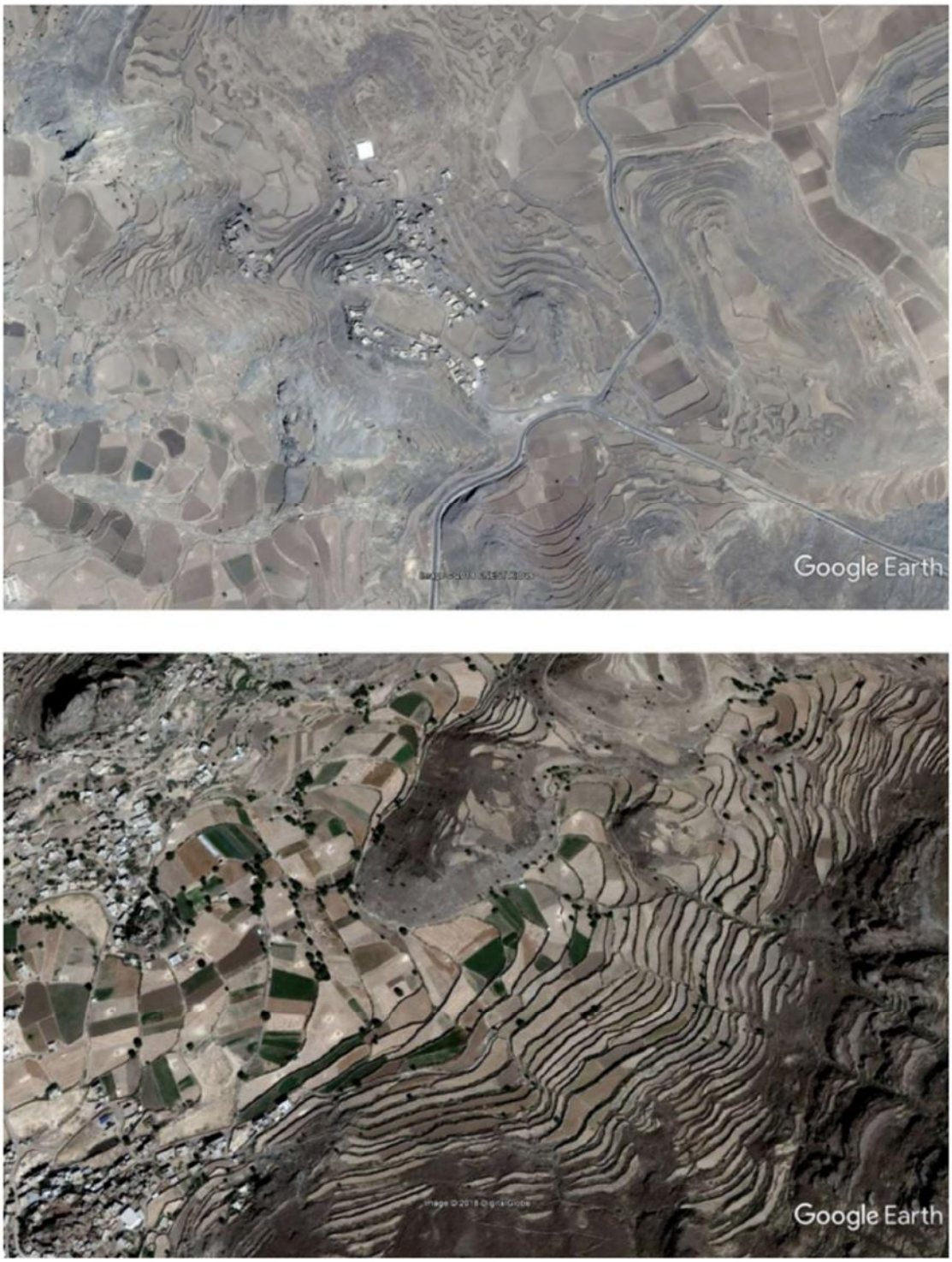

Figure 38. Google Earth images of terraces in Yemen. The majority of these terraces have been used during the last two millennia.

Since agriculture was a primary aspect of the local and regional economies, low agricultural yields during dry years would have affected the stability of these economies and undermined the political influence of Himyar's rulers. The amount of labour is one key factor for high agricultural productivity, and the maintenance of hydraulic infrastructures, in both the highlands and desert margins, required substantial resources and planning which only a well-organized and stable society could provide. For instance, the structural integrity of terraced fields depends on the maintenance of the whole system of hillside terraces. Furthermore, the intensive terrace and irrigation systems of Himyar were clearly a source of great pride for the inhabitants and political leaders as evidenced by abundant inscriptions (Kopp, 1981). This is also true for the numerous dams, which had to be repaired regularly. Thus, a proper functioning of the irrigation systems was of eminent importance for the functioning of the Himyarite society and only a centralized political entity could control and maintain these systems effectively. A simultaneous significant reduction in spring and summer rainfall at the end of the fifth and beginning of the sixth centuries C.E. would have had a profound impact on socio-economic conditions and all aspects of economic life in Himyar. The combination of drought, neglect of irrigation systems and terraced fields can thereby exacerbate socio-economic problems. Thus, agricultural productivity in Himyar was highly dependent on rainfall and on stable socio-economic conditions; both were intrinsically linked as the majority of Himyar's population were peasants.

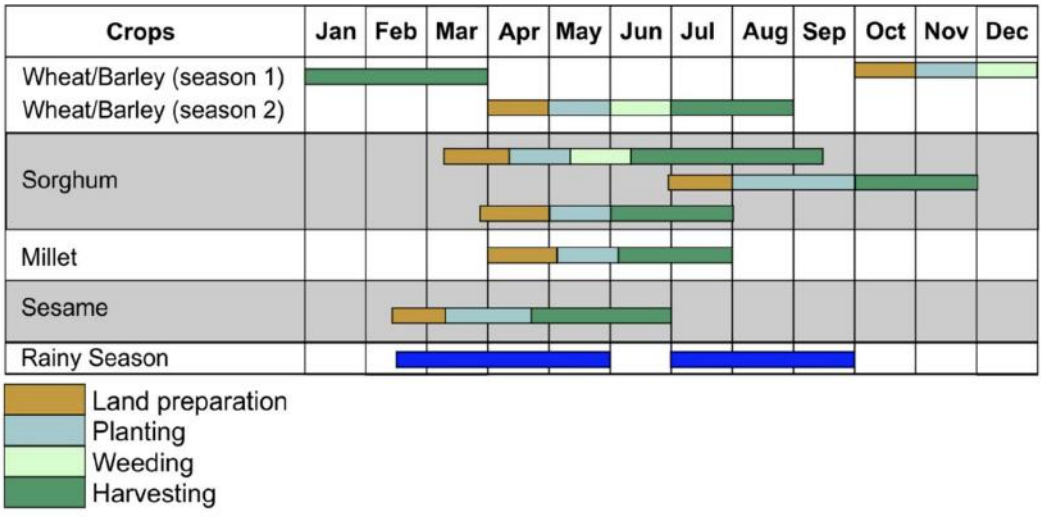

Figure 39. Schematic figure of the farming calendar for the most important cereals in Himyar.

5.3.4. Historical and archaeological evidence for droughts and rainfall fluctuations in the Middle East between the 3rd and 6th century C.E.

Though droughts are a frequent phenomenon in the Middle East, the number of historical accounts of droughts increased markedly at the end of the 5th and first half of 6th century C.E. in the Levant and other parts of the Middle East (Stathakopoulos, 2004). Though care is required when using historical sources and individual accounts for climate reconstructions, they are nevertheless useful and support the evidence for severe and persistent droughts in the hydrological reconstructions from the Middle East (Figure 30).

Water was the most valuable commodity across the Arabian Peninsula and the relationships between the Arabs and the Byzantine and Sasanian empires in the north were significantly influenced by droughts as they triggered Arab raids in the frontier regions. Historical documents (letters) suggest that such raids in the areas belonging to the Byzantine and Sasanian empires became more frequent at the end of the 5th and beginning of the 6th century and also contributed to the increasing tensions between the Byzantine and Sasanian Empires, such as in 484/5 C.E. when Arab raids near Nisibis (modern Syria) occurred (Edwell, 2015; Stathakopoulos, 2004). During this time, the bishop of Nisibis wrote in a letter to Mar Acacius, the catholicos at Seleucia-Ctesiphon, to explain the reasons for his absence at a synod organized by Acacius. "*For two successive years we have been afflicted by a shortage of rain and a lack of necessary commodities. The mob of the tribes from the south has assembled, and because of the multitude of people and their animals, they have destroyed the villages of the countryside and of the mountain*."

Further evidence for both drought and deteriorating environmental conditions at the beginning of the 6th century can be found in a letter of Procopius of Gaza (450-528 C.E.) to his close friend Jerome of Elusa. This letter is a vivid testament to the environmental conditions in the southern Levant at the beginning of the 6th century C.E. In one of his letters Procopius states "*For there will be a day when you will see Elusa again and you will weep at the sand being shifted by the wind and stripping the vines naked to their roots. The nymphs of the dry land and of the sea, and Zeus the Bringer of Rain, are nowhere there at all*." (Mayerson, 1983), a clear indication of severe and prolonged drought and the damage inflicted on vineyards by wind and sand. The mention of "*nymphs of the dry land*" most likely

referred to the periodic flow of flood water in wadis in winter/spring, which could be diverted onto the fields to grow crops and also into reservoirs to deliver potable water to the inhabitants. Furthermore, by writing "*as for the nymphs of the sea*", Procopius was referring to brackish well-water, as he remarked in the previously mentioned letter to Jerome, "*those who drink of it are reminded of the sea*". It is most likely that the severe droughts depleted ground water levels and caused a rise in salinity. Procopius' letter may provide us with a terminus a quo for a radical change in the physical environment in the region around Elusa: the encroachment of sand dunes onto its cultivable lands. Later accounts from 570 C.E. suggest that the entire region around Elusa was invaded by shifting sands and that the desert extended to Sinai. Additional support for a major change in the regional environment comes from excavations at the coastal site of Deir elBalah, just west of Gaza, where large deposits of Byzantine pottery were found under sand dunes 13m in height. Nothing from later periods was found. The distinct climate-induced socioeconomic transformations are also evidenced in settlements which were abandoned around the mid-sixth century C.E. according to systematic archaeological excavations (Bar-Oz et al., 2019).

Between ~516 and 520 C.E. the area around the Lavra of Mar Saba (Monastery of the Cave; Bir el Qattar; "Well of drops") in Palestine was affected by a severe multi-year drought. Documents report frictions between shepherds and monks as the shepherds were grazing their flocks within the bounds of the monastery. Furthermore, they also bothered the monks with repeated demands for food until their flocks stopped giving milk and their kids and lambs starved to death. In 520 C.E., the fourth year of the drought, the cisterns of the monastery were empty and the monks planned to abandon the monastery (Hirschfeld, 2004; Patrich, 1995).

Further evidence for drier climatic conditions at the beginning of the 6th century comes from the Levant, where Cyril of Scythopolis reports that in the 520s C.E., "*…in the fifth year of a drought, "so great was the lack of water that the poor of the Holy City (τῆς ἁγίας πόλεως) were begging for water and dying of thirst. In fact, because of the long drought and lack of rain the water had disappeared from the Siloam Pool and the Lucillian Pool; moreover, the springs of Colonia and Nephtho were much diminished.*" The drought is believed to have lasted from 516 to 520 C.E. (Hirschfeld, 2004; Telelis, 2008).

In 536 C.E. the contemporary Latin writer Marcellinus Comes reports that two Arab chieftains (~15.000 people in total) from central Arabia appeared in Mesopotamia on the search for pastures due to an excessive drought (Hirschfeld, 2004; Stathakopoulos, 2004). Increasing aridity during the 5th and 6th centuries C.E. is also evident in archaeological and geoarchaeological records from southern Oman. At Khawr Rawri (Figure 40), for example, there is direct evidence for a marked reduction in freshwater run-off as a result of decreasing summer monsoon precipitation sometime between 270-420 C.E. This is indicated by a shift from an open estuary to a barrier dominated estuary (Hoorn & Cremaschi, 2004). Until then monsoonal rainfall and fluvial discharge from Wadi Darbat was sufficiently high to prevent siltation until a sand barrier formed between 270 and 420 C.E and led to the abandonment of the Samhuram citadel (Figure 40). Furthermore, there is a distinct lack of archaeological records from this period compared to almost all others going back as far as the Bronze Age. All of this suggests that the arrival of Islam occurred during one of the most arid periods in over 3500 years of Umani (modern Oman and the United Arab Emirates) settlement history (Hoorn & Cremaschi, 2004).

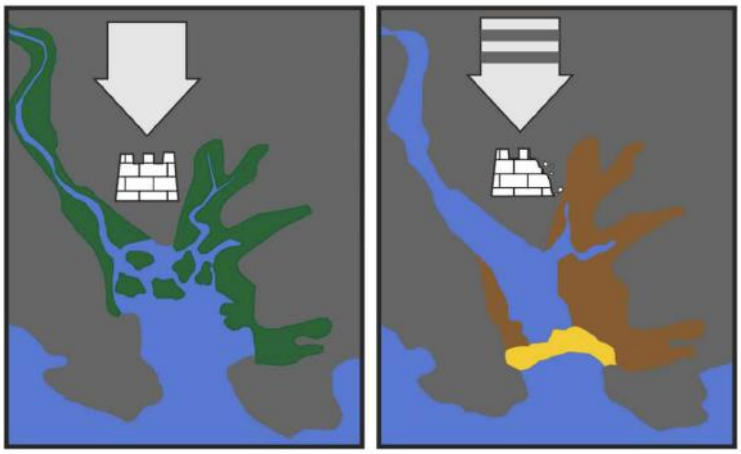

Figure 40. Paleogeographical development of Khawr Rawri in Southern Oman. Left figure shows the environmental situation during the pre-Islamic period between 100 B.C.E and 100 C.E. when the estuary was fully opened to the sea and surrounded by vegetation. The estuary was a natural harbor and supported by the settlement of Samhuram. Right figure shows the geographical situation between 270 and 420 C.E. (uncertainties arise from radiocarbon dates) when the estuary was blocked by a sand barrier and Samhuram was abandoned.

5.3.5. Historical context

The context in which Islam appeared and expanded is both complex and in many respects – because of substantial difficulties with the written source tradition – obscure (Robinson, 2003, 2011). It includes as background a socio-cultural and local as well as international political situation that had been changing rapidly across the period from the early sixth into the early seventh century. This consisted of religious/tribal conflict, especially between Judaism and Christianity; political upheaval and shifting economic relationships (Patrich, 1995; Whittow, 2011); external – imperial – interference in local power politics resulting in shifts in the political configuration of states and tribal groupings within the peninsula; and an increasingly arid climate from the later fifth and early sixth century that challenged established lifeways and economic relationships, rendering traditional loyalties and relationships more fragile and less resilient to stress. The increasing aridity described here should thus be seen as just one of several elements that without doubt contributed to a major transformation of the established configuration of political-economic relationships and played a key role in setting the scene for the dramatic events described under the rubric 'the rise of Islam'.

Geostrategic, economic, and demographic context

To understand the bigger picture and to appreciate the significance of the environmental data it will be helpful to sketch out the wider historical and geographical context for the century leading into the rise of Islam (Macdonald et al., 2015). The Arabian Peninsula was of strategic, economic and ideological importance to both the major powers of the late ancient Middle East: the eastern Roman (Byzantine) empire, with its capital in faraway Constantinople (mod. Istanbul) and the Sasanian Persian empire, centred on the capital of its ruler, the Shāhānshāh (king of kings), at Ctesiphon on the Tigris in Iraq (Whittow, 2011; Wiesehöfer, 2010). Strategically the northern regions of the Arabian Peninsula were home to tribes who acted as a buffer between the two empires and who also served as mercenaries in their armies. Economically the southern coastal towns also offered access to a rich long-distance trade as well as some agricultural products. Commercial centres such as Ṣanʿā' in Yemen maintained regular trading contacts across the Indian Ocean as well as with the east

African littoral and the Aksumite kingdom of Ethiopia, and the Sasanian Persian kings actively encouraged commercial links via the Indian Ocean trade (Crone, 2007). In the north the clans and tribes of the Ḥijāz were key players in trading a variety of goods, including perfumes as well as some non-luxuries, to the Roman provinces of Palestine, Syria and Arabia, and possibly beyond. The semi-nomadic populations of these northern regions occasionally posed a threat as small-scale raiders, but were also traders on a substantial scale to both Roman and Sasanian markets. The Quraysh of Mecca – Muḥammad's clan - in particular were involved in what had by the later sixth century C.E. become a lucrative trade in leather, possibly supplying the Roman military. But gold and silver were also produced and traded, apparently in substantial quantities – indeed, the Sasanians depended on the mines of central Arabia for bullion for their silver coinage (Heck, 1999; Shahîd, 2010). The importance of this commerce partially accounts for the economic importance of Mecca and the pre-eminence of the Quraysh (Crone, 1987, 2007). As a focus for exchange and the long-distance trade to both Rome's eastern provinces and Sasanian Iraq, the significance of the region was clearly recognised (Lecker, 2010; Schiettecatte, 2016; Shahid, 1989, 1995).

The population of Arabia included many Persians, especially in the east (Oman and Bahrain), Judaism was well-established in parts of western Arabia, and there were substantial Christian communities in the south. Society throughout the peninsula was structured around the tribe and focused heavily on its constituent clans and lineages. Tribes varied considerably in extent and territory as well as in ascribed status, but had little purchase on daily life, where it was the clan or lineage group that offered solidarity against external threat, and within which pasture and camp were shared and justice meted out. Tribal identities did play a role, of course, at a broader level of political and economic interests, and leaders were chosen from established ruling lineages on the basis of talent and effectiveness. In the centre and north of the peninsula the symbiotic relationship between nomads and sedentary populations involved benefits in both directions, with the nomads providing warriors and military resources to their settled neighbours (Donner, 1981; Kennedy, 2004). In the south, where until the collapse of Himyar an organised state dominated such relationships, the nomads tended to be subordinate to the kings and their vassals and far less powerful politically.

Geographically the Arabian Peninsula can be divided very roughly into four zones. Yemen in the south includes a coastal plain in the west (important because of its ports) and inland highlands; to the east lies Ḥaḍramawṭ. The north-western part of the peninsula, the Ḥijāz, includes desert as well as oases, many substantial, and its population comprised sedentary, nomadic and semi- nomadic tribes, mostly pagan, but some Jewish and Christian. Here there were a number of important oasis settlements, including Ṭā'if and Yathrib (Medina), Khaybar and Fadak and several others. The commercial wealth of Mecca, until the early sixth century relatively unimportant, appears to have become more significant after the early decades, based largely on trans-peninsular caravan trade and finance, while agriculture and local commerce were the mainstay of the remaining settlement economies. With each settlement or town there was associated a group of nomadic or seminomadic clans and tribes. Political, economic and religious leadership tended to lie in the towns, in particular Mecca, rather than with the nomadic tribes. The third zone is constituted by the central and eastern regions of Najd, remote and populated largely by nomadic groups, and to the east Yamāma, a densely populated, cultivated area, the main towns of which were Hajar and al-Jaww (or al-Khiḍrima). Yamāma was important both because trade routes from Iraq, the Yemen and the Ḥijāz passed through it as well as the fact that it is supposed to have supplied wheat to the Ḥijāz. To the east lay the coastal regions and the island of Bahrain, whose economy was dominated by agriculture, fishing and trade, and whose populations were a mix of pagan, Christian, Zoroastrian and some Jews. Finally, Oman, lying on the south eastern corner of the Arabian Peninsula, consists of a coastal plain, desert and mountains. The coastal area is easily accessible from Iraq, eastern Africa and the Indian Ocean, and the economy included fishing, trade, pearl production, textiles as well as agriculture. It was heavily influenced by Persia both culturally and in terms of language (Lecker, 2010; Potts, 1997).

Political context

With a few short periods of disruption and raiding, the Roman and Persian 'frontiers' (in reality, wide zones of semi-desert and highland) with the Arabs remained stable from the fourth to the seventh centuries. On the Roman side a system of allied tribes or clans organised as foederati, or federates, under a paramount group or tribe (the Tanukhids in the

fourth century, the Salihids in the fifth century C.E., and the Ghassanids into the later sixth century C.E.) served to defend Roman interests. On the Persian side the kings of al-Ḥīra and their clan, the Lakhmids, played a similar role. The Ghassanids, and many of their subordinate clans, were Miaphysite Christian (thus of a different confession from the Byzantine church) (Gajda, 2009; Robin, 2015; Shahîd, 2010); by the 580s C.E. many of those under the Lakhmids had likewise converted (but to Nestorian Christianity, heretical from the Byzantine point of view), but the conversion of the ruler Nu'man III towards the end of the century provoked a breach with the Persians and the Lakhmid dynasty was replaced. The Ghassanids also saw their political and military power dramatically reduced at this time as the result of a split between the Roman emperor and their 'phylarch', the client warlord/king of the confederacy. But a long-term result of Roman and Persian subsidizing Arab client leaders and confederacies, combined with the wealth generated by Arab commerce with both empires, was to make the clans and tribes of the desert fringe of empire far more powerful, and far more knowledgeable about their patrons, their strategic organisation and their military capabilities (Donner, 1981; Kennedy, 2004; Potts, 1997; Shahîd, 2010).

These factors account for the sustained interest of the great powers in the S. Arabian Peninsula and in particular for the political and military interventions that took place in the sixth century C.E. The petty states or confederacies of Aden and the Yemen (Himyar) were a focus for diplomatic activity, and the kingdom of Himyar in particular, with its centre in Yemen, was a bone of contention between Persia and Rome, primarily because of its location in respect of the commercial interests of both powers and their access to the Indian Ocean trade. Himyar, historically referred to as the Homerite Kingdom in Greek and Roman sources, had a long and chequered history, having been founded in 110 B.C.E. During the fifth century the royal dynasty, followed by many of the inhabitants of the Yemen, converted to Judaism. This led to increasing tension between the Jewish and Christian populations of the region.

It was no accident that a state evolved in one of the few regions that enjoyed a predictable annual rainfall, and where water resources can only be maintained through dams and other irrigation projects that require some degree of centralised management and resourcing (Kervan, 1994; Robin, 2015). By the end of the second century C.E., Himyar was the dominant power in the southern part of the peninsula, extending its influence over its neighbours through warrior allies such as the central Arabian nomad tribes of Kinda and

Madhḥij. These seem to have formed the mainstay of its military power in spite of occasional defeats at the hands of northern tribal confederacies. They continued in this role into the sixth century. But during the first half of the sixth century C.E. increasing East Roman interference in central Arabian politics, internecine strife within the Kinda elite in the 530s C.E., together with the conflict between the rival great power allies, the Ghassanids and Lakhmids, resulted in the retreat of Himyarite power in the region. Himyarite interests in the Ḥijāz, and international competition for influence, and over access to the resources of the peninsula between the Sasanian Persians, the Ethiopian Aksumite kingdom, and the eastern Roman empire greatly complicated the political situation from the early sixth century onwards (Bowersock, 2013; Harper, 2017; Hatke, 2011; Whitehouse & Williamson, 1973).

The Aksumite kingdom of Ethiopia (named after its capital, Aksum, in the north Ethiopian highlands), Christian since its conversion in the fourth century, played a prominent role in the politics and commerce of the Arabian Peninsula-Red Sea region. Its rulers acted in particular to enhance their own advantage from the flourishing trans-Peninsula and coastal commerce. Although East Roman rulers regarded the kingdom of Aksum as a legitimate part of their sphere of influence, the Aksumite rulers themselves remained entirely independent. Aksumite intervention in the later fifth century was fended off by Himyar, but further Aksumite pressure during the reign of Marthad'īlān Yanūf (c. 500-515 C.E.) eventually led to invasion and temporary conquest, with a Christian king, Ma'dīkarib Yafur (519-522 C.E.) being imposed by the Aksumites. In 522/23 C.E. the Jewish Himyarite leader Yūsuf 'As'ar Yath'ar, also known as Dhū Nuwās (c. 522-525 C.E.) was enthroned, but then challenged Aksumite influence. His massacre of the Christians of Najran in 522/523 C.E. worsened the tensions between Jewish and Christian communities. In retaliation, the negus (emperor) of Aksum, Kaleb 'Ella 'Asbeha (ca. 510-540 C.E.), invaded and imposed a Christian king. Yusuf was crushed and Aksumite forces reestablished their hold (Nebes, 2010) through the puppet Himyarite ruler, Sumuyafa' 'Ashwa'. In 527 C.E., however, the Aksumite commander Abreha rebelled, seized power as king and ruled independently until sometime between the later 550s and ~570 C.E. (the chronology is extremely uncertain) (Bowersock, 2013; Hoyland, 2001; Schippmann, 2001). Relations between the Jewish communities and Christians in Himyar were stabilised until the 620s C.E., and the Himyarite kingdom, while nominally tributary to Aksum, was able to reassert its autonomy for a while. Abreha conducted a number of military

campaigns in efforts to secure his authority in central Arabia (Korotayev et al., 1999), the last one in ~570 C.E. aiming at destroying pagan religious centers and thus enhancing the importance of Ṣanʿā' as a Christian sanctuary (Hoyland, 2001; Korotayev et al., 1999). The fact that the expeditions had to be repeated four times does, however, suggest that Himyarite authority in the region was largely a fiction in the absence of its military.

The short-lived slight increase in winter/spring precipitation between 530-545 C.E. might have contributed to a brief revival of Himyar under Aksumite or rebel Aksumite power, and conditions up to the 590s C.E. were not as bad as before 530 C.E. But it seems likely that there was no full and lasting recovery: the key structural damage had been done, first in terms of political stability in the south, and secondly in respect of the maintenance of the irrigation infrastructure and dependent agriculture. For the dynamics of the social-political system, the clock could not simply be turned back, even had conditions improved very markedly - which they did not. By the middle decades of the century Himyarite power was substantially weakened, major irrigation and infrastructural projects were abandoned, epigraphic evidence ceased, the king was unable to marshal the resources to resist external interference, and the extension of Sasanian Persian power into the Ḥijāz as well as the south deepened (Robin, 2012). The absence of effective Himyarite power in central Arabia opened up the whole region to the potential or likelihood of violent competition between tribal interests. In 570 C.E. a Persian force was invited in by opponents of the king (a son of Abraha), who was slain in battle, and Persia became the pre-eminent power in the region (Bowersock, 2013; Kervan, 1994). By the later sixth century C.E. the Sasanians controlled, directly through the placement of garrisons and the building of forts, or indirectly through client kings, most of the eastern coast of the Arabian Peninsula including Bahrain and Oman, as well as the Yemen (Kervan, 1994; Potts, 1997; Robin, 2012). Whatever the exact causes, the Arabian Peninsula was once more in a state of disunity and inter-tribal conflict by the later sixth century. The arrival of a virulent and recurrent pandemic disease, the Justinianic Plague, in the early 540s C.E. may have been yet another aggravating factor, although the evidence is problematic: some hold that this plague travelled up Arabia's Red Sea coast before it irrupted in the eastern Nile Delta in 541 C.E. and spread throughout the Mediterranean world (although there is no textual evidence to confirm this pattern) (Harper, 2017; Hatke, 2011; McCormick, 2007; Sussman, 2016). As noted, lack of any centralised authority able to

mobilise resources meant that major irrigation facilities such as the Ma'rib dam were no longer maintained, with significant negative consequences for local agriculture and political authority (Robin, 2012).

Islam

The origins of Islam lie in the Ḥijāz, where different forms of Christianity and Judaism had competed and co-existed with indigenous beliefs for centuries, in particular in the much-travelled trading and caravan communities of Mecca and Medina in the west and in Hajar in the east, where the major permanent settlement of the Ḥanīfa tribe included a shrine as well as an important commercial centre. But Mecca itself became a significant commercial centre only in the course of the sixth century C.E., enhancing thereby also the power and influence of those branches of the Quraysh clan who had hereditary responsibility for the sacred Ka'ba, to the extent that the Meccan elite had come by the early seventh century C.E. to represent a powerful and influential body of commercial financiers able to conclude effective trading agreements with foreign sources, using their religious authority and financial influence to collaborate with the nomads of the Ḥijāz and beyond in protecting their trade to Yemen, Syria and Iraq. Muḥammad, was himself a respected and established merchant who had several times accompanied the trade caravans north to Roman Syria. But at the time of his first revelations, he was only one of a number of similar holy men or prophets, self-proclaimed or not, who seem to have been responding to the exigencies of the times. His success was due at least in part to the establishment of an organized community in Medina, one that was attractive both in respect of the order and social justice it offered as well as the respect it garnered – one of the prophet's most significant achievements was acting as arbitrator between rival clans and factions, for example (Donner, 1981; Kennedy, 2004; Montgomery-Watt, 1953; Robinson, 2003).

Syria and Palestine already had substantial populations of Arabs, mostly Christian, both farmers and herdsmen, as well as mercenary soldiers serving the eastern Roman (Byzantine) empire as clients and as a buffer against the Persians. It is important to bear several key points in mind when considering the origins and expansion of Islam.

First, it evolved in a situation of comparative social-economic and cultural uncertainty in the region, and more widely, one of anxiety about the future reflected in a number of contemporary apocalyptic writings (Bowersock, 2017; Crone, 1987; Harper, 2017; Kennedy, 2004; Wiesehöfer, 2010). Muḥammad met with stiff resistance from his own clan, the Quraysh, who dominated Mecca and its trade (as well as the holy Ka'ba), which is why he was forced to leave for Yathrib (Medina) in 622 C.E., the year of the Hijra (flight/departure/emigration). Only after developing his power-base there and allying himself with local tribes, both pagan and Jewish in faith, was he able to challenge Mecca and, after defeating them in battle, persuade them to collaborate with him and become allies and eventually supporters. By the end of the year 630 C.E. he had established his authority over most of the peninsula primarily through negotiation and occasionally by military threat as his power expanded.

But second, Muslim control was still precarious and dependent in many cases on Muḥammad's personal efforts. On his death in 632 C.E. there followed a brief period of warfare (the so-called Ridda wars, or wars of apostasy) during which his immediate successors as leaders of the Muslim community had to fight hard to re-assert Islamic authority against a variety of different alliances and groups of tribes who attempted to re-assert their autonomy, free themselves from paying tribute or tax to the Muslims, or simply return to the earlier order. Among these the Banu Hanīfa in Yamāma rejected Islamic authority in favour of their own prophet, Musaylima, who was eventually killed in a decisive battle in 632 C.E. Acceptance of Islamic leadership on the part of many tribes and clans throughout the peninsula had to be constantly reinforced through threats or negotiation (Donner, 1981; Kennedy, 2004).

Third, the Islamic leadership was able relatively rapidly between about 630 and 634 C.E. to weld the disparate, fractured, warring and unruly tribes of the Arabian Peninsula together into a single identifiable community of interests with, at least in theory, a common focus for religious zeal and a common identity as Arabs under an Islamic leadership. This was the first time in the history of the peninsula that such had been the case, and the hitherto unrealised military potential of these groups was enormous.

Fourth, the Quraysh, whose elite members stood at the pinnacle of the early Islamic power hierarchy, undoubtedly had a powerful vested interest in expanding their economic and political power and commercial interests. There is little doubt that while religious zeal may have inspired the leadership, the pragmatic need to hold this new, easily fractured community together played a key role in encouraging attacks on the imperial powers outside the peninsula - and the desire for booty, new lands and glory certainly drew many to the prophet's banners. Many fighters in the first 'Islamic' armies were not yet 'Muslim', for example (indeed, the first generation of Muḥammad's followers referred to themselves not as Muslims but simply as 'believers'), and while acceptance of Islam was achieved remarkably rapidly, it was neither universal at first nor a foregone conclusion (Bowersock, 2017; Crone, 2007; Donner, 1981; Kennedy, 2004).

Chapter 6: Climate change and the Sasanian Empire (224 - 651 CE): a review

6.1. Preface

This chapter was prepared in the style of a journal article to be submitted to the *Journal of Interdisciplinary History* (*JIH*). Authorship: Matthew J Jacobson

6.2. Journal Article

6.2.1. Introduction

Scholarship on the societal impacts of climate change in Late Antiquity (3rd-7th centuries CE) has been extensive across much of the northern hemisphere (e.g. Chen, 2015; Haldon et al., 2014; McCormick et al., 2012). Significant periods of climatic change, which are sometimes named (e.g the DACP: Dark Ages Cold Period, 450-800 CE and LALIA: Late Antique Little Ice Age, 536-660 CE), are argued to relate to agricultural and economic change, migrations, conflict (both inter- and intra-state), and the end of empires (Büntgen et al., 2016; Harper, 2017; Chapters 4 and 5). The Sasanian Empire (SE hereafter: 224-651 CE; Figures 40 and 41) was a significant polity in socio-political developments in the Middle East during Late Antiquity and the impact on it of climatic factors requires assessment for several reasons. Firstly, there are eight palaeoclimate proxy records within the core territories of the empire, which enable reconstruction of climatic conditions. Secondly, significant climate shifts have been identified in these proxies, and in surrounding regions, which contributed to societal change in the contemporaneous Byzantine Empire (Büntgen et al., 2016; Haldon et al., 2014) and Kingdom of Himyar (Chapter 5). Thirdly, climate in this region has been linked to societal change during other historical periods (Appendix B.2) and is arguably implicated in recent geo-political instability (Gleick, 2014; Kelley et al., 2015). Finally, the empire contains some of the driest and hottest places on earth (Djamali et al., 2011; Mildrexler et al., 2006), where societies can only thrive through intense water management, and regions with annual

precipitation close to the minimum for rainfed agriculture (250mm/yr: Hole, 2007), suggesting small hydroclimatic fluctuations could have significant impacts.

Despite the increasing consideration and importance of climate factors in other regions and periods, and the potential susceptibility of the empire to fluctuations, examination of the History of Climate and Society (HCS: Degroot et al., 2021) for the Sasanian Empire has been limited. Previous consideration has been limited to statements on how general climatic conditions impact agricultural potential (Mashkour et al., 2017; Shumilovskikh et al., 2017) and temporal correlations, sometimes paired with environmentally-deterministic comments about 'collapse' (Büntgen et al., 2016, 2020; Peregrine, 2020; Sharifi et al., 2015). The former has been useful for characterising constraints on agriculture but ignores the spatio-temporally heterogenous nature of climate (Chapter 3; Appendix B.1). Environmental determinism has already been comprehensively critiqued; establishing causal links and examining societal resilience are now considered crucial for successful studies (Contreras, 2016; Coombes & Barber, 2005; Haldon et al., 2020; Izdebski et al., 2016a; Moreland, 2018; Sluyter, 2003).

This interdisciplinary paper presents an investigation into societal and climatic change in the SE, alongside assessment of the quality of available historical, archaeological, palaeoenvironmental and palaeoclimatic evidence. First, key periods of societal changes are identified. Second, the vulnerability of the SE to climatic variability is assessed, through examination of modern climatic conditions and Sasanian agricultural practices. Third, palaeoclimatic proxy data from within the SE are synthesised to establish Late Antique climate changes. Finally, conclusions regarding specific impacts from climate change and future research agendas are outlined.

The potential influences of climate on the history of the SE are evaluated on a polity-wide scale (Figure 41) and for three diverse case-study regions (Figure 43). These are centred in the western territories of the SE due to greater availability of strong archaeological, palaeoenvironmental and palaeoclimatic datasets (Figures 40 and 42).

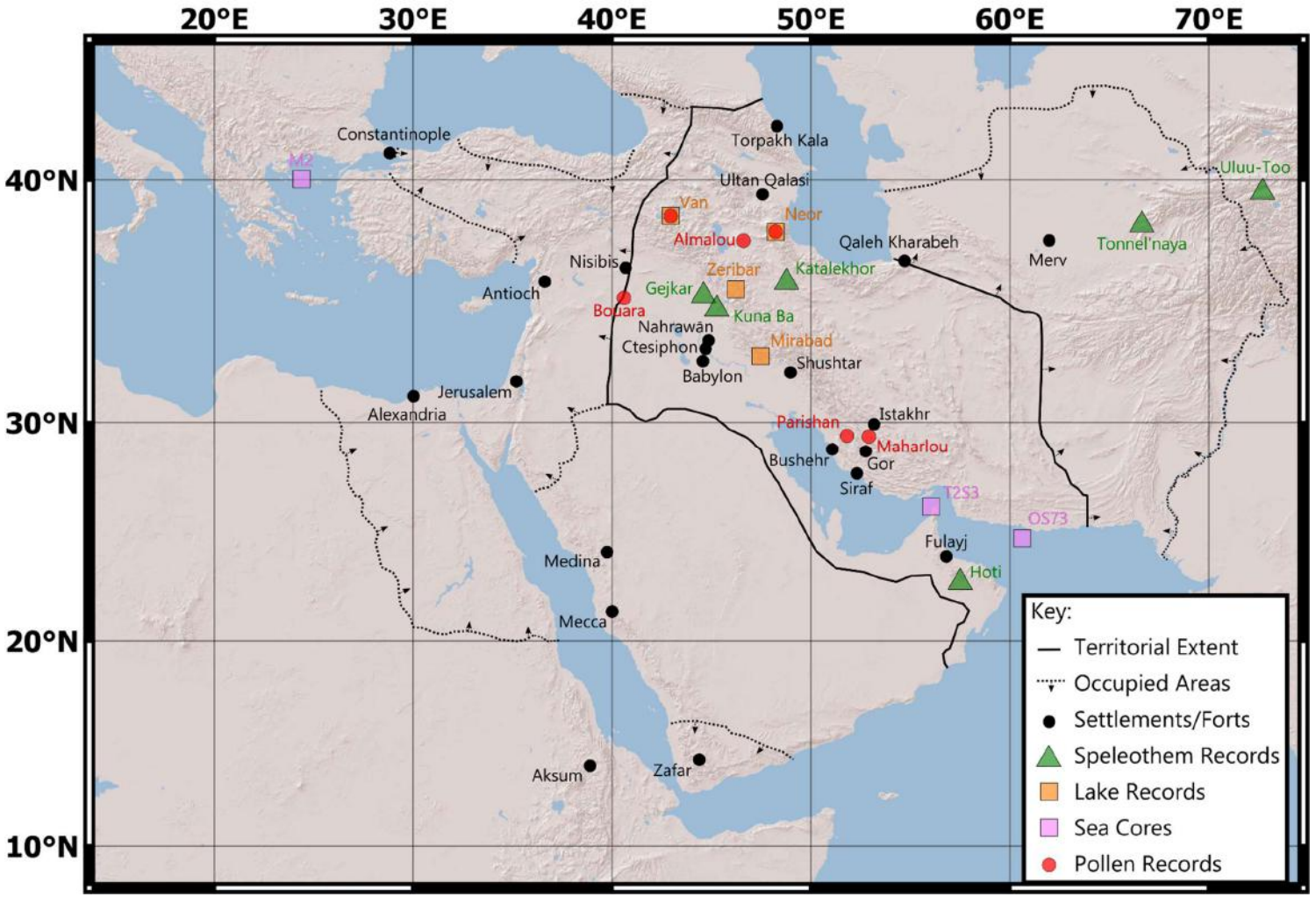

Figure 41. Map indicating the approximate territorial extent of the Sasanian Empire, with palaeo-climate and pollen records, and locations mentioned in text. Extent does not indicate established borders.

(1) Lower Mesopotamia. This region, on the border of Iraq and Iran, was the administrative centre of the SE, containing Ctesiphon, the capital (Daryaee & Rezakhani, 2016). The Tigris-Euphrates River system, and associated canals, provide flowing water for agriculture and transport routes (Tamburrino, 2010). Irrigation, combined with fertile alluvial soils and suitably warm temperatures, led to this region being the long-term "breadbasket" of the SE and multiple other states (Adams, 2006; Altaweel, 2019; P. Christensen, 1993; Soroush, 2020; Wilkinson et al., 2012).

(2) The Persian Gulf (PG) and Fars. This is an important region with port cities established during the Sasanian Period (e.g. Bushehr, Siraf) that reworked raw materials and agricultural products into high-value commodities to trade with east Africa and across the Indian Ocean (Daryaee, 2003; Fakhar & Hesari, 2013; Hojabri-Nobari et al., 2011; Pashazanous et al., 2014; Pourshariati, 2008). Nearby, the World Heritage Site of "Sassanid Archaeological Landscape of Fars Region", inscribed in 2018 (UNESCO, 2018), includes Gor (the homeland of the empire) and was an important Zoroastrian religious centre (Potts, 2018).

(3) Mughan Steppe. An extensively studied region in NW Iran and Azerbaijan (to the west of the Caspian Sea), this low plain along the south of the Araxes River was a Sasanian borderland colony populated by rectangular fortified settlement complexes (e.g. Ultan Qalası, Torpakh Qala) with associated large feeder canals (Alizadeh & Ur, 2007; Lawrence & Wilkinson, 2017; E. Sauer et al., 2017; Ur & Alizadeh, 2013).

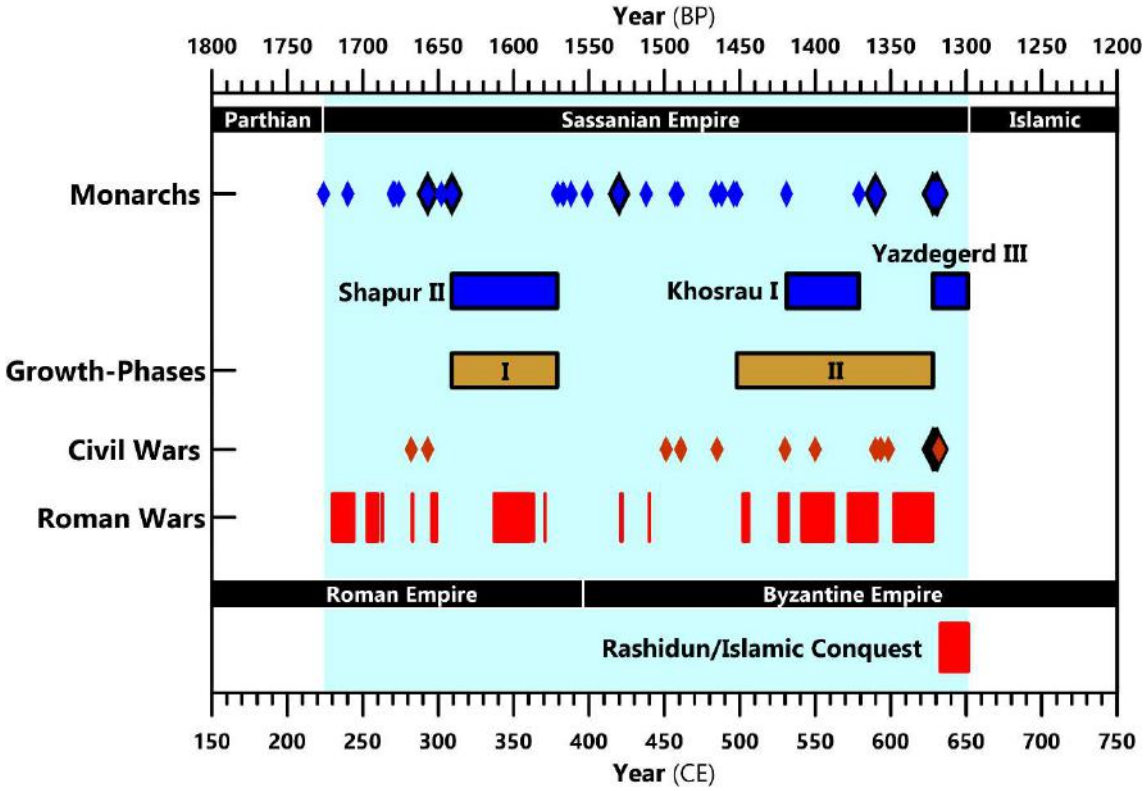

Figure 42. Timeline of the Sasanian Empire. Black diamonds indicate years when multiple monarchs were coronated or multiple civil wars occurred (data from Daryaee and Rezakhani, 2016).

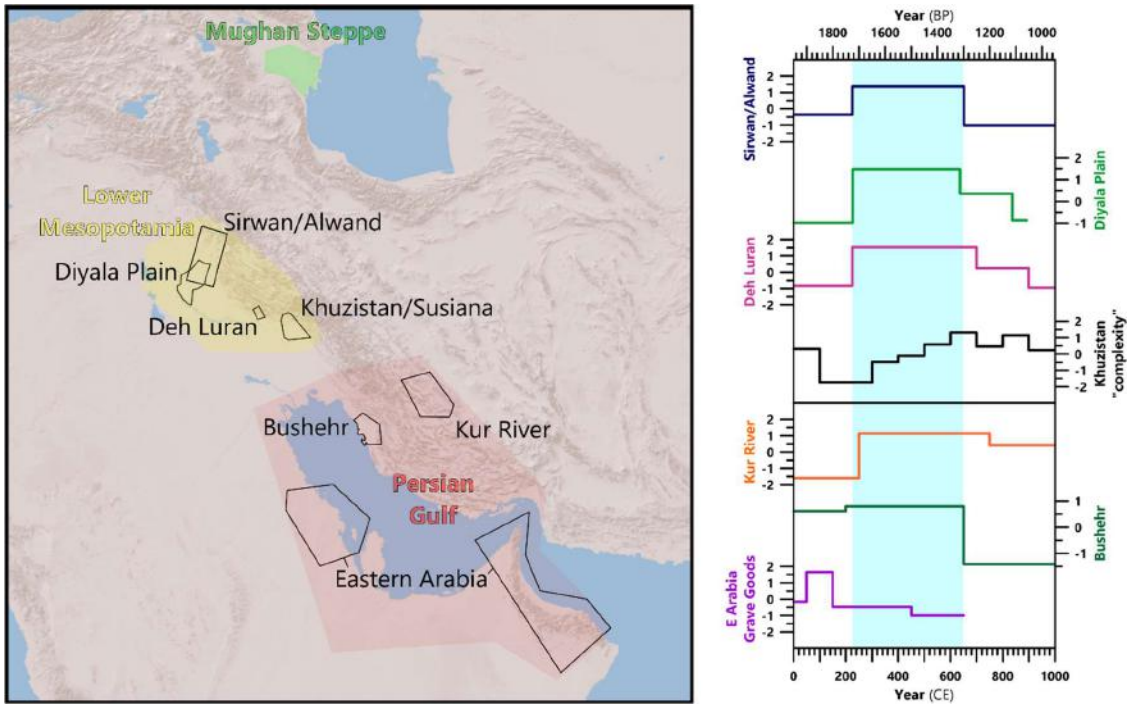

Figure 43. Map showing case-study regions and the locations of surveys (left). Standardised survey data (right), settlement counts unless otherwise stated. References in main text.

6.2.2. The Sasanian Empire

Background

Ardashir I, the first *Shahanshah* (King of the Sasanians), overthrew the Parthian Empire, weakened following internal strife and conflict with the Roman Empire, in 224 CE (Bivar, 1983; Frye, 2005; Katouzian, 2009; Olbrycht, 2016). The SE quickly established a large spatial extent, which encompassed the eastern Fertile Crescent (FC) to eastern Iran, including eastern Arabia and the Caucasus. Surrounding regions were controlled by the Sasanians discontinuously, including parts of Central Asia (CA), Pakistan, Yemen, Egypt, the Levant and Anatolia (Cameron, 2012; Canepa & Wiesehöfer, 2018; Rezakhani, 2017; E. Sauer et al., 2017). Sasanian kings claimed a divine right to rule, both as heirs to the Achaemenid dynasty which they frequently imitated, similarly naming themselves *Eranshahr* (the Empire of the Iranians), and through the state-religion of Zoroastrianism (Altaweel & Squitieri, 2018; Bosworth, 1999; Crone, 2012; Daryaee, 2019).

The SE had a more centralised structure than their Parthian predecessors (A. Christensen, 1944; Daryaee & Rezakhani, 2016) and was hierarchical, with the *Shahanshah* at the top, followed by nobles (the rulers of smaller regions within the empire), clergy/secretariats (the administrative class), members of the military, and wealth producers (i.e. civilians) (Karimian, 2008, 2010). Zoroastrian fire temples were built as economic institutions, with clergy managing regional administration (Payne, 2014). Via these institutions, the state funded the construction, restoration, and maintenance of cities, irrigation infrastructure and military structures, and then taxed their use (Canepa & Daryaee, 2018; Gyselen, 1998; Manuel et al., 2018; Maresca, 2019). Increased use of irrigation was at least partially driven by the Zoroastrian religion, which encourages agriculture and sanctifies water (Adamo & Al-ansari, 2020). The empire also colonised and invested in areas on their borderlands, such as the Mughan Steppe and Khorasan, southeast of the Caspian Sea (Alizadeh, 2014; Ur & Alizadeh, 2013). Sasanian society became highly monetised, with soldiers, Zoroastrian administrative officials, and taxes, paid in high-quality silver coins (Kennedy, 2002; Payne, 2018). Minting of these coins necessitated recruitment and management of miners to extract the required silver (Darley & Canepa, 2018; Khademi

Nadooshan & Khazaie, 2011; Nezafati & Pernicka, 2012). Complex trade networks were developed, selling agricultural produce and high-value commodities, such as silver artefacts, glassware, linen and cotton, carpets, and oils (Fakhar & Hesari, 2013; Payne, 2018; S. J. Simpson, 2000).

Conflict with the Roman, later Byzantine, Empire was virtually continuous (Sicker, 2000), although the two empires viewed each other as equal rivals; the terms *Basileús* and *Caesar* were reserved exclusively in diplomatic documents for Sasanian kings and Roman emperors (Brockley, 1984, 1992; Canepa, 2009; Chrysos, 1978). The two empires exchanged lands in their frontier zone around western Mesopotamia and in the Caucasus and Arabia, as well as launching invasions into each other's home territories (Canepa & Wiesehöfer, 2018; Sicker, 2000). The Sasanians also warred to their east, initially against the Kushan Empire and later against Hunnic tribal confederations such as the Göktürks and Hephthalite Khanate (Cameron, 2012; Rezakhani, 2017). Constant military campaigns at great distances and the threat of attacks from all sides were costly (Adams, 2006), necessitating agricultural surpluses, construction of military bases and coinage for payment (Howard-Johnston, 2014).

Expansion

Investment in the construction and maintenance of irrigation infrastructure, new cities and colonies, military defences, trade networks and mining activities was labour intensive, with many workers forcefully deported from conquered territories (Canepa & Daryaee, 2018; Morony, 2004). As a result, settlement and irrigation infrastructure peaks in the Sasanian Period in many archaeological surveys (Figure 43). In Lower Mesopotamia, a peak of settlement is observed in surveys in the Sirwan/Alwand river basin (Casana & Glatz, 2017; Panahipour, 2021), Diyala Plain (Adams, 1965), Deh Luran (Neely, 2016) and Khuzistan Plain (Adams, 1962; Wenke, 1987). Around the Persian Gulf and Fars, settlement numbers also peak at Bushehr (Carter et al., 2006) and the Kur River basin (Hartnell, 2014). In the Mughan Steppe, no raw settlement number datasets are available; but evidence nonetheless suggests that this region was part of the state's expansion strategy; especially well-evidenced are canal systems and associated settlement along the Araxes River (Alizadeh & Ur, 2007; Ur &

Alizadeh, 2013). Elsewhere in the empire, unprecedented expansion of river-fed canal systems and installation of qanats occurred during the Sasanian Period (Campopiano, 2017)

Unfortunately, settlement surveys, which date identified settlements primarily with ceramics and are used to date associated irrigation infrastructure, rarely provide chronologies that are more precise than just 'Sasanian' (visible in Figure 43), other ceramics are ascribed even broader chronologies that also encompass the Parthian and/or the early Islamic periods (Mousavi & Daryaee, 2012; Neely, 2016). This regards settlements as occupied for an entire period, although they may in fact have been occupied throughout, for only a short duration, or at multiple times throughout the period (Dewar, 1991; Plog, 1973) Thus, sites that were not contemporaneous may appear so (Premo, 2014; Schacht, 1984). Tighter chronological ceramic typologies have been established in some regions (Boucharlat & Haerinck, 1991; Kennet, 2002; Ucko & Puschnigg, 2006); however, diversity of traditions, a lack of distinctive forms, and inadequate examination and publication have hampered Sasanian ceramic studies (Mousavi & Daryaee, 2012). The names of some cities act as chronological indicators, associating them with the king who founded or re-established them; for example, Gor (now Firuzabad) was renamed Ardashir-Kwarrah by Ardashir I, and nearby Bishapur was founded by Shapur I in 266 CE (Karimian, 2010). Smaller settlements can sometimes be dated more precisely through rare coin finds attributed to specific rulers (Mousavi & Daryaee, 2012); however, on their own, coins only evidence occupation during a very small period, not what occurred earlier or later than the coin issue date.

Expanding population and settlement, as well as long-distance military campaigning, necessitated agricultural surpluses. To investigate past flora and agriculture, palynological (pollen) records are utilised. There are numerous pollen records in the SE's territory (Figures 40 and 43), however, there are limitations to these records (Shumilovskikh et al., 2017). Of the six pollen records near the case-study regions, only two have numerous palynological samples during the Sasanian Period (Almalou: 7; Maharlou: 6) whilst the others are more limited (Parishan: 1, Neor: 1; Van: 2; Bouara: 3) (Djamali et al., 2009a, 2009b, 2016; Gremmen & Bottema, 1991; Ponel et al., 2013; Van Zeist & Woldring, 1978). Zeribar was not included in this study as there are no palynological samples relevant to the Sasanian Period (Van Zeist, 1967). Excluding Van, which is dated by varve counts (Van Zeist & Woldring, 1978), these records were dated by means of varying numbers of radiocarbon dates, which have large

chronological uncertainties (often ± centuries) and bring further uncertainty when a small number are used to date a long record. In the discussed pollen records, the Sasanian Period is a peak of arboriculture, particularly walnuts (Juglans) and pistachios, and of cereal cultivation in some regions (Shumilovskikh et al., 2017; see Figure 44).

Whilst the Sasanian Period is perceived as a peak of settlement, irrigation infrastructure, and agricultural productivity, this is potentially misleading due to broad ceramic periodisation and additional chronological uncertainties. Assigning specific causes to these changes (including climatic factors) requires the establishment of a tighter chronology.

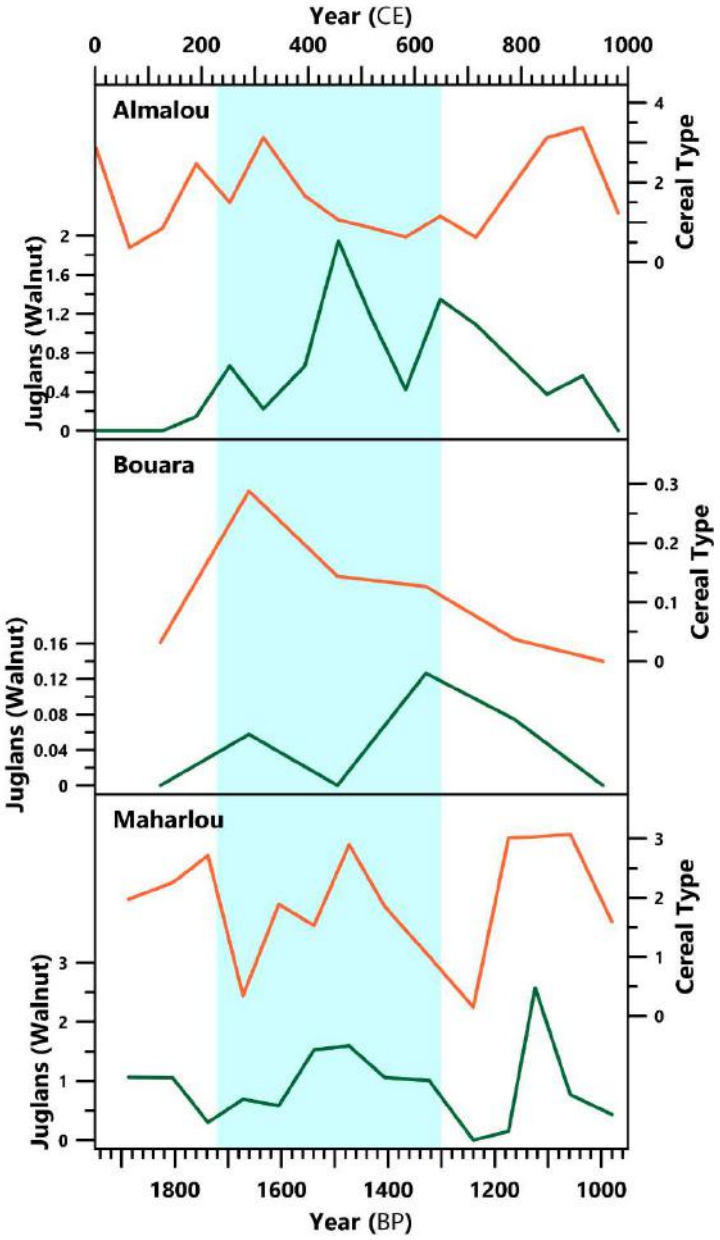

Figure 44. Cereal (orange) and walnut (green) pollen percentages from lake palaeoenvironmental records from the European Pollen Database: Almalou, Bouara and Maharlou (Djamali et al., 2009a; Saeidi Ghavi Andam et al., 2020)

When was the expansion?

The Seshat databank, a systematic synthesis of archaeological and historical knowledge of historical polities into nine multi-variate characteristics, has been statistically assessed with Principle Component Analysis (PCA) and the first component (PC1) was found

to reflect societal "complexity", The SE is one of the databanks case-studies, with the nine variables assessed for each century: polity population, polity territory, capital population (Ctesiphon), hierarchical levels, government complexity, infrastructure, information systems (i.e. record keeping), texts (publishing of literature), and sophistication of currency (Turchin et al., 2017, 2015; "complexity" data in Figure 43). Though historical quantification in projects such as Seshat suffers from inherent subjectivity and value judgments, and will require updating as future research is conducted, the record is useful for contextualising and summarising current understanding of broad societal change (Slingerland et al., 2020; Turchin, 2018; Turchin et al., 2012). The largest increase in PC1 is observed in the 4th century CE, with two further large increases in the 6th and 7th centuries CE (Figure 43). These correspond to two historically-attested periods of economic growth and military success ("growth-phase" hereafter) for the SE: 309-379 CE and 498-622/628 CE (Figure 42).

Growth-Phase I

The first growth-phase is coincident with Shapur II (309-379 CE), the longest reigning monarch in Iranian history, who expanded Sasanian territory into eastern Arabia, Mesopotamia, the Caucasus, and Central Asia (Daryaee, 2009a; Pourshariati, 2008; Rezakhani, 2017). Eastern Arabia had been partially under the control of the Sasanians from the start of their reign, with cities founded there by Ardashir I (Potts, 1990). By the start of the 4th century CE, regions on the western and southern Persian Gulf (now NE Saudi Arabia, Bahrain, Qatar, UAE and N Oman) were no longer under Sasanian control and Arab tribes raided the coast of Fars (Gignoux, 1971; Kennet, 2007; Potts, 1990). Shapur II retaliated by leading a campaign across Arabia from 325 CE, reaching as far as Mecca and Medina, and founded cities in eastern Arabia by forced relocation of Arab tribesmen (Bosworth, 1983, 1999; Shayegan, 2004). It has been suggested that eastern Arabia experienced a marked decline in Late Antiquity, however (Kennet, 2007; Ulrich, 2011; see grave goods in Figure 43). Shapur II reignited wars with the Roman Empire, eventually expanding Sasanian territory further into Mesopotamia, Georgia and Armenia (Daryaee & Rezakhani, 2016; Sicker, 2000). In the east, the empire expanded into Gandhara-Punjab to the north and to Sakistan-Sindh and past the Indus River in the south, with the construction of cities in these regions. This followed an

invasion of eastern Iran by the Chionites, who had previously removed the Kushano-Sasanians from these regions (Rezakhani, 2017). The 4th-century increase in PC1 in the Seshat data can largely be interpreted as resulting from expansion into new territories and associated increases in population (Turchin et al., 2017). However, Shapur II also ordered the construction of new cities in the core territories (e.g. Eranshahr-Shapur) and the rebuilding of destroyed cities (e.g. Nisibis, Susa) (Daryaee, 2009a). Large-scale military complexes, forts and defensive walls were built from the 4th century CE, for example, Qal'eh Kharabeh and Fulayj (Al-Jahwari et al., 2018; E. Sauer et al., 2013, 2017). Expansion and construction, in addition to the establishment of the Sasanian hierarchical system and the completion of the Avesta, the sacred texts of Zoroastrianism, contributed to the rise in PC1 observed in the Seshat dataset (Daryaee, 2018; Turchin et al., 2015).

Growth-Phase II

The second growth-phase (498-622/628 CE) started with the second reign of Kavad I (498-531 CE) and ended following the second reign of Khosrau II (591-628 CE) (Rezakhani, 2016). Kavad I originally ruled from 488-496 CE but was usurped following exploitation of the beliefs of Mazdak, a Zoroastrian high priest, to enact reforms that undermined the power of the nobles and clergymen (Crone, 2012, 2016; Daryaee & Canepa, 2018). He collaborated with the Hephthalites to reclaim his throne and resumed administrative reforms, which were completed under his son and successor Khosrau I (531-579 CE; see below) (Schindel, 2013a). Kavad I's reforms included a re-evaluation of agricultural tax to ensure parity (Axworthy, 2008), creation of a Zoroastrian institution to aid the lower classes (Daryaee & Rezakhani, 2017), as well as infrastructure investment and a policy to block Byzantine trading in the Indian Ocean (Howard-Johnston, 2017; Seland, 2012). Proliferation of the Sasanian trade network is evidenced by 5th-7th century CE Sasanian silver coins, which are found in abundance across the Eastern Mediterranean and Middle East (Schindel, 2013b; Sears & Ariel, 2000), as well as further afield in China (Li, 2006; Skaff, 1998), Central Asia (R.N. Frye, 1993; T. Li, 2021), and even in Britain (Abdy & Williams, 2006). Kavad I also reignited the war with the Byzantines, capturing land in the Caucaus where he founded new cities and forts, for example, Ultan Qalası most likely dates to this period (Alizadeh, 2011). He also reclaimed

Khorasan from the Hephthalites (Rezakhani, 2017). Peace was made with the Byzantines following the succession of Khosrau I in 531 CE, which allowed a continuation of reforms and a focus on centralisation and consolidation of power (Canepa & Wiesehöfer, 2018; Sicker, 2000). A fixed agricultural tax was introduced, which meant that the treasury had a predictable income; the military was also reorganised with the establishment of the *dehqan* (entrepreneurial elite) class and their recruitment as cavalrymen (Farrokh, 2005, 2007). It was following these reforms that the perceived centralised and organised SE (described above) took shape. This enabled further successful military campaigning against the Byzantines c. 540-562 CE (Lawrence & Wilkinson, 2017; Sicker, 2000), the Hephthalites from 557-560 CE (Rezakhani, 2017), and the Kingdom of Aksum in Yemen from 570 CE (Bowersock, 2013; Schippmann, 2001; Yule, 2007). In the late-6th and early-7th centuries CE, wars with the Byzantines continued and the Sasanians conquered significant swaths of land. The Sasanian army fought battles to take important cities in Byzantine territory, including Antioch, Jerusalem, and Alexandria, and they even laid siege to Constantinople. The empire was at its greatest extent between 619 and 628 CE, including Yemen, the previous frontier zone in Mesopotamia, the Levant, and Egypt (Cameron et al., 2012; Whittow, 2011; Figure 41). The consistent military successes and increases in the state's territorial extent, administrative reforms, and infrastructure investment led to the increases observed in the Seshat PC1 variable from the 5th-7th centuries CE (Turchin et al., 2017, 2015; data in Figure 43).

The end of the Sasanian Empire

Following the end of the second growth-phase, the SE experienced a rapid decline. The Byzantine Emperor Heraclius retaliated against the Sasanians, invading Mesopotamia, and raiding towns along the Tigris (Sicker, 2000). This led to the humiliation of Khosrau II (590-628 CE) and a *coup d'état* against him by his son Shērōē, who later renamed himself Kavad II (Daryaee & Rezakhani, 2017; Pourshariati, 2008). Shērōē had his father and brothers executed, and made peace with the Byzantines by returning all their lost territories (Payne, 2014). After the death of Shērōē to the plague a few months later (Shahraki et al., 2016), civil wars broke out in the empire with 11 monarchs taking the throne between 628 and 632 CE (Daryaee and Rezakhani, 2016; Figure 42). Shērōē's Plague (627/8 CE) was centred on

Mesopotamia and is reported to have caused significant loss of life in the SE (>100,000 people) and was followed by another outbreak from 634-642 CE, which may be the same outbreak as the Amwas Plague in Syria (Bray, 2004; P. Christensen, 1993; Shahraki et al., 2016). Similar theories of mass death from plague in the Byzantine Empire have recently been questioned, however, and further investigation into these plagues for the SE is required to confidently establish impacts (Eisenberg & Mordechai, 2019; J. Luterbacher et al., 2020; Meier, 2020; Mordechai et al., 2019). The civil wars culminated with Yazdegerd III inheriting the throne at eight years old; however, many regional kings and governors had proclaimed independence, notably those in Arabia, and the empire had returned to a system akin to Parthian feudality (Kia, 2016; Pourshariati, 2008). The empires weakness emboldened attacks from the Göktürks in Central Asia and Khazars in the Caucasus, with Yazdegerd III eventually murdered in 651 CE in the city of Merv whilst attempting to flee from the invading Rashidun Caliphate (Wiesehöfer, 2010).

The actual impact of these developments on communities within Sasanian territories has been hotly debated (e.g. Soroush, 2020). A reduction in settlement numbers is observed in archaeological surveys (Figure 43) and it is suggested that irrigation infrastructure, which required governmental organisation for successful maintenance, "collapsed" in the early Islamic period as it was no longer maintained (Asadi et al., 2013). Similar trends towards the end of Late Antiquity are observed in the Byzantine Empire (e.g. Baird, 2004; Decker, 2018) and Kingdom of Himyar (see Fleitmann et al., 2021; Schippmann, 2001). However, as mentioned above, ceramic chronologies are often broad for the Sasanian Period, so an overlap with the early Islamic period is common. Identifying the "end" of occupation therefore presents a significant challenge (Mousavi & Daryaee, 2012; Neely, 2016). For example, in Deh Luran only 54% of Sasanian/7th century CE Islamic settlements contain evidence of 8th/9th century CE Islamic occupation (Neely, 2016). Whilst this perhaps demonstrates a significant decline, it can be only vaguely dated to some point during the late Sasanian and early Islamic periods, which could be before, during, or after the Rashidun invasion at any given site. However, Soroush (2020, 2014) convincingly argues that infrastructure was less influenced by the invasions than often presumed, with consistent investment in Lower Mesopotamia throughout the Sasanian Period and after. She suggests that a gradual decline in the quality of irrigation infrastructure occurred in the 9th/10th

centuries CE associated with downcutting of river beds that increased the cost of maintenance (Soroush, 2020; Walstra et al., 2010), whereas others suggest the same phenomenon may have resulted from power struggles and inter-dynastic wars (Alizaddeh et al., 2004; P. Christensen, 1993). Similarly, in the Mughan Steppe the chronology of abandonment of Sasanian settlements is unclear and may have occurred before or after the Islamic conquest of the region (Alizadeh et al., 2021). In the Persian Gulf, a reduction in site numbers at Bushehr (Carter et al., 2006) is mirrored in the Mohr, Lamerd, Dezhgah and Bastak districts (Asadi, 2010; Asadi et al., 2013; Askari Chaveri & Azarnoush, 2004). The abandonment of fortified sites in this region following the conquests, which acted as administrative centres for local agriculture, is suggested to have led to the observed reduction in settlements (Asadi et al., 2013).

In the palaeoenvironmental records described above, broadly speaking, pastoralism increased following the Islamic conquest, with a scaling back of arboriculture (Shumilovskikh et al., 2017). However, these changes are not clear in all records, being hampered by low sampling resolution and chronological uncertainties. The records also show varied changes; for example, peak cereal pollen is observed around the turn of the 4th century CE in Almalou and Bouara, followed by a decline (Figure 44; Djamali et al., 2009a; Gremmen & Bottema, 1991). Both Almalou and Maharlou suggest a reinvigoration of cereal agriculture around the start of the 9th century CE (Djamali et al., 2009a, b; Saeidi Ghavi Andam et al., 2020). More samples from existing records, new records, and tighter chronological precision are required to improve our understanding of these changes.

6.2.3. Climatic fluctuations and agricultural resilience in the Sasanian Empire

This section examines the ability of the SE to withstand climatic fluctuations (resilience hereafter; Brand and Jax, 2007). Firstly, modern spatial and seasonal variability of climate are summarised to establish "baseline conditions"; these are crucial for the following assessment of which climatic variables will be most impactful. Secondly, mechanisms through which climate could impact the SE are investigated. Finally, adaptations that improve resilience to climatic fluctuations are assessed.

Modern Climate

The region previously occupied by the SE was large. Currently this area has large ranges of precipitation and temperature, various seasonal patterns, and high inter-annual variability, with many regions being water-stressed (Barlow et al., 2016; Gerlitz et al., 2020). Hydrological conditions are the focus here, due to their relative heterogeneity, importance for agriculture, and propensity to be recorded in high-resolution palaeoclimate proxies.

To establish spatial and seasonal variability, annual and monthly precipitation data from 10 weather stations were collected from the KNMI Climate Explorer (van Oldenborgh, 2020; Peterson & Vose, 1997), and are collated in Figure 45. Stations across the western SE with >50 years of data (r=52-120, m=86) were selected. Average annual precipitation is relatively low (82-380mm) in most of the analysed weather stations; Lenkoran is the exception (1181mm) due to its coastal location (-13m asl) and influence from the Caspian Sea. The two northern stations, Yerevan (Armenia) and Lenkoran (Azerbaijan), have a winter-spring wet season and experience an autumn precipitation peak (Figure 45). Cyclones from the Black Sea and Caspian Sea transport moisture through the Caucasus and northern Iran, which precipitates as air masses rise over the regions mountains (Evans et al., 2004; Maslova et al., 2020; Molanejad et al., 2015; Molavi-Arabshahi et al., 2016). All other weather stations have a single winter-spring wet season (Nov-Mar; 72-95% of annual precipitation) and very dry summers (Jun-Aug; 0.02-2.89%). Winter precipitation originates from westward storm tracks and winter cyclones originating in the North Atlantic or Mediterranean, and is enhanced as these air masses rise over mountains (Ulbrich et al., 2012). Inversely, precipitation is reduced on the lee side of the mountains and further away from the coasts due to rainout (Evans et al., 2004). For stations near the southern coasts (Basrah, Bushehr, Jask, Seeb), the wet season has a distinct winter peak (Nov/Dec-Feb), whereas at the inland stations (Mosul, Tehran, Baghdad, Kerman) precipitation is more evenly distributed across winter and spring (Nov-Apr). Conditions are exceptionally hot and dry in Iran, and especially in the southern deserts (e.g. average annual precipitation at Jask and Seeb is 115 and 82mm, respectively; Djamali et al., 2011; Mildrexler et al., 2006), caused by the subtropical high system blocking westerly frontal systems in the summer (Babaeian & Rezazadeh, 2018).

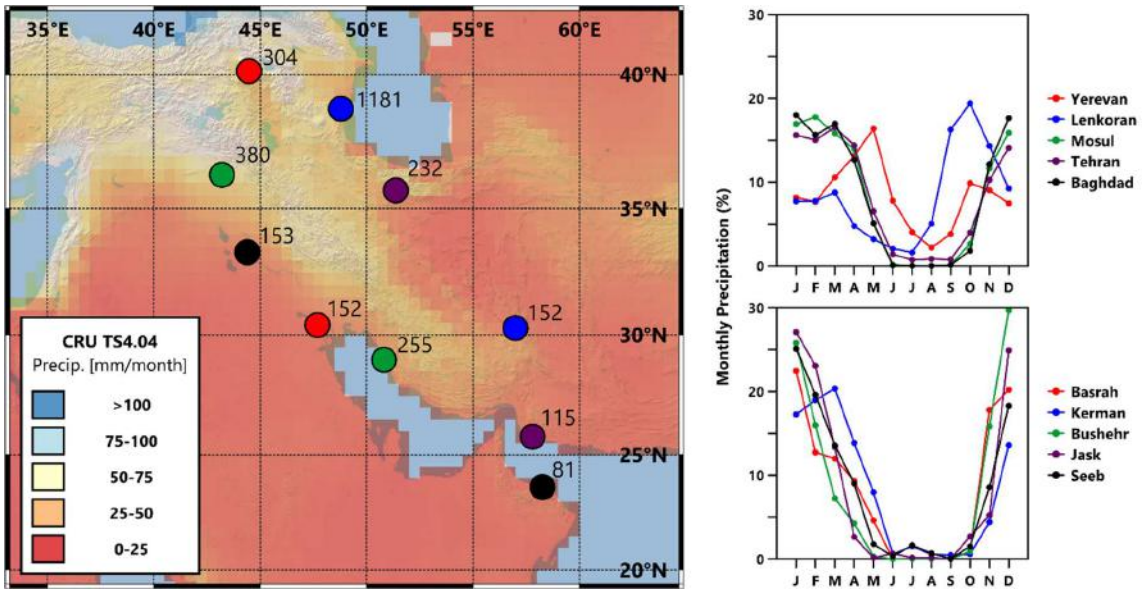

Figure 45. Modern precipitation in Sasanian territories. Map shows CRU TS4.04 (1901-2019) averaged monthly precipitation (University of East Anglia Climatic Research Unit et al., 2020). Coloured circles represent weather stations, labelled with their average monthly precipitation and matching with their seasonality of precipitation graphs (right). Weather stations with the greatest number of years with data (>50) were selected (Range: 52-120, Mean: 86). Weather station data from (Peterson and Vose, 1997). All data collected from the KMNI climate explorer (van Oldenborgh, 2020).

Positive phases of the North Atlantic Oscillation (NAO) may decrease precipitation and Tigris-Euphrates streamflow (Cullen et al., 2002; Cullen & DeMenocal, 2000); however, examination by Evans et al. (2004) suggests this influence from the NAO may be limited to the southern Zagros region. Total solar irradiance (TSI) and volcanic activity also influence climatic conditions in the Middle East, with particularly strong cooling and drying from volcanic eruptions during positive phases of the NAO (Dogar et al., 2017; Mendoza, 2005). The relationship between precipitation, temperature, and forcing mechanisms – the influences which determine climatic conditions – is ultimately, however, poorly understood.

Agricultural Productivity

Direct societal impacts from climate change are caused either by alterations of agricultural productivity, or loss of human life and infrastructural damage during short-term

cataclysmic events (SCEs: heat-waves, storms, floods) (Mordechai, 2018). Consequently, secondary impacts are experienced through agricultural productivity's relevance to the economy (see below; Zhang et al., 2011). Potential Agricultural Productivity (PAgP: Contreras et al., 2019) is determined by many natural factors, with the agricultural strategies employed by humans contributing to the actualised productivity of a region (discussed below). For PAgP (also called bio-productivity or plant growth), three climatic variables have differing importance by region: water availability, temperature, and sunlight. Across the SE, the primary climatic constraint to PAgP is water availability (precipitation-evapotranspiration; "effective moisture" hereafter). However, temperature is a secondary constraint across the Fertile Crescent and sunlight is important in the Caucasus (see Nemani et al., 2003).

Whilst it is often assumed that higher temperatures and increased effective moisture will increase agricultural productivity, this relationship is not simple, especially in (semi-) arid regions (Haldon et al., 2014). The diverse conditions described above mean that impacts from specific climate changes vary per region. For example, relatively low average annual precipitation in most of the examined weather stations (82-380mm, see above) and the importance of effective moisture to bio-productivity, mean that drier phases could be potentially devastating to agriculture in many regions. However, northern regions that experience high precipitation (e.g. 1181mm/yr at Lenkoran), may be relatively unafflicted by hydroclimatic fluctuations. Inversely, whilst warmer temperatures in northern regions may promote high bio-productivity, in the exceptionally hot deserts, cooler temperatures may promote plant growth by reducing evaporation, thus increasing effective moisture (Gohari et al., 2013). Rainfed agriculture, which requires minimum precipitation of 250mm/yr (Hole, 2007), is not possible in many regions under current climatic conditions (Gholikandi et al., 2013). The three most northern weather stations (Yerevan, Lenkoran and Mosul) and Bushehr on the western Persian Gulf experience >250mm/yr on average (Figure 45), opening the possibility for rainfed agriculture. Regions with precipitation close to the minimum may be particularly vulnerable to increased climatic variability, if a community adapts to utilise rainfed agriculture and conditions subsequently deteriorate (Hole, 2007). Extreme heat and low precipitation led to a reliance on hydraulic infrastructure and diverse agro-pastoral strategies to overcome deficiency of effective moisture (Seyf, 2006; Shumilovskikh et al., 2017; Soroush, 2020).

Agricultural Adaptations

In Mesopotamia, the Babylonian Talmud, written about Jewish communities during the 3rd-5th centuries CE and completed around the turn of the 6th century CE, reveals an extensive list of cultivated crops and animals (Listed in Table 5; Elman, 2004). Palaeoenvironmental records suggest that arboriculture was important, particularly walnuts (Juglans pollen) and pistachios (Shumilovskikh et al., 2017). Animal exploitation, as discussed in the Talmud and revealed by zooarchaeological remains, was also extensive and relied mainly on sheep/goats and cattle, with pigs largely absent from peoples diet perhaps as a result of Semitic influence on Zoroastrianism (Foltz, 2010; Gignoux, 1994; Mashkour et al., 2017). Agricultural strategies included: fallowing ground, i.e. leaving it unplanted for a year; crop rotation, i.e. planting different crops sequentially to improve soil quality; intercropping, i.e. growing crops in proximity that benefit one another; and manuring fields, normally by arrangement between land owners and herders (Adamo & Al-ansari, 2020; Decker, 2009a; Elman, 2004).

Table 5. List of agricultural produce and animals raised and bred for meat, in order of importance, in Sasanian Mesopotamia (3rd-5th centuries CE). Information is from the Babylonian Talmud, a description of contemporary Jewish communities (Adamo & Al-ansari, 2020; Elman, 2004)

	Grains	Other crops	Animals
1	Wheat	Pulses	Sheep
2	Barley	Vines	Cows
3	Spelt	Dates	Oxen
4	Rye	Sesame	Chicken
5	Oats	Flax	Ducks
6	Rice	Vegetables	Geese
7	Millet		

Perhaps more important was the organised use, installation and maintenance of irrigation structures, such canals, dams, weirs, and qanats (Gyselen, 2002; Manuel et al., 2018;

Payne, 2014). Investments in irrigation unparalleled until modernity (Casana & Glatz, 2017) meant large areas of previously inarable land was now cultivated, and regions where rainfed agriculture was previously practiced had increased agricultural productivity. River-fed canal systems associated with the Tigris-Euphrates River system expanded. One of the largest Sasanian imperial projects was the hydraulic system at Shushtar, which comprised the Gargar canal and the Shadurwan weir-bridge. The Shadurwan is over 500m in length and created a reservoir in the Karun River (Alizaddeh et al., 2004; Campopiano, 2017; Moghaddam, 2012; Soroush, 2014, 2020). The canal system at Shushtar,and others such as the Nahrawān, systematically gridded huge swaths of land, spanning hundreds of kilometres (Altaweel et al., 2019; Asadi et al., 2013; Hartnell, 2014). Canal systems and associated infrastructure were also common in the Mughan Steppe, along the Araxes River, and around the Persian Gulf, especially in Fars (Alizadeh & Ur, 2007; Carter et al., 2006; Hartnell, 2014; E. Sauer et al., 2017; Ur & Alizadeh, 2013).

Qanats, which utilise gravity transport of water from upland regions to arid plains through underground tunnels, were frequently used in the SE. They are particularly abundant in the Central Plateau east of the Zagros mountains (Beaumont, 1971), but are also found in the southern Iranian deserts, eastern Arabia, Mesopotamia and further west in Syria (Lightfoot, 1996; Manuel et al., 2018). Qanats are insensitive to hydroclimatic fluctuations, as they draw water from aquifers rather than rivers or rainfall, and, due to their subterranean nature, resistant to evaporation. This causes them to have a near-continuous flow that only varies slightly between wet and dry years (Kheirabadi, 1991; Manuel et al., 2014, 2018). Qanats require careful planning, construction, and maintenance but when managed successfully they significantly enhance both agricultural potential and security from short-term climate fluctuations (Beaumont, 1971; Semsar Yazdi & Semsar Yazdi, 2020).

Climatic factors are especially important for regions where agriculture is the key component of the economy, which is common in SW Asia and the history of Iran (Hijioka et al., 2014; Seyf, 2006). The Sasanian economy was primarily agricultural, which was enhanced by the irrigation described above (Canepa & Daryaee, 2018; Fakhar & Hesari, 2013; Hartnell, 2014). Centres with specialised artisans were established to manufacture commodities, which, in addition to agricultural produce and rare resources such as Persian Gulf pearls and precious metals, were traded across Eurasia and east Africa via maritime routes in the Arabian

and Caspian Seas, Indian Ocean, and Mediterranean, as well as over land on the Silk Route (Daryaee, 2003, 2009b; Frye, 1993; Richard N Frye, 1972; Howard-Johnston, 2017; T. Li, 2021; Majd & Taheri Sarparvar, 2016). Investments in the irrigation infrastructure, in addition to foundation of new cities and trade networks, all created institutions that could be taxed (Canepa & Daryaee, 2018). Taxation by the SE created exceptional wealth for the treasury, especially in the Late Sasanian Period following the reforms of Khosrau I.

In summary, as agriculture was the primary component of the Sasanian economy and the empire contains exceptionally hot and dry regions, hydroclimatic fluctuations had the potential to cause significant damage. However, careful management of irrigation infrastructure, diverse agro-pastoral strategies and techniques, and trade of non-agricultural products may have mitigated against some impacts.

6.2.4. Climate change in the Sasanian Period

Palaeohydrological conditions

For Sasanian Persia, eight available continental palaeohydrological records (Table 6) are the focus of this paper, due to the importance of effective moisture in determining potential agricultural productivity. Environmental and erosive conditions in arid environments lead to scarcity and unevenly distributed palaeoclimate records, mainly due to continental records (speleothems, lakes, trees) requiring adequate effective moisture to form (for speleothems, see Burstyn et al., 2019; Appendix B.1). The eight available records are thus limited to the western regions around the FC (Figure 41) and at high elevations (650-2500m asl), due to their intermontane nature. Of these, four are high-resolution (Neor, Gejkar, Kuna Ba, Hoti) and the other four are low-resolution (Van, Katalekhor, Zeribar, Mirabad). The high-resolution (33.5-46 samples/100y) group has an average of 2.63 years between each sample, whereas the low-resolution (0.3-1.5 samples/100y) group averages 111 years between each sample. The high-resolution records are utilised more frequently here as they are more reliable, with precise age-models and proxies which are confidently linked to regional hydroclimatic fluctuations at scales appropriate for analysis of human-environment interactions (Finné et al., 2011; Knapp & Manning, 2016). The reliability of the high-resolution

records is increased as each contains multiple proxies that corroborate each other. Furthermore, the Kuna Ba and Neor records are replicated across multiple speleothems and lake cores, respectively (Comas-Bru & Harrison, 2019; Sharifi et al., 2015; Sinha et al., 2019). The low-resolution records cannot be used to characterise short term palaeoclimate change; however, they can be utilised for assessing climatic differences between centuries.

Table 6. Palaeohydrological records in Sasanian Persia (see Figure 41 for locations). Interpretation is that given by the original authors. Resolution is averaged across all data for the first millennium and high-resolution archives are in bold. All records, except Neor, will show a winter-bias due to seasonality of precipitation.

Archive	Proxy	Interpretation	Resolution (samples/100y)	Elev. (m asl)	Reference(s)
Lakes:					
Van	$\delta^{18}O$	Humidity	0.8	1648	Wick et al., 2003 Barlas Şimşek & Çağatay, 2018
Neor	Ti	Dust Influx/ Aridity	**33.5**	2500	Sharifi et al., 2015
Zeribar	$\delta^{18}O$	Seasonality/ Precipitation Amount	1	1300	Stevens et al., 2001
Mirabad	$\delta^{18}O$	Seasonality/ Precipitation Amount	0.3	800	Stevens et al., 2006
Caves:					
Katalekhor	$\delta^{18}O$	Precipitation Amount	1.5	1719	Andrews et al., 2020
Gejkar	$\delta^{18}O$	Effective Moisture	**46**	650	Flohr et al., 2017
Kuna Ba	$\delta^{18}O$	Precipitation Amount	**33.6**	660	Sinha et al., 2019
Hoti	$\delta^{18}O$	Precipitation Amount	**39**	800	Chapter 5

From the raw palaeoclimate proxy data (Figure 46), centurial z-score averages were calculated for all records (Figure 47a) and decadal z-score averages were calculated for the high-resolution records (Figure 47b). Z-scores are standardised units which enable simpler comparison of different variables, calculated by dividing the difference between a value and the dataset's mean by its standard deviation. In the records discussed in this paper, positive

(negative) z-scores represent conditions drier (wetter) than mean conditions. An average of all z-scores was calculated for each resolution, which broadly characterises climatic conditions across western Sasanian Persia. However, as records are not always in agreement, likely due to spatial heterogeneity of climatic conditions and the different character of each record (emphasised in Chapter 3), this calculated variable will miss sub-regional palaeoclimate change.

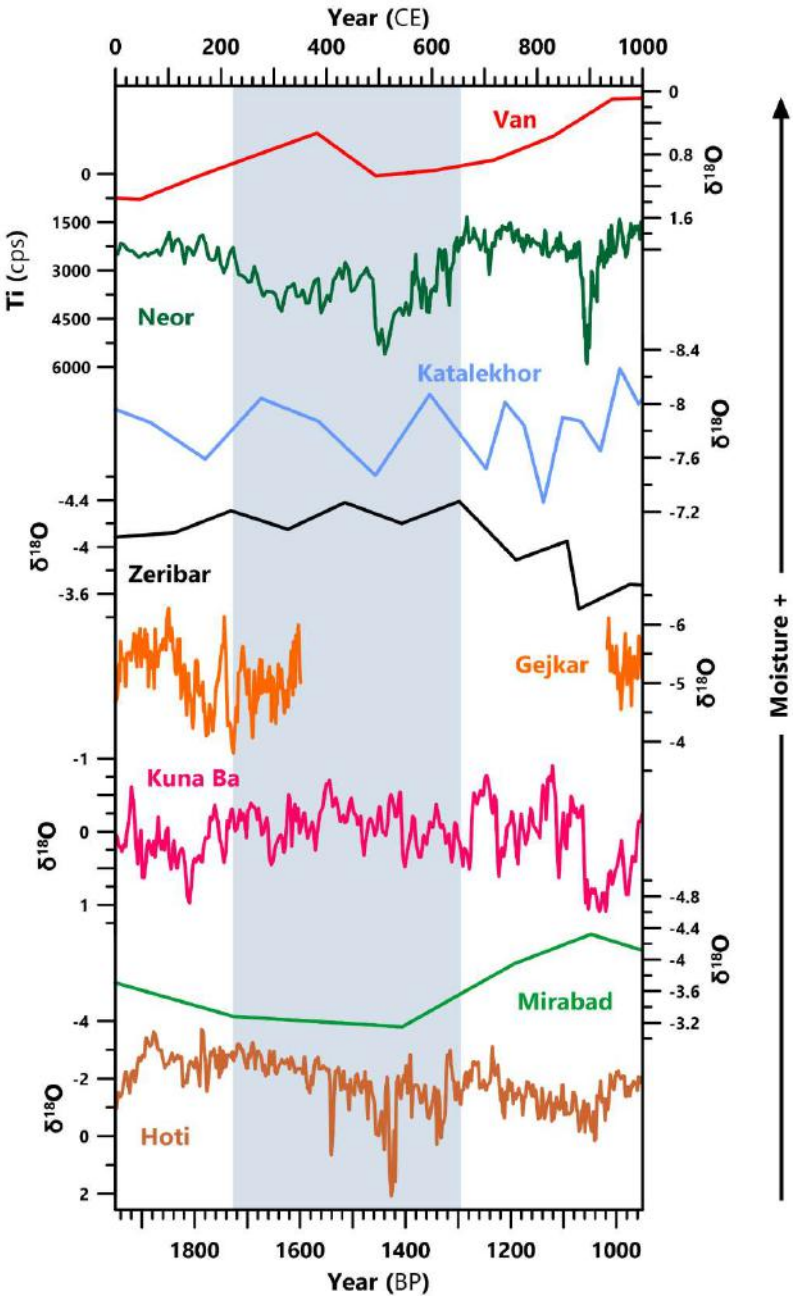

Figure 46. Palaeoclimate records in the Sasanian Empire, aligned from N-S. Records are aligned so that peaks represent enhanced precipitation/wet winters. Locations in Figure 41 and metadata in Table 6.

The palaeoclimate proxy records reveal significant variability during the Sasanian Period (Figures 45 and 46). From the start of the common era, the high-resolution records indicate that effective moisture was increasing, until a peak in the first century CE. Following this, effective moisture declines at Katalekhor, Gejkar, Kuna Ba and Hoti caves, reaching a low between 125 CE and 175 CE, which is reflected in the centurial average z-score (Figure 47a). A short-lived amelioration of climate is then observed, in the Kuna Ba and Gejkar records, before a return to arid conditions preceding the Sasanian takeover from the Parthians (200-220 CE). For the remainder of the third century, effective moisture is more stable and is increasing in some records (Van, Katalekhor, Gejkar, Kuna Ba) but decreasing in others (Neor, Zeribar, Hoti). From 300-480 CE, effective moisture is relatively stable (Figure 47b), with increases in some records (Van, Neor Zeribar, Gejkar, Kuna Ba). The centurial average z-score shows a generally dry 5th century CE, influenced by the declines at Van and Katalekhor, as well as the drier conditions in the late-5th century CE suggested by Neor and Hoti. Drying from ~480 CE is arguably the most significant of the palaeoclimatic shifts in these records. A period of very low effective moisture is suggested by the Van, Neor, Katalekhor and Hoti records at ~480-540 CE. In the Neor and Hoti decadal averages, the 510s and 520s have the driest conditions, respectively. However, in the high-resolution Kuna Ba record a less significant shift is observed and comes later at ~540 CE. Somewhat drier conditions are observed in all records during the 6th century CE, enhancing the centurial and decadal averages (Figures 46a and 46b).

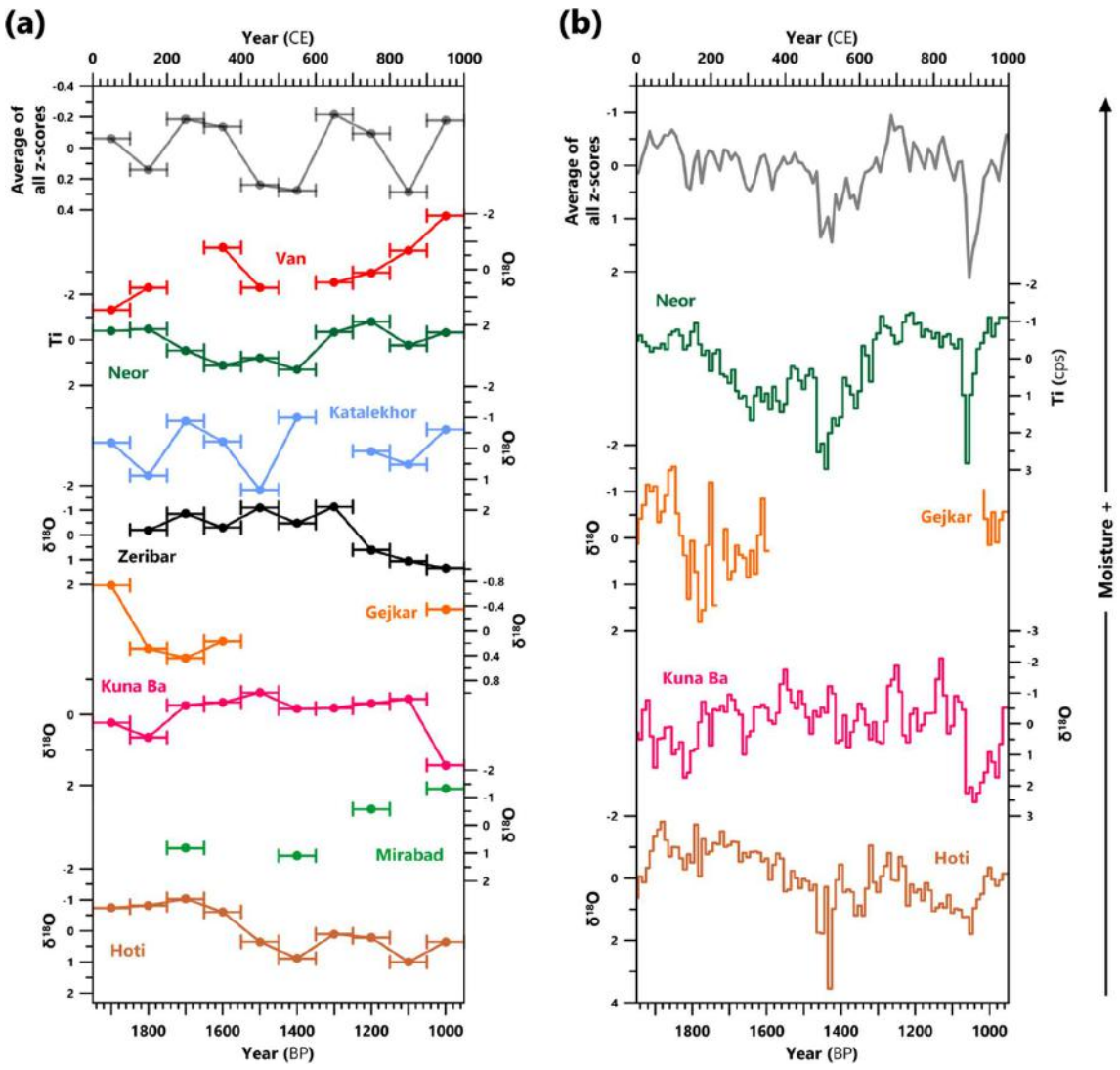

Figure 47. Centurial (left) and decadal (right) average z-scores for palaeoclimate records in the Sasanian Empire, aligned from N-S. Records are aligned so that peaks represent enhanced precipitation/wet winters. Averages of all z-scores are displayed at the top of both graphs, decadal average was calculated using only the high-resolution records.

It is striking that most of the palaeoclimate proxies suggest a dry phase that starts prior to the 536 CE dust-veil event (DVE)(see below). This historically-attested event arose from three volcanic eruptions, which added aerosol to the stratosphere causing significant global forcing and triggering cold conditions across much of the northern hemisphere (Sigl et al., 2015; Toohey and Sigl, 2017). The end-date of this period is uncertain, possibly being sustained for over a century due to ocean and sea-ice feedbacks or further eruptions (The "Late Antique Little Ice Age" (LALIA); 536-650 CE) (Büntgen et al., 2016; Helama et al., 2018;

Peregrine, 2020) or lasting just over a decade "536-550 CE climate downturn" (Newfield, 2018). Whilst it is a possibility that the drying observed prior to 536 CE is merely due to dating inaccuracies and the reduction in effective moisture in all records is caused by the DVE, it is unlikely that a similar error would occur in multiple records dated with different techniques (radiocarbon, uranium-series). Furthermore, palaeoclimate proxies from surrounding regions - the Aegean (Skala Marion, Trichonida, Mavri Trypa), Anatolia (Sofular, Nar, Kocain), the Levant (Jeita, Kfar Giladi, Soreq), and Central Asia (Tonnel'naya, Uluu-Too) – also suggest reduced effective moisture prior to 536 CE (Bar-Matthews et al., 2003; Cheng et al., 2016, 2015; Dean et al., 2018; Finné et al., 2017; Fleitmann et al., 2009; Morin et al., 2019; Psomiadis et al., 2018; Seguin et al., 2020; Wolff et al., 2017; Chapter 3). Further evidence comes from historical records, with an increase in the number of references to droughts in the Middle East from 500-540 CE (see Chapter 5; McCormick et al., 2012). Specific to Persia, there was a famine in 527-529 CE and a drought in 536 CE that ruined pasturage and forced 15,000 Arabs to cross into Byzantine territory (McCormick et al., 2012; Teleles, 2008).

After a brief amelioration of climate around ~560 CE, another slightly drier period is observed in the high-resolution records that ends 620 CE at Neor and Hoti, and 670 CE at Kuna Ba. The 7th century CE experienced further amelioration of climate, with the wettest conditions suggested by centurial average z-scores and, more specifically, in the 680s in the decadal average (Figure 47). After the end of the SE, another period of low effective moisture stands out from the palaeoclimate records. Between ~860-960 CE, exceptionally dry conditions are observed in all records except Van. Although not relevant for Sasanian history, this arid phase is especially pronounced and causes the 9th century CE average z-score and 890-920 CE decadal averages to be the driest of the entire first millennium CE (Figure 47). The onset of drier conditions around the start of the 10th century CE are also suggested by sea sediment core OS73 from the Gulf of Oman (Miller et al., 2016). This may be related to the start of the Medieval Climate Anomaly (MCA) (see Xoplaki et al., 2016).

Temperature and forcing mechanisms

The links between palaeohydrological changes, temperature, and forcing mechanisms are poorly understood in Southwest Asia (Chapter 3). In Figure 48, the decadal z-score

average of high-resolution effective moisture records is compared to temperature reconstructions and forcing variables (aligned W-E). High-resolution temperature reconstructions are primarily derived from studies of tree-ring width, which currently do not extend into the first millennium CE in Southwest Asia due to aridity. Within the region, reconstructions are all sea surface temperatures (SSTs) from sea cores and are thus low resolution records: the Aegean (Gogou et al., 2016: Figure 48e) and the Persian Gulf (Safarkhani et al., 2021: Figure 48g). External temperature reconstructions are also included as they are higher resolution and temperature variability is more homogenous than hydroclimatic fluctuations (Jürg Luterbacher et al., 2012). The PAGES 2k Consortium (2019) temperature anomaly dataset (Figure 48a) utilises 257 archives, of which none are from the Middle East. Summer temperature anomalies from tree-rings in the Alps (Figure 48d) and Altai (Figure 48h) mountain ranges are included (Büntgen et al., 2016). Records of total solar irradiance (TSI: Figure 48b) calculated from Greenland ice cores, the North Atlantic Oscillation (NAO: Figure 48c) and global volcanic forcing (GVF: Figure 48i) are also included for comparison (Franke et al., 2017; Sigl et al., 2015; F Steinhilber et al., 2009; Friedhelm Steinhilber et al., 2012; Vieira et al., 2011).

There is broad disagreement between the high-resolution (and external) temperature reconstructions and those produced from Middle Eastern archives. It is unclear whether these are caused by regional variation in climate, or chronological uncertainties in the sea sediment cores. Of note is relative stability in the high-resolution archives (especially from the Altai) until a decline in temperatures ~536 CE, coincident with the volcanically induced DVE. A relative stability is also observed in the decadal average z-scores (Figure 48f); however, fluctuations are seen in the individual palaeohydrological records (see above; Figures 45 and 46). Sea surface temperatures (SSTs) from the nearby Persian Gulf suggest more fluctuating conditions, with notable colder (~200, 380, 460, 710 CE) and warmer (~280-340, 410, 560-610 CE) phases (Safarkhani et al., 2021). Colder conditions from the mid-7th century CE are also suggested by low TSI (Figure 48b) and Aegean core M2 SSTs (Figure 48e).

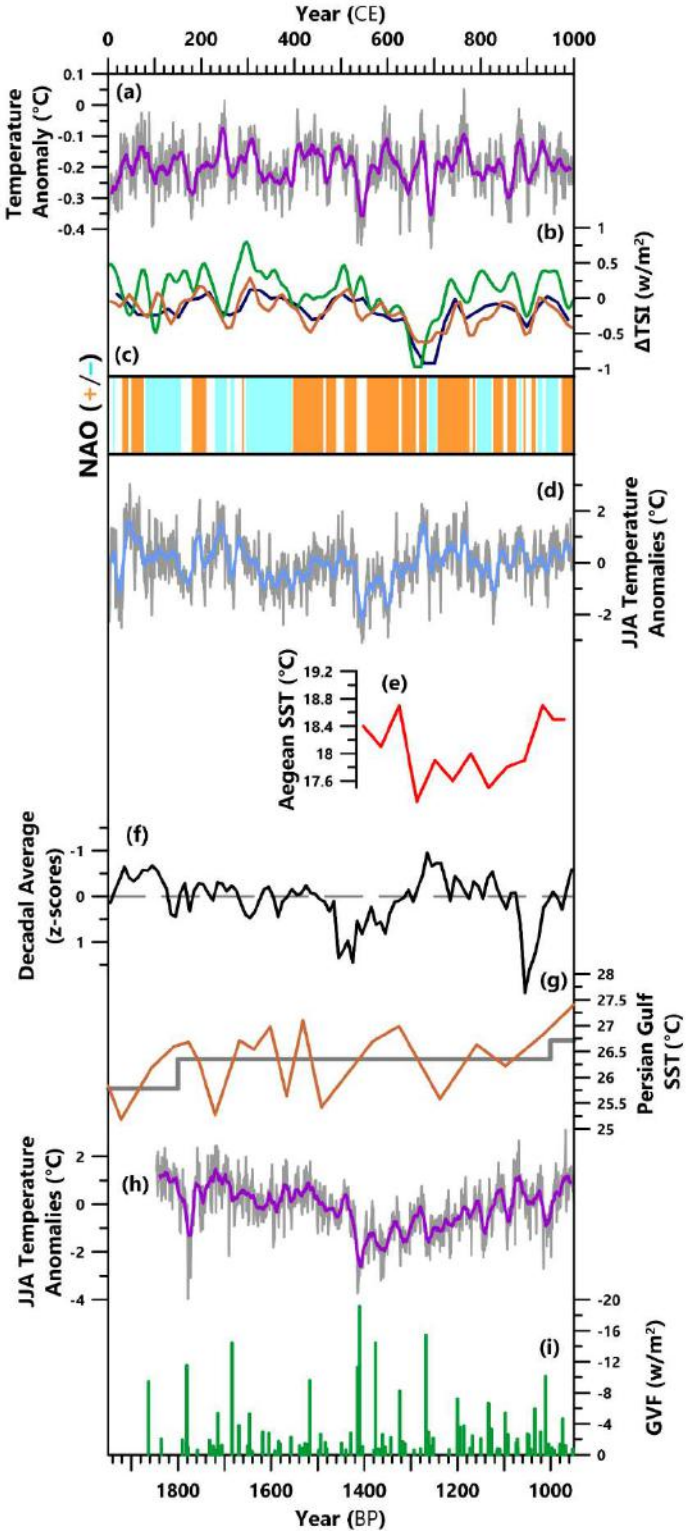

Figure 48. Temperature and forcing mechanism records, aligned from W-E. (a) Global temperature anomaly record (PAGES 2k Consortium et al., 2019). (b) Total Solar Irradiance as deviations from the 1986 value of 1365.57 w/m^{-2} (F Steinhilber et al., 2009; Friedhelm Steinhilber et al., 2012; Vieira et al., 2011). (c) Positive and negative states of the North Atlantic Oscillation (Franke et al., 2017). (d) European Alps summer (June-August) temperature anomalies (Büntgen et al., 2016). (e) Aegean sea

surface temperature sea sediment core record (Gogou et al., 2016). (f) Decadal z-score averages (from Figure 47b). (g) Persian Gulf sea surface temperature sea sediment core record, grey lines represent averages from sedimentary units (Safarkhani et al., 2021). (h) Russian Altai summer (June-August) temperature anomalies (Büntgen et al., 2016). (i) Global volcanic forcing from known volcanic eruptions (Sigl et al., 2015). Tree-ring temperature anomaly reconstructions with respect to 1961-1990 CE (a, d, h), displayed as annual records (grey) and 15-year averages (colour).

6.2.5. Socio-economic impacts from climate change?

In the previous sections, the complex and detailed history of the SE and high-quality palaeoclimate evidence from the Middle East has been contrasted with weaknesses in the archaeological and palaeoenvironmental data that is essential to establishing causal mechanisms between climatic and societal change. Expansion and, especially, the end of Middle Eastern empires and communities, are frequently studied in relation to environmental factors (e.g., Kaniewski and Van Campo, 2017; Sinha et al., 2019; Chapter 5). However, the enduring success and subsequent rapid decline of the SE has not been examined within its climatic context. Here, I present a discussion of climatic influences on the history of the SE, followed by suggestions for future research.

Climate-driven growth?

Disentangling the factors contributing to the two growth-phases for the SE is challenging. Considering current evidence, the role of climate appears negligible. The first growth-phase occurred during a relatively stable period of effective moisture, with a low centurial average z-score and increasing effective in some records (Van, Neor, Zeribar, Gejkar, Kuna Ba). Additionally, there is a peak of cereal pollen percentages during the 4th century CE in lake palaeoenvironmental records from Van, Almalou and the Bouara salt marsh (Djamali et al., 2009b, 2009a; Saeidi Ghavi Andam et al., 2020; Van Zeist and Woldring, 1978; Figure 44). From an environmentally-deterministic standpoint, it could be tempting to say that stable climatic conditions enabled the first growth-phase through increased agricultural productivity. However, the situation is more complicated. Wild grasses, which are the ancestors of cultivated cereals, release pollen in large quantities which is indistinguishable from that of domesticates (Bottema et al., 1990; Shumilovskikh et al., 2017; Zohary et al.,

2012). Persistently cooler temperatures are suggested for this period in the high-resolution global temperature reconstruction (PAGES 2k Consortium et al., 2019; Figure 48a) and the Alps temperature anomalies (Büntgen et al., 2016; Figure 48d), possibly related to a persistently negative NAO (Franke et al., 2017). Cool temperatures can have more severe effects on human health and societies than warming (McMichael, 2012), although maybe not in arid locations (Haldon et al., 2014; see above). Furthermore, the second growth-phase occurs alongside some of the driest (and possibly coolest) conditions of the entire Sasanian Period. The highest (driest) centurial z-score average for the Sasanian Period is the 6th century CE, influenced by particularly dry conditions in the period 490-550 CE (Figure 47). These are the same conditions that contributed to a significant decline in the Kingdom of Himyar (From ~480 CE; Chapter 5). Interestingly, Peregrine (2020) argued for both a negligible temperature change and no significant social change at the start of the LALIA in Sasanian Khuzestan – looking at the decades 525-535 and 536-546 CE. However, he also utilises the PAGES 2k Consortium et al. (2019) dataset for establishing temperature, but their 5° spatial reconstruction which is weak for this region due to lack of suitable temperature proxy datasets.

This second growth-phase presents many important questions that deserve future research: Did the Sasanians truly expand during this period of drier climatic conditions? What made the SE resilient to this period compared to other polities which experienced decline during similar climatic conditions? Is there any evidence to suggest drier climatic conditions were a *civilising factor* (Rosen, 2007) in this period, necessitating adaptation which contributed to growth? And, if climatic conditions had relatively little impact (as seems likely), then what were the important factors behind the growth-phases of the SE? This final question is the most complicated, but with current evidence it could be suggested that certain economic policies and military aspirations from particularly effective kings (Shapur II, Kavad I and Khosrau I) were important.

Climate-driven "collapse"?

Perhaps the most common hypothesis regarding climatic impacts on societies is that "extreme" hydroclimatic changes, combined with warming or cooling, caused failed harvests

thus leading to "collapse" (Degroot et al., 2021; Haldon et al., 2020). Whilst the overwhelming focus on negative impacts from climate mischaracterises human-environment relationships and these arguments often suffer from inherent environmental determinism, they remain sensational and frequent due to the current significance and fear of climate change. Studying factors that contribute to a polity or region's "collapse" – commonly interpreted as a loss of socio-economic complexity, inter-connectivity, and settlement and/or demographic density – is important however, to prevent negative events in the future.

As discussed above, the driest climatic conditions during the Sasanian Period pre-date the empires decline (from 628 CE) and end (651 CE) by over a century. The role of climate in the end of the SE thus also seems negligible. Internal conflict, protracted wars with the Byzantine Empire and Hunnic tribal confederations, and perhaps plague epidemics, that lowered the Sasanians' defensive capabilities before the invasion by the Rashidun Caliphate were more important. Additionally, the experience of this "collapse" on local levels appears to have been varied, with recent research suggesting settlement and investment in irrigation structures continued through the Late Sasanian and into the Early Islamic periods. Furthermore, degradation of infrastructure is often considered to result from harsh climatic conditions. In the SE, damage to infrastructure is later than the drier conditions and appears to represent a symptom of decline rather than a cause, with the requirement for organisation and planning no longer provided by the fragmented SE. It has previously been suggested that nomadic groups in Central Asia and the conquest by the early Caliphate may have been enabled or "pushed" by climatic conditions (Bulliet, 2009; Büntgen et al., 2016, 2020). Current evidence (Figure 49), however, shows no simple correlation with wars/invasions and climatic conditions.

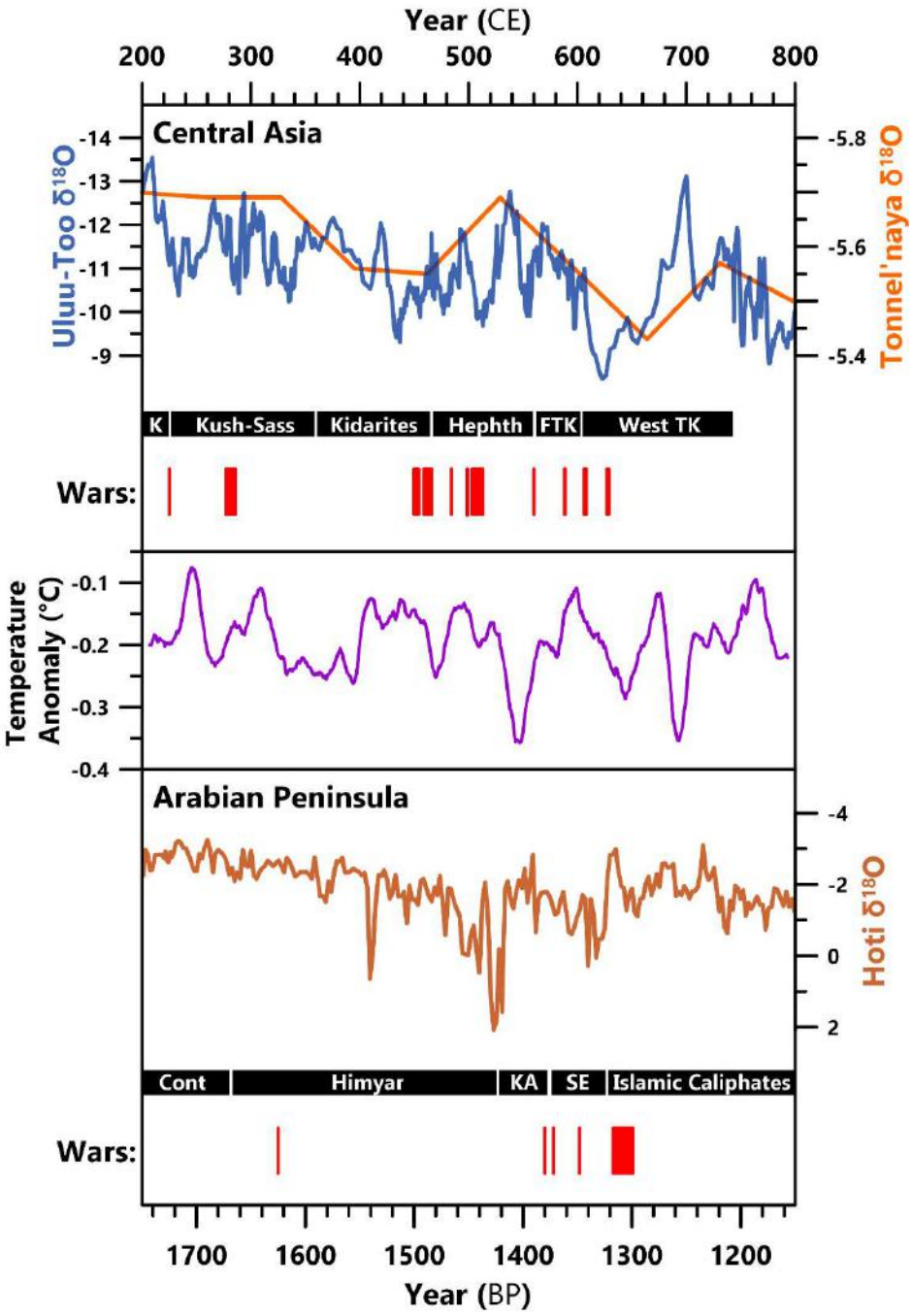

Figure 49. Sasanian wars with empires and kingdoms from Central Asia and the Arabian Peninsula compared to 15-year averages of global temperature anomalies (PAGES 2k Consortium et al., 2019; same as Figure 48a) and palaeohydrological records from Uluu-Too Cave (Wolff et al., 2017), Tonnel'naya Cave (Cheng et al., 2016), and Hoti Cave (Chapter 5). Records are aligned so that peaks represent enhanced precipitation/wet winters.

A useful comparison with the SE is the preceding Parthian Empire. Prior to their replacement by the Sasanians in 224 CE, they were distracted and exhausted which enabled

Ardashir I, and his father Papak, to consolidate their power in the south unabated (R.N. Frye, 2005). Firstly, conflict with Rome has been occurring since 54 BCE, but escalated in their final century, with invasions of Mesopotamia in 164-165 CE, 195-197 CE, and 216-217 CE, leading to the loss of northern Mesopotamia (Bivar, 1983; Katouzian, 2009; Sicker, 2000). Secondly, a maritime trade-route between India and the Red Sea became dominant; this diminished the Parthian economy which was centred around acting as conduits for international trade (Sicker, 2000). Thirdly, the Antonine plague (an outbreak of smallpox), likely had a devastating impact inside the Parthian Empire. The outbreak had spread along trade-routes to China, India and Mesopotamia, and was contracted by a Roman soldier during an attack on Parthian Seleucia 165 CE (Bivar, 1970, 1983; de Crespigny, 2007). In the Roman Empire, conservative estimates predict the disease killed ~1 million people (Gilliam, 1961; Haldon et al., 2018c). Evidence for the impact inside the Parthian Empire is lacking, however. The final factor previously considered is internal strife (civil wars and rebellions). In 207 CE, Vologeses VI inherited the Parthian Empire, but in 212 CE his brother, Artabanus V, rebelled and established himself as an independent ruler over Mesopotamia (Bivar, 1983). However, inversely to the Sasanian Period, current evidence suggests that climatic fluctuations do correlate temporally with these changes. Two periods of low effective moisture (125-175 CE and 200-220 CE) can be seen in Figures 45 and 46, especially in the Kuna Ba and Gejkar Cave records (Flohr et al., 2017; Sinha et al., 2019) and are perhaps also evidenced in the Neor, Katalekhor and Hoti records (Andrews et al., 2020; Fleitmann et al., 2021; Sharifi et al., 2015). A cold spell is also observed in the high resolution temperature reconstructions from 175-200 CE (Figure 48). Hatred of the Parthians by Ardashir I and subsequent Sasanian kings, however, appears to have been more related to a belief in a divine right to rule and the non-traditional Parthian decentralised system of leadership (see Bosworth, 1999). There is no clear link between these factors and the climate change discussed above. The decline and eventual end of the Parthian Empire does not require climatic change to be explained. Future work may highlight it as one of several factors leading to rebellion against Parthian; however, this seems unlikely as new historical sources (which are lacking) would be required to ascertain a causal connection.

6.2.6. Conclusions and future research agendas

In conclusion, current evidence suggests that the impact of climate change on the SE was negligible, despite experiencing the same conditions that had significant societal impacts on other contemporaneous polities (e.g. Chapter 5). However, it must be stressed that further work is needed is four important research areas to increase the confidence of conclusions.

1. Palaeoclimate records: Due to high spatial variability of climatic conditions, additional palaeoclimate records are required. More records from the Zagros Mountains and Fertile Crescent (Gejkar, Kuna Ba, Shalaii caves) covering Late Antiquity are required to discern what makes the Kuna Ba record different. The shift to drier conditions observed pre-500 CE is observed at Hoti Cave (Oman) and Neor Lake (N Iran), as well as in records from the Aegean, SW Turkey, and the Levant, appears to be a large-scale phenomenon. Disentangling the various influences (cave-specific, the NAO, shifts in the storm track, topography etc.) on records will be crucial for understanding climatic variability. More strikingly, there are large gaps in the network of records that need filling: the eastern parts of the SE (no records between 50-70°E), the Caucasus, the Persian Gulf. Furthermore, there are no high-resolution palaeotemperature records from the Middle East, and the lower-resolution records appear to disagree with reconstructions from external regions.

2. Archaeology: chronological uncertainty in archaeological evidence is one of the biggest challenges to assessing the HCS for the SE. Additional excavations in the region are challenging due to geopolitical tensions (Bernbeck, 2012). However, targeted excavation of a large Sasanian city could provide a tighter ceramic chronology, which could then be utilised to re-evaluate and improve existing datasets (Adams, 2006).

3. Agricultural productivity: To establish causal links between climatic change and societal impacts for the SE, examination of PAgP and agricultural resilience would be invaluable; however, more data is required for this (Turchin et al., 2021). Additional pollen or plant macrofossil datasets with higher sampling resolutions are required to reconstruct past agricultural practices. Whilst a few of these datasets have stronger sampling resolution (Almalou, Maharlou), most only contain one or two palynological samples during the Sasanian Period and all suffer from significant chronological uncertainties. Stronger datasets of agricultural change (and productivity) would enable examination of the link between

climatic and environmental change, which is the primary mechanism through which climate impacts people.

4. Micro-regional case studies: Perhaps the most important next step would be to identify regions with high-quality archaeological, palaeoenvironmental and palaeoclimate datasets, and study influences on a micro-regional scale. The importance of this strategy has been emphasised (Chapter 3) and demonstrated (Chapter 4) elsewhere. Suggested regions, which fulfil most of the data requirements, are the Diyala Plain (requires a stronger archaeological chronology), Mughan Steppe (requires pollen data) and the areas surrounding the Gorgān Wall (requires a palaeoclimate proxy).

Further investigation of climatic impacts on the SE, Iran, and the Middle East more broadly, may provide information that can help to mitigate against future climate change. For example, increased use of qanats may be crucial for continued occupation of arid regions (Gholikandi et al., 2013; Manuel et al., 2018; Seyf, 2006). This will be especially important as the region is projected to experience some of the most extreme local conditions resulting from climate change (Giorgi, 2006; Mansouri Daneshvar et al., 2019).

Acknowledgements and data

This work was supported by the AHRC South, West and Wales Doctoral Training Partnership (Grant AH/L503939/1 to MJJ).

This research employed data from the European Pollen Database (europeanpollen-database.net) and the work of contributors to the database is gratefully acknowledge. I would like to thank Maria Rabbani for her assistance with the pollen data and useful feedback.

This research employed data from the Seshat Databank (seshatdatabank.info) under Creative Commons Attribution Non-Commercial (CC By-NC SA) licensing. I would like to thank Daniel Hoyer for his assistance understanding the codebook and datasets.

This research employed data from the KNMI Climate Explorer (climexp.knmi.nl) and the work of contributors, particularly Peterson & Vose (1997) is gratefully appreciated.

Chapter 7: Summary discussion and conclusions

The overall aim of this thesis was to improve understanding of the socio-economic impacts of climate change during Late Antiquity (3rd-7th centuries CE). There were two key avenues of research, as described in the introduction. Firstly, two new speleothem-based palaeoclimate archives were produced to address spatio-temporal gaps in coverage (from Kocain and Hoti caves: Chapters 3 and 5) and existing palaeoclimate records were compiled to establish current understanding of Late Antique climate (Chapters 2, 3, 5 and 6). Secondly, palaeoclimate data was compared with palaeoenvironmental, archaeological, and historical evidence of socio-economic change on both micro- and macro-regional (polity-wide) scales (Chapters 4, 5, and 6). Production of the Kocain Cave palaeoclimate record (Chapter 3) and a settlement dataset based on volume 8 of the *Tabula Imperii Byzantini* (Chapter 4), made available high-quality and proximate evidence for climatic, environmental, and socio-economic change for Byzantine SW Turkey. This enabled micro-regional analysis, which had previously been stated as an important next step to confidently establish human-environment interactions (Haldon et al., 2014). Two further, larger-scale, case studies were then explored for states which had previously seen little investigation of HCS: the Kingdom of Himyar (Chapter 5) and Sasanian Empire (Chapter 6). The three case-studies were examined in chapters presented as individual journal articles containing their own discussion and conclusion sections. In this final chapter, the key findings from each discussion are summarised to address four key research questions:

1. **Palaeoclimatology** (Section 7.1):
    a. How did climatic conditions change in the EMME region during Late Antiquity?
2. **History of Climate and Society** (Section 7.2):
    a. To what extent did changing climatic conditions impact societies and their economies?

b. Was climatic change an important factor in the decline of empires and kingdoms in the 6th and 7th centuries CE?
c. Do micro-regional case-studies improve our understanding of socio-economic impacts from climate change?

By these means, the overall contribution of this thesis to our understanding of Late Antique palaeoclimate and its relative impact on socio-economic changes, recurrent themes, and directions for future research are examined.

7.1. Palaeoclimatology

7.1.1. Kocain Cave

Multi-proxy data from Kocain Cave (Figure 50; Chapter 3; Appendix A.1) provides the first highly-resolved (sub-annual) and well-dated palaeohydrological record covering the late Holocene for SW Turkey. Existing records either did not cover this period, in the case of tree-rings, Lake Salda and Dim Cave (Akkemik & Aras, 2005; Danladi & Akçer-Ön, 2018; Heinrich et al., 2013; Köse et al., 2011; Rowe et al., 2020; Touchan et al., 2007; Ünal-İmer et al., 2015, 2016), or had lower resolutions (Gölhisar: Eastwood et al., 2007). From the Ko-1 stalagmite, 25 uranium-series ages were extracted to establish the sample chronology; eight suffered from significant detrital contamination ($^{230}Th/^{232}Th$ ratios <30) and were excluded from the *StalAge* model. The age-depth model was supported by two lateral shifts in the speleothem growth-axis which could be linked to historically-attested earthquakes in the region. Whilst growth-axis deviations and other impacts from earthquakes, such as breakages, have previously been used to date earthquakes (Ferranti et al., 2019), they have not been linked to catalogues of known earthquakes to support speleothem age-models. Stable-isotope samples ($\delta^{18}O$ and $\delta^{13}C$) were micromilled from Ko-1 at 0.3 and 0.5mm increments, providing a total of 370 measurements that cover 3,366 years, 1366 BCE – 2000 CE (3316 – -50 BP) at an average resolution of ~9.3 years between samples (0.11 samples per year). $\delta^{18}O$ and $\delta^{13}C$ were interpreted as being influenced by effective moisture, as well as precipitation amount and biological activity, respectively.

LA-ICP-MS was utilised along 25 laser-ablation paths to extract 31,503 samples of Ca, Mg, Sr, P, and Fe, at a 0.00516mm resolution. This covered 2,978 years, 973 – 2005 CE (2923 – -55 BP), with an average of 10.6 samples per year. LA-ICP-MS has seen extensive use in the geosciences (Chew et al., 2021; YongSheng Liu et al., 2013), forensics (Orellana et al., 2013), and archaeology (Dussiubieux et al., 2016), and its utility in speleothem analysis has been well-understood for over two decades (e.g. Roberts et al., 1999; Treble et al., 2005; Weber et al., 2017). However, prior to study of the Ko-1 speleothem, it had not been utilised to provide an ultra-high resolution, long-duration, record. The trace elements were presented as ratios with calcium and have individual interpretations. Mg/Ca and Sr/Ca were interpreted as having an inverse relationship to effective moisture, due to enhanced PCP during drier intervals (Fairchild et al., 2006; Treble et al., 2003; Tremaine & Froelich, 2013). Mg/Ca was the stronger record due to dissolution of dolomitic limestones with longer residence times, and less influence from other factors (Fairchild & Treble, 2009). P/Ca is enhanced when increased effective moisture promotes biological activity, releasing bio-available P that is transported during intense soil infiltration (Fairchild et al., 2001, 2007). Whilst P/Ca has previously been utilised successfully as a palaeoclimate indicator in speleothems (Fairchild et al., 2001; K. Johnson et al., 2006; Lewis et al., 2011; Treble et al., 2003), its significance and interpretation has been debated (Frisia et al., 2012). The Ko-1 speleothem provides an additional example of a sample where increases in P/Ca can confidently be linked to enhanced effective moisture via impacts from biological activity and soil infiltration, supported by strong negative correlations with Mg/Ca ($r=-0.60$, $p<0.05$) and Sr/Ca ($r=-0.87$, $p<0.05$), and visual similarities with the stable-isotope records. It is important to note that P/Ca may have also been impacted by accumulation of P on mineral surfaces during PCP (Lewis et al., 2011), which could account for the correlations. However, the interpretation of P/Ca as reflecting effective moisture would remain the same.

Important late Holocene climate changes were revealed by the Ko-1 record, including a double peak of arid conditions centred on 1150 and 800 CE and a dry/wet MCA/LIA pattern (noted as significant shifts in Chapter 3), as well as low effective moisture and precipitation during the 1st century BCE (discussed in Chapter 4). In Late Antiquity, a period of high effective moisture between ~330 and 460 CE is suggested by the Ko-1 proxies, followed by a

shift to lower effective moisture from ~460 CE, with further drying that lasted until at least 830 CE.

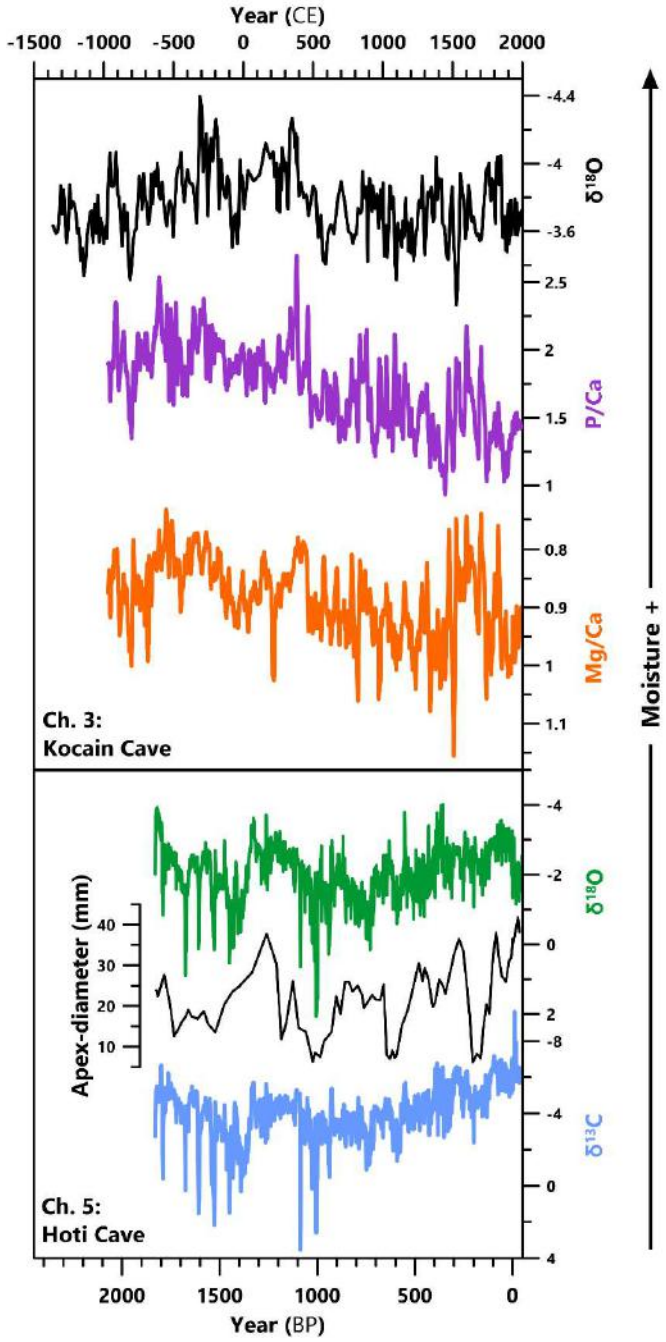

Figure 50. Summary of new speleothem-based palaeoclimate data resulting from the papers in this thesis. Kocain Cave trace-element ratios are displayed as 15-year averages, all other data is displayed in full.

7.1.2. Hoti Cave

Analysis of speleothem H12 from Hoti Cave (Chapter 5) similarly detailed important climatic changes during Late Antiquity, as the first highly-resolved and well-dated late Holocene record from Oman (Figure 50; Appendix A.3). Records in arid regions are especially sparse, or provide longer but lower-resolution records, due to the requirement of effective moisture for their formation (Appendix B.1). Existing speleothem records in the Arabian Peninsula either evidence climatic variability during wetter phases in the early Holocene or before, such as other samples from Hoti Cave and those from Mukallah Cave, and/or are from the southern extremities of Arabia where variations in the Indian or African summer monsoons are the key driver of their variability; for example, Qunf Cave and Defore Cave or the caves on Socotra Island (Hoq, Casecas, Dimarshim and Moomi caves) (Fleitmann et al., 2007; Nicholson et al., 2020; Rampelbergh et al., 2013; Shakun et al., 2007; see Appendices B.1 and B.4). Speleothem H12 is thus the only highly resolved and accurately dated record of Mediterranean influence in Late Antique Arabia. From the sample, 29 uranium-series ages were extracted to establish the chronology, with 9 that suffered from significant detrital contamination ($^{230}Th/^{232}Th$ ratios <30) not being utilised in the *StalAge* model. Stable-isotope samples ($\delta^{18}O$ and $\delta^{13}C$) were micromilled from H12 at 0.2 and 0.5mm increments providing a total of 1360 measurements that cover 2,627 years, 631 BCE – 1996 CE (2581 – -46 BP) at an average resolution of ~2.3 years. Apex diameter measurements were taken from H12, where possible, totalling 88 measurements with an average resolution of ~30 years between samples. Isotopes were interpreted as reflecting precipitation amount ($\delta^{18}O$) and effective moisture ($\delta^{13}C$), whereas apex diameter width reflects drip rates and precipitation. Key periods of persistently lower effective moisture were identified, one between 250 BCE – 25 CE and another between 480 – 1400 CE, with the driest period of the entire record dated to ~520 – 532 CE (Figure 50).

7.1.3. Comparison with other records

Examination of speleothem Ko-1 in comparison with other Turkish palaeoclimate records further stressed the marked heterogeneity of climatic conditions in the Eastern Mediterranean (Luterbacher et al., 2012; Ulbrich et al., 2012; Xoplaki et al., 2018; for the

Middle East, see Appendix B.1). Variation between records also results from the complexities of palaeoclimate analysis, including different responses from each record to palaeohydrological change and chronological uncertainties (Jones et al., 2019). In Turkey, there are two other high-resolution late Holocene records, one from Lake Nar (Dean et al., 2015, 2018; Jones et al., 2006) and another from Sofular Cave (Fleitmann et al., 2009; Göktürk et al., 2011). These records and low-resolution archives from Turkey frequently exhibit inverse climate changes to the Ko-1 record (Figure 51). In Late Antiquity, a marked drier phase is observed starting ~300-350 CE, followed by a shift to wetter conditions at ~500-550 CE (Nar, Sofular, Tecer, Van) (Barlas Şimşek & Çağatay, 2018; Dean et al., 2018; Fleitmann et al., 2009; Kuzucuoğlu et al., 2011). During the MCA and LIA, a wet/dry pattern is evidenced by other Turkish archives (Nar, Sofular, Burdur, Salda, Iznik) (Danladi & Akçer-Ön, 2018; Dean et al., 2015; Fleitmann et al., 2009; Tudryn et al., 2013; Ülgen et al., 2012). Discrepancies among these records illustrate high spatio-temporal heterogeneity of climatic conditions and our limited understanding of the mechanisms behind these differences. A dense network of highly-resolved and precisely-dated palaeoclimate records is required to address these challenges, as stated in Chapter 2. Speleothems Ko-1 and H12 address two of the identified gaps in coverage, but many remain for Late Antiquity (the eastern Aegean, eastern Turkey and the Caucasus, Syria and western Iraq, across the northern AP and eastward of the FC) and other periods.

The persistent wetter phase during Late Antiquity (330-460 CE) revealed by Ko-1 is supported by evidence from the cave and local palaeoenvironmental records, and is likewise observed in coastal records around the Eastern Mediterranean. Inside the cave, a large Roman cistern dated after 312 CE and high Fe/Ca ratios on Ko-1 that evidence mobilised dust from the cave floor, combined with a regional increase in mountainside goat herding (De Cupere et al., 2017; Fuller et al., 2012; Izdebski, 2012; Poblome, 2015) and soot layers that demonstrate fires in the cave (Koç et al., 2020), suggest use of the cave during a period of greater spring flow. This emphasises the importance of understanding cave history for the interpretability of speleothem records. Locally, high effective moisture is evidenced in palaeoenvironmental records from Sagalassos, the Bereket Valley, Gravgaz Marsh and Lake Burdur (Bakker et al., 2012, 2013; Van Geel et al., 1989; Kaniewski et al., 2007; Kaptijn et al., 2013; Tudryn et al., 2013; Vermoere et al., 2002). Coastal palaeohydrological records from

western Greece (Trichonida, Mavri Trypa), the northern Aegean (Skala Marion), and the Levant (Kfar Giladi, Jeita Cave), also demonstrate high effective moisture in the 4th/5th centuries CE (Cheng et al., 2015; Finné et al., 2017; Morin et al., 2019; Psomiadis et al., 2018; Seguin et al., 2020a). In the Middle East (Chapter 6), the period 300 to 410 CE has relatively stable effective moisture in all records, with increases observed in the high-resolution FC archives (Gejkar and Kuna Ba) (Flohr et al., 2017; Sinha et al., 2019). From 410 to 480 CE, conditions are spatially variable, with drying (Van, Katalekhor, Hoti), stable conditions (Kuna Ba) and increasing effective moisture (Neor) observed (Andrews et al., 2020; Barlas Şimşek & Çağatay, 2018; Sharifi et al., 2015; Sinha et al., 2019).

Perhaps the most significant shift observed in this thesis is the Late Antique transition to consistently drier conditions, evidenced in the Ko-1 and H12 records from 460 and 480 CE respectively. Principal component analysis of Mediterranean palaeohydrological records performed by Labuhn et al. (2018) indicated that the most significant palaeohydrological change of the first millennium CE occurred between 450 and 550 CE. They propose this may be linked to the 536 CE DVE and the start of the LALIA (Büntgen et al., 2016; Labuhn et al., 2018; Sigl et al., 2015). As discussed in Chapters 3, 5 and 6, for all records except Nar and possibly Kuna Ba, the shift in conditions starts before 536 CE (Figure 51). This suggest another factor was responsible for changing climatic conditions in the late-5th/early-6th centuries CE. In Chapter 5, it is argued that the contrast between the continental Anatolian (Nar, Sofular) and other records results from a northward displacement of storm tracks in the Eastern Mediterranean at the beginning of the 6th century CE. The broad similarities between the Ko-1 and H12 records suggest fewer rain-bearing storms crossed the Eastern Mediterranean; cyclones originating in Central Europe, the Black Sea, and the Gulf of Genoa, which transport precipitation to northern regions of Greece and Turkey (Appendix B.1; Karaca et al., 2000; Trigo et al., 2002), perhaps became more dominant. However, palaeoclimate records from the Balkans (Ascunsă Cave, Ceremonsja, Uzuntarla) and northern Greece (Skala Marion, Dojran, Prespa) do not appear to show an increase in effective moisture coincident with the changes at Nar and Sofular (Göktürk, 2011; Kern et al., 2019; Labuhn et al., 2018). Further research is needed in this region to disentangle the causes of significant change between 450 and 550 CE. Statistical analysis similar to Labuhn et al. (2018), but focused on the EMME region and including newer records would be informative, especially if containing

the Balkan and Greek records mentioned above, archives from the Peloponnese (e.g. Trichonida, Mavri Trypa, Stymphalia), Skala Marion, the Lake Salda and Kocain Cave records from SW Turkey, and the high-resolution ME records (Gejkar, Kuna Ba, Hoti).

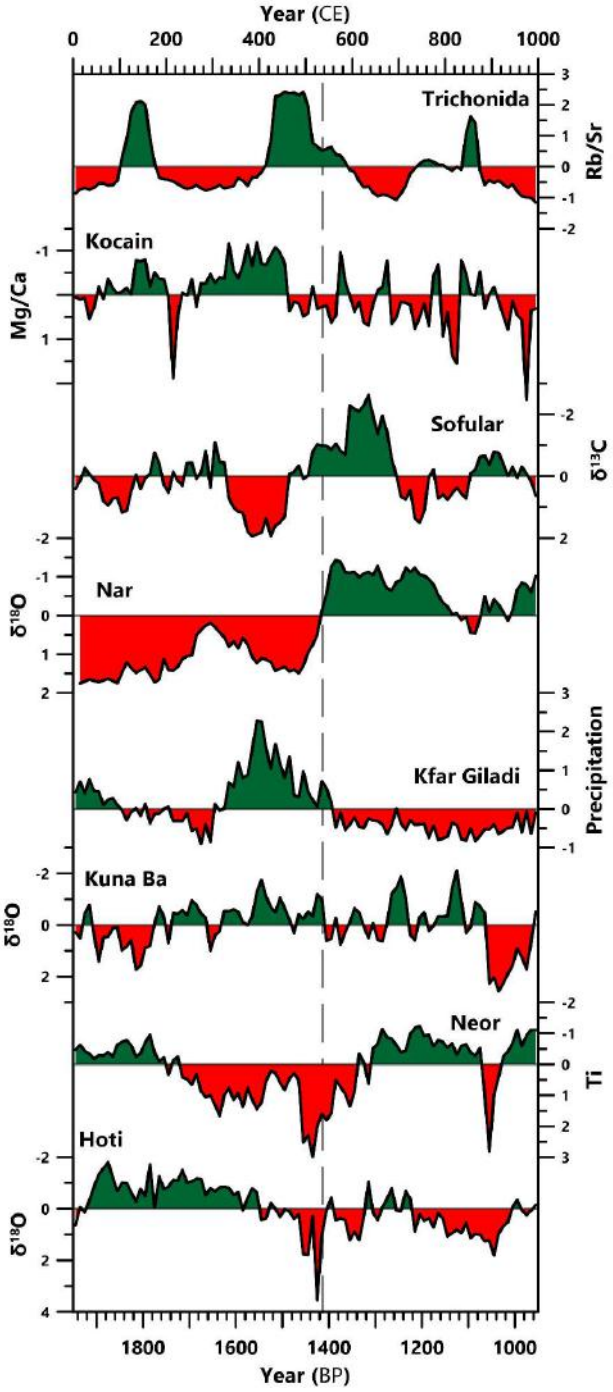

Figure 51. Decadal averages of high-resolution EMME hydrological archives, ordered from west to east, standardised to z-scores (for the first millennium) for simpler comparison. The dashed line indicates the DVE in 536 CE.

7.2. History of Climate and Society

Understanding the societal impacts of past climate change, and the factors which determine a society's resilience, can provide useful insights for mitigation of future climate change (Holm & Winiwarter, 2017; Marston, 2015). Climate is increasingly recognised as a potential factor in societal change, with more nuanced and critical perspectives arising over the past few decades (see Chapter 2). In this thesis, deterministic arguments and observations of correlations were avoided in favour of establishing causal links through examination of agricultural impacts, the contribution of other factors and societal resilience. This required examination of palaeoenvironmental, archaeological, and historical evidence of socio-economic change to assess human consequences from, and responses to, climate change.

In this section, the case-studies of this thesis are summarised utilising the "Adaptive Cycle", a conceptual framework for understanding system change. This model, originally developed for studies of ecosystems, defines the nature of a system according to four key phases: growth (r), conservation (K), release (Ω) and reorganisation (α) (Holling & Gunderson, 2002). In human systems, the phases are defined as follows (Allcock, 2017; Haldon & Rosen, 2018; Roberts et al., 2018b):

- **r-phase** – growth of the system and exploitation of resources, with increasing complexity and interconnectivity.
- **K-phase** – the system has stabilised into a strong and highly productive structure. However, over-connectivity and -rigidity reduce the resilience of the system.
- **Ω-phase** – a stressor forces a catastrophic shift in the system, opening the system up for reorganisation.
- **α-phase** –reorganisation, in which the system becomes loosely structured and highly resilient, leading to the start of a new Adaptive Cycle.

Application of this framework emphasises resilience, adaptation and fragility, which are important for avoiding environmental determinism (Lewit, 2020). The Adaptive Cycle operates at different scales in human systems (communities, regions, society, inter-state networks), and these link up into multi-scalar systems known as 'Panarchy' (Holling & Gunderson, 2002; Marston, 2015); catastrophic change will only result when high fragility is exhibited among all the constituent adaptive cycles of a society (Haldon & Rosen, 2018).

Below, this framework is applied to the case-studies of this thesis (Figure 52), as has been done comprehensively for other regions and periods in Anatolia (Allcock, 2017; Bogaard et al., 2017; Marston, 2011, 2015, 2021; Roberts et al., 2018b; Shin et al., 2021).

7.2.1. SW Anatolia

Chapter 4 provided a micro-regional case-study of HCS (SW Anatolia), the need for which has long been recognised (Haldon et al., 2014; Horden & Purcell, 2000) but is challenging due to the requirement for proximate high-quality palaeoclimatic, palaeoenvironmental and archaeological/historical datasets. The required high-quality palaeoclimatic evidence was produced in Chapter 3 (Kocain Cave), whilst pre-existing palaeoenvironmental datasets were synthesised into a variable for human agricultural activity (OJCV values) and an archaeological settlement dataset was produced from volume 8 of the *Tabula Imperii Byzantini* (TIB). Three periods of broad societal change for the Roman/Byzantine Empire that had previously been associated with climatic change were then assessed.

Imperial Roman expansion (late 1stc. BCE - early 4th c. CE) can be considered part of the r-phase. The Roman Climatic Optimum (RCO), a proposed period of consistently warm and wet conditions that led to Roman expansion in the 1st c. BCE – 2nd c. CE (Harper, 2017), was found to be false for SW Anatolia. Whilst expansion did take place, as evidenced by increasing settlement numbers, agricultural productivity and interconnectivity between regions (De Cupere et al., 2017; Dündar, 2018; Poblome et al., 2017; Vandam et al., 2019a), the palaeoclimate evidence showed no evidence for warm or wet conditions. Low effective moisture and precipitation were observed in the Ko-1 record during 100 BCE – 100 CE, with average conditions thereafter until a short-lived drier phase at 220 CE. Annexation of the region by the Roman Empire in 43 CE (Bennett, 2011; Brandt & Kolb, 2005) appears to have been the important factor for growth. The empire invested in agricultural and trade infrastructure (Adak & Şahin, 2007; Kokkinia, 2000; Rice, 2020) and increased regional security from banditry (Çevik & Bulut, 2007). Their takeover of the region brought increased demand for agricultural surplus to feed the Roman army (Akyürek, 2016), and technology and knowledge which increased agricultural productivity (Curtis, 2008; Greene, 2000).

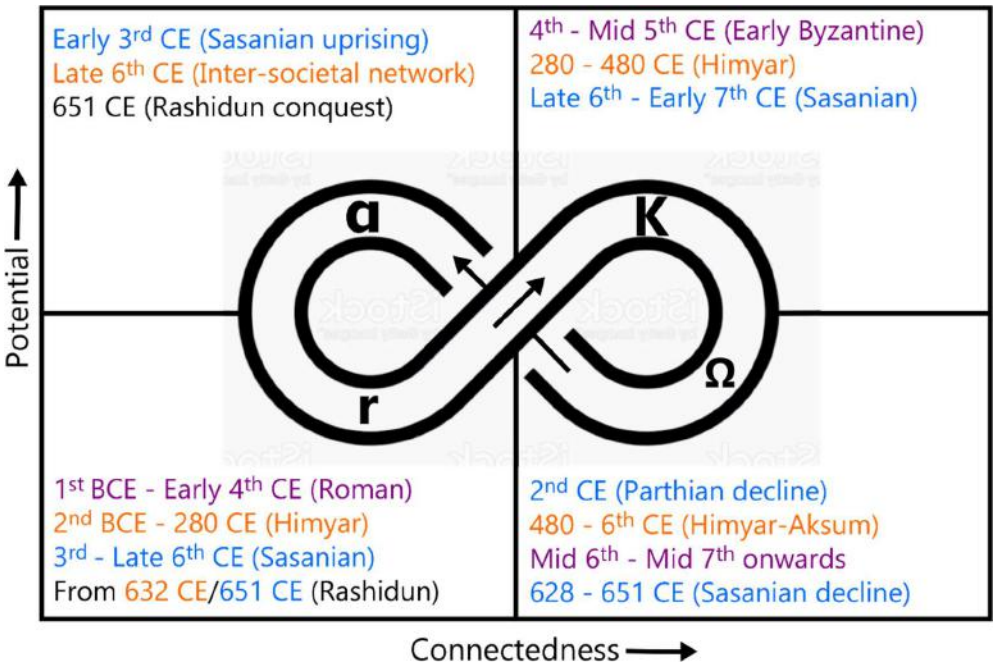

Figure 52. The Adaptive Cycle (adapted from Holling & Gunderson, 2002) with phases for Chapters 4 (Purple), 5 (Orange) and 6 (Blue), as well as for the Rashidun Caliphate (Black).

The Late Antique phases are more complicated under the Adaptive Cycle framework. It has previously been argued that a period of enhanced precipitation in the 4th-6th c. CE was an enabling factor for Late Antique "prosperity" in the Eastern Mediterranean (Decker, 2009b; Haldon et al., 2018a; Izdebski, 2013b; Izdebski et al., 2016b). In other regions of Anatolia, this period is considered the K-phase with diverse agricultural activities, economic prosperity, and increasing importance of long-distance trade (Roberts et al., 2018b). However, from the mid-5th c. CE in SW Anatolia, the character of local settlement changes, coincident with a shift to drier conditions evidenced in the Ko-1 record from 460 CE and by modifications to urban water supply. Older Roman cities lose their monumental aspect, with previous public buildings no longer maintained and instead utilised as workshops. Interior regions experience a decline in settlement numbers, whereas increased settlement density is observed on the coast, perhaps resulting from increasing importance of maritime trade routes (Cassis et al., 2018; Foss, 1993, 1994; Terpoy, 2019a, b). These changes do not indicate "prosperity" in SW Anatolia and appear to reflect adaptive responses to drier conditions.

Whilst utilisation of the Adaptive Cycle framework for the above changes is challenging, a marked decline (Ω-phase) is visible between the Early and Middle Byzantine periods (starting 550-650 CE), with a reduction in settlement numbers, settlement size, and interregional exchange, and increased importance of pastoralism (De Cupere et al., 2017; W. J. Eastwood et al., 1998; Izdebski, 2011). This decline occurred at least a century after the shift to drier conditions, with further drying until a minimum of precipitation around the start of the 7th century CE, reflected by Ko-1 $\delta^{18}O$ and Ca/Fe ratios from Lake Salda (Danladi & Akçer-Ön, 2018). Drier conditions in SW Anatolia endured until at least 830 CE and were part of a complex web of interconnected factors (earthquakes, epidemics, insecurity from interstate conflict), all of which may have contributed to settlement decline, but regarding which it is hard to establish causal links (Ambraseys, 2009; Baird, 2004; Eisenberg & Mordechai, 2019; C. Mango et al., 1997; Mordechai & Pickett, 2018; Stathakopoulos, 2004).

The concept of Panarchy is important for understanding the Byzantine Empire in Anatolia. Although the empire as a whole had become vulnerable due to over-connectivity, smaller systems (micro-regions) were relatively resilient and adapted by shifting strategies (from agriculture to pastoralism) and by reducing the complexity of settlement (contraction and renucleation). Further research is required on this topic, but it may help to explain why the Byzantine Empire survived into the 2nd millennium, whilst other empires and kingdoms did not.

7.2.2. The Kingdom of Himyar

In Chapter 5, palaeoclimate data from Hoti Cave (see above) was examined alongside the history of the Kingdom of Himyar. Phases of the Adaptive Cycle occurred earlier in this region; Himyar consolidated its power in southern Arabia by ~280 CE (r-phase) from its homeland in Yemen and exerted power further north through alliances with the Kinda and Madhhjj tribes (Cameron, 2012; Phillipson, 2012; Yule, 2007). In the subsequent K-phase, settlement numbers expanded, the kingdom invested in agricultural infrastructure and its elite were important players in Indian Ocean trade (Brunner, 1997; Charbonnier, 2011; Edwell, 2015; Schippmann, 2001; Shahîd, 2010). The kingdom was more reliant on interconnectivity

with Arabian tribes, the Byzantine and Sasanian Empires, and Indian Ocean trade. From ~480 CE the region declined (Ω-phase); settlement numbers were reduced (Schiettecatte, 2008), irrigation infrastructure fell into disrepair (Brunner, 1997; Charbonnier, 2011), and conflict erupted over control of Yemen, with involvement from the Kingdom of Aksum and the Byzantine and Sasanian empires (Hatke, 2011; Robin, 2015; Whittow, 2011; Wiesehöfer, 2010). These changes correspond with the start of persistently drier conditions (~480-1400 CE) overlain by a severe drought (~520-532 CE), evidenced by the Hoti Cave record, other Middle Eastern palaeoclimate records (Bookman et al., 2004; Cheng et al., 2015; Sharifi et al., 2015) and historical references to droughts (McCormick et al., 2012; Telelis, 2008). The highly dependent nature of this region on rainfed agriculture and reduced agricultural yields caused by aridification suggest that the decline of Himyar should be viewed in the context of climatic change. Subsequently, across the Arabian Peninsula, there was a much faster transition to the α-phase, with removal of supra-tribal political structures (kings and lords) and the development of an intersocietal network with increased importance of regional pilgrimage and economic centres (Korotayev et al., 1999; Schippmann, 2001; Yule, 2007). This reconfiguration of the political systems was highly adaptive and resilient, and also created the context within which Islam could flourish, the start of the next r-phase.

7.2.3. The Sasanian Empire

In Chapter 6, an investigation into the history and resilience of the Sasanian Empire was conducted and palaeoclimate records were examined to highlight avenues for future research. The Parthian Empire entered an Ω-phase during the 2nd c. CE and the initial years of the Sasanian Empire can be considered an α-phase, an adaptation to Parthian decline. The r-phase for the Sasanian Empire was long-lasting, with increasing settlement numbers, agricultural productivity, interregional exchange, and irrigation infrastructure, with territorial expansion during the 3rd-early 7th centuries CE (Altaweel & Squitieri, 2018; Howard-Johnston, 2017; Neely, 2016; Panahipour, 2021; Shumilovskikh et al., 2017). This was focused in two established growth-phases (309-379 and 498-628 CE), during which particularly effective kings launched military campaigns, invested in construction of settlements and infrastructure, and reformed political systems to ensure greater wealth for the state (Axworthy, 2008;

Daryaee & Rezakhani, 2017). Whilst in the first growth-phase effective moisture was relatively stable in most records, tempting an argument for climate-driven prosperity, the second (and arguably more significant) is coincident to the driest (and maybe coldest) conditions of the entire Sasanian Period. These are the same conditions that contributed to a significant decline in the Kingdom of Himyar (From ~480 CE; Chapter 5). A short K-phase is observed for the Sasanian Empire, which started to overextend towards the end of the 6th c. CE. The Sasanian Empire's decline (Ω-phase) occurred later than in other regions (~628-651 CE) and no evidence suggests a local climatic influence. However, if drought conditions in Arabia were implicated in the downfall of Himyar and the initial success of Islam, then the caliphates conquest of Persia may be seen as consequential. Similar arguments have been made for invasions of the EMME region by nomadic groups from the Caucasus and CA being "pushed" by climatic deterioration (Büntgen et al., 2016, 2020). Although the conquest was the ultimate cause of the end of the Sasanian Empire, its overextension and aggressive taxation, as well as protracted conflict with the Byzantine Empire and civil wars (Wiesehöfer, 2010), were crucial in lowering the Sasanians' defensive capabilities. The impact of the decline and eventual end of the Sasanian Empire on smaller regions may have been negligible, however. Further research is required to improve chronological resolution for archaeological and palaeoenvironmental developments, which can only be broadly dated to around the end of the Sasanian Period. Furthermore, theories of climatic "push" factors should be tested in Late Antiquity and other periods.

7.2.4. Recurrent themes

Throughout the case-studies there are several recurrent themes. Firstly, there appears to be a requirement for a combination of factors to coalesce before significant societal change is observed; in other words, a "perfect storm". Communities in SW Anatolia adapted to the shift to drier conditions from ~460 CE through changing the character of settlement and modifying water infrastructure; however, decline was observed after protracted drying, the appearance of plague, earthquakes, and regional insecurity. In addition to the climate change preceding the decline by at least a century, there were earlier instances of earthquakes, epidemics, and conflicts, where the population appears to have been relatively

unafflicted. Similarly, the Kingdom of Himyar resisted invasions by the Aksumites in the late 5th century CE but was overwhelmed by them in the early 6th century CE, following deterioration of climate, the arrival of plague and deterioration of infrastructure. In the Sasanian Empire, the driest conditions pre-date weakening of the empire, which enabled its rapid conquest of the Caliphate, by around a century. Reduction in Sasanian power resulted from multiple factors including long-lasting wars with the Romans/Byzantines and Hunnic tribal confederations, internal conflict, changes in the trade economy, and epidemics. This was also analogous to the preceding Parthian Empire, which was replaced by the Sasanians whilst weakened by conflict with Rome, an increase in the importance of the Indian Ocean trade route, the Antonine Plague (smallpox) and internal conflict (Bivar, 1983; de Crespigny, 2007; Olbrycht, 2016). In each of these examples, disentangling the relative influence of individual factors is challenging, and perhaps their combination was important. Variations between the impacts of similar events at different times and between the different case studies in this thesis emphasise the need for critical examination of climate changes, other factors, and societal responses, in each instance to mitigate against simplistic narratives.

Degradation of agricultural infrastructure is often associated with climate change. In the case studies of this thesis, infrastructure failure appears more as a symptom of decline as opposed to a direct impact of climatic or environmental occurrences. Maintenance, repair work and modifications to hydraulic infrastructure required central organisation and mobilisation of large work forces which was only possible through state intervention. Following the dissolution of states, no repair work was attempted on damaged large-scale irrigation structures, the most prominent example being the collapse of the Ma'rib dam in ~580 CE (Brunner, 2000a). In the Mughan Steppe, flood damage to the Araxes River canals was remedied by constructing a new wall and canal head, but after a subsequent flood, no repair occurred and the entire Sasanian irrigation system was abandoned (Alizadeh et al., 2021).

7.3. Concluding remarks

In summary, by taking an interdisciplinary approach, this thesis has made significant contributions to the fields of palaeoclimatology, archaeology, and history, through the

development of two new speleothem-based palaeoclimate records, comparison of existing records, and multi-scalar analysis of climatic impacts on socio-economic change.

For palaeoclimatologists, there are several important implications from this thesis. Firstly, for those developing speleothem records, novel methodologies (speleoseismology, LA-ICP-MS for long records) and proxies (P/Ca, apex diameter) can be utilised and built upon in future speleothem proxy records. Secondly, new palaeoclimate data from speleothems Ko-1 and H12 address two previous spatio-temporal gaps in coverage which help our understanding of climate dynamics and can be input into palaeoclimate models. Thirdly, and most importantly, heterogeneity of both climatic conditions and interpretations of proxies has been stressed. This emphasises the necessity for further analysis, of both more palaeoclimate records, and updated regional syntheses. Our understanding of past regional responses to changing global climatic conditions will be critical for predicting and responding to future climate change (Masson-Delmotte et al., 2013).

For those concerned with climatic influences on societal change – archaeologists and historians, but also environmental managers and policy makers (Hambrecht et al., 2020; Moser & Hart, 2015) – there are additional important implications from this thesis. The climate change demonstrated by the new records and the emphasis on heterogeneity indicate that care should be taken in selection of palaeoclimatic datasets for HCS analysis. Varied climate, as well as the diverse responses to climate observed between regions, stresses the importance of micro-regional case studies, which were demonstrated to be useful in Chapter 4. Uncertainties when using datasets from disparate regions must be considered more transparently and producing palaeoclimate datasets alongside archaeological projects should become customary.

Climate change, and societal responses to it, are a generation-defining research area. Humans will struggle to adapt to future climate change, with the world's poorer regions and communities facing disproportionately extreme challenges. The EMME region is one such locality, expected to experience significant climate change (Giorgi, 2006; Lelieveld et al., 2012) and severe societal consequences including water shortages, crop failures and geo-political instability (Gleick, 2014; Kelley et al., 2015). Continuing to examine the diversity of impacts from climate change in the ancient EMME, in addition to other contributing environmental

and human factors, is essential for understanding the dynamics of human-environment-climate interactions and thus for preparing to face future climate change. Strategies for mitigating against social problems resulting from climate change will be as vital for continued human flourishment as constructing physical defences and reducing greenhouse gas emissions. The research presented in this thesis contributes to these conversations through investigation of multi-scalar impacts and human responses during Late Antiquity and sets future research agendas.

Bibliography

Abdy, R., & Williams, G. (2006). A catalogue of hoards and single finds from the British Isles c. AD 410–675. In B. J. Cook & G. Williams (Eds.), *Coinage and History in the North Sea World, c. AD 500–1250: Essays in Honour of Marion Archibald* (pp. 11–74). Leiden: Brill.

Adak, M., & Şahin, S. (2007). *Stadiasmus Patarensis: Itinera Romana Provinciae Lyciae*. Istanbul: Ege Yayınları.

Adamo, N., & Al-ansari, N. (2020). The Greeks and the Sassanids - A new Glorious Era for Agriculture (330-625 AD). *Journal of Earth Science and Geotechnical Engineering*, *10*(3), 113–135.

Adams, R. M. (1962). Agriculture and Urban Life in Early Southwestern Iran. *Science*, *136*, 109–122.

Adams, R. M. (1965). *Land Behind Baghdad: A History of Settlement on the Diyala Plains*. London: University of Chicago Press.

Adams, R. M. (2006). Intensified Large-Scale Irrigation as an Aspect of Imperial Policy: Strategies of Statecraft on the Late Sasanian Mesopotamian Plain. In J. Marcus & C. Stanish (Eds.), *Agricultural Strategies* (pp. 17–37). Los Angeles: Cotsen Institute of Archaeology, University of California.

Akkemik, Ü.¨, & Aras, A. (2005). Reconstruction (1689-1994 AD) of April-August precipitation in the southern part of central Turkey. *International Journal of Climatology*, *25*(4), 537–548. https://doi.org/10.1002/joc.1145

Akyürek, E. (2016). Andriake: The Port of Myra in Late Antiquity. In P. Magdalino & N. Necipoğlu (Eds.), *Trade in Byzantium: Papers from the Third International Sevgi Gönül Byzantine Studies Symposium* (pp. 465–487). Istanbul: Köc University Research Center for Anatolian Civilizations.

Akyürek, E., & Tiryaki, A. (2010). Rhodiapolis Piskoposluk Kilisesi Kazılarından Üç Mimari Plastik Eser Üzerine Değerlendirmeler. *Adalya*, *13*, 398–403.

Al-Jahwari, N. S., Kennet, D., Priestman, S., & Sauer, E. (2018). Fulayj: a Late Sasanian fort on the Arabian coast. *Antiquity*, *92*(363), 724–741. https://doi.org/10.15184/aqy.2018.64

Alanyalı, H. S. (2010). Work at and around Side Theater in 2009. *ANMED*, *8*, 94–103.

Alanyalı, H. S. (2011). Excavations at Side in 2010. *ANMED*, *9*, 100–112.

Alcock, S., & Cherry, J. (2016). *Side-by-Side Survey: Comparative Regional Studies in the Mediterranean World*. Oxford: Oxbow Books.

Aldrich, D. P. (2012). *Building resilience: social capital in post-disaster recovery*. Chicago: University of Chicago Press.

Alizaddeh, A., Kouchoukos, N., Bauer, A. M., Wilkinson, T. J., & Mashkour, M. (2004). Human-Environment Interactions on the Upper Khuzestan Plains, Southwest Iran. Recent Investigations. *Paléorient*, *30*, 69–88.

Alizadeh-Choobari, O. (2017). Contrasting global teleconnection features of the eastern Pacific and central Pacific El Niño events. *Dynamics of Atmospheres and Oceans*, *80*, 139–154. https://doi.org/10.1016/j.dynatmoce.2017.10.004

Alizadeh, K. (2011). Ultan Qalası: A Fortified Site in the Sasanian Borderlands (Mughan Steppe, Iranian Azerbaijan). *Iran*, *49*, 55–77.

Alizadeh, K. (2014). Borderland Projects of Sasanian Empire: Intersection of Domestic and Foreign Policies. *Journal of Ancient History*, *0*(0), 93–115. https://doi.org/10.1515/jah-2014-0015

Alizadeh, K., & Ur, J. A. (2007). Formation and destruction of pastoral and irrigation landscapes on the Mughan Steppe, north-western Iran. *Antiquity*, *81*(311), 148–160.

Alizadeh, K., Rouhollah Mohammadi, M., Maziar, S., & Feizkhah, M. (2021). The Islamic Conquest or Flooding? Sasanian Settlements and Irrigation Systems Collapse in Mughan, Iranian Azerbaijan. *Journal of Field Archaeology*, *46*(5), 316–332. https://doi.org/10.1080/00934690.2021.1913314

Allcock, S. L. (2017). Long-term socio-environmental dynamics and adaptive cycles in Cappadocia, Turkey during the Holocene. *Quaternary International*, *446*, 66–82. https://doi.org/10.1016/j.quaint.2017.06.065

Almazroui, M., Nazrul Islam, M., Athar, H., Jones, P. D., & Rahman, M. A. (2012). Recent climate change in the Arabian Peninsula: Annual rainfall and temperature analysis of Saudi Arabia for 1978-2009. *International Journal of Climatology*, *32*(6), 953–966. https://doi.org/10.1002/joc.3446

AlSarmi, S., & Washington, R. (2011). Recent observed climate change over the Arabian Peninsula. *Journal of Geophysical Research: Atmospheres*, *116*(D11), 11109. https://doi.org/10.1029/2010JD015459

Altaweel, M. (2019). Southern Mesopotamia: Water and the rise of urbanism. *WIREs Water*, *6*(4), e1362. https://doi.org/10.1002/wat2.1362

Altaweel, M., & Squitieri, A. (2018). *Revolutionizing a World: From Small States to Universalism in the Pre-Islamic Near East* (Vol. 148). London: University College London Press.

Altaweel, M., Marsh, A., Jotheri, J., Hritz, C., Fleitmann, D., Rost, S., et al. (2019). New insights on the role of environmental dynamics shaping southern Mesopotamia: from the pre-Ubaid to the early Islamic period. *Iraq*, *81*, 23–46. https://doi.org/10.1017/irq.2019.2

Altinok, Y., Alpar, B., Özer, N., & Aykurt, H. (2011). Revision of the tsunami catalogue affecting Turkish coasts and surrounding regions. *Natural Hazards and Earth System Science*, *11*(2), 273–291. https://doi.org/10.5194/nhess-11-273-2011

Ambraseys, N. (2009). *Earthquakes in the eastern Mediterranean and the Middle East: a multidisciplinary study of 2000 years of seismicity*. Cambridge: Cambridge University Press.

Anderson, D. M., Baulcomb, C. K., Duvivier, A. K., & Gupta, A. K. (2010). Indian summer monsoon during the last two millennia. *Journal of Quaternary Science*, *25*(6), 911–917. https://doi.org/10.1002/jqs.1369

Andrews, J. E., Carolin, S. A., Peckover, E. N., Marca, A., Al-Omari, S., & Rowe, P. J. (2020). Holocene stable isotope record of insolation and rapid climate change in a stalagmite from the Zagros of Iran. *Quaternary Science Reviews*, *241*, 106433. https://doi.org/10.1016/j.quascirev.2020.106433

Arjava, A. (2005). The Mystery Cloud of 536 CE in the Mediterranean Sources. *Dumbarton Oaks Papers*, *59*(2005), 73–94.

Armstrong, P. (2009). Trade in the east Mediterranean in the 8th century. In M. M. Mango (Ed.), *Byzantine Trade, 4th-12th Centuries* (pp. 157–178). Aldershot: Ashgate Publishing.

Armstrong, P. (2012). The survey pottery: Hellenistic and later. In J. J. Coulton (Ed.), *The Balboura Survey and Settlement in Highland Southwest Anatolia: Volume 2. The Balboura survey: detailed studies and catalogues* (pp. 31–82). London: British Institute of Archaeology at Ankara.

Arthur, P. (2008). Form, Function And Technology In Pottery Production From Late Antiquity To The Early Middle Ages. In Luke Lavan, E. Zanini, & A. Sarantis (Eds.), *Technology in Transition A.D. 300-650* (pp. 159–186). Leiden: Brill. https://doi.org/10.1163/ej.9789004165496.i-573.66

Asadi, A. (2010). The Settlement Pattern and Land Use in Bastak Plain, Hormozgan Province/Olguy-e Esteghrary va Karbari-e Arazi dar Dasht-e Bastak, Hormozgan (Persian, with English summary). *Majale Bastanshenasi va Tarikh [Iranian Journal of Archaeology and History]*, *45*, 3–32.

Asadi, A., Mousavi Kouhpar, S. M., Neyestani, J., & Hojabri-Nobari, A. (2013). Sasanian and early Islamic settlement patterns north of the Persian Gulf. *Vicino Oriente*, *XVII*, 21–38.

Asano, K. (2010). *Island of St. Nicholas. Excavation and Survey of the Gemiler Island Area, Lycia, Turkey*. Osaka: Osaka University Press.

Askari Chaveri, A., & Azarnoush, M. (2004). Survey in the Hinterland of the Persian Gulf: Lamerd and Mohr Districts /Barresi-e Bastanshenakhti-e Mohavatehaye Bastani-e Pas Karanehaye Khalij-e Fars: Lamerd va Mohr: Fars" (Persian, with English summary). *Majale Bastanshenasi va Tarikh [Iranian Journal of Archaeology and History]*, *36*, 3–19.

Axworthy, M. (2008). *A History of Iran: Empire of the Mind*. New York: Basic Books.

Aydın, S., Şimşek, M., Çetinkaya, G., & Öztürk, M. Z. (2019). Erinç Yağış Etkinlik İndisi'ne Göre Belirlenen Türkiye İklim Bölgelerinin Rejim Karakteristikleri (Regime Characteristiscs of Turkey's Climatic Regions Determined Using the Erinç Precipitation Efficiency Index). In *1st Istanbul International Geography Congress Proceedings Books* (pp. 752–760). Istanbul: Istanbul University Press. https://doi.org/10.26650/PB/PS12.2019.002.074

Babaeian, I., & Rezazadeh, P. (2018). On the relationship between Indian monsoon withdrawal and Iran's fall precipitation onset. *Theoretical and Applied Climatology*, *134*(1–2), 95–105. https://doi.org/10.1007/s00704-017-2260-0

Badertscher, S., Borsato, A., Frisia, S., Cheng, H., Edwards, R. L., Tüysüz, O., & Fleitmann, D. (2014). Speleothems as sensitive recorders of volcanic eruptions - the Bronze Age Minoan eruption recorded in a stalagmite from Turkey. *Earth and Planetary Science Letters*, *392*, 58–66. https://doi.org/10.1016/j.epsl.2014.01.041

Baird, D. (2004). Settlement expansion on the Konya Plain, Anatolia 5th-7th centuries AD. In L Lavan & W. Bowden (Eds.), *The Late Antique Countryside* (pp. 219–246). Oxford: Brill.

Bakker, J, Kaniewski, D., Verstraeten, G., De Laet, V., & Waelkens, M. (2011). Numerically derived evidence for late-Holocene climate change and its impact on human presence in the southest Taurus Mountains, Turkey. *Holocene*, *22*(4), 425–438. https://doi.org/10.1177/0959683611425546

Bakker, J, Paulissen, E., Kaniewski, D., Poblome, J., De Laet, V., Verstraeten, G., & Waelkens, M. (2013). Climate, people, fire and vegetation: New insights into vegetation dynamics in the Eastern Mediterranean since the 1st century AD. *Climate of the Past*, *9*(1), 57–87. https://doi.org/10.5194/cp-9-57-2013

Bakker, Johan, Paulissen, E., Kaniewski, D., de Laet, V., Verstraeten, G., & Waelkens, M. (2012). Man, vegetation and climate during the Holocene in the territory of Sagalassos, Western Taurus Mountains, SW Turkey. *Vegetation History and Archaeobotany*, *21*(4–5), 249–266. https://doi.org/10.1007/s00334-011-0312-4

Ball, W. (2016). *Rome in the East: Transformation of an Empire* (2nd editio). New York: Routledge.

Bar-Matthews, M., & Ayalon, A. (2011). Mid-holocene climate variations revealed by high-resolution speleothem records from soreq cave, israel and their correlation with cultural changes. *Holocene*, *21*(1), 163–171. https://doi.org/10.1177/0959683610384165

Bar-Matthews, M., Ayalon, A., Gilmour, M., Matthews, A., & Hawkesworth, C. J. (2003). Sea–land oxygen isotopic relationships from planktonic foraminifera and speleothems in the Eastern Mediterranean region and their implication for paleorainfall during interglacial intervals. *Geochimica et Cosmochimica Acta*, *67*(17), 3181–3199.

Bar-Oz, G., Weissbrod, L., Erickson-Gini, T., Tepper, Y., Malkinson, D., Benzaquen, M., et al. (2019). Ancient trash mounds unravel urban collapse a century before the end of Byzantine hegemony in the southern Levant. *Proceedings of the National Academy of Sciences of the United States of America*, *116*(17), 8239–8248.

https://doi.org/10.1073/pnas.1900233116

Barlas Şimşek, F., & Çağatay, M. N. (2018). Late Holocene high resolution multi-proxy climate and environmental records from Lake Van, eastern Turkey. *Quaternary International*, *486*, 57–72. https://doi.org/10.1016/j.quaint.2017.12.043

Barlow, M., Zaitchik, B., Paz, S., Black, E., Evans, J., & Hoell, A. (2016). A review of drought in the Middle East and southwest Asia. *Journal of Climate*, *29*(23), 8547–8574. https://doi.org/10.1175/JCLI-D-13-00692.1

Barton, C. M., Bernabeu, J., Aura, J. E., & Garcia, O. (1999). Land-use dynamics and socioeconomic change: an example from the Polop Alto Valley. *American Antiquity*, *64*(4), 609–634.

Beaumont, P. (1971). Qanat systems in Iran. *Hydrological Sciences Journal*, *16*, 39–50.

Beck, H. E., Zimmermann, N. E., McVicar, T. R., Vergopolan, N., Berg, A., & Wood, E. F. (2018). Present and future köppen-geiger climate classification maps at 1-km resolution. *Scientific Data*, *5*. https://doi.org/10.1038/sdata.2018.214

Becker, A., Davenport, C. A., Eichenberger, U., Gilli, E., Jeannin, P. Y., & Lacave, C. (2006). Speleoseismology: A critical perspective. *Journal of Seismology*, *10*(3), 371–388. https://doi.org/10.1007/s10950-006-9017-z

Bell, M., & Walker, M. J. C. (2005). *Late Quaternary Environmental Changes: Physical and Human Perspectives* (2nd editio). Harlow: Pearson Education Limited.

Bengtsson, L. (2012). Water balance of lakes. In B. L., H. R.W., & F. R.W. (Eds.), *Encyclopedia of Lakes and Reservoirs. Encyclopedia of Earth Science Series* (pp. 869–872). Dordrecht: Springer. https://doi.org/10.1007/978-1-4020-4410-6_244

Bennett, J. (2011). Why did Claudius Annex Lycia? *Adalya*, *14*, 119–136.

Berger, A., & Loutre, M. F. (1991). Insolation values for the climate of the last 10 million years. *Quaternary Science Reviews*, *10*(4), 297–317. https://doi.org/10.1016/0277-3791(91)90033-Q

Bernal, J. P., Cruz, F. W., Stríkis, N. M., Wang, X., Deininger, M., Catunda, M. C. A., et al. (2016). High-resolution Holocene South American monsoon history recorded by a speleothem from Botuverá Cave, Brazil. *Earth and Planetary Science Letters*, *450*, 186–196. https://doi.org/10.1016/j.epsl.2016.06.008

Bernbeck, R. (2012). The Political Dimension of Archaeological Practices. In D. Potts (Ed.), *A Companion to the Archaeology of the Ancient Near East* (pp. 87–105). Chichester: Wiley-Blackwell.

Bewley, R. A., Wilson, D., Kennedy, D., Mattingly, R., Banks, M., Bishop, J., et al. (2016). Endangered Archaeology in the Middle East and North Africa: Introducing the EAMENA Project. In S. Campana, R. Scopigno, G. Carpentiero, & M. Cirillo (Eds.), *CAA2015. Keep the Revolution Going: Proceedings of the 43rd Annual Conference on Computer*

Applications and Quantitative Methods in Archaeology (pp. 919–932). Oxford: Archaeopress.

Binford, M. W., Kolata, A. L., Brenner, M., Janusek, J. W., Seddon, M. T., Abbott, M., & Curtis, J. H. (1997). Climate variation and the rise and fall of an Andean civilization. *Quaternary Research*, *47*, 235–248.

Bivar, A. D. H. (1970). Hāritī and the Chronology of the Kuṣāṇas. *Bulletin of the School of Oriental and African Studies, University of London*, *33*(1), 10–21.

Bivar, A. D. H. (1983). The political history of Iran under the Arsacids. In E. Yarshater (Ed.), *The Cambridge History of Iran. Volume 3: The Seleucid, Parthian and Sasanid Periods, Part 1* (pp. 21–99). Cambridge University Press.

Bocinsky, R. K., & Kohler, T. A. (2014). A 2,000-year reconstruction of the rain-fed maize agricultural niche in the US Southwest. *Nature Communications*, *5*. https://doi.org/10.1038/ncomms6618

Bogaard, A., Filipović, D., Fairbairn, A., Green, L., Stroud, E., Fuller, D., & Charles, M. (2017). Agricultural innovation and resilience in a long-lived early farming community: The 1,500-year sequence at Neolithic to early Chalcolithic Çatalhöyük, central Anatolia. *Anatolian Studies*, *67*(March), 1–28. https://doi.org/10.1017/S0066154617000072

Bonifay, M. (2008). Ceramic production in Africa during late antiquity: Continuity and change. In Luke Lavan, E. Zanini, & A. Sarantis (Eds.), *Technology in Transition A.D. 300-650* (pp. 143–158). Leiden: Brill. https://doi.org/10.1163/EJ.9789004165496.I-573.58

Bookman, R., Enzel, Y., Agnon, A., & Stein, M. (2004). Late Holocene lake levels of the dead sea. *Bulletin of the Geological Society of America*, *116*(5–6), 555–571. https://doi.org/10.1130/B25286.1

Borchhardt, J. (1975). *Myra: eine Lykische Metropole in antiker und byzantinischer Zeit. Gebr.* Berlin: Mann Verlag.

Borsato, A., Frisia, S., Fairchild, I. J., Somogyi, A., & Susini, J. (2007). Trace element distribution in annual stalagmite laminae mapped by micrometer-resolution X-ray fluorescence: Implications for incorporation of environmentally significant species. *Geochimica et Cosmochimica Acta*, *71*(6), 1494–1512. https://doi.org/10.1016/j.gca.2006.12.016

Bosworth, C. E. (1983). Iran and the Arabs before Islam. In E. Yarshater (Ed.), *The Cambridge History of Iran. Volume 3: The Seleucid, Parthian and Sasanid Periods, Part 1* (pp. 593–612). Cambridge: Cambridge University Press.

Bosworth, C. E. (1999). *The History of al-Tabari. Volume V: The Sasanids, the Byzantines, the Lakmids, and Yemen (translation)*. New York: State University of New York.

Bottema, S., Entjes-Nieborg, G., & van Zeist, W. (eds. . (1990). *Man's role in the shaping of the eastern Mediterranean landscape*. Rotterdam: A.A. Balkema.

Boucharlat, R. (2014). Fire altars and fire temples in the first millennia BC/AD in the Iranian

world: some remarks. In P. Bieliński, M. Gawlikowski, R. Koliński, D. Ławecka, A. Sołtysiak, & Z. Wygnańska (Eds.), *Proceedings of the 8th International Congress on the Archaeology of the Ancient Near East. Volume 1: Plenary Sessions, Township and Villages, High and Low - The Minor Arts for the Elite and for the Populace* (pp. 7–26). Wiesbaden: Harrassowitz.

Boucharlat, R., & Haerinck, E. (1991). Ceramics in Iran. The Parthian and Sasanian periods. In E. Yarshater (Ed.), *Encyclopaedia Iranica* (pp. 304–307). New York: Encyclopaedia Iranica Foundation.

Bowden, W. (2001). A new urban élite? Church builders and church building in late-antique Epirus. In L. Lavan & W. Bowden (Eds.), *Recent research in late-antique urbanism* (pp. 57–67). Portsmouth: Journal of Roman Archaeology.

Bowersock, G. W. (2013). *The Throne of Adulis: Red Sea Wars on the Eve of Islam*. Oxford: Oxford University Press.

Bowersock, G. W. (2017). *The crucible of Islam*. Oxford: Harvard University Press.

Bowersock, G. W., Brown, P., & Grabar, O. (1999). *Late antiquity: A guide to the postclassical world*. Cambridge: Harvard University Press.

Boyce, M. (1975). On the Zoroastrian Temple Cult of Fire. *Journal of the American Oriental Society*, *95*(3), 454–465.

Bradley, R. S. (2015). Paleoclimatic Reconstruction. In *Paleoclimatology* (pp. 1–11). Academic Press. https://doi.org/10.1016/b978-0-12-386913-5.00001-6

Brand, F. S., & Jax, K. (2007). Focusing the meaning(s) of resilience: Resilience as a descriptive concept and a boundary object. *Ecology and Society*, *12*(1), 23.

Brandt, H., & Kolb, F. (2005). *Lycia et Pamphylia: eine römische Provinz im südwesten Kleinasiens*. Mainz: Verlag Philipp von Zabern.

Bray, R. S. (2004). *Armies of pestilence: the impact of disease on history*. Camrbidge: Clarke & Co.

Brayshaw, D. J., Hoskins, B., & Black, E. (2010). Some physical drivers of changes in the winter storm tracks over the North Atlantic and Mediterranean during the Holocene. *Philosophical Transactions. Series A, Mathematical, Physical, and Engineering Sciences*, *368*(1931), 5185–223. https://doi.org/10.1098/rsta.2010.0180

Brock, S. P. (1982). Christians in the Sasanian empire: a case of divided loyalties. *Studies in Church History*, *18*, 1–19. https://doi.org/10.1017/S0424208400016004

Brockley, R. C. (1984). The Romano-Persian peace treaties of AD 299 and 363. *Florilegium*, *6*, 28–49.

Brockley, R. C. (1992). *East Roman Foreign Policy*. Leeds: Francis Cairns Publications.

Broecker, W. S. (1975). Climatic change: Are we on the brink of a pronounced global warming? *Science*, *189*(4201), 460–463. https://doi.org/10.1126/science.189.4201.460

Brown, P. (1971). *The World of Late Antiquity from Marcus Aurelius to Muhammad*. London: Thames and Hudson.

Brown, P. (1978). *The Making of Late Antiquity*. Cambridge, MA: Harvard University Press.

Brubaker, L., & Haldon, J. (2011). *Byzantium in the iconoclast era c. 680-850: a history*. Cambridge: Cambridge University Press.

Brunner, U. (1997). Geography and human settlements in ancient South Arabia. *Arabian Archaeology and Epigraphy*, *8*, 190–202.

Brunner, U. (2000a). The Great Dam and the Sabean Oasis of Ma'rib. *Irrigation and Drainage Systems*, *14*(3), 167–182. https://doi.org/10.1023/A:1026583213688

Brunner, U. (2000b). The sustainability of the ancient Great Dam of Ma'rib in Yemen. *Icid Journal*, *49*, 49–61.

Bulliet, R. W. (2009). *Cotton, Climate, and Camels in Early Islamic Iran: A Moment in World History*. New York: Columbia University Press.

Büntgen, U., Myglan, V. S., Ljungqvist, F. C., McCormick, M., Di Cosmo, N., Sigl, M., et al. (2016). Cooling and societal change during the Late Antique Little Ice Age from 536 to around 660 AD. *Nature Geoscience*, *9*(3), 231–236. https://doi.org/10.1038/ngeo2652

Büntgen, U., Arseneault, D., Boucher, É., Churakova (Sidorova), O. V., Gennaretti, F., Crivellaro, A., et al. (2020). Prominent role of volcanism in Common Era climate variability and human history. *Dendrochronologia*, *64*(September). https://doi.org/10.1016/j.dendro.2020.125757

Burstyn, Y., Martrat, B., Lopez, Jordi, F., Iriarte, E., Jacobson, M. J., Lone, M. A., & Deininger, M. (2019). Speleothems from the Middle East: An Example of Water Limited Environments in the SISAL Database. *Quaternary*, *2*(16). https://doi.org/10.3390/quat2020016

Butzer, K. W., & Endfield, G. H. (2012). Critical perspectives on historical collapse. *Proceedings of the National Academy of Sciences*, *109*(10), 3628–3631. https://doi.org/10.1073/PNAS.1114772109

Cadorin, J. F., Jongmans, D., Plumier, A., Camelbeeck, T., Delaby, S., & Quinif, Y. (2001). Modelling of speleothems failure in the Hotton cave (Belgium). Is the failure earthquake induced? *Netherlands Journal of Geosciences*, *80*(3–4), 315–321. https://doi.org/10.1017/S001677460002391X

Cameron, A. (2012). *The Mediterranean World in Late Antiquity: AD 395-700* (2nd Editio). New York: Routledge.

Cameron, A., & Hall, S. (1999). *Eusebius of Caesarea: Vita Constantini (Life of Constantine)*. New York: Oxford University Press.

Campopiano, M. (2017). Cooperation and private enterprise in water management in Iraq: Continuity and change between the Sasanian and early Islamic periods (sixth to tenth centuries). *Environment and History*, *23*(3), 385–407. https://doi.org/10.3197/096734017X14979473873867

Canepa, M. P. (2009). *The Two Eyes of the Earth: art and ritual of kingship between Rome and Sasanian Iran*. Berkeley: University of California Press.

Canepa, M. P., & Daryaee, T. (2018). Persia, economic history of. In O. Nicholson (Ed.), *The Oxford Dictionary of Late Antiquity* (p. 1160). Oxford: Oxford University Press.

Canepa, M. P., & Wiesehöfer, J. (2018). Persian Empire. In O. Nicholson (Ed.), *The Oxford Dictionary of Late Antiquity* (p. 1190). Oxford: Oxford University Press.

Cardille, J., Coe, M. T., & Vano, J. A. (2004). Impacts of Climate Variation and Catchment Area on Water Balance and Lake Hydrologic Type in Groundwater-Dominated Systems: A Generic Lake Model. *Earth Interactions*, *8*(13), 1–24.

Carolin, S. A., Walker, R. T., Day, C. C., Ersek, V., Alastair Sloan, R., Dee, M. W., et al. (2019). Precise timing of abrupt increase in dust activity in the Middle East coincident with 4.2 ka social change. *Proceedings of the National Academy of Sciences of the United States of America*, *116*(1), 67–72. https://doi.org/10.1073/pnas.1808103115

Carter, R. A., Challis, K., Priestman, S. M. N., & Tofighian, H. (2006). The Bushehr Hinterland Results of the First Season of the Iranian-British Archaeological Survey of Bushehr Province, November-December 2004. *Iran*, *44*(1), 63–103. https://doi.org/10.1080/05786967.2006.11834681

Casana, J., & Glatz, C. (2017). The land behind the land behind Baghdad: archaeological landscapes of the Upper Diyala (Sirwan) river valley. *Iraq*, *79*, 47–69. https://doi.org/10.1017/irq.2017.3

Cassis, M., Doonan, O., Elton, H., & Newhard, J. (2018). Evaluating Archaeological Evidence for Demographics, Abandonment, and Recovery in Late Antique and Byzantine Anatolia. *Human Ecology*, *46*(3), 381–398. https://doi.org/10.1007/s10745-018-0003-1

Cavalier, L. (2006). Observations sur l'architecture de Xanthos a l'époque archaïque. *Revue Des Etudes Anciennes*, *108*, 327–354.

Cerling, T. E. (1984). The stable isotopic composition of modern soil carbonate and its relationship to climate. *Earth and Planetary Science Letters*, *71*, 229–240.

Cesaretti, R., Lobo, J., Bettencourt, L., Ortman, S., & Smith, M. E. (2016). Population-Area Relationship for Medieval European Cities. *PLoS ONE*, *11*(10). https://doi.org/https://doi.org/10.1371/journal.pone.0162678

Çevik, N., & Bulut, S. (2007). The Belen and Kelbessos farmsteads with towers on the border of Pisidia-Lycia and some thoughts on security in the countryside. *Adalya*, *10*, 105–130.

Çevik, N., & Bulut, S. (2011). Excavations at Myra and Andriake in 2010. *ANMED*, *9*, 59–70.

Charbonnier, J. (2009). Dams in the western mountains of Yemen: a Himyarite model of water management. *Proceedings of the Seminar for Arabian Studies*, *39*, 81–93.

Charbonnier, J. (2011). The distribution of storage and diversion dams in the western mountains of South Arabia during the Himyarite period. *Proceedings of the Seminar for Arabian Studies*, *41*, 35–46.

Chen, Q. (2015). Climate shocks, dynastic cycles and nomadic conquests: Evidence from historical China. *Oxford Economic Papers*, *67*(2), 185–204. https://doi.org/10.1093/oep/gpu032

Cheng, H., Edwards, R. L., Hoff, J., Gallup, C. D., Richards, D. A., & Asmerom, Y. (2000). The half-lives of uranium-234 and thorium-230. *Chemical Geology*, *169*(1–2), 17–33. https://doi.org/10.1016/S0009-2541(99)00157-6

Cheng, H., Lawrence Edwards, R., Shen, C. C., Polyak, V. J., Asmerom, Y., Woodhead, J., et al. (2013). Improvements in 230 Th dating, 230 Th and 234 U half-life values, and U-Th isotopic measurements by multi-collector inductively coupled plasma mass spectrometry. *Earth and Planetary Science Letters*, *371–372*, 82–91. https://doi.org/10.1016/j.epsl.2013.04.006

Cheng, H., Sinha, A., Verheyden, S., Nader, F. H., Li, X. L., Zhang, P. Z., et al. (2015). The climate variability in northern Levant over the past 20,000 years. *Geophysical Research Letters*, *42*(20), 8641–8650. https://doi.org/10.1002/2015GL065397

Cheng, H., Spötl, C., Breitenbach, S. F. M., Sinha, A., Wassenburg, J. A., Jochum, K. P., et al. (2016). Climate variations of Central Asia on orbital to millennial timescales. *Scientific Reports*, *5*, 1–11. https://doi.org/10.1038/srep36975

Cheung, C., Zhang, H., Hepburn, J. C., Yang, D. Y., & Richards, M. P. (2019). Stable isotope and dental caries data reveal abrupt changes in subsistence economy in ancient China in response to global climate change. *PLOS ONE*, *14*(7), e0218943. https://doi.org/10.1371/JOURNAL.PONE.0218943

Chevalier, M., Davis, B. A. S., Heiri, O., Seppä, H., Chase, B. M., Gajewski, K., et al. (2020). Pollen-based climate reconstruction techniques for late Quaternary studies. *Earth-Science Reviews*, *210*, 103384. https://doi.org/10.1016/J.EARSCIREV.2020.103384

Chew, D., Drost, K., Marsh, J. H., & Petrus, J. A. (2021). LA-ICP-MS imaging in the geosciences and its applications to geochronology. *Chemical Geology*, *559*, 119917. https://doi.org/10.1016/J.CHEMGEO.2020.119917

Christensen, A. (1944). *L'Iran sous les Sassanides*. Copenhagen: E. Munksgaard.

Christensen, P. (1993). *The Decline of Iranshahr: Irrigation and Environments in the History of the Middle East, 500 B.C. to A.D. 1500*. Copenhagen: Museum Tusculanum Press.

Chrysos, E. (1978). The Title [basileús] in Early Byzantine International Relations. *Dumbarton Oaks Papers*, *32*, 30–75.

Çiner, A. (2019). Coastal Landforms and Landscapes of Turkey. In C. Kuzucuoğlu, A. Çiner, & N. Kazancı (Eds.), *Landscapes and Landforms of Turkey* (pp. 233–247). New York: Springer. https://doi.org/10.1007/978-3-030-03515-0_9

Cline, E. H. (2014). *1177 B.C.: The Year Civilization Collapsed*. Princeton, New Jersey: Princeton University Press.

Çolak, E., & Sunar, F. (2020). Evaluation of forest fire risk in the Mediterranean Turkish forests: A case study of Menderes region, Izmir. *International Journal of Disaster Risk Reduction*, *45*, 101479. https://doi.org/10.1016/J.IJDRR.2020.101479

Comas-Bru, L., & Harrison, S. P. (2019). SISAL: Bringing Added Value to Speleothem Research. *Quaternary*, *2*(1), 7. https://doi.org/10.3390/quat2010007

Commito, A. (2019). The cities of southern Asia Minor in the sixth century. *Asia Minor in the Long Sixth Century*, (2019), 109–142. https://doi.org/10.2307/j.ctvjsf69w.10

Conrad, L. (2000). The Arabs. In A. Cameron, B. Ward-Perkins, & M. Whitby (Eds.), *The Cambridge Ancient History, Vol. 14: Late Antiquity: Empire and Successors AD 425–600* (pp. 678–700). Cambridge: Cambridge University Press.

Contreras, D. A. (2016). *The Archaeology of Human-Environment Interactions: Strategies for Investigating Anthropogenic Landscapes, Dynamic Environments, and Climate Change in the Human Past*. (D. A. Contreras, Ed.). New York: Routledge. https://doi.org/10.4324/9781315697697

Contreras, D. A., Hiriart, E., Bondeau, A., Kirman, A., Guiot, J., Bernard, L., et al. (2018). Regional paleoclimates and local consequences: Integrating GIS analysis of diachronic settlement patterns and processbased agroecosystem modeling of potential agricultural productivity in Provence (France). *PLoS ONE*, *13*(12), e0207622. https://doi.org/10.1371/journal.pone.0207622

Contreras, D. A., Bondeau, A., Guiot, J., Kirman, A., Hiriart, E., Bernard, L., et al. (2019). From paleoclimate variables to prehistoric agriculture: Using a process-based agro-ecosystem model to simulate the impacts of Holocene climate change on potential agricultural productivity in Provence, France. *Quaternary International*, *501*, 303–316. https://doi.org/10.1016/j.quaint.2018.02.019

Cook, E. R., Seager, R., Kushnir, Y., Briffa, K. R., Büntgen, U., Frank, D., et al. (2015). Old World megadroughts and pluvials during the Common Era. *Science Advances*, *1*(10), e1500561. https://doi.org/10.1126/sciadv.1500561

Coombes, P., & Barber, K. (2005). Environmental determinism in Holocene research: Causality or coincidence? *Area*, *37*(3), 303–311. https://doi.org/10.1111/j.1475-4762.2005.00634.x

Cornwell, H. (2017). *Pax and the Politics of Peace: Republic to Principate*. Oxford: Oxford University Press.

Costa, S. (2015). The Late Antique economy: ceramics and trade. In Luke Lavan (Ed.), *Local Economies?: Production and Exchange of Inland Regions in Late Antiquity* (pp. 91–130).

Leiden: Brill.

Coulton, J. J. (2012a). *The Balboura Survey and Settlement in Highland Southwest Anatolia: Volume 1. Balboura and the history of highland settlement*. London: British Institute of Archaeology at Ankara.

Coulton, J. J. (2012b). *The Balboura Survey and Settlement in Highland Southwest Anatolia: Volume 2. The Balboura survey: detailed studies and catalogues*. London: British Institute of Archaeology at Ankara.

de Crespigny, R. (2007). *A Biographical Dictionary of Later Han to the Three Kingdoms (23–220 AD)*. Leiden: Brill.

Crone, P. (1987). *Meccan Trade and the Rise of Islam*. Piscataway, New Jersey: Gorgias Press.

Crone, P. (2007). Quraysh and the Roman army: Making sense of the Meccan leather trade. *Bulletin of the School of Oriental and African Studies*, *70*(1), 63–88. https://doi.org/10.1017/S0041977X0700002X

Crone, P. (2012). *The Nativist Prophets of Early Islamic Iran: Rural Revolt and Local Zoroastrianism*. Cambridge: Cambridge University Press.

Crone, P. (2016). Kavād's Heresy and Mazdak's Revolt. In P. Crone (Ed.), *The Iranian Reception of Islam: The Non-Traditionalist Strands* (pp. 1–49). Leiden: Brill.

Cullen, H. M., & DeMenocal, P. B. (2000). North Atlantic influence on Tigris-Euphrates streamflow. *International Journal of Climatology*, *20*(8), 853–863. https://doi.org/10.1002/1097-0088(20000630)20:8<853::AID-JOC497>3.0.CO;2-M

Cullen, H. M., Kaplan, A., Arkin, P. A., & DeMenocal, P. B. (2002). Impact of the North Atlantic Oscillation on Middle Eastern Climate and Streamflow. *Climatic Change*, *55*, 315–338. https://doi.org/10.1002/hyp.9960

Cumming, G. S., & Peterson, G. D. (2017). Unifying research on social-ecological resilience and collapse. *Trends in Ecology and Evolution*, *32*(9), 695–713.

De Cupere, B., Frémondeau, D., Kaptijn, E., Marinova, E., Poblome, J., Vandam, R., & Van Neer, W. (2017). Subsistence economy and land use strategies in the Burdur province (SW Anatolia) from prehistory to the Byzantine period. *Quaternary International*, *436*, 4–17. https://doi.org/10.1016/j.quaint.2015.11.097

Curtis, R. (2008). Food Processing and Preparation. In J. P. Oleson (Ed.), *Oxford Handbook of Engineering and Technology in the Classical World* (pp. 369–392). Oxford: Oxford University Press.

Dalezios, N. R., Gobin, A., Tarquis Alfonso, A. M., & Eslamian, S. (2017). Agricultural Drought Indices: Combining Crop, Climate, and Soil Factors. In S. Eslamian & F. Eslamian (Eds.), *Handbook of Drought and Water Scarcity: Environmental Impacts and Analysis of Drought and Water Scarcity* (pp. 73–89). Boca Raton: CRC Press. https://doi.org/10.1201/9781315404219-5

Danladi, I. B., & Akçer-Ön, S. (2018). Solar forcing and climate variability during the past millennium as recorded in a high altitude lake: Lake Salda (SW Anatolia). *Quaternary International*, *486*, 185–198. https://doi.org/10.1016/j.quaint.2017.08.068

Dansgaard, W. (1964). Stable isotopes in precipitation. *Tellus*, *16*(4), 436–468. https://doi.org/10.3402/tellusa.v16i4.8993

Dark, K. (2007). Globalizing Late Antiquity. Models, metaphors and the realities of long-distance trade and diplomacy. In A. Harris (Ed.), *Incipient Globalization? Long-distance trade in the sixth century AD* (pp. 3–14). Oxford: BAR International Series.

Darley, R., & Canepa, M. P. (2018). coinage, Persian. In Oliver Nicholson (Ed.), *The Oxford Dictionary of Late Antiquity* (p. 367). Oxford: Oxford University Press.

Daryaee, T. (2003). The Persian Gulf Trade in Late Antiquity. *Journal of World History*, *14*(1), 1–16. https://doi.org/10.1353/jwh.2003.0005

Daryaee, T. (2009a). *Sasanian Persia: The Rise and Fall of an Empire*. London: I.B. Tauris & Co Ltd.

Daryaee, T. (2009b). The Persian Gulf in Late Antiquity: The Sasanian Era (200–700 c.e.). *The Persian Gulf in History*, 57–70. https://doi.org/10.1057/9780230618459_3

Daryaee, T. (2018). Persian Literature. In Oliver Nicholson (Ed.), *The Oxford Dictionary of Late Antiquity* (pp. 1168–1172). Edinburgh: Edinburgh University Press.

Daryaee, T. (2019). *The Sasanian Empire*. *The Syriac World*. https://doi.org/10.4324/9781315708195-3

Daryaee, T., & Canepa, M. P. (2018). Mazdak and Mazdakism. In Oliver Nicholson (Ed.), *The Oxford Dictionary of Late Antiquity* (p. 996). Oxford: Oxford University Press.

Daryaee, T., & Rezakhani, K. (2016). *From Oxus to Euphrates: The World of Late Antique Iran*. Irvine, California: Jordan Centre for Persian Studies.

Daryaee, T., & Rezakhani, K. (2017). The Sasanian Empire. In T. Daryaee (Ed.), *King of the Seven Climes: A History of the Ancient Iranian World (3000 BCE - 651 CE)* (pp. 155–197). Irvine, California: UCI Jordan Centre for Persian Studies.

Dean, J. R., Jones, M. D., Leng, M. J., Noble, S. R., Metcalfe, S. E., Sloane, H. J., et al. (2015). Eastern Mediterranean hydroclimate over the late glacial and Holocene, reconstructed from the sediments of Nar lake, central Turkey, using stable isotopes and carbonate mineralogy. *Quaternary Science Reviews*, *124*, 162–174. https://doi.org/10.1016/j.quascirev.2015.07.023

Dean, J. R., Jones, M. D., Leng, M. J., Metcalfe, S. E., Sloane, H. J., Eastwood, W. J., & Roberts, C. N. (2018). Seasonality of Holocene hydroclimate in the Eastern Mediterranean reconstructed using the oxygen isotope composition of carbonates and diatoms from Lake Nar, central Turkey. *Holocene*, *28*(2), 267–276. https://doi.org/10.1177/0959683617721326

Decker, M. J. (2009a). Plants and Progress : Rethinking the Islamic Agricultural Revolution. *Journal of World History*, *20*(2), 187–206.

Decker, M. J. (2009b). *Tilling the Hateful Earth: Agricultural Production and Trade in the Late Antique East*. Oxford: Oxford University Press.

Decker, M. J. (2017a). Approaches to the environmental history of Late Antiquity, part 1: The rise of Islam. *History Compass*, *15*(10), e12407. https://doi.org/10.1111/hic3.12407

Decker, M. J. (2017b). Approaches to the environmental history of Late Antiquity, part II: Climate Change and the End of the Roman Empire. *History Compass*, *15*(10), e12425. https://doi.org/10.1111/hic3.12425

Decker, M. J. (2018a). Settlement patterns. In O. Nicholson (Ed.), *The Oxford Dictionary of Late Antiquity* (pp. 1364–1365). Oxford: Oxford University Press.

Decker, M. J. (2018b). The current state of Byzantine archeology. *History Compass*, *16*(9), e12459. https://doi.org/10.1111/hic3.12459

Decker, M. J., & Cooper, J. E. (2012). *Life and Society in Byzantine Cappadocia*. Basingstoke: Palgrave Macmillan.

Dee, D. P., Uppala, S. M., Simmons, A. J., Berrisford, P., Poli, P., Kobayashi, S., et al. (2011). The ERA-Interim reanalysis: configuration and performance of the data assimilation system. *Quarterly Journal of the Royal Meteorological Society*, *137*(656), 553–597. https://doi.org/10.1002/QJ.828

Degroot, D., Anchukaitis, K. J., Bauch, M., Burnham, J., Carnegy, F., Cui, J., et al. (2021). Towards a rigorous understanding of societal responses to climate change. *Nature*, *591*(March), 539–550. https://doi.org/10.1038/s41586-021-03190-2

deMenocal, P. B. (2001). Cultural Responses to Climate Change During the Late Holocene. *Science*, *292*(5517), 667–673. https://doi.org/10.1126/SCIENCE.1059287

Demer, S., Elitok, Ö., & Memiş, Ü. (2019). Origin and geochemical evolution of groundwaters at the northeastern extend of the active Fethiye-Burdur fault zone within the ophiolitic Teke nappes, SW Turkey. *Arabian Journal of Geosciences*, *12*(24). https://doi.org/10.1007/s12517-019-4963-2

Dewar, R. E. (1991). Incorporating Variation in Occupation Span into Settlement-Pattern Analysis. *American Antiquity*, *56*(4), 604–620.

Diamond, J. (1997). *Guns, Germs, and Steel: The Fates of Human Societies*. New York: W.W. Norton.

Diamond, J. (2005). *Collapse: How Societies Choose to Fail or Succeed*. New York: Penguin Books.

Dimbleby, G. W. (1985). *The palynology of archaeological sites*. London: Academic Press.

Djamali, M., de Beaulieu, J. L., Andrieu-Ponel, V., Berberian, M., Miller, N. F., Gandouin, E., et al. (2009a). A late Holocene pollen record from Lake Almalou in NW Iran: evidence for changing land-use in relation to some historical events during the last 3700 years. *Journal of Archaeological Science*, *36*(7), 1364–1375. https://doi.org/10.1016/j.jas.2009.01.022

Djamali, M., de Beaulieu, J.-L., Miller, N. F., Andrieu-Ponel, V., Lak, R., Sadeddin, M., et al. (2009b). Vegetation History of the SE Section of Zagros Mountains During the Last Five Millennia: A Pollen Record from the Maharlou Lake, Fars Province, Iran. *Vegetation History and Archaeobotany*, *18*, 123–136.

Djamali, M., Akhani, H., Khoshravesh, R., Andrieu-Ponel, V., Ponel, P., & Brewer, S. (2011). Application of the Global Bioclimatic Classification to Iran: implications for understanding the modern vegetation and biogeography. *Ecologia Mediterranea*, *37*(1), 91–114. https://doi.org/10.3406/ECMED.2011.1350

Djamali, M., Jones, M. D., Migliore, J., Balatti, S., Fader, M., Contreras, D., et al. (2016). Olive Cultivation in the Heart of the Persian Achaemenid Empire: New Insights to Agricultural Practices and Environmental Changes Reflected in a Late Holocene Pollen Record from Lake Parishan, SW Iran. *Vegetation History and Archaeobotany*, *25*(3), 255–269.

Dogar, M. M., Stenchikov, G., Osipov, S., Wyman, B., & Zhao, M. (2017). Sensitivity of the regional climate in the Middle East and North Africa to volcanic perturbations. *Journal of Geophysical Research*, *122*(15), 7922–7948. https://doi.org/10.1002/2017JD026783

Donner, F. M. (1981). *The early Islamic conquests*. Princeton, New Jersey: Princeton University Press.

Doonan, O. P. (2004). *Sinop Landscapes: Exploring Connection in a Black Sea Hinterland*. Philadelphia: University of Pennsylvania Museum of Archaeology and Anthropology.

Dorale, J. A., Edwards, R. L., Alexander, E. C., Shen, C.-C., Richards, D. A., & Cheng, H. (2004). Uranium-Series Dating of Speleothems: Current Techniques, Limits, & Applications. *Studies of Cave Sediments*, 177–197. https://doi.org/10.1007/978-1-4419-9118-8_10

Drake, B. L. (2012). The influence of climatic change on the Late Bronze Age Collapse and the Greek Dark Ages. *Journal of Archaeological Science*, *39*(6), 1862–1870. https://doi.org/10.1016/j.jas.2012.01.029

Dündar, E. (2018). The Maritime of Roman Patara. Preliminary Remarks on the Amphorae. *Skyliss*, *2*, 166–173.

Dussiubieux, L., Golitko, M., & Gratuze, B. (Eds.). (2016). *Recent Advances in Laser Ablation ICP-MS for Archaeology*. New York: Springer.

Eastwood, W. J., Roberts, N., & Lamb, H. F. (1998). Palaeoecological and archaeological evidence for human occupance in southwest Turkey: the Beyşehir occupation phase. *Anatolian Studies*, *48*, 69–86. https://doi.org/10.2307/3643048

Eastwood, Warren J., Leng, M. J., Roberts, N., & Davis, B. (2007). Holocene climate change in

the eastern Mediterranean region: A comparison of stable isotope and pollen data from Lake Gölhisar, southwest Turkey. *Journal of Quaternary Science*, *22*(4), 327–341. https://doi.org/10.1002/jqs.1062

Edgell, H. S. (2006). *Arabian Deserts: Nature, Origin and Evolution*. Dordrecht, The Netherlands: Springer.

Edwell, P. (2015). Arabs in the conflict between Rome and Persia. In G. Fisher (Ed.), *Arabs and empires before Islam, 491-630* (pp. 214–275). Oxford: Oxford University Press.

Eisenberg, M., & Mordechai, L. (2019, October 1). The Justinianic Plague: An interdisciplinary review. *Byzantine and Modern Greek Studies*. Cambridge University Press. https://doi.org/10.1017/byz.2019.10

Elias, S. A. (1994). *Quaternary insects and their environments*. Washington, D.C.: Smithsonian Institution Press.

Elias, S. A. (2021). Introduction to Paleoclimates. *Encyclopedia of Geology*, 288–298. https://doi.org/10.1016/B978-0-08-102908-4.00013-8

Ellenblum, R. (2012). *The Collapse of the Eastern Mediterranean: Climate Change and the Decline of the East, 950-1072*. Cambridge: Cambridge University Press.

Elman, Y. (2004). "Up to the ears" in horses' necks (B.M. 108a): On Sasanian agricultural policy and private "eminent doman." *Jewish Studies Internet Journal*, *3*, 95–149.

Elton, H. (2019). The countryside in southern Asia Minor in the long sixth century. In H. Elton & I. Jacobs (Eds.), *Asia Minor in the Long Sixth Century: Current Research and Future Directions* (pp. 91–108). Oxford: Oxbow Books. https://doi.org/10.2307/j.ctvjsf69w

Enzel, Y., Bookman, R., Sharon, D., Gvirtzman, H., Dayan, U., Ziv, B., & Stein, M. (2003). Late Holocene climates of the Near East deduced from Dead Sea level variations and modern regional winter rainfall. *Quaternary Research*, *60*(3), 263–273. https://doi.org/10.1016/j.yqres.2003.07.011

Erdoğan, O., & Ceylan, B. (2019). Church in Church: The Reuse of Late Antique Basilicas in Lycia in the Middle Ages (in Turkish). *Cedrus*, *7*, 663–679.

Erel, T., & Adatepe, F. (2007). Traces of historical earthquakes in the ancient city life at the Mediterranean region. *Journal of Black Sea / Mediterranean Environment*, *13*(3), 241–252.

Ergin, K., Guclu, U., & Uz, Z. (1967). *A Catalog of Earthquakes for Turkey and the Surrounding Area (11 A.D. to 1964 A.D.)*. Istanbul: Istanbul Technical Univeristy.

Ertuğrul, M., Varol, T., & Barış Özel, H. (2018). The Analysis of the Forest Fires in Turkey with Statistical Quality Control Method. *Modern Management Forum*, *2*(1), 1–12. https://doi.org/10.18686/mmf.v2i1.975

Evans, J. P., Smith, R. B., & Oglesby, R. J. (2004). Middle East climate simulation and dominant

precipitation processes. *International Journal of Climatology*, *24*(13), 1671–1694. https://doi.org/10.1002/joc.1084

Fairchild, I. J., & Baker, A. (2012). *Speleothem Science: From Process to Past Environments (Volume 3)*. New York: John Wiley & Sons, Ltd.

Fairchild, I. J., & Treble, P. C. (2009). Trace elements in speleothems as recorders of environmental change. *Quaternary Science Reviews*, *28*(5–6), 449–468. https://doi.org/10.1016/j.quascirev.2008.11.007

Fairchild, I. J., Baker, A., Borsato, A., Frisia, S., Hinton, R. W., McDermott, F., & Tooth, A. F. (2001). Annual to sub-annual resolution of multiple trace-element trends in speleothems. *Journal of the Geological Society*, *158*(5), 831–841. https://doi.org/10.1144/jgs.158.5.831

Fairchild, I. J., Smith, C. L., Baker, A., Fuller, L., Spötl, C., Mattey, D., & McDermott, F. (2006). Modification and preservation of environmental signals in speleothems. *Earth-Science Reviews*, *75*(1–4), 105–153. https://doi.org/10.1016/j.earscirev.2005.08.003

Fairchild, I. J., Frisia, S., Borsato, A., & Tooth, A. F. (2007). Speleothems. In D. J. Nash & S. J. McLaren (Eds.), *Geochemical Sediments and Landscapes* (pp. 200–245). Oxford: Blackwell Publishing Ltd.

Fakhar, Z., & Hesari, M. (2013). *Sasanian Exchange an Archaeological Perspective*. *Advances in Environmental Biology* (Vol. 7).

Farquhar, G. D. (1983). On the Nature of Carbon Isotope Discrimination in C4 Species. *Australian Journal of Plant Physiology*, *10*, 205–226.

Farquhar, G. D., Ehleringer, J. R., & Hubick, K. T. (1989). Carbon Isotope Discrimination and Photosynthesis. *Annual Review of Plant Physiology and Plant Molecular Biology*, *40*, 503–537.

Farrokh, K. (2005). *Sassanian Elite Cavalry AD 224-642*. Oxford: Osprey Publishing.

Farrokh, K. (2007). *Shadows in the Desert: Ancient Persia at War*. Oxford: Osprey Publishing.

Fellows, C. (1840). *An account of discoveries in Lycia, being a journal kept during a second excursion in Asia Minor*. London: J. Murray.

Feng, X., Faiia, A. M., & Posmentier, E. S. (2009). Seasonality of isotopes in precipitation: A global perspective. *Journal of Geophysical Research*, *114*(D8), D08116. https://doi.org/10.1029/2008JD011279

Ferranti, L., Pace, B., Valentini, A., Montagna, P., Pons-branchu, E., Tisnérat-laborde, N., & Maschio, L. (2019). Speleoseismological constraints on ground shaking threshold and seismogenic sources in the pollino range (Calabria, southern Italy). *Journal of Geophysical Research: Solid Earth*, *124*(5), 5192–5216. https://doi.org/10.1029/2018JB017000

Fetter, C. W. (1994). *Applied Hydrogeology*. Upper Saddle River: Prentice-Hall Inc.

Findlater, J. (1969). Interhemispheric transport of air in the lower troposphere over the western Indian Ocean. *Quarterly Journal of the Royal Meteorological Society*, *95*(404), 400–403. https://doi.org/10.1002/qj.49709540412

Finné, M., Holmgren, K., Sundqvist, H. S., Weiberg, E., & Lindblom, M. (2011). Climate in the eastern Mediterranean, and adjacent regions, during the past 6000 years - A review. *Journal of Archaeological Science*, *38*(12), 3153–3173. https://doi.org/10.1016/j.jas.2011.05.007

Finné, M., Bar-Matthews, M., Holmgren, K., Sundqvist, H. S., Liakopoulos, I., & Zhang, Q. (2014). Speleothem evidence for late Holocene climate variability and floods in Southern Greece. *Quaternary Research (United States)*, *81*(2), 213–227. https://doi.org/10.1016/j.yqres.2013.12.009

Finné, M., Holmgren, K., Shen, C. C., Hu, H. M., Boyd, M., & Stocker, S. (2017). Late Bronze Age climate change and the destruction of the Mycenaean palace of Nestor at Pylos. *PLoS ONE*, *12*(12), e0189447. https://doi.org/10.1371/journal.pone.0189447

Fleitmann, D., & Matter, A. (2009). The speleothem record of climate variability in Southern Arabia. *Comptes Rendus - Geoscience*, *341*(8–9), 633–642. https://doi.org/10.1016/j.crte.2009.01.006

Fleitmann, D., Burns, S. J., Mudelsee, M., Neff, U., Kramers, J., Mangini, A., & Matter, A. (2003). Holocene forcing of the Indian monsoon recorded in a stalagmite from Southern Oman. *Science*, *300*(5626), 1737–1739. https://doi.org/10.1126/SCIENCE.1083130

Fleitmann, D., Burns, S. J., Neff, U., Mudelsee, M., Mangini, A., & Matter, A. (2004). Palaeoclimatic interpretation of high-resolution oxygen isotope profiles derived from annually laminated speleothems from Southern Oman. In *Quaternary Science Reviews* (Vol. 23, pp. 935–945). Pergamon. https://doi.org/10.1016/j.quascirev.2003.06.019

Fleitmann, D., Burns, S. J., Mangini, A., Mudelsee, M., Kramers, J., Villa, I., et al. (2007). Holocene ITCZ and Indian monsoon dynamics recorded in stalagmites from Oman and Yemen (Socotra). *Quaternary Science Reviews*, *26*(1–2), 170–188. https://doi.org/10.1016/j.quascirev.2006.04.012

Fleitmann, D., Cheng, H., Badertscher, S., Edwards, R. L., Mudelsee, M., Göktürk, O. M., et al. (2009). Timing and climatic impact of Greenland interstadials recorded in stalagmites from northern Turkey. *Geophysical Research Letters*, *36*(19), 1–5. https://doi.org/10.1029/2009GL040050

Flohr, P., Fleitmann, D., Zorita, E., Sadekov, A., Cheng, H., Bosomworth, M., et al. (2017). Late Holocene droughts in the Fertile Crescent recorded in a speleothem from northern Iraq. *Geophysical Research Letters*, *44*(3), 1528–1536. https://doi.org/10.1002/2016GL071786

Fohlmeister, J., Voarintsoa, N. R. G., Lechleitner, F. A., Boyd, M., Brandtstätter, S., Jacobson, M. J., & Oster, J. L. (2020). Main controls on the stable carbon isotope composition of speleothems. *Geochimica et Cosmochimica Acta*, *279*, 67–87.

https://doi.org/10.1016/j.gca.2020.03.042

Foltz, R. (2010). Zoroastrian Attitudes toward Animals. *Society and Animals*, *18*, 367–378.

Ford, D., & Williams, P. (2007). *Karst Hydrogeology and Geomorphology*. Hoboken, New Jersey: John Wiley & Sons, Ltd.

Forti, P., & Postpischl, D. (1984). Seismotectonic and paleoseismic analyses using karst sediments. *Marine Geology*, *55*(1–2), 145–161. https://doi.org/10.1016/0025-3227(84)90138-5

Foss, C. (1991). Attaleia. In A.P. Kazhdan (Ed.), *The Oxford Dictionary of Byzantium*. Oxford: Oxford University Press.

Foss, C. (1993). Lycia in history. In J. Morganstern (Ed.), *The Fort at Dereağzı and Other Material Remains in its Vicinity: From Antiquity to the Middle Ages* (pp. 5–25). Tubingen: Ernst Wasmuth Verlag.

Foss, C. (1994). The Lycian Coast in the Byzantine Age. *Dumbarton Oaks Papers*, *48*, 1. https://doi.org/10.2307/1291721

Franke, J. G., Werner, J. P., & Donner, R. V. (2017). Reconstructing Late Holocene North Atlantic atmospheric circulation changes using functional paleoclimate networks, *13*, 1593–1608. https://doi.org/10.5194/cp-13-1593-2017

Frisia, S., Borsato, A., Drysdale, R. N., Paul, B., Greig, A., & Cotte, M. (2012). A re-evaluation of the palaeoclimatic significance of phosphorus variability in speleothems revealed by high-resolution synchrotron micro XRF mapping. *Climate of the Past*, *8*(6), 2039–2051. https://doi.org/10.5194/cp-8-2039-2012

Frye, R.N. (1993). Sasanian-central Asian trade relations. *Bulletin of the Asia Institute*, *7*, 73–77.

Frye, R.N. (2005). The Sassanians. In A. Bowman, A. Cameron, & P. Garnsey (Eds.), *The Crisis of Empire, AD 193-337* (2nd ed., pp. 461–480). Cambridge: Cambridge University Press.

Frye, Richard N. (1972). Byzantine and Sasanian Trade Relations with Northeastern Russia. *Source: Dumbarton Oaks Papers*, *26*, 263–269.

Fuller, B. T., De Cupere, B., Marinova, E., Van Neer, W., Waelkens, M., & Richards, M. P. (2012). Isotopic reconstruction of human diet and animal husbandry practices during the Classical-Hellenistic, imperial, and Byzantine periods at Sagalassos, Turkey. *American Journal of Physical Anthropology*, *149*(2), 157–171. https://doi.org/10.1002/ajpa.22100

Gajda, I. (2009). *Le royaume de Ḥimyar à l'époque monothéiste. l'histoire de l'Arabie du sud ancienne de la fin du IVe siècle de l'ère chrétienne jusqu'à l'avènement de l'Islam*. Paris: Académie des Inscriptions et Belles-Lettres.

Gallaher, C., Dahlman, C. T., Gilmartin, M., Mountz, A., & Shirlow, P. (2009). Introduction. In C. Gallaher, C. T. Dahlman, M. Gilmartin, A. Mountz, & P. Shirlow (Eds.), *Key Concepts in*

Political Geography (pp. 1–16). London: SAGE Publications Ltd.

Gardberg, C. J. (2001). *Late Nubian Sires: Churches and Settlements (The Scandinavian Joint Expedition to Sudanese Nubia, Vol. 7)*. Gothenburg: Astrom.

Garvey, R. (2018). Current and potential roles of archaeology in the development of cultural evolutionary theory. *Philosophical Transactions of the Royal Society B: Biological Sciences*, *373*(1743). https://doi.org/10.1098/RSTB.2017.0057

Gascoyne, M. (1992). Palaeoclimate determination from cave calcite deposits. *Quaternary Science Reviews*, *11*, 609–632.

Gasse, F. (2000). Hydrological changes in the African tropics since the Last Glacial Maximum. *Quaternary Science Reviews*, *19*(1–5), 189–211. https://doi.org/10.1016/S0277-3791(99)00061-X

Gates, M.-H. (1997). Archaeology in Turkey. *American Journal of Archaeology*, *101*(2), 241. https://doi.org/10.2307/506511

Van Geel, B., Coope, G. R., & Van Der Hammen, T. (1989). Palaeoecology and stratigraphy of the lateglacial type section at Usselo (the Netherlands). *Review of Palaeobotany and Palynology*, *60*(1–2). https://doi.org/10.1016/0034-6667(89)90072-9

Genito, B. (2016). A modern archaeology of the Sasanian Period: former limitations and new perspectives. *Newsletter Di Archeologia CISA*, *7*, 35–88.

Genty, D., Baker, A., Massault, M., Proctor, C., Gilmour, M., Pons-Branchu, E., & Hamelin, B. (2001). Dead carbon in stalagmites: Carbonate bedrock paleodissolution vs. ageing of soil organic matter. Implications for 13C variations in speleotherms. *Geochimica et Cosmochimica Acta*, *65*(20), 3443–3457. https://doi.org/10.1016/S0016-7037(01)00697-4

Gerlitz, L., Vorogushyn, S., & Gafurov, A. (2020). Climate informed seasonal forecast of water availability in Central Asia: State-of-the-art and decision making context. *Water Security*, *10*(July 2019), 100061. https://doi.org/10.1016/j.wasec.2020.100061

Geyh, M. (2000). Groundwater: Saturated and unsaturated zone. In W. Mook, J. Gat, H. Meijer, K. Rozanski, K. Frolich, M. Geyh, et al. (Eds.), *Environmental isotopes in the hydrological cycle* (1st editio, pp. 311–424). Paris: UNESCO.

Gholikandi, G. B., Sadrzadeh, M., Jamshidi, S., & Ebrahimi, M. (2013). Water resource management in ancient Iran with emphasis on technological approaches: a cultural heritage. *Water Science and Technology: Water Supply*, *13*(3), 582–589. https://doi.org/10.2166/ws.2013.084

Gignoux, P. (1971). *La liste des provinces de l'Eran dans les inscriptions de Sabuhr et de Kirdir*. Budapest: Academiae Scientarium Hungaricae.

Gignoux, P. (1994). Dietary Laws in Pre-Islamic and Post-Sasanian Iran: A Comparative Survey. *Jerusalem Studies in Arabic and Islam*, *17*, 16–42.

Gilbertson, D. D., Schwenninger, J. L., Kemp, R. A., & Rhodes, E. J. (1999). Sand-drift and Soil Formation Along an Exposed North Atlantic Coastline: 14,000 Years of Diverse Geomorphological, Climatic and Human Impacts. *Journal of Archaeological Science*, *26*(4), 439–469. https://doi.org/10.1006/JASC.1998.0360

Gilli, É. (2004). Glacial causes of damage and difficulties to use speleothems as palaeoseismic indicators. *Geodinamica Acta*, *17*(3), 229–240. https://doi.org/10.3166/ga.17.229-240

Gilli, É. (2005). Point sur l'utilisation des spéléothèmes comme indicateurs de paléosismicité ou de néotectonique. *Comptes Rendus - Geoscience*, *337*(13), 1208–1215. https://doi.org/10.1016/j.crte.2005.05.008

Gilliam, J. F. (1961). The Plague under Marcus Aurelius. *The American Journal of Philology*, *82*(3), 225–251.

Gilmartin, M. (2009). Colonialism/Imperialism. In C. Gallaher, C. T. Dahlman, M. Gilmartin, A. Mountz, & P. Shirlow (Eds.), *Key Concepts in Political Geography* (pp. 115–123). London: SAGE Publications Ltd.

Giorgi, F. (2006). Climate change hot-spots. *Geophysical Research Letters*, *33*(8), 1–4. https://doi.org/10.1029/2006GL025734

Giray, H. (2012). Turkish agriculture at a glance. *Journal of Food, Agriculture & Environment*, *10*(3–4), 292–295.

Gleick, P. H. (2014). Water, Drought, Climate Change, and Conflict in Syria. *Weather, Climate, and Society*, *6*(3), 331–340. https://doi.org/10.1175/WCAS-D-13-00059.1

Gogou, A., Triantaphyllou, M., Xoplaki, E., Izdebski, A., Parinos, C., Dimiza, M., et al. (2016). Climate variability and socio-environmental changes in the northern Aegean (NE Mediterranean) during the last 1500 years. *Quaternary Science Reviews*, *136*, 209–228. https://doi.org/10.1016/j.quascirev.2016.01.009

Gohari, A., Eslamian, S., Abedi-Koupaei, J., Massah Bavani, A., Wang, D., & Madani, K. (2013). Climate change impacts on crop production in Iran's Zayandeh-Rud River Basin. *Science of the Total Environment*, *442*, 405–419. https://doi.org/10.1016/j.scitotenv.2012.10.029

Göktürk, O. M. (2011). *Climate in the Eastern Mediterranean through the Holocene inferred from Turkish stalagmites (PhD Thesis)*. University of Bern, Switzerland.

Göktürk, O. M., Bozkurt, D., Şen, Ö. L., & Karaca, M. (2008). Quality control and homogeneity of Turkish precipitation data. *Hydrological Processes*, *22*(16), 3210–3218. https://doi.org/10.1002/HYP.6915

Göktürk, O. M., Fleitmann, D., Badertscher, S., Cheng, H., Edwards, R. L., Leuenberger, M., et al. (2011). Climate on the southern Black Sea coast during the Holocene: Implications from the Sofular Cave record. *Quaternary Science Reviews*, *30*(19–20), 2433–2445. https://doi.org/10.1016/j.quascirev.2011.05.007

Goldsworthy, A. (2016). *Pax Romana: War, Peace and Conquest in the Roman World*. New

Haven: Yale University Press.

Gore, A., Guggenheim, D., David, L., Bender, L., Burns, S. Z., Skoll, J., et al. (2006). *An Inconvenient Truth*. Hollywood, California: Paramount.

Gornall, J., Betts, R., Burke, E., Clark, R., Camp, J., Willett, K., & Wiltshire, A. (2010). Implications of climate change for agricultural productivity in the early twenty-first century. *Philosophical Transactions of the Royal Society B: Biological Sciences*, *365*(1554), 2973–2989. https://doi.org/10.1098/rstb.2010.0158

Grainger, J. D. (2009). *The Cities of Pamphylia*. Oxford: Oxbow Books.

Green, P. (1996). *The Greco-Persian Wars*. Oakland: University of California Press.

Greene, K. (2000). Technological Innovation and Economic Progress in the Ancient World: M. I. Finley Re-Considered. *Economic History Review*, *53*(1), 29–59.

Gremmen, W. H. E., & Bottema, S. (1991). Palynological Investigations in the Syrian Gazira. In H. Kühne, A. Mahmoud, & W. Röllig (Eds.), *Berichte der Ausgrabung Tall Šeh Hamad und Daten zur Umweltrekonstruktionen der assyrischen Stadt Dur-Katlimmu* (pp. 105–116). Berlin: Reimer.

Grossmann, P., & Severin, H.-G. (2003). *Frühchristliche und byzantinische Bauten im südöstlichen Lykien: Ergebnisse zweier Surveys. Istanbuler Forschungen Bd. 46.* Tübingen: Ernst Wasmuth Verlag.

Von Gunten, L., Grosjean, M., Beer, J., Grob, P., Morales, A., & Urrutia, R. (2009). Age modeling of young non-varved lake sediments: Methods and limits. Examples from two lakes in Central Chile. *Journal of Paleolimnology*, *42*(3), 401–412. https://doi.org/10.1007/s10933-008-9284-5

Gupta, A. K., Anderson, D. M., & Overpeck, J. T. (2003). Abrupt changes in the Asian southwest monsoon during the Holocene and their links to the North Atlantic Ocean. *Nature*, *421*, 354–357. https://doi.org/doi:10.1038/nature01340

Gwynn, D., & Bangert, S. (2010). Religious Diversity In Late Antiquity: An Introduction. In *Religious Diversity in Late Antiquity* (pp. 1–12). Leiden: Brill. https://doi.org/10.1163/ej.9789004180000.i-570.6

Gyselen, R. (1998). Economy IV. In the Sasanian Period. In *Encyclopaedia Iranica* (Volume VII, pp. 104–107). Enyclopaedia Iranica Foundation, Brill.

Gyselen, R. (2002). *Nouveaux materiaux pour la geographie historique de l'empire sassanide: sceaux administratifs de la collection Ahmad Saeedi*. Paris: Association pour l'avancement des etudes iraniennes.

Haas, C. (2008). Mountain Constantines; The Christianization of Aksum and Iberia. *Journal of Late Antiquity*, *1*(1), 101–126.

Haas, C. (2018). trade, Red Sea and Arabian. In O. Nicholson (Ed.), *The Oxford Dictionary of*

Late Antiquity (pp. 1516–1517). Oxford: Oxford University Press.

Haldon, J. (2016). *The Empire That Would Not Die: The Paradox of Eastern Roman Survival, 640–740*. Cambridge: Harvard University Press. https://doi.org/10.1093/ehr/cex279

Haldon, J., & Rosen, A. (2018). Society and Environment in the East Mediterranean ca 300–1800 CE. Problems of Resilience, Adaptation and Transformation. Introductory Essay. *Human Ecology 2018 46:3*, *46*(3), 275–290. https://doi.org/10.1007/S10745-018-9972-3

Haldon, J., Roberts, N., Izdebski, A., Fleitmann, D., McCormick, M., Cassis, M., et al. (2014). *The climate and environment of Byzantine Anatolia: Integrating science, history, and archaeology*. *Journal of Interdisciplinary History* (Vol. 45). https://doi.org/10.1162/JINH_a_00682

Haldon, J., Mordechai, L., Newfield, T. P., Chase, A. F., Izdebski, A., Guzowski, P., et al. (2018a). History meets palaeoscience: Consilience and collaboration in studying past societal responses to environmental change. *Proceedings of the National Academy of Sciences of the United States of America*, *115*(13), 3210. https://doi.org/10.1073/PNAS.1716912115

Haldon, J., Elton, H., Huebner, S. R., Izdebski, A., Mordechai, L., & Newfield, T. P. (2018b). Plagues, climate change, and the end of an empire: A response to Kyle Harper's The Fate of Rome (1): Climate. *History Compass*, *16*(12), e12508. https://doi.org/10.1111/hic3.12508

Haldon, J., Elton, H., Huebner, S. R., Izdebski, A., Mordechai, L., & Newfield, T. P. (2018c). Plagues, climate change, and the end of an empire. A response to Kyle Harper's The Fate of Rome (2): Plagues and a crisis of empire. *History Compass*, *16*(12), e12506. https://doi.org/10.1111/hic3.12506

Haldon, J., Chase, A. F., Eastwood, W., Medina-Elizalde, M., Izdebski, A., Ludlow, F., et al. (2020). Demystifying Collapse: Climate, environment, and social agency in pre-modern societies. *Millennium*, *17*(1), 1–33. https://doi.org/10.1515/mill-2020-0002

Hambrecht, G., Anderung, C., Brewington, S., Dugmore, A., Edvardsson, R., Feeley, F., et al. (2020). Archaeological sites as Distributed Long-term Observing Networks of the Past (DONOP). *Quaternary International*, *549*, 218–226. https://doi.org/10.1016/J.QUAINT.2018.04.016

Hansen, M. H. (2006). *Polis: An Introduction to the Ancient Greek City-State*. Oxford: Oxford University Press.

Harper, K. (2017). *The Fate of Rome*. Princeton, New Jersey: Princeton University Press.

Harris, J. (2007). *Constantinople: Capital of Byzantium*. London: Continuum.

Harris, J. (2010). *The End of Byzantium*. New Haven: Yale University Press.

Harrison, M. (2001). *Mountain and Plain*. Ann Arbor: University of Michigan Press.

Hartnell, T. (2014). Agriculture in Sasanian Persis: ideology and practice. *Journal of Ancient History*, *2*(2), 182–208. https://doi.org/10.1515/jah-2014-0028

Hatke, G. (2011). *Africans in Arabia Felix: Aksumite relations with Himyar in the sixth century C.E.* Princeton.

Hayes, J. W. (2000). From Rome to Beirut and Beyond: Asia Minor and Eastern Mediterranean Trade Connections. *Rei Cretariae Romanae Fautorum Acta*, *36*, 285–298.

Heather, P. (2005). *The Fall of the Roman Empire: A New History of Rome and the Barbarians*. Oxford: Oxford University Press.

Heck, G. W. (1999). Gold mining in Arabia and the rise of the Islamic state. *Journal of the Economic and Social History of the Orient*, *42*(3), 364–395.

Heinrich, I., Touchan, R., Dorado Liñán, I., Vos, H., & Helle, G. (2013). Winter-to-spring temperature dynamics in Turkey derived from tree rings since AD 1125. *Climate Dynamics*, *41*(7–8), 1685–1701. https://doi.org/10.1007/s00382-013-1702-3

Helama, S., Jones, P. D., & Briffa, K. R. (2017). Dark Ages Cold Period: A literature review and directions for future research. *Holocene*. https://doi.org/10.1177/0959683617693898

Helama, S., Arppe, L., Uusitalo, J., Holopainen, J., Mäkelä, H. M., Mäkinen, H., et al. (2018). Volcanic dust veils from sixth century tree-ring isotopes linked to reduced irradiance, primary production and human health. *Scientific Reports*, *8*(1), 1–12. https://doi.org/10.1038/s41598-018-19760-w

Hellenkemper, H., & Hild, F. (2004). *Tabula Imperii Byzantini 8: Lykien und Pamphylien*. Vienna: Austrian Academy of Sciences Press.

Henderson, S. A., von Caemmerer, S., & Farquhar, G. D. (1992). Short-term Measurements of Carbon Isotope Discrimination in Several C4 Species. *Australian Journal of Plant Physiology*, *19*, 263–285.

Hendy, C. H. (1971). The isotopic geochemistry of speleothems-I. The calculation of the effects of different modes of formation on the isotopic composition of speleothems and their applicability as palaeoclimatic indicators. *Geochimica et Cosmochimica Acta*, *35*(8), 801–824. https://doi.org/10.1016/0016-7037(71)90127-X

Hennekam, R., Jilbert, T., Schnetger, B., & de Lange, G. J. (2014). Solar forcing of Nile discharge and sapropel S1 formation in the early to middle Holocene eastern Mediterranean. *Paleoceanography*, *29*(5), 343–356. https://doi.org/10.1002/2013PA002553

Herrera, A. (2009). Crassulacean acid metabolism and fitness under water deficit stress: if not for carbon gain, what is facultative CAM good for? *Annals of Botany*, *103*(4), 645–653. https://doi.org/10.1093/aob/mcn145

Hijioka, Y., Lin, E., Pereira, J. J., Corlett, R. T., Cui, X., Insarov, G. E., et al. (2014). Asia. In V. R. Barros, C. B. Field, D. J. Dokken, M. D. Mastrandrea, K. J. Mach, T. E. Bilir, et al. (Eds.),

Climate Change 2014: Impacts, Adaptation, and Vulnerability. Part B: Regional Aspects. Contribution of Working Group II to the Fifth Assessment Report of the Intergovernmental Panel on Climate Change (pp. 1327–1370). Cambridge: Cambridge University Press.

Hirschfeld, Y. (2004). A Climatic Change in the Early Byzantine Period? Some Archaeological Evidence. *Palestine Exploration Quarterly*, *136*(2), 133–149. https://doi.org/10.1179/003103204225014184

Hirschfeld, Y. (2006). The Crisis of the Sixth Century: Climatic Change, Natural Disasters and the Plague. *Mediterranean Archaeology and Archaeometry*, *6*(1), 19–32.

Hirschon, R. (2003). *Crossing the Aegean: An Appraisal of the 1923 Compulsory Population Exchange Between Greece and Turkey*. Oxford: Berghahn Books.

Hojabri-Nobari, A., Khosrowzadeh, A., Mehdi Mousavi Kouhpar, S., & Vahdatinasab, H. (2011). Trade and Cultural Contacts between Northern and Southern Persian Gulf during Parthians and Sasanians: A Study Based on Pottery from Qeshm Island, *18*(2), 89–115.

Hole, F. (2007). Agricultural sustainability in the semi-arid Near East. *Climate of the Past*, *3*(2), 193–203. https://doi.org/10.5194/cp-3-193-2007

Hollander, D. B. (2019). *Farmers and Agriculture in the Roman Economy*. Abingdon: Routledge.

Hollesen, J., Matthiesen, H., Møller, A. B., Westergaard-Nielsen, A., & Elberling, B. (2016). Climate change and the loss of organic archaeological deposits in the Arctic. *Scientific Reports 2016 6:1*, *6*(1), 1–9. https://doi.org/10.1038/srep28690

Holling, C. ., & Gunderson, L. H. (2002). Resilience and adaptive cycles. In L. H. Gunderson & C. . Holling (Eds.), *Panarchy: Understanding Transformations in Human and Natural Systems* (pp. 25–62). Washington, D.C.: Island Press.

Holm, P., & Winiwarter, V. (2017). Climate change studies and the human sciences. *Global and Planetary Change*, *156*, 115–122. https://doi.org/10.1016/J.GLOPLACHA.2017.05.006

Hoorn, C., & Cremaschi, M. (2004). Late Holocene palaeoenvironmental history of Khawr Rawri and Khawr Al Balid (Dhofar, Sultanate of Oman). *Palaeogeography, Palaeoclimatology, Palaeoecology*, *213*(1–2), 1–36. https://doi.org/10.1016/J.PALAEO.2004.03.014

Hörandner, W., & Carr, A. W. (2005). Chi Rho. In Alexander P. Kazhdan (Ed.), *The Oxford Dictionary of Byzantium*. Oxford: Oxford University Press.

Horden, P., & Purcell, N. (2000). *The Corrupting Sea: A Study of Mediterranean History*. Oxford: Blackwell Publishing Ltd.

Houston, M. S. (2000). Chinese Climate, History, and State Stability in AD 536. In J. D. Gunn (Ed.), *The Years without Summer: Tracing AD 536 and Its Aftermath* (pp. 71–77). Oxford: BAR International Series.

Howard-Johnston, J. (1995). The Two Great Powers in Late Antiquity: A Comparison. In A. Cameron (Ed.), *The Byzantine and Early Islamic Near East, III, States, Resources, and Armies* (pp. 157–226). Princeton, New Jersey: Darwin Press.

Howard-Johnston, J. (2014). The Sasanian state: the evidence of coinage and military construction. *Journal of Ancient History*, *2*(2), 144–181. https://doi.org/10.1515/jah-2014-0032

Howard-Johnston, J. (2017). The India Trade in Late Antiquity. In E. Sauer (Ed.), *Sasanian Persia: Between Rome and Steppes of Eurasia* (pp. 284–304). Edinburgh: Edinburgh University Press.

Hoyland, R. G. (2001). *Arabia and the Arabs from the Bronze Age to the coming of Islam*. Princeton, New Jersey: Princeton University Press.

Hoyland, R. G. (2012). Early Islam as a Late Antique Religion. In S. F. Johnson (Ed.), *The Oxford Handbook of Late Antiquity* (pp. 1053–1077). Oxford: Oxford University Press. https://doi.org/10.1093/oxfordhb/9780195336931.013.0032

Hozhabri, A., & Watson, G. (2013). The evolution of religious architecture in the Sasanian Period. *Sasanika Archaeology*, *18*.

Huntington, E. (1913). Changes of Climate and History. *The American Historical Review*, *18*(2), 213–232.

Huntington, E. (1915). *Civilization and Climate*. New Haven: Yale University Press.

Huntington, E. (1917). Climatic change and agricultural exhaustion as elements in the fall of Rome. *The Quarterly Journal of Economics*, *31*(2), 173–208.

Huppert, A., & Solow, A. R. (2004). A method for reconstructing climate from fossil beetle assemblages. *Proceedings of the Royal Society B: Biological Sciences*, *271*(1544), 1125–1128. https://doi.org/10.1098/rspb.2004.2706

Hurrell, J. W. (1995). Decadal trends in the North Atlantic oscillation: Regional temperatures and precipitation. *Science*, *269*(5224), 676–679. https://doi.org/10.1126/science.269.5224.676

Hutter, M. (1993). Manichaeism in the Early Sasanian Empire. *Numen*, *40*(1), 2–15.

IAEA/WMO. (2021). Global Network of Isotopes in Precipitation. Retrieved July 17, 2020, from http://www.iaea.org/water

Inglebert, H. (2012). Introduction: Late Antique Conceptions of Late Antiquity. In S. F. Johnson (Ed.), *The Oxford Handbook of Late Antiquity* (pp. 4–30). Oxford: Oxford University Press. https://doi.org/10.1093/oxfordhb/9780195336931.013.0000

IPCC, & Houghton, T. J. (1990). *IPCC first assessment report*. Geneva: WMO.

Işkan, H. (2013). Neue Ergebnisse zur Wasserleitung von Patara / Türkei. In G. Wiplinger (Ed.),

Historische Wasserleitungen. Gestern – Heute – Morgen. Tagungsband des internationalen Frontinus-Symposiums, Wien 19. – 23. Oktober 2011 (pp. 93–103). Leuven: Peeters.

Izdebski, A. (2011). Why did agriculture flourish in the late antique East? The role of climate fluctuations in the development and contraction of agriculture in Asia Minor and the Middle East from the 4th till the 7th c. AD. *Millennium*, *8*(2011), 291–312. https://doi.org/10.1515/9783110236453.291

Izdebski, A. (2013a). *A rural world in transition: Asia Minor from Late Antiquity into the early Middle Ages*. Berlin: Taubenschlag Foundation.

Izdebski, A. (2013b). The Economic Expansion of the Anatolian Countryside in Late Antiquity: The Coast Cersus Inland Regions. In *Local Economies?: Production and Exchange of Inland Regions in Late Antiquity* (pp. 343–376). https://doi.org/10.1163/22134522-12340036

Izdebski, A., Holmgren, K., Weiberg, E., Stocker, S. R., Büntgen, U., Florenzano, A., et al. (2016a). Realising consilience: How better communication between archaeologists, historians and natural scientists can transform the study of past climate change in the Mediterranean. *Quaternary Science Reviews*, *136*, 5–22. https://doi.org/10.1016/j.quascirev.2015.10.038

Izdebski, A., Pickett, J., Roberts, N., & Waliszewski, T. (2016b). The environmental, archaeological and historical evidence for regional climatic changes and their societal impacts in the Eastern Mediterranean in Late Antiquity. *Quaternary Science Reviews*, *136*, 189–208. https://doi.org/10.1016/j.quascirev.2015.07.022

Jackson, M., Zelle, M., Vandeput, L., & Köse, V. (2012). Primary evidence for Late Roman D Ware production in southern Asia Minor: a challenge to 'Cypriot Red Slip Ware.' *Anatolian Studies*, *62*, 89–114.

Johnson, K., Hu, C., Belshaw, N. S., & Henderson, G. M. (2006). Seasonal trace-element and stable-isotope variations in a Chinese speleothem: The potential for high-resolution paleomonsoon reconstruction. *Earth and Planetary Science Letters*, *244*(1–2), 394–407. https://doi.org/10.1016/j.epsl.2006.01.064

Jones, M. D., & Roberts, N. (2008). Interpreting lake isotope records of Holocene environmental change in the Eastern Mediterranean. *Quaternary International*, *181*(1), 32–38. https://doi.org/10.1016/j.quaint.2007.01.012

Jones, M. D., Roberts, N., Leng, M. J., & Türkeş, M. (2006). A high-resolution late Holocene lake isotope record from Turkey and links to North Atlantic and monsoon climate. *Geology*, *34*(5), 361–364. https://doi.org/10.1130/G22407.1

Jones, M. D., Abu-Jaber, N., AlShdaifat, A., Baird, D., Cook, B. I., Cuthbert, M. O., et al. (2019). 20,000 years of societal vulnerability and adaptation to climate change in southwest Asia. *Wiley Interdisciplinary Reviews: Water*, *6*(2), e1330. https://doi.org/10.1002/wat2.1330

Kaniewski, D., & Van Campo, E. (2017). 3.2 ka BP Megadrought and the Late Bronze Age Collapse. In H. Weiss (Ed.), *Megadrought and Collapse: From Early Agriculture to Angkor* (pp. 161–182). Oxford: Oxford University Press.

Kaniewski, D., Paulissen, E., De Laet, V., Dossche, K., & Waelkens, M. (2007). A high-resolution Late Holocene landscape ecological history inferred from an intramontane basin in the Western Taurus Mountains, Turkey. *Quaternary Science Reviews*, *26*(17–18), 2201–2218. https://doi.org/10.1016/j.quascirev.2007.04.015

Kaniewski, D., Van Campo, E., & Weiss, H. (2012). Drought is a recurring challenge in the Middle East. *Proceedings of the National Academy of Sciences*, *109*(10), 3862–3867. https://doi.org/10.1073/pnas.1116304109

Kaniewski, D., Van Campo, E., Guiot, J., Le Burel, S., Otto, T., & Baeteman, C. (2013). Environmental Roots of the Late Bronze Age Crisis. *PLoS ONE*, *8*(8), 1–10. https://doi.org/10.1371/journal.pone.0071004

Kaniewski, D., Marriner, N., Cheddadi, R., Morhange, C., Bretschneider, J., Jans, G., et al. (2019). Cold and dry outbreaks in the eastern Mediterranean 3200 years ago. *Geology*, *47*(10), 933–937. https://doi.org/10.1130/g46491.1

Kaptijn, E., Poblome, J., Vanhaverbeke, H., Bakker, J., & Waelkens, M. (2013). Societal changes in the Hellenistic, Roman and early Byzantine periods. Results from the Sagalassos Territorial Archaeological Survey 2008 (southwest Turkey). *Anatolian Studies*, *63*(January), 75–95. https://doi.org/10.1017/S0066154613000057

Karaca, M., Deniz, A., & Tayanç, M. (2000). Cyclone track variability over Turkey in association with regional climate. *International Journal of Climatology*, *20*(10), 1225–1236. https://doi.org/10.1002/1097-0088(200008)20:10<1225::AID-JOC535>3.0.CO;2-1

Karami, N. (2019). The Modality of Climate Change in the Middle East: Drought or Drying up? *The Journal of Interrupted Studies*, *2*(1), 118–140. https://doi.org/10.1163/25430149-00201003

Karimian, H. (2008). Iranian society in the Sasanian period. In D. Kennet & P. Luft (Eds.), *Current research in Sasanian archaeology, art and history* (pp. 99–107). Oxford: Archaeopress.

Karimian, H. (2010). Cities and social order in Sasanian Iran - The archaeological potential. *Antiquity*, *84*, 453–466. https://doi.org/10.1017/S0003598X00066709

Katouzian, H. (2009). *The Persians: Ancient, Mediaeval and Modern Iran*. New Haven: Yale University Press.

Kazancı, N., & Roberts, N. (2019). The Lake Basins of South-west Anatolia. In C. Kuzucuoğlu, A. Çiner, & N. Kazancı (Eds.), *Landscapes and Landforms of Turkey* (pp. 325–337). New York: Springer. https://doi.org/10.1007/978-3-030-03515-0_15

Kelley, C. P., Mohtadi, S., Cane, M. A., Seager, R., & Kushnir, Y. (2015). Climate change in the Fertile Crescent and implications of the recent Syrian drought. *Proceedings of the*

National Academy of Sciences, *112*(11), 3241–3246. https://doi.org/10.1073/pnas.1421533112

Kennedy, H. (1999). Islam. In G. W. Bowersock, P. Brown, & O. Grabar (Eds.), *Late antiquity: a guide to the postclassical world*. Cambridge: Harvard University Press.

Kennedy, H. (2002). Military pay and the economy of the early Islamic state. *Historical Research*, *75*, 155–169.

Kennedy, H. (2004). *The Prophet and the Age of the Caliphates*. London: Pearson-Longman.

Kennet, D. (2002). Sasanian Pottery in Southern Iran and Eastern Arabia. *Journal of the British Institute of Persian Studies*, *40*(1), 153–162.

Kennet, D. (2007). The decline of eastern Arabia in the Sasanian period. *Arabian Archaeology and Epigraphy*, *18*(1), 86–122. https://doi.org/10.1111/j.1600-0471.2007.00274.x

Kern, Z., Demény, A., Perşoiu, A., & Hatvani, I. G. (2019). Speleothem Records from the Eastern Part of Europe and Turkey—Discussion on Stable Oxygen and Carbon Isotopes. *Quaternary 2019, Vol. 2, Page 31*, *2*(3), 31. https://doi.org/10.3390/QUAT2030031

Kern, Z., Hatvani, I. G., Czuppon, G., Fórizs, I., Erdélyi, D., Kanduč, T., et al. (2020). Isotopic "altitude" and "continental" effects in modern precipitation across the Adriatic-Pannonian region. *Water (Switzerland)*, *12*(6). https://doi.org/10.3390/w12061797

Kervan, M. (1994). Forteresses, entrepôts et commerce : Une histoire à suivre depuis les rois sassanides jusqu'aux princes d'Ormuz. In R. Curie & R. Gyselen (Eds.), *Itinéraires d'Orient: Hommages à Claude Cahen* (pp. 325–351). Leuven: Group pour l'Etude de la Civilisation du Moyen-Orient.

Keys, D. (1999). *Catastrophe: A quest for the origins of the modern world*. New York: Ballantine.

Khademi Nadooshan, F., & Khazaie, M. (2011). Probable Sources and Refining Technology of Parthian and Sasanian Silver Coins. *Interdisciplinaria Archaeologica - Natural Sciences in Archaeology*, *II*(2/2011), 101–107. https://doi.org/10.24916/iansa.2011.2.3

Kheirabadi, M. (1991). *Iranian Cities: Formation and Development*. Austin: University of Texas Press.

Kia, M. (2016). *The Persian Empire: A Historical Encyclopedia*. Santa Barbara: ABC-CLIO.

Knapp, A. B., & Manning, S. W. (2016). Crisis in Context: The End of the Late Bronze Age in the Eastern Mediterranean. *American Journal of Archaeology*, *120*(1), 99–149. https://doi.org/10.3764/aja.120.1.0099

Koç, K., Koşun, E., Cheng, H., Demirtaş, F., Lawrence Edwards, R., & Fleitmann, D. (2020). Black carbon traces of human activities in stalagmites from Turkey. *Journal of Archaeological Science*, *123*, 105255. https://doi.org/10.1016/J.JAS.2020.105255

Kokkinia, C. (2000). *Die Opramoas-Inschrift von Rhodiapolis: Euergetismus und Soziale Elite in Lykien*. Bonn: Rudolf Habelt.

Kopp, H. (1981). *Die Agrargeographie der Arabischen Republik Jemen*. Erlangen: Selbstverlag der Fränkischen Geographischen Gesellschaft.

Korotayev, A. V., Klimenko, V., & Proussakov, D. (1999). Origins of Islam: political-anthropological and environmental context. *Acta Orientalia Academiae Scientiarum Hungaricae*, *52*, 243–276.

Köse, N., Akkemik, Ü., Dalfes, H. N., & Özeren, M. S. (2011). Tree-ring reconstructions of May-June precipitation for western Anatolia. *Quaternary Research*, *75*(3), 438–450. https://doi.org/10.1016/j.yqres.2010.12.005

Kowalewski, S. A. (2008). Regional Settlement Pattern Studies. *Source: Journal of Archaeological Research*, *16*(3), 225–285. https://doi.org/10.1007/S10814-008-9020-8

Külzer, A. (2020). Ein historischer Atlas zum byzantinischen Reich: Anfänge und Entwicklung der Tabula Imperii Byzantini (TIB). In A. Külzer, V. Polloczek, & M. St. Popović (Eds.), *Raum und Geschichte: der historische Atlas 'Tabula Imperii Byzantini (TIB)' an der Österreichischen Akademie der Wissenschaften (Studies in Historical Geography and Cultural Heritage 3)* (pp. 11–30). Vienna-Novi Sad: Akademska knjiga.

Kutiel, H., & Benaroch, Y. (2002). North Sea-Caspian pattern (NCP) - An upper level atmospheric teleconnection affecting the Eastern Mediterranean: Identification and definition. *Theoretical and Applied Climatology*, *71*(1–2), 17–28. https://doi.org/10.1007/s704-002-8205-x

Kutiel, H., & Türkeş, M. (2005). New evidence for the role of the North Sea - Caspian Pattern on the temperature and precipitation regimes in continental Central Turkey. *Geografiska Annaler, Series A: Physical Geography*, *87*(4), 501–513. https://doi.org/10.1111/j.0435-3676.2005.00274.x

Kutiel, H., Maheras, P., Türkeş, M., & Paz, S. (2002). North Sea - Caspian Pattern (NCP) - An upper level atmospheric teleconnection affecting the eastern Mediterranean - Implications on the regional climate. *Theoretical and Applied Climatology*. https://doi.org/10.1007/s00704-002-0674-8

Kuzucuoğlu, C., Dörfler, W., Kunesch, S., & Goupille, F. (2011). Mid- to late-Holocene climate change in central Turkey: The tecer lake record. *Holocene*, *21*(1), 173–188. https://doi.org/10.1177/0959683610384163

Kwarteng, A. Y., Dorvlo, A. S., & Kumar, G. T. V. (2009). Analysis of a 27-year rainfall data (1977-2003) in the Sultanate of Oman. *International Journal of Climatology*, *29*(4), 605–617. https://doi.org/10.1002/joc.1727

Labuhn, I., Finné, M., Izdebski, A., Roberts, N., & Woodbridge, J. (2018). Climatic Changes and Their Impacts in the Mediterranean during the First Millennium AD. *Late Antique Archaeology*, *12*(1), 65–88. https://doi.org/10.1163/22134522-12340067

Lachniet, M. S. (2009). Climatic and environmental controls on speleothem oxygen-isotope values. *Quaternary Science Reviews*, *28*(5–6), 412–432. https://doi.org/10.1016/j.quascirev.2008.10.021

Laiou, A. E. (2002). Writing the eocnomic history of Byzantium. In A. E. Laiou (Ed.), *The economic history of Byzantium* (pp. 3–8). Washington, D.C.: Dumbarton Oaks.

Landes, D. S. (1998). *The wealth and poverty of nations*. New York: W.W. Norton.

Last, W. M., & Smol, J. P. (Eds.). (2001). *Tracking Environmental Change Using Lake Sediments. Volume 2: Physical and Geochemical Methods.* Dordrecht, The Netherlands: Kluwer Academic Publishers.

Lawrence, D., & Wilkinson, T. J. (2017). The Northern and Western Borderlands of the Sasanian Empire: Contextualising the Roman/Byzantine and Sasanian Frontier. In E. Sauer (Ed.), *Sasanian Persia: Between Rome and Steppes of Eurasia* (pp. 99–125). Edinburgh: Edinburgh University Press.

Lechterbeck, J., & Jensen, C. E. (2020). Exploring the potential of palynology in archaeological contexts: proceedings of the session held at the 24th Annual Meeting of the European Association of Archaeologists in Barcelona 2018. *Vegetation History and Archaeobotany 2020 29:2*, *29*(2), 111–112. https://doi.org/10.1007/S00334-020-00773-3

Lecker, M. (2010). Pre-Islamic Arabia. *The New Cambridge History of Islam: Volume 1: The Formation of the Islamic World Sixth to Eleventh Centuries*, (April), 153–170. https://doi.org/10.1017/CHOL9780521838238.006

Lelieveld, J., Hadjinicolaou, P., Kostopoulou, E., Chenoweth, J., El Maayar, M., Giannakopoulos, C., et al. (2012). Climate change and impacts in the Eastern Mediterranean and the Middle East. *Climatic Change*, *114*(3–4), 667–687. https://doi.org/10.1007/s10584-012-0418-4

Leng, M. J., & Henderson, A. C. G. (2013). Recent advances in isotopes as palaeolimnological proxies. *Journal of Paleolimnology 2013 49:3*, *49*(3), 481–496. https://doi.org/10.1007/S10933-012-9667-5

Leng, M. J., Lamb, A. L., Heaton, T. H. E., Marshall, J. D., Wolfe, B. B., Jones, M. D., et al. (2006). Isotopes in lake sediments. In M. J. Leng (Ed.), *Isotopes in Palaeoenvironmental Research (Volume 10)* (pp. 147–184). Dordrecht, The Netherlands: Springer.

Levine, X. J., Schneider, T., Levine, X. J., & Schneider, T. (2015). Baroclinic Eddies and the Extent of the Hadley Circulation: An Idealized GCM Study. *Journal of Atmospheric Science*, *72*, 2744–2761.

Lewis, S. C., Gagan, M. K., Ayliffe, L. K., Zhao, J. xin, Hantoro, W. S., Treble, P. C., et al. (2011). High-resolution stalagmite reconstructions of Australian-Indonesian monsoon rainfall variability during Heinrich stadial 3 and Greenland interstadial 4. *Earth and Planetary Science Letters*, *303*(1–2), 133–142. https://doi.org/10.1016/j.epsl.2010.12.048

Lewit, T. (2020). A view point on Eastern Mediterranean villages in late antiquity: Applying the

lens of community resilience theory. *Studies in Late Antiquity*, *4*(1), 44–75. https://doi.org/10.1525/sla.2020.4.1.44

Li, S. (2006). The distribution and significance of Sassanid silver currency in China. *Chinese Archaeology*, *6*, 190–194.

Li, T. (2021). Sasanian's Role in the Trading Network of the Silk Roads: An Insight into the Coins Found along the Silk Roads. *The Frontiers of Society, Science and Technology*, *3*(2), 56–59. https://doi.org/10.25236/FSST.2021.030210

Lightfoot, D. R. (1996). Syrian qanat Romani. *Journal of Arid Environments*, *33*, 321–336.

Lionello, P. (2012). *The Climate of the Mediterranean Region: From the Past to the Future*. London: Elsevier Inc.

Liu, YongSheng, Hu, Z., Li, M., & Gao, S. (2013). Applications of LA-ICP-MS in the elemental analyses of geological samples. *Chinese Science Bulletin 2013 58:32*, *58*(32), 3863–3878. https://doi.org/10.1007/S11434-013-5901-4

Liu, Yuyun, Wang, L., Zhou, W., & Chen, W. (2014). Three Eurasian teleconnection patterns: Spatial structures, temporal variability, and associated winter climate anomalies. *Climate Dynamics*, *42*(11–12), 2817–2839. https://doi.org/10.1007/s00382-014-2163-z

Luterbacher, J., Newfield, T. P., Xoplaki, E., Nowatzki, E., Luther, N., Zhang, M., & Khelifi, N. (2020). Past pandemics and climate variability across the Mediterranean. *Euro-Mediterranean Journal for Environmental Integration*, *5*(2), 5–7. https://doi.org/10.1007/s41207-020-00197-5

Luterbacher, Jürg, Garcia-Herrera, R., Akçer-Ön, S., Allan, R., Alvarez-Castro, M. C., Benito, G., et al. (2012). A review of 2000 years of paleoclimatic evidence in the Mediterranean. In P. Lionello (Ed.), *The Climate of the Mediterranean region: from the past to the future* (pp. 87–185). Amsterdam: Elsevier.

Macdonald, M. C. A., Corcella, A., Daryaee, T., Fisher, G., Gibbs, M., Lewin, A., et al. (2015). Arabs and Empires before the Sixth Century. In Greg Fisher (Ed.), *Arabs and Empires before Islam* (pp. 11–89). Oxford: Oxford University Press. https://doi.org/10.1093/acprof:oso/9780199654529.003.0002

Mackensen, M., & Scheider, G. (2006). Production centres of African Red Slip ware (2nd–3rd c.) in northern and central Tunisia: archeological provenance and reference groups based on chemical analysis. *Journal of Roman Archaeology*, *19*, 163–190.

Majd, S. R., & Taheri Sarparvar, A. (2016). An Overview on Commercial Relations between Iran and China in the era of Empires Sassanid. *International Academic Journal of Humanities*, *3*(11), 36–40. Retrieved from www.iaiest.com

Malalas, J. (2017). *The Chronicle of John Malalas*. (E. Jeffreys, M. Jeffreys, & R. Scott, Eds.), *The Chronicle of John Malalas*. Melbourne: Australian Association for Byzantine Studies. https://doi.org/10.1163/9789004344600

Mango, C., Scott, R., & Greatrex, G. (1997). *The Chronicle of Theophanes Confessor: Byzantine and Near Eastern History, AD 284-813*. Oxford: Oxford University Press.

Manning, S. W., Lorentzen, B., Welton, L., Batiuk, S., & Harrison, T. P. (2020). *Beyond megadrought and collapse in the Northern Levant: The chronology of Tell Tayinat and two historical inflection episodes, around 4.2ka BP, and following 3.2ka BP*. *PLoS ONE* (Vol. 15). https://doi.org/10.1371/journal.pone.0240799

Mannocchi, F., Todisco, F., & Vergni, L. (2004). Agricultural drought: indices, definition and analysis. In *The Basis of Civilization-Water Science? (Proceedings of the UNESCO/IAIIS/IWIIA symposium held in Rome. December 2003)* (Vol. 286). Rome: IAHS Publ.

Mansouri Daneshvar, M. R., Ebrahimi, M., & Nejadsoleymani, H. (2019). An overview of climate change in Iran: facts and statistics. *Environmental Systems Research 2019 8:1*, *8*(1), 1–10. https://doi.org/10.1186/S40068-019-0135-3

Manuel, M., Coningham, R. A. E., Gillmore, G. K., & Fazeli, H. (2014). Societal change and sustainability within the Central Plateau of Iran: an archaeological viewpoint. In P. Sillitoe (Ed.), *Sustainable development: an appraisal from the Gulf Region* (pp. 38–61). London: Berghahn Books.

Manuel, M., Lightfoot, D., & Fattahi, M. (2018). The sustainability of ancient water control techniques in Iran: an overview. *Water History*, *10*(1), 13–30. https://doi.org/10.1007/s12685-017-0200-7

Maresca, G. (2019). Hydraulic Infrastructures in South-Western Iran during the Sasanian Period: some Archaeological Remarks. *Vicino Oriente*, *XXIII*, 207–222. https://doi.org/10.4000/abstractairanica.52090

Marshall, M. H., Lamb, H. F., Davies, S. J., Leng, M. J., Kubsa, Z., Umer, M., & Bryant, C. (2009). Climatic change in northern Ethiopia during the past 17,000 years: A diatom and stable isotope record from Lake Ashenge. *Palaeogeography, Palaeoclimatology, Palaeoecology*, *279*(1–2), 114–127. https://doi.org/10.1016/j.palaeo.2009.05.003

Marston, J. M. (2011). Archaeological markers of agricultural risk management. *Journal of Anthropological Archaeology*, *30*(2), 190–205. https://doi.org/10.1016/j.jaa.2011.01.002

Marston, J. M. (2015). Modeling Resilience and Sustainability in Ancient Agricultural Systems. *Journal of Ethnobiology*, *35*(3), 585–605. https://doi.org/10.2993/etbi-35-03-585-605.1

Marston, J. M. (2021). Archaeological Approaches to Agricultural Economies. *Journal of Archaeological Research*, *29*(3), 327–385. https://doi.org/10.1007/s10814-020-09150-0

Martens, F. (2008). Water Abundance and Shortage at Sagalassos (SW-Turkey). In C. Ohlig (Ed.), *Cura Aquarum in Jordanien. Beiträge des 13. Internationalen Symposiums zur Geschichte der Wasserwirtschaft und des Wasserbaus im Mediterranen Raum. Petra/Amman 31. März – 09 April 2007* (p. 247=262). Siegburg: DWhG.

Martín-Chivelet, J., Muñoz-García, M. B., Cruz, J. A., Ortega, A. I., & Turrero, M. J. (2017).

Speleothem Architectural Analysis: Integrated approach for stalagmite-based paleoclimate research. *Sedimentary Geology*, *353*, 28–45. https://doi.org/10.1016/j.sedgeo.2017.03.003

Martin, G. J. (2005). *All possible worlds: A history of geographic ideas*. New York: Oxford University Press.

Marx, W., Haunschild, R., & Bornmann, L. (2018). Climate and the decline and fall of the Western Roman Empire: A bibliometric view on an interdisciplinary approach to answer a most classic historical question. *Climate*, *6*(4), 1–34. https://doi.org/10.3390/cli6040090

Mashkour, M., Khazeli, R., Fathi, H., Amiri, S., Decruyenaere, D., Mohaseb, A., et al. (2017). Animal Exploitation and Subsistence on the Borders of the Sasanian Empire: From the Gorgan Wall (Iran) to the Gates of the Alans (Georgia). In E. Sauer (Ed.), *Sasanian Persia: Between Rome and Steppes of Eurasia* (pp. 74–98). Edinburgh: Edinburgh University Press.

Maslova, V. N., Voskresenskaya, E. N., Lubkov, A. S., Yurovsky, A. V., Zhuravskiy, V. Y., & Evstigneev, V. P. (2020). Intense cyclones in the black sea region: change, variability, predictability and manifestations in the storm activity. *Sustainability (Switzerland)*, *12*(11). https://doi.org/10.3390/su12114468

Masson-Delmotte, V., Schulz, M., Abe-Ouchi, A., Beer, J., Ganopolski, A., Gonzalez-Rouco, J. F., et al. (2013). Information from Paleoclimate Archives. In T. F. Stocker, D. Qin, G.-K. Plattner, M. Tignor, S. K. Allen, J. Boschung, et al. (Eds.), *Climate Change 2013: The Physical Science Basis. Contribution of Working Group I to the Fifth Assessment Report of the Intergovernmental Panel on Climate Change* (pp. 383–464). Cambridge: Cambridge University Press.

Maxwell, J. (2012). Paganism and Christianization. In S. F. Johnson (Ed.), *The Oxford Handbook of Late Antiquity* (pp. 849–875). Oxford: Oxford University Press. https://doi.org/10.1093/OXFORDHB/9780195336931.013.0026

Mayerson, P. (1983). The City of Elusa in the Literary Sources of the Fourth–Sixth Centuries. *Israel Exploration Journal*, *33*(3/4), 247–253.

Mayewski, P. A., Rohling, E. E., Stager, J. C., Karlén, W., Maasch, K. A., Meeker, L. D., et al. (2004). Holocene climate variability. *Quaternary Research*, *62*(3), 243–255. https://doi.org/10.1016/j.yqres.2004.07.001

McCormick, M. (2007). Towards a Molecular History of the Justinianic Pandemic. In L. K. Little (Ed.), *Plague and the End of Antiquity: The Pandemic of 541-750* (pp. 290–312). Cambridge: Cambridge University Press.

McCormick, M. (2011). History's Changing Climate: Climate Science, Genomics, and the Emerging Consilient Approach to Interdisciplinary History. *The Journal of Interdisciplinary History*, *42*(2), 251–273. https://doi.org/10.1162/jinh_a_00214

McCormick, M. (2012). Movements and Markets in the First Millennium Information, Containers, and Shipwrecks. In C. Morrisson (Ed.), *Trade and Markets in Byzantium* (pp.

51–98). Washington, D.C.: Dumbarton Oaks.

McCormick, M., Büntgen, U., Cane, M. A., Cook, E. R., Harper, K., Huybers, P., et al. (2012). Climate Change during and after the Roman Empire: Reconstructing the Past from Scientific and Historical Evidence. *Journal of Interdisciplinary History*, *43*(2), 169–220. https://doi.org/10.1162/JINH_a_00379

McDermott, F. (2004). Palaeo-climate reconstruction from stable isotope variations in speleothems: A review. *Quaternary Science Reviews*, *23*(7–8), 901–918. https://doi.org/10.1016/j.quascirev.2003.06.021

McDermott, F., Schwarcz, H. P., & Rowe, P. J. (2006). Isotopes in speleothems. In M. J. Leng (Ed.), *Isotopes in Palaeoenvironmental Research (Volume 10)* (pp. 185–226). Dordrecht, The Netherlands: Springer.

McDonald, J., Drysdale, R., & Hill, D. (2004). The 2002-2003 El Niño recorded in Australian cave drip waters: Implications for reconstructing rainfall histories using stalagmites. *Geophysical Research Letters*, *31*(22), 1–4. https://doi.org/10.1029/2004GL020859

McMichael, A. J. (2012). Insights from past millennia into climatic impacts on human health and survival. *Proceedings of the National Academy of Sciences*, *109*(13), 4730–4737. https://doi.org/10.1073/pnas.1120177109

McNeill, J. R. (1992). *The Mountains of the Mediterranean World*. Cambridge: Cambridge University Press.

Meier, M. (2004). Prokop, Agathias, die Pest und das 'Ende' der antiken Historiographie. Naturkatastrophen und Geschichtsschreibung in der ausgehenden Spätantike. *Historische Zeitschrif*, *278*, 281–310.

Meier, M. (2016). The 'Justinianic Plague'. The Economic Consequences of the Pandemic in the Eastern Roman Empire and Its Cultural and Religious Effects. *Early Medieval Europe*, *24*(267–292).

Meier, M. (2020). The 'Justinianic Plague': An "Inconsequential Pandemic"? A Reply. *Medizinhistorisches Journal*, *55*(2), 172–199. https://doi.org/10.25162/MHJ-2020-0006

Mellado-Cano, J., Barriopedro, D., García-Herrera, R., Trigo, R. M., & Hernández, A. (2019). Examining the north atlantic oscillation, east atlantic pattern, and jet variability since 1685. *Journal of Climate*, *32*(19), 6285–6298. https://doi.org/10.1175/JCLI-D-19-0135.1

Mendoza, B. (2005). Total solar irradiance and climate. *Advances in Space Research*, *35*(5), 882–890. https://doi.org/10.1016/J.ASR.2004.10.011

Mercuri, A. M., Sadori, L., & Blasi, C. (2010). Archaeobotany for cultural landscape and human impact reconstructions. *Plant Biosystems*, *144*(4), 860–864. https://doi.org/10.1080/11263504.2010.514137

Mercuri, A. M., Bandini Mazzanti, M., Florenzano, A., Montecchi, M. C., & Rattighieri, E. (2013). Olea, Juglans and Castanea: The OJC group as pollen evidence of the development of

human-induced environments in the Italian peninsula. *Quaternary International*, *303*, 24–42. https://doi.org/10.1016/J.QUAINT.2013.01.005

Meyer, J. C. (2013). City and hinterland. Villages and estates north of Palmyra. New Perspectives. *Study of Palmyra*, *12*, 269–286.

Meyer, W. B., & Guss, D. M. T. (2017). *Neo-Environmental Determinism*. London: Palgrave Macmillan.

Mildrexler, D. J., Zhao, M., & Running, S. W. (2006). Where are the hottest spots on Earth? *Eos, Transactions American Geophysical Union*, *87*(43), 461–467. https://doi.org/10.1029/2006EO430002

Miller, C. B., & Wheeler, P. A. (2012). *Biological Oceanography*. Hoboken, New Jersey: Wiley-Blackwell.

Miller, C. S., Leroy, S. A. G., Collins, P. E. F., & Lahijani, H. A. K. (2016). Late Holocene vegetation and ocean variability in the Gulf of Oman. *Quaternary Science Reviews*, *143*, 120–132. https://doi.org/10.1016/j.quascirev.2016.05.010

Milner, N. P. (2016). Building Roman Lycia: new inscriptions and monuments from the baths and peristyle buildings Ml 1 and Ml 2 at Oinoanda. *Anatolian Studies*, *66*, 91–124.

Mitchell, D. (2000). *Cultural geography: a critical introduction*. Oxford: Blackwell Publishing Ltd.

Mitchell, S. (2005). The Treaty between Rome and Lycia of 46 BC (MS 2070). In R. Pintaudi (Ed.), *Papyri Graecae Schøyen. The Schøyen Collection V: Greek Papyri Vol. I.* (pp. 165–258). Florence: Gonnelli.

Mitchell, S. (2018). The Great Plague of Late Antiquity in Asia Minor. In C. Şimşek & T. Kaçar (Eds.), *The Lykos Valley and Neighborhood in Late Antiquity* (pp. 27–36). Istanbul: Ege Yayınları.

Moghaddam, A. (2012). *Later Village Period Settlement Development in the Karun River Basin, Upper Khuzestan Plain, Greater Susiana, Iran*. Oxford: Archaeopress.

Molanejad, M., Soltani, M., Ranjbar Saadat Abadi, A., Babu, C. A., Sohrabi, M., & Martin, M. V. (2015). Climatology of cyclones and their tracking over southern coasts of Caspian Sea. *International Journal of Environmental Research*, *9*(1), 117–132. https://doi.org/10.22059/ijer.2015.881

Molavi-Arabshahi, M., Arpe, K., & Leroy, S. A. G. (2016). Precipitation and temperature of the southwest Caspian Sea region during the last 55 years: Their trends and teleconnections with large-scale atmospheric phenomena. *International Journal of Climatology*, *36*(5), 2156–2172. https://doi.org/10.1002/joc.4483

Montgomery-Watt, W. (1953). *Muhammad at Mecca*. Oxford: Oxford University Press.

Mordechai, L. (2018). Short-term Cataclysmic Events in Premodern Complex Societies. *Human*

Ecology, *46*(3), 323–333. https://doi.org/10.1007/s10745-018-9971-4

Mordechai, L., & Pickett, J. (2018). Earthquakes as the Quintessential SCE: Methodology and Societal Resilience. *Human Ecology*, *46*(3), 335–348. https://doi.org/10.1007/s10745-018-9985-y

Mordechai, L., Eisenberg, M., Newfield, T. P., Izdebski, A., Kay, J. E., & Poinar, H. (2019). The Justinianic Plague: An inconsequential pandemic? *Proceedings of the National Academy of Sciences of the United States of America*, *116*(51), 25546–25554. https://doi.org/10.1073/pnas.1903797116

Moreland, J. (2018). Ad536 – Back To Nature? *Acta Archaeologica*, *89*(1), 91–111. https://doi.org/10.1111/j.1600-0390.2018.12194.x

Morin, E., Ryb, T., Gavrieli, I., & Enzel, Y. (2019). Mean, variance, and trends of Levant precipitation over the past 4500 years from reconstructed Dead Sea levels and stochastic modeling. *Quaternary Research (United States)*, *91*(2), 751–767. https://doi.org/10.1017/qua.2018.98

Morony, M. G. (2004). Economic Boundaries? Late Antiquity and Early Islam. *Journal of the Economic and Social History of the Orient*, *47*(2), 166–194.

Morris, S. (2005). Greek Towers and Slaves: An Archaeology of Exploitation. *Journal of Archaeology*, *109*(2), 155–225.

Morrisson, C., & Sodini, J.-P. (2002). The Sixth-Century Economy. In A. E. Laiou (Ed.), *The Economic History of Byzantium* (pp. 171–220). Washington, D.C.: Dumbarton Oaks.

Moser, S. C., & Hart, J. A. F. (2015). The long arm of climate change: societal teleconnections and the future of climate change impacts studies. *Climatic Change 2015 129:1*, *129*(1), 13–26. https://doi.org/10.1007/S10584-015-1328-Z

Mousavi, A., & Daryaee, T. (2012). The Sasanian Empire: An Archaeological Survey, c.220-AD 640. In D. Potts (Ed.), *A Companion to the Archaeology of the Ancient Near East* (pp. 1076–1094). London: Blackwell Publishing Ltd.

Muñoz-García, M. B., Cruz, J., Martín-Chivelet, J., Ortega, A. I., Turrero, M. J., & López-Elorza, M. (2016). Comparison of speleothem fabrics and microstratigraphic stacking patterns in calcite stalagmites as indicators of paleoenvironmental change. *Quaternary International*, *407*, 74–85. https://doi.org/10.1016/J.QUAINT.2016.02.036

Nebes, N. (2010). The martyrs of Najrān and the end of the himyar: On the political history of South Arabia in the early sixth century. In A. Neuwirth, N. Sinai, & M. Marx (Eds.), *The Qur'an in Context. Historical and Literary Investigations into the Qur'anic Milieu* (pp. 27–59). Boston: Brill.

Neely, J. A. (2016). Parthian and Sasanian settlement patterns on the Deh Luran Plain, Khuzistan Province, southwestern Iran. *Iranica Antiqua*, *51*, 235–300. https://doi.org/10.2143/IA.51.0.3117836

Nemani, R. R., Keeling, C. D., Hashimoto, H., Jolly, W. M., Piper, S. C., Tucker, C. J., et al. (2003). Climate-driven increases in global terrestrial net primary production from 1982 to 1999. *Science*, *300*(5625), 1560–1563. https://doi.org/10.1126/science.1082750

Newfield, T. P. (2018). The Climate Downturn of 536-50. In S. Whites, C. Pfister, & F. Mauelshagen (Eds.), *The Palgrave Handbook of Climate History* (pp. 447–493). London: Palgrave Macmillan. https://doi.org/10.1057/978-1-137-43020-5

Nezafati, N., & Pernicka, E. (2012). Early silver production in Iran. *Iranian Archaeology*, *3*, 37–45.

Nicholson, S. L., Pike, A. W. G., Hosfield, R., Roberts, N., Sahy, D., Woodhead, J., et al. (2020). Pluvial periods in Southern Arabia over the last 1.1 million-years. *Quaternary Science Reviews*, *229*, 106112. https://doi.org/10.1016/J.QUASCIREV.2019.106112

Oikonomides, N. (1983). The Usual Lead Seal. *Dumbarton Oaks Papers*, *37*, 147–157.

Olbrycht, M. J. (2016). Dynastic Connections in the Arsacid Empire and the Origins of the House of Sasan. In *The Parthian and Early Sasanian Empires: Adaptation and Expansion* (pp. 23–35). Oxford: Oxbow Books.

van Oldenborgh, G. J. (2020). KNMI Climate Explorer. Retrieved July 17, 2020, from https://climexp.knmi.nl/start.cgi

Orellana, F. A., Gálvez, C. G., Orellana, F. A., Gálvez, C. G., Roldán, M. T., García-Ruiz, C., et al. (2013). Applications of laser-ablation-inductively-coupled plasma-mass spectrometry in chemical analysis of forensic evidence. *TrAC Trends in Analytical Chemistry*, *42*, 1–34. https://doi.org/10.1016/J.TRAC.2012.09.015

Orland, I. J., Bar-Matthews, M., Kita, N. T., Ayalon, A., Matthews, A., & Valley, J. W. (2009). Climate deterioration in the Eastern Mediterranean as revealed by ion microprobe analysis of a speleothem that grew from 2.2 to 0.9 ka in Soreq Cave, Israel. *Quaternary Research*. https://doi.org/10.1016/j.yqres.2008.08.005

Orton, C., & Hughes, M. (2013). *Pottery in Archaeology* (2nd Editio). Cambridge: Cambridge University Press.

Österreichischen Archäologischen Instituts. (2017). *Wissenschaftlicher Jahresbericht des Österreichischen Archäologischen Instituts*. Vienna: ÖAW.

Ousterhout, R. (2019). *Eastern Medieval Architecture. The Building Traditions of Byzantium and Neighboring Lands*. Oxford: Oxford University Press.

Öztürk, M. Z., Çetınkaya, G., & Aydin, S. (2017). Köppen-Geiger İklim Sınıflandırmasına Göre Türkiye'nin İklim Tipleri - (Climate Types of Turkey According to Köppen-Geiger Climate Classification). *Istanbul University Journal of Geography*, *35*, 17–27. https://doi.org/10.26650/jgeog330955

PAGES 2k Consortium, Neukom, R., Barboza, L. A., Erb, M. P., Shi, F., Emile-Geay, J., et al. (2019). Consistent multidecadal variability in global temperature reconstructions and

simulations over the Common Era. *Nature Geoscience*, *12*(8), 643–649. https://doi.org/10.1038/s41561-019-0400-0

Palmisano, A., Bevan, A., & Shennan, S. (2017). Comparing archaeological proxies for long-term population patterns: An example from central Italy. *Journal of Archaeological Science*, *87*, 59–72. https://doi.org/10.1016/j.jas.2017.10.001

Panahipour, M. (2021). Land Use and Environment in a Zone of Uncertainty: A Case of the Sasanian Expansion in Eastern Iraq–Western Iran. *Iran*, *59*(1), 90–108. https://doi.org/10.1080/05786967.2019.1657781

Papadopoulos, G. A., Daskalaki, E., Fokaefs, A., & Giraleas, N. (2007). Tsunami hazards in the Eastern Mediterranean: Strong earthquakes and tsunamis in the East Hellenic Arc and Trench system. *Natural Hazards and Earth System Science*, *7*(1), 57–64. https://doi.org/10.5194/nhess-7-57-2007

Pashazanous, H. R., Zohouri, M. M., & Ahmadi, T. (2014). Sea Trade between Iran and China in the Persian Gulf based on the Excavations of Sīrāf City. *Indian Journal of Economics and Development*, *2*(2), 6–13.

Patrich, J. (1995). *Sabas, Leader of Palestinian Monasticism. A Comparative Study in Eastern Monasticism, Fourth to Seventh Centuries*. Washington, D.C.: Dumbarton Oaks Research Library and Collection.

Payne, R. (2014). The archaeology of Sasanian politics. *Journal of Ancient History*, *2*(2), 80–92. https://doi.org/10.1515/jah-2014-0029

Payne, R. (2018). The silk road and the Iranian political economy in late antiquity: Iran, the Silk Road, and the problem of aristocratic empire. *Bulletin of the School of Oriental and African Studies*, *81*(2), 227–250. https://doi.org/10.1017/S0041977X18000459

Peel, M. C., Finlayson, B. L., & McMahon, T. A. (2007). Updated world map of the Köppen-Geiger climate classification. *Hydrology and Earth System Sciences*. https://doi.org/10.5194/hess-11-1633-2007

Peregrine, P. N. (2020). Climate and social change at the start of the Late Antique Little Ice Age. *The Holocene*, *30*(11), 1643–1648. https://doi.org/10.1177/0959683620941079

Peschlow, U. (2017). Patara. In P. Niewöhner (Ed.), *The Archaeology of Byzantine Anatolia: From the End of Late Antiquity until the Coming of the Turks* (pp. 280–291). Oxford: Oxford University Press.

Peterson, T. C., & Vose, R. S. (1997). An Overview of the Global Historical Climatology Network Temperature Database. *Bulletin of the American Meteorological Society*, *78*(12), 2837–2849. https://doi.org/10.1175/1520-0477(1997)078<2837:AOOTGH>2.0.CO;2

Philippsen, B. (2013). The freshwater reservoir effect in radiocarbon dating. *Heritage Science 2013 1:1*, *1*(1), 1–19. https://doi.org/10.1186/2050-7445-1-24

Phillipson, D. W. (2012). *Foundations of an African Civilisation*. New York: James Currey.

Pickett, J. (2017). Water and empire in the de aedificiis of procopius. *Dumbarton Oaks Papers*, *71*, 95–125.

Pickett, J. (2020). Hydraulic Landscapes of Cities in the East Roman World. In J. Beardsley & G. Farhat (Eds.), *Landscapes of Pre-industrial Urbanism*. Washington, D.C.: Dumbarton Oaks.

Pieri, D. (2012). Regional and Interregional Exchanges in the Eastern Mediterranean during the Early Byzantine Period The Evidence of Amphorae. In C. Morrisson (Ed.), *Trade and Markets in Byzantium* (pp. 27–50). Washington, D.C.: Dumbarton Oaks.

Piotrovsky, M. B. (1994). Late ancient and early medieval Yemen: settlement traditions and innovations. In G. R. D. King & A. Cameron (Eds.), *The Byzantine and early Islamic Near East, II. Land use and settlement patterns* (pp. 213–220). Princeton, New Jersey: Princeton University Press.

Pirazzoli, P. A., Laborel, J., & Stiros, S. C. (1996). Earthquake clustering in the eastern Mediterranean during historical times. *Journal of Geophysical Research: Solid Earth*, *101*(B3), 6083–6097. https://doi.org/10.1029/95jb00914

Plog, F. T. (1973). Diachronic Anthropology. In C. L. Redman (Ed.), *Research and Theory in Current Archaeology* (pp. 181–198). New York: John Wiley & Sons, Ltd.

Poblome, J. (2015). The Economy of the Roman World as a Complex Adaptive System: Testing the Case in Second to Fifth Century CE Sagalassos. In P. Erdkamp & K. Verboven (Eds.), *Structure and Performance in the Roman Economy: Models, Methods, and Case Studies* (pp. 97–140). Brussels: Éditions Latomus.

Poblome, J., Talloen, P., & Kaptijn, E. (2017). Sagalassos. In P. Niewöhner (Ed.), *The Archaeology of Byzantine Anatolia: From the End of Late Antiquity until the Coming of the Turks* (pp. 302–311). Oxford: Oxford University Press.

Ponel, P., Andrieu-Ponel, V., Djamali, M., Lahijani, H., Leydet, M., & Mashkour, M. (2013). Fossil beetles as possible evidence for transhumance during the middle and late Holocene in the high mountains of Talysch (Talesh) in NW Iran. *Environmental Archaeology*, *18*(3), 201–210. https://doi.org/10.1179/1749631413Y.0000000007

Ponton, C., Giosan, L., Eglinton, T. I., Fuller, D. Q., Johnson, J. E., Kumar, P., & Collett, T. S. (2012). Holocene aridification of India, *39*(December 2011), 1–6. https://doi.org/10.1029/2011GL050722

Potts, D. (1990). *The Arabian Gulf in Antiquity 2: From Alexander the Great to the coming of Islam*. Oxford: Clarendon Press.

Potts, D. (1997). Late Sasanian armament from southern Arabia. *Electrum*, *1*, 127–137.

Potts, D. (2018). Fars (MP Pārs; Gk. Persis). In Oliver Nicholson (Ed.), *The Oxford Dictionary of Late Antiquity* (p. 586). Oxford: Oxford University Press.

Pourshariati, P. (2008). *Decline and Fall of the Sasanian Empire: The Sasanian-Parthian*

Confederacy and the Arab Conquest of Iran. London: I.B. Tauris & Co Ltd.

Preiser-Kapeller, J. (2015). A collapse of the Eastern Mediterranean? New results and theories on the interplay between climate and societies in Byzantium and the Near East, ca. 1000-1200 AD. *Jahrbuch Der Österreichischen Byzantinistik*, *65*, 195–242. https://doi.org/10.1126/science.1235367

Premo, L. S. (2014). Reports Cultural Transmission and Diversity in Time-Averaged Assemblages. *Current Anthropology*, *55*(1). https://doi.org/10.1086/674873

Psomiadis, D., Dotsika, E., Albanakis, K., Ghaleb, B., & Hillaire-Marcel, C. (2018). Speleothem record of climatic changes in the northern Aegean region (Greece) from the Bronze Age to the collapse of the Roman Empire. *Palaeogeography, Palaeoclimatology, Palaeoecology*, *489*(January), 272–283. https://doi.org/10.1016/j.palaeo.2017.10.021

Quézel, P., & Médail, F. (2003). *Ecologie et biogéographie des forêts du bassin méditerranéen*. Paris: Elsevier.

Raith, M. M., Hoffbauer, R., Euler, H., Yule, P. A., & Damgaard, K. (2013). Archaeometric Study of the Aqaba Late Roman Period Pottery Complex and Distribution in the 1st Millennium CE. *Zeitschrift Für Orient-Archäologie*, *6*, 320–350.

Rampelbergh, M. Van, Fleitmann, D., Verheyden, S., Cheng, H., Edwards, L., Geest, P. De, et al. (2013). Mid- to late Holocene Indian Ocean Monsoon variability recorded in four speleothems from Socotra Island , Yemen. *Quaternary Science Reviews*, *65*, 129–142. https://doi.org/10.1016/j.quascirev.2013.01.016

Ratzel, F. (1882). *Anthropogeographie. Volume 1.* Stuttgart: J. Englehorn.

Ratzel, F. (1891). *Anthropogeographie. Volume 2.* Stuttgart: J. Englehorn.

Rees, R. (2004). Diocletian and the tetrarchy, 219.

Regattieri, E., Zanchetta, G., Drysdale, R. N., Isola, I., Hellstrom, J. C., & Dallai, L. (2014). Lateglacial to Holocene trace element record (Ba, Mg, Sr) from Corchia Cave (Apuan Alps, central Italy): Paleoenvironmental implications. *Journal of Quaternary Science*, *29*(4), 381–392. https://doi.org/10.1002/jqs.2712

Rezakhani, K. (2016). The Arab Conquests and Sasanian Iran. *Mizan*, 1–16.

Rezakhani, K. (2017). *ReOrienting the Sasanians*. Edinburgh: Edinburgh University Press.

Rice, C. (2020). The ports of Roman Lycia: Urbanism, networks, and hierarchies. In M. E. Flohrr (Ed.), *Urban Space and Urban History in the Roman World* (pp. 241–265). New York: Routledge.

Riehl, S., Pustovoytov, K. E., Weippert, H., Klett, S., & Hole, F. (2014). Drought stress variability in ancient Near Eastern agricultural systems evidenced by δ 13 C in barley grain, *111*(34), 12348–12353. https://doi.org/10.1073/pnas.1409516111

Ritter, C. (1832). *Die Erdkunde im Verhältniss zur Natur und zur Geschichte des Menschen. Volumen 1.* Berlin: G. Reimer.

Robert, M. S., Smart, P. L., Hawkesworth, C. J., Perkins, W. T., & Pearce, N. J. G. (1999). Trace element variations in coeval Holocene speleothems from GB Cave, southwest England. *Holocene*, *9*(6), 707–713. https://doi.org/10.1191/095968399672615014

Roberts, N. (2018). Revisiting the Beyşehir Occupation Phase: Land-Cover Change and the Rural Economy in the Eastern Mediterranean During the First Millennium AD. *Late Antique Archaeology*, *11*(1), 53–68. https://doi.org/10.1163/22134522-12340052

Roberts, N., Jones, M. D., Benkaddour, A., Eastwood, W. J., Filippi, M. L., Frogley, M. R., et al. (2008). Stable isotope records of Late Quaternary climate and hydrology from Mediterranean lakes: the ISOMED synthesis. *Quaternary Science Reviews*, *27*(25–26), 2426–2441. https://doi.org/10.1016/j.quascirev.2008.09.005

Roberts, N., Moreno, A., Valero-Garcés, B. L., Corella, J. P., Jones, M., Allcock, S., et al. (2012). Palaeolimnological evidence for an east-west climate see-saw in the Mediterranean since AD 900. *Global and Planetary Change*, *84–85*, 23–34. https://doi.org/10.1016/j.gloplacha.2011.11.002

Roberts, N., Woodbridge, J., Bevan, A., Palmisano, A., Shennan, S., & Asouti, E. (2018a). Human responses and non-responses to climatic variations during the last Glacial-Interglacial transition in the eastern Mediterranean. *Quaternary Science Reviews*, *184*, 47–67. https://doi.org/10.1016/j.quascirev.2017.09.011

Roberts, N., Cassis, M., Doonan, O., Eastwood, W., Elton, H., Haldon, J., et al. (2018b). Not the End of the World? Post-Classical Decline and Recovery in Rural Anatolia. *Human Ecology*, *46*(3), 305–322. https://doi.org/10.1007/s10745-018-9973-2

Roberts, N., Woodbridge, J., Palmisano, A., Bevan, A., Fyfe, R., & Shennan, S. (2019). Mediterranean landscape change during the Holocene: Synthesis, comparison and regional trends in population, land cover and climate. *Holocene*, *29*(5), 923–937. https://doi.org/10.1177/0959683619826697

Robin, C. J. (2006). South Arabia, Religions in Pre-Islamic. In J. D. McAuliffe (Ed.), *Encyclopaedia of the Qurʾān*. Leiden: Brill.

Robin, C. J. (2012). Arabia and Ethiopia. In *The Oxford Handbook of Late Antiquity* (pp. 247–333). Oxford: Oxford University Press.

Robin, C. J. (2015). Ḥimyar, Aksūm, and Arabia Deserta in late antiquity: the epigraphic evidence. In Greg Fisher (Ed.), *Arabs and empires before Islam* (pp. 127–171). Oxford: Oxford University Press.

Robinson, C. F. (2003). Reconstructing early Islam: Truth and consequences. In H. Berg (Ed.), *Method and theory in the study of Islamic origins* (pp. 101–134). Leiden: Brill.

Robinson, C. F. (2011). The rise of Islam, 600-705. In C. F. Robinson (Ed.), *The New Cambridge History Of Islam (Vol. 1): The Formation of the Islamic World Sixth to Eleventh Centuries*

(pp. 173–225). Cambridge: Cambridge University Press.

Rosen, A. M. (2007). *Civilizing Climate: Social Responses to Climate Change in the Ancient Near East*. Lanham: AltaMira Press.

Rowe, P. J., Wickens, L. B., Sahy, D., Marca, A. D., Peckover, E., Noble, S., et al. (2020). Multi-proxy speleothem record of climate instability during the early last interglacial in southern Turkey. *Palaeogeography, Palaeoclimatology, Palaeoecology*, *538*, 109422. https://doi.org/10.1016/J.PALAEO.2019.109422

Rozanski, K., Araguãs-Araguãs, L., & Gonfiantini, R. (1992). Relation between long-term trends of oxygen-18 isotope composition of precipitation and climate. *Science*, *258*(5084), 981–985. https://doi.org/10.1126/SCIENCE.258.5084.981

Sadori, L., Bertini, A., Combourieu-Nebout, N., Kouli, K., Mariotti Lippi, M., Roberts, N., & Mercuri, A. M. (2013). Palynology and Mediterranean vegetation history. *Flora Mediterranea*, *23*(December), 141–156. https://doi.org/10.7320/FlMedit23.141

Saeidi Ghavi Andam, S., Djamali, M., Nelle, O., Naderi Beni, A., Haghighifard, M., Brisset, E., & Poschlod, P. (2020). Vegetation history of the Maharlou Lake basin (SW Iran) with special reference to the Achaemenid period (550–330 BC). *Vegetation History and Archaeobotany*. https://doi.org/10.1007/s00334-020-00810-1

Safarkhani, E., Yarahmadi, D., Hamzeh, M. A., & Sharafi, S. (2021). Reconstruction of the Persian Gulf SST variability over the last five millennia. *Quaternary International*. https://doi.org/10.1016/j.quaint.2021.01.028

Sandweiss, D. H., & Kelley, A. R. (2012). Archaeological contributions to climate change research: The archaeological record as a paleoclimatic and paleoenvironmental archive. *Annual Review of Anthropology*, *41*, 371–391. https://doi.org/10.1146/annurev-anthro-092611-145941

Saradi, H. G. (2006). *The Byzantine City in the Sixth Century: Literary Images and Historical Reality*. Athens: Society for Messenian Archaeological Studies.

Sariş, F., Hannah, D. M., & Eastwood, W. J. (2010). Spatial variability of precipitation regimes over Turkey. *Hydrological Sciences Journal*, *55*(2), 234–249. https://doi.org/10.1080/02626660903546142

Sarris, P. (2018). taxation, Roman and post-Roman. In Oliver Nicholson (Ed.), *The Oxford Dictionary of Late Antiquity* (pp. 1458–1459). Oxford: Oxford University Press.

Sarris, Peter. (2015). Integration and disintegration in the late Roman economy: The role of markets, emperors, and aristocrats. *Local Economies?: Production and Exchange of Inland Regions in Late Antiquity*, 167–188. https://doi.org/10.1163/22134522-12340031

Sauer, C. O. (1925). The Morphology of Landscape. *University of California Publications in Geography*, *2*(2), 19–53.

Sauer, E. (2017). Sasanian Persia: Introduction. In E. Sauer (Ed.), *Sasanian Persia : between*

Rome and the steppes of Eurasia. Edinburgh: Edinburgh University Press.

Sauer, E., Omrani Rekavandi, H., Wilkinson, T. J., & Nokandeh, J. (2013). *Persia's Imperial Power in Late Antiquity: The Great Wall of Gorgān and Frontier Landscapes of Sasanian Iran*. Oxford: Oxbow Books.

Sauer, E., Nokandeh, J., Pitskhelauri, K., & Omrani Rekavandi, H. (2017). Innovation and Stagnation: Military Infrastructure and the Shifting Balance of Power Between Rome and Persia. In *Sasanian Persia: Between Rome and Steppes of Eurasia* (pp. 241–267).

Schacht, R. M. (1984). The Contemporaneity Problem. *American Antiquity*, *49*, 678–695.

Schiettecatte, J. (2008). L' èvolution du peuplement sudarabique du 1er au VIe siècle. In C. F. Robinson & J. Schiettecatte (Eds.), *L'Arabie à la veille d l'Islam* (pp. 217–249). Paris: CNRS.

Schiettecatte, J. (2016). Les barrages des hautes-terres. In G. Charloux & J. Schiettecatte (Eds.), *Yémen, Terre d'archéologiee* (pp. 190–199). Paris: Geuthner.

Schiettecatte, J. (2018). Himyar (Sabaic Hmyrm, Lat. Himyarites, Homeritae). In O. Nicholson (Ed.), *The Oxford Dictionary of Late Antiquity* (p. 723). Oxford: Oxford University Press.

Schindel, N. (2013a). KAWĀD I i. Reign. In E. Yarshater (Ed.), *Encyclopaedia Iranica. Vol. XVI. Fasc. 2.* (pp. 136–141). New York: Encyclopaedia Iranica Foundation.

Schindel, N. (2013b). Sasanian Coinage. In D. Potts (Ed.), *Oxford Handbook of Ancient Iran* (pp. 814–839). Oxford: Oxford University Press.

Schippmann, K. (2001). *Ancient South Arabia – From the Queen of Sheba to the advent of Islam*. Princeton, New Jersey: Markus Wiener Publishers.

Scholz, D., & Hoffmann, D. L. (2011). StalAge - An algorithm designed for construction of speleothem age models. *Quaternary Geochronology*, *6*(3–4), 369–382. https://doi.org/10.1016/j.quageo.2011.02.002

Sears, S. D., & Ariel, D. T. (2000). Finds of Late Sasanian and Early Muslim drachms in historical Palestine. *Atiqot*, *40*, 135–150.

Seguin, J., Bintliff, J. L., Grootes, P. M., Bauersachs, T., Dörfler, W., Heymann, C., et al. (2019). 2500 years of anthropogenic and climatic landscape transformation in the Stymphalia polje, Greece. *Quaternary Science Reviews*, *213*, 133–154. https://doi.org/10.1016/J.QUASCIREV.2019.04.028

Seguin, J., Avramidis, P., Dörfler, W., Emmanouilidis, A., & Unkel, I. (2020a). A 2600-year high-resolution climate record from Lake Trichonida (SW Greece). *E&G Quaternary Science Journal*, *69*(2), 139–160. https://doi.org/10.5194/egqsj-69-139-2020

Seguin, J., Avramidis, P., Haug, A., Kessler, T., Schimmelmann, A., & Unkel, I. (2020b). Reconstruction of palaeoenvironmental variability based on an inter-comparison of four lacustrine archives on the Peloponnese (Greece) for the last 5000 years. *E&G Quaternary Science Journal*, *69*(2), 165–186. https://doi.org/10.5194/egqsj-69-165-2020

Seland, E. H. (2012). Trade and Christianity in the Indian Ocean during Late Antiquity, *5*(1), 72–86.

Semsar Yazdi, A. A., & Semsar Yazdi, S. (2020). An introduction to Qanats of Yazd Province. In A. Alehashemi, J.-F. Coulais, & G. Hubert (Eds.), *Water & City: Hydraulic Systems and Urban Structures* (pp. 23–30). Paris: Editions L'Œil d'or.

Ševčenko, I., & Ševčenko, N. P. (1984). *The Life of Saint Nicholas of Sion. Text and Translation (Archbishop Iakovos Library of Ecclesiastical and Historical Sources 10)*. Brookline, Mass.: Hellenic Collage Press.

Seyf, A. (2006). On the importance of irrigation in Iranian agriculture. *Middle Eastern Studies*, *42*(4), 659–673. https://doi.org/10.1080/00263200600642399

Sezen, C., & Partal, T. (2019). The impacts of Arctic oscillation and the North Sea Caspian pattern on the temperature and precipitation regime in Turkey. *Meteorology and Atmospheric Physics*, *131*(6), 1677–1696. https://doi.org/10.1007/s00703-019-00665-w

Shahid, I. (1989). *Byzantium and the Arabs in the fifth century*. Washington, D.C.: Dumbarton Oaks Research Library and Collection.

Shahid, I. (1995). *Byzantium and the Arabs in the sixth century, I, pts. 1-2*. Washington, D.C.: Dumbarton Oaks Research Library and Collection.

Shahîd, I. (2010). *Byzantium and the Arabs in the Sixth Century. Volume 2, Part 2: Economic, Social, and Cultural History*. Georgetown: Dumbarton Oaks.

Shahraki, A. H., Carniel, E., & Mostafavi, E. (2016). Plague in Iran: its history and current status. *Epidemiology and Health*, *38*, e2016033. https://doi.org/10.4178/EPIH.E2016033

Shakun, J. D., Burns, S. J., Fleitmann, D., Kramers, J., Matter, A., & Al-Subary, A. (2007). A high-resolution, absolute-dated deglacial speleothem record of Indian Ocean climate from Socotra Island, Yemen. *Earth and Planetary Science Letters*, *259*(3–4), 442–456. https://doi.org/10.1016/j.epsl.2007.05.004

Sharifi, A., Pourmand, A., Canuel, E. A., Ferer-Tyler, E., Peterson, L. C., Aichner, B., et al. (2015). Abrupt climate variability since the last deglaciation based on a high-resolution, multi-proxy peat record from NW Iran: The hand that rocked the Cradle of Civilization? *Quaternary Science Reviews*, *123*, 215–230. https://doi.org/10.1016/j.quascirev.2015.07.006

Shayegan, M. R. (2004). On the Rationale behind the Roman Wars of Šābuhr II the Great. *Bulletin of the Asia Institute*, *18*, 111–133.

Shin, N., Marston, J. M., Luke, C., Roosevelt, C. H., & Riehl, S. (2021). Agricultural practices at Bronze Age Kaymakçı, western Anatolia. *Journal of Archaeological Science: Reports*, *36*(January), 102800. https://doi.org/10.1016/j.jasrep.2021.102800

Shumilovskikh, L. S., Djamali, M., Andrieu-Ponel, V., Ponel, P., de Beaulieu, J.-L., Naderi-Beni, A., & Sauer, E. (2017). Palaeoecological Insights into Agri-Horti-Cultural and Pastoral

Practices Before, During and After the Sasanian Empire. In E. Sauer (Ed.), *Sasanian Persia: Between Rome and Steppes of Eurasia* (pp. 51–73). Edinburgh: Edinburgh University Press.

Sicker, M. (2000). *Pre-Islamic Middle East*. London: Greenwood Publishing Group.

Sigl, M., Winstrup, M., McConnell, J. R., Welten, K. C., Plunkett, G., Ludlow, F., et al. (2015). Timing and climate forcing of volcanic eruptions for the past 2,500 years. *Nature*, *523*(7562), 543–549. https://doi.org/10.1038/nature14565

Similox-Tohon, D., Sintubin, M., Muchez, P., Verhaert, G., Vanneste, K., Fernandez, M., et al. (2006). The identification of an active fault by a multidisciplinary study at the archaeological site of Sagalassos (SW Turkey). *Tectonophysics*, *420*(3), 371–387. https://doi.org/10.1016/j.tecto.2006.03.026

Simpson, J. (2005). Christians at Nineveh in Late Antiquity. *Iraq*, *67*(1), 285–294.

Simpson, S. J. (2000). Mesopotamia in the Sasanian Period: Settlement Patterns, Arts and Crafts. In R. Curtis (Ed.), *Mesopotamia and Iran in the Parthian and Sasanian Periods. rejection and Revival c. 238 BC – AD 642* (pp. 57–66). London: British Museum Press.

Sinha, A., Kathayat, G., Cheng, H., Breitenbach, S. F. M., Berkelhammer, M., Mudelsee, M., et al. (2015). Trends and oscillations in the Indian summer monsoon rainfall over the last two millennia. *Nature Communications 2015 6:1*, *6*(1), 1–8. https://doi.org/10.1038/ncomms7309

Sinha, A., Kathayat, G., Weiss, H., Li, H., Cheng, H., Reuter, J., et al. (2019). Role of climate in the rise and fall of the Neo-Assyrian Empire. *Sci. Adv*, *5*(November), 6656–6669.

Skaff, J. K. (1998). The Sasanian and Arab-Sasanian silver coins from Turfan: their relationship to international trade and the local economy. *Asia Major*, *11*(2), 67–115.

Slingerland, E., Monroe, M. W., Sullivan, B., Walsh, R. F., Veidlinger, D., Noseworthy, W., et al. (2020). Historians respond to Whitehouse et al. (2019), "Complex societies precede moralizing gods throughout world history." *Journal of Cognitive Historiography*, *5*(1–2), 124–141. https://doi.org/https://doi.org/10.1558/jch.39393

Sluyter, A. (2003). Neo-Environmental Determinism, Intellectual Damage Control, and Nature/Society Science. *Antipode*, *35*, 813–817.

Smith, M. E. (2010). The archaeological study of neighbourhoods and districts in ancient cities. *Journal of Anthropological Archaeology*, *29*(2), 137–154. https://doi.org/https://doi.org/10.1016/j.jaa.2010.01.001

Sodini, J.-P., Canbilen, H., & Lebouteiller, P. (1996). La basilique de l'acropole haute de Xanthos. *Anatolia Antiqua*, *4*, 201–229.

Soroush, M. (2014). Irrigation in Khuzistan after the Sasanians: Continuity, Decline, or Transformation? In A. Gnasso, E. E. Intagliata, & T. J. Macmaster (Eds.), *Te Long Seventh Century: Continuity and Discontinuity in an Age of Transition* (pp. 269–289). Bern: Peter

Land Publishing Incorporated.

Soroush, M. (2020). Urban Resilience and Hydraulic Continuity Against a Backdrop of Wars and Conquests, the Susiana Plain of Iran in the First Millennium CE. In A. Alehashemi, J.-F. Coulais, & G. Hubert (Eds.), *Water & City: Hydraulic Systems and Urban Structures* (pp. 69–81). Paris: Editions L'Œil d'or.

Spate, M. (2019). Reconsidering Archaeological and Environmental Proxies for Long Term Human-Environment Interactions in the Valley of Kashmir. *Socio-Environmental Dynamics Along the Historical Silk Road*, 123–149. https://doi.org/10.1007/978-3-030-00728-7_6

Spötl, C., & Boch, R. (2019). Uranium-series dating of speleothems. In W. B. White, D. C. Culver, & T. Pipan (Eds.), *Encyclopedia of Caves* (Third Edit, Vol. 37, pp. 1096–1102). London: Elsevier. https://doi.org/10.1016/b978-0-12-814124-3.00128-x

Stathakopoulos, D. C. (2004). *Famine and Pestilence in the Late Roman and Early Byzantine Empire: A Systematic Survey of Subsistence Crises and Epidemics (Birmingham Byzantine and Ottoman Studies)*. Aldershot: Ashgate Publishing.

Staubwasser, M., Sirocko, F., Grootes, P. M., & Segl, M. (2003). Climate change at the 4.2 ka BP termination of the Indus valley civilization and Holocene south Asian monsoon variability. *Geophysical Research Letters*, *30*, 1425.

Steinhilber, F, Beer, J., & Fröhlich, C. (2009). Total solar irradiance during the Holocene. *Geophysical Research Letters*, *36*(19), 1–5. https://doi.org/10.1029/2009GL040142

Steinhilber, Friedhelm, Abreu, J. A., Beer, J., Brunner, I., Christl, M., Fischer, H., et al. (2012). 9,400 years of cosmic radiation and solar activity from ice cores and tree rings. *Proceedings of the National Academy of Sciences*, *109*(16), 5967–5971. https://doi.org/10.1073/PNAS.1118965109

Stevens, L. R., Wright, J., & Ito, E. (2001). Proposed changes in seasonality of climate during the Lateglacial and Holocene at Lake Zeribar, Iran. *Holocene*, *11*(6), 747–755. https://doi.org/10.1191/09596830195762

Stevens, Lora R., Ito, E., Schwalb, A., & Wright, H. E. (2006). Timing of atmospheric precipitation in the Zagros Mountains inferred from a multi-proxy record from Lake Mirabad, Iran. *Quaternary Research*, *66*(3), 494–500. https://doi.org/10.1016/j.yqres.2006.06.008

Stiros, S. C. (2001). The AD 365 Cret earthquake and possible seismic clustering during the fourth to sixth centuries AD in the Eastern Mediterranean: A review of historical and archaeological data. *Journal of Structural Geology*, *23*(2–3), 545–562. https://doi.org/10.1016/S0191-8141(00)00118-8

Stoll, H. M., Müller, W., & Prieto, M. (2012). I-STAL, a model for interpretation of Mg/Ca, Sr/Ca and Ba/Ca variations in speleothems and its forward and inverse application on seasonal to millennial scales. *Geochemistry, Geophysics, Geosystems*, *13*(9), 9004. https://doi.org/10.1029/2012GC004183

Stothers, R. B. (2002). Cloudy and clear stratospheres before A.D. 1000 inferred from written sources. *Journal of Geophysical Research: Atmospheres*, *107*(D23). https://doi.org/10.1029/2002JD002105

Stroumsa, G. G. (2015). *The Making of the Abrahamic Religions in Late Antiquity*. Oxford: Oxford University Press.

Sussman, G. (2016). Scientists Doing History: Central Africa and the Origins of the First Plague Pandemic. *Journal of World History*, *26*, 325–354.

Takaoğlu, T. (2020). Adapting to a Diverse Landscape: Agriculture in Hellenistic and Roman Anatolia. In D. B. Hollander & T. Howe (Eds.), *A Companion to Ancient Agriculture* (pp. 363–382). Hoboken, New Jersey: John Wiley & Sons, Ltd. https://doi.org/10.1002/9781118970959.ch17

Talloen, P. (2015). *Cult in Pisidia. Religious Practice in Southwestern Asia Minor from Alexander the Great to the Rise of Christianity. (Studies in Eastern Mediterranean Archaeology, 10)*. Turnhout: Brepols.

Tamburrino, A. (2010). Water Technology in Ancient Mesopotamia. In L. Mays (Ed.), *Ancient Water Technologies* (pp. 29–51). Dordrecht: Springer.

Tan, O., Tapirdamaz, M. C., & Yörük, A. (2008). The earthquake catalogues for Turkey. *Turkish Journal of Earth Sciences*, *17*(2), 405–418.

Tanner, S. D., Baranov, V. I., & Bandura, D. R. (2002). Reaction cells and collision cells for ICP-MS: A tutorial review. *Spectrochimica Acta - Part B Atomic Spectroscopy*, *57*(9), 1361–1452. https://doi.org/10.1016/S0584-8547(02)00069-1

Taylor, R. E., & Bar-Yosef, O. (2014). *Radiocarbon Dating* (2nd Editio). Walnut Creek, California: Left Coast Press.

Tekeli, F. O., & Gokce, A. F. (2016). Endemic plants and wild Allium species in Turkey. In *Acta Horticulturae* (Vol. 1143, pp. 327–332). International Society for Horticultural Science. https://doi.org/10.17660/ActaHortic.2016.1143.46

Telelis, I. G. (2008). Climatic Fluctuations in the Eastern Mediterranean and the Middle East AD 300–1500 from Byzantine Documentary and Proxy Physical Paleoclimatic Evidence – A Comparison. *Jahrbuch Der Österreichischen Byzantinistik*, *58*(January 2008), 167–208. https://doi.org/10.1553/joeb58s167

Terpoy, K. (2019a). Questioning Late Antique prosperity: The case of Lycia (southwest Turkey). *Byzantine and Modern Greek Studies*, *43*(1), 1–23. https://doi.org/10.1017/byz.2018.22

Terpoy, K. (2019b). Studying Asia Minor in the sixth century. Methodological considerations for an economic analysis. In H. Elton & I. Jacobs (Eds.), *Asia Minor in the Long Sixth Century: Current Research and Future Directions* (pp. 63–78). Oxford: Oxbow Books. https://doi.org/https://doi.org/10.2307/j.ctvjsf69w

Tomber, R. (2007). Rome and Mesopotamia – importers into India in the first millennium AD.

Antiquity, *81*, 972–988.

Toohey, M., & Sigl, M. (2017). Volcanic stratospheric sulfur injections and aerosol optical depth from 500ĝ€BCE to 1900ĝ€CE. *Earth System Science Data*, *9*(2), 809–831. https://doi.org/10.5194/essd-9-809-2017

Tooth, A. F., & Fairchild, I. J. (2003). Soil and karst aquifer hydrological controls on the geochemical evolution of speleothem-forming drip waters, Crag Cave, southwest Ireland. *Journal of Hydrology*, *273*(1–4), 51–68. https://doi.org/10.1016/S0022-1694(02)00349-9

Touchan, R., Akkemik, Ü., Hughes, M. K., & Erkan, N. (2007). May-June precipitation reconstruction of southwestern Anatolia, Turkey during the last 900 years from tree rings. *Quaternary Research*, *68*(2), 196–202. https://doi.org/10.1016/j.yqres.2007.07.001

Touchan, R., Meko, D. M., & Anchukaitis, K. J. (2014a). Dendroclimatology in the Eastern Mediterranean. *Radiocarbon*, *56*(4), S61–S68. https://doi.org/10.2458/azu_rc.56.18321

Touchan, R., Anchukaitis, K. J., Shishov, V. V., Sivrikaya, F., Attieh, J., Ketmen, M., et al. (2014b). Spatial patterns of eastern Mediterranean climate influence on tree growth. *Holocene*, *24*(4), 381–392. https://doi.org/10.1177/0959683613518594

Treble, P., Shelley, J. M. G., & Chappell, J. (2003). Comparison of high resolution sub-annual records of trace elements in a modern (1911-1992) speleothem with instrumental climate data from southwest Australia. *Earth and Planetary Science Letters*, *216*(1–2), 141–153. https://doi.org/10.1016/S0012-821X(03)00504-1

Treble, P., Chappell, J., & Shelley, J. M. G. (2005). Complex speleothem growth processes revealed by trace element mapping and scanning electron microscopy of annual layers. *Geochimica et Cosmochimica Acta*, *69*(20), 4855–4863.

Tremaine, D. M., & Froelich, P. N. (2013). Speleothem trace element signatures: A hydrologic geochemical study of modern cave dripwaters and farmed calcite. *Geochimica et Cosmochimica Acta*, *121*, 522–545. https://doi.org/10.1016/j.gca.2013.07.026

Trigo, I. F., Bigg, G. R., & Davies, T. D. (2002). Climatology of Cyclogenesis Mechanisms in the Mediterranean. *Monthly Weather Review*, *130*, 549–569.

Tudryn, A., Tucholka, P., Özgûr, N., Gibert, E., Elitok, O., Kamaci, Z., et al. (2013). A 2300-year record of environmental change from SW Anatolia, Lake Burdur, Turkey. *Journal of Paleolimnology*, *49*(4), 647–662. https://doi.org/10.1007/s10933-013-9682-1

Turchin, P. (2018). *Translating Knowledge about Past Societies into Seshat Data*. *Cliodynamics* (Vol. 9).

Turchin, P., Whitehouse, H., Francois, P., Slingerland, E., & Collard, M. (2012). A Historical Database of Sociocultural Evolution. *Cliodynamics*, *3*(2). https://doi.org/10.21237/C7CLIO3215770

Turchin, P., Brennan, R., Currie, T. E., Feeney, K. C., François, P., Hoyer, D., et al. (2015). Seshat:

The global history databank. *Cliodynamics*, *6*(1), 77–107. https://doi.org/10.21237/C7CLIO6127917

Turchin, P., Currie, T. E., Whitehouse, H., François, P., Feeney, K., Mullins, D., et al. (2017). Quantitative historical analysis uncovers a single dimension of complexity that structures global variation in human social organization. *Proceedings of the National Academy of Sciences of the United States of America*, *115*(2), E144–E151. https://doi.org/10.1073/pnas.1708800115

Turchin, P., Currie, T., Collins, C., Levine, J., Oyebamiji, O., Edwards, N. R., et al. (2021). An integrative approach to estimating productivity in past societies using Seshat: Global History Databank. *Holocene*, *31*(6), 1055–1065. https://doi.org/10.1177/0959683621994644

Türkeş, M., & Erlat, E. (2003). Precipitation changes and variability in Turkey linked to the North Atlantic oscillation during the period 1930-2000. *International Journal of Climatology*, *23*(14), 1771–1796. https://doi.org/10.1002/joc.962

Türkeş, M., & Erlat, E. (2009). Winter mean temperature variability in Turkey associated with the North Atlantic Oscillation. *Meteorology and Atmospheric Physics*, *105*(3–4), 211–225. https://doi.org/10.1007/s00703-009-0046-3

Turner, S. (2021). Agricultural terraces in the Mediterranean: medieval intensification revealed by OSL profiling and dating. *Antiquity*, *95*(381), 773–790.

Ucko, P. J., & Puschnigg, G. (Eds.). (2006). *Ceramics of the Merv Oasis*. New York: Routledge.

Ulbrich, U., Lionello, P., Belušić, D., Jacobeit, J., Knippertz, P., Kuglitsch, G., et al. (2012). Climate of the Mediterranean: Synoptic Patterns, Temperature, Precipitation, Winds and their Extremes. In P. Lionello (Ed.), *The Climate of the Mediterranean Region: From the Past to the Future* (pp. 301–346). Amsterdam: Elsevier.

Ülgen, U. B., Franz, S. O., Biltekin, D., Çagatay, M. N., Roeser, P. A., Doner, L., & Thein, J. (2012). Climatic and environmental evolution of Lake Iznik (NW Turkey) over the last ~4700 years. *Quaternary International*, *274*, 88–101. https://doi.org/10.1016/j.quaint.2012.06.016

Ulrich, B. (2011). Oman and Bahrain in late antiquity: the Sasanians' Arabian periphery. *Proceedings of the Seminar for Arabian Studies*, *41*, 377–385.

Ünal-İmer, E., Shulmeister, J., Zhao, J.-X., Uysal, I. T., Feng, Y.-X., Nguyen, A. D., & Yüce, G. (2015). An 80 kyr-long continuous speleothem record from Dim Cave, SW Turkey with paleoclimatic implications for the Eastern Mediterranean. *Scientific Reports 2015 5:1*, *5*(1), 1–11. https://doi.org/10.1038/srep13560

Ünal-İmer, E., Shulmeister, J., Zhao, J. X., Uysal, I. T., & Feng, Y. X. (2016). High-resolution trace element and stable/radiogenic isotope profiles of late Pleistocene to Holocene speleothems from Dim Cave, SW Turkey. *Palaeogeography, Palaeoclimatology, Palaeoecology*, *452*, 68–79. https://doi.org/10.1016/j.palaeo.2016.04.015

Unal, Y. S., Deniz, A., Toros, H., & Incecik, S. (2012). Temporal and spatial patterns of precipitation variability for annual, wet, and dry seasons in Turkey. *International Journal of Climatology*, *32*(3), 392–405. https://doi.org/10.1002/joc.2274

UNESCO. (2018). Sassanid Archaeological Landscape of Fars Region. Retrieved October 5, 2021, from https://whc.unesco.org/en/list/1568/

University of East Anglia Climatic Research Unit, Harris, I. C., Jones, P. D., & Osborn, T. (2020). *CRU TS4.04: Climatic Research Unit (CRU) Time-Series (TS) version 4.04 of high-resolution gridded data of month-by-month variation in climate (Jan. 1901- Dec. 2019)*. Norwich. Retrieved from https://catalogue.ceda.ac.uk/uuid/89e1e34ec3554dc98594a5732622bce9

Unkel, I., Schimmelmann, A., Shriner, C., Forsén, J., Heymann, C., & Brückner, H. (2014). The environmental history of the last 6500 years in the Asea Valley (Peloponnese, Greece) and its linkage to the local archaeological record. *Zeitschrift Für Geomorphologie, Supplementary Issues*, 89–107. https://doi.org/10.1127/0372-8854/2014/S-00160

Ur, J. A., & Alizadeh, K. (2013). The Sasanian Colonization of the Mughan Steppe, Ardebil Province, Northwestern Iran. *Iranian Archaeology*, *4*, 98–110.

Vaiglova, P., Hartman, G., Marom, N., Ayalon, A., Bar-Matthews, M., Zilberman, T., et al. (2020). Climate stability and societal decline on the margins of the Byzantine empire in the Negev Desert. *Scientific Reports 2020 10:1*, *10*(1), 1–13. https://doi.org/10.1038/s41598-020-58360-5

Vandam, R., Kaptijn, E., Broothaerts, N., De Cupere, B., Marinova, E., Van Loo, M., et al. (2019a). "Marginal" Landscapes: Human Activity, Vulnerability, and Resilience in the Western Taurus Mountains (Southwest Turkey). *Journal of Eastern Mediterranean Archaeology and Heritage Studies*, *7*(4), 432–450. https://doi.org/doi: 10.5325/jeasmedarcherstu.7.4.0432

Vandam, R., Kaptijn, E., Willet, R., & Willett, P. T. (2019b). The Countryside - Where Are The People? In J. Poblome, E. Torun, P. Talloen, & M. Waelkens (Eds.), *Meanwhile in the Mountains: Sagalassos* (pp. 275–284). Istanbul: Yapı Kredi Yayınları.

Vandam, R., Willett, P. T., & Poblome, J. (2019c). The Results of the 2017 Dereköy Archaeological Survey by the Sagalassos Project in the Western Taurus Mountains. *The Archaeology of Anatolia Volume III: Recent Discoveries (2017-2018)*, (February), 260–269.

Varisco, D. M. (1983). Sayl and Ghayl: The Ecology of Water Allocation in Yemen. *Human Ecology*, *11*(4), 365–383.

Vermoere, M., Bottema, S., Vanhecke, L., Waelkens, M., Paulissen, E., & Smets, E. (2002). Palynological evidence for late-Holocene human occupation recorded in two wetlands in SW Turkey. *The Holocene*, *12*(5), 569–584. https://doi.org/10.1191/0959683602hl568rp

Vicente-Serrano, S. M., Beguería, S., & López-Moreno, J. I. (2010). A multiscalar drought index

sensitive to global warming: The standardized precipitation evapotranspiration index. *Journal of Climate*, *23*(7), 1696–1718. https://doi.org/10.1175/2009JCLI2909.1

Vieira, L. E. A., Solanki, S. K., Krivova, N. A., & Usoskin, I. (2011). Evolution of the solar irradiance during the Holocene. *Astronomy & Astrophysics*, *531*, A6. https://doi.org/10.1051/0004-6361/201015843

Van de Vijver, K. (2018). Fiziksel antropoloji çalışmaları. In *39 Kazı sonuçları toplantısı 22–26 Mayış 2017 Bursa* (pp. 227–228). Ankara: T.C. Kültür ve Turizm Bakanlığı.

Vionis, A. K., Poblome, J., & Waelkens, M. (2009). The hidden material culture of the Dark Ages. Early medieval ceramics at Sagalassos (Turkey): new evidence (ca AD 650–800). *Anatolian Studies*, *59*, 147–165. https://doi.org/10.1017/S0066154600000946

Vroom, J. (2011). The Other Dark Ages: Early Medieval Pottery Finds in the Aegean as an Archaeological Challenge. In R. Attoui (Ed.), *When did Antiquity End? Archaeological Case Studies in Three Continents* (pp. 137–158). Oxford: Archaeopress.

Waelkens, M. (2000). *Sagalassos V. Report on the Survey and Excavation Campaigns of 1996 and 1997*. Leuven: Leuven University Press.

Waelkens, M. (2002). Romanization in the East. A Case Study: Sagalasso and Pisidia. *Istanbuler Mitteilungen*, *52*, 311–368.

Waelkens, M. (2019). Sagalassos, Archaeology of. In C. Smith (Ed.), *Encyclopedia of Global Archaeology* (2nd editio, pp. 1121–1123). Basel: Springer.

Waelkens, M., Sintubin, M., Muchez, P., & Paulissen, E. (2000). Archaeological, geomorphological and geological evidence for a major earthquake at Sagalassos (SW Turkey) around the middle of the seventh century AD. *Geological Society Special Publication*, *171*, 373–383. https://doi.org/10.1144/GSL.SP.2000.171.01.27

Walstra, J., Heyvaert, V., & Verkinderen, P. (2010). Assessing Human Impact on Alluvial Fan Development: A Multidisciplinary Case-Study from Lower Khuzestan (SW Iran). *Geodinamica Acta*, *23*(5), 267–285.

Wang, P., Tian, J., & Lourens, L. J. (2010). Obscuring of long eccentricity cyclicity in Pleistocene oceanic carbon isotope records. *Earth and Planetary Science Letters*, *290*(3–4), 319–330. https://doi.org/10.1016/j.epsl.2009.12.028

Wang, Y., Cheng, H., Edwards, R. L., He, Y., Kong, X., An, Z., et al. (2005). The holocene Asian monsoon: Links to solar changes and North Atlantic climate. *Science*, *308*(5723), 854–857. https://doi.org/10.1126/SCIENCE.1106296

Wanner, H., Wanner, H., Mercolli, L., Mercolli, L., Grosjean, M., Grosjean, M., & Ritz, S. P. (2015). Holocene climate variability and change; a data-based review. *Journal of the Geological Society*, *172*(2), 254–263. https://doi.org/10.1144/jgs2013-101

Ward-Perkins, B. (2005). *The fall of Rome and the end of civilisation*. Oxford: Oxford University Press.

Wassenburg, J. A., Immenhauser, A., Richter, D. K., Niedermayr, A., Riechelmann, S., Fietzke, J., et al. (2013). Moroccan speleothem and tree ring records suggest a variable positive state of the North Atlantic Oscillation during the Medieval Warm Period. *Earth and Planetary Science Letters*, *375*, 291–302. https://doi.org/10.1016/j.epsl.2013.05.048

Wassenburg, J. A., Riechelmann, S., Schröder-Ritzrau, A., Riechelmann, D. F. C., Richter, D. K., Immenhauser, A., et al. (2020). Calcite Mg and Sr partition coefficients in cave environments: Implications for interpreting prior calcite precipitation in speleothems. *Geochimica et Cosmochimica Acta*, *269*, 581–596. https://doi.org/10.1016/j.gca.2019.11.011

Weber, M., Scholz, D., Wassenburg, J. A., Jochum, K. P., & Breitenbach, S. (2017). Application of LA-MC-ICP-MS for analysis of Sr isotope ratios in speleothems. *EGUGA*, *19*, 12278. Retrieved from https://ui.adsabs.harvard.edu/abs/2017EGUGA..1912278W/abstract

Weiberg, E., & Finné, M. (2018). Resilience and persistence of ancient societies in the face of climate change: a case study from Late Bronze Age Peloponnese. *World Archaeology*, *50*(4), 584–602. https://doi.org/10.1080/00438243.2018.1515035

Weiberg, E., Unkel, I., Kouli, K., Holmgren, K., Avramidis, P., Bonnier, A., et al. (2016). The socio-environmental history of the Peloponnese during the Holocene: Towards an integrated understanding of the past. *Quaternary Science Reviews*, *136*, 40–65. https://doi.org/10.1016/j.quascirev.2015.10.042

Weiss, H. (Ed.). (2017). *Megadrought and Collapse: From Early Agriculture to Angkor*. Oxford: Oxford University Press.

Weiss, H., Courty, M.-A., Wetterstrom, W., Guichard, F., Senior, L., Meadow, R., & Curnow, A. (1993). The genesis and collapse of third millennium North Mesopotamian civilization. *Science*, *261*, 995–1004.

Wenke, R. J. (1987). Western Iran in the Partho-Sasanian Period: The Imperial Transformation. In F. Hole (Ed.), *The Archaeology of Western Iran: Settlement and Society from Prehistory to the Islamic Conquest* (pp. 251–281). Washington, D.C.: Smithsonian Institution Press.

Whitcomb, D. (2014). Landscape signatures in Sasanian archaeology. *Journal of Ancient History*, *2*(2), 209–215. https://doi.org/10.1515/jah-2014-0030

White, W. B. (1976). Cave Minerals and Speleothems. In D. Ford & C. H. D. Cullingford (Eds.), *The Science of Speleology* (pp. 267–327). London: Academic Press.

White, W. B. (2012). Speleothems. In W. B. White & D. Culver (Eds.), *Encyclopedia of Caves* (pp. 1006–1017). Chennai: Elsevier Inc.

White, W. B. (2016). Chemistry and karst. *Acta Carsologica*, *44*(3), 349–362.

Whitehouse, D., & Williamson, A. (1973). Sasanian Maritime Trade. *Iran*, *11*, 29–49.

Whittow, M. (2011). The late Roman/early Byzantine Near East. In C. F. Robinson (Ed.), *The*

New Cambridge History Of Islam (Vol. 1): The Formation of the Islamic World Sixth to Eleventh Centuries (pp. 72–97). Cambridge: Cambridge University Press.

Wick, L., Lemcke, G., & Sturm, M. (2003). Evidence of Lateglacial and Holocene climatic change and Human impact in Eastern Anatolia. *The Holocene*, *13*(5), 665–675.

Wiesehöfer, J. (2010). The late Sasanian Near East. In *The New Cambridge History of Islam: Volume 1: The Formation of the Islamic World Sixth to Eleventh Centuries* (pp. 98–152). Cambridge University Press. https://doi.org/10.1017/CHOL9780521838238.005

Wilkinson, T. J. (2011). Empire and Environment in the Northern Fertile Crescent. In I. P. Martini & W. Chesworth (Eds.), *Landscapes and Societies: Selected Cases* (pp. 135–152). Dordrecht: Springer.

Wilkinson, T. J., Edens, C., & Gibson, M. (1997). The archaeology of the Yemen High Plains: a preliminary chronology. *Arabian Archaeology and Epigraphy*, *8*(1), 99–142. https://doi.org/10.1111/j.1600-0471.1997.tb00149.x

Wilkinson, T. J., Boucharlat, R., Ertsen, M. W., Gillmore, G., Kennet, D., Magee, P., et al. (2012). From human niche construction to imperial power: long-term trends in ancient Iranian water systems. *Water History*, *4*(2), 155–176. https://doi.org/10.1007/s12685-012-0056-9

Wolff, C., Plessen, B., Dudashvilli, A. S., Breitenbach, S. F., Cheng, H., Edwards, L. R., & Strecker, M. R. (2017). Precipitation evolution of Central Asia during the last 5000 years. *Holocene*, *27*(1), 142–154. https://doi.org/10.1177/0959683616652711

Woodbridge, J., Roberts, C. N., Palmisano, A., Bevan, A., Shennan, S., Fyfe, R., et al. (2019). Pollen-inferred regional vegetation patterns and demographic change in Southern Anatolia through the Holocene. *Holocene*, *29*(5), 728–741. https://doi.org/10.1177/0959683619826635

Xanthopoulos, G., & Nikolov, N. (2019). Wildfires and fire management in the Eastern Mediterranean, Southeastern Europe, and Middle East regions. *Fire Management Today*, *1*(1), 29–38.

Xoplaki, E., González-Rouco, J. F., Luterbacher, J., & Wanner, H. (2004). Wet season Mediterranean precipitation variability: Influence of large-scale dynamics and trends. *Climate Dynamics*, *23*(1), 63–78. https://doi.org/10.1007/s00382-004-0422-0

Xoplaki, E., Fleitmann, D., Luterbacher, J., Wagner, S., Haldon, J. F., Zorita, E., et al. (2016). The Medieval Climate Anomaly and Byzantium: A review of the evidence on climatic fluctuations, economic performance and societal change. *Quaternary Science Reviews*, *136*, 229–252. https://doi.org/10.1016/j.quascirev.2015.10.004

Xoplaki, E., Luterbacher, J., Wagner, S., Zorita, E., Fleitmann, D., Preiser-Kapeller, J., et al. (2018). Modelling Climate and Societal Resilience in the Eastern Mediterranean in the Last Millennium. *Human Ecology*, *46*(3), 363–379. https://doi.org/10.1007/s10745-018-9995-9

Yener-Marksteiner, B. (2009). Surveys in Andriake 2008. *ANMED*, *7*, 105–107.

Yılmaz, E., & Çiçek, İ. (2018). Türkiye'nin detaylandırılmış Köppen-Geiger iklim bölgeleri (Detailed Köppen-Geiger climate regions of Turkey). *Journal of Human Sciences*, *15*(1), 225–242. https://doi.org/10.14687/jhs.v15i1.5040

Yoffee, N. (2019). *The Evolution of Fragility: Setting the Terms*. Cambridge: McDonald Institute for Archaeological Research.

Yule, P. A. (2007). *Late Antique Yemen*. Aichwald: Linden Soft.

Yule, P. A. (2013). *Late antique Arabia - Ẓafār, capital of Ḥimyar: rehabilitation of a "decadent" society. Excavations of the Ruprecht-Karls-Universität Heidelberg 1998-2010 in the highlands of Yemen*. Wiesbaden: Harrassowitz.

Zarins, J., Kabawi, A., & Murad, M. (1983). Preliminary Report on the Najran / Ukhdud Survey and Excavations (1402/1982). *Aṭlāl: The Journal of Saudi Arabian Archaeology*, *7*, 22–40.

Van Zeist, W. (1967). Late Quaternary Vegetation History of Western Iran. *Review of Palaeobotany and Palynology*, *2*, 301–311.

Van Zeist, W., & Woldring, H. (1978). A Postglacial Pollen Diagram from Lake Van in East Anatolia'. *Review of Palaeobotany and Palynology*, *26*, 249–276.

Zhang, D. D., Lee, H. F., Wang, C., Li, B., Pei, Q., Zhang, J., & An, Y. (2011). The causality analysis of climate change and large-scale human crisis. *Proceedings of the National Academy of Sciences of the United States of America*, *108*(42), 17296–17301. https://doi.org/10.1073/pnas.1104268108

Zohary, D., Hopf, M., & Weiss, E. (2012). *Domestication of Plants in the Old World* (4th Editio). Oxford: Oxford University Press.

Zolitschka, B., Francus, P., Ojala, A. E. K., & Schimmelmann, A. (2015). Varves in lake sediments—A review. *Quaternary Science Reviews*, *117*, 1–41.

Appendices

Appendix A - Data

A.1. Chapter 3 Data: Kocain Cave geochemistry dataset

From speleothem Ko-1 from Kocain Cave, southwest Turkey, 17 uranium-series dates were utilised to produce an age-depth model, 370 stable-isotope measurements were performed, and LA-ICP-MS produced 31,503 trace-element samples. These datasets are available on the NOAA palaeoclimate database (https://www.ncdc.noaa.gov/paleo-search/study/33854) and can be found on the attached CD. File name: Appendix A1_Ko1 dataset.xlsm

A.2. Chapter 4 Data: Southwest Turkey settlement change dataset

Settlement toponyms from volume 8 of the Tabula Imperii Byzantini (TIB 8: Lycia and Pamphylia) were tabulated to create a record of settlement change between the Bronze Age and the Middle Byzantine period. The records metadata, full list of settlements, and elevation data, with a record of Byzantine lead seals and coin hoards, can be found on the attached CD. File name: Appendix A2_TIB settlement dataset.xlsx

A.3. Chapter 5 Data: Hoti Cave geochemistry dataset

From speleothem H12 from Hoti Cave, northern Oman, 20 uranium-series dates were utilised to produce an age-depth model, 1,360 stable-isotope measurements were performed, and 88 apex diameter measurements were taken. These datasets will be available on the NOAA palaeoclimate database once the paper is published and can be found on the attached CD. File name: Appendix A3_H12 dataset.xlsx

Appendix B – Publications

Additional publications worked on during production of this thesis. Author contributions are outlined in Chapter 2. Publications are in the format of the journal to which they were submitted, figures are not listed in the thesis list of figures. Supplementary materials are not included, all are available on the online versions of the articles.

B.1. Speleothems from the Middle East: An Example of Water Limited Environments in the SISAL Database

Burstyn, Y., Martrat, B., Lopez, Jordi, F., Iriarte, E., **Jacobson, M.J.**, Lone, M. A., & Deininger, M. (2019). Speleothems from the Middle East: An Example of Water Limited Environments in the SISAL Database. *Quaternary*, *2*(16). https://doi.org/10.3390/quat2020016

quaternary

MDPI

Review

Speleothems from the Middle East: An Example of Water Limited Environments in the SISAL Database

Yuval Burstyn [1,2,*], Belen Martrat [3], Jordi F. Lopez [3], Eneko Iriarte [4], Matthew J. Jacobson [5], Mahjoor Ahmad Lone [6,7] and Michael Deininger [8]

1 Geological Survey of Israel, 30 Malchei Israel Street, Jerusalem 95501, Israel

2 Institute of Earth Sciences, Hebrew University of Jerusalem, Edmond Y. Safra Givat Ram Campus, Jerusalem 91904, Israel

3 Department of Environmental Chemistry, Spanish Council for Scientific Research (CSIC), Institute of Environmental Assessment and Water Research (IDAEA), 08034 Barcelona, Spain; belen.martrat@idaea.csic.es (B.M.); jlfqam@idaea.csic.es (J.F.L.)

4 Laboratorio de Evolución Humana, Universidad de Burgos, 09001 Burgos, Spain; eiriarte@ubu.es

5 Department of Archaeology and Centre for Past Climate Change, University of Reading, Reading RG6 6UR, UK; m.j.jacobson2@pgr.reading.ac.uk

6 High-Precision Mass Spectrometry and Environment Change Laboratory (HISPEC), Department of Geosciences, National Taiwan University, Taipei 10617, Taiwan; lonemahjoor@gmail.com

7 Research Center for Future Earth, National Taiwan University, Taipei 10617, Taiwan

8 Institute of Geosciences, Johannes Gutenberg University Mainz, J.-J.-Becher-Weg 21, 55128 Mainz, Germany; michael.deininger@uni-mainz.de

* Correspondence: yuval.burstyn@mail.huji.ac.il; Tel.: +972-544-331745

Received: 30 January 2019; Accepted: 4 April 2019; Published: 22 April 2019

Abstract: The Middle East (ME) spans the transition between a temperate Mediterranean climate in the Levant to hyper-arid sub-tropical deserts in the southern part of the Arabian Peninsula (AP), with the complex alpine topography in the northeast feeding the Euphrates and Tigris rivers which support life in the Southeastern Fertile Crescent (FC). Climate projections predict severe drying in several parts of the ME in response to global warming, making it important to understand the controls of hydro-climate perturbations in the region. Here we discuss 23 ME speleothem stable oxygen isotope (δ^{18}Occ) records from 16 sites from the SISAL_v1 database (Speleothem Isotope Synthesis and Analysis database), which provide a record of past hydro-climatic variability. Sub-millennial changes in ME δ^{18}Occ values primarily indicate changes in past precipitation amounts the result of the main synoptic pattern in the region, specifically Mediterranean cyclones. This pattern is superimposed on change in vapor source δ^{18}O composition. The coherency (or lack thereof) between regional records is reviewed from Pleistocene to present, covering the Last Glacial Maximum (~22 ka), prominent events during deglaciation, and the transition into the Holocene. The available δ^{18}Occ time-series are investigated by binning and normalizing at 25-year and 200-year time windows over the Holocene. Important climatic oscillations in the Holocene are discussed, such as the 8.2 ka, 4.2 ka and 0.7 ka (the Little Ice Age) Before Present events. Common trends in the normalized anomalies are tested against different climate archives. Finally, recommendations for future speleothem-based research in the region are given along with comments on the utility and completeness of the SISAL database.

Keywords: SISAL database; speleothem; cave; isotopes; Middle East; palaeoclimate

1. Introduction

The climate conditions across the Middle East (ME) are markedly heterogeneous for its relatively small geographical extension, encompassing the Eastern coasts of the Mediterranean (hereafter the Levant) and the Fertile Crescent (FC) (often considered in tandem,) as well as parts of the Arabian Peninsula (AP) and North-East Africa [1,2]. The region spans the transition between a temperate Mediterranean climate in the Levant to hyper-arid sub-tropical deserts in the south, with complex alpine topography in the northeast feeding the Euphrates and Tigris rivers which support life in the Southeastern FC (Figure 1). Climate projections predict severe drying in major parts of the ME in response to global climate change, with a considerable impact for societies [3–5]. Climate reconstructions and archaeological information, suggest that changes in the regional hydroclimate was a primary driver in human expansion out of Africa [6], the Neolithic revolution, and the development of the first complex societies [7]. The ME has plentiful archeological records of human settlement throughout much of the Quaternary, and well into the Holocene [8–14]. Initially, the predominantly semi to hyper-arid climate of the region served as a bottle-neck for early hominin dispersion out of Africa, allowing migrations onto the Levant and the AP pathways only during wetter periods that were identified using speleothem growth (wet)/non-growth (dry) patterns in desert and water-limited settings [15–18]. These events are also recognized using other methods and different climate archives [10,19,20]. Since the Last Glacial Maximum from c. 25 to 20 ka BP (Before Present, calibrated in the SISAL database to the year 1950 of the Common Era, hereafter CE) and the following transition into the Holocene interglacial, there has been considerable evidence that variations in climate served as a driver in Homo Sapiens' cultural evolution. The most notable is the "Neolithic Revolution", where it has been suggested that post-glacial hunter-gatherers were able to cultivate a number of food plants due to the trend towards warmer and possibly wetter climate [21], whereas succeeding abrupt cooling events may have forced proto-agrarian societies to turn to the cultivation of wild cereals and fruit [21–23]. Wheat was cultivated in the FC around 9500 years BP, suggesting that the ME was the first region to cultivate plants and support sedentary human communities [24,25]. The ME localities, specifically the FC, were also the earliest locations where sophisticated civilizations, city-states and complex empire systems appeared during the mid- to late-Holocene [26,27]. It has been argued that the expansion and subsequent collapse of these civilizations was partly driven by rapid climate change events [14,28–32] superimposed on more gradual millennial climatic shifts. Furthermore, recent studies have suggested an association between a contemporary increase in the frequency and intensity of droughts in recent decades, to geopolitical unrest in the region, e.g., the Syrian Civil War [29,33,34]. These correlations highlight the importance of understanding both past and future climate perturbations in the ME. This can be achieved by use of large spatio-temporal networks/datasets of terrestrial hydro-climate archives. Regional-scale coherency would greatly improve our understanding of past variations in the spatio-temporal precipitation pattern of the ME, thereby resolving some of the contradictions between different records in the region [1,35].

The first version of the Speleothem Isotope Synthesis and Analysis database (SISAL_v1) [36,37], contains 376 isotope entity records derived from speleothems (secondary cave deposits) worldwide. Speleothems are commonly used as archives of past terrestrial climatic variability. This is because speleothems can be accurately dated and preserve multiple climate-sensitive proxies, which can be sampled at high spatial and temporal resolution. In temperate regions speleothem time-series are often continuous even under dry conditions [38,39]. By contrast, in semi-arid environments where the effective infiltration (i.e., precipitation minus evaporation or evapotranspiration) is negative throughout most of the year, the site specific hydrology and reservoir properties are emphasized in the palaeo-record and decadal, annual and often seasonal hiatuses (or seasonal biases) can be found [31,40,41]. Similarly, arid to hyper-arid environments particularly highlight growth/non-growth events. This gives speleothem records a distinct advantage over alternative palaeoclimate proxies (e.g., lake cores, tree-rings, corals), specifically for inter-comparison of the different climate settings found in the ME.

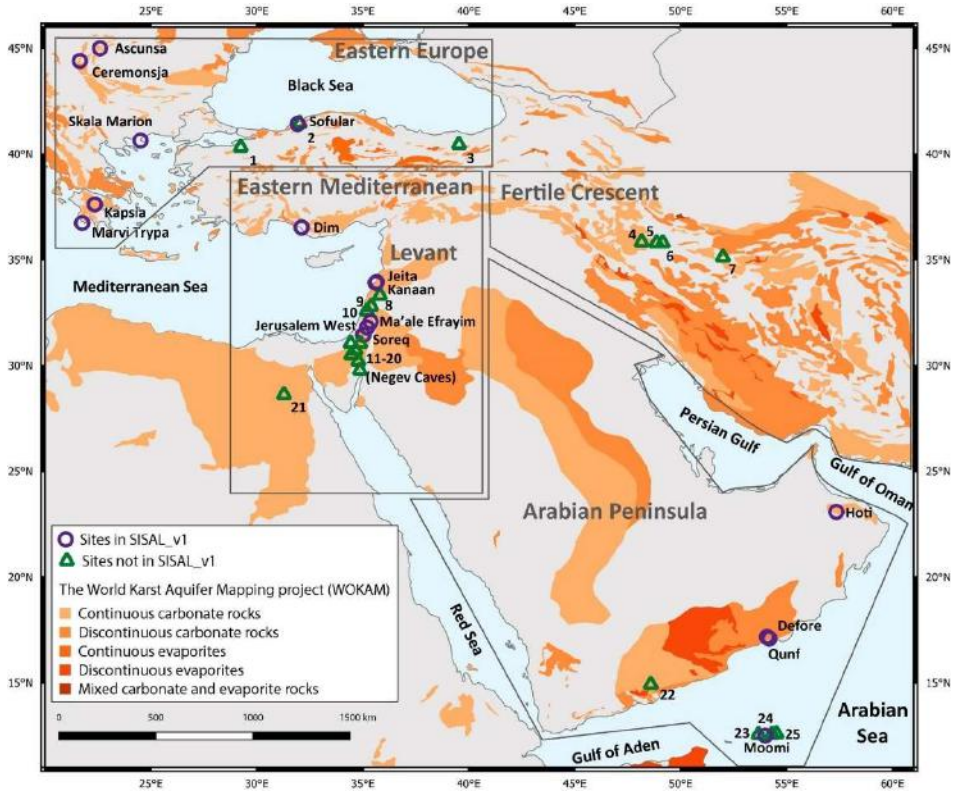

Figure 1. Location of the Middle East (ME) speleothem records that are included in SISAL_v1 (purple circles) and other identified records, not yet included in the database (green triangles). The base map shows the distribution of carbonate and evaporite rocks in the ME, as provided by the World Karst Aquifer Mapping project (WOKAM), adapted with permission from [42]. Cave sites with entities not included in the SISAL database are numbered (Table 1): (1) Karaca (2) Ovacik (3) Akçakale (4) Katleh Khor (5) Qal'e Kord (6) Gejkar (7) Gol-e Zard (8) Mitzpe Shlagim (9) Peqiin (10) Zalmon (11) Ashalim (12) Even Sid (13) Hol-Zakh (14) Izzim (15) Ma'ale Ha-Mishar (16) Ma'ale Dargot (17) Makhtesh ha-Qatan (18) Shizfon mini-caves (19) Tzavoa (20) Wadi Lotz (21) Wadi Sannur (22) Mukalla (23) Dimarshim (24) Casecas (25) Hoq.

In this work we review 17 speleothem isotope records (hereafter entities) that are in SISAL_v1 for the ME, which includes sites in Lebanon, Israel, the West Bank, Oman, Yemen, and Southwest Turkey (entities from the AP and Egypt are also reviewed by Braun et al. [43]). An additional six sites from Eastern Europe and Northern Turkey (see Kern et al. [44]) are included here as these sites are along the dominant Eastern Mediterranean (EM) Sea storm tracks, the major climate patterns controlling precipitation in the region (Figures 1 and 2; Table 1). The aim of this work is to highlight the applicability of speleothems from the ME currently logged in the SISAL_v1 database to resolve regional-scale consistencies and inconsistencies and to test for spatial coherency between speleothems and additional climate recorders (i.e., Arctic ice sheets and Mediterranean surface temperatures). The available speleothem stable oxygen isotope ratio (hereafter δ^{18}Occ) Holocene time-series are investigated via binning and normalizing (providing median, the 25th and 75th quantiles of the data) at 25-year and 200-year time windows, as used previously in the context of the PAGES 2k databases [45]. This method is used to better understand how different Holocene climatic events are differentiated regionally with the context of a normalized ME composite time-series from multiple records analysis (hereafter, ME composite), i.e., Sapropel 1, the 8.2 ka and the 4.2 ka event or the Little Ice Age at 0.7 ka BP. Finally, we highlight sites and entities that are not logged in SISAL_v1 and identify potential regions for the generation of new speleothem proxy time-series, suggestions regarding future speleothem-based research using the SISAL database are given accordingly.

Table 1. List of all speleothem records which include SISAL metadata: site (or cave) name and id number, latitude, longitude, entity (or speleothem) name and id number. Additional information includes; location of site (country or region), site height Above Mean Sea Level (AMSL) in meters, minimum and maximum ages given in years BP (1950), and published references. The top table are records available in SISAL_v1 (with annotations of some entities in those sites as yet to be added to SISAL_v1). The bottom table lists additional sites and speleothems not included in in SISAL_v1. A minimum age of "~present" is designated where a younger than 1950 CE sample is presented without an exact minimum age for the age model or a removal date. When ages beyond U/Th dating method are reported, the table notes these as >U/Th.

Site_name	Site _id	Location	Latitude °N	Longitude °E	Elevation (m AMSL)	Entity _name	Entity _id	Min. Age (yrs BP)	Max. Age (yrs BP)	Ref.
Ascunsa	72	Romania	45.00	22.60	1050	POM-2	161	−32	8169	[46]
Ceremosjna	76	Serbia	44.40	21.65	530	CC-1	165	−48	2426	[47]
Defore	170	Oman	17.17	54.08	150	S3	366	−46	731	[48]
						S4		9095	10,693	[49]
Dim	79	Turkey	36.53	32.11	232	Dim-E2	168	9738	13,094	[50]
						Dim-E3	169	12,575	89,714	
						Dim-E4	170	12,020	14,555	
Hoti	152	Oman	23.08	57.35	800	H5	327	6026	9607	[49,51]
						H1		78,000	82,000	[49,52]
						H2		~present	5000	
						H3		~present	5000	
						H4		117,000	130,000	
						H10		6200	10,500	
						H11		6200	10,500	
						H12		164	6277	
								117,000	130,000	
						H13		180,000	210,000	
								300,000	325,000	
						H14		6200	10,500	
						flowstone		117,000	130,000	
Jeita	11	Lebanon	33.95	35.65	100	Jeita-1	58	1137	12,288	[53,54]
						Jeita-2	59	13,330	20,367	
						Jeita-3	60	372	847	
						JeG-Stm-1		1100	11,900	[54]
Jerusalem West	68	Israel	31.80	35.20	700	AF-12	152	−16	168,714	[55]
Kanaan	19	Lebanon	33.91	35.61	98	Kanaan_MIS5	81	83,125	128,847	[56]
						Kanaan_MIS6	82	154,455	193,498	
Kapsia	44	Greece	37.62	22.35	700	GK-09-02	120	1115	2904	[57]
Ma'ale Efrayim	110	West Bank	32.08	35.37	250	ME-12	218	16,548	66,948	[18]
						36 samples				
Mavri Trypa	156	Greece	36.74	21.76	70	S1	347	1296	4687	[58]
Moomi	138	Yemen	12.50	54.00	400	M1-5	293	11,086	27,370	[59]
						M1-2		40,000	53,000	[59]
Qunf	159	Oman	17.10	54.18	650	Q5	351	308	10,558	[49]
Skala Marion	56	Greece	40.64	24.51	41	MAR_L	136	1481	5534	[60]
Sofular	141	Turkey	41.42	31.93	700	SO-1	305	−56	50,275	[61]

Table 1. *Cont.*

Site_name	Site _id	Location	Latitude °N	Longitude °E	Elevation (m AMSL)	Entity _name	Entity _id	Min. Age (yrs BP)	Max. Age (yrs BP)	Ref.
						SO-2 SO-4 SO-6SO-10 SO-14BSO-17A		~60 1080 93,572 ~present 475,910 86,190	59,510 307,030 133,200 2200 670,000 122,930	[62,63]
Soreq	160	Israel	31.45	35.03	400	Soreq composite	354	~present	30,031	[64]
						2N	353	4440	33,804	[31]
						2–6	352	743	2086	[14]
						Numerous samples		~present	250,000	[13,28,65–72]

Sites identified but currently not in SISAL_v1 (see Figure 1)

Cave Name	Figure 1 id	Country	Latitude (N)	Longitude (E)	Elevation (masl)	Identified speleothems	Min. Age	Max. Age	Ref.
Ashalim	11	Israel	30.94	34.74	400		116,700	>U/Th	[73]
Akcakale	3	Turkey	40.45	39.54		2p	~55	189	[74]
Casecas	24	Yemen	12.56	54.31		STM5	12	856	[75]
Dimarshim	23	Yemen	12.55	53.68		D1	~present	4530	[49]
Even Sid	12	Israel	30.64	34.81	800		87,700	>U/Th	[73]
Gejkar	6	Iraq	35.80	49.16		Gej-1	~63	2380	[29]
Gol-e Zard	7	Iran	35.13	52.00	2530	-	3700	5100	[76]
Hol-Zakh	13	Israel	31.16	35.20	150		111,700	349,100	[73]
Hoq	25	Yemen	12.59	54.53		Hq1 STM1 STM6	~50 ~53 ~56	6900 5600 4500	[75]
Izzim	14	Israel	31.14	35.06	500		372,600	500,100	[73]
Karaca	1	Turkey	40.32	29.24		K1	6000	77,300	[77]
Kataleh Khor	4	Iran	35.84	48.16		(2 samples)	214,000	500,000	[78]
Ma'ale ha-Meyshar	15	Israel	30.49	34.93	450		110,600	>U/Th	[73]
Ma'ale Dragot	16	Israel	31.4	35.00	300	MD (6 samples)	<500	426,440	[79]
Makhtesh ha-Qatan	17	Israel	30.95	35.22	~20		140,000	>U/Th	[73]
Mitzpe Shlagim	8	Israel/Syria	33.32	35.81	2224	MS-1 MS-2 MS-3	4300 8800 8500	88,000 89,000 49,100	[80]
Mukalla Cave	22	Yemen	14.92	48.59	1500	Y99 Y97-4 Y97-5	119,141 5630 8790	358,887 185,600 233,300	[16]
Ovacik	2	Turkey	41.46	32.02		O-1	4472	9796	[61]
Peqiin	9	Israel	32.58	35.19	650	PEK-5 PEK-6 PEK-9 PEK-10	5620 24,710 47,810 55,630	6780 223,700 283,650 288,160	[72]
Qal'e Kord	5	Iran	35.80	48.86		QK 8 QK 14	78,104 6581	99,182 127,012	[78,81]
Shizafon mini-caves	18	Israel	30.04	35.00	400		333,400	>U/Th	[73]
Tzavoa	19	Israel	31.20	35.20	550	TZ (15 samples)	14,400	204,760	[79]
Wadi Lotz	20	Israel	30.47	34.58	900	LOTS-3	-	>U/Th	[73]
Wadi Sannur	21	Egypt	28.62	31.28		WSS 1 to 6	136,460	188,120	[82]
Zalmon	10	Israel	32.80	35.40		ZAL-1 to ZAL-7 and ZAL-11	5100	165,000	[83]

2. Climate of the Middle East

The Middle East (ME) is located within the subtropical high-pressure belt between the Northern Hemisphere tropical (Hadley cell) and the mid-latitude atmospheric circulation, which is generally associated with dry climates (i.e., the global desert belt). However, while most of the region is indeed semi to hyper arid, the modern climate of the Levant is less arid and much milder than would be expected from its location. This is mainly due to Mediterranean cyclones delivering precipitation to the Levant, Fertile Crescent (FC), and on rare instances the Arabian Peninsula (AP), the genesis of which is triggered by the interplay between the Mediterranean lows and the major North Atlantic synoptic systems [84]. Furthermore, the Mediterranean Sea is characterized by an eastward gradient of increasing salinity and sea surface temperatures (SST). This SST gradient and the cooler (compared to the Mediterranean SSTs) surrounding land are key drivers for the Mediterranean cyclogenesis [85].

The EM coastal areas receive most precipitation during Northern Hemisphere winter months, on average about 95% of rainfall occurs between October and May [86]. Mean annual precipitation (climatological mean, last 30 years) in the Levant displays a steep gradient, from hyper-arid in the south with less than 100mm/y (e.g., Egypt, Southern Negev), through semi-arid with 500–600mm/y (e.g.,Soreq, Jerusalem) to humid in the north with >1000 mm (Lebanon and Southeast Turkey) (Figure 2A,B). Precipitation in the Levant is mainly sourced from eastward moving storm tracks generated inside the Mediterranean region, Cyprus low systems, when cold and dry air from continental Euro-Asia interfaces with the relatively warm Mediterranean Sea (Figure 2A compared to Figure 2B) [87,88]. A smaller fraction of cyclones enter on a southeastern trajectory from the Atlantic crossing the Southern EM Sea (Figure 2B), but rarely reach all the way to the Levant and FC [89]. Greece and Turkey (>38° N) also receive cyclones originating to the northwest over Central Europe, the Black Sea and in the Gulf of Genoa [84,90]. The semi-arid to hyper-arid FC currently receives most of its moisture during winter (98% of the precipitation occurs between October-May; [29]) from Mediterranean storm tracks [91]; while summer precipitation from tropical systems is virtually absent (Figure 2B).

The modern AP receives rainfall from the Mediterranean frontal systems (Dec-Mar), and rarely from the Indian summer monsoon (Figure 2A). In the Late Pleistocene, however, groundwater evidence suggests that the precipitation was sourced mainly from the Indian Ocean [92]. The modern climate at the Southern AP is largely dependent on the annual migration of the Inter-tropical Convergence Zone (ITCZ), which reaches its northern-most position in August. During this period, the Somali Jet brings large quantities of precipitation to the southernmost parts of the AP [93]. This is particularly important in the southwest where rainfall can occur all year round due to the orographic features of the region and moisture advected from the Red Sea [94,95]. The dominance of the Indian Ocean source in late Pleistocene suggests a northwards migration of the ITCZ.

The ME water-balance (Figure 2C,D) plays an important role in the development of cave records in the region. This becomes immediately visible when comparing the Mediterranean seasonality for summer (dry) and winter (wet), highlighting that even in regions that receive summer rainfall (Figure 2A), there will be little to no summer recharge under modern climate conditions (Figure 2C). The importance of the sub-regions reviewed in this work is emphasized when inspecting the patterns of winter potential recharge throughout the ME. The Levant, specifically the EM coastal region, is clearly on the desert-Mediterranean climate seamline with positive TP-E in the northernmost parts and negative TP-E in the south. The Israeli and Lebanese caves are situated in such a way where even a slight migration of the storm tracks shifts the water-balance from positive to negative and vice-versa. This sensitivity has been used to describe the Negev humid periods, however, Negev entities are not yet logged in the SISAL_v1 database) [73], climate controlled vegetation changes in the Levant [28] and changes in the dominant storm tracks [83]. The FC caves may track a similar transition between Mediterranean and monsoonal sources using Katleh Khor, Qal'e Kord and Gejkar caves, which appear to experience a positive winter water-balance compared to Gol-e Zard Cave, located further east and

experiencing more water-limited conditions. The predominantly year-round negative water-balance in the AP stresses the importance of local physiographic settings and individual storms.

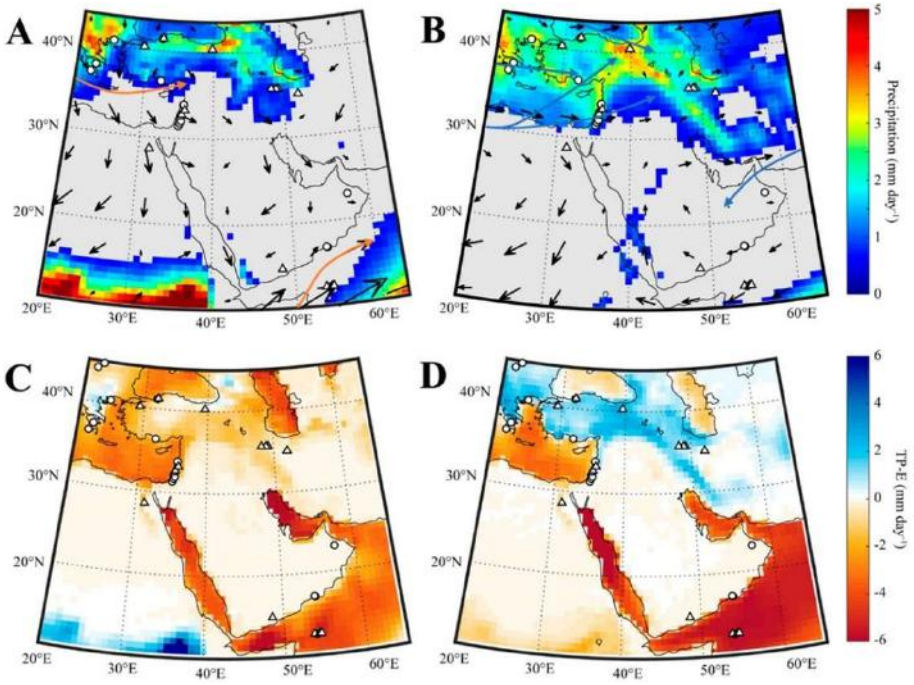

Figure 2. Maps showing seasonal precipitation amounts and water balance in the study region. Panel (**A**) and (**B**) illustrate seasonal precipitation amounts from June to September (JJAS) and from December to March (DJFM), respectively. Grey areas indicate regions where the daily precipitation amount is smaller than 0.5 mm. These panels also show the seasonal 850 hPa wind fields in the EM, AP and FC. Common storm trajectories are superimposed on the image and shown by the black arrows. Panels (**C**) and (**D**) show the seasonal water-balance: Total Precipitation (TP) minus Evaporation (E), for the periods JJAS (C) and DJFM (D), to best estimate the potential recharge (or "effective infiltration"). All data was retrieved from the ERA-Interim reanalysis dataset (1979 to 2015 CE) [96]. Following Figure 1, circles show the locations of speleothem records that are included in SISAL_v1, while triangles mark identified sites not included in SISAL_v1.

Due to the high SST and low atmospheric moisture above the Mediterranean Sea, the ratio of oxygen to deuterium isotopes in precipitation yields a unique regional water line, the Mediterranean Meteoric Water Line (MMWL, $\delta D = 8 \times \delta^{18}O + \sim 22$ [%VSMOW], [97]). The majority of Levant precipitation indicates a local vapor source, [86,97–99]. Atlantic storms traversing the Mediterranean Sea are overprinted with the MMWL signal, obscuring the original vapor source. There is no clear indication that alternative trajectories for the Levant, such as tropical plumes or Red Sea troughs (see Armon et al. [100]) maintain their source vapor, even though these storms travel very short distances over the EM [98]. Considering that the vadose aquifer mixes the rainwater of different storms, identifying shifts in trajectories of Mediterranean storms using water stable isotopes would be nearly impossible. However, using other tracers such as dust deposition rates its composition and Sr isotopes in speleothem may prove valuable [101–103]). Another important consideration is the effect of the aforementioned strong evaporative climate. In a long-term rainfall sampling campaign at the Soreq Cave site mean rainfall $\delta^{18}O$-δD relationship seemed to fall on the MMWL (slope ~8, deuterium excess of ~20–30%) [41,86], however, when events of <20 mm (and higher than 10 ˚C surface temperature) are

examined separately their slope and deuterium excess suggested to be the result of evaporative processes underneath the cloud. Whether the signature of the isotopically light events is transferred to the karst reservoir is still unclear, but a 2013 re-analysis of $\delta^{18}O$ time-series of Soreq Cave drip water suggests evaporation effect to be minimal [41].

In contrast, precipitation at the southern tip of the AP and the southernmost parts of the Levant is associated with the annual migration of the ITCZ and precipitation derived from tropical cyclones (Figure 2). These are isotopically enriched compared to the $\delta^{18}O$ of the Atlantic/Mediterranean systems and fall closer to the Global Meteoric Water Line ($\delta D = 8 \times \delta^{18}O + 10$, [104]). If, however, changes in atmospheric ITCZ and associated precipitation occurred simultaneously in the Levant/FC and the AP, the variation recorded in $\delta^{18}Occ$ time-series should be synchronized (see Section 4.1 for details).

3. Spatial/Temporal Setting of Middle East Speleothems

We define the ME roughly from 10° N to 45° N and from 20° E to 65° E. This includes the Eastern parts of Europe that are relevant for understanding of the ME climate, as described in Section 2. We use records from 16 caves and 23 individual speleothems from SISAL_v1 (Table 1), of which 10 sites and 17 entities are from the ME and highlighted in Figure 1. There are additional entities that are not in the SISAL_v1 database (Table 1), including sites in Turkey, Israel, Egypt, Yemen, Iran and Iraq [37]. All $\delta^{18}Occ$ values are reported in ‰ (per mille) and reported in the Vienna Pee Dee Belemnite (VPDB) standard.

The geographic coverage of the sites is uneven, with the majority of sites and entities from the EM, and a smaller proportion from the AP and FC. The geographical distribution of SISAL_v1 sites in the ME region is centered on areas of continuous carbonate rocks (Figure 1). However, other factors also have an influence. First, much of the region is arid to hyper arid (Figure 2), which inhibits the formation of speleothems, or limits formation to pluvial periods only [6,105]. Second, the recent unstable geopolitical situation in parts of the ME has allowed for limited scientific exploration.

The time intervals covered by the SISAL_v1 entities in the ME range from 0.056 ka BP (Sofular Cave, Turkey) to 193 ka BP (Kanaan Cave, Lebanon). The temporal distribution of samples is skewed towards the Holocene, with an almost linear increase in $\delta^{18}O$ data in SISAL_v1 from ~40 ka BP to the present (Figure 3B). Only six entities extend to and beyond the last interglacial (south to north): Jerusalem West Cave AF-12, Ma'ale Efrayim ME-12, Kanaan Cave MIS5 and MIS6, Dim Cave Dim-E3 and Sofular SO-1 (Figure 3C). The remaining 17 entities are largely confined to the interval between the Last Glacial Maximum (LGM, ~22 ka BP) and present day (Table 1). The skewed distribution may be the result of publication bias, as most studies have focused on the link between climate and human civilizations [14,106], coupled with the fact that younger speleothems are more naturally abundant as older samples are either covered by the younger deposits, or destroyed by dissolution, alteration, earthquakes etc. [107]. Large parts of the Late Pleistocene have generally been obtained specifically in sites where long-term continuous research has been carried out over multiple overlapping entities (e.g., Israel, Lebanon and Oman).

The median temporal resolution of all ME samples is close to decadal with a 7.7-year temporal gap between data points (Figure 3A), the distribution of temporal gaps for all existing entities varies between sub-annual to >500 year gaps, as indicated by the dark purple gaps in Figure 3C,D. Caution is needed when analyzing close to millennial gaps, as they may be the result of prolonged growth hiatuses or problematic sampling methodology. Temporal resolution for all entities is given in Figure 3C,D (up to 1000-year gaps), showing that most entities maintain a relatively constant growth-rate, with the exception of entities from Levant sites (i.e., Soreq, Ma'ale Efrayim, Kanaan Jeita and Dim caves). This highlights the hydrological sensitivity of the Levant records to changes in storm tracks, rainfall amount and evapotranspiration [29,40,48].

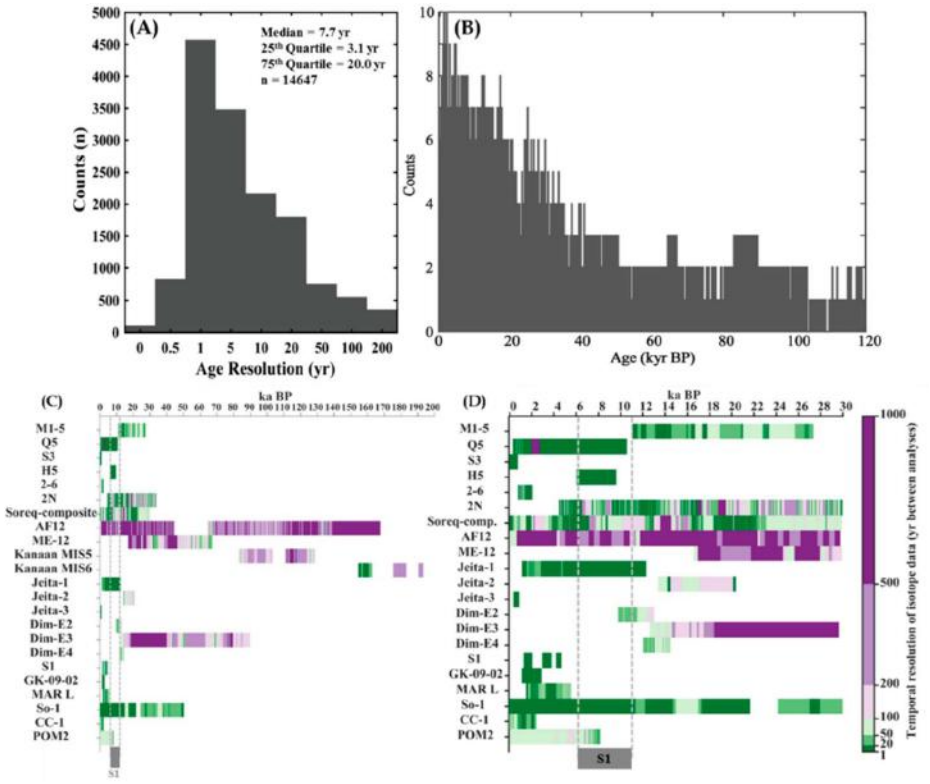

Figure 3. (**A**) Histogram showing the distribution of temporal difference between two consecutive data points for all ME SISAL_v1 entities, in bins of smaller than 0.5 years, between 0.5 and 1.0 years, between 1 and 5 years, between 5 and 10 years, between 10 and 20 years, between 20 and 50 years, between 50 and 100 years, between 100 and 200 years and over 200 years. (**B**) Histogram of speleothem records during the last 120 kyr subdivided in 250-year bins, available speleothem isotope time-series were counted if at least one $\delta^{18}O$ value was within a bin [108]. (**C**) Temporal coverage and temporal difference of studied entities covering the pre-Holocene time periods (up to 200 ka BP) and (**D**) entities from the last 30 ka BP. Sapropel 1 period is bracketed by the dashed lines in (**C**,**D**) [109].

Following the analysis of spatial distribution of the SISAL_v1 entities (Figure 1), as well as the temporal distribution and resolution (Figure 3), we will focus our discussion on the last 30 kyr of available SISAL_v1 data, and the regional ME composite for the last 12 kyr, from the Younger Dryas (YD) to present day. The temporal potential of climatological analysis is, in most entities, limited to decadal perturbations. However, the additional entities reported in Table 1 should allow for regional compilations and coherence tests to extend beyond the late-Pleistocene and Holocene to the last interglacial and beyond. Moreover, the regional dataset analyzed here is mainly affected by the Mediterranean storm tracks, with little information on the Indian Summer Monsoon (ISM) (see Kaushal et al. [110]). Questions concerning the intrusion of the Siberian High and migration of the ISM would be easier to tackle with the inclusion of the FC entities and the Negev caves (Table 1).

The inclusion of these sites could be used to construct a regional-comparison traverse between Eastern Europe and the Balkans, EM, FC and AP. For this reason, we limit this review to the last glacial period and Holocene, and in Section 5 we provide suggestions to achieve a complete regional coherence analysis for the Late Pleistocene.

4. SISAL_v1 Entities: Site-Specific Trends and Regional Interpretations

While variations of speleothem $\delta^{18}O$ values are a response to changes in climate parameters (rainfall amount and seasonal distribution, temperature, evaporation etc.), the absolute value of precipitation $\delta^{18}O$ values ($\delta^{18}Op$) can vary between different sites, even if they respond to similar regional climate trends. As a result, even if near-equilibrium deposition is assumed, the absolute value of $\delta^{18}Occ$ from different sites may not be identical. Hence, we focus on trends and excursions (i.e., on the variability) rather than absolute $\delta^{18}Occ$ values of the time-series plotted in Figure 4 (LGM to present) and Figure 5 (last 12 kyrs), these are then expended on using a normalized ME composite described in Section 4.3 and plotted in Figure 6.

4.1. Controls on Speleothem $\delta^{18}O$

For the Levant, Southwest and Northwest Turkey, as well as parts of Eastern Europe, two main processes were suggested to dictate the composition of $\delta^{18}Op$–the source and "amount" effect [53,111,112].

The potential vapor sources available for Middle East (ME) precipitation are the Mediterranean and the Indian Ocean (including the Arabian and Red Seas). Another source for the entities included from Turkey, Greece and Eastern Europe is the Black Sea (see Section 2). The modern Levant rainfall is limited to winter cold fronts with strong wet-winter/dry-summer seasonality. These fronts quickly inherit the isotopic signature of the Eastern Mediterranean (EM). This is commonly referred to as the source effect, where $\delta^{18}Op$ and (and the resulting $\delta^{18}O$ recorded in speleothems) is strongly influenced by the marine reservoir that contributes its vapor to rain formation. This effect is dominant over millennial time-scales, specifically glacial-interglacial cycles, where the isotopically light (low $\delta^{18}O$) polar ice-sheet meltwater deplete the overall composition of oceanic surface water and the resulting cloud forming vapor [111]. Specifically for the EM there is also a precessional time-scale effect where the isotopically light Nile flux (during Sapropels, African Humid Periods) results in lighter surface water [113]. $\delta^{18}Occ$ palaeo-data from Soreq, Pequiin and Jeita that show a visual first order millennial control on $\delta^{18}Occ$, predominantly reflect the change in composition of the vapor source, i.e., the EM Sea. Often, the glacial-interglacial transitions in speleothem records follow the depletion of sea surface $\delta^{18}O$ as resolved from planktonic foraminifera [53,112]. A similar, but isotopically opposite, millennial trend is also observed in Sofular Cave, where the vapor source is the Black Sea [62,63] (for additional discussion see Kern et al. [44]).

The "amount" effect is considered the dominant driver of short-term $\delta^{18}Op$ variations in the Levant and was empirically evaluated using modern measurements in numerous locations on the EM coastline [98,114]. Rainfall amount and isotopic compositions from the Israeli coastal plains and mountains display strong negative empirical correlations between rainfall amount, site altitude, and distance from the sea (all result in more negative values). The three are the underlying parameters controlling the rainout-distillation process (Rayleigh distillation) of the cloud [86,114]. There is no similar correlation for desert sites possibly due to desert rainfall being strongly affected by evaporation at the base of the cloud [98]. This observation was made using data from the EM coastline sites, where long-term rainfall sampling programs (amount and $\delta^{18}Op$) and modern cave water monitoring have been established. Regarding the sites in the SISAL_v1 database, only three of the seven Levant sites reviewed here had a long-term monitoring program (Kanaan, Soreq and Ma'ale Efraim). Three other sites (Mitzpe Shlagim, Pequiin and Dim) have had cave water sampled sporadically, when access to those sites was granted.

To evaluate the controlling mechanisms on decadal to seasonal $\delta^{18}O$ variability in Levant records, we refer to the extensive monitoring dataset from Soreq Cave collected between 1989 and 2016. The monitoring included the logging of rainfall amount, analysis of its isotopic composition, as well as sampling of local ground water and host rock and measurements of cave pCO_2, relative humidity and temperature of the cave air, seasonal cave drip and pool water sampling in multiple locations and the collection of modern speleothems and calcites [40,41,86,114–117]. The modern data from Soreq Cave reveals that on an annual time-scale, the rainfall amount is linearly correlated with more negative annual

δ^{18}Op (weighted average), and that this trend is then transferred into the cave. High mean annual rainfall amount results in more negative δ^{18}Op values of the water in the vadose zone for that year, while prolonged droughts shifts the baseline seepage water to more positive δ^{18}Op values [41]. The decadal to seasonal variations were validated in a modern stalagmite sample [40] and also observed in Soreq Cave fossil speleothem records, with seasonal to centennial resolution [14,28,31]. A similar control of the "amount" effect was also suggested in Western Mediterranean caves [118–121].

As a result of the modern strong seasonality pattern of the Levant region, the δ^{18}O of cave water represents mostly winter rainfall. For seasonal studies, this simplifies the evaluation of the δ^{18}Occ records by removing the by omitting the summer's contribution to annual δ^{18}Op variability (i.e., rainfall source seasonality [122,123]) and potentially avoiding δ^{18}O enrichment following evaporation in the epikarst and karst reservoirs (as it is often reported as negligible in winter storms [86,98,114]). Consequently, the resulting speleothem record is strongly biased towards negative winter δ^{18}Op. The implementation of the modern observation on paleorecords relies on the hypothesis which a suggests that the physiography of the Levant enforces the wet-winters/dry-summers seasonality of the region throughout the Pleistocene [124]. However, we note recent contrasting evidence by speleothem palaeoclimate studies resolved in seasonal resolution and other studies utilizing isotopically enabled climate models, which suggest the possibility of significant summer rainfall and positive summer effective infiltration for the Levant during the interglacials and interstadials [14,31,125].

In the Northern AP, Hoti cave records are mainly confined to the interglacial, with modern rainfall derived from similar Mediterranean cyclones (Figure 2A,B). Regional δ^{18}Op however is much higher than in the EM coastline caves, ranging between 0 and −2%. The current hypothesis to explain why the Hoti records have significantly lower δ^{18}Occ values is that speleothem growth occurs under the highly pluvial conditions brought by the ISM, as the most recent period of deposition in the cave, the early to mid - Holocene is regarded as a period of increased monsoonal activity [52]. The Southern AP sites (Defore, Moomi, Qunf), record the intensity and duration of the ISM as well as the location of the ITCZ [49], as suggested by the modern synoptic systems and rainfall regime, and corroborated by examination of multiple δ^{18}Occ records. These variations have been linked to solar output [48] and orbital forcing [75], and are synchronous global millennial scale events as recorded in the Greenland ice cores, EM Sea planktonic records and regional terrestrial records (i.e., the Dead Sea level curve [126]).

Unlike the Levant and AP records, the FC rainfall patterns vary from annual rainfall to distinct wet-dry seasonality, depending on the topography and proximity to the vapor sources [127]. Positive effective infiltration is limited to the autumn and winter months. δ^{18}Op values vary between −10% (winter) and −2% (summer), with heavier events as being high as +5% in spring and summer [81,127]. Records from Qal'e Kord Cave are similar to Soreq Cave and link to changes in monsoonal precipitation in China. This suggests a teleconnection between Eastern Europe and Asia as a result of the meridional migration of the Westerly Jet. The main vapor source for the Levant sites and the FC sites the same (the Mediterranean Sea), however, the average δ^{18}Occ values from the previous interglacial and glacial in Qal'e Kord Cave are ~2% lighter than coeval Soreq Cave records. This is ascribed mainly to the Rayleigh distillation of atmospheric vapor as it moves east over the land mass [81].

4.2. The Last Glacial Maximum, Deglaciation and the Transition into the Holocene (30 kyr BP to 12 kyr)

Levant records for the glacial-interglacial transition of the Late Pleistocene (deglaciation) follow the Mediterranean planktonic curves, indicating that these speleothem δ^{18}O records primarily reflect sea surface δ^{18}O changes [55,70,111,112]. The glacial period is characterized by a mean δ^{18}Occ that is several permille more positive as a result of the enriched δ^{18}O composition of the vapor source, i.e., the Mediterranean Sea (source effect), variations of the vapor source of ~1%–1.5% are observed in the Holocene as well, but as shown by Almogi-Labin et al. [112] " ... *source effect is not directly recorded in*

δ^{18}Osea–δ^{18}Oland values, which would remained constant if the source effect were the only control of rainwater δ^{18}O. The influences of rainfall, the amount, sea–land distance and elevation changes are thus superimposed on sea surface water δ^{18}O change". This shift is most pronounced in the Soreq Cave, where a sharp decrease in δ^{18}Occ is visible starting at the Last Glacial Maximum (LGM) from −3.0% towards Holocene values of −5.5% (Figure 4). This depletion trend stabilizes at ~15 kyr BP (circa the Bølling-Allerød warm event), followed by a pronounced response to the Younger Dryas (YD), which is the sharpest response observed to event in the SISAL_v1 records from the region, with an enrichment of >1.5%, but still 1–1.5% lower than LGM values (Figure 4).

The Jeita, Ma'ale Efrayim and Jerusalem West entities all have lower temporal resolution during the LGM and deglaciation, which makes the identification of major climatic events difficult (Figure 4). On centennial and longer time-scale, we observe a gradual transition in the δ^{18}Occ values, from −2.5% after the LGM (~17.5 ka BP) to between ~−5 and −7% in the Holocene in Dim, Jeita and West Jerusalem caves (Figure 4). The expected "back to glacial" excursion of the YD, described for the Soreq composite record (~ +1.5%), is harder to identify in the neighboring Levant (Figure 4). The identical trends observed across Levant records suggest that they respond to the same drivers, specifically, changing storm tracks, encroaching coastlines and changes in EM Sea surface isotopic composition [53,54,83,98]. This can be seen in Jeita Cave, which displays a visual correlation with the EM marine foraminifera δ^{18}O and in the trend of the ME composite (Figure 4 vs. Figure 6D,E). However, during prominent climatic events (LGM, H1) Jeita-2 δ^{18}Occ time-series shows opposite trends to the marine records [128,129]. These excursions towards lighter δ^{18}Occ are often in tandem with lower δ^{13}Ccc and Sr/Ca values and are suggested to reflect increased infiltration (i.e., high TP or higher TP-E). Evidence of changes in palaeo-infiltration highlight the inconsistencies found between the climate as inferred from the marine vs. terrestrial records, and also emphasizes that the source effect is not the only parameter influencing variations in δ^{18}Occ.

Sofular Cave entity SO-1, however, is the only time-series which does not agree with this glacial to interglacial regional trend, towards more positive values in the transition to the Holocene (Figure 4). The distinct imprint of Greenland interstadials on the MIS2 50-kyr record suggests that SO-1 captures decadal to centennial-scale events. This means that on glacial time-scales SO-1 reflects Black Sea surface water composition rather than Mediterranean source [61]. Additional discussion on Sofular Cave, including the Holocene cycle documented in the speleothem δ^{13}C time-series, can be found in the review of Eastern European records in SISAL_v1 [44].

The majority of entities from the AP grew only during interglacial periods. The only entity growing from the LGM to the Holocene is M1-5 from Moomi Cave (Socotra Island) spanning from 27 ka to 11 ka BP (Figure 3). The North-Easterly autumn rains sourced from the ITCZ are the main source of infiltrating water for Moomi Cave. Most of the Moomi δ^{18}Occ record is strongly correlated with the Greenland ice cores, suggesting a possible Atlantic driver of these monsoonal shifts [59]. The LGM is dated in the record as occurring circa 23–22 ka BP, which is interpreted as an arid period with pronounced decrease in precipitation over the Island. After the LGM there is an increase in rainfall, as deduced from a trend towards more negative δ^{18}Occ values, that is similar but more gradual than the trend seen in the Soreq Cave composite (Figure 4). The post-LGM warming and wetting trend is interrupted by the warm/dry H1 event (~16.4 ka BP), followed by the wet Bølling-Allerød event (14.5 ka BP) and then the dry YD (12.9–11.7 ka BP [130]) (Figure 4). The entity terminates soon after the commencement of the Holocene (dated to 11.4 ka BP), when a sharp decrease in δ^{18}Occ, interpreted as an increase in monsoonal rainfall is observed. The Levant records (Soreq, Jerusalem West and Ma'ale Efrayim) do not show a concomitant abrupt change of ~30 years transition from YD to the Holocene.

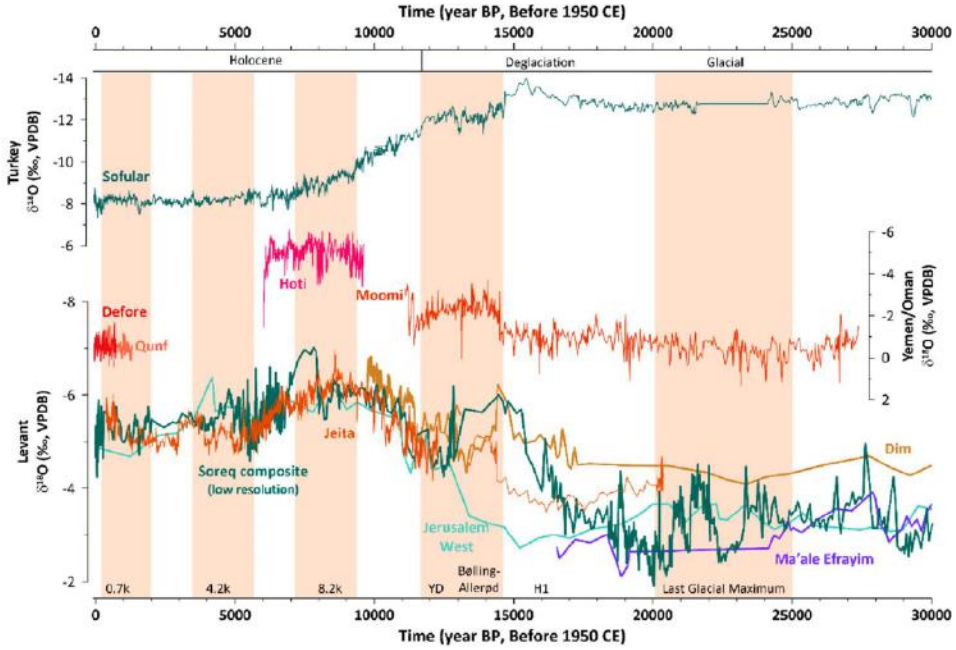

Figure 4. Time-series of δ^{18}Occ of speleothem records from the AP (Yemen/Oman), Levant including Turkeys' Mediterranean coast, i.e., Dim Cave) and Northern Turkey (Sofular). The climatic events highlighted on the plot are based on the interpretations from references [30,131].

4.3. Holocene Climatic Events and Spatial Heterogeneity across the Middle East

When interpreting the post-YD, early Holocene time-series, we note that although there is still an effect of changes in source δ^{18}O (seen in the planktonic curves of the EM Sea, Figure 6E), this is not as significant as during deglaciation. Thus, in this work we follow the conviction which determines that the dominant driver of δ^{18}Op variations is likely the "amount" effect [53,112]. The Holocene is characterized by a general trend towards increasing aridity in the ME region [46,49,51,57,61,66,70,132]. The wettest period in the EM, and the Levant in particular, occurred from ~10.8 to ~6.1 ka BP, coeval to the formation of Mediterranean Sapropel 1 and the African Humid Period (AHP) [68,133,134]. The entities from Jeita Cave (Figure 5A) show increasing precipitation during the early Holocene (from 12 to 10 ka BP) and wet conditions between ~10 to ~7 ka BP with peak precipitation amounts at ~8.5 ka BP. Between 7.5 and 6.5 ka BP, the δ^{18}Occ time-series from Jeita Cave indicates progressively decreasing precipitation amounts until 5 ka BP. Late Holocene δ^{18}Occ values in these entities reveal a generally dry period that is interrupted by shorter and longer wet-periods, e.g., from 4.0 to 3.0 ka BP, when precipitation amounts were increased. The hydroclimate changes recorded by the speleothems at Jeita Cave are in general agreement with other speleothem δ^{18}Occ time-series from the region, such as the speleothem records from Soreq Cave (Israel) [64] and Dim Cave (Turkey) [50] (Figure 5A). All these records indicate that the most arid conditions in the Holocene occurred after ~3.2 ka BP [54,58].

The only other record from the Levant that spans the entire Holocene is SO-1 from Sofular Cave (Figure 5A). This record shows increasing δ^{18}Occ values during the early- and mid-Holocene, until ~6 ka BP. However, compared to other records from the EM, long-term δ^{18}Occ trends in SO-1 are not related to variations in precipitation amounts, but instead reflect changes in the mean δ^{18}O value of the Black Sea, which is the main moisture source for this site, rather than the EM Sea [61,62]. Therefore,

while periodic coupling of the Mediterranean and Black Sea system can be observed in the regional records, it is difficult to directly link long-term δ^{18}Occ changes in SO-1 to δ^{18}Occ variations from EM speleothems [62]. Only one speleothem record from Eastern Europe, Ascunsa Cave (Romania), shows similar long-term trends similar to SO-1 (Figure 5A), likely reflecting also δ^{18}O changes of the Black Sea [46].

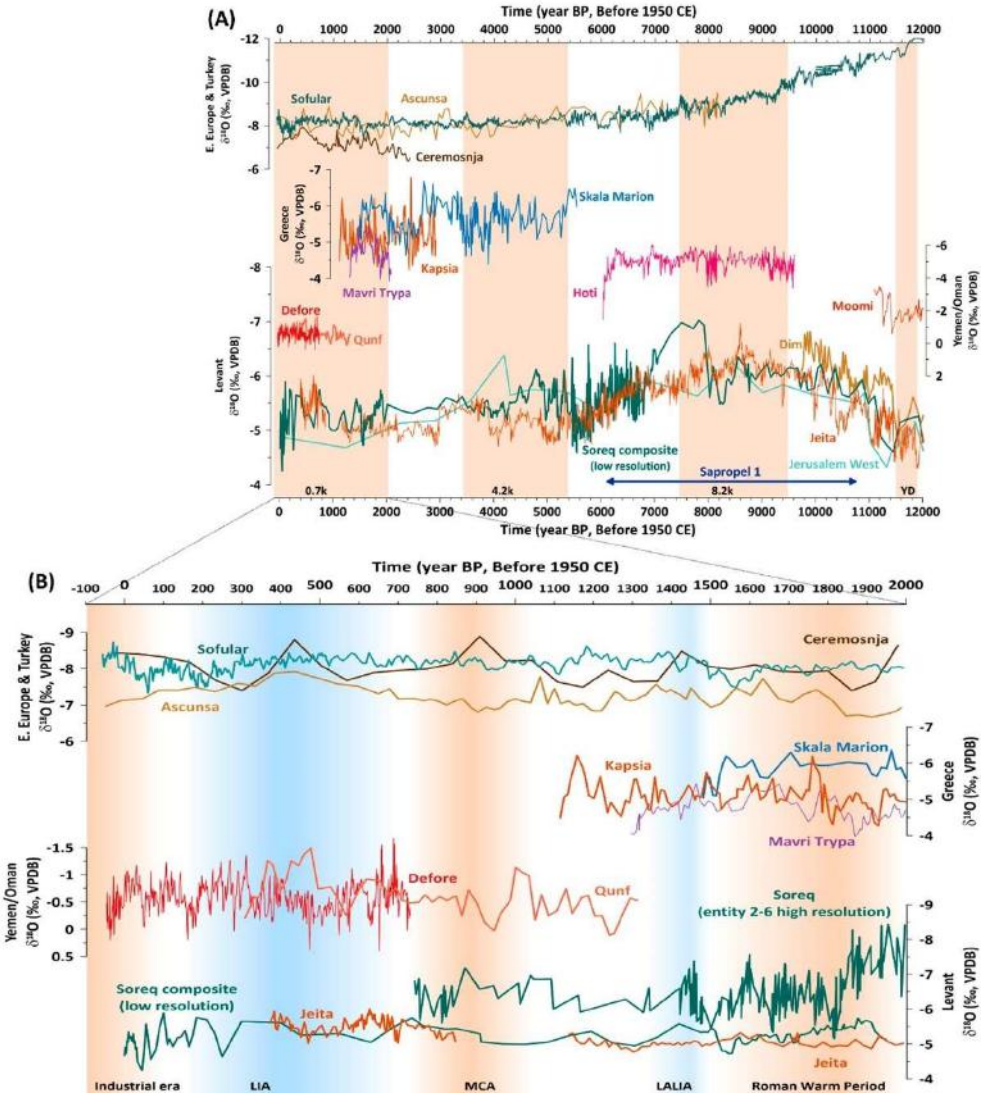

Figure 5. (**A**) Time-series of δ^{18}Occ of speleothem records for the last 12 kyr. speleothem records are the same than in Figure 4, which are on the modern dominant storm trace to the ME region shown in Figure 2. (**B**) Temporal variability of entities in panel A for the last 2 kyr. The seasonally-resolved entity 2–6 (Soreq Cave) is added for discussion [14]. The climatic events highlighted on the plot are based on the interpretations from references [30,131].

For the last 2 kyr, entities from Sofular Cave, Kapsia Cave, Mavri Trypa Cave, Soreq Cave, Jeita Cave, Qunf Cave and Defore Cave are available (Figure 6). From these records, only SO-1 (Sofular Cave) covers the entire period at 1 to 50-year resolution. The seasonally resolved Soreq entity 2–6, which was generated using Secondary Ion Mass Spectrometry (SIMS) [14,71], has more negative δ^{18}Occ values compared to the δ^{18}Occ of the Soreq composite record and the SIMS time-series variability is much higher. This is possibly related to the SIMS-sampling methodology, which targets multiple analyses in a

single ~50–100 µm thick annual band, which emphasizes the bias toward the negative winter values (~ −2.15% offset) [14]. The Soreq 2–6 δ^{18}Occ indicates a steep drying trend from 2.0 to 1.8 ka BP that is not observed in the other δ^{18}Occ time-series from the EM (Figure 5B), probably due to the relatively low temporal resolution of the other records, which are able to resolve only pronounced changes in δ^{18}Occ. Lechleitner et al. [135], find the opposite trend in their stacked records of Western Europe speleothem records. The finer climate variations during the Medieval Climate Anomaly (MCA) and the Late Antique Little Ice Age (LALIA) [131] are only identifiable in Soreq 2–6. The Little Ice Age (LIA) is recorded by the EM coastline entities (mainly Jeita Cave) and the record from Defore Cave (Figure 5B) with a positive excursion, that is again opposite to the observation from the Western European stack [135].

The comparison between the AP and the Levant over the past 2000 years is limited by the overlap of the entities that are available. The transition from the LALIA to the MCA is characterized by variable δ^{18}Occ values in Soreq 2–6. At the beginning of the LALIA δ^{18}Occ values are the most negative measured in Soreq 2–6, indicating a generally wet conditions in the Southern Levant (consistent with the Soreq composite record). By contrast, δ^{18}Occ values are more positive at the end of the LALIA, indicating dryer conditions in the transition period from the LALIA to the MCA. At the MCA, precipitation amounts increased again in the EM. This is indicated by the negative trend in δ^{18}Occ values in Soreq 2–6 [14,53,136]. During the MCA, δ^{18}Occ changes in the Qunf record and in Soreq 2–6 are anti-correlated, suggesting opposite precipitation variations at the southern tip of the AP and in the EM, to be considered further when additional high-resolution entities become available.

Analyses of regional composites have yielded useful results in the study of the Holocene [32,35] and the past 2000 years [45,137,138], because they mitigate the effect of age uncertainties and focus on detectable climate variability. Here we construct a composite of Holocene ME speleothem records (Figure 6E) and compare them with reconstructions of solar and volcanic activity, respectively (Figure 6A), the sum of glacier advances as well as cold and dry periods [32] (Figure 6B). The ME composite was produced as follows: first, data from each of the reconstructions were averaged into bins (at 25-year and 200-year intervals); second, each binned series was normalized. The normalized anomalies are visualized as boxes that are connected with a 3-point running average of 25-year bin means (Figure 6D). The same process is applied to Greenland ice cores [139] (Figure 6C). EM planktonic δ^{18}Occ profiles are also shown in order to highlight the source vapor isotopic variability, if recorded [64,109,140] (Figure 6E).

Rapid, prominent events observed in both continental and marine palaeo-archives during glacial periods are also evident during the Holocene, although less pronounced. This persistent rapid variability is suggested to be in response to an internal rhythmic throbbing of the climatic system at centennial scales [141]. In the scope of this review, three reference Holocene events are reviewed: ca. 8200 years BP (referred to here as the 8.2 ka event), ca. 4200 years BP (4.2 ka event) and ca. 700 years BP (0.7 ka or LIA). These events are concomitant with major glacier advances in the Northern Hemisphere [32,142] (Figure 6B).

The base of the Holocene is defined in the North Greenland Ice Core Project's NGRIP2 ice core, at 11,650 years BP [143]. The Early Holocene goes from the base to the 8.2 ka event [144], coeval with a final drainage of northern ice-dammed lakes causing a freshwater outburst into the North Atlantic [145] and the formation of Sapropel 1 in the Mediterranean [109,146]. The tail-end of Sapropel 1 in the EM (roughly 8.2 ka BP until a little after 7 ka BP) is seen in the normalized ME composite as trending toward more positive δ^{18}Occ values, the result of superposition of a general drying trend [109] and the enrichment trend of sea surface water δ^{18}O (Figure 6E). The normalized ME speleothem composite during this period displays the highest variability (i.e., the difference 25–75% percentiles) observed for the entire 12 kyr time-series (Figure 6D). This high variability indicates disagreement between the time-series of the various entities, hence increased regional heterogeneity. Sapropels are recorded in marine sediments due to a change either in the flux of organic matter to the sea floor from productivity changes or in preservation by low oxygen levels in bottom-waters [147,148]. Factors such as monsoon intensification, increased runoff from North Africa into the Mediterranean Sea and preconditioning due

to meltwater events/sea-level rise are potential factors leading to sapropels [109,146]. In addition, the particular geomorphology and hydrology of the Mediterranean basin favours their deposition [147].

The 8.2 ka event marks the mid-point of Sapropel 1–a generally humid period in the ME–and is indicated by a rapid positive anomaly in most ME entities (interpreted as cold/dry) (Figure 6C–E). The 25-year bin line of the normalized ME composite analysis does not indicate a pronounced 8.2 ka event, while the 200-year bin box highlight it as an interruption of this generally humid period, with distinct heterogeneity in the records (Figure 6D). In the marine sediment $\delta^{18}O$ record (Figure 6E), the 8.2 ka event is not as dominant as in other marine proxies [146], but Sapropel 1 appears as a negative 'hump' in the $\delta^{18}O$ time-series, where peak negative values are in agreement with the 8.2 ka event as well as cold reversal consistent in the North Atlantic context (Figure 6B,C) [32,149,150]. The 8.2 ka event is recorded in multiple records as a pronounced cold temperatures lasting ca. 160 years (Greenland, Figure 6C), together with a decreased snow-accumulation rate [151]. The 8.2 ka event is preceded by a remarkable minimum in solar activity [152] and an increase in the magnitude and frequency of volcanic eruptions [139] (Figure 6A). The Dead Sea level was sustained at low during the 8.2 ka event, which would suggest anomalously low rainfall intensities [153]. Thus, the 8.2 ka event is placed within a distinct cooling of the Aegean-Levantine regions from 8.6 to 8.0 ka BP, when African monsoon indicators suggest a change from an increased moisture availability to a decline towards a modern-type aridity reached at around 6 to 5.5 ka BP (Rohling et al. [142] and references therein) with a discontinuously wet and vegetated Sahara [154–156]. In the Levant, this behaviour of the ITCZ (African and Indian monsoon driver) could explain why the 8.2 ka event results in differentiated records across the ME region. In the Levant, the 8.2 ka event is suggested to be coeval with Neolithic revolution traits (e.g., the transition from the Pre-Pottery to the Pottery period) [157].

The 4.2 ka event is one of several decadal to centennial scale, regional to global, Rapid Climate Change (RCC) events that characterize the mid to late -Holocene [30,158]. The 4.2 ka marks the transition into the late-Holocene and is generally considered as a cold drought event, between ~4.2 and ~3.8 ka. The drought event lead to considerable environmental stress, most notably in Mediterranean and Levant societies, with cultural changes and settlement abandonment are seen from the Near East to Northern Mesopotamia as part of the end-phases of the Bronze age [28,159–161]. Although the 4.2 ka is a widely studied event, identifiable in multiple records and proxies, there is still considerable debate regarding the timing, nature and drivers of the event (or 4.2 to ~3.8 cycle) [28,158]. Thus, the SISAL entities timing if the event is also not as straight forward and ubiquitous. Comparing the $\delta^{18}Occ$ time-series of Soreq Cave to that of Jeita Cave, there is a close to centennial offset between the positive $\delta^{18}Occ$ excursion found in the Soreq composite (~4.2 ka), and the positive shift in Jeita Cave $\delta^{18}Occ$

(Figure 5A). The Soreq $\delta^{18}Occ$ excursion is superimposed on a prolonged drying trend starting circa 4.8 ka, when in contrast during the Soreq 4.2 ka itself, Jeita Cave expressed a rapid negative $\delta^{18}Occ$ excursion, commonly regarded as a wet condition (which Cheng et al., interpret to last until 2.9 ka [53]). The offset between the caves could also be a naturally occurring time transgressive phenomena, similar termination of the African Humid Period which progressed from north to south, following a gradual reduction in monsoon rainfall [162,163]. Inconsistencies between the Jeita and Soreq records have been suggested to be consistent with the progressive southward decrease in the regional humidity [53]. With the offset in mind, both caves appear to produce a close to W-shape event, with cold-warm/dry-wet episodes lasting decades to centuries, rather than a major single event (Figure 5A). This is in agreement with observation from Skala Marion Cave [164] and highlighted in regional multi-record compilations, such as a Dead Sea level drop lasting close to five centuries [153,158,165]. In this regard, the ME composite suggests that circa 3.8 ka marks the culmination of the observed gradual increase in aridity starting after the termination of Sapropel 1 (Figure 6D). The period between ~4.8 and ~4.0 ka has minor spatial heterogeneity which can be indicative of a less regionally unique event, weaker than the previous one circa 5.6 ka. However, as there is a gap in SISAL_v1 AP records for the duration of the event/cycle and the available records have much lower resolution for this specific time period [28],

we would recommend additional records to be included in the ME composite before any significant conclusions be drawn for this climate period.

The Little Ice Age (LIA) is the most recent climate anomaly of the Late Holocene and had strong impacts on European societies [166,167]. Greenland ice cores show the coldest individual bins of the past 2000 years during this period and a similar pattern is observed for EM marine profiles (Figure 6C–E). Over the past 2 kyrs, the ME composite (Figure 6D) shows a high variability (i.e., the difference 25–75% percentiles), as regional heterogeneity intensifies around what seem to be the coldest periods in the North Atlantic since the early Holocene [32]. Unlike the previous cold events reviewed (8.2 ka and 4.2 ka), the LIA shows a tendency towards more moisture availability, consistent with higher lake-levels at the Dead Sea [153]. Forcing simulations suggest that this pattern is consistent with a global cooling trend arising from an increased frequency of volcanic activity and/or land use change [137] (Figure 6B). Studies in the North Atlantic show year-to-year variability during the Little Ice Age: severe droughts, floods, intense storm activity during late summer-early autumn, cold/heat waves that showed significant spatio-temporal variation and exceptional wintertime conditions, with sea ice expansion and reduced northward heat transport by the subpolar gyre [168–170]. In the Levant, the onset of the Little Ice Age coincides with the end of the Crusades and reinforcement of the Mamluk sultanate and Ottoman empire, between the 14th and early 20th centuries [161], similar to the rise and subsequent fall of the Roman rule over the Levant during the "Roman Humid Period" [14].

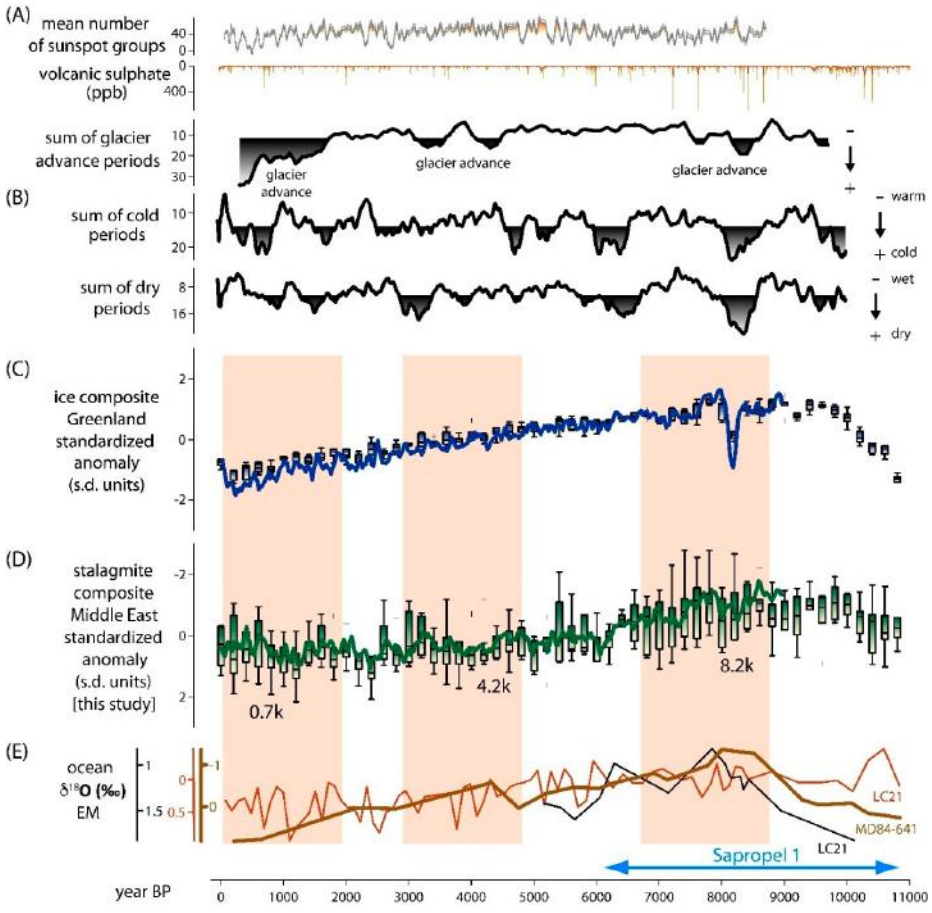

Figure 6. Holocene overview of the δ^{18}Occ of ME speleothem records in comparison with additional terrestrial and marine palaeo-archives. (**A**) Reconstructed sunspot number along with its 68% confidence interval [152] and volcanic aerosol based on empirical orthogonal function analysis performed in ice cores from Greenland [139,171]. (**B**) Sum of ice glacier advances, cold and dry periods [32]. (**C**) Composite δ^{18}O data from Greenland ice-cores [172]. (**D**) Composite of the SISAL δ^{18}Occ from ME and

Eastern Europe speleothems reviewed in this study. The composites in (**C**,**D**) are shown as normalized anomalies (standard units) with a box width: 200-year intervals; central mark: median; edges of the box: 25th & 75th percentiles; whiskers: extreme values (~99% of data); plusses: outliers (~1% of data); boxes connected with a 3-point running average of 25-year bin means. (**E**) Eastern Mediterranean planktonic $\delta^{18}O$ profiles of site LC21 [64,109] (light brown line: *Globigerinoides ruber*, black line: *Neogloboquadrina pachyderma*) and site MD84-641 [140] covering the Holocene. The shaded areas highlight important early, middle and late Holocene climate events discussed in the text (8.2, 4.2 and 0.7 ka, respectively).

5. Conclusions and Future of SISAL Project in the Middle East

5.1. Emphasis for Future Speleothem Research in the Middle East

The main goal for future speleothem research in the Middle East (ME) would be to increase spatial coverage in the region (Figure 1, Table 1), specifically in the Fertile Crescent (FC), Arabian Peninsula (AP) and Saharan belt (Egypt, Negev) sub-regions where current site density is considerably lower than the Levant. Efforts in these environments are specifically important as the spatial distribution of carbonate bedrock is not continuous so without regional continuity, improved entity density would improve regional analysis coherency.

Additionally, emphasis should be placed on including additional entities to increase the temporal coverage and generate longer time-series from the region as most of the records cover only the last 40–30 kyr (Figure 3B). This should be done in tandem with application of high temporal-resolution analysis methodologies (conventional and novel) to increase the resolution of the available geological paleorecords (see Figure 3C) and allow detection of changes in seasonality [14,31] and decadal scale variations [28,48]. This will enable future studies to conduct more accurate coherence regional investigations to reveal coherent and robust climate variations over longer time periods, including glacial-interglacial cycles in the Pleistocene.

Achieving these goals will allow SISAL based studies could better constrain teleconnections amongst the hydroclimate of remote regions such as Northern Africa, the Levant and the FC, which should all be influenced by Mediterranean cyclones and ITCZ migration, as the spatial scale of the ITCZ migration and the overall effect it might have had on rainfall amount in the Southern AP is still debated [173] and a regional compilation incorporating crucial missing records to the SISAL database will enable us to shed light on this topic. Furthermore, considering the location of the Levant at the border between the tropical Hadley cell and the mid-latitude Ferrel cell, hydroclimate change in this region is supposed to be very sensitive to shifts in the Hadley-Ferrel-cell border, which should be ultimately imprinted in the speleothem palaeoclimate record. Hence, future speleothem-based reconstructions and synthesis of past hydroclimate changes from North Africa, the Levant and the FC will allow testing of theoretical concepts on how the Hadley-Ferrel-cell border shifts in response to changes in insolation [174].

The ability to simulate the rhythm of climate variability and specific events (such as sapropels, the 8.2 ka or 4.2 ka events and the LIA) depends on the availability of high-quality databases, with high enough temporal resolution to make relevant inferences from a human perspective. In this regard, completion of the above-mentioned information will help in answering challenging questions and in understanding future changes to water limited environments.

Though this work does not review the carbon isotope climate proxy ($\delta^{13}C$), it should be noted that the $\delta^{18}O$ record is often 'noisy' in fast growing speleothems which provide high-resolution Holocene records, as it reflects seasonal and annual variations in $\delta^{18}O$, while the $\delta^{13}C$ record is less sensitive to such short time-scale variations and reflects variations in the soil CO_2 composition, which can be used to identify and characterize Holocene centennial and millennial climate variability [28].

5.2. The Importance of Fertile Crescent Speleothem Data

The publication of more speleothem-based proxy records from the FC is a priority in palaeoclimate research for several reasons. First, additional FC entities would make it easier to establish the role of the Siberian High and Indian Summer Monsoon in the regional palaeo-hydrology. Whereas there is no influence from the ISM on precipitation in the modern-day FC, it has been theorized that in the early Holocene (and before) the picture was more complicated–the FC received rainfall more evenly from two sources instead of the simple single-sourced nature of precipitation today [175], SISAL records could help researching this question.

Second, the late Holocene δ^{18}Occ records from the FC reflect winter-spring precipitation, the main hydrological season, while records such as lake sediments, pollen and tree-rings often reflect annual precipitation, summer precipitation or temperature changes. They can also suffer from other inadequacies such as lacking the required temporal resolution, not covering the researched period, or suffering from considerable chronological uncertainties [175]. These problems are especially limiting when using palaeoclimate proxies in archaeological discussions, as tying climatic events to specific human developments requires maximum chronological precision and precipitation during the growing period (spring) will be most important for human flourishing. Seeing the FC as one of the most important regions worldwide for human development, producing highly-resolved and accurately-dated speleothem records is of vital concern. Here we identified five sites in the FC, from Turkey, Iran and Iraq. The entities from these publications have already contributed to the understanding of the prevailing continental climatic conditions over the Holocene and as far back as 500 ka BP. Increasing the number of datasets available in SISAL would provide an important tool for answering the questions raised in this section.

5.3. SISAL Outlook for the Middle East

As Table 1 suggests, there is an excellent opportunity to include more records from the ME in the SISAL database. This would allow the application of statistical analyses, e.g., standardization techniques to synthesize common trends in the stable isotope time-series [137] or coherence analysis using Monte Carlo Principal Component Analyses (MC-PCA) [35]. Such analyses will enable better constraints on the relationships between different archives such as between the speleothem hydroclimate records and reconstructed SSTs. It would also allow the identification of common modes of hydroclimate variability and better insights into the climate dynamics/mechanisms and its forcing. Coherence analyses could also be extended to incorporate Western Mediterranean as well as European stable isotope time-series, and validate the teleconnection between hydroclimate changes that also depend on mid-latitude cyclones [176–178].

Author Contributions: Y.B. designed the concept of this study and led the synthesis and writing of this manuscript with support of all co-authors; Y.B., B.M., J.F.L., M.D. extracted, collated and evaluated the data and performed statistical analyses; Y.B., B.M., E.I., M.A.L., M.D. worked on the design and visualization of the figures; Y.B., B.M., M.J.J., M.D. worked on editing the text and all authors reviewed the manuscript.

Funding: Y.B. acknowledges support of FFB grant #3-323/4532211. B.M. acknowledges support from the CSIC Ramón y Cajal postdoctoral programme RYC-2013-14073. M.A.L. acknowledges support from the Ministry of Science and Technology (MOST), Taiwan (107-2119-M-002-051). M.D. acknowledges funding by the German Research Foundation (DFG) grant DE 2398/3-1.

Acknowledgments: The SISAL is a working group of the Past Global Changes (PAGES) programme and we thank PAGES for their support of this activity. We thank Laia Comas-Bru for assistance in Figure 1, sharing and producing Figure 3. The authors thank the members of the World Karst Aquifer Mapping project for providing the carbonate aquifer maps used by in for Figure 1. We are grateful to Sandy Harrison and Laia Comas Bru for their editorial handling of the manuscript and endless patience. We also wish to thank Andrea Columbu and three anonymous reviewers for their support and suggestions. The authors offer the secret speleo handshake to Andy Baker donated of his time to review this work and share his insight on water-limited environments. Assistant Editor Mark Guo for his time and kind help in publishing this manuscript. Y.B. wishes to thank Kerstin Braun and Zoltán Kern for coordination in preparation of the African and Eastern European review papers included in this special issue [43,44], and Miryam Bar-Matthews for her support in the SISAL Middle East team efforts to advance the input of regional datasets into SISAL.

Conflicts of Interest: The authors declare no conflict of interest. The funders had no role in the design of the study; in the collection, analyses, or interpretation of data; in the writing of the manuscript, or in the decision to publish the results.

References

1. Katrantsiotis, C.; Kylander, M.E.; Smittenberg, R.; Yamoah, K.K.A.; Hättestrand, M.; Avramidis, P.; Strandberg, N.A.; Norström, E. Eastern Mediterranean hydroclimate reconstruction over the last 3600 years based on sedimentary n-alkanes, their carbon and hydrogen isotope composition and XRF data from the Gialova Lagoon, SW Greece. *Quat. Sci. Rev.* **2018**, *194*, 77–93. [CrossRef]
2. Lionello, P.; Abrantes, F.; Congedi, L.; Dulac, F.; Gacic, M.; Gomis, D.; Goodess, C.; Hoff, H.; Kutiel, H.; Luterbacher, J.; et al. Introduction: Mediterranean Climate – Background Information. In *The Climate of the Mediterranean Region: From The Past to the Future*; Lionello, P., Ed.; Elsevier: London, UK, 2012.
3. Giorgi, F. Climate change hot-spots. *Geophys. Res. Lett.* **2006**, *33*, 1–4. [CrossRef]
4. Giorgi, F.; Lionello, P. Climate change projections for the Mediterranean region. *Glob. Planet. Chang.* **2008**, *63*, 90–104. [CrossRef]
5. Lionello, P.; Scarascia, L. The relation between climate change in the Mediterranean region and global warming. *Reg. Environ. Chang.* **2018**, *18*, 1481–1493. [CrossRef]
6. Vaks, A.; Bar-Matthews, M.; Ayalon, A.; Matthews, A.; Halicz, L.; Frumkin, A. Desert speleothems reveal climatic window for African exodus of early modern humans. *Geology* **2007**, *35*, 831. [CrossRef]
7. Rosen, A.M. *Civilizing Climate: Social Responses to Climate Change in the Ancient Near East*; Altamira Press: Plymouth, UK, 2007; ISBN 978-07591-0494-5.
8. Berger, J.F.; Lespez, L.; Kuzucuog˘lu, C.; Glais, A.; Hourani, F.; Barra, A.; Guilaine, J. Interactions between climate change and human activities during the Early to Mid Holocene in the East Mediterranean basins. *Clim. Past* **2016**, *12*, 1847–1877.
9. Schilman, B.; Bar-Matthews, M.; Almogi-Labin, A.; Luz, B. Global climate instability reflected by Eastern Mediterranean marine records during the late Holocene. *Palaeogeogr. Palaeoclimatol. Palaeoecol.* **2001**, *176*, 157–176. [CrossRef]
10. Langgut, D.; Almogi-Labin, A.; Bar-Matthews, M.; Pickarski, N.; Weinstein-Evron, M. Evidence for a humid interval at ~56–44 ka in the Levant and its potential link to modern humans dispersal out of Africa. *J. Hum. Evol.* **2018**, *124*, 75–90. [CrossRef]
11. Brierley, C.M.; Manning, K.; Maslin, M. Pastoralism may have delayed the end of the green Sahara. *Nat. Commun.* **2018**, *9*, 4018. [CrossRef] [PubMed]
12. Weiss, H.; Bradley, R.S. What drives societal collapse? *Science* **2001**, *291*, 609–610. [CrossRef]
13. Bar-Matthews, M.; Ayalon, A. Climatic Conditions in the Eastern Mediterranean During the Last Glacial (60–10 ky) and Their Relations to the Upper Palaeolithic in the Levant as inferred from Oxygen and Carbon Isotope Systematics of Cave Deposits. In *More Than Meets the Eye: Studies on Upper Palaeolithic Diversity in the Near East*; Goring-Morris, N.A., Belfer-Cohen, A., Eds.; Oxbow: Oxford, UK, 2003; pp. 13–18.
14. Orland, I.J.; Bar-Matthews, M.; Kita, N.T.; Ayalon, A.; Matthews, A.; Valley, J.W. Climate deterioration in the Eastern Mediterranean as revealed by ion microprobe analysis of a speleothem that grew from 2.2 to 0.9 ka in Soreq Cave, Israel. *Quat. Res.* **2009**, *71*, 27–35. [CrossRef]
15. Rosenberg, T.M.; Preusser, F.; Fleitmann, D.; Schwalb, A.; Penkman, K.E.H.; Schmid, T.W.; Al-Shanti, M.A.; Kadi, K.; Matter, A. Humid periods in southern Arabia: Windows of opportunity for modern human dispersal. *Geology* **2011**, *39*, 1115–1118. [CrossRef]
16. Fleitmann, D.; Burns, S.J.; Pekala, M.; Mangini, A.; Al-Subbary, A.A.; Al-Aowah, M.; Kramers, J.; Matter, A. Holocene and Pleistocene pluvial periods in Yemen, southern Arabia. *Quat. Sci. Rev.* **2011**, *30*, 783–787. [CrossRef]

17. Vaks, A.; Woodhead, J.D.; Bar-Matthews, M.; Ayalon, A.; Cliff, R.A.; Zilberman, T.; Matthews, A.; Frumkin, A. Pliocene–Pleistocene climate of the northern margin of Saharan–Arabian Desert recorded in speleothems from the Negev Desert, Israel. *Earth Planet. Sci. Lett.* **2013**, *368*, 88–100. [CrossRef]

18. Vaks, A.; Bar-Matthews, M.; Ayalon, A.; Schilman, B.; Gilmour, M.A.; Hawkesworth, C.J.; Frumkin, A.; Kaufman, A.; Matthews, A. Paleoclimate reconstruction based on the timing of speleothem growth and oxygen and carbon isotope composition in a cave located in the rain shadow in Israel. *Quat. Res.* **2003**, *59*, 182–193. [CrossRef]

19. Rosenberg, T.M.; Preusser, F.; Risberg, J.; Plikk, A.; Kadi, K.A.; Matter, A.; Fleitmann, D. Middle and Late Pleistocene humid periods recorded in palaeolake deposits of the Nafud desert, Saudi Arabia. *Quat. Sci. Rev.* **2013**, *70*, 109–123. [CrossRef]

20. Drake, N.A.; Breeze, P.; Parker, A. Palaeoclimate in the Saharan and Arabian Deserts during the Middle Palaeolithic and the potential for hominin dispersals. *Quat. Int.* **2013**, *300*, 48–61. [CrossRef]

21. Weisdorf, J.L. From Foraging To Farming: Explaining The Neolithic Revolution. *J. Econ. Surv.* **2005**, *19*, 561–586. [CrossRef]

22. Lev-Yadun, S.; Gopher, A.; Abbo, S. The Cradle of Agriculture. *Science* **2000**, *288*, 1602 LP-1603. [CrossRef] [PubMed]

23. Kislev, M.E.; Hartmann, A.; Bar-Yosef, O. Early domesticated fig in the Jordan Valley. *Science* **2006**, *312*, 1372–1374. [CrossRef] [PubMed]

24. Tanno, K.I.; Willcox, G. How fast was wild wheat domesticated? *Science* **2006**, *311*, 1886. [CrossRef] [PubMed]

25. Zohary, D.; Hopf, M. Domestication of Pulses in the Old World: Legumes were companions of wheat and barley when agriculture began in the Near East. *Science* **1973**, *182*, 887–894. [CrossRef] [PubMed]

26. Liverani, M. *The Ancient Near East: History, Society and Economy*; Routledge: New York, NY, USA, 2014.

27. Mellaart, J. *The Neolithic of the Near East*; Scribner's: New York, NY, USA, 1975; ISBN 0-684-14484-0.

28. Bar-Matthews, M.; Ayalon, A. Mid-Holocene climate variations revealed by high-resolution speleothem records from Soreq Cave, Israel and their correlation with cultural changes. *Holocene* **2011**, *21*, 163–171. [CrossRef]

29. Flohr, P.; Fleitmann, D.; Zorita, E.; Sadekov, A.; Cheng, H.; Bosomworth, M.; Edwards, R.L.; Matthews, W.; Matthews, R. Late Holocene droughts in the Fertile Crescent recorded in a speleothem from northern Iraq. *Geophys. Res. Lett.* **2017**, *44*, 1528–1536. [CrossRef]

30. Mayewski, P.A.; Rohling, E.J.; Curt Stager, J.; Karlén, W.; Maasch, K.A.; David Meeker, L.; Meyerson, E.A.; Gasse, F.; Van Kreveld, S.; Holmgren, K.; et al. Holocene climate variability. *Quat. Res.* **2004**, *62*, 243–255. [CrossRef]

31. Orland, I.J.; Bar-Matthews, M.; Ayalon, A.; Matthews, A.; Kozdon, R.; Ushikubo, T.; Valley, J.W. Seasonal resolution of Eastern Mediterranean climate change since 34ka from a Soreq Cave speleothem. *Geochim. Cosmochim. Acta* **2012**, *89*, 240–255. [CrossRef]

32. Wanner, H.; Solomina, O.; Grosjean, M.; Ritz, S.P.; Jetel, M. Structure and origin of Holocene cold events. *Quat. Sci. Rev.* **2011**, *30*, 3109–3123. [CrossRef]

33. Kelley, C.P.; Mohtadi, S.; Cane, M.A.; Seager, R.; Kushnir, Y. Climate change in the Fertile Crescent and implications of the recent Syrian drought. *Proc. Natl. Acad. Sci. USA* **2015**, *112*, 3241–3246. [CrossRef]

34. Trigo, R.M.; Gouveia, C.M.; Barriopedro, D. The intense 2007-2009 drought in the Fertile Crescent: Impacts and associated atmospheric circulation. *Agric. For. Meteorol.* **2010**, *150*, 1245–1257. [CrossRef]

35. Deininger, M.; McDermott, F.; Mudelsee, M.; Werner, M.; Frank, N.; Mangini, A. Coherency of late Holocene European speleothem δ18O records linked to North Atlantic Ocean circulation. *Clim. Dyn.* **2017**, *49*, 595–618. [CrossRef]

36. Atsawawaranunt, K.; Comas-Bru, L.; Amirnezhad Mozhdehi, S.; Deininger, M.; Harrison, S.P.; Baker, A.; Boyd, M.; Kaushal, N.; Masood Ahmad, S.; Ait Brahim, Y.; et al. The SISAL database: A global resource to document oxygen and carbon isotope records from speleothems. *Earth Syst. Sci. Data* **2018**, *10*, 1687–1713. [CrossRef]

37. Comas-Bru, L.; Harrison, S.P. SISAL: Bringing Added Value to Speleothem Research. *Quaternary* **2019**, *2*, 7. [CrossRef]
38. Baker, A.; Smith, C.L.; Jex, C.N.; Fairchild, I.J.; Genty, D.; Fuller, L. Annually Laminated Speleothems: A Review. *Int. J. Speleol.* **2008**, *37*, 193–206. [CrossRef]
39. Fairchild, I.J.; Baker, A. *Speleothem Science: From Process to Past Environments*; John Wiley & Sons: New York, NY, USA, 2012; Volume 3, ISBN 9781444361094.
40. Orland, I.J.; Burstyn, Y.; Bar-Matthews, M.; Kozdon, R.; Ayalon, A.; Matthews, A.; Valley, J.W. Seasonal climate signals (1990–2008) in a modern Soreq Cave stalagmite as revealed by high-resolution geochemical analysis. *Chem. Geol.* **2014**, *363*, 322–333. [CrossRef]
41. Burstyn, Y. *Multi-decade to Seasonal Climate Change Recorded by Stable Isotope and Trace Element Variability in Modern Cave-waters and Calcite of Soreq Cave, Israel*; Geological Survey of Israel: Jerusalem, Israel, 2013.
42. Chen, Z.; Auler, A.S.; Bakalowicz, M.; Drew, D.; Griger, F.; Hartmann, J.; Jiang, G.; Moosdorf, N.; Richts, A.; Stevanovic, Z.; et al. The World Karst Aquifer Mapping project: concept, mapping procedure and map of Europe. *Hydrogeol. J.* **2017**, *25*, 771–785. [CrossRef]
43. Braun, K.; Nehme, C.; Pickering, R.; Rogerson, M.; Scroxton, N. A Window into Africa's Past Hydroclimates: The SISAL_v1 Database Contribution. *Quaternary* **2019**, *2*, 4. [CrossRef]
44. Kern, Z.; Demény, A.; Hatvani, I.G. Speleothem stable isotope records from Eastern Europe & Turkey. *Preprints* **2018**, 2018120038. [CrossRef]
45. Emile-Geay, J.; McKay, N.P.; Kaufman, D.S.; von Gunten, L.; Wang, J.; Anchukaitis, K.J.; Abram, N.J.; Addison, J.A.; Curran, M.A.J.; Evans, M.N.; et al. A global multiproxy database for temperature reconstructions of the Common Era. *Sci. Data* **2017**, *4*, 170088. [CrossRef]
46. Dragus¸in, V.; Staubwasser, M.; Hoˇ ffmann, D.L.; Ersek, V.; Onac, B.P.; Veres, D. Constraining Holocene hydrological changes in the Carpathian-Balkan region using speleothem δ18O and pollen-based temperature reconstructions. *Clim. Past* **2014**, *10*, 1363–1380. [CrossRef]
47. Kacanski, A.; Carmi, I.; Shemesh, A.; Kronfeld, J.; Yam, R.; Flexer, A. Late Holocene Climatic Change in the Balkans: Speleothem Isotopic Data from Serbia. *Radiocarbon* **2001**, *43*, 647–658. [CrossRef]
48. Burns, S.J.; Fleitmann, D.; Mudelsee, M.; Neff, U.; Matter, A.; Mangini, A. A 780-year annually resolved record of Indian Ocean monsoon precipitation from a speleothem from south Oman. *J. Geophys. Res.* **2002**, *107*, ACL-9. [CrossRef]
49. Fleitmann, D.; Burns, S.J.; Mangini, A.; Mudelsee, M.; Kramers, J.; Villa, I.; Neff, U.; Al-Subbary, A.A.; Buettner, A.; Hippler, D.; et al. Holocene ITCZ and Indian monsoon dynamics recorded in stalagmites from Oman and Yemen (Socotra). *Quat. Sci. Rev.* **2007**, *26*, 170–188. [CrossRef]
50. Ünal-Imer, E.; Shulmeister, J.; Zhao, J.X.; Tonguç Uysal, I.; Feng, Y.-X.; Duc Nguyen, A.; Yüce, G. An 80 kyr-long continuous speleothem record from Dim Cave, SW Turkey with paleoclimatic implications for the Eastern Mediterranean. *Sci. Rep.* **2015**, *5*, 1–9.
51. Neff, U.; Burns, S.J.; Mangini, A.; Mudelsee, M.; Fleitmann, D.; Matter, A. Strong coherence between solar variability and the monsoon in Oman between 9 and 6 kyr ago. *Nature* **2001**, *411*, 290–293. [CrossRef]
52. Burns, S.J.; Fleitmann, D.; Matter, A.; Neff, U.; Mangini, A. Speleothem evidence from Oman for continental pluvial events during interglacial periods. *Geology* **2001**, *29*, 623–626. [CrossRef]
53. Cheng, H.; Sinha, A.; Verheyden, S.; Nader, F.H.; Li, X.L.; Zhang, P.-Z.; Yin, J.J.; Yi, L.; Peng, Y.B.; Rao, Z.G.; et al. The climate variability in northern Levant over the past 20,000 years. *Geophys. Res. Lett.* **2015**, *42*, 8641–8650. [CrossRef]
54. Verheyden, S.; Nader, F.H.; Cheng, H.; Edwards, R.L.; Swennen, R. Paleoclimate reconstruction in the Levant region from the geochemistry of a Holocene stalagmite from the Jeita cave, Lebanon. *Quat. Res.* **2008**, *70*, 368–381. [CrossRef]
55. Frumkin, A.; Ford, D.C.; Schwarcz, H.P. Continental Oxygen Isotopic Record of the Last 170,000 Years in Jerusalem. *Quat. Res.* **1999**, *51*, 317–327. [CrossRef]

56. Nehme, C.; Verheyden, S.; Noble, S.R.; Farrant, A.R.; Sahy, D.; Hellstrom, J.C.; Delannoy, J.J.; Claeys, P. Reconstruction of MIS 5 climate in the central Levant using a stalagmite from Kanaan Cave, Lebanon. *Clim. Past* **2015**, *11*, 1785–1799. [CrossRef]

57. Finné, M.; Bar-Matthews, M.; Holmgren, K.; Sundqvist, H.S.; Liakopoulos, I.; Zhang, Q. Speleothem evidence for late Holocene climate variability and floods in Southern Greece. *Quat. Res.* **2014**, *81*, 213–227. [CrossRef]

58. Finné, M.; Holmgren, K.; Shen, C.C.; Hu, H.M.; Boyd, M.; Stocker, S. Late bronze age climate change and the destruction of the mycenaean palace of nestor at pylos. *PLoS ONE* **2017**, *12*, 1–18.

59. Shakun, J.D.; Burns, S.J.; Fleitmann, D.; Kramers, J.; Matter, A.; Al-Subary, A.A. A high-resolution, absolute-dated deglacial speleothem record of Indian Ocean climate from Socotra Island, Yemen. *Earth Planet. Sci. Lett.* **2007**, *259*, 442–456. [CrossRef]

60. Psomiadis, D.; Dotsika, E.; Albanakis, K.; Ghaleb, B.; Hillaire-Marcel, C. Speleothem record of climatic changes in the northern Aegean region (Greece) from the Bronze Age to the collapse of the Roman Empire. *Palaeogeogr. Palaeoclimatol. Palaeoecol.* **2018**, *489*, 272–283. [CrossRef]

61. Fleitmann, D.; Cheng, H.; Badertscher, S.; Edwards, R.L.; Mudelsee, M.; Göktürk, O.M.; Fankhauser, A.; Pickering, R.; Raible, C.C.; Matter, A.; et al. Timing and climatic impact of Greenland interstadials recorded in stalagmites from northern Turkey. *Geophys. Res. Lett.* **2009**, *36*, 1–5. [CrossRef]

62. Göktürk, O.M.; Fleitmann, D.; Badertscher, S.; Cheng, H.; Edwards, R.L.; Leuenberger, M.; Fankhauser, A.; Tüysüz, O.; Kramers, J. Climate on the southern Black Sea coast during the Holocene: Implications from the Sofular Cave record. *Quat. Sci. Rev.* **2011**, *30*, 2433–2445. [CrossRef]

63. Badertscher, S.; Fleitmann, D.; Cheng, H.; Edwards, R.L.; Göktürk, O.M.; Zumbühl, A.; Leuenberger, M.; Tüysüz, O. Pleistocene water intrusions from the Mediterranean and Caspian seas into the Black Sea. *Nat. Geosci.* **2011**, *4*, 236–239. [CrossRef]

64. Grant, K.M.; Rohling, E.J.; Bar-Matthews, M.; Ayalon, A.; Medina-Elizalde, M.; Ramsey, C.B.; Satow, C.; Roberts, A.P. Rapid coupling between ice volume and polar temperature over the past 50,000 years. *Nature* **2012**, *491*, 744–747. [CrossRef]

65. Bar-Matthews, M.; Ayalon, A.; Kaufman, A. Late Quaternary Paleoclimate in the Eastern Mediterranean Region from Stable Isotope Analysis of Speleothems at Soreq Cave, Israel. *Quat. Res.* **1997**, *47*, 155–168. [CrossRef]

66. Bar-Matthews, M.; Ayalon, A.; Kaufman, A. Middle to Late Holocene (6500 Years Period) Paleoclimate in The Eastern Mediterranean Region From Stable Isotopic Composition Of Speleothems From Soreq Cave, Israel. *Isot. Tech. Study Environ. Chang.* **1998**, 673–682.

67. Bar-Matthews, M.; Ayalon, A.; Kaufman, A.; Wasserburg, G.J. The Eastern Mediterranean paleoclimate as a reflection of regional events: Soreq cave, Israel. *Earth Planet. Sci. Lett.* **1999**, *166*, 85–95. [CrossRef]

68. Bar-Matthews, M.; Ayalon, A.; Kaufman, A. Timing and hydrological conditions of Sapropel events in the Eastern Mediterranean, as evident from speleothems, Soreq cave, Israel. *Chem. Geol.* **2000**, *169*, 145–156. [CrossRef]

69. Ayalon, A.; Bar-Matthews, M.; Kaufman, A. Climatic conditions during marine oxygen isotope stage 6 in the eastern Mediterranean region from the isotopic composition of speleothems of Soreq Cave, Israel. *Geology* **2002**, *30*, 303–306. [CrossRef]

70. Schilman, B.; Ayalon, A.; Bar-Matthews, M.; Kagan, E.J.; Almogi-Labin, A. Sea-land paleoclimate correlation in the Eastern Mediterranean region during the late Holocene. *Israel J. Earth Sci.* **2002**, *51*, 181–190. [CrossRef]

71. Kolodny, Y.; Bar-Matthews, M.; Ayalon, A.; McKeegan, K.D. A high spatial resolution d18O profile of a speleothem using an ion-microprobe. *Chem. Geol.* **2003**, *197*, 21–28. [CrossRef]

72. Bar-Matthews, M.; Ayalon, A.; Gilmour, M.A.; Matthews, A.; Hawkesworth, C.J. Sea–land oxygen isotopic relationships from planktonic foraminifera and speleothems in the Eastern Mediterranean region and their implication for paleorainfall during interglacial intervals. *Geochim. Cosmochim. Acta* **2003**, *67*, 3181–3199. [CrossRef]

73. Vaks, A.; Bar-Matthews, M.; Matthews, A.; Ayalon, A.; Frumkin, A. Middle-Late Quaternary paleoclimate of northern margins of the Saharan-Arabian Desert: reconstruction from speleothems of Negev Desert, Israel. *Quat. Sci. Rev.* **2010**, *29*, 2647–2662. [CrossRef]

74. Jex, C.N.; Baker, A.; Fairchild, I.J.; Eastwood, W.J.; Leng, M.J.; Sloane, H.J.; Thomas, L.; Bekaroglu, E. Calibration of speleothem δ18O with instrumental climate records from Turkey. *Glob. Planet. Chang.* **2010**, *71*, 207–217. [CrossRef]

75. Van Rampelbergh, M.; Fleitmann, D.; Verheyden, S.; Cheng, H.; Edwards, R.L.; De Geest, P.; De Vleeschouwer, D.; Burns, S.J.; Matter, A.; Claeys, P.; et al. Mid- to late Holocene Indian Ocean Monsoon variability recorded in four speleothems from Socotra Island, Yemen. *Quat. Sci. Rev.* **2013**, *65*, 129–142. [CrossRef]

76. Carolin, S.A.; Walker, R.T.; Henderson, G.M.; Maxfield, L.; Ersek, V.; Sloan, A.; Talebian, M.; Fattahi, M.; Nezamdoust, J. Decadal-scale Climate Variability on the Central Iranian Plateau Spanning the So-called 4.2 ka BP Drought Event. In Proceedings of the 2015 AGU Fall Meeting, San Francisco, CA, USA, 14–18 December 2015; American Geophysical Union: Washington, DC, USA, 2015.

77. Rowe, P.J.; Mason, J.E.; Andrews, J.E.; Marca, A.D.; Thomas, L.; Van Calsteren, P.; Jex, C.N.; Vonhof, H.B.; Al-Omari, S. Speleothem isotopic evidence of winter rainfall variability in northeast Turkey between 77 and 6 ka. *Quat. Sci. Rev.* **2012**, *45*, 60–72. [CrossRef]

78. Mehterian, S.; Pourmand, A.; Sharifi, A.; Lahijani, H.A.K.; Naderi, M.; Swart, P.K. Reconstruction of Pleistocene Paleo-Hydrology and Climate Variations in Western Asia as Recorded in Speleothems from West-Central Iran. In Proceedings of the 2014 AGU Fall Meeting Abstracts Fall Meeting, San Francisco, CA, USA, 15–19 December 2014; American Geophysical Union: Washington, DC, USA, 2014.

79. Vaks, A.; Bar-Matthews, M.; Ayalon, A.; Matthews, A.; Frumkin, A.; Dayan, U.; Halicz, L.; Almogi-Labin, A.; Schilman, B. Paleoclimate and location of the border between Mediterranean climate region and the Saharo–Arabian Desert as revealed by speleothems from the northern Negev Desert, Israel. *Earth Planet. Sci. Lett.* **2006**, *249*, 384–399. [CrossRef]

80. Ayalon, A.; Bar-Matthews, M.; Frumkin, A.; Matthews, A. Last Glacial warm events on Mount Hermon: the southern extension of the Alpine karst range of the east Mediterranean. *Quat. Sci. Rev.* **2013**, *59*, 43–56. [CrossRef]

81. Mehterian, S.; Pourmand, A.; Sharifi, A.; Lahijani, H.A.K.; Naderi, M.; Swart, P.K. Speleothem records of glacial/interglacial climate from Iran forewarn of future Water Availability in the interior of the Middle East. *Quat. Sci. Rev.* **2017**, *164*, 187–198. [CrossRef]

82. Rifai, R.I. Reconstruction of the Middle Pleistocene climate of south Mediterranean using the Wadi Sannur speleothem, eastern Desert, Egypt. *Carbonates Evaporites* **2007**, *22*, 73–85. [CrossRef]

83. Keinan, J. Paleo-Environment of the Northern Jordan Rift Region Based on Speleothems from Zalmon Cave. Master's Thesis, Hebrew University of Jerusalem, Jerusalem, Israel, 2016.

84. Trigo, I.F.; Bigg, G.R.; Davies, T.D. Climatology of Cyclogenesis Mechanisms in the Mediterranean. *Mon. Weather Rev.* **2002**, *130*, 549–569. [CrossRef]

85. Brayshaw, D.J.; Hoskins, B.; Black, E. Some physical drivers of changes in the winter storm tracks over the North Atlantic and Mediterranean during the Holocene. *Philos. Trans. R. Soc. A Math. Phys. Eng. Sci.* **2010**, *368*, 5185–5223. [CrossRef]

86. Ayalon, A.; Bar-Matthews, M.; Sass, E. Rainfall-recharge relationships within a karstic terrain in the Eastern Mediterranean semi-arid region, Israel: δ180 and δD characteristics. *J. Hydrol.* **1998**, *207*, 18–31. [CrossRef]

87. Gat, J.R.; Klein, B.; Kushnir, Y.; Roether, W.; Wernli, H.; Yam, R.; Shemesh, A. Isotope composition of air moisture over the Mediterranean Sea: An index of the air-sea interaction pattern. *Tellus, Ser. B Chem. Phys. Meteorol.* **2003**, *55*, 953–965. [CrossRef]

88. Alpert, P.; Neeman, B.U.; Shay-El, Y. Climatological analysis of Mediterranean cyclones using ECMWF data. *Tellus A Dyn. Meteorol. Oceanogr.* **1990**, *42*, 65–77. [CrossRef]

89. Lionello, P.; Trigo, I.F.; Gil, V.; Liberato, M.L.R.; Nissen, K.M.; Pinto, J.G.; Raible, C.C.; Reale, M.; Tanzarella, A.; Trigo, R.M.; et al. Objective climatology of cyclones in the Mediterranean region: A consensus view

among methods with different system identification and tracking criteria. *Tellus Ser. A Dyn. Meteorol. Oceanogr.* **2016**, *68*, 29391. [CrossRef]

90. Karaca, M.; Deniz, A.; Tayanç, M. Cyclone track variability over Turkey in association with regional climate. *Int. J. Climatol.* **2000**, *20*, 1225–1236. [CrossRef]
91. Ulbrich, U.; Lionello, P.; Belusic´, D.; Jacobeit, J.; Knippertz, P.; Kuglitsch, F.G.; Leckebusch, G.C.; Luterbacher, J.;ˆ Maugeri, M.; Maheras, P.; et al. Climate of the Mediterranean: Synoptic Patterns, Temperature, Precipitation, Winds, and Their Extremes. In *The Climate of the Mediterranean Region: From The Past to the Future*; Lionello, P., Ed.; Elsevier: Amsterdam, The Netherlands, 2012; pp. 301–346.
92. Weyhenmeyer, CE; Burns, S.J.; Waber, H.N.; Aeschbach-Hertig, W.; Kipfer, R.; Loosli, H.H.; Matter, A. Cool glacial temperatures and changes in moisture source recorded in Oman groundwaters. *Science* **2000**, *287*, 842–845. [CrossRef] [PubMed]
93. Findlater, J. Interhemispheric transport of air in the lower troposphere over the western Indian Ocean. *J. R. Met. Soc* **1969**, *95*, 400–403. [CrossRef]
94. Almazroui, M.; Nazrul Islam, M.; Athar, H.; Jones, P.D.; Rahman, M.A. Recent climate change in the Arabian Peninsula: Annual rainfall and temperature analysis of Saudi Arabia for 1978–2009. *Int. J. Climatol.* **2012**, *32*, 953–966. [CrossRef]
95. Almazroui, M. The Relationship between Atmospheric Circulation Patterns and Surface Climatic Elements in Saudi Arabia. Ph.D. Thesis, University of East Anglia, Norwich, UK, 2006.
96. Berrisford, P.; Dee, D.; Poli, P.; Brudgge, R.; Fielding, K.; Fuentes, M.; Kallberg, P.; Kobayashi, S.; Uppala, S.; Simmons, A. *The ERA-Interim archive Version 2.0*; ECMWF: Reading, UK, 2011; p. 23.
97. Gat, J.R.; Carmi, I. *Effect of Climate Changes on the Precipitation Patterns and Isotopic Composition of Water in a Climate Transition Zone: Case of the Eastern Mediterranean Sea Area*; IAHSPubl. no. 168; IAHS: Vancouver, BC, Canada, 1987; pp. 513–524.
98. Goldsmith, Y.; Polissar, P.J.; Ayalon, A.; Bar-Matthews, M.; de Menocal, P.B.; Broecker, W.S. The modern and Last Glacial Maximum hydrological cycles of the Eastern Mediterranean and the Levant from a water isotope perspective. *Earth Planet. Sci. Lett.* **2017**, *457*, 302–312. [CrossRef]
99. Gat, J.R.; Dansgaard, W. Stable isotope survey of the fresh water occurrences in Israel and the Northern Jordan Rift Valley. *J. Hydrol.* **1972**, *16*, 177–211. [CrossRef]
100. Armon, M.; Dente, E.; Smith, J.A.; Enzel, Y.; Morin, E. Synoptic-Scale Control over Modern Rainfall and Flood Patterns in the Levant Drylands with Implications for Past Climates. *J. Hydrometeorol.* **2018**, *19*, 1077–1096. [CrossRef]
101. Haliva-Cohen, A.; Stein, M.; Goldstein, S.L.; Sandler, A.; Starinsky, A. Sources and transport routes of fine detritus material to the Late Quaternary Dead Sea basin. *Quat. Sci. Rev.* **2012**, *50*, 55–70. [CrossRef]
102. Ben-Israel, M.; Enzel, Y.; Amit, R.; Erel, Y. Provenance of the Various Grain-Size Fractions in the Negev Loess and Potential changes in Major dust Sources to the Eastern Mediterranean. *Quat. Res.* **2015**, *83*, 105–115. [CrossRef]
103. Ayalon, A.; Bar-Matthews, M.; Kaufman, A. Petrography, strontium, barium and uranium concentrations, and strontium and uranium isotope ratios in speleothems as palaeoclimatic proxies: Soreq Cave, Israel. *Holocene* **1999**, *9*, 715–722. [CrossRef]
104. Craig, H. Isotopic Variations in Meteoric Waters. *Science* **1961**, *133*, 1702–1703. [CrossRef]
105. Bar-Matthews, M.; Ayalon, A.; Vaks, A.; Frumkin, A. Climate and Environment Reconstruction Based on Speleothems from the Levant. In *Quaternary of the Levant, Environments, Climate Change, and Humans*; Bar-Yosef, O., Enzel, Y., Eds.; Cambridge University Press: Cambridge, UK, 2017; pp. 151–164, ISBN 9781316106754.
106. Bar-Yosef, O. On the Nature of Transitions: the Middle to Upper Palaeolithic and the Neolithic Revolution. *Camb. Archaeol. J.* **1998**, *8*, 63–141. [CrossRef]
107. Scroxton, N.; Gagan, M.K.; Dunbar, G.B.; Ayliffe, L.K.; Hantoro, W.S.; Shen, C.-C.; Hellstrom, J.C.; Zhao, J.; Cheng, H.; Edwards, R.L.; et al. Natural attrition and growth frequency variations of stalagmites in

southwest Sulawesi over the past 530,000 years. *Palaeogeogr. Palaeoclimatol. Palaeoecol.* **2016**, *441*, 823–833. [CrossRef]

108. Deininger, M.; Ward, B.M.; Novello, V.F.; Cruz, F.W. Late Quaternary Variations in the South American Monsoon System as Inferred by Speleothems—New Perspectives using the SISAL Database. *Quaternary* **2019**, *2*, 6. [CrossRef]

109. Rohling,E.J.; Marino,G.; Grant,K.M.Mediterranean climate and oceanography, and the periodic development of anoxic events (sapropels). *Earth-Sci. Rev.* **2015**, *143*, 62–97. [CrossRef]

110. Breitenbach, S.F.M.; Lechleitner, F.A.; Sinha, A.; Hills, D.; Ahmad, S.M. The Indian Summer Monsoon from a Speleothem d18O Perspective—A Review. *Quaternary* **2018**, *1*, 29.

111. Kolodny, Y.; Stein, M.; Machlus, M. Sea-rain-lake relation in the Last Glacial East Mediterranean revealed by δ18O-δ13C in Lake Lisan aragonites. *Geochim. Cosmochim. Acta* **2005**, *69*, 4045–4060. [CrossRef]

112. Almogi-Labin, A.; Bar-Matthews, M.; Shriki, D.; Kolosovsky, E.; Paterne, M.; Schilman, B.; Ayalon, A.; Aizenshtat, Z.; Matthews, A. Climatic variability during the last ~90 ka of the southern and northern

Levantine Basin as evident from marine records and speleothems. *Quat. Sci. Rev.* **2009**, *28*, 2882–2896. [CrossRef]

113. Wang, P.; Tian, J.; Lourens, L.J. Obscuring of long eccentricity cyclicity in Pleistocene oceanic carbon isotope records. *Earth Planet. Sci. Lett.* **2010**, *290*, 319–330. [CrossRef]

114. Ayalon, A.; Bar-Matthews, M.; Schilman, B. *Rainfall Isotopic Characteristics At Various Sites In Israel And The Relationships With Unsaturated Zone Water*; 04; The Geological Survey of Israel: Jerusalem, Israel, 2004; Volume GSI/16/04.

115. Kaufman, A.; Bar-Matthews, M.; Ayalon, A.; Carmi, I. The vadose flow above Soreq Cave, Israel: A tritium study of the cave waters. *J. Hydrol.* **2003**, *273*, 155–163. [CrossRef]

116. Bar-Matthews, M.; Ayalon, A.; Matthews, A.; Sass, E.; Halicz, L. Carbon and oxygen isotope study of the active water-carbonate system in a karstic Mediterranean cave: Implications for paleoclimate research in semiarid regions. *Geochim. Cosmochim. Acta* **1996**, *60*, 337–347. [CrossRef]

117. Affek, H.P.; Matthews, A.; Ayalon, A.; Bar-Matthews, M.; Burstyn, Y.; Zaarur, S.; Zilberman, T. Accounting for kinetic isotope effects in Soreq Cave (Israel) speleothems. *Geochim. Cosmochim. Acta* **2014**, *143*, 303–318. [CrossRef]

118. Regattieri, E.; Zanchetta, G.; Drysdale, R.N.; Isola, I.; Hellstrom, J.C.; Roncioni, A. A continuous stable isotope record from the penultimate glacial maximum to the Last Interglacial (159-121ka) from Tana Che Urla Cave (Apuan Alps, central Italy). *Quat. Res.* **2014**, *82*, 450–461. [CrossRef]

119. Drysdale, R.N.; Hellstrom, J.C.; Zanchetta, G.; Fallick, A.E.; Sánchez Goñi, M.F.; Couchoud, I.; Donald, J.; Maas, R.; Lohmann, G.; Isola, I. Evidence for obliquity forcing of glacial Termination II. *Science* **2009**, *325*, 1527–1531. [CrossRef] [PubMed]

120. Zanchetta, G.; Drysdale, R.N.; Hellstrom, J.C.; Fallick, A.E.; Isola, I.; Gagan, M.K.; Pareschi, M.T. Enhanced rainfall in the Western Mediterranean during deposition of sapropel S1: stalagmite evidence from Corchia cave (Central Italy). *Quat. Sci. Rev.* **2007**, *26*, 279–286. [CrossRef]

121. Columbu, A.; Sauro, F.; Lundberg, J.; Drysdale, R.N.; De Waele, J. Palaeoenvironmental changes recorded by speleothems of the southern Alps (Piani Eterni, Belluno, Italy) during four interglacial to glacial climate transitions. *Quat. Sci. Rev.* **2018**, *197*, 319–335. [CrossRef]

122. Braun, K.; Bar-Matthews, M.; Ayalon, A.; Zilberman, T.; Matthews, A. Rainfall isotopic variability at the intersection between winter and summer rainfall regimes in coastal South Africa (Mossel Bay, Western Cape Province). *S. Afr. J. Geol.* **2017**, *120*, 323–340. [CrossRef]

123. Braun, K.; Bar-Matthews, M.; Matthews, A.; Ayalon, A.; Cowling, R.M.; Karkanas, P.; Fisher, E.C.; Dyez, K.; Zilberman, T.; Marean, C.W. Late Pleistocene records of speleothem stable isotopic compositions from Pinnacle Point on the South African south coast. *Quat. Res.* **2019**, *91*, 265–288. [CrossRef]

124. Enzel, Y.; Amit, R.; Dayan, U.; Crouvi, O.; Kahana, R.; Ziv, B.; Sharon, D. The climatic and physiographic controls of the eastern Mediterranean over the late Pleistocene climates in the southern Levant and its neighboring deserts. *Glob. Planet. Chang.* **2008**, *60*, 165–192. [CrossRef]

125. Orland, I.J.; He, F.; Bar-Matthews, M.; Chen, F.; Ayalon, A. Valley Resolving paleorainfall proxies in the Eastern Mediterranean with seasonal-resolution model and proxy analyses. In Proceedings of the AGU Fall Meeting 2018, Washington, DC, USA, 10–14 December 2018; p. PP12B-04.

126. Torfstein, A.; Goldstein, S.L.; Kushnir, Y.; Enzel, Y.; Haug, G.; Stein, M. Dead Sea drawdown and monsoonal impacts in the Levant during the last interglacial. *Earth Planet. Sci. Lett.* **2015**, *412*, 235–244. [CrossRef]

127. Wickens, L.B. Geochemistry and Petrography of Speleothems From Turkey and Iran: Palaeoclimate and Diagenesis. Ph.D. Thesis, University of East Anglia, Norwich, UK, 2013.

128. Cheng, H.; Sinha, A.; Wang, X.; Cruz, F.W.; Edwards, R.L. The Global Paleomonsoon as seen through speleothem records from Asia and the Americas. *Clim. Dyn.* **2012**, *39*, 1045–1062. [CrossRef]

129. Ziegler, M.; Tuenter, E.; Lourens, L.J. The precession phase of the boreal summer monsoon as viewed from the eastern Mediterranean (ODP Site 968). *Quat. Sci. Rev.* **2010**, *29*, 1481–1490. [CrossRef]

130. Broecker, W.S.; Denton, G.H.; Edwards, R.L.; Cheng, H.; Alley, R.B.; Putnam, A.E. Putting the Younger Dryas cold event into context. *Quat. Sci. Rev.* **2010**, *29*, 1078–1081. [CrossRef]

131. Büntgen, U.; Myglan, V.S.; Ljungqvist, F.C.; McCormick, M.; Di Cosmo, N.; Sigl, M.; Jungclaus, J.; Wagner, S.; Krusic, P.J.; Esper, J.; et al. Cooling and societal change during the Late Antique Little Ice Age from 536 to around 660 AD. *Nat. Geosci.* **2016**, *9*, 231–236. [CrossRef]

132. Wanner, H.; Beer, J.; Bütikofer, J.; Crowley, T.J.; Cubasch, U.; Flückiger, J.; Goosse, H.; Grosjean, M.; Joos, F.; Kaplan, J.O.; et al. Mid- to Late Holocene climate change: an overview. *Quat. Sci. Rev.* **2008**, *27*, 1791–1828. [CrossRef]

133. Box, M.R.; Krom, M.D.; Cliff, R.A.; Bar-Matthews, M.; Almogi-Labin, A.; Ayalon, A.; Paterne, M. Response of the Nile and its catchment to millennial-scale climatic change since the LGM from Sr isotopes and major elements of East Mediterranean sediments. *Quat. Sci. Rev.* **2011**, *30*, 431–442. [CrossRef]

134. Siani, G.; Magny, M.; Paterne, M.; Debret, M.; Fontugne, M.R. Paleohydrology reconstruction and Holocene climate variability in the South Adriatic Sea. *Clim. Past* **2013**, *9*, 499–515. [CrossRef]

135. Lechleitner, F.A.; Amirnezhad-Mozhdehi, S.; Columbu, A.; Comas-Bru, L.; Labuhn, I.; Pérez-Mejías, C.; Rehfeld, K.; Lechleitner, F.A.; Amirnezhad-Mozhdehi, S.; Columbu, A.; et al. The Potential of Speleothems from Western Europe as Recorders of Regional Climate: A Critical Assessment of the SISAL Database. *Quaternary* **2018**, *1*, 30. [CrossRef]

136. Nicholson, S.E.; Nash, D.J.; Chase, B.M.; Grab, S.W.; Shanahan, T.M.; Verschuren, D.; Asrat, A.; Lézine, A.M.; Umer, M. Temperature variability over Africa during the last 2000 years. *Holocene* **2013**, *23*, 1085–1094. [CrossRef]

137. McGregor, H.V.; Evans, M.N.; Goosse, H.; Leduc, G.; Martrat, B.; Addison, J.A.; Mortyn, P.G.; Oppo, D.W.; Seidenkrantz, M.S.; Sicre, M.A.; et al. Robust global ocean cooling trend for the pre-industrial Common Era. *Nat. Geosci.* **2015**, *8*, 671–677. [CrossRef]

138. Abram, N.J.; McGregor, H.V.; Tierney, J.E.; Evans, M.N.; McKay, N.P.; Kaufman, D.S.; the PAGES 2k Consortium; Thirumalai, K.; Martrat, B.; Goosse, H.; et al. Early onset of industrial-era warming across the oceans and continents. *Nature* **2016**, *536*, 411–418. [CrossRef] [PubMed]

139. Zielinski, G.A.; Mayewski, P.A.; Meeker, L.D.; Grönvold, K.; Germani, M.S.; Whitlow, S.; Twickler, M.S.; Taylor, K. Volcanic aerosol records and tephrochronology of the Summit, Greenland, ice cores. *J. Geophys. Res. Ocean.* **1997**, *102*, 26625–26640. [CrossRef]

140. Fontugne, M.R.; Calvert, S.E. Late Pleistocene Variability of the Carbon Isotopic Composition of Organic Matter in the Eastern Mediterranean: Monitor of Changes in Carbon Sources and Atmospheric CO2 Concentrations. *Paleoceanography* **1992**, *7*, 1–20. [CrossRef]

141. Bond, G.; Kromer, B.; Beer, J.; Muscheler, R.; Evans, M.N.; Showers, W.; Hoffmann, S.; Lotti-Bond, R.; Hajdas, I.; Bonani, G. Persistent solar influence on North Atlantic climate during the Holocene. *Science* **2001**, *294*, 2130–2136. [CrossRef]

142. Rohling, E.J.; Marino, G.; Grant, K.M.; Mayewski, P.A.; Weninger, B. A model for archaeologically relevant Holocene climate impacts in the Aegean-Levantine region (easternmost Mediterranean). *Quat. Sci. Rev.* **2019**, *208*, 38–53. [CrossRef]

143. Walker, M.J.C.; Johnsen, S.; Rasmussen, S.O.; Popp, T.; Steffensen, J.P.; Gibbard, P.; Hoek, W.; Lowe, J.; Andrews, J.; Björck, S.; et al. Formal definition and dating of the GSSP (Global Stratotype Section and Point) for the base of the Holocene using the Greenland NGRIP ice core, and selected auxiliary records. *J. Quat. Sci.* **2009**, *24*, 3–17. [CrossRef]

144. Head, M.J.; Gibbard, P.L. Formal subdivision of the Quaternary System/Period: Past, present, and future. *Quat. Int.* **2015**, *383*, 4–35. [CrossRef]

145. Kleiven, H.K.F.; Kissel, C.; Laj, C.; Ninnemann, U.S.; Richter, T.O.; Cortijo, E. Reduced North Atlantic deep water coeval with the glacial Lake Agassiz freshwater outburst. *Science* **2008**, *319*, 60–64. [CrossRef]

146. Grant, K.M.; Grimm, R.; Mikolajewicz, U.; Marino, G.; Ziegler, M.; Rohling, E.J. The timing of Mediterranean sapropel deposition relative to insolation, sea-level and African monsoon changes. *Quat. Sci. Rev.* **2016**, *140*, 125–141. [CrossRef]

147. Rohling, E.J. Review and new aspects concerning the formation of eastern Mediterranean sapropels. *Mar. Geol.* **1994**, *122*, 1–28. [CrossRef]

148. de Lange, G.J.; Thomson, J.; Reitz, A.; Slomp, C.P.; Speranza Principato, M.; Erba, E.; Corselli, C. Synchronous basin-wide formation and redox-controlled preservation of a Mediterranean sapropel. *Nat. Geosci.* **2008**, *1*, 606–610. [CrossRef]

149. Martrat, B.; Jimenez-Amat, P.; Zahn, R.; Grimalt, J.O. Similarities and dissimilarities between the last two deglaciations and interglaciations in the North Atlantic region. *Quat. Sci. Rev.* **2014**, *99*, 122–134. [CrossRef]

150. Jalali, B.; Sicre, M.-A.; Bassetti, M.-A.; Kallel, N. Holocene climate variability in the North-Western Mediterranean Sea (Gulf of Lions). *Clim. Past* **2016**, *12*, 91–101. [CrossRef]

151. Thomas, E.R.; Wolff, E.W.; Mulvaney, R.; Steffensen, J.P.; Johnsen, S.J.; Arrowsmith, C.; White, J.W.C.; Vaughn, B.; Popp, T. The 8.2 ka event from Greenland ice cores. *Quat. Sci. Rev.* **2007**, *26*, 70–81. [CrossRef]

152. Wu, C.J.; Usoskin, I.G.; Krivova, N.; Kovaltsov, G.A.; Baroni, M.; Bard, E.; Solanki, S.K. Solar activity over nine millennia: A consistent multi-proxy reconstruction. *Astron. Astrophys.* **2018**, *615*, A93. [CrossRef]

153. Torfstein, A.; Goldstein, S.L.; Stein, M.; Enzel, Y. Impacts of abrupt climate changes in the Levant from Last Glacial Dead Sea levels. *Quat. Sci. Rev.* **2013**, *69*, 1–7. [CrossRef]

154. de Menocal, P.B.; Ortiz, J.; Guilderson, T.; Adkins, J.; Sarnthein, M.; Baker, L.; Yarusinsky, M. Abrupt onset and termination of the African Humid Period: rapid climate responses to gradual insolation forcing. *Quat. Sci. Rev.* **2002**, *19*, 347–361. [CrossRef]

155. de Menocal, P.B. Palaeoclimate: End of the African Humid Period. *Nat. Geosci.* **2015**, *8*, 86–87. [CrossRef]

156. Quade, J.; Dente, E.; Armon, M.; Ben Dor, Y.; Morin, E.; Adam, O.; Enzel, Y. Megalakes in the Sahara? A Review. *Quat. Res.* **2018**, *90*, 253–275. [CrossRef]

157. Kuper, R.; Kröpalin, S. Climate-controlled holocene occupation in the Sahara: Motor of Africa's evolution. *Science* **2006**, *313*, 803–807. [CrossRef]

158. Bini, M.; Zanchetta, G.; Persoiu, A.; Cartier, R.; Català, A.; Cacho, I.; Dean, J.R.; Di Rita, F.; Drysdale, R.N.;

Finnè, M.; et al. The 4.2 ka BP Event in the Mediterranean Region: an overview. *Clim. Past Discuss.* **2018**, *15*, 555–577. [CrossRef]

159. Zanchetta, G.; Regattieri, E.; Isola, I.; Drysdale, R.N.; Bini, M.; Baneschi, I.; Hellstrom, J.C. The so-called "4.2 event" in the central mediterranean and its climatic teleconnections. *Alp. Mediterr. Quat.* **2016**, *29*, 5–17.

160. Carolin, S.A.; Walker, R.T.; Day, C.C.; Ersek, V.; Sloan, R.A.; Dee, M.W.; Talebian, M.; Henderson, G.M. Precise timing of abrupt increase in dust activity in the Middle East coincident with 4.2 ka social change. *Proc. Natl. Acad. Sci. USA* **2019**, *116*, 67–72. [CrossRef]

161. Issar, A.S.; Zohar, M. *Climate Change—Environment and History of the Near East*; Springer: Berlin/Heidelberg, Germany, 2007; ISBN 9783540698517.

162. Renssen, H.; Brovkin, V.; Fichefet, T.; Goosse, H. Simulation of the Holocene climate evolution in Northern Africa: The termination of the African Humid Period. *Quat. Int.* **2006**, *150*, 95–102. [CrossRef]

163. Shanahan, T.M.; McKay, N.P.; Hughen, K.A.; Overpeck, J.T.; Otto-Bliesner, B.; Heil, C.W.; King, J.; Scholz, C.A.; Peck, J. The time-transgressive termination of the African Humid Period. *Nat. Geosci.* **2015**, *8*, 140–144. [CrossRef]

164. Magny, M.; Vannière, B.; Zanchetta, G.; Fouache, E.; Touchais, G.; Petrika, L.; Coussot, C.; Walter-Simonnet, A.V.; Arnaud, F. Possible complexity of the climatic event around 4300-3800 cal. BP in the central and western Mediterranean. *Holocene* **2009**, *19*, 823–833. [CrossRef]

165. Kaniewski, D.; Marriner, N.; Cheddadi, R.; Guiot, J.; Van Campo, E. The 4.2 ka BP event in the Levant. *Clim. Past* **2018**, *14*, 1529–1542. [CrossRef]

166. Hughes, P. 1816 the Year without a Summer. *Weatherwise* **2010**, *32*, 108–111. [CrossRef]

167. Zhang, D.D.; Lee, H.F.; Wang, C.; Li, B.; Pei, Q.; Zhang, J.; An, Y. The causality analysis of climate change and large-scale human crisis. *Proc. Natl. Acad. Sci. USA* **2011**, *108*, 17296–17301. [CrossRef]

168. Alonso-Garcia, M.; Kleiven, H.K.F.; McManus, J.F.; Moffa-Sanchez, P.; Broecker, W.S.; Flower, B.P. Freshening of the Labrador Sea as a trigger for Little Ice Age development. *Clim. Past* **2017**, *13*, 317–331. [CrossRef]

169. Moreno-Chamarro, E.; Zanchettin, D.; Lohmann, K.; Luterbacher, J.; Jungclaus, J.H. Winter amplification of the European Little Ice Age cooling by the subpolar gyre. *Sci. Rep.* **2017**, *7*, 9981. [CrossRef]

170. Dezileau, L.; Sabatier, P.; Blanchemanche, P.; Joly, B.; Swingedouw, D.; Cassou, C.; Castaings, J.; Martinez, P.; Von Grafenstein, U. Intense storm activity during the Little Ice Age on the French Mediterranean coast. *Palaeogeogr. Palaeoclimatol. Palaeoecol.* **2011**, *299*, 289–297. [CrossRef]

171. Gao, C.; Robock, A.; Ammann, C. Volcanic forcing of climate over the past 1500 years: An improved ice core-based index for climate models. *J. Geophys. Res.* **2008**, *113*, D23111. [CrossRef]

172. Steffensen, J.P.; Dahl-Jensen, D.; Vinther, B.M.; Svensson, A.M.; Clausen, H.B.; Buchardt, S.L.; Rasmussen, S.O.; Andersen, K.K.; Lipenkov, V.; Blunier, T.; et al. Holocene thinning of the Greenland ice sheet. *Nature* **2009**, *461*, 385–388.

173. Enzel, Y.; Kushnir, Y.; Quade, J. The middle Holocene climatic records from Arabia: Reassessing lacustrine environments, shift of ITCZ in Arabian Sea, and impacts of the southwest Indian and African monsoons. *Glob. Planet. Chang.* **2015**, *129*, 69–91. [CrossRef]

174. Levine, X.J.; Schneider, T.; Levine, X.J.; Schneider, T. Baroclinic Eddies and the Extent of the Hadley Circulation: An Idealized GCM Study. *J. Atmos. Sci.* **2015**, *72*, 2744–2761. [CrossRef]

175. Marsh, A.; Fleitmann, D.; Al-Manmi, D.A.M.; Altaweel, M.; Wengrow, D.; Carter, R. Mid- to late-Holocene archaeology, environment and climate in the northeast Kurdistan region of Iraq. *Holocene* **2018**, *28*, 955–967. [CrossRef]

176. Wassenburg, J.A.; Dietrich, S.; Fietzke, J.; Fohlmeister, J.; Jochum, K.P.; Scholz, D.; Richter, D.K.; Sabaoui, A.; Spötl, C.; Lohmann, G.; et al. Reorganization of the North Atlantic Oscillation during early Holocene deglaciation. *Nat. Geosci.* **2016**, *9*, 602–605. [CrossRef]

177. Deininger, M.; Werner, M.; McDermott, F. North Atlantic Oscillation controls on oxygen and hydrogen isotope gradients in winter precipitation across Europe; Implications for palaeoclimate studies. *Clim. Past* **2016**, *12*, 2127–2143. [CrossRef]

178. Hurrell, J.W. Decadal Trends in the North Atlantic Oscillation: Regional Temperatures and Precipitation. *Science* **1995**, *269*, 676–679. [CrossRef] [PubMed]

B.2. New insights into the role of environmental dynamics shaping southern Mesopotamia: From the Pre-Ubaid to the Early Islamic Period

Altaweel, M., Marsh, A., Jotheri, J., Hritz, C., Fleitmann, D., Rost, S., Lintner, S.F., Gibson, M., Bosomworth, M., **Jacobson, M.J.**, Garzanti, E., Limonta, M., Radeff, G., 2019. New insights on the role of environmental dynamics shaping southern Mesopotamia: From the Pre-Ubaid to the Early Islamic Period. Iraq 81, 23–46. https://doi.org/10.1017/irq.2019.2

NEW INSIGHTS ON THE ROLE OF ENVIRONMENTAL DYNAMICS SHAPING SOUTHERN MESOPOTAMIA: FROM THE PRE-UBAID TO THE EARLY ISLAMIC PERIOD

By MARK ALTAWEEL, ANKE MARSH, JAAFAR JOTHERI, CARRIE HRITZ, DOMINIK FLEITMANN, STEPHANIE ROST, STEPHEN F. LINTNER, MCGUIRE GIBSON, MATTHEW BOSOMWORTH, MATTHEW JACOBSON, EDUARDO GARZANTI, MARA LIMONTA AND GIUDITTA RADEFF

Recent fieldwork and archival sedimentary materials from southern Iraq have revealed new insights into the environment that shaped southern Mesopotamia from the pre-Ubaid (early Holocene) until the early Islamic period. These data have been combined with northern Iraqi speleothem, or stalagmite, data that have revealed relevant palaeoclimate information. The new results are investigated in light of textual sources and satellite remote sensing work. It is evident that areas south of Baghdad, and to the region of Uruk, were already potentially habitable between the eleventh and early eighth millennia B.C., suggesting there were settlements in southern Iraq prior to the Ubaid. Date palms, the earliest recorded for Iraq, are evident before 10,000 B.C., and oak trees are evident south of Baghdad in the early Holocene but disappeared after the mid-sixth millennium B.C. New climate results suggest increased aridity after the end of the fourth millennium B.C. For the third millennium B.C. to first millennium A.D., a negative relationship between grain and date palm cultivation in Nippur is evident, suggesting shifting cultivation emphasising one of these crops at any given time in parts of the city. The Shatt en-Nil was also likely used as a channel for most of Nippur's historical occupation from the third millennium B.C. to the first millennium A.D. In the early to mid-first millennium A.D., around the time of the Sasanian period, a major increase in irrigation is evident in plant remains, likely reflecting large-scale irrigation expansion in the Nippur region. The first millennium B.C. to first millennium A.D. reflects a relatively dry period with periodic increased rainfall. Sedimentary results suggest the Nahrawan, prior to it becoming a well-known canal, formed an ancient branch of the Tigris, while the region just south of Baghdad, around Dalmaj, was near or part of an ancient confluence of the Tigris and Euphrates.

Keywords: southern Mesopotamia, Nippur, Uruk, environment, palaeochannels, climate, speleothems, phytoliths, sediments, date palm, oak

Introduction

New fieldwork focusing on the paleoenvironment and past channel systems was carried out during 2016–2017 in southern Iraq. This work focused on gaining a better understanding of long-term palaeochannel and environmental development during prehistoric and historic periods. Boreholes were drilled in the Dalmaj and Nahrawan regions south of Baghdad (Fig. 1) in order to obtain sedimentary samples for analyses. The new samples were combined with previously recovered sediments from Nippur's ancient channel (Shatt en-Nil) that ran through the city and with sediments recovered from a borehole near Uruk. Sediments were analysed for their structure, petrography, mineralogy, and microfossil remains, with phytoliths being a particular focus, and absolute dates were obtained using Accelerator Mass Spectrometry (AMS) methods where possible. New results also include palaeoclimate proxy data obtained from a speleothem (stalagmite) sample from Shalaii cave in the Kurdistan region of Iraq,

dated using Uranium- Thorium dating. These combined data provide a long-term, environmental and hydrologic history in southern Mesopotamia that can now be juxtaposed to archaeological and historical data. Results provide insights into the plant ecology and human-environmental interactions that shaped southern Mesopotamia in different millennia. In this article, we summarize the new results while also focusing on particular periods and instances where novel insights are gained. Up to this point, much of southern Mesopotamia's environmental history has been determined through evident surface remains, such as ancient river courses or canals dated by spatial association with archaeological sites, or geomorphological techniques that assess sedimentary remains. Furthermore, there is a lack of knowledge of Iraq's ancient botanical remains, including prehistoric and historic periods. For the first time in the study of ancient southern Mesopotamia, we focus on microfossil and sedimentary data and combine terrestrial proxy climate data from cave speleothems to gain novel insight into wider environmental and landscape change. This article begins by presenting existing research on the palaeolandscapes and environmental history of southern Mesopotamia. This includes geoarchaeological, archaeological, remote sensing, and some textual analysis. Our methods are then presented, demonstrating where our work builds from these earlier efforts, and our new results are described. Finally, a discussion on the novel insights obtained and benefits of this type of research for understanding Mesopotamian environmental history is given, in light of previous archaeological and historical data.

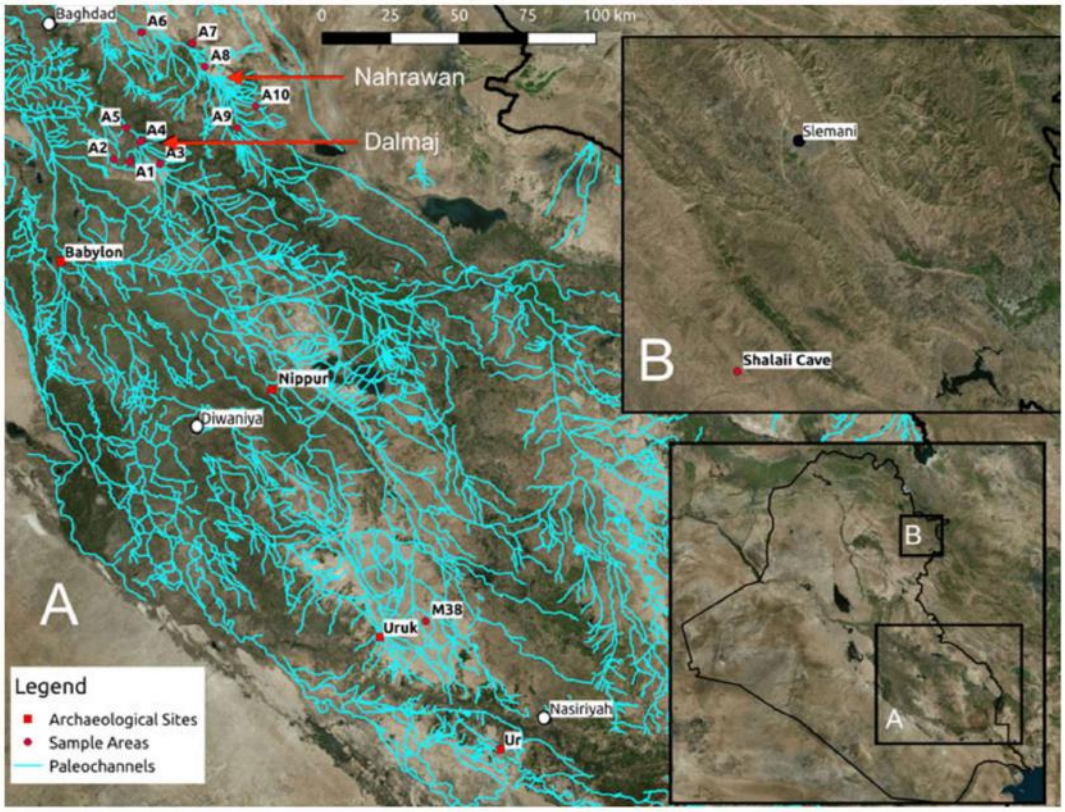

Fig. 1 Locations offieldwork areas in southern Iraq. Inset A: numbers prefixed with A are sites of boreholes on the Naharwan and Dalmaj channels. Nippur and borehole M38 near Uruk are also indicated. Inset B: location of Shalaii cave in the Kurdish region of Iraq.

Archaeology, Geoarchaeology and History

Beginning in the 1950s and continuing nearly unabated until 1990, archaeologists endeavoured to document and understand the settlement and environmental history of

southern Mesopotamia. Work initially focused on excavation of large mounded sites (tells) that mark the landscape and represent the accumulated material remains of long-term occupation (Adams 1981; Gibson 1972; Hritz 2010; Wright 1980). While these features reflect the importance of place in the long history of southern Mesopotamia, archaeologists also recognized the important role of landscape and environment, specifically the ancient rivers and canals, in shaping settlement history. The guiding premise in these earlier works was that durable human settlement in ancient Mesopotamia was only possible along river channels and canals, and that changes in watercourses would be accompanied by changes in settlement locations.

The first attempts to associate tells with relict river channels, thereby providing dates of visible relict channels by association with dated tell sites and demonstrating the linkages between channels, canals, and settlement history, were made by the Diyala Basin Archaeological project begun in 1937 and led by Thorkild Jacobsen (1982) and Robert McC. Adams (1965). Adams and Jacobsen postulated that by systematically mapping all mounded sites in the region, dating them by examining visible pottery on the surface, associating them with locations mentioned in textual records, and plotting them on period maps, any linear patterns that emerged would represent the major routes of ancient water courses. In other words, spatial distributions of tells were used to infer the location of channels and canals that were no longer visible or only partially visible on the ground. Using this method, archaeologists surveyed around one third of the entire alluvial plain, plotting and postulating key hydrologic events, including avulsion, siltation, and salinisation, while associating these changes to changes in the fortunes of settlements (Adams 1981; Gibson 1972; Jacobsen 1960; Jacobsen and Adams 1958). Work by Adams (1965) in the Diyala used archaeological survey and historical data together to understand periods of environmental stress affecting settlements, where channel abandonment, including that of canals, was seen as related to settlement abandonment. Another frequently cited environmental reason explaining the abandonment of settlements and even the collapse of major early states is salinisation induced by irrigation (Jacobsen 1982; Jacobsen and Adams 1958). The primary evidence for salinisation comes from the analysis of ancient texts. The term ki-mun ('saline ground') was used to classify the fertility of soils from 2500 B.C. onwards. Surveys of agricultural ground delineate parcels as saline ground that remained uncultivated due to salinisation (Jacobsen 1982:8–9). Scholars have also compared texts recording crop yield and yield projections and used changing amounts to suggest cycles of progressive salinisation, including impact on the health of early states' economies (Algaze 1993:4–5, 104–106; Civil 1987:39–44; Gibson 1974; Maekawa 1974; Sallaberger 1999: 175–177). The most comprehensive study of ancient crop yields and projections (third millennium B.C. through first millennium A.D.) was made by Jacobsen (1982). He argued that progressive salinisation promoted the switch at the beginning of the Akkadian Period (2335-2120 B.C.) from cultivating primarily emmer wheat to farming almost exclusively more salt tolerant barley in the alluvial plain (Jacobsen 1982:15–17; see also Helbaek 1960: 195). This conclusion has been questioned by Powell (1985), who criticized not only the translation of key elements of the textual data but also noted that the preference for barley in southern Mesopotamia might have been related to its greater productivity, better adaptability and greater tolerance to seasonal variation (see also Helbaek 1959: 370).

Building on the earlier extant approaches to understanding environmental and settlement

pattern changes over time and space, a few local-scale survey and excavation projects demonstrated the importance of diverse micro-topography and environment within the alluvial plains. For example, field studies by Mahringer, Lintner and Brandt undertaken as part of the Nippur Expedition in the 1970s-80s (Gibson 1976, 1977 and 1978) focused on examination of historical and contemporary environmental processes in the central alluvial plain landscape, on both a local and regional level, and the relationship of these processes to the city, including how they might have influenced the course of the ancient Euphrates in relation to the urban (Brandt 1990). Work around Abu Salabikh also focused on channel change, as well as settlement and landscape change, demonstrating the important interplay between processes and cycles of erosion, plain scour, sedimentation, and marsh development in a seemingly homogeneous agricultural landscape (Wilkinson 1990). Collaborative geoarchaeological, archaeological, and historical analysis around Tell ed-Dēr in the 1970s focused on reconstructing and better understanding the relationship of the Euphrates and Tigris-Euphrates belt around the site (Paepe 1971; Paepe and Baeteman 1978), demonstrating the presence of layers of contemporaneous and diachronic relict river levees, identified through multiple datasets. Later efforts combined textual and archaeological sources with continued geoarchaeological work (Heyvaert et al. 2008; Cole and Gasche 1998; Morozova 2005; Verhoeven 1998). Taken together, the interdisciplinary work at Nippur, Tell ed- Dēr and Abu Salabikh, along with the shift to closer analysis of sediments to understand channel change, demonstrated the value of landscape and environmental proxy records for micro-topographic analysis of natural and ecological data. The outcome of these efforts is the broad recognition that the Mesopotamian landscape is a palimpsest, where the premise that linear site alignments always demarcate canals provides only a small portion of palaeochannel and settlement history. During the late 1990s, although foreign work had largely stopped in southern Iraq, new access to high resolution satellite imagery, in particular CORONA imagery, allowed palaeochannels to be more easily identified and encouraged archaeologists to analyse areas beyond survey boundaries. CORONA satellites were in operation from the 1950s to 1970s, giving researchers the opportunity to map palaeochannels across Mesopotamia before the large landscape altering land reclamation projects of the 1970s. Later satellite data included higher resolution imagery, including QuickBird, and relatively easy access to digital elevation models (DEM) provided by different satellite and radar systems, such as the Shuttle Radar Topography Mission (SRTM). For the first time, these datasets provided archaeologists with a broad and encompassing view of the alluvial plains, including its micro-topography, enabling base images for time-series comparisons. Work by Pournelle (2003), Hritz (2005) and al-Hamdani (2014) focused on areas previously unsurveyed by archaeologists, including the former Haur al-Hawiza and Hammar marshes, the Shatt al-Gharraf, and Tigris and Euphrates levees. Using remote datasets and applying geoarchaeological principles of landscape change (Wilkinson 2003), these studies identified possible new archaeological sites and landscape features such as irrigation works or habitable regions.

Beginning in 2010, Hritz et al. (2013) began ground truthing features detected on imagery, both validating the methodological approach and illustrating the complexity of landscape evolution in southern Mesopotamia. Collecting targeted samples from archaeological sites and relict visible canals, this work demonstrated that (1) preservation in southern Iraq is such that sections exposed in historical excavations may still yield reliable AMS dates, and (2) proxy records such as shell and sediment cores can shed light on long-standing questions

about landscape, such as the evolution and extent of marsh formation and canal development in antiquity (Hritz et al. 2012: 77). Jotheri (2016) has greatly added to our knowledge about palaeochannels, including relict rivers and canals, through imagery analysis and subsequent ground truthing, including dating these features using augering, structural remains in sediments, mineralogy, and AMS dating.

On the historical side, considerable progress has been made in gathering textual sources to reconstruct ancient environments and historical geographies (Blaschke 2018; Cancik-Kirschbaum and Ziegler 2009; |Reculeau 2008, 2015, 2011; Rost 2015; Schrakamp 2015, 2017; Vanderroost 2012). This progress is largely due to the recent availability of online databases of ancient texts (e.g., Database of Neo-Sumerian Texts [BDTNS], Cuneiform Digital Library Initiative [CDLI], Ebla Digital Archives, Archives Babyloniennes [ARCHIBAB], etc.), which allow for the digital sourcing and more systematic analysis of entire text corpora. The success of integrating textual and archaeological data in the reconstruction of ancient environments has been demonstrated by Cole and Gasche (1998), and currently there are several ongoing projects adopting such a combined approach (e.g., Historische Geographie Obermesopotamiens [HIGEOMES]; Cancik- Kirschbaum and Hess 2016; Fink 2016; Ziegler and Langlois 2016).

These studies demonstrate the value of environmental data collection and analysis. With renewed foreign access to southern Iraq and the emergence of different techniques to collect, integrate, and analyse data, a large, regional-scale sampling program is possible, to reconstruct a general picture of long-term social, environmental, and historical change in southern Mesopotamia.

Methods

Most previous work in southern Mesopotamia focused on macro-remains, visible to the naked eye. Our work, while using satellite imagery (i.e., CORONA and QuickBird imagery) to identify palaeochannels, has also focused on combing microfossil, petrographic, and heavy mineral composition. Furthermore, new proxy data on the paleoclimate from cave speleothems now allow us to contextualize some results with climate trends, including their relation to the hydrologic cycle. Table 1 summarizes the dated sediments and samples discussed below, showing sample numbers, sediment types, dates, coordinates (in UTM 38N), and materials used for absolute dating.

TABLE 1 Summary of remains, key contents, locations (UTM 38N), and dated levels for sediments and speleothem samples. The Sample column indicates the sample number (e.g., A3) and depth (e.g., A3-4, with '4' being depth in metres), where present. Not all samples are given in detail here; the list mostly provides dated samples and samples discussed in the text. Calibration for AMS dates employs IntCal13 (Reimer et al. 2013) and was conducted by Beta Analytic.

Region	*Sample*	*Sediment/ Reference*	*Without d13C Correction*	*Calibrated Date*	*X*	*Y*	*Dated Material*
Dalmaj	A1				470713	3635889	
Dalmaj	A1-5	Sandy-Silty-Clay			470713	3635889	
Dalmaj	A2				465005	3636683	
Dalmaj	A2-3	Fine Sand			465005	3636683	

Dalmaj	A3				481449	3634876	
Dalmaj	A3-2	Silty-Clay			481449	3634876	
Dalmaj	A3-3	Silty-Clay	6770 +/− 30 BP	c. 5743-5645 BC (95%)	481449	3634876	Gyttja
Dalmaj	A3-4	Sandy-Clay	8520 +/− 30 BP	c. 7601-7546 BC (95%)	481449	3634876	Gyttja
Dalmaj	A4				474667	3642892	
Dalmaj	A4-4	Fine Sand			474667	3642892	
Dalmaj	A5	Silty-Clay			469557	3647641	
Nahrawan	A6				475064	3681522	
Nahrawan	A7				493050	3677679	
Nahrawan	A8				497536	3669338	
Nahrawan	A9				509095	3647704	
Nahrawan	A9-2	Sandy-Clay	6210 +/− 30 BP	c. 5306-5204 BC (75%); 5167 - 5076 cal BC (20.7%)	509095	3647704	Gyttja
Nahrawan	A9-3	Fine Sand			509095	3647704	
Nahrawan	A9-4	Sandy-Clay	10430 +/− 30 BP	c. 10,488-10,175 BC (79%); 10577 - 10511 BC (16.2%)	509095	3647704	Gyttja
Nahrawan	A10				515553	3655370	
Nahrawan	A10-4	Fine Sand			515553	3655370	
Nippur	300-311	Mostly silty-clay, some sand			5034796	3780305	
Nippur	310 (0.5m)	Silty-Clay	1210 +/− 30BP	c. 766-898 (89%); 924- 945 (3.5%); 722-740 (2.9%)	5034796	3780305	Charcoal
Nippur	307 (2.0m)	Silty-Clay	1270 +/− 30 BP	c. 662-778 (92%); 842- 859 (1.6%); 792-804 (1.3%); 818-821 (0.2%)	5034796	3780305	Charcoal
Nippur	304 (3.5m)	Silty-Clay	1580 +/− 30 BP	c. 85-235 (95%)	5034796	3780305	Shell
Nippur	301 (5.0m)	Silty-Clay Fine Sand	3720 +/− 30 BP	c. 2578-2457 BC (95%)	5034796	3780305	Shell
Nippur	300 (5.5m)	Silty-Clay Fine Sand	3730 +/− 30 BP	c. 2577-2468 BC (95%)	5034796	3780305	Shell
Uruk Region	M38	see Jotheri *et al.* 2017			577390	3472026	
Uruk Region	M38-5	see Jotheri *et al.* 2017		c. 3980-3940 BC (95%)	577390	3472026	Shell
Uruk Region	M38-7	see Jotheri *et*		c. 4900-4860 BC (95%)	577390	3472026	Shell

		al. 2017					
Uruk Region	M38-12.5	see Jotheri *et al.* 2017		c. 7750-7600 BC (95%)	577390	3472026	Shell
Shalaii Cave	SHC-1	see Marsh *et al.* 2018		c. 938 (±42)-1456 (±29)	526935	3889333	Stalagmite
Shalaii Cave	SHC-2	see Marsh *et al.* 2018		c. 6075 (±38)-5027 (±219) BC	526935	3889333	Stalagmite
Shalaii Cave	SHC-3			~ 8500 BC-present	526935	3889333	Stalagmite

Geoarchaeology and Satellite Imagery

The primary goal of fieldwork was identifying and sampling from palaeochannels across southern Mesopotamia, as these channels act as environmental traps that allow dating and also contain microfossils that reflect the surrounding paleoenvironment. Palaeochannels were identified and selected using CORONA and QuickBird images, where channels can be seen as sinuous linear features that cast shadows on imagery. Identified paleochannels were then selected for fieldwork based on their visibility in the floodplain as well as possible historical relevance. Figure 1 shows the palaeochannels identified and the areas where fieldwork was conducted. This includes areas that were sampled using hand augering in the Dalmaj (A1-5) and Nahrawan (A6-10) regions. Figure 2 shows the sedimentary results from fieldwork. Boreholes A1-A10 were taken to a depth of six meters, with the exception of A2 and A3 that were shallower (three and four meters respectively), due to difficulty in penetrating deeper levels. For the samples, elevations were obtained using a level and theodolite during field surveys. The design of the augers used meant that each 0.5 m in depth resulted in a single sample being recovered. While this method is generally not enough accurate to develop a fine-scale reconstruction of deposition, it is possible to recognize the main depositional environments. Since the Dalmaj and Nahrawan areas are part of the Mesopotamian floodplain, riverine are the main type of deposits. Based on the sediments' grain sizes, colours, microfossils, and organic matter, this environment can be divided into channel, floodplain, crevasse splay, and marsh sub-environments (Jotheri et al. 2017). The channel deposits consist of coarse grain sediments that are mainly grey-fine sand; floodplain deposits consist of massive blocks of clay and sandy to silty clay; crevasse splay deposits are characterized by very light grey fine sand, silty sand to fine silt; marsh deposits are of clay to silty clay. Deposits were dated using AMS, where possible, using shells, charcoal, or gyttja. Problems with dating accuracy can occur in all of these materials, although shells and gyttja can be particularly problematic, where introduced carbon may not give a date of deposition (Lougheed et al. 2017). While acknowledging such issues, we have minimized this by presenting results where we feel there is some relative accuracy given by the fact that dates follow a chronological order (e.g., bottom layers are older) or there is good context, such as ceramics being found between dates obtained that suggest a general accuracy of dates (e.g., see Nippur below).

The samples from the Shatt en-Nil, the large channel running north to south that divides Nippur into massive western and eastern tells, were recovered from excavations during Seasons 13–14 (1975– 1976) of the Nippur Expedition, although the results presented here are new. The channel is believed to be the remains of an ancient Euphrates channel or canal; it is famously known from a Kassite map of Nippur and very likely existed for most of the

history of the site (Kramer 1956: 271–275; Gibson 1985). In order to examine historic environmental conditions in the vicinity of this feature, a trench was excavated with heavy mechanical equipment normally used for construction and maintenance of large irrigation canals and drainage structures. The excavation, "Trench 2," was approximately 200 by 2 meters, with a maximum depth of5.5 meters (Fig. 3). In some locations at the bottom of the trench, hand-excavated pits were used to allow sampling at a greater depth.

Petrography

Analyses of sediments included grain size and structural analysis, including composition and morphology. Samples from Dalmaj and Nahrawan were sent to the Department of Earth and Environmental Sciences, University of Milano-Bicocca in Italy for bulk petrography and heavy mineral analysis. The intent was to determine the likely origin of the sampled area's palaeochannels, specifically if the samples derived from one of the major rivers such as the Tigris or Euphrates, using mineralogy from given regions. Samples A1-5, A2-3, and A4-4 were analysed from the Dalmaj area; the Nahrawan samples A9-3 and A10-4 were also used. Mineral compositions of the samples were compared with samples from the Tigris, Euphrates and Diyala rivers. Quantitative petrographic analysis of sand within samples was carried out by point- counting in thin section (Gazzi-Dickinson method; Ingersoll et al. 1984). Sands were classified according to the relative proportions of quartz, feldspars, and lithic fragments (Garzanti 2016). Heavy mineral analyses were carried out using a 32-500 μm size window obtained by dry sieving.

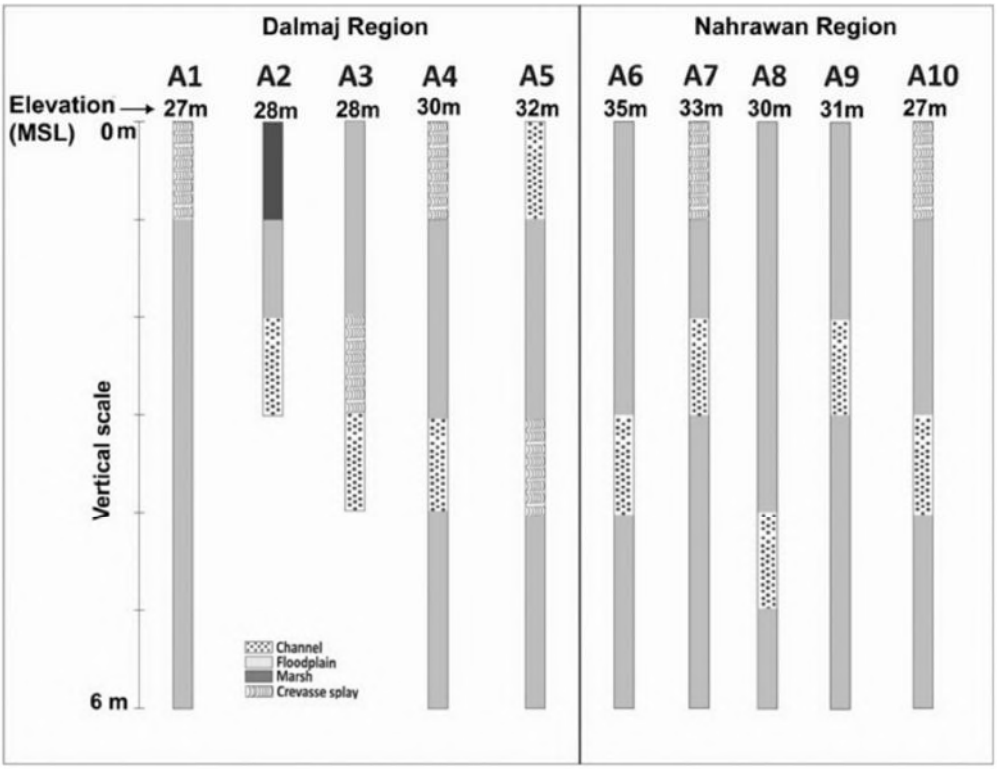

Fig. 2 Boreholes from the Dalmaj (A1-5) and Nahrawan (A6-10) regions. Elevation (mean sea level; MSL) is provided for the boreholes

Detrital grains denser than 2.90 g/cm3 were separated by centrifuging in sodium polytungstate and recovered by partial freezing with liquid nitrogen. On grain mounts, ~250

transparent heavy mineral grains were point-counted at suitable regular spacing to obtain real volume percentages using Galehouse's (1971) method. Compositional data of sediments carried by the Euphrates, Tigris, and Diyala Rivers used for comparison are from Garzanti et al. (2016). Relative sediment contributions from these rivers were assessed by forward mixing models based on integrated bulk petrography and heavy mineral data (Garzanti et al. 2012).

Phytoliths

Another analysis conducted involved identifying phytoliths from sediments. Phytoliths, which are silicified plant cells that are deposited into sediment when plants decay, were extracted from samples using a protocol by Rosen (1992, 2005; Fig. 4). Each sediment sample analysed, which contained phytoliths, was about 2.5 g. Hydrochloric acid (10%) was added to eliminate the carbonates. Clays were then separated out, using the manual settling method, and the samples were dried and then furnaced at 500 degrees Celsius for two hours to burn off any organic material. The phytoliths and other silica microfossils were separated from the remaining sediment using sodium polytungstate. The extracted microfossils were then placed on slides and mounted with Merck New Entellan. Slides were examined under an Alpha shot transmitted light microscope. Phytoliths were identified and counted, with an ideal minimum of 400 for single cells and 100 for multicells. Count size is important as a too-low count can introduce biases into the results, mainly via misidentification and under-representation of taxa that do not produce as many phytoliths (Strömberg 2009). Monocotyledons (i.e., grasses, reeds, sedges, palms, etc.) generally produce the largest numbers of phytoliths, both single- and multicells; many trees and shrubs (dicotyledons) also produce them although generally in smaller numbers (Piperno 2006). Differential preservation may also introduce biases. Sediment geochemistry, sediment deposition, sediment transport, soil formation and phytolith types all can impact preservation, with some more robust morphotypes, such as bulliforms, being over-represented. This is somewhat mitigated with higher minimum counts where possible. In addition to the boreholes from the Dalmaj and Nahrawan regions, previously excavated sediments from a machine cut near the Uruk region (Jotheri et al. 2017; M38) are used to provide phytoliths newly studied here. Sediment samples from Nippur's Shatt en-Nil (Trench 2) are also analysed for their phytoliths.

Speleothems

An approximately three meter long stalagmite sample was recovered from Shalaii cave from the Kurdistan region of Iraq (SHC-3) and was analysed for proxy palaeoclimate data. This provides proxy paleoclimate data relevant for informing on rainfall that would have affected southern Mesopotamia's river systems. Analysis of the speleothems included measuring thickness of annual growth bands in the stalagmites, measured in high-resolution (4,800 dpi) with the software ImageJ. Stable carbon ($\delta^{13}C$) and oxygen ($\delta^{18}O$) isotope analyses were also applied; samples were micromilled at 1 cm increments. The powdered samples were then measured using a Finnigan Delta V Advantage mass spectrometer equipped with an automated carbonate preparation system (Gas Bench II) from the Chemical Analytical Facilities (CAF) at the University of Reading. The reported values are provided relative to the international Vienna Peedee Belemnite (VPDB) standard. The methodology is the same as Flohr et al. 2017 and Marsh et al. 2018. Stable isotopes of oxygen and carbon ($\delta^{18}O$ and $\delta^{13}C$) are among the most widely used proxies for palaeoclimate research and provide a 'common currency' that can be used to link records from across a region (Roberts et al. 2018). Oxygen isotope variation in calcite can be caused by changes in a number of variables, including

moisture source, temperature, rainfall amount and effective- moisture (P:E; Lachniet 2009). $\delta^{18}O$ calcite values from Near Eastern speleothems are thought to reflect changes in the amount of rainfall and effective moisture (P-E; Bar-Matthews et al. 1997; Cheng et al. 2015; Flohr et al. 2017), although the source effect is a significant control on long- term time-scales. This is the case with Shalaii cave, where previous monitoring has established calcite growth, moisture level change, temperature and $\delta^{18}O$ of cave drip water. These values were used to calculate the theoretical calcite value of $\delta^{18}O$, which indicated the speleothems were deposited very close to isotopic equilibrium (Marsh et al. 2018). Speleothems formed at or close to isotopic equilibrium are primarily influenced by variations in drip-water $\delta^{18}O$, which, in turn, are primarily influenced by rainfall amount (McDermott et al. 2006).

Fig. 3 Trench 2, excavated across the Shatt en-Nil at Nippur. Sediment characteristics were generally homogeneous

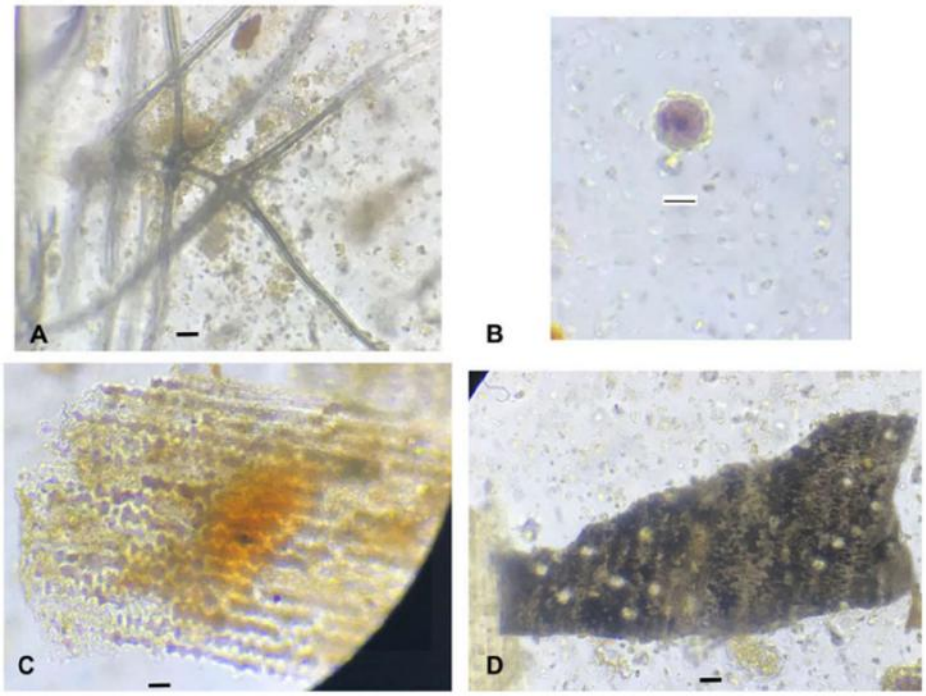

Fig. 4 Phytoliths; A) trichome from an oak (Quercus sp.), B) date palm (Phoenix dactylifera), C) multicell grass husk, and D) burnt cereal (probably barley)

Results

Below, we summarize the new results obtained by our work and present a discussion that brings in outside data.

The Dalmaj Samples

The sediments are mainly clay, with varying components of silt and sands. The sediments indicate generally low velocity flow, which is typical for a low-lying region. Figure 2 shows switching between channel and floodplain deposits, with A1 and A3-5 showing evidence of crevasse splays and A2 showing evidence of marsh deposits. Three samples were collected for mineralogical analysis from the Dalmaj area (A1-5, A2-3, A4-4). The samples were found to be quartzofeldspathic lithic sands (i.e., comprised of silica and feldspars), characterised by common plagioclase (feldspar), carbonate rock fragments, and intermediate to mafic volcanic grains. Relative to the Nahrawan samples (see below), they have higher quartz (monocrystalline/ polycrystalline quartz ratio), K-feldspar, volcanic, plutonic rock fragments, and medium-rank to high-rank metasedimentary grains. Cellular serpentinite and serpentine-schist grains are particularly distinctive. Micas are common, with biotite dominating over muscovite. Heavy mineral assemblages are moderately rich, with amphibole prevailing over epidote and clinopyroxene, and minor garnet, Cr-spinel, apatite, hypersthene, and enstatite. Dalmaj palaeochannel sands are richer in volcanic detritus than Tigris sand and richer in sedimentary detritus than Euphrates sand. Mica is more common, and quartz and heavy mineral concentrations are lower than in both Euphrates and Tigris bedload, which is accounted for by the fine grain size of the samples analysed (Garzanti et al. 2010). Forward compositional modelling indicates equal contribution of the Euphrates and Tigris rivers in the formation of the Dalmaj sediments. This suggests that the Dalmaj region was likely located close to or downstream of a confluence between the Tigris and Euphrates in earlier parts of the Holocene. As we could not obtain dates for those samples, we do not know when this

would have occurred, but given the depths and dating we have from A3, we suggest a early to mid-Holocene date (i.e., pre-Ubaid up to the Uruk period). Throughout much of the Holocene, the two rivers were generally near each other in this part of the plain.

Figure 5A shows the absolute phytolith and microfossil counts per gramme. For all of the samples, it is quite low, likely due to soil processes. As can be seen from Figure 5B, monocotyledons (mainly grasses) outnumber dicotyledons (mainly trees and shrubs), which is to be expected given that monocotyledons produce more phytoliths overall. The proportions fluctuate in all of the samples, although no pattern is evident. Figure 5C shows the proportions of grasses (wild and cereals), wetland plants (reeds and sedges), date palms and dicotyledons, while excluding other monoctyledons. As can be seen, there are temporal fluctuations in the proportions, with increasing grasses in relatively more recent times (i.e., A1-1, A1-2; A2-1, A2-2). Figure 5D shows the numbers of other types of silica microfossils found in these cores. Other microfossils include non- diatom algae and sponges, all of which indicate aquatic conditions, indicating the Dalmaj has long been an alluvial area.

Dalmaj samples, A3-4 and A3-3, dated to approximately 7600-7550 cal. B.C. and 5750-5650 cal. B.C. respectively. Overall, we see that the plant communities changed, with changing proportions of dicotyledons, wetland plants and grasses, and a hint of fruit cultivation through the presence of date palm in some samples. The samples generally indicate a more temperate climate (as compared to the present) with C3 grasses dominating and few C4 grasses. There are also few reeds (mainly Arundo donax). From A3-4, dicotyledons found include Quercus sp., what appears to be oak (i.e., similar to Figure 4A), while date palm (Phoenix dactylifera; similar to Figure 4B) was also found. Date palm in southern Iraq is expected, although in the eighth millennium B.C. this is relatively early. What is particularly unexpected is the presence of oak this far south. These results also suggest likely more humid conditions in southern Iraq between the eighth and sixth millennia B.C. Oak disappears above A3-3, indicating that sometime after approximately 5750-5650 cal. B.C. oak is no longer present.

The Nahrawan Samples

In general, the Nahrawan samples show a similar pattern of channel and floodplain deposits as the Dalmaj samples and have similar characteristics in grain size, colour and composition. More specifically, samples A9-2 and A9-4 were both clay, indicating a low velocity depositional environment, such as a backswamp floodplain, located away from the main channel. A9-3 consisted of silty fine sands, indicating a slight increase in velocity and more characteristic of overbank channel deposits. This indicates some movement in the river channel. Sample A10-4 consisted of sandy silts and fine sand, which are indicative of channel deposits. Samples from A9-3 and A10-4 were used for heavy mineral analysis. The Nahrawan palaeochannel sands are quartzo-feldspatho-lithic like Dalmaj sands, but much richer in limestone and chert grains. Heavy mineral assemblages are similar but much poorer and contain kaersutite and oxy-hornblende but lack orthopyroxenes. Chert abundance indicates significant supply from the Diyala River, whereas low heavy mineral concentration and relative abundance of Cr-spinel indicates recycling of foreland- basin sediments accreted to the Zagros foothills (Garzanti et al. 2016). Quartz, serpentinite, medium/high-rank metamorphic rock fragments, and mica are lower than in Tigris sand; forward compositional modelling indicates contribution from the Tigris and Diyala in about a 2:1 ratio. In other

words, during the time these channels were active, between about 10,500-5200 cal. B.C., they were influenced by those two rivers, with a likelihood that the Nahrawan was a part of the ancient Tigris prior to it becoming a canal. This would substantiate claims by Hritz (2010) about the Nahrawan's origin being linked to an ancient branch of the Tigris and the canal's reuse of an older, relict channel.

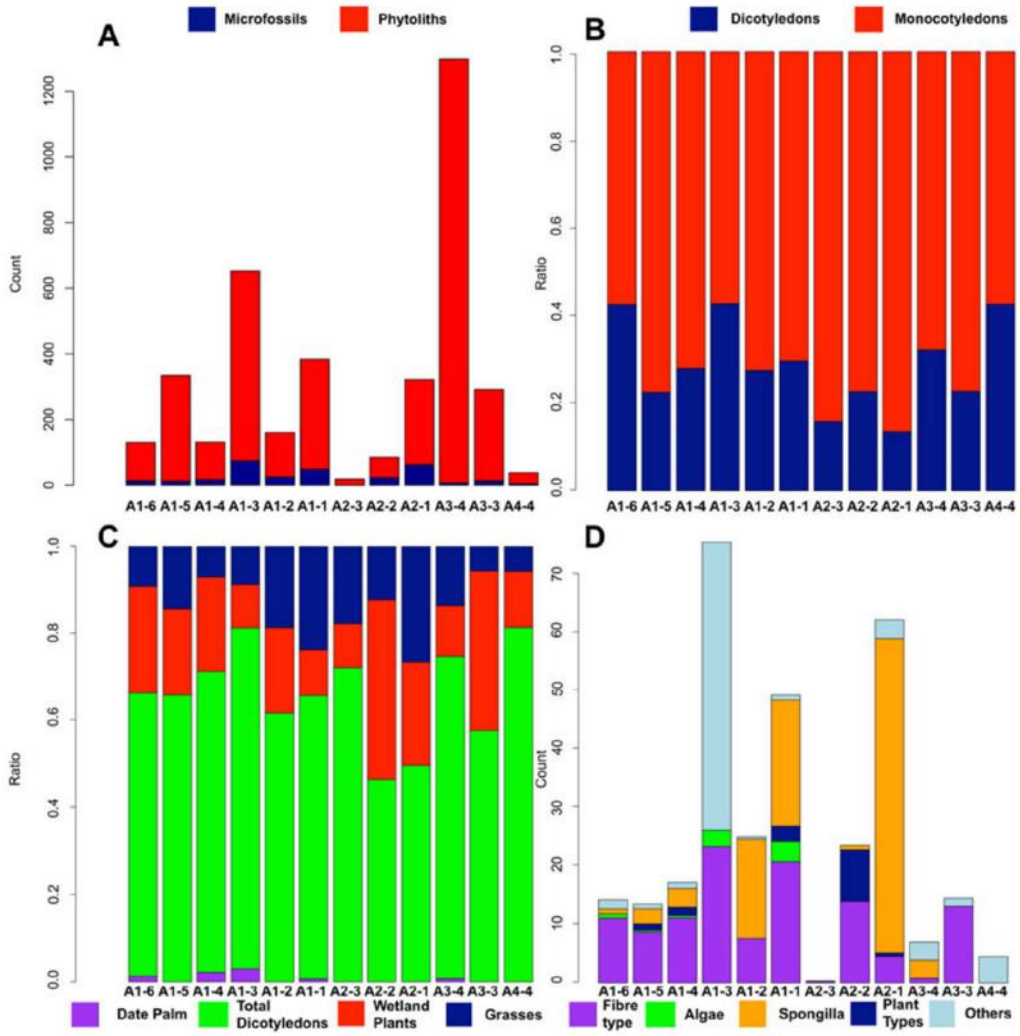

Fig. 5 Dalmaj: A) phytolith counts, B) proportion of monocotyledons to dicotyledons, C) types of plants, and D) other types of silica microfossils

Figure 6A shows the phytolith counts per gramme for the Nahrawan. Single cells dominate, with very few multicells represented (Fig. 6B). Figure 6C shows the ratios of monocotyledons (grasses, wetland plants, palms) and dicotyledons (mostly trees and shrubs); monocotyledons dominate, but dicotyledons are significant. There is some fluctuation through time as indicated by borehole A9. Figure 6D compares proportions of dicotyledons, grasses (cereals and wild), wetland plants and date palms. We were also able to obtain two dates from A9: about 10,500-10,175 cal. B.C. (A9-4) and 5300-5200 cal. B.C. (A9-2), which also indicates that about two meters of sediment was deposited in about 5000 years and two meters was deposited in the subsequent 7000 years, not accounting for erosion and compaction. The sediments reflect a changing river course, shifting from clay (distal backswamp) to fine sands

(overbank deposits) and back to clay. In the first clay sample (A9-4), there are far more wetland plants, but in A9-2, the other clay sample, dicotyledons are much more dominant. The first sample dates to around 10,000 B.C., near the beginning of the Holocene, which was particularly wet and warm, so the results are not surprising.

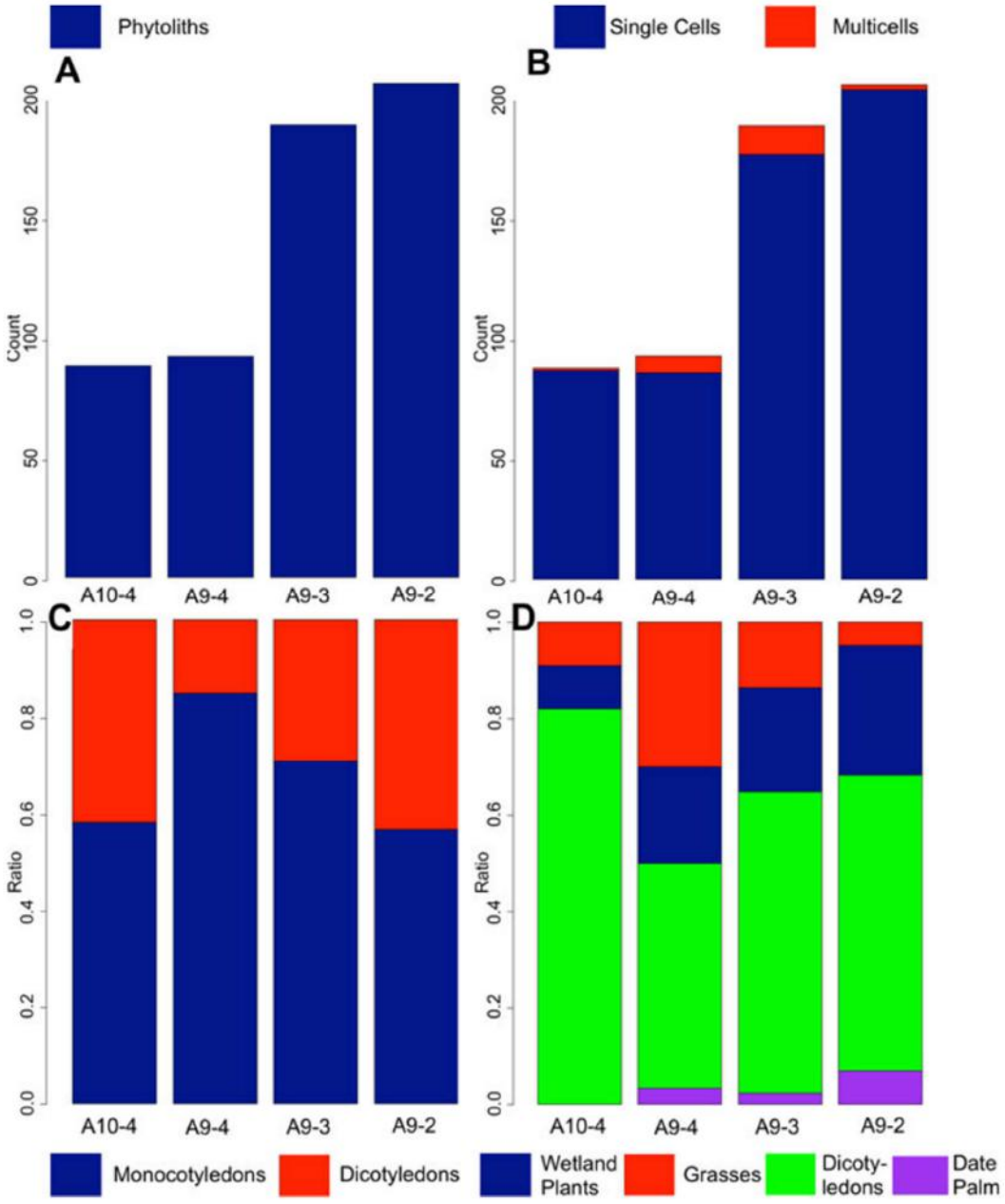

Fig. 6 Nahrawan: A) phytolith counts, B) proportion of single cell vs. multicell phytoliths, C) monocotyledons versus dicotyledons, and D) plant types

In borehole A9, there is a trend of increasing numbers of dicotyledons and date palms; increases in date palms could reflect increased cultivation in the late sixth millennium B.C. or early Ubaid. In all of the samples, there is also a correspondence between dicotyledons and date palm (which is a monocotyledon). The presence of date palm (Phoenix dactylifera) in sample A9-4 is significant because it shows that the tree was present in Iraq at a very early

period. In fact, as far as we are aware, this is the earliest Holocene date for the presence of date palm in Iraq, indicating that it was likely a native species.

Once again, C3 grasses dominate, with very few C4 grasses, indicating, as with the other samples, that a more temperate climate regime operated, as compared to the present. There were also other types of silica microfossils, including diatoms and sponge spicules, which indicate a wet environment, typical for an alluvial environment.

Uruk Region Borehole

Borehole M38 comes from an area near Uruk and Larsa. The samples analysed date from just after about 7750-7600 cal. B.C. (M38-12.5) and to before about 4900-4860 cal. B.C. (M38-7). Additional samples from this borehole (not analysed here) were previously assessed for microfossils including diatoms (Jotheri et al. 2017). The total number of phytoliths and other silica microfossils in this borehole is the highest of all samples analysed for off-site materials. They also fluctuate in a corresponding manner (Fig. 7A), which could be a result of preservation conditions, due to, for instance, sedimentation rates and soil processes; the numbers for both are highest from 10 to 11.5 m, which correspond to after about 7750 cal. B.C. and before 4900 cal. B.C.

Figure 7B shows the proportions between monocotyledons and dicotyledons. The proportions fluctuate through time, starting near 60/40 at 12 m, shifting to 90/10 at 11.5 m and 11 m, 80/20 (10.5 m), then back to 90/10 and finally to 50/50 at 9 m. The proportions also vary for single cells versus multicells, with the highest numbers of multicells found at 12 and 9 m depth. Figure 7C shows the varying proportions of grasses (cereals/wild grasses), wetland plants (sedges and reeds), dicotyledons and date palms. The results here are interesting in that they again reflect a changing environment. For example, at 12 m, the proportion of dicotyledons increases. This reflects a typical riparian environment, consisting of trees, shrubs, grasses and wetland plants. At 11 and 11.5 m, the number of dicotyledons decreases, while the numbers of grasses and wetland plants increase, reflecting a more marshy/wetlands type environment. At 10.5 m, dicotyledons increase again, indicating an increase in riparian type environment, one that is positioned more closely to the channel. This could be overbank or a crevasse splay deposit. In the 10m sample, once again, oak is present, but disappears from the later samples. Interestingly, barley is also evident, showing grain cultivation was happening nearby and was contemporary with the presence of oak. At 9.5 to 9 m, we again have a marshy environment (channel likely moving away), as reflected by an increase in wetland plants and grasses, and finally at 9 m, we have an increase of dicotyledons. The sediment here is a reddish clay, interpreted as floodplain deposits. These would be distal deposits and likely were exposed to oxygen (i.e., drier conditions) for the majority of the time due to their colour. The lack of water could also explain the reduction in wetland plants. Date palm is evident in most samples. They appear early on (just after 7750 cal. B.C.) and indicate firstly a fluctuating climate, followed by increasing seasonality towards the mid-Holocene. The numbers of sponge spicules are very high, especially at 11.5, 11 and 10 m, with high numbers as well at 10.5 m. The sponges are most prevalent in the marshy sediments, indicating standing or flowing freshwater; the presence of diatoms also supports this. In fact, in Jotheri et al. (2017), the diatoms from the 12.5 m level indicate the area was a possible swamp. The previous results published from M38-12.5 (Jotheri et al. 2017) and the phytoliths analysed here indicate that the area of M38 remained a freshwater environment

between approximately 7750 cal. B.C. and 4900 cal. B.C. This supports conclusions that the region was conducive for settlement as early as the early eighth millennium B.C., with favourable freshwater conditions persisting afterwards.

Nippur Samples

Trench 2 showed limited stratification, with relatively homogeneous deposits ofmostly buff-coloured clay and silt (Fig. 3). In several locations, there were concentrations ofsmall shell fragments that were originally attributed to desiccation ofmarshes and deposits ofhighly wind-eroded pottery fragments, probably washed from the mound of Nippur. Identifiable cultural material in the trench included fragments of Kassite goblets in several locations, mostly concentrating at or around the levels of samples 302 and 303. The earliest sample is 300 and is at 5.5 m depth, and sample 311 was the last sample, near the surface; other samples come from 0.5 m intervals above 300. Sample 301, for instance, is at 5.0 m depth. Dates for samples are in Table 1. Interestingly, no abandonment of Nippur is evident in the sediments, but this could mean such evidence may have been eroded or even dug out. The dated levels suggest that the Shatt-en Nil existed for much of Nippur's history. While the sediments appeared largely undifferentiated, clear differences in plant remains were evident from phytolith analysis. The numbers of phytoliths per gramme far exceeded those from the other samples and are dominated (at around 80%) by monocotyledons (mainly grasses; Fig. 8A–B). Wetland plants remain fairly consistent throughout the samples, but grasses and date palms fluctuate much more and seem to be negatively correlated (when there are more grasses, there are fewer palms and vice versa). There are fewer dicotyledons present in these samples than the other areas investigated, which could indicate a decline in trees/shrubs in the region (Fig. 8C). The overall high presence of date palms in the samples suggests these were grown very near Nippur's main channel throughout much of its history.

The negative correlation between date palm and grasses, which includes cereals, could indicate landscape management, whereby the main focus in this area switched between date palm and cereal cultivation. The presence of date palm is certainly more obvious in samples dating from the 26th century B.C. and onwards, where this represents extensive cultivation likely occurring near or within Nippur. Date cultivation seemed to intensify after the mid-third millennium B.C., as indicated by samples 302, 303, and especially 304 (Parthian). Based on the ceramics from the levels of 302 and 303, we can roughly assume that 302 and 303 date to the late second millennium B.C.

The presence of the date palm and Arundo donax, reeds, as well as other C3 plants indicates the continuing presence of water and likely use of the channel for almost the entire recorded history of Nippur. There were also a few samples with large multicells (consisting of 10+ cells), which is an indicator of increased water availability according to Rosen and Weiner (1994). Additionally, Madella et al. (2009) showed that the ratio of fixed to sensitive forms of phytoliths can also be used to detect irrigation, while more recently Jenkins et al. (2016) showed similar results to Madella et al. Given that rainfall levels are generally low in this region at this point, we suggest the presence of multicells likely resulted from irrigation from the channel that leads to increasingly saturated soils. It should be noted that not all samples contained these larger multicells, so there is an indication of either changing agriculture management strategies (i.e., less reliance on irrigation). There is a sudden increase in large multicells from sample 305 to 306, sometime around the Sasanian period (Fig. 8D).

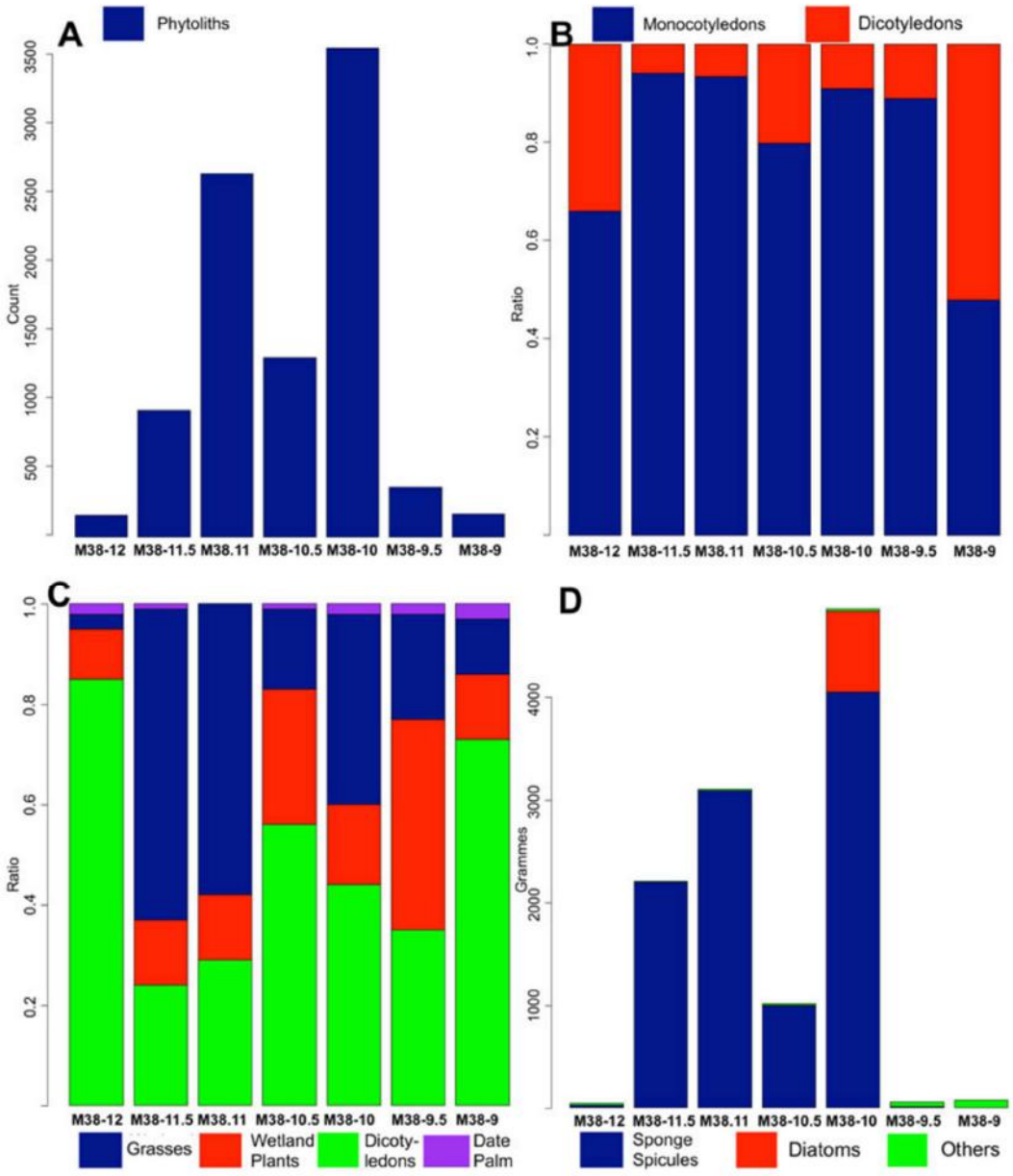

Fig. 7 M38 : A) phytolith counts, B) proportion of monocotyledons to dicotyledons, C) types of plants, and D) other evidence for freshwater microfossils

Analysis of the Nippur samples indicates an environment where the climate regime was more set, although variable over time. The continued presence of C3 grasses and Arundo donax indicate a more temperate climate; however, it is likely that these are present due to irrigation/agriculture and the general dampness of the immediate vicinity, rather than reflecting regional climatic trends. The area was also much more intensively managed. Fluctuations in grains and date palm phytoliths seem to reflect agricultural strategies, rather than the result of natural environmental change from major shifts in climate. Date palms and grains appear to show a clear negative relationship, suggesting that land management and choice of cultivation of one affected the other. The increase in multicells during roughly the Sasanian period, or samples 305–306, is likely evidence for the intensification of the use of irrigation, at a rate likely more intense than earlier periods. In other words, this likely reflects

irrigation expansion in the vicinity with more intense water flow. Overall, the results from Nippur are important because they span a long period (around three millennia) and illustrate the shifting agricultural strategies used at least in one area in and around the site.

Speleothem Climate Results

Our results for SHC-3, dated from about 8500 B.C. to today, are preliminary and require more work for accuracy, but a general assessment is made here. The SHC-3 recordwould appear to be the longest and most complete paleoclimate record for all ofMesopotamia during the Holocene. Figure 9 shows results from Shalaii's speleothems as well as additional regional data; it is further discussed below. Like existing records, the $\delta^{18}O$ variation values are thought to reflect changes in rainfall amount (Marsh et al. 2018) and, therefore, evidence of a wetter early-mid Holocene climate relative to today is evident, while the more recent sample shows drying conditions similar to today but with volatile climate conditions. $\delta^{18}O$ trends show that after the end of the fourth millennium B.C., there could be a shift towards generally drier conditions. These conditions could have prevailed for much of the rest of the Holocene, although periods of enhanced rainfall exist during this time. By the mid-first millennium B.C., and particularly over the last two thousand years, dry conditions appear evident, but conditions were volatile as well, sometimes reflecting short, wetter periods. These results need to be analysed further to develop a more detailed understanding for different climate trends within key archaeological periods and palaeoclimate events (e.g., 4.2 kya event).

Discussion and Conclusion

North Iraq Climate Discussion

This section summarises evidence for general changes in regional hydrological conditions using existing palaeoclimate records and other investigated records from northern Iraq. The Near East is still relatively neglected in terms of palaeoclimate investigations. High resolution palaeoclimate records that cover the Holocene are rare, and there exist large spatiotemporal gaps between those that do exist (Finné et al. 2011); this leaves a lot of uncertainty in our knowledge of hydrological conditions during the Holocene.

The $\delta^{18}O$ records from the region show significant shifts in climate during the Holocene and are generally coeval, which are also supported by other proxy evidence, although there were likely some fine-scale, regional variations. In fact, these variations necessitate local collection of palaeoclimate data. However, we can summarise a general picture of the region, which can then be compared to the records from southern Iraq. Following a short recovery after the Younger Dryas glacial reversal, the early Holocene ~9,700 – ~4,000 B.C. was characterised by relatively depleted δ 18Oin speleothem and lake sediment records, an indication of wetter conditions; some of this depletion was caused by a change in source (Eastern Mediterranean) $\delta^{18}O$, that is rain deriving from the Mediterranean region (Cheng et al. 2015). A decrease in dust flux evident from a lake record in northern Iran (Sharifi et al. 2015), where abundance of titanium (Ti) generally reflects wind blown dust, supports evidence of increased rainfall for the early Holocene, similar to our results. During the end of the mid-Holocene to late Holocene, by around ~3,000 B.C., there was a shift to more enriched $\delta^{18}O$ values, similar to the present day. This is suggestive of drier conditions prevailing. Values remain similar for much of the rest of the Holocene, although there were periods of enhanced rainfall and prolonged drought, with a few records indicating that a wet phase prevailed between ~2,000

and ~1,000 B.C. (Cheng et al. 2015; Roberts et al. 2011). $\delta^{18}O$ values from lake sediments also support this trend (e.g., Roberts et al. 2011).

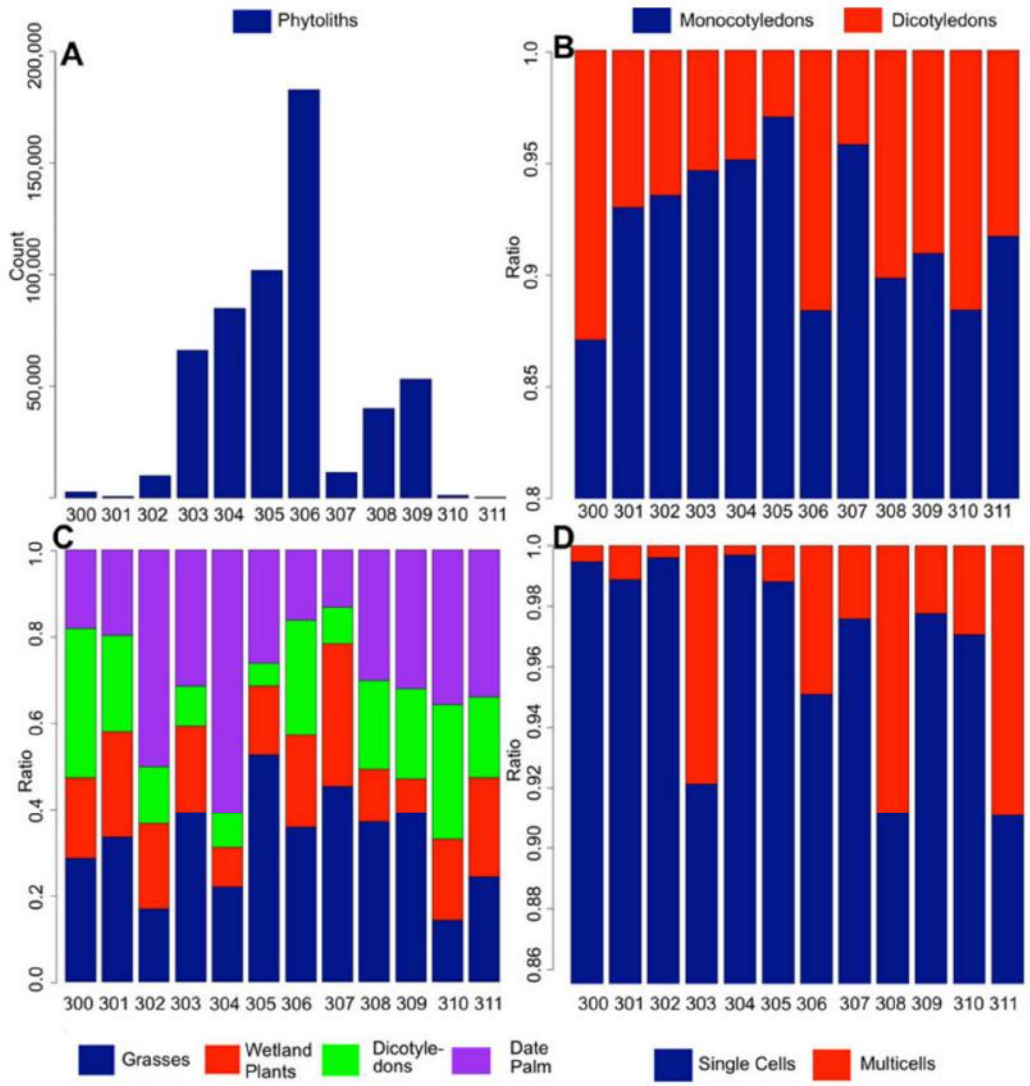

Fig. 8 Nippur: A) phytolith counts, B) proportion of monocotyledons to dicotyledons, C) types of plants, and D) single and multicells

The $\delta^{18}O$ records from the region show significant shifts in climate during the Holocene and are generally coeval, which are also supported by other proxy evidence, although there were likely some fine-scale, regional variations. In fact, these variations necessitate local collection of palaeoclimate data. However, we can summarise a general picture of the region, which can then be compared to the records from southern Iraq. Following a short recovery after the Younger Dryas glacial reversal, the early Holocene ~9,700 – ~4,000 B.C. was characterised by relatively depleted δ 18Oin speleothem and lake sediment records, an indication of wetter conditions; some of this depletion was caused by a change in source (Eastern Mediterranean) $\delta^{18}O$, that is rain deriving from the Mediterranean region (Cheng et al. 2015). A decrease in dust flux evident from a lake record in northern Iran (Sharifi et al. 2015), where abundance of titanium (Ti) generally reflects wind blown dust, supports evidence of increased rainfall for the early Holocene, similar to our results. During the end of the mid-Holocene to late

Holocene, by around ~3,000 B.C., there was a shift to more enriched $\delta^{18}O$ values, similar to the present day. This is suggestive of drier conditions prevailing. Values remain similar for much of the rest of the Holocene, although there were periods of enhanced rainfall and prolonged drought, with a few records indicating that a wet phase prevailed between ~2,000 and ~1,000 B.C. (Cheng et al. 2015; Roberts et al. 2011). $\delta^{18}O$ values from lake sediments also support this trend (e.g., Roberts et al. 2011).

Previous analysis was conducted on speleothem samples from Shalaii cave, Kurdistan region of Iraq (Fig. 9). Two samples (SHC-1 and SHC-2; Marsh et al. 2018) cover different periods of the Holocene and allow for an insight into the change of $\delta^{18}O$ and $\delta^{13}C$ values between these periods in Northern Iraq. One sample, SHC-2, which was deposited between 8,025 B.P. (6,075 B.C.) ± 38 and 6,977 B.P. (5,027 B.C.) ± 219, has a mean oxygen isotope value of −6.54‰ (VPDB). The younger sample, SHC-1, which grew between 1,012 B.P. (938) ± 42 and 494 B.P. (1456) ± 29 B.P., shows an average enrichment of ~1.10% from SHC-02, correlating well with other speleothem records from the region, which show similar $\delta^{18}O$ decreases of between 0.6% (Jeita) – 1.10% (Soreq) during the same period. While these two samples are relatively short in time, the third (SHC-3) more detailed sample shows some similar trends to the regional picture, although evidence for regional variations affecting northern Iraq are also evident (Table 1).

Southern Mesopotamia Environment

Several noteworthy results relevant to the environmental history of southern Iraq are presented in this work. We see similar environmental patterns in the alluvial regions of the Nahrawan and Dalmaj. The general trend from phytolith and sedimentary results shows a more temperate (i.e., as compared to the present) climate regime was established early in the Holocene (c. 10,000 B.C.) in Iraq. The microfossils all indicate changes within alluvial and surrounding environments, changing from marsh/riverine, with mainly wetland plants and grasses, to floodplain and switching to river banks, with trees often composed of date palm. South of Baghdad and the region of Nahrawan are likely to already have been habitable by the eleventh millennium B.C. To the south around Uruk, the region was habitable for settlement at least by the early eighth millennium B.C. These results suggest early habitation prior to the earliest phases of the Ubaid was likely to be present south of Baghdad, even if material culture is lacking. A lack of evidence for the Persian Gulf in areas investigated and favourable settlement conditions from phytolith and diatom results suggest that by the early Holocene, and before the Ubaid, settlement was likely in many regions south of Baghdad and as far as the regions near Uruk. It is possible that earlier, pre-Ubaid cultures used less mud brick and, given the presence of more abundant wood and other building materials such as reeds, simply relied on these perishable resources more, thus making the detection of these cultures difficult using standard archaeological methods. The sediments suggest a very different Tigris-Euphrates system once existed. The Dalmaj region suggests the Tigris and Euphrates could have been joined near this area, sometime in the early to mid-Holocene, while the Nahrawan appears to have been a branch or part of the ancient Tigris prior to the development of the canal.

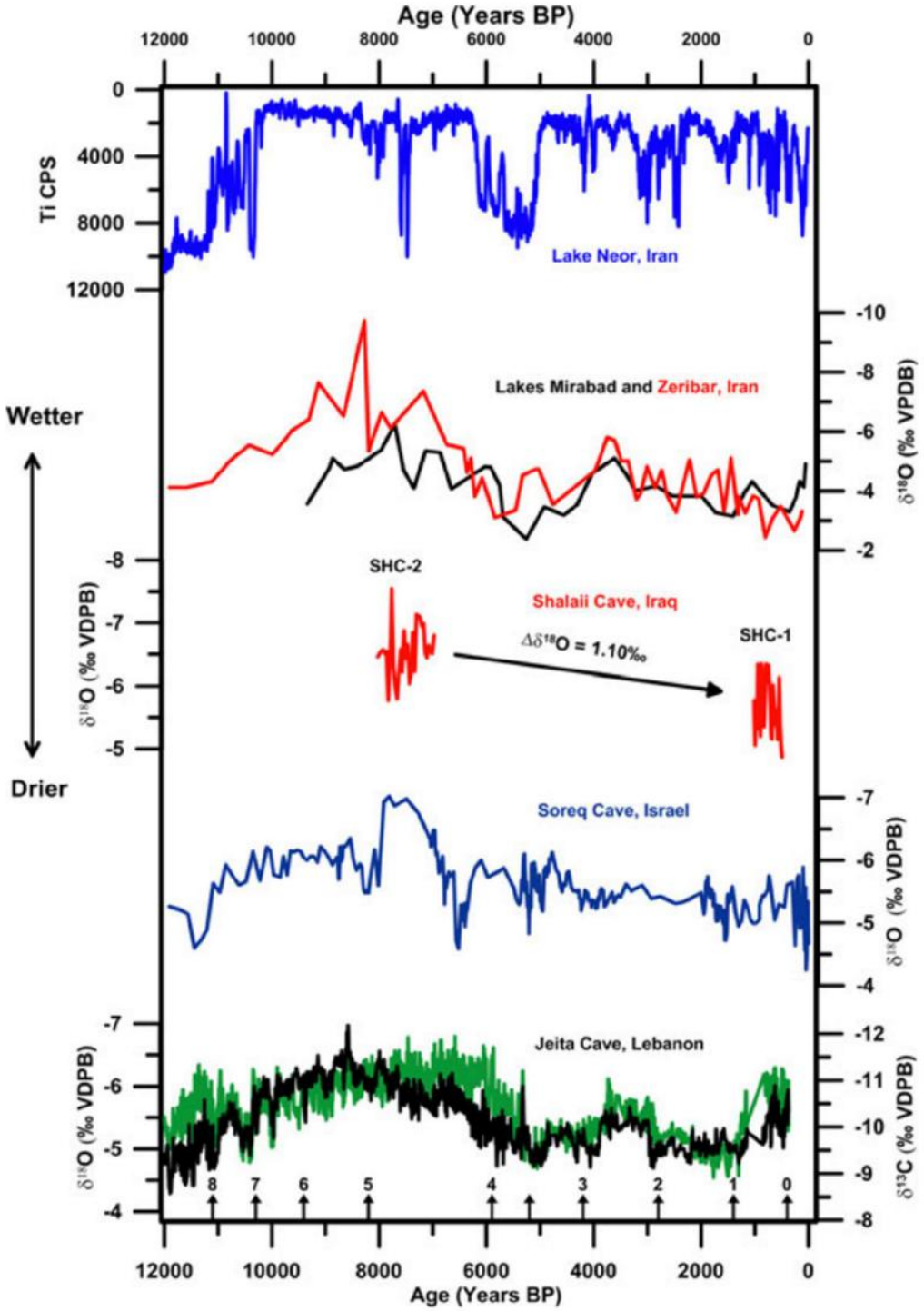

Fig. 9 Summary of palaeoclimate data from Shalaii cave reflecting trends from recovered speleothems and showing similarity to regional data (see Sharifi et al. 2015)

Another novel result is that oak was also present in southern Iraq, both in the Dalmaj and Uruk regions, between the eighth and sixth millennia B.C. No previous archaeological or historical data have discussed oak this far south in Iraq. Moreover, oak disappeared from later samples, which could occur due to increased aridity and/or increased human activity in southern Mesopotamia. From our results, we note that oak disappeared in records by the

time of the earlier Ubaid and later Uruk expansions (Stein 2012; Algaze 2008). In other words, part of the motivation for expansion or even colonization/trade could have been the lack of quality wood materials in southern Iraq after the sixth millennium B.C.

At Nippur, the Shatt en-Nil was a long-lived channel that existed as an active canal/river channel throughout much of the city's history. The remains from Nippur suggest that during the late second millennium B.C. and Parthian period, date palms would have been substantially cultivated in parts of Nippur, with some date palm cultivation happening in the mid-third millennium B.C. Dates, in general, do not appear very frequently in textual sources from the third and second millennia B.C. Administrative texts from the third millennium B.C. indicate the use of date palm, via indirect citation in legal contexts such as transactions or agreements (Cocquerillat 1968; Landsberger 1967). Date palms were grown in irrigated orchards along with other fruit trees, such as figs, grapes, pomegranates, and apples in the late third millennium B.C. (Focke 2015; Greco 2015; Postgate 1987; Powell 1992). Given that most of the written records from the third and second millennia B.C. derive from public/state institutions, the lack of information on date cultivation is not entirely surprising. State and public institutions in the third and second millennia B.C. were heavily invested in cereal cultivation and to a much lesser degree in horticulture, as for example the cultivation of dates. There are some texts suggesting institutional involvement in date cultivation in the late third millennium B.C. (Focke 2015; Greco 2015), but it has been assumed that date cultivation was a more private/individual enterprise, as was true for example in pharaonic Egypt (Moreno Garcia, in press). However, until now, there were no empirical data that could provide a clue about the size of the non-institutional sector of early states' economies that was based on date cultivation. Hence, one result of the presented study is a more nuanced and holistic understanding of these early state economies. Additionally, trees were grown for timber in irrigated lands in the third millennium B.C. (Selz 2011). Textual sources suggest that dates were part of the regular diet, but the volume of grain-related texts has generally minimized the importance of dates. Our results suggest dates were relatively important for the Bronze Age economy, although in the mid-third millennium B.C. they were not as prevalent as in the second millennium B.C. (Kassite) levels, and their importance continued well into the first millennium A.D. Overall, there appears to be a negative relationship between date palm and grain cultivation in the area sampled.

The most detailed insight into the agricultural regime of the Nippur region is provided by the archive of the Murašu agricultural firm, which managed large amounts of arable land around Nippur in the fifth century B.C. on behalf of their owners. A major shift towards intensive horticulture of date palms at the expense of cereal cultivation took place during that period in other areas of the alluvial plain. From texts in the first millennium B.C., during the Achaemenid and Hellenistic periods, there is evidence of widespread date cultivation, in particular in more northern regions such as around Sippar, with even a cash crop economy revolving around the date palm (Jursa 2006). However, the Murašu archive deals primarily with cereal cultivation, with very little direct information on date cultivation (Jursa 2010: 407). References to the cultivation of dates are only found in debt notes, in which those to be paid by members of the Murašu agricultural firm were reckoned in large quantities of dates. Other references to date cultivation are rents collected in the form of quantities of dates for the leasing of garden plots (Jursa 2010: 410–411). Furthermore, Jursa (2010: 409, 413) suggests that date cultivation was not as prevalent in the Nippur region as elsewhere, consisting

probably of medium to modest sized gardens tended to by individual families. The large quantities of dates listed in debt notes are thus to be understood as the obligation of a collective of tenants or farmers.

Although irrigation was present in Nippur in the earliest levels from the phytoliths analysed, it greatly expanded around the time of the Sasanian period, from the third century A.D. or later. This is supported by historical sources from the region that show expansion of irrigation during the Sasanian period (Campopiano 2017). Our results likely reflect the major irrigation works that began to be created by this period. Volatile climate could have been one problem faced in irrigation, as evident from climate data, where alternating periods of high rainfall and very dry years could have been frequent at least by the first millennium B.C., and into later periods. From a methodological view, phytolith analysis proved useful in differentiating the homogeneous remains from the Shatt en-Nil.

What the results most clearly demonstrate is the potential use of these multidisciplinary approaches, applied here in southern Mesopotamia. Furthermore, linkages between rainfall patterns in northern Iraq, via speleothem data, can be made to events in southern Iraq, including changes in the hydrologic regime and changes to the environment and plant communities (e.g., the disappearance of oak in southern Iraq). Future work should certainly focus on validating the observations presented here, as we recognize that remains from a limited number of samples do not mean wide-scale trends across southern Mesopotamia. Nevertheless, we are now better able to reconstruct plant communities and the local environments and how they were affected/modified by human activity and natural climate variations.

Acknowledgements
We are deeply grateful to the Neubauer Collegium for Culture and Society at the University of Chicago for funding the fieldwork, analysis and a 2018 conference that allowed collaborators to share results. The Neubauer also generously organized and hosted the conference. In addition, earlier funding from the Japanese Society for the Promotion of Science (JP26283012: CE Watanabe) helped fund our work near Uruk. The National Geographic Society also provided funding to conduct fieldwork and analysis. Funding from the British Institute for the Study of Iraq helped cover our work in Shalaii cave.

References
Adams, R.M. 1981. Heartland of Cities: Surveys of Ancient Settlement and Land Use on the Central Floodplain of the Euphrates. Chicago: University of Chicago Press.
——1965. Land Behind Baghdad: A History of Settlement on the Diyala Plains. Chicago: University of Chicago Press.
Algaze, G. 2008. Ancient Mesopotamia at the Dawn of Civilization: The Evolution of An Urban Landscape. Chicago: University of Chicago Press.
—— 1993. The Uruk World System: The Dynamics of Expansion of Early Mesopotamian Civilization. Chicago: University of Chicago Press.
al-Hamdani, A. 2014. The Shadow States: The Archaeology of Power in the Marshes of Southern Mesopotamia. PhD Dissertation, State University of New York Stony Brook.

Bar-Matthews, M., A. Ayalon, and A. Kaufman. 1997. "Late Quaternary Paleoclimate in the Eastern Mediterranean Region from Stable Isotope Analysis of Speleothems at Soreq Cave, Israel". Quaternary Research 47(2): 155–168.

Blaschke, T. 2018. Euphrat und Tigris im Alten Orient. Leipziger Altorientalische Studien 6. Wiesbaden: Harrassowitz Verlag.

Brandt, M. C. 1990. "Nippur: Building an Environmental Model". Journal of Near East Studies 49(1): 67–73.

Campopiano, M. 2017. "Cooperation and Private Enterprise in Water Management in Iraq: Continuity and Change between the Sasanian and Early Islamic Periods (Sixth to Tenth Centuries)". Environment and History 23(3): 385–407.

Cancik-Kirschbaum, E. and N. Ziegler, eds. 2009. Entre les Fleuves I. Untersuchungen zur Historischen Geographie Obermesopotamiens im 2. Jahrtausend v. Chr. Berliner Beiträge zum Vorderer Orient 20. Gladbeck: PeWe-Verlag.

Cancik-Kirschbaum, E. and C. Hess (with collaboration of K. Petrow). 2016. Toponyme der Mittelassyrischen Texte: Der Westen des Mittelassyrischen Reiches: Obermesopotamien im 2. Jt. v.Chr. Materialien zu Toponyme und Topographie I/2 [online]. Paris: Collège de France.

Cheng, H., A. Sinha, S. Verheyden, F. H. Nader, X. L. Li, P. Z. Zhang, L. Yin, L. Yi, Y. B. Peng, Z. G. Rao, Y. F. Ning and R. L. Edwards. 2015. "The climate variability in northern Levant over the past 20,000 years". Geophysical Research Letters 42(20): 8641–8650.

Civil, M. 1987. "Ur III Bureaucracy" in M. Gibson and R.D. Biggs, eds. The Organisation of Power: Aspects of Bureaucracy in the Ancient Near East. Studies in Ancient Oriental Civilization 46. Chicago: the University of Chicago Press, pp. 43–53.

Cocquerillat, D. 1968. "Palmeraies et cultures de l'Eanna d'Uruk (559-520)". Ausgrabungen der Deutschen Forschungsgemeinschaft in Uruk-Warka 8. Berlin: Gebr. Mann Verlag. pp. 72–74.

Cole, S. W. and H. Gasche. 1998. "Second- and first-millennium B.C. rivers in northern Babylonia" in H. Gasche and M. Tanret, eds. Changing watercourses in Babylonia. Towards a reconstruction of the ancient environment in lower Mesopotamia. Chicago: University of Chicago Press, pp. 1–158.

Fink, C. 2016. Fundorte und Karten. Materialien zu Toponyme und Topographie I/3 [online]. Paris: Collège de France.

Finné, M., K. Holmgren, H. S. Sundqvist, E. Weiberg and M. Lindblom. 2011. "Climate in the Eastern Mediterranean, and Adjacent Regions, During the Past 6000 years–A Review". Journal of Archaeological Science 38(12): 3153–3173.

Flohr, P., D. Fleitmann, E. Zorita, A. Sadekov, H. Cheng, M. Bosomworth, L. Edwards, W. Matthews and R. Matthews. 2017. "Late Holocene droughts in the Fertile Crescent recorded in a speleothem from northern Iraq: Late Holocene Droughts". Geophysical Research Letters 44(3): 1528–1536.

Focke, K. 2015. Der Garten in Neusumerischer Zeit. Alter Orient and Altes Testament 53. Münster: Ugarit- Verlag.

Galehouse, J. S. 1971. "Point counting" in R.E. Carver, ed. Procedures in sedimentary petrology. New York: Wiley, pp. 385–407.

Garzanti, E. 2016. "From Static to Dynamic Provenance Analysis: Sedimentary Petrology Upgraded". Sedimentary Geology 336: 3-13.

Garzanti, E., A. I. Al-Juboury, Y. Zoleikhaei, P. Vermeesch, J. Jotheri, D. B. Akkoca and G. Vezzoli. 2016. "The Euphrates-Tigris-Karun River System: Provenance, Recycling and

Dispersal of Quartz-Poor Foreland-Basin Sediments in Arid Climate". Earth-Science Reviews 162: 107–128.
Garzanti, E., A. Resentini, G. Vezzoli, S. Andó, M. Malusà and M. Padoan. 2012. "Forward Compositional Modelling of Alpine Orogenic Sediments". Sedimentary Geology 280: 149–164.
Garzanti, E., S. Andò,C. France-Lanord,G. Vezzoli, P. Censi, V. Galy andY. Najman. 2010. "Mineralogical and Chemical variability of Fluvial Sediments. Bedload sand (Ganga–Brahmaputra, Bangladesh)". Earth and Planetary Science Letters 299(3–4): 368–381.
Gibson, M. 1985. "Nippur. Back to Tablet Hill: Sixteenth Season at Nippur, 1985" in J.H. Johnson, ed. The Oriental Institute 1984–85 Annual Report. Chicago: Orient Institute, pp. 20–30.
—— 1974. "Violation of Fallow and Engineered Disaster in Mesopotamian Civilization" in T.E. Downing and McG. Gibson, eds. Irrigation's Impact on Society. Tuscon: The University of Arizona Press, pp. 7–20.
—— 1972. The City and Area of Kish. Field Research Projects. Miami, FL: Coconut Grove. —— 1978. "Nippur Regional Project: Umm Al-Hafriyat" in J.A. Brinkman, ed., The Oriental Institute 1977–78 Annual Report. Chicago: Oriental Institute, pp. 20–26.
—— 1977. "The Nippur Expedition" in J.A. Brinkman, ed., The Oriental Institute 1976–77 Annual Report. Chicago: Oriental Institute, pp. 24–34.
—— 1976. "The Nippur Expedition" in J.A. Brinkman, ed., The Oriental Institute 1976–77 Annual Report. Chicago: Oriental Institute, pp. 22–28.
Greco, A. 2015. Garden Administration in the Ĝirsu Province During the Neo-Sumerian Period. Biblioteca del Próximo Orient Antiguo 12. Madrid: Consejo Superior de Investigaciones Científicas.
Helbaek, H. 1960. "The Palaeoethnobotany of the Near East and Europe" in R.J. Braidwood and B. Howe, eds. Prehistoric Investigation in Iraqi Kurdistan. Chicago: University of Chicago Press, pp. 100–118.
—— 1959. "Domestication of Food Plants in the Old World." Science 130 (3372): 365–372. Heyvaert, V. M. A. and C. Baeteman. 2008. "A Middle to Late Holocene avulsion history of the Euphrates River: A Case Study from Tell ed-Dēr, Iraq, Lower Mesopotamia". Quaternary Science Reviews 27 (25–26): 2401–2410.
Hritz, C., J. Pournelle and J. Smith. 2013. "Revisiting the Sealands: Report of Preliminary Ground Reconnaissance in the Hammar District, Dhi Qar and Basra Governorates, Iraq". Iraq 74: 37–49.
Hritz, C., J. Pournelle, J. Smith, B. Albadran, B. M. Issa, and A. al-Handal. 2012. "Mid-Holocene Dates for Organic-Rich Sediment, Palustrine Shell, and Charcoal from Southern Iraq". Radiocarbon 54(01): 65–79.
Hritz, C. 2010. "Tracing settlement patterns and channel systems in southern Mesopotamia using remote sensing". Journal of Field Archaeology 35(2): 184–203.
—— 2005. Landscape and Settlement in Southern Mesopotamia: A Geoarchaeological Analysis. PhD Dissertation, University of Chicago.
Ingersoll, R. V., T. F. Bullard, R. L. Ford, J. P. Grimm, J. D. Pickle and S. W. Sares. 1984. "The effect of grain size on detrital modes: A test of the Gazzi-Dickinson point-counting method". Journal of Sedimentary Petrology 54: 103–116.
Jacobsen, T. 1960. "The waters of Ur". Iraq 22: 174–185. Jacobsen, T. and R. M. Adams. 1958. "Salt and Silt in Ancient Mesopotamian Agriculture: Progressive Changes in Soil

Salinity and Sedimentation Contributed to the Breakup of Past Civilizations". Science 128 (3334): 1251–1258.

Jacobsen, T. 1982. Salinity and Irrigation Agriculture in Antiquity, Diyala Basin Archaeological Projects: Report on Essential Results, 1957–58. Bibliotheca Mesopotamica, v. 14. Malibu: Undena Publications.

Jenkins, E., K. Jamjoum, S. Nuimat, R. Stafford, S. Nortcliff, and S. Mithen. 2016. "Identifying Ancient Water Availability through Phytolith Analysis: An Experimental Approach". Journal of Archaeological Science 73 (September): 82–93.

Jotheri, J., M. Altaweel, A. Tuji, R. Anma, B. Pennington, S. Rost and C. Watanabe. 2017. "Holocene Fluvial and Anthropogenic Processes in the Region of Uruk in Southern Mesopotamia". Quaternary International 483: 57–69.

Jotheri, J., M. B. Allen and T. J. Wilkinson. 2016. "Holocene Avulsions of the Euphrates River in the Najaf Area of Western Mesopotamia: Impacts on Human Settlement Patterns". Geoarchaeology 31(3): 175–193.

Jotheri, J. 2016. Holocene Avulsion History of the Euphrates and Tigris Rivers in the Mesoptamian Floodplain. PhD dissertation, Durham University.

Jursa, M. (with contributions by J. Hackl, B. Janković, K. Kleber, E. E. Payne, C. Waerzeggers and M.Weszeli). 2010. Aspects of the Economic History of Babylonia in the First Millennium BC: Economic Geography, Economic Mentalities, Agriculture, the Use of Money and the Problem of Economic Growth. Alter Orient and Altes Testament 377. Münster: Ugarit-Verlag.

Jursa, M. 2006. "Agricultural management, tax farming and banking: Aspects of entrepreneurial activity in Babylonia in the Late Achaemenid and Hellenistic periods" in P. Briant and F. Joannès, eds. La transition entre l'Empire achéménide et les royaumes hellénistiques. Paris: De Boccard, pp. 137–222.

Kennett, D. J. and J. P. Kennett. 2006. "Early State Formation in Southern Mesopotamia: Sea Levels, Shorelines, and Climate Change". Journal of Island & Coastal Archaeology 1(1): 67–99.

Kramer, S. 1956. From the Tablets of Sumer. Indian Hills: Falcon's Wing Press. Lachniet, M. S. 2009. "Climatic and Environmental Controls on Speleothem Oxygen-Isotope Values". Quaternary Science Reviews 28(5–6): 412–432.

Landsberger, B. 1967. The Date Palm and Its By-Products According to Cuneiform Sources. Archiv für Orientforschung. Beiheft 17. Graz: Selbstverlag E.Weidner.

Lougheed, B. C., S. P. Obrochta, C. Lenz, A. Mellström, B. Metcalfe, R. Muscheler, M. Reinholdsson, I. Snowball and L. Zillén. 2017. "Bulk Sediment 14C Dating in an Estuarine Environment: How Accurate Can It Be?: Estuarine Bulk Sediment 14C Dating." Paleoceanography 32 (2): 123–31.

Madella, M., M. K. Jones, P. Echlin, A. Powers-Jones and M. Moore. 2009. "Plant Water Availability and Analytical Microscopy of Phytoliths: Implications for Ancient Irrigation in Arid Zones". Quaternary International 193 (1–2): 32–40.

Maekawa, K. 1974. "Agricultural Production in Ancient Sumer: Chiefly from Lagash Materials". Zinbun 13: 1–60.

Marsh, A., D. Fleitmann, D. A. M. al-Manmi, M. Altaweel, D. Wengrow and R. Carter. 2018. "Mid- to late- Holocene archaeology, environment and climate in the northeast Kurdistan region of Iraq". The Holocene. https://doi.org/10.1177/0959683617752843.

McDermott, F., H. Schwarcz and P.J. Rowe. 2006. "Isotopes in speleothems". in M. J. Leng, ed. Isotopes in Palaeoenvironmental Research. Vol. 10. Dordrecht: Springer, pp. 185–226.

Moreno García, J.-C. (in press). "Wells, Small-Scale Private Irrigation and Agricultural Strategies in the 3rd and 2nd Millennium BC Egypt" in S. Rost, ed. Irrigation in Early States: New Directions. Oriental Institute Seminars 13. Chicago: Oriental Institute of the University of Chicago.

Morozova, G. S. 2005. "A Review of Holocene Avulsions of the Tigris and Euphrates Rivers and Possible Effects on the Evolution of Civilizations in Lower Mesopotamia". Geoarchaeology 20(4): 401–423.

Paepe, R. 1971. "Geological approach of the Tell ed-Dēr area, Mesopotamian plain, Iraq". Tell ed-DērI. Leuven: Peeters, pp. 19–27.

Paepe, R. and C. Baeteman. 1978. "Fluvial system between Tell ed-Dēr and Tell Abu Habbah". Tell Ed-DērII. Leuven: Peeters, pp. 37–56.

Piperno, D. R. 2006. Phytoliths: A Comprehensive Guide for Archaeologists and Paleoecologists. Lanham, MD: AltaMira Press.

Postgate, J. N. 1987. "Notes on Fruits in the Cuneiform Sources". Bulletin on Sumerian Agriculture 3: 115–144. Pournelle, J. 2003. Marshland of Cities: Deltaic Landscapes and the Evolution of Early Mesopotamian Civilization. PhD Dissertation, University of California San Diego.

Powell, M. A. 1992. "Timber Production in Presargonic Lagaš". Bulletin on Sumerian Agriculture 4: 99–122. ——1985. "Salt, Seed and Yields in Sumerian Agriculture: A Critique of the Theory of Progressive Salinization". Zeitschrift für Assyriologie 75: 7–38.

Reculeau, H. 2015. "Middle Assyrian Agrarian Management in theWest in the Light of its Forerunners" in B. S. Düring, ed. Understanding Hegemonic Practices ofthe Early Assyrian Empire. Publications de l'Institut Historique-Archéologique Néerlandaise de Stamboul 125. Leiden: Nederlands Instituut voor het Nabije Oosten, pp. 199–219.

—— 2011. Climate, Environment and Agriculture in Assyria in the 2nd half of the 2nd Millennium BCE. Wiesbaden: Harrassowitz.

——2008. "Late Bronze Age Rural Landscapes ofthe Euphrates According to the Emar Texts" in L. d'Alfonso, Y. Cohen and D. Sürenhagen. eds. The City ofEmar Among the Late Bronze Age Empires. Alter Orient und Altes Testament 349. Münster: Ugarit Verlag, pp. 129–140.

Reimer, P. J, E. Bard, A. Bayliss, J. W. Beck, P. G. Blackwell, C. B. Ramsey, C. E. Buck. 2013. "IntCal13 and Marine13 Radiocarbon Age Calibration Curves 0–50,000 Years Cal BP." Radiocarbon 55 (04): 1869–87.

Roberts, N., J. Woodbridge, A. Bevan, A. Palmisano, S. Shennan and `E. Asouti. 2018. "Human responses and non-responses to climatic variations during the last glacial-interglacial transition in the eastern Mediterranean". Quaternary Science Reviews 184: 47–67.

Roberts, N., W. J. Eastwood, C. Kuzucuoğlu, G. Fiorentino and V. Caracuta. 2011. "Climatic, Vegetation and Cultural Change in the Eastern Mediterranean During the Mid-Holocene Environmental Transition". The Holocene 21(1): 147–162.

Rosen, A. M. 2005. "Phytolith Indicators of Plant and Landuse at Catalhoyuk" in I. Hodder, ed. Inhabiting Catalhoyuk: Reports from the 1995–99 Seasons. London and Cambridge: McDonald Institute for Archaeological Research and British Institute of Archaeology at Ankara, pp. 203–212.

Rosen, A. M. and S. Weiner. 1994. "Identifying Ancient Irrigation: A New Method Using Opaline Phytoliths from Emmer Wheat". Journal ofArchaeological Science 21(1): 125–32.

Rosen, A. M. 1992. "Preliminary Identification of Silica Skeletons from Near Eastern Archaeological Sites: An Anatomical Approach" in G.R. Rapp, S.C. Mulholland, eds. Plenum Press: New York, pp. 129–147.

Rost, S. 2015. Watercourse Management and Political Centralization in Third-millennium B.C. Southern Mesopotamia: A Case study of the Umma Province of the Ur III period (2112–2004 B.C.). PhD Dissertation, State University of New York at Stony Brook, New York.

Sallaberger, W. 1999. "Ur III-Zeit" in W. Sallaberger and A. Westenholz, eds. Mesopotamien: Annäherungen 3, Akkade-Zeit und Ur III-Zeit. Orbis Biblicus et Orientalis 160/3. Freiburg Schw.; Göttingen: Universitätsverlag; Vandenhoeck & Ruprecht, pp. 119–390.

Schrakamp, I. 2017. Das Bewässerungssystem des Präsargonischen Staates von Lagaš (ca. 2475-2310 v. Chr.). Habilitationsschrift, Freie Universität Berlin.

—— 2015. "Geographical Horizons of the Presargonic and Sargonic Archives" in W. Sallaberger and I. Schrakamp, eds. Associated Regional Chronologies for the Ancient Near East and the Eastern Mediterranean 3. Turnhout: Brepols, pp. 197–270.

Selz, G. 2011. "Zur Holzwirtschaft im Altsumerischen Lagaš" in L. Vacín, ed. U4 du11-ga-ni sa2 mu-ni-ib2-du11: Ancient Near Eastern Studies in Memory ofBlahoslav Hruška. Dresden: Islet Verlag, pp. 213–246.

Sharifi, A., A. Pourmand, E. A. Canuel, E. Ferer-Tyler, L. C. Peterson, B. Aichner and H. A. Lahijani. 2015. "Abrupt Climate Variability Since the Last Deglaciation Based on a High-Resolution, Multi-Proxy Peat Record from NW Iran: The Hand that Rocked the Cradle of Civilization?" Quaternary Science Reviews 123: 215–230.

Stein, G. J. 2012. "The Development ofIndigenous Social Complexity in Late Chalcolithic Upper Mesopotamia in the 5th-4th millennia BC – An Initial Assessment. Origini 24(5): 115–142.

Strömberg, C. A. E. 2009. "Methodological Concerns for Analysis of Phytolith Assemblages: Does Count Size Matter?" Quanternary International 193: 124–140.

Vanderroost, N. 2012. Organisation Administrative du Bureau de l'Agriculture d'Umma à l'Époque de la Troisième Dynastie d'Ur. Ph.D., Faculté de Philosophie et Lettres, Université Libre de Bruxelles.

Verhoeven, K. 1998. "Geomorphological Research in the Mesopotamia Plain" in H. Gasche and M. Tanret, eds. Changing Watercourses in Babylonia: Towards a Reconstruction ofthe Ancient Environment in Lower Mesopotamia. Chicago: Oriental Institute University of Chicago, pp. 159–204.

Wilkinson, T. J. 2003. Archaeological Landscapes ofthe Near East. Tucson: University of Arizona Press. Wilkinson, T.J. 1990. "Early Channels and Landscape Development around Abu Salabikh, a Preliminary Report". Iraq 52: 75–83.

Wright, H. 1980. "Problems of Absolute Chronology in Protohistoric Mesopotamia". Paléorient 6: 93–98. Ziegler, N. and A.-I. Langlois (avec la collaboration de J. Patrier et A. Jacquet). 2016. Les Toponymes Paléo- Babyloniens de la Haute-Mésopotamie. Materialien zu Toponyme und Topographie I/2 [online]. Paris: Collège de France.

Zohary, D., M. Hopf and E. Weiss. 2013. Domestication of Plants in the Old World: The Origin and Spread of Domesticated Plants in South-West Asia, Europe and the Mediterranean Basin. Oxford: Oxford University Press.

B.3. Main controls on the stable carbon isotope composition of speleothems

Fohlmeister, J., Voarintsoa, N.R.G., Lechleitner, F.A., Boyd, M., Brandtstätter, S., **Jacobson, M.J.**, Oster, J.L., 2020. Main controls on the stable carbon isotope composition of speleothems. Geochimica et Cosmochimica Acta 279, 67–87. https://doi.org/10.1016/j.gca.2020.03.042

Available online at www.sciencedirect.com

ScienceDirect

Geochimica et Cosmochimica Acta 279 (2020) 67–87

Geochimica et Cosmochimica Acta

Main controls on the stable carbon isotope composition of speleothems

Jens Fohlmeister [a,b,*], Ny Riavo G. Voarintsoa [c], Franziska A. Lechleitner [d,i], Meighan Boyd [e], Susanne Brandtstätter [f], Matthew J. Jacobson [g], Jessica L. Oster [h]

[a]Potsdam Institute for Climate Impact Research, Telegrafenberg, 14473 Potsdam, Germany

[b]GFZ German Research Centre for Geosciences, Section 'Climate Dynamics and Landscape Development', Telegrafenberg, 14473 Potsdam, Germany

[c]Department of Earth and Environmental Sciences, Katholieke Universiteit Leuven, Leuven, Belgium

[d]Department of Earth Sciences, University of Oxford, South Parks Road, Oxford OX1 3AN, UK

[e]Department of Earth Sciences, Royal Holloway University of London, Egham TW20 0EX, UK

[f]Institute of Geology, University of Innsbruck, Innrain 52, 6020 Innsbruck, Austria

[g]Department of Archaeology and Centre for Past Climate Change, University of Reading, Reading RG6 6UR, UK

[h]Department of Earth and Environmental Sciences, Vanderbilt University, Nashville, TN 37240, USA

[i]Department of Chemistry and Biochemistry, University of Bern, Freiestrasse 3, 3012 Bern, Switzerland

Received 30 July 2019; accepted in revised form 29 March 2020; available online 6 April 2020

Abstract

The climatic controls on the stable carbon isotopic composition ($\delta^{13}C$) of speleothem carbonate are less often discussed in the scientific literature in contrast to the frequently used stable oxygen isotopes. Various local processes influence speleothem $\delta^{13}C$ values and confident and detailed interpretations of this proxy are often complex. A better understanding of speleothem $\delta^{13}C$ values is critical to improving the amount of information that can be gained from existing and future records. This contribution aims to disentangle the various processes governing speleothem $\delta^{13}C$ values and assess their relative importance. Using a large data set of previously published records we examine the spatial imprint of climate-related processes in speleothem $\delta^{13}C$ values deposited post-1900 CE, a period during which global temperature and climate data is readily available. Additionally, we investigate the causes for differences in average $\delta^{13}C$ values and growth rate under identical climatic conditions by analysing pairs of contemporaneously deposited speleothems from the same caves. This approach allows to focus on carbonate dissolution and fractionation processes during carbonate precipitation, which we evaluate using existing geochemical models. Our analysis of a large global data set of records reveals evidence for a temperature control, likely driven by vegetation and soil processes, on $\delta^{13}C$ values in recently deposited speleothems. Moreover, data-model intercomparison shows that calcite precipitation occurring along water flow paths prior to reaching the top of the speleothem can explain the wide $\delta^{13}C$ range observed for concurrently deposited samples from the same cave. We demonstrate that using the combined information of contemporaneously growing speleothems is a powerful tool to decipher controls on $\delta^{13}C$ values, which facilitates a more detailed discussion of speleothem $\delta^{13}C$ values as a proxy for climate conditions and local soil-karst processes.

Keywords: Stable carbon isotopes; Speleothems; SISAL; Vegetation; Temperature; Rayleigh modelling approach; Prior calcite precipitation

* Corresponding author at: Potsdam Institute for Climate Impact Research, Telegrafenberg, 14473 Potsdam, Germany.

E-mail address: jens.fohlmeister@pik-potsdam.de (J. Fohlmeister).

1. INTRODUCTION

Speleothems, secondary cave carbonates, are valuable archives for reconstructing past climate conditions (e.g., Wong and Breecker, 2015). Of the various geochemical parameters they preserve, speleothem $\delta^{13}C$ values can provide information on climate and vegetation conditions (e.g., McDermott, 2004; Ridley et al., 2015). However, it is often difficult to disentangle the various processes that influence speleothem $\delta^{13}C$ values, especially as some may be interdependent (e.g., vegetation type/density and rainfall amount/moisture availability). This complexity poses a significant challenge for the accurate interpretation of speleothem $\delta^{13}C$ values, and often limits its utility as a paleoclimate proxy to generalised discussions on overall conditions or broad vegetative transitions (e.g., Genty et al., 2003; Holmgren et al., 2003). However, in some cases $\delta^{13}C$ time series proved to be easier to interpret than corresponding $\delta^{18}O$ time series, in particular at sites where $\delta^{18}O$ is affected by multiple and competing effects (e.g., Genty et al., 2003, 2006; Scholz et al., 2012; Ridley et al., 2015; Mischel et al., 2017).

Although carbon transfer dynamics in cave systems have been extensively studied (e.g., Hendy, 1971; Genty et al., 1998; Oster et al., 2010; Fohlmeister et al., 2011; Rudzka et al., 2011; Lechleitner et al., 2016; Mattey et al., 2016; Bergel et al., 2017; Carlson et al., 2019), it is difficult to attribute individual processes as the driving force behind speleothem $\delta^{13}C$ variations (Griffiths et al., 2012; Spötl et al., 2016). The $\delta^{13}C$ composition of soil gas CO_2 is influenced by the type and density of vegetation above the cave, depending on the dominant photosynthetic pathway (C3, C4 or CAM plants), and by soil respiration rate (e.g., Cerling, 1984). The soil gas CO_2 is dissolved in percolating meteoric water, introducing a temperature-dependent fractionation effect on $\delta^{13}C$. This acidic water dissolves the underlying host rock carbonate until the solution is in equilibrium with respect to Ca^{2+}. The dissolution can occur under ''open" conditions, where enough gaseous CO_2 is available in the soil or karst to allow for complete carbon exchange with the dissolved inorganic carbon species, or under ''closed" conditions, where no gaseous CO_2 is present and carbon exchange is absent (Hendy, 1971). Intermediate conditions generally prevail in natural systems as often only a limited amount of gaseous CO_2 is available (e.g., Genty et al.,1998; Rudzka et al., 2011). Once the solution reaches the cave atmosphere with lower partial pressure of CO_2 (pCO_2), CO_2 starts to degas from the solution,

triggering $CaCO_3$ precipitation. This process is accompanied by temperature dependent carbon isotope fractionation processes, which have been largely investigated by modelling studies (Dreybrodt et al., 2016; Dreybrodt and Scholz, 2011; Hansen et al., 2017; Mühlinghaus et al., 2009; Scholz et al., 2009) and laboratory studies (e.g., Polag et al., 2010; Wiedner et al., 2008; Hansen et al., 2019). Carbonate precipitation occurring before reaching the apex of the stalagmite is known as prior calcite precipitation (PCP) or, more rarely, prior aragonite precipitation. The degree of PCP usually depends on two parameters: (I) on the pCO_2 gradient between the water and the gaseous phase and (II) on length of the period the water in contact with the cave air before dripping.

There are several approaches to better constrain speleothem $\delta^{13}C$ variability. First, applying a multi-proxy approach that considers other proxies than $\delta^{13}C$, such as $\delta^{18}O$, radiocarbon or trace elements, and mineralogy or petrography, can shed light on the dominant processes that influence $\delta^{13}C$ variability in a given cave system (e.g., Oster et al., 2010; Rudzka et al., 2011; Griffiths et al., 2012; Fohlmeister et al., 2017; Voarintsoa et al., 2017c). Often, interpreting speleothem $\delta^{13}C$ values requires critical knowledge about the cave system, including potential anthropogenic impacts (e.g., Baldini et al., 2005; Mattey et al., 2008, 2010; Hartmann et al., 2013; Burns et al., 2016; Voarintsoa et al., 2017c). A second approach lies in the investigation of the acting processes through analysis of a large and spatially extensive network of speleothem records (Breecker, 2017). This has the potential to remove highly localised, site-specific variability, and allow detection of more general relationships between speleothem $\delta^{13}C$ composition and climate or ecosystem conditions.

Here, we use speleothem $\delta^{13}C$ records compiled in the first version of the SISAL database (Atsawawaranunt et al., 2018a,b), henceforth denoted SISAL_v1. This database was compiled to provide a comprehensive understanding of speleothem $\delta^{18}O$ and $\delta^{13}C$ records for climate reconstruction and model evaluation (e.g., Comas-Bru et al., 2019). From this database, several papers have already been published that assess data coverage and investigate regional patterns in stalagmite $\delta^{18}O$ records from specific regions and continents (e.g., Lechleitner et al., 2018; Oster et al., 2019; Braun et al., 2019; Burstyn et al., 2019; Appendix B.1). To constrain the governing processes influencing speleothem $\delta^{13}C$ values in the SISAL records we focus on two subsets of the data of the SISAL_v1 database. First, we analyse globally distributed records that cover the period between

1900 and 2014 CE (hereafter denoted post- 1900 CE), to investigate the spatial relationship between $\delta^{13}C$ and climate by comparing the speleothem records with available instrumental data. Second, we analyse records from contemporaneously growing speleothems from the same cave to shed light on karst and cave processes and to evaluate the utility of Rayleigh isotope fractionation models (e.g., Deininger et al., 2012; Deininger and Scholz, 2019) for understanding speleothem $\delta^{13}C$ records.

2. THE SISAL_V1 DATA

2.1. Post- 1900 CE speleothem $\delta^{13}C$ data

We extracted $\delta^{13}C$ data of all speleothems that grew after 1900 CE from SISAL_v1, resulting in 59 speleothem records from 50 individual caves (Table 1) and yielding about 3600 individual $\delta^{13}C$ measurements. Three speleothems have only one data point in the according time window, but were nonetheless included in the analysis. The record with the highest number has 659 data points (stalagmite YOK-G, Ridley et al., 2015).

2.2. Speleothem $\delta^{13}C$ data from contemporaneous samples

The second data sub-set extracted from SISAL_v1 com-prises speleothems which grew at the same time in the same cave for at least 20 consecutive years, without upper limitations on the time period of growth. In total, 94 speleothems from 32 caves fulfil this requirement (Table 2). Up to seven at least pairwise coevally growing speleothems from a single cave are available. With our search criteria we extracted approximately 57,000 individual $\delta^{13}C$ data points. For each data point we also extracted its depth along the speleothem profile and its age.

The shortest time period of overlap is about 100 years for Rukiessa Cave (Baker et al., 2007) and the longest period of overlap is for the Kesang Cave (Cheng et al., 2016), where stalagmites grew contemporaneously for about 50000 years. Most stalagmite pairs grew contemporaneously for 1000– 10000 years. The number of $\delta^{13}C$ data points per stalagmite in coeval growth phases is between 7 (Paraiso Cave; Wang et al., 2017) and more than 3500 (Yok Balum Cave, Ridley et al., 2015). Most stalagmites provide data between 100 to 300 data points for the coeval growth phases.

Table 1
Speleothem $\delta^{13}C$ records growing after 1900 CE extracted from SISAL_v1. Speleothems marked by an (*) consist of aragonite. Column 'Comments on dating': number of U-Th dating points in the post 1900 CE period/ actively dripping or layer counting (LC)/evidence through radiocarbon bomb peak detection (14C-BPD) or ^{210}Pb dating.

Cave	Speleothem	number of data point	$\delta^{13}C$	MAT [°C]	Precipitation [mm/a]	Altitude [m asl]	Comments on dating	reference
Anjohibe Cave	AB3	12	3.38	27.2	1496	100	1/-/-	Burns et al., 2016
Anjohibe Cave	AB2	191	3.49	27.2	1496	100	1/-/-	Scroxton et al., 2017
Ascunsa Cave	POM2	2	-10.37	8.2	600	1050	0/dripping/-	Dragusin et al., 2014
Bero Cave	Bero-1	135	-4.61	18.9	1030	1363	0/LC/14C-BPD	Asrat et al., 2008
Bir-Uja Cave	Keklik1	58	-4.89	12.1	353	1325	0/-/14C-BPD	Fohlmeister et al., 2017
Botuverá Cave	BT-2	1	-6.16	19.5	1300	230	0/-/-	Cruz et al., 2005
Brown's Follymine	Boss	17	-9.63	10	842	150	0/LC/-	Baldini et al., 2005
Brown's Follymine	BFM-9	12	-9.31	10	842	150	0/LC/14C-BPD	Baldini et al., 2005
Brown's Follymine	F2	17	-8.83	10	842	150	0/LC/-	Baldini et al., 2005
Bunker Cave	Bu4	8	-5.86	10.8	950	184	0/-/14C-BPD	Fohlmeister et al., 2012
Cango Cave	V3	2	-6.32	17.5	172	650	0/dripping/-	Talma and Vogel, 1992
Ceremosnja Cave	CC-1	3	-7.84	11.6	695	530	0/dripping/-	Kacinski et al., 2001
Cold Air Cave	T8	13	-6.09	17.3	521	1420	0/-/-	Holmgren et al., 2008
Cold Air Cave	T7_2013	106	-7.12	17.3	521	1420	1/LC/14C-BPD	Sundquist et al., 2013
Crag Cave	CC3	2	-7.41	10.5	1475	60	0/-/-	McDermott et al., 1999
Dante Cave	DP1_2016	31	-10.70	21	532	1300	2/-/-	Voarintsoa et al., 2017
Defore Cave	S3	83	-10.16	25.7	500	150	0/LC/-	Burns, 2002
DeSoto Caverns	DSSG-4	33	-9.50	17.4	1406	170	0/-/-	Aharon et al., 2013
Furong Cave	FR-0510	9	-5.32	18.3	1086	260	0/-/-	Li et al., 2011
Guillotine Cave	GT05-5	9	-9.23	9.6	2400	740	0/-/-	Whittaker, 2008
Han-sur-Lesse Cave	Han-stm5b	15	-9.37	8.9	787	180	0/LC/14C-BPD	Genty et al., 1998
Heshang Cave	HS4_2008	102	-12.08	18	1460	694	0/LC/14C-BPD	Hu et al., 2008

Ifoulki Cave	IFK1	66	-7.93	17	400	1265	1/-/-	Ait Brahim et al., 2017
Jhumar Cave	JHU-1	70	-11.92	25.5	1503	600	1/-/-	Sinha et al., 2011
Kesang Cave	KS08-1-H	2	-6.20	4.5	500	2000	0/-/-	Cheng et al., 2016
Kinderlinskaya Cave	KC-3	2	-8.16	3	560	240	0/-/-	Baker et al., 2017
Klapferloch Cave	PFU6	38	-2.54	4.8	600	1140	0/LC/-	Boch and Spötl, 2011
Korallgrottan Cave	K11	5	-6.25	1.4	866	600	0/-/-	Sundqvist et al., 2010
Leviathan Cave	LC-1	3	-4.18	8.3	106	2400	0/-/-	Lachniet et al., 2015
Liang Luar Cave	LR06-B1_2016	58	-9.90	25	1200	550	1/-/14C-BPD	Griffiths et al., 2016
Macal Chasm	MC01	15	-11.02	21	2095	550	0/active/210Pb	Webster et al., 2007
Modric Cave	MOD-22	6	-7.25	16	960	32	0/dripping/-	Rudzka et al., 2012
Munagamanu Cave	Mun-stm2	44	-5.72	27.6	526	475	1/-/-	Genty et al., unpublished
Munagamanu Cave	Mun-stm1	21	-4.29	27.6	526	475	2/-/-	Genty et al., unpublished
Natural Bridge Caverns	NBJ	6	-7.71	21	740	315	0/-/-	Wong et al., 2015
New St Michael's Cave	Gib04a	443	-11.04	18.3	767	426	0/LC/14C-BPD	Mattey et al., 2008
Okshola Cave	FM3	2	-6.56	3.2	1000	165	0/-/-	Linge et al., 2009
Palestina Cave	PAL3	10	-11.40	22.8	1570	870	0/-/-	Apaéstegui et al., 2014
Paraiso Cave	PAR03	19	-8.97	26	2400	60	2/-/-	Wang et al., 2017
Perdida Cave	PDR-1	86	-5.53	27.3	1375	400	0/active/-	Winter et al., 2011
Postojna Cave	POS-STM-4	10	-9.59	8	1500	529	0/event/14C-BPD	Genty et al., 1998
Rukiessa Cave	Merc-1	84	-5.15	18.9	1030	1618	0/LC/14C-BPD	Baker et al., 2007
Rukiessa Cave	Asfa-3	83	-6.44	18.9	1030	1618	0/LC/14C-BPD	Baker et al., 2007
Sahiya Cave	SAH-AB	110	0.24	22	1600	1190	1/-/-	Sinha et al., 2015
Sofular Cave	So-1	56	-9.57	13.8	1200	400	0/-/-	Fleitmann et al., 2009
Soreq Cave	Soreq-	20	-10.17	20	500	400	0/-/-	Grant et al., 2012

	composite							
Soylegrotta Cave	SG95	4	-3.60	3.5	1450	280	0/-/-	Linget al., 2001
Tamboril Cave	TM0	10	-11.09	22.5	1400	575	1/-/-	Wortham et al., 2017
Taurius Cave	Taurius	293	-11.71	26	2735	230	4/-/210Pb	Partin et al., 2013
Tonnelnaya Cave	TON-2	2	1.38	3.1	355	3226	0/-/-	Cheng et al., 2016
Uamh an Tartair	SU967	39	-11.16	7.1	1900	220	-/LC/-	Baker et al., 2012
Uamh an Tartair	SU032	101	-11.89	7.1	1900	220	-/LC/-	Baker et al., 2011
Ursilor Cave	PU-2	1	-10.81	9.7	950	482	0/-/-	Onac et al., 2002
Villars Cave	Vil-stm6	1	-9.06	12.5	1005	175	0/-/-	D. Genty, unpublished
Villars Cave	Vil-stm1	21	-8.56	12.5	1005	175	0/LC/14C-BPD	Labuhn et al., 2015
Wah Shikhar Cave	WS-B	72	-2.59	17	2150	1290	0/-/-	Sinha et al., 2011
Xinya Cave	XY07-8	75	-4.74	16.1	1130	1250	0/dripping/-	Li et al., 2017
Yok Balum Cave	YOKI	174	-9.86	22.9	2950	366	3/-/14C-BPD	Kennett et al., 2012
Yok Balum Cave	YOKG	659	-10.52	22.9	2950	366	6/-/14C-BPD	Ridley et al., 2015

3. METHODS

3.1. Climate influence on speleothem $\delta^{13}C$

We analyse the SISAL_v1 $\delta^{13}C$ dataset covering the period post-1900 CE and compare it to instrumental climate data to investigate the influence of temperature, rainfall amount, altitude or vegetation on speleothem $\delta^{13}C$ values. We calculate the average $\delta^{13}C$ value and its variance, to prevent over-interpretation of individual $\delta^{13}C$ values that may contain temporally restricted outliers. As carbon isotope fractionation effects are different for aragonite and calcite, the $\delta^{13}C$ values of aragonitic speleothems (Table 2) were corrected to the corresponding $\delta^{13}C$ value of calcite by using the fractionation offset between both polymorphs established in a laboratory study (Romanek et al., 1992). This fractionation offset was recently confirmed by a speleothem study, where calcite-aragonite transitions occurred along individual growth layers (Fohlmeister et al., 2018).

Climate data, i.e., present-day mean annual temperature, rainfall amount, and altitude (Table 1), were obtained either directly from the original papers or - where necessary - from companion papers reporting on the same cave. Vegetation data is derived from SPOT-VEGETATION satellite imagery from the Global Land Cover 2000 Project (GLC2000), used in Aaron and Gibbs (2008). The data, available online from the Carbon Dioxide Information Analysis Center (http://cdias.ess-dive.lbl.gov), were imported to ArcGIS 10.5 as shapefile, and plotted using the coordinate reference system WGS-84. To ease comparison with speleothem $\delta^{13}C$ averages, we grouped each polygon based on vegetation cover categories (e.g., steppe, dry forest, shrub land, rainforest). The average speleothem $\delta^{13}C$ values were binned into 1‰ increments, yielding ten categories, ranging from data lower than -11.00‰ VPDB (Vienna PeeDee Belemnite) to data higher than -3.00‰ VPDB.

It is important to note that age uncertainties related to either U-Th dating uncertainties and/or interpolation techniques may complicate interpretation of the results from this study. To address this, however, we have tested how chronological uncertainty may influence $\delta^{13}C$ values, by calculating the $\delta^{13}C$ averages of the last 100 years (i.e., back to 1919 CE), in comparison with the interval back to 1900 CE (our initial boundary set for this study). This 19-year change in the applied time interval refers to a change in relative age uncertainty of 16% and thus well represents the

typical U-Th derived age uncertainty during this period. This simple test suggests that the average $\delta^{13}C$ values did not change by more than 0.1‰ between the two intervals studied. Therefore, we presume that chronological uncertainty is insignificant at this temporal scale.

3.2. Influence of local processes on speleothem $\delta^{13}C$ values

The investigation of karst and fractionation processes during $CaCO_3$ dissolution and precipitation is more technical. Contemporaneously growing speleothems from the same cave were used on the assumption that temperature, rainfall amount and vegetation above the cave should influence their $\delta^{13}C$ value in a similar way. In that case, any variability in $\delta^{13}C$ values between individual speleothems must be related to the conditions under which carbonate is dissolved and precipitated.

To explore this, we use the second dataset extracted from SISAL_v1, and calculate the average growth rate along with the average and standard deviation of $\delta^{13}C$ of contemporaneous growth sections in the speleothems. For the growth rate, the standard deviation could not be calculated as unfortunately most SISAL_v1 records lack information on interpolated age uncertainties. Where speleothems from individual caves exist in calcitic and aragonitic form, we correct for calcite-aragonite fractionation effects using present-day cave temperatures, as all specimens that needed to be corrected are of late Holocene age. Those speleothems are marked by (**) in Table 2.If all speleothems from one cave consist entirely of aragonite (marked (*) in Table 2), we performed no correction for fractionation effects. Some isotope samples were referred to as consisting of a ‘mixed’ mineralogy in SISAL. Those samples were removed from the data set.

3.2.1. Influence of carbonate dissolution conditions

Different pathways of carbonate dissolution affect the carbon isotope composition of drip water (Hendy, 1971; Fohlmeister et al., 2010; Minami et al., 2015). Carbonate dissolution conditions can be similar in the same cave for the same time period, as deduced by radiocarbon reservoir effects of contemporaneously growing speleothems from the same cave (e.g., Fohlmeister et al., 2012; Lechleitner et al., 2016; Cheng et al., 2018; Riechelmann et al., 2019). Furthermore, modelling

studies have shown that slight differences in carbonate dissolution conditions have only a small effect on $\delta^{13}C$ values (Hendy, 1971; Fohlmeister et al., 2011; Griffiths et al., 2012). This was recently corroborated by a study on speleothems from Baradla Cave, Hungary (Demény et al., 2017b), where large differences in open to closed dissolution system conditions (10 pmC difference in radiocarbon) had nearly no appreciable effect on $\delta^{13}C$ values.

Here, we further test the influence of carbonate dissolution on $\delta^{13}C$ composition using CaveCalc, a recently developed model for speleothem chemistry and isotopes (Owen et al., 2018). CaveCalc is a numerical model based on PHREEQC, and importantly allows direct quantitative modelling of semi-open dissolution conditions (Owen et al., 2018). Thus, we can test the sensitivity of drip water $\delta^{13}C$ values to system ''openness" by varying the volume of soil gas the aqueous solution is in contact with during dissolution (the larger the volume of air, the more open the system).

Table 2
$\delta^{13}C$ records from speleothems growing contemporaneously in the same cave from SISAL_v1. The records are grouped by cave, and the number of overlapping samples is indicated

Cave	Stalagmites	Number of overlap (#)	Reference
Abaco Island Cave	AB-DC-01, AB-DC-03, AB-DC-09	2	Arienzo et al., 2017
Abaliget Cave	ABA_1, ABA_2	1	Koltai et al., 2017
Anjohibe Cave	AB3, AB2, MA3, ANJB-2	6	Scroxton et al., 2017; Voarintsoa et al., 2017b,c; Burns et al., 2016
Antro del Corchia	CC-1_2009, CC-5_2009, CC-7	2	Drysdale et al., 2009
Baradla Cave	BAR-IIL,BAR-IIB	1	Demény et al., 2017
Bittoo Cave	BT-1, BT-2.1, BT-2.2	2	Kathayat et al., 2016
Botuverá Cave	BTV21a, BT-2	1	Bernal et al., 2016; Cruz et al., 2005
Brown's Follymine	Boss, F2, BFM-9	3	Baldini et al., 2005
Buckeye Creek	BCC-8, BCC-10	1	Springer et al., 2014
Bunker Cave	Bu1, Bu2, Bu4, Bu6	3	Fohlmeister et al., 2012
Devils Hole	DH2, DH2-D, DH2-ETerminal1, DH2-ETerminal2	3	Moseley et al., 2016
Dim Cave	Dim-E2, Dim-E3, Dim-E4	3	Ünal-İmer et al., 2015

Gueldaman Cave	stm2, stm4	1	Ruan et al., 2016
Katerloch Cave	K1, K3	1	Boch et al., 2009
Kesang Cave	KS06-A-H, KS08-2-H, KS06-A, KS06-B, KS08-1, KS08-2,	5	Cheng et al., 2016
Kinderlinskaya Cave	KC-1, KC-3	1	Baker et al., 2017
Lancaster Hole	LH-70s-1, LH-70s-2, LH-70s-3	3	Atkinson and Hopley, 2013; Atkinson and Hoffmann, unpubl.
Liang Luar Cave	LR07-A8, LR07-A9, LR07-E11, LR06-B1_2016, LR06-B3_2016	4	Griffiths et al., 2013; 2016
Mairs Cave	MC-S1, MC-S2	1	Treble et al., 2017
Milchbach Cave	MB-2, MB-3, MB-5	3	Luetscher et al., 2011
Molinos Cave	Mo-1, Mo-7	1	Moreno et al., 2017
Munagamanu Cave	Mun-stm1, Mun-stm2	1	Genty et al., unpubl.
Okshola Cave	FM3, Oks82	1	Linge et al., 2009
Palestina Cave	PAL3, PAL4	1	Apaéstegui et al., 2014
Paraiso Cave	PAR01, PAR03, PAR06, PAR07, PAR08, PAR16, PAR24	7	Wang et al., 2017
Rukiessa Cave	Merc-1, Asfa-3	1	Baker et al., 2007
Tamboril Cave	TM0, TM2	1	Worthham et al., 2017
Tonnel'naya Cave	TON-1, TON-2	1	Cheng et al., 2016
Uamh an Tartair	SU967, SU032	1	Baker et al., 2011; 2012
Villars Cave	Vil-stm1, Vil-stm6, Vil-stm9, Vil-stm11, Vil-stm14, Vil-stm27, Vil-car1	11	Labuhn et al., 2015; Wainer et al., 2011; Genty et al., 2003; 2006; 2013; Genty, unpubl.;
Yok Balum Cave	YOK-I, YOK-G	1	Kennett et al., 2012; Ridley et al., 2015
Zhuliuping Cave	ZLP1, ZLP2	1	Huang et al., 2016

3.2.2. Influence of $CaCO_3$ precipitation processes on $\delta^{13}C$ values

Fractionation effects during degassing of CO_2 and carbonate precipitation (including PCP) can lead to substantial variability in speleothem $\delta^{13}C$ values. We assume that temperature, vegetation cover and carbonate dissolution conditions are sufficiently similar for drip sites feeding two or more speleothems from the same cave as long as the cave system is not too large. Thus, we expect the pCO_2 in equilibrium with initial drip water to be similar for individual drip locations. Here, initial drip water refers to water that has just achieved Ca^{2+} saturation following dissolution of the carbonate host rock, but where no CO_2 has degassed and no carbonate has yet been precipitated. As most stalagmites in our dataset grew in the deep interior of the cave (>100 m distance from any entrance) or close to each other (>5 m distance), when nearer to the entrance, it is also reasonable to assume that the pCO_2 level of air is sufficiently constant within the cave. Keeping these assumptions in mind, the only sources of variability in $\delta^{13}C$ data of coevally growing speleothems should be the drip interval and the presence/extent of PCP, the latter defining the degree of supersaturation of $[Ca^{2+}]$ in the solution reaching the top of the speleothem. These two factors also strongly affect growth rate (e.g., Kaufmann, 2003; Mühlinghaus et al., 2007; and Romanov et al., 2008). Once drip water is in equilibrium with cave air CO_2 levels, which takes only a few seconds (Dreybrodt and Scholz, 2011; Day and Henderson, 2011), a faster speeothem growth rate requires a shorter drip interval. Furthermore, speleothems with a higher growth rate should have lower $\delta^{13}C$ values as the time for isotopic enrichment of the dissolved inorganic carbon (DIC) and the precipitating $CaCO_3$ is reduced. Thus, we expect a $\delta^{13}C$ offset in contemporaneously growing speleothems with different growth rates. We can quantify this offset by calculating the slope between $\delta^{13}C$ average and average growth rate for two contemporaneously growing speleothems from the same cave. According to the above argument the slope is expected to be negative, given that the initial conditions are similar.

The growth rate– $\delta^{13}C$ offsets obtained from speleothem data were evaluated by first principles of carbonate precipitation and carbon isotope fractionation. We applied a Rayleigh distillation model for $\delta^{13}C$ and an exponential approach for carbonate precipitation, closely following the ISOLUTION modelling approach (Deininger et al., 2012; Deininger and Scholz, 2019). The Ca^{2+} concentration at time t, $[Ca^{2+}](t)$, after the solution is in contact with CO_2,

decreases progressively and can be approximated by an exponential decay (e.g., Dreybrodt, 1980).

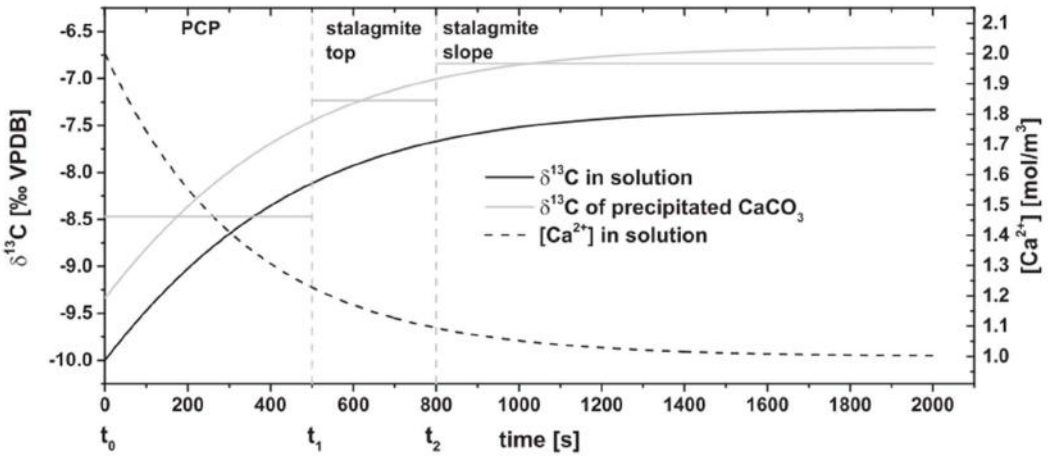

Fig. 1. Evolution of $\delta^{13}C$ and $[Ca^{2+}]$ in drip water and the respective $\delta^{13}C$ composition of precipitated $CaCO_3$ at 20 °C. Between t_0 and t_1, the water evolves before the droplet reaches the stalagmite top (PCP). Between t_1 and t_2 (dashed grey lines) carbonate precipitation at the top of the speleothem occurs. After t_2, carbonate precipitation takes place along the slopes of the stalagmite, when the drop has been replaced by a new one. The horizontal solid grey lines indicate the average $\delta^{13}C$ isotopic composition of $CaCO_3$ at those three stages.

$$[Ca^{2+}](t) = ([Ca^{2+}](t_0) - [Ca^{2+}]_{app})exp(-t/\tau) + [Ca^{2+}]_{app}\ in\ moles/m^3 \quad (1)$$

where $[Ca^{2+}](t_0)$ is the initial Ca^{2+} concentration before any carbon is lost from the solution ($t = t_0 = 0$). $[Ca^{2+}]app$ is the Ca^{2+} concentration in equilibrium with cave air pCO_2, modulated by inhibiting effects (Dreybrodt et al., 1997; Kaufmann, 2003). The time constant, s, refers to calcite precipitation rate.

The role of PCP on Eq. (1) is important. While in earlier approaches (Dreybrodt 2008; Mühlinghaus et al., 2009; Scholz et al., 2009; Deininger et al., 2012) carbonate precipitation at the top of a speleothem was considered to be important from t_0 to a time point t_1, we here use a different approach in order to account for PCP, which is an important process in most caves (e.g., Fairchild et al., 2000; Johnson et al., 2006; Sherwin and Baldini, 2011). In our approach, we define PCP to be acting from $t = t_0$ to $t = t_1$. At $t = t_1$ the droplet is falling onto the stalagmite top and is replaced by the next one at time $t = t_2$ (Fig. 1). Thus, for growth rate calculation purposes, we are only interested in the amount of calcite precipitating between t_1

and t_2. The amount of precipitated Ca^{2+} (F), between the two time points, t_1 and t_2, can be calculated by:

$$F = ([Ca^{2+}](t_1) - [Ca^{2+}](t_2)) \; in \; moles/m^3 \qquad (2)$$

The growth rate (GR) of a stalagmite can be determined by F, the typical thickness of the water film layer, R, which is in the order of 10^{-2} cm (e.g., Dreybrodt, 1980; Baker et al., 1998), the time interval of precipitation, $t_2 - t_1$, the density of precipitating calcite, rho (for calcite q = 2.689 g/cm^3) and the molecular weight, M, of $CaCO_3$ (100.09 g/mol). To express GR in cm/a we have to account for conversion factors (1a is $3.15*10^7$s and 1 m^3 =10^6 cm^3; Dreybrodt, 1980).

$$GR = R * F * M/\rho/(t_2 - t_1) * 3.15 * 10^7/10^6 \qquad (3)$$

The temporal evolution of the $\delta^{13}C$ of DIC in drip water ($\delta^{13}C$ (t)) is determined by:

$$\delta^{13}C(t) = ((\delta^{13}C(t_0)/1000 + 1) * ([Ca^{2+}](t)/[Ca^{2+}](t_0))^{\varepsilon} - 1) * 1000 \qquad (4)$$

where $\delta^{13}C$ (t_0) is the initial $\delta^{13}C$ of DIC in the drip water and e is the combined fractionation factor for 13C, composed from carbon fractionation factors for the transition between HCO^{3-} and gaseous CO_2 as well as between HCO^{3-} and $CaCO_3$ (e.g., Mühlinghaus et al., 2009; Deininger et al., 2012). In order to account for PCP, we do not integrate the $\delta^{13}C$ values of precipitated $CaCO_3$ from t = t_0 (the initial drip water) to t = t_1 but allow the solution to lose some carbon through degassing and precipitation before the drip impinges on the stalagmite top (Fig. 1). As for the $CaCO_3$ growth rate we focus on the $\delta^{13}C$ value of precipitating $CaCO_3$ at the top of the stalagmite between t = t_1 and t = t_2 and Eq. (4) is transferred to:

$$\delta^{13}C(t_2) = ((\delta^{13}C(t_1)/1000 + 1) * ([Ca^{2+}](t_2)/[Ca^{2+}](t_1))^{\varepsilon} - 1) * 1000 \qquad (5)$$

Therefore, the $\delta^{13}C$ composition of $CaCO_3$ precipitating at the stalagmite top (between t_1 and t_2, Fig. 1) is the weighted mean of the $\delta^{13}C$ of precipitating $CaCO_3$ and the amount of precipitated $CaCO_3$:

$$\delta^{13}C_{CaCO3}(t_1,t_2) = \sum \delta^{13}C(t_i') * F(t_i') / \sum F(t_i'), \qquad (6)$$

where t_0i =[t_1, t_1 +1, t_1 +2, ..., t_2].

4. RESULTS

4.1. Post-1900 CE speleothem $\delta^{13}C$ data

The speleothems in our dataset are from cave sites with an annual average air temperature ranging from 1 to 27 °C, average annual precipitation between 100 and 3000 mm, and altitude between 60 and 3100 m above sea level.

The average $\delta^{13}C$ values of speleothems vary between -12.1 and +3.5‰ VPDB. The minimum standard deviation of the average $\delta^{13}C$ is 0.11‰, and the maximum standard deviation is 2.5‰. To check for systematic trends towards lighter or heavier $\delta^{13}C$ values, which would complicate our analysis, we calculated the slope of $\delta^{13}C$ with time for each stalagmite record (Fig. 2A). While the mean of all records is slightly shifted towards a negative slope (-0.0035‰/a), the ensemble is nearly Gaussian distributed (Fig. 2B) with a standard deviation of 0.0177. This indicates that applying an ensemble approach can level out various local processes in individual cave environments.

4.2. Speleothem $\delta^{13}C$ values from contemporaneously growing speleothems

The average speleothem $\delta^{13}C$ values from this subset vary between ~-13‰ and ~+3, and average growth rates vary between ~$2*10^{-5}$ and 1 mm/a (Fig. 3A). The slopes vary between average $\delta^{13}C$ values and average growth rate of two contemporaneously growing speleothems reveal a bimodal distribution (Fig. 3B). This bimodal distribution is an artefact of the logarithmic scale, which however is necessary to show all data adequately. With the 94 speleothems extracted from the SISAL_v1 database we were able to calculate 76 $\delta^{13}C$ -growth rate slopes between coeval speleothems. 52 out of 76 slopes were negative, i.e., faster growing speleothems have lower $\delta^{13}C$ values, while 24 slopes were positive (Fig. 3A). The positive slopes can vary between 0.2 and 6200‰/(mm/a), while negative slopes span a range between -33000 and -0.1‰/(mm/a). The frequency maximum of the slopes is between 10 and 100‰/ (mm/a) for both positive and negative slopes (Fig. 3B).

In the next step, we defined a maximum duration of overlap. If the analysed interval of contemporaneous growth is too long, various environmental and cave parameters may have changed (even if in a similar manner for both speleothems) potentially complicating the interpretation. Thus, we split periods of contemporaneous growth of speleothems into periods of 1000 years. For example, when the duration of contemporaneous growth between two stalagmites is 10000 years, we divided this interval into ten phases and calculated the $\delta^{13}C$ -growth rate lines for each of the 10 phases instead of one slope for the entire 10000 year interval. This modification greatly increased the number of calculated slopes ($\delta^{13}C$ vs. growth rate, Fig. 3C). Encouragingly, the general $\delta^{13}C$ -growth rate relationship (i.e., the slope) is well reproduced even when using this larger dataset (Fig. 3C and D), and suggests that these relationships are robust at different timescales.

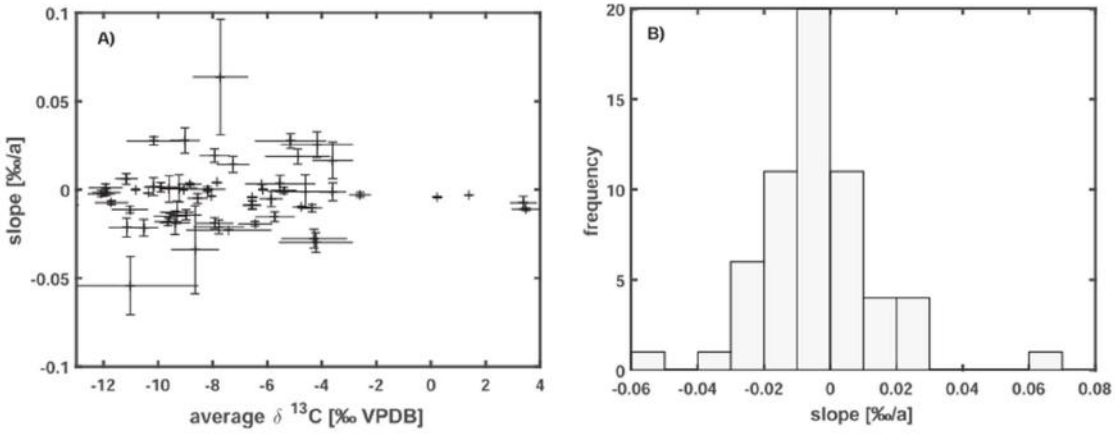

Fig. 2. (A) Slope ($\delta^{13}C$ /time) of speleothem $\delta^{13}C$ values for the post-1900 CE records in comparison to their average $\delta^{13}C$ composition. (B) Histogram showing the frequency distribution of the slope for individual speleothems.

5. DISCUSSION

5.1. Controls on modern speleothem $\delta^{13}C$ values

As speleothem $\delta^{13}C$ values can have a large biogenic component originating from vegetation and/or soil activity above the cave, we compare the average $\delta^{13}C$ values of modern speleothems (post-1900 CE) with instrumental climate and vegetation data. Although it is possible to convert each category of vegetation from the colour code on the map into numbers, defining the correlation factors or other statistical quantification of the

relationship between vegetation cover and speleothem $\delta^{13}C$ values is less reliable. The map resolution is too coarse to provide accurate correlation with the local vegetation at the cave site, and although some sites have better description of the local type of vegetation cover, the interpretation may be biased due to the limited information from the other sites where complete vegetation description of the cave surrounding is lacking. Hence, we use general observations by comparing the vegetation zones and speleothem $\delta^{13}C$ values, which were also colour coded for every per mil change (Fig. 4). This qualitative observation suggests that higher speleothem $\delta^{13}C$ values tend to be associated with vegetation zones that are generally characterized by less vegetation, and vice versa, and it could be used as a general framework to set the baseline and range of $\delta^{13}C$ values for modern speleothems. Nevertheless, caution should be taken when interpreting $\delta^{13}C$ in regions where vegetation cover is more heterogeneous.

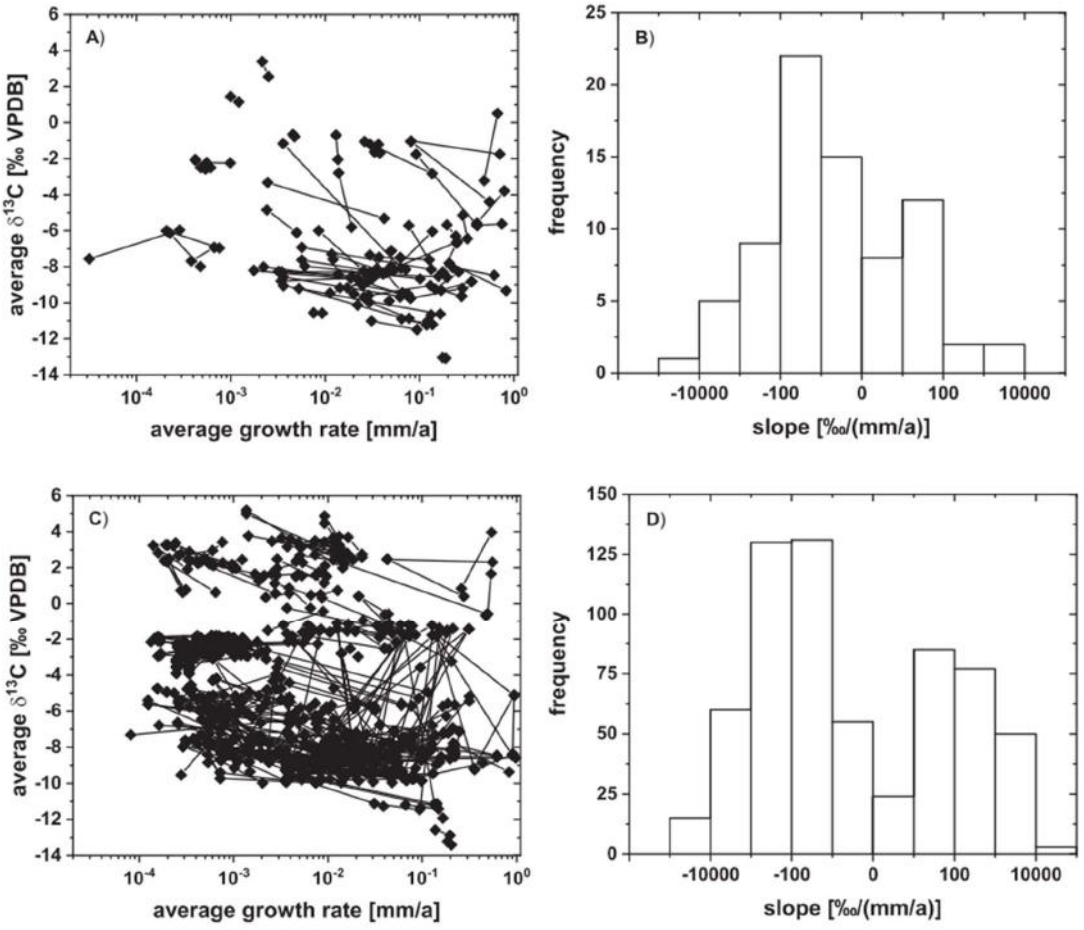

Fig. 3. (A) Average $\delta^{13}C$ values and average growth rates for periods of contemporaneous speleothem growth. Speleothem pairs from the same cave are connected by a straight line. Error estimates for

growth rate are about 10 % for those records with large age errors. (B) Histogram showing the frequency distribution for the slopes ($\delta^{13}C$ – growth rate). Please note the logarithmic scale on the x-axes. A stability analysis with using at maximum 1000 year periods (see text for details) suggests that this pattern is robust (C as in A, D as in B only with analysing 1000 year long windows).

Because vegetation type and density strongly depend on the amount of precipitation, site altitude and local air temperature, we also assess the relationships between speleothem $\delta^{13}C$ averages and these three variables. First we focus on altitude and annual precipitation (Fig. 5).

With respect to altitude, there appears to be no significant relationship with speleothem $\delta^{13}C$ data. When using the Spearman rank correlation, which better assesses monotonic relationships in general and is thus less sensitive to outliers, a correlation coefficient of 0.2 with p = 0.13 is obtained. Nevertheless, the marked absence of low $\delta^{13}C$ values at high-altitude sites is interesting (Fig. 5A). These results agree with findings from a locally confined set of caves, monitored above an altitude gradient in the southern European Alps (Johnston et al., 2013). In that study, lower speleothem $\delta^{13}C$ values are not found in high-altitude caves, while at lower altitudes, the entire range of $\delta^{13}C$ values is present. This speleothem $\delta^{13}C$ behaviour with respect to altitude may be related to vegetation cover and/or soil thickness, which becomes sparser at higher altitudes. Other cave site specific aspects like drip interval or cave ventilation are viewed as having minimal influence within such a large set of data. A relationship between $\delta^{13}C$ and altitude is also suggested by a principal component analysis (PCA, Fig. S1), where the $\delta^{13}C$ values and altitude vectors point approximately to the same direction.

We found a weak but significant negative relationship between speleothem $\delta^{13}C$ values and the amount of precipitation (q = ?0.27, p = 0.04, Fig. 5B). This is also consistent with the PCA results where $\delta^{13}C$ and precipitation show contrasting behaviour on PC1 (Fig. S1). The full range of speleothem $\delta^{13}C$ values is observed for caves located in regions with annual precipitation below 1500 mm. Another remarkable feature is that high $\delta^{13}C$ values (>?8‰) are not found in regions receiving more than ~1500 mm of precipitation per year. From this observation, we deduce that high amounts of precipitation favour the development of high-density vegetation, which promotes lower speleothem $\delta^{13}C$ values. The only exception is Wah Shikhar Cave with a mean $\delta^{13}C$ value of ~-2.6 and an average annual precipitation of ~2150 mm/a (Sinha et al., 2011). Although the area above Wah Shikhar Cave

is also densely vegetated (Sinha et al., 2011), processes in the cave and karst must have strong influence on speleothem $\delta^{13}C$ values, favouring the transition from the light isotopic soil CO_2 values towards heavy isotopic values in the speleothem.

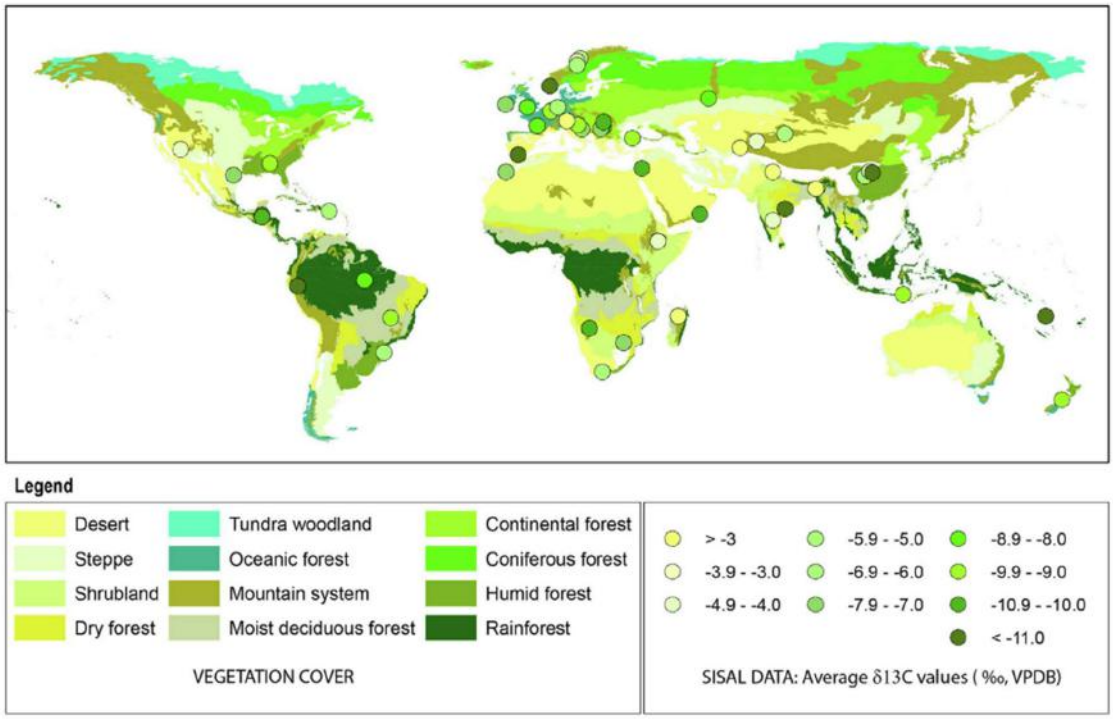

Fig. 4. Global map showing the relationship between vegetation cover and average speleothem $\delta^{13}C$ data post-1900 CE. Vegetation map is from Global Land Cover 2000 Project (GLC2000) based on SPOT-VEGETATION satellite imagery (Aaron and Gibbs, 2008).

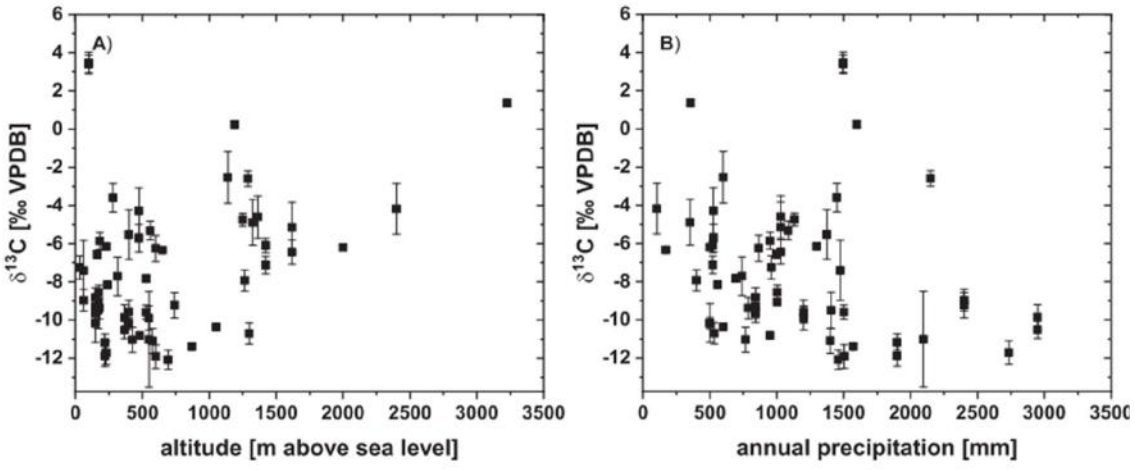

Fig. 5. Average speleothem $\delta^{13}C$ data post-1900 CE vs altitude of the cave (A) and vs amount of precipitation (B).

5.2. Temperature and speleothem $\delta^{13}C$

The most interesting and complex pattern evolves when we compare the $\delta^{13}C$ averages of speleothems in the post 1900 CE era with the present day mean annual temperature.

Although there is no clear relationship in the data (p = -0.07, p = 0.62), as also confirmed by the PCA (Fig. S1), temperature has the potential to be responsible for the overall sensitivity of speleothem $\delta^{13}C$ to vegetation and climate conditions. As photosynthesis and respiration depend on temperature, we expect differences in the $\delta^{13}C$ values of speleothems from cold and warm/hot sites (indicated as tracks A and B in Fig. 6). From this general pattern several cave specific processes can contribute to a deviation from this relationship and might be summarised by three categories in our dataset (labelled #1, #2, #3 in Fig. 6). Four out of these five general clusters are also well identified (Fig. S3) by an unsupervised machine learning algorithm (DBSCAN; Ester et al., 1996), suggesting that our grouping is objective. Details and results of this algorithm are provided in the supplement.

For the cold temperature branch (labelled A in Fig. 6), one possible explanation could be the production of soil gas CO_2. The soil gas $\delta^{13}C$ composition is very sensitive to diffusion of CO_2 into soils when soil respiration rates are small and the atmospheric component becomes more important (Cerling, 1984). Soil respiration rates between ~0 and 1 mmoles/m^2/hr can easily explain $\delta^{13}C$ variations of about 12‰ in soil gas CO_2 (between -21 and -9‰ for soil respiration rates between 0 and 1 mmoles/m^2/hr). At low temperatures, soil respiration rates are generally lower than under warmer temperatures for similar vegetation cover (Raich and Schlesinger, 1992; Raich and Potter, 1995; Kätterer et al., 1998). For comparison, soil respiration rates for grassland soils during the growing season can reach values between 6 and 9 mmoles/m^2/hr, while during the dry or cool non-growing season they are typically about 1 mmoles/m^2/hr (Singh and Gupta, 1977; Schlesinger, 1977; Parker et al., 1983). At freezing conditions, soil respiration rates can drop close to 0 mmoles/m^2/hr (Kucera and Kirkham, 1971).

Thus, it appears likely that diffusion of atmospheric CO_2 into soils at low soil respiration rate sites can explain the large spread of $\delta^{13}C$ data we observe for low temperature sites (below 5 °C MAT; Fig. 6). Speleothems from these caves show a wide $\delta^{13}C$

range, varying from -8to+2‰, despite the small sample size (i.e., only seven speleothems were available for evaluation). This group has no significant correlation to temperature, but roughly follows the expected trend. The average speleothem $\delta^{13}C$ values at these cold sites are higher than those at slightly warmer caves (around 7–10 °C).

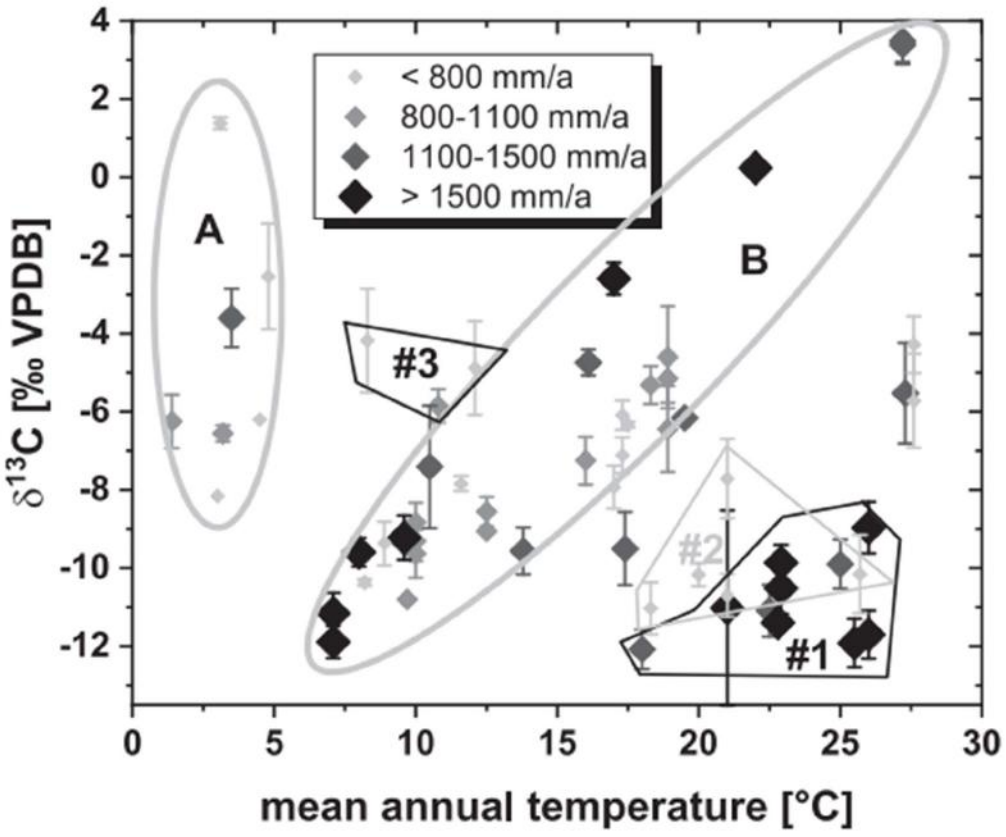

Fig. 6. Clustering pattern between $\delta^{13}C$ averages and mean annual temperature (diamonds), highlighting the highly non-linear relationship between both parameters. Grey-tone and size of the diamonds refer to the amount of annual precipitation at the cave location. The two near-linear branches (A and B), discussed in the text, for low and high temperatures are indicated by the grey lines (labelled A and B). The three marked clusters (#1, #2 and #3) highlight special characteristics of those speleothem $\delta^{13}C$ values. See section 5.2 for details.

Speleothems following the warm temperature branch (~7 to 27 °C, Fig. 6), also show a wide range in $\delta^{13}C$ values temperatures, $\delta^{13}C$ values also increase, following an (between ~-12 and +3‰). With increasing mean annual approximately linear relationship. Optimal conditions for where most speleothems cluster, with low $\delta^{13}C$ values speleothem growth appear to be between ~7 and 15 °C, (-12 to -8‰) that suggest a large imprint from soil respired CO_2. One possible mechanism to explain the high $\delta^{13}C$ values (-2 to +4‰) at high temperatures is increasing heat and drought stress on vegetation. As opposed to soils from

cold regions, those from higher temperature regions (>15 °C) can be affected by enhanced evaporation, which can quickly reduce the water stored in soils, which in turn is responsible for changing fractionation strength during photosynthesis (Bowling et al., 2002; Hartman and Danin, 2010; Buchmann et al., 1996). Temperature can thus be responsible for reduced vegetation density and soil respiration rates, even when the overall amount of precipitation is high. This in turn affects the soil gas $\delta^{13}C$ via the earlier discussed fractionation effects during CO_2 diffusion out of the soil into the free atmosphere. Another reason for increased speleothem $\delta^{13}C$ values might be that C4 type plants become more likely at higher temperatures as seen at Anjohibe Cave (Madagascar), which is nearly completely covered by C4 plants (average $\delta^{13}C$ of stalagmites AB2 and AB3 = +3.4 and +3.5‰; MAT = 27.2 °C; Burns et al., 2016; Scroxton et al., 2017; Voarintsoa et al., 2017c). As the C4 metabolic pathway fractionates the carbon isotopes less strongly, a higher proportion of C4 plants can also explain the trend towards higher speleothem $\delta^{13}C$ values at high temperatures.

We observe significant deviations in speleothem $\delta^{13}C$ values from the warm temperature branch. One category of data (region '#10) forms a cluster with very negative $\delta^{13}C$ values (around –12‰) at high temperature sites (Fig. 6). These samples are from climates experiencing strong precipitation seasonality, e.g., monsoonal, and high amounts of annual precipitation as in Jhumar Cave, India (Sinha et al., 2011), Liang Luar Cave, Indonesia (Griffiths et al., 2016) or Taurius Cave, Vanuatu (Partin et al., 2013). In this case, it is likely that despite the high temperatures reigning at the sites, enough water is available to maintain a dense vegetation, which translates to high soil respiration rates, and low $\delta^{13}C$ values in soil gas and speleothems.

Of special interest are the five speleothem $\delta^{13}C$ data points in region '#2' (Fig. 6), which largely overlap with region #1. These samples have low $\delta^{13}C$ values (-7.5 to -11‰) and high temperatures, but are affected by a much more arid climate than the samples in region '#1'. Two of the five samples are from St. Michaels Cave, Gibraltar (Mattey et al., 2008) and Natural Bridge Caverns, Texas (Wong et al., 2015). These two sites are well monitored and their dominant cave processes and carbon fluxes are well understood (Mattey et al., 2016; Breecker et al., 2012, Meyer et al., 2014; Bergel et al., 2017). For both caves, it has been recognised that a deep, ^{13}C depleted carbon source in the karst must exist in addition to the surface soil CO_2. This would explain the relatively low speleothem $\delta^{13}C$ values at these sites,

despite the warm and arid local conditions and relatively sparse vegetation at present. The other three data points are from Dante Cave, Namibia (Voarintsoa et al., 2017a), Soreq Cave, Israel (Bar-Matthews et al., 2003) and Defore Cave, Oman (Burns et al., 2002). Unfortunately, no detailed monitoring data of carbon transfer dynamics is hitherto available for these three caves, and therefore we cannot test whether they are also affected by the presence of deep carbon reservoirs. This proves how important cave monitoring is for understanding individual proxy time series but also to understand data in a more general context like this compilation.

Finally, the cluster in region '#3' (Fig. 6) is composed of three speleothems characterised by unusually high $\delta^{13}C$ values compared to other speleothems in the same temperature range. These three speleothems are from Bunker Cave, Germany (Fohlmeister et al., 2012), Bir-Uja Cave, Kyrgyzstan (Fohlmeister et al., 2017), and Leviathan Cave, Nevada (Lachniet et al., 2014). Bunker Cave was artificially opened after its discovery in 1860 CE, which likely lead to stronger ventilation and an increase in $\delta^{13}C$ values (Riechelmann et al., 2011; Fohlmeister et al., 2012). Speleothem values prior to 1860 CE average around -9‰ (instead of -5.9‰ in the period after 1860 CE), which better matches predictions based on vegetation cover (Fig. 4) and temperature (Fig. 6). A similar explanation is provided for the Bir-Uja Cave stalagmite, where fractionation processes within a small cave with a large opening are dominant (Fohlmeister et al., 2017). Such strong fractionation effects are often reported for well ventilated caves (Spötl et al., 2005; Frisia et al., 2011; Tremaine et al., 2011). Little information about fractionation processes is available for Leviathan Cave, therefore we cannot make final statements about the reason for its relatively high $\delta^{13}C$ values. However, site descriptions suggest that vegetation cover at this site is sparse and dominated by grasses, as expected for the very arid conditions in the Great Basin (Lachniet et al., 2014). This suggests that again, the low soil respiration rate at this high elevation site (2400 m above sea level) might be contributing to the high average $\delta^{13}C$ values.

5.3. Governing processes in karst and speleothem $\delta^{13}C$ values

In the previous subsections we analysed the influence of vegetation, temperature, precipitation and altitude on carbonate $\delta^{13}C$ values. In order to eliminate these site-specific external factors from our analysis, we compare $\delta^{13}C$ values of contemporaneously grown speleothems from the same cave. Thus, any differences in the average $\delta^{13}C$ values of

contemporaneously grown speleothems can be attributed to changes in the type of host rock dissolution and fractionation processes during PCP or CO_2 degassing.

In this section and in section 5.4 we will focus on the direction and steepness of the slope between the average $\delta^{13}C$ value and the average growth rate of two contemporaneously growing speleothems (Fig. 3A). The detected bimodal distribution in the frequency of the slopes (Fig. 3B) is surprising under the given boundary conditions of similar drip water and cave air characteristics. More than 2/3 of all analysed speleothem pairs show a negative slope between $\delta^{13}C$ and growth rate (as expected from previous modelling studies, e.g., Mühlinghaus et al., 2007; Romanov et al., 2008; Dreybrodt and Scholz 2011 and the description in Section 3.2.2), while the remaining show a positive slope. This is an interesting result and raises the question for the driving mechanism behind these relationships.

First, we evaluate the possibility that carbonate dissolution processes can explain the observed behaviour in the slopes of $\delta^{13}C$ values vs. growth rates. For this purpose, we use the forward model CaveCalc (Owen et al., 2018) to model the evolution of $\delta^{13}C$ during carbonate dissolution processes in the karst. In this model the degree of open to closed carbonate dissolution conditions is represented by an adjustable amount of soil gas, which is able to supply CO_2 during the dissolution of carbonate bed rock and contribute CO_2 for the exchange of carbon between the dissolved carbon species and the specified gas volume. The larger the specified gas volume, the more open the carbonate dissolution conditions.

For the modelling, we assumed soil gas $\delta^{13}C$ values of -25‰ with a concentration of 10,000 ppm, which are typical values for soils (e.g., Spötl et al., 2005, Frisia et al., 2011, Mattey et al., 2016). We specify a calcitic bedrock and a temperature of 10 °C. While the previous parameters were kept constant, we varied the amount of gas volume (between 1 and 500 L) that is in contact with the acidic solution during the dissolution of the host rock (Fig. 7), to simulate changes in the carbonate dissolution system (open vs closed conditions).

Under more open carbonate dissolution systems, e.g. when the gas volume is larger, $\delta^{13}C$ values decrease and $[Ca^{2+}]$ increases. This is because more soil CO_2 is available for bedrock dissolution, leading to more $CaCO_3$ dissolution (increase in $[Ca^{2+}]$), while providing a large reservoir of low- $\delta^{13}C$ air with which the solution can re-equilibrate. The relationship between $\delta^{13}C$ values and $[Ca^{2+}]$ is non- linear with a stronger increase in $[Ca^{2+}]$ than a

decrease in $\delta^{13}C$ values for small gas volumes (near completely closed system). For large gas volumes, $[Ca^{2+}]$ increases more slowly than for small gas volumes, while $\delta^{13}C$ decreases more rapidly. This behaviour can be explained by the highly nonlinear dissolution of $CaCO_3$ with respect to the available gaseous CO_2 (Dreybrodt, 1988). The $[Ca^{2+}]$- $\delta^{13}C$ relationship found by CaveCalc is in agreement with an alternative carbon isotope enabled karst dissolution model (Fohlmeister et al., 2011).

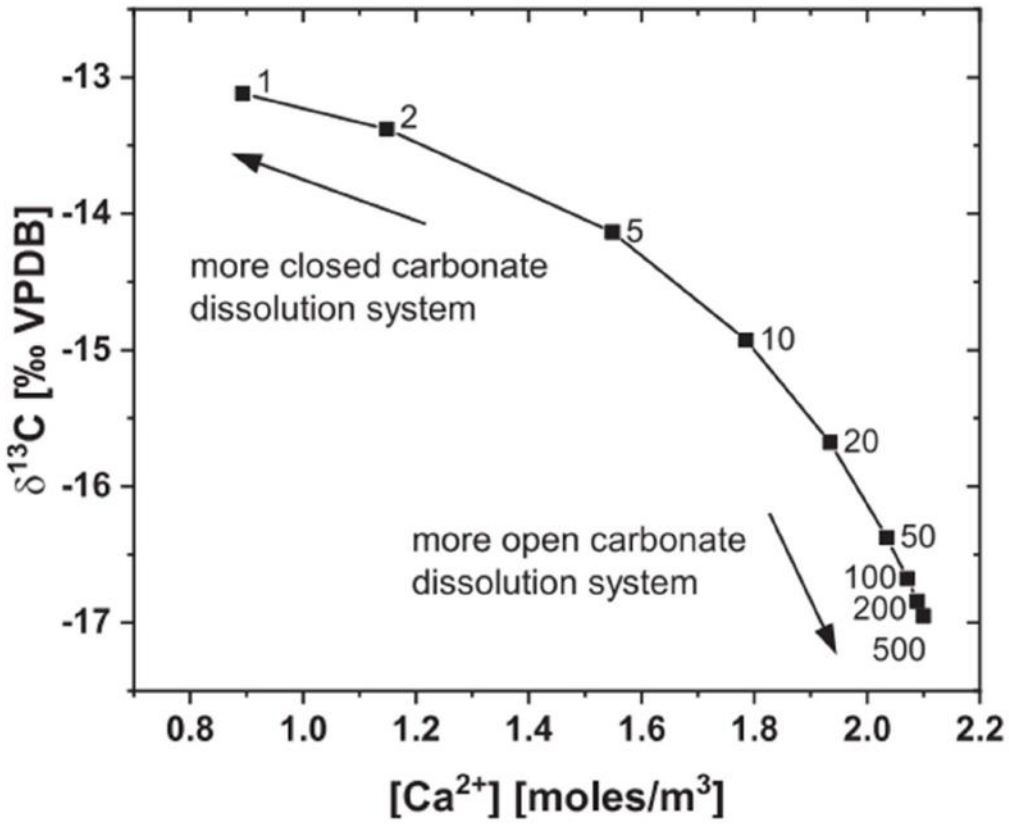

Fig. 7. Carbonate dissolution under various degrees of open/closed conditions using CaveCalc (Owen et al., 2018). Numbers refer to the volume of gas (in l) in contact with the water during dissolution. The more open the carbonate dissolution system (larger gas volume), the higher $[Ca^{2+}]$ and the lower the $\delta^{13}C$ of DIC of the $[Ca^{2+}]$ saturated drip water. The resulting range of slopes ($\delta^{13}C$ vs growth rate) is between -6 and -61‰/(mm/a).

Higher $[Ca^{2+}]$ in the solution entering the cave favours higher growth rates. If we assume for simplicity that both drip sites have similar drip intervals, which is also an important factor for growth rate and $\delta^{13}C$ evolution (see Section 5.4), a negative slope between $\delta^{13}C$ values and growth rate is established by a variation in dissolution conditions, i.e., a more open system dissolution leads to lower $\delta^{13}C$ values and higher $[Ca^{2+}]$ and thus

higher growth rates, and vice versa for more closed system conditions. This is in line with the majority of the $\delta^{13}C$ -growth rate slopes found in contemporaneously growing speleothems from the same cave (ca. two thirds of datasets have negative slope, Fig. 3B). To test our assumption, we use the relationship between $\delta^{13}C$ values and $[Ca^{2+}]$ to calculate the slope expected from the simulated dissolution regimes. The concentration of Ca^{2+} can be transferred to growth rates by applying equation (3). If we assume a typical cave air pCO_2 of 500 ppm, the equilibrium $[Ca^{2+}]$ is about $0.77*10^{-3}$ moles/l. Furthermore, we assume there is one drip per second for both sites. We choose this short interval in order to only focus on the effect of $CaCO_3$ dissolution. The effect of carbonate precipitation under different drip intervals is discussed later (Sections 5.4 and 5.5). This allows us to calculate the precipitation rate. The extreme values for the slope are -6‰/(mm/a) for near closed dissolution conditions (gas volume = 1 and 2 l) and -63‰/(mm/ a) for close to completely open dissolution conditions (gas volume = 200 and 500 l). Those values fall very closely to the frequency maximum of the observed frequency distribution for the branch with the negative slope (Fig. 3B). Thus, the steepest negative slopes (-200 to -1000‰/(mm/a), Fig. 3B) calculated from the SISAL_v1 dataset cannot be explained by carbonate dissolution systematics. Furthermore, variations in dissolution systematics can also not explain the positive slopes obtained in about one third of cases in our dataset. Thus, the positive slope must be related to processes occurring during degassing of CO_2 and $CaCO_3$ precipitation in the cave after the dissolution of $CaCO_3$ is completed.

5.4. Governing processes on speleothem $\delta^{13}C$ values during CO_2 degassing and $CaCO_3$ precipitation

Studies focusing on radiocarbon analysis of contemporaneously growing speleothems have shown that variations in the open/closed ratio are often small between speleothems from the same cave (Lechleitner et al., 2016, Demeny et al., 2017a,b, Riechelmann et al., 2019; Markowska et al., 2019). This requires that initial $\delta^{13}C$ values and $[Ca^{2+}]$ are approximately equal for two drip sites when the water just reaches Ca^{2+}-saturation. Where there are small differences in the open-closed carbonate dissolution system for two drip sites, we have shown that $\delta^{13}C$ and $[Ca^{2+}]$ of the Ca-saturated solution is not expected to change significantly (Fig. 7).

When considering the effects of CO_2 degassing and $CaCO_3$ precipitation, the only variable parameters are the time interval during which the water is in contact with cave air before reaching the top of the speleothem and the time interval during which the drop is on the top of the speleothem before it is replaced by the next incoming drop. The first time period essentially falls within the time the drip water solution is affected by PCP. Its duration will influence the isotopic composition and growth rate of the speleothem. For our analysis, we first assume that no PCP occurs, e.g., water is not in contact with air prior to reaching the top of the stalagmite (Fig. 8). To model the resulting slopes in two contemporaneously growing speleothems with different drip intervals, we simulate the chemical evolution of two drip sites, by systematically changing cave temperature (T = 5, 10 and 20 °C), $[Ca^{2+}]$ in drip water (equivalent to a cave air pCO_2 = 500 and 1000 ppm) in the same way for both speleothems. Additionally, we change the drip interval difference between the two speleothems, and calculate how these factors will affect the slope between two contemporaneously growing speleothems using a Rayleigh model (Section 3.2.2).

The Rayleigh model predicts that the greater the drip interval difference between the two speleothems, the less negative the slope (Fig. 8). If both drip intervals are long (i.e., both are above 1000 s), the slope also becomes less negative. Both observations can be explained by the different rate of change for $\delta^{13}C$ values and $[Ca^{2+}]$ during $CaCO_3$ precipitation. The used parameters for calcite precipitation rate, s (Eq. (1)) and for fractionation factors, e (Eq. (4)) require that $\delta^{13}C$ values of DIC reaches equilibrium faster than $[Ca^{2+}]$(Fig. 1). This behaviour is even more pronounced in the $\delta^{13}C$ evolution of precipitated $CaCO_3$ and growth rate (supplementary Fig. S4). Thus, under the scenario of a large difference in drip intervals between two speleothems, the difference between DIC $\delta^{13}C$ values at different time steps increases more slowly than that of $[Ca^{2+}]$ (and therefore growth rate), resulting in a smaller absolute value of the slope. When the oversaturation of the $[Ca^{2+}]$ saturated solution is larger (i.e., cave air CO_2 is 500 instead of 1000 ppm) the slope will only be slightly more negative. The largest effect on slope magnitude results from temperature variations. Increasing temperatures lead to less negative slopes, and the effect is stronger at lower T. An explanation for this behaviour is provided by the temperature-dependent parameters s and e, which lead to a more pronounced difference in the rate of change for $\delta^{13}C$ values in DIC and $[Ca^{2+}]$ during degassing of CO_2 and precipitation of $CaCO_3$. As for the carbonate

dissolution conditions (Section 5.3), the slope is always negative and fits well to the majority of the slopes analysed for the speleothems extracted from SISAL (between -1 to -100‰/(mm/a) – see Fig. 3B).

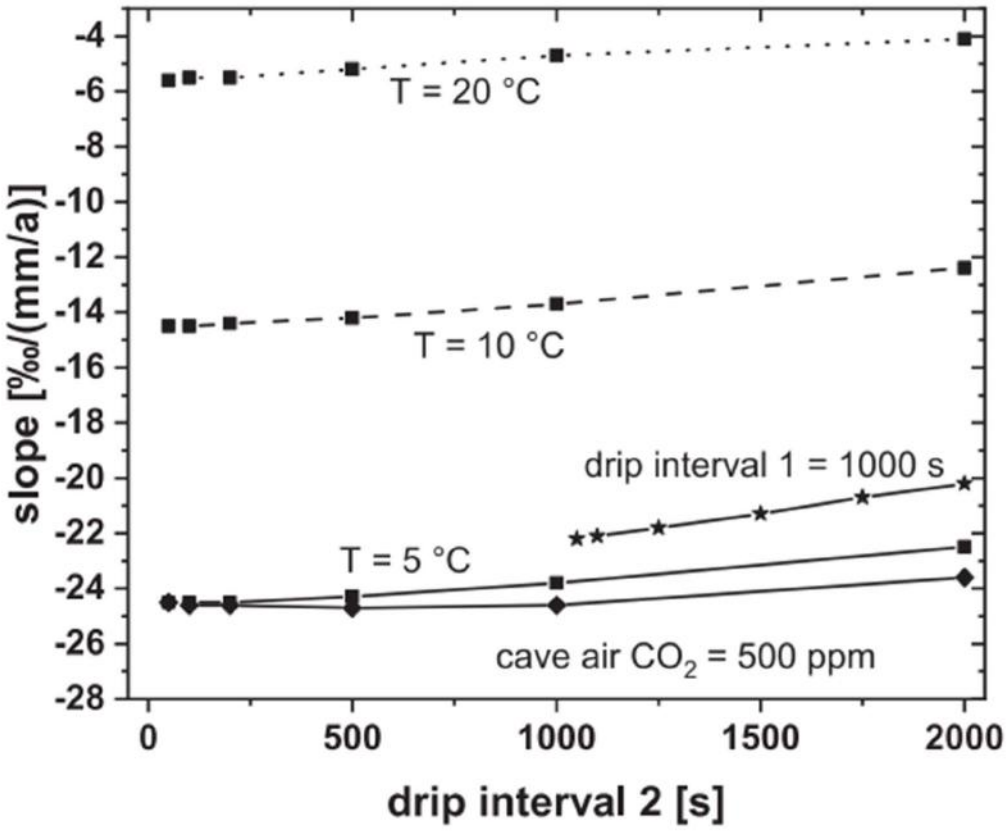

Fig. 8. The slope of $\delta^{13}C$ over growth rate for two contemporaneously growing speleothems over drip interval variations of the second speleothem. When not explicitly modelled, T is set to 5 °C, cave air pCO_2 to 1000 ppm and drip interval of the first speleothem to 1s. Initial drip water $\delta^{13}C$ composition is -10‰ and $[Ca^{2+}]$is 2 moles/m^3, which corresponds to a solution in equilibrium with approximately 5000 ppm of CO_2.

However, this process fails to provide a mechanism for the observed positive slopes in about one third of the data set on contemporaneously growing speleothems, suggesting that another factor must be at play to generate this behaviour. Thus, we allow for a variable period of PCP in our model experiments but keep the duration of PCP at equal length for both speleothems. In addition, temperature and cave air pCO_2 were kept constant (Fig. 9).

The main features of the slope with respect to drip intervals (Fig. 8) remain valid even when accounting for PCP. We observe that the slope in $\delta^{13}C$ values vs growth rate becomes more negative with increasing time for PCP. It is likely that the different rate of change in the evolution of cave drip water with respect to $\delta^{13}C$ and $[Ca^{2+}]$ is again responsible for this behaviour. While this analysis also reveals slopes that are in agreement with most of our analysed $\delta^{13}C$ data, it remains impossible to produce the observed positive slopes.

Therefore, in the next step we applied a more comprehensive approach, which likely reflects more general conditions in a cave system, by allowing individual variability in the duration for PCP at the two drip sites. First, we investigate the slopes when the time for PCP is longer for drip site 2 compared to drip site 1 and when drip site 2 also has a longer drip interval than drip site 1. This approach produces similar relationships as compared to results from an equal time for PCP for both drip locations, and thus cannot explain positive slopes (Figs. 8 and 9). We then prescribed longer duration for PCP for drip site 1 than for drip site 2, but still leaving the drip interval of site 1 shorter than for site 2 (Fig. 10). These conditions could reflect a drip site 1 where water is in contact with cave air pCO_2 for a prolonged period of time, e.g. water running down a cascade of cave-roof carbonates, and a drip site 2 where a slowly dripping soda straw would result in only a short exposure of drip water to cave air CO_2.

When drip site 1 experiences a longer period of PCP and a longer drip interval than drip site 2, a complex hyperbola-like behaviour of the slope is observed (Fig. 10). The asymptotes, which are parallel to the x-axis, have a range in the slope as observed earlier in the modelling approach (Figs. 8 and 9) and as most of the analysed pairs of speleothems. However, with longer drip intervals the slope rapidly decreases and reaches very large values, which are also found, albeit rarely, in our dataset, e.g., Abaco Island Cave, Bahamas (-2163‰/(mm/a); Arienzo et al., 2017) or Kesang Cave, China (-7462‰/(mm/a); Cheng et al., 2016). At even longer drip intervals, strongly positive slopes appear and rapidly decreases to either an asymptote with a slightly negative (-14‰/(mm/a); grey, Fig. 10) or slightly positive value for the slope (4‰/(mm/a); black, Fig. 10). Similar to those two examples, there are many further cases possible, where the same behaviour is observed. Similar as explained for the examples calculated without accounting for PCP or an equal PCP for the two drip sites,

this behaviour is a result of the interplay between the rate of changes for $\delta^{13}C$ values and $[Ca^{2+}]$ during CO_2 degassing and $CaCO_3$ precipitation.

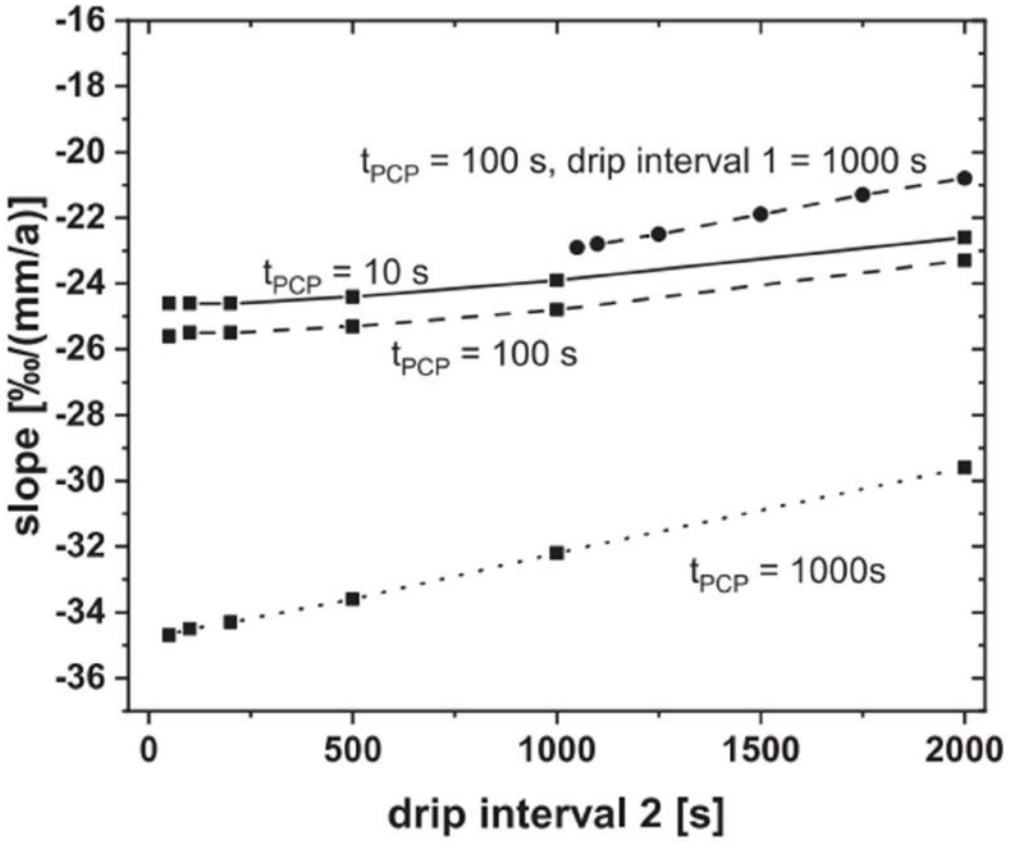

Fig. 9. The slope of $\delta^{13}C$ over growth rate for two contemporaneously growing speleothems over drip interval variations of the second speleothem. In contrast to Fig. 8, PCP is enabled and the time for PCP is varied (but both speleothems experience equal PCP duration). Temperature is set to 5 °C, cave air pCO_2 to 1000 ppm and when not explicitly modelled drip interval of the first speleothem to 1 s. Initial drip water $\delta^{13}C$ composition is ?10‰ and $[Ca^{2+}]$ is 2 moles/m^3, which corresponds to a solution in equilibrium with approximately 5 000 ppm of CO_2.

This result provides a possible mechanism for the positive slopes observed in the SISAL extracted $\delta^{13}C$ data for contemporaneously growing speleothems from the same cave. In addition to this, our model experiments with different time periods of PCP and drip interval can also explain the large positive and negative slopes observed in some of the speleothem data (Fig. 3B). As the range of combinations of time periods for PCP and drip intervals, where such large positive or negative values are observed, is relatively small (only a few 100 seconds for drip interval 2), this might also provide an explanation why only few speleothem pairs show such large slopes.

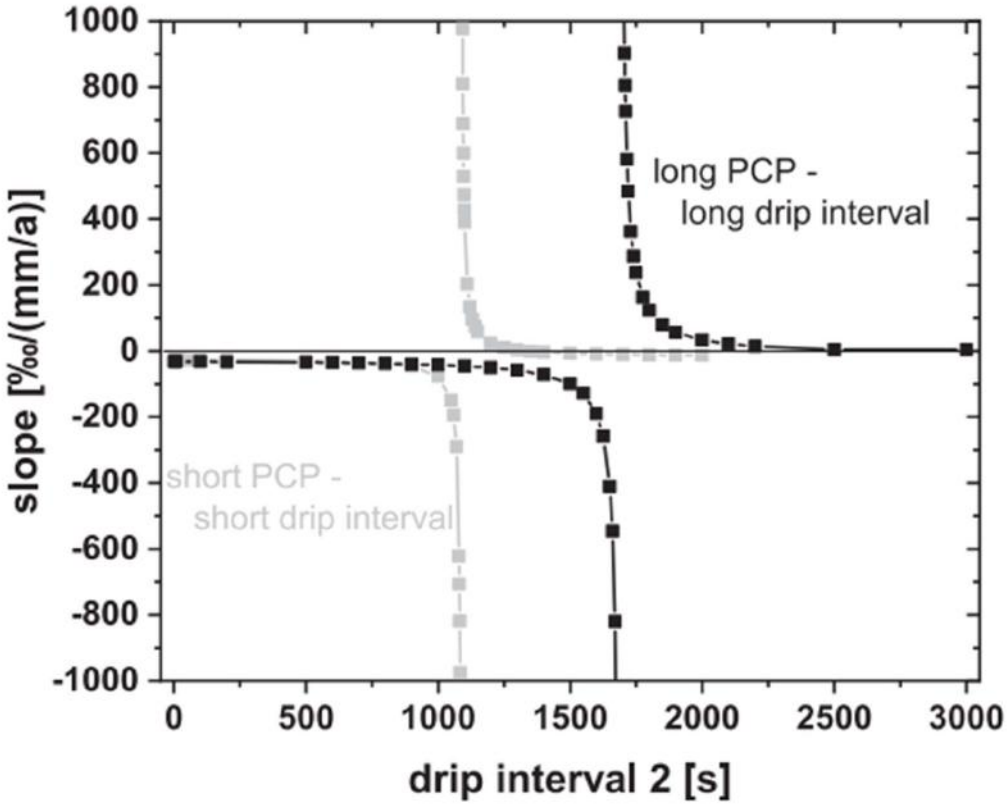

Fig. 10. The slope of $\delta^{13}C$ over growth rate for two contemporaneously growing speleothems over drip interval variations of the second speleothem for two examples. Example 1 (grey): ''short PCP – short drip interval" describes the situation where the time for PCP was fixed at drip site 1 to 100 s and at drip site 2 to 0 s, while drip interval 1 was set to 1 s (drip interval 2 varies). Example 2 (black): ''long PCP – long drip interval" describes the situation where the time for PCP is 1000 s for drip site 1 and 500 s for drip site 2, while keeping the drip interval of site 1 at 500 s. Temperature is 5 °C and cave air pCO_2 is 1000 ppm. Furthermore, initial drip water $\delta^{13}C$ composition is ?10‰ and $[Ca^{2+}]$ is 2 moles/m^3, which corresponds to a solution in equilibrium with approximately 5 000 ppm of CO_2. The $\delta^{13}C$ vs growth rate slope vary over a large range and changes the sign.

From our modelling results we can now more confidently interpret the processes driving the slope between $\delta^{13}C$ data and growth rate. The slope is a measure of differences in the amount of fractionation between two contemporaneously growing speleothems, with which we can quantify the influence of cave processes on individual $\delta^{13}C$ time series. Analysing the slope in reproduced $\delta^{13}C$ time series of speleothems will give additional information on drip site characteristics. We found that the slope is sensitive to temperature, pCO_2, drip interval and the duration of PCP, but together with other proxies and the individual $\delta^{13}C$ time series, a more thorough evaluation of climatic conditions can be drawn.

5.5. Combination of $CaCO_3$ dissolution and re-precipitation

Another possibility to obtain positive slopes between $\delta^{13}C$ values and growth rates of two contemporaneously growing speleothems is through the combined effect of carbonate dissolution under different open-closed conditions and Rayleigh fractionation during PCP or $CaCO_3$ precipitation on the stalagmite top. Let us assume that the host rock is dissolved in nearly completely closed carbonate conditions with only slightly different degrees of openness between two speleothem drip sites (e.g., gas volume = 1 and 2 l; Fig. 7). For a drip interval of 1 s for those two sites we obtained negative slopes (Section 5.3). Here, we want to investigate the effects on the slope, if drip intervals are considerably longer.

For different gas volumes of 1 and 2 l and a drip interval of 1 s for both stalagmite sites, the slope was about -6‰/ (mm/a). When drip interval was about 100 s the slope increased to -5‰/(mm/a) and to +16‰/(mm/a) if one drip is falling each 2000 s. Thus, the combined effect of different carbonate dissolution conditions near the completely closed system and fractionation effects is also able to provide positive slopes.

When doing the same exercise for a nearly completely open carbonate dissolution system (gas volume = 200 and 500 l; Fig. 7) for drip intervals of 1, 100 and 2000 s, the slopes for $\delta^{13}C$ vs growth rates are -63, -67 and -170‰/(mm/a). Thus, positive slopes cannot be obtained by the combined effect of dissolution and re-precipitation under nearly completely open dissolution conditions.

In a last case, we do the calculations for two speleothems, where the carbonate dissolution occurred during nearly completely open and completely closed conditions (gas volume = 1 and 500 l; Fig. 7). For drip intervals of 1, 100 and 2000 seconds the slope remains always negative (-19, -20, -36‰/(mm/a)). However, as those extreme dissolution conditions were never observed, we render this calculation only as a hypothetical example. Further, very different carbonate dissolution conditions have not been observed within the same cave. In addition, in most caves carbonate dissolution conditions occur mostly under more open conditions (e.g., Genty et al., 1998; Griffiths et al., 2012; Lechleitner et al., 2016), where it is not possible to obtain positive slopes for $\delta^{13}C$ values and growth rates, when combined with Rayleigh fractionation effects. Only in the rare cases where dissolution occurs under near-completely closed conditions, the combined effects of dissolution and Rayleigh effects can produce positive slopes. Radiocarbon measurements on each of the two stalagmites can

reveal the carbonate dissolution conditions and thus can help to guide through the choice of which effect is responsible for a positive slope (dissolution and Rayleigh fractionation or the effect of decoupled length of PCP and drip intervals).

6. CONCLUSIONS

We have discussed the main factors influencing speleothem $\delta^{13}C$ values. With the $\delta^{13}C$ records extracted from the SISAL_v1 database and modelling results we were able to disentangle and quantify various processes affecting speleothem $\delta^{13}C$ values from a large number of speleothems from globally distributed caves. First, we focused on average $\delta^{13}C$ values of recently grown speleothems, accounting only for material deposited post-1900 CE. We found that $\delta^{13}C$ values are mainly affected by vegetation cover and temperature, but both relationships are subject to noise introduced by competing additional effects. The $\delta^{13}C$ - temperature relationship can be explained by temperature- vegetation and temperature-soil respiration rate dependencies, with additional modulation by the amount of precipitation for monsoonal areas. Although we applied a comprehensive approach, we nevertheless found extreme cases, which deviate from the main relationships. This is especially conspicuous for caves which are shown to have deep carbon sources or extreme ventilation that drives fractionation processes.

In the second part of our analysis, we focused on contemporaneously growing speleothems from individual caves. We observed a bimodal distribution of positive and negative slopes of $\delta^{13}C$ values vs growth rates. While negative slopes are expected, based on previously published incave fractionation model studies, positive slopes were more difficult to explain. By considering CO_2 degassing and $CaCO_3$ precipitation effects also for PCP and accounting for drip interval, we extended the Rayleigh fractionation approach of earlier in-cave fractionation models and we demonstrated that positive slopes between $\delta^{13}C$ values and growth rate can be explained by decoupling the time available for PCP and the drip interval for the individual drip sites or by the combined effect of nearly closed carbonate dissolution systems and long drip intervals.

Our data-model intercomparison highlights the various influences of in-situ processes and external climate conditions on speleothem $\delta^{13}C$ values. Not surprisingly, vegetation cover is an important driver of speleothem $\delta^{13}C$ values, but temperature emerges as a second

factor that has a large effect, likely via its influence on the soil respiration rate. Soil respiration rate however, is also affected by the amount of precipitation, which was shown to be an important factor in warm regions. Furthermore, we showed that fractionation effects, especially via PCP, are important to explain the results of $\delta^{13}C$ differences in contemporaneously growing speleothems from the same cave. We propose that PCP should be implemented in next-generation $CaCO_3$ precipitation models, as this process can explain much of the variations observed in our analysed dataset. Also, for climate reconstruction this process should be discussed in more detail, especially in combination with Mg/Ca or Sr/Ca ratio - $\delta^{13}C$ variations are a powerful tool to evaluate the strength of this process.

7. DATA AVAILABILITY

The used speleothem data were extracted from the SISAL_v1 data base obtained from their repository (https://doi.org/10.17864/1947.147). The code for extraction can be downloaded from the supplemental material. The extended Rayleigh-model for in-cave fractionation models are provided as an excel file in the supplement to this contribution or on request to the corresponding author. Eight free parameters can be used to fit the model to the cave conditions - temperature, initial and equilibrium $[Ca^{2+}]$ as well as initial $\delta^{13}C$ composition. In addition, the time for PCP and drip interval for the two drip sites can be adjusted.

Declaration of Competing Interest

The authors declare that they have no known competing financial interests or personal relationships that could have appeared to influence the work reported in this paper.

ACKNOWLEDGEMENTS

The authors acknowledge the speleothem community effort to establish the SISAL database, without which this contribution would not be possible. SISAL is an international working group of the Past Global Changes (PAGES) programme, and the authors gratefully acknowledge their support of this activity. JF is supported by DFG grant FO 809/4-1. NRGV is currently supported by EU-HORIZON Marie Curie Fellowship no. 796707. FAL gratefully acknowledges support from the Swiss National Science Foundation (SNSF) grant P400P2_180789. This project is TiPES contribution #9: This project has received funding from

the European Union's Horizon 2020 research and innovation programme under grant agreement No 820970.

APPENDIX A. SUPPLEMENTARY MATERIAL

Supplementary data to this article can be found online at https://doi.org/10.1016/j.gca.2020.03.042.

REFERENCES

Aaron, R., Gibbs, H. K. (2008) New IPCC Tier-1 Global Biomass Carbon Map for the Year 2000. Available online from the Carbon Dioxide Information Analysis Center [http://cdiac.ess- dive.lbl.gov], Oak Ridge National Laboratory, Oak Ridge, Tennessee.

Aharon P., Aldridge D. and Hellstrom J. (2013) Rainfall Variability and the Rise and Collapse of the Mississippian Chiefdoms: Evidence from a Desoto Caverns Stalagmite, in Climates, Landscapes, and Civilizations. American Geophysical Union, pp. 35–42.

Ait Brahim Y., Cheng H., Sifeddine A., Wassenburg J. A., Cruz F. W., Khodri M., Sha L., Pe´rez-Zano´n N., Beraaouz E. H., Apaéstegui J., Guyot J.-L., Jochum K. P. and Bouchaou L. (2017) Speleothem records decadal to multidecadal hydroclimate variations in southwestern Morocco during the last millennium, Earth Planet. Sci. Lett. 476, 1–10.

Apae´stegui J., Cruz F. W., Sifeddine A., Vuille M., Espinoza J. C., Guyot J. L., Khodri M., Strikis N., Santos R. V., Cheng H., Edwards L., Carvalho E. and Santini W. (2014) Hydroclimate variability of the northwestern Amazon Basin near the Andean foothills of Peru related to the South American Monsoon System during the last 1600 years. Climate ofthe Past 10, 1967– 1981.

Arienzo M. M., Swart P. K., Broad K., Clement A. C., Pourmand A. and Kakuk B. (2017) Multi-proxy evidence of millennial climate variability from multiple Bahamian speleothems. Quat. Sci. Rev. 161, 18–29.

Asrat A., Baker A., Leng M., Gunn J. and Umer M. (2008) Environmental monitoring in the Mechara caves, Southeastern Ethiopia: implications for speleothem palaeoclimate studies. Int. J. Speleol. 37, 207–220.

Atkinson T. C. and Hopley P. J. (2013) Speleothems and Palaeoclimates. In Caves and Karst of the Yorkshire Dales. Wiley-Blackwell, Buxton, pp. 181–186.

Atsawawaranunt, K., Harrison, S. and Comas Bru, L. (2018a) SISAL (Speleothem Isotopes Synthesis and AnaLysis Working Group) database Version 1.0. University of Reading. Dataset. http://dx.doi.org/10.17864/1947.139.

Atsawawaranunt K., Comas-Bru L., Amirnezhad Mozhdehi S., Deininger M., Harrison S. P. and Baker A., et al. (2018b) The SISAL database: A global resource to document oxygen and carbon isotope records from speleothems. Earth Syst. Sci. Data 10, 1687–1713.

Baker A., Asrat A., Fairchild I. J., Leng M. J., Wynn P. M., Bryant C., Genty D. and Umer M. (2007) Analysis of the climate signal contained within $\delta^{18}O$ and growth rate parameters in two Ethiopian stalagmites. Geochim. Cosmochim. Acta 71, 2975– 2988.

Baker A., Bradley C., Phipps S. J., Fischer M., Fairchild I. J., Fuller L., Spötl C. and Azcurra C. (2012) Millennial-length forward models and pseudoproxies of stalagmite $\delta^{18}O$: an example from NW Scotland. Climate of the Past 8, 1153–1167.

Baker A., Genty D., Dreybrodt W., Barnes W. L., Mockler N. J. and Grapes J. (1998) Testing theoretically predicted stalagmite growth rate with recent annually laminated samples: Implications for past stalagmite deposition. Geochim. Cosmochim. Acta 62, 393–404.

Baker A., Wilson R., Fairchild I. J., Franke J., Spötl C., Mattey D., Trouet V. and Fuller L. (2011) High resolution $\delta^{18}O$ and $\delta^{13}C$ records from an annually laminated Scottish stalagmite and relationship with last millennium climate. Glob. Planet. Change 79(3–4), 303–311.

Baker J. L., Lachniet M. S., Chervyatsova O., Asmerom Y. and Polyak V. J. (2017) Holocene warming in western continental Eurasia driven by glacial retreat and greenhouse forcing. Nat. Geosci. 10, 430–435.

Baldini J., McDermott F., Baker A., Baldini L., Mattey D. and Railsback L. (2005) Biomass effects on stalagmite growth and isotope ratios: A 20th century analogue from Wiltshire, England, Earth Planet. Sci. Lett. 240, 486–494.

Bar-Matthews M., Ayalon A., Gilmour M., Matthews A. and Hawkesworth C. J. (2003) Sea–land oxygen isotopic relationships from planktonic foraminifera and speleothems in the Eastern Mediterranean region and their implication for paleorainfall during interglacial intervals. Geochim. Cosmochim. Acta 67, 3181–3199.

Bergel S. J., Carlson P. E., Larson T. E., Wood C. T., Johnson K. R., Banner J. L. and Breecker D. O. (2017) Constraining the subsoil carbon source to cave-air CO_2 and speleothem calcite in central Texas. Geochim. Cosmochim. Acta 217, 112–127.

Bernal J. P., Cruz F. W., Strikis N. M., Wang X., Deininger M., Catunda M. C. A., Ortega-Obregon C., Cheng H., Edwards R. L. and Auler A. S. (2016) High-resolution Holocene South American monsoon history recorded by a speleothem from Botuvera Cave, Brazil, Earth Planet. Sci. Lett. 450, 186–196.

Boch R. and Spötl C. (2011) Reconstructing palaeoprecipitation from an active cave flowstone. J. Quat. Sci. 26, 675–687.

Boch R., Spötl C. and Kramers J. (2009) High-resolution isotope records of early Holocene rapid climate change from two coeval stalagmites of Katerloch Cave, Austria. Quat. Sci. Rev. 28, 2527–2538.

Bowling D. R., McDowell N. G., Bond B. J., Law B. E. and Ehleringer J. R. (2002) 13C content of ecosystem respiration is linked to precipitation and vapor pressure deficit. Oecologia 131, 113–124.

Braun K., Nehme C., Pickering R., Rogerson M. and Scroxton N. (2019) A window into Africa's past hydroclimates: the SISAL_V1 database contribution. Quaternary 2, 4.

Breecker D. O. (2017) Atmospheric ρCO_2 control on speleothem stable carbon isotope compositions. Earth Planet. Sci. Lett. 458, 58–68.

Breecker D. O., Payne A. E., Quade J., Banner J. L., Ball C. E., Meyer K. W. and Cowan B. D. (2012) The sources and sinks of CO_2 in caves under mixed woodland and grassland vegetation. Geochim. Cosmochim. Acta 96, 230–246.

Buchmann N., Brooks J. R., Rapp K. D. and Ehleringer J. R. (1996) Carbon isotope composition of C4 grasses is influenced by light and water supply. Plant, Cell Environ. 19, 392–402.

Burns S. J., Fleitmann D., Mudelsee M., Neff U., Matter A. and Mangini A. (2002) A 780-year annually resolved record of Indian Ocean monsoon precipitation from a speleothem from south Oman. J. Geophys. Res. 107.

Burns S. J., Godfrey L. R., Faina P., McGee D., Hardt B., Ranivoharimanana L. and Randrianasy J. (2016) Rapid human-induced landscape transformation in Madagascar at the end of the first millennium of the Common Era. Quat. Sci. Rev. 134, 92–99.

Burstyn Y., Martrat B., Lopez J. F., Iriarte E., Jacobson M. J., Lone M. A. and Deininger M. (2019) Speleothems from the Middle East: an example of water limited environments in the SISAL database. Quaternary 2, 16.

Carlson P. E., Banner J. L., Johnson K. R., Casteel R. C. and Breecker D. O. (2019) Carbon cycling of subsurface organic matter recorded in speleothem 14C records: Maximizing bomb- peak model fidelity. Geochim. Cosmochim. Acta 246, 436–449.

Cerling T. E. (1984) The stable isotopic composition of modern soil carbonate and its relationship to climate. Earth Planet. Sci. Lett. 71, 229–240.

Cheng H., Edwards R. L., Southon J., Matsumoto K., Feinberg J. M., Sinha A., Zhou W. J., Li H., Li X., Xu Y., Chen S., Tan M., Wang Y. and Ning Y. (2018) Atmospheric 14C/12C changes during the last glacial period from Hulu Cave. Science 362, 1293–1297.

Cheng H., Spötl C., Breitenbach S. F. M., Sinha A., Wassenburg J. A., Jochum K. P., Scholz D., Li X., Yi L., Peng Y., Lv Y., Zhang P., Votintseva A., Loginov V., Ning Y., Kathayat G. and Edwards R. L. (2016) Climate variations of Central Asia on orbital to millennial timescales. Sci. Rep. 6, 36975.

Cruz F. W., Burns S. J., Karmann I., Sharp W. D., Vuille M., Cardoso A. O., Ferrari J. A., Dias P. L. S. and Viana O. (2005) Insolation-driven changes in atmospheric circulation over the past 116,000 years in subtropical Brazil. Nature 434, 63–66.

Comas-Bru L., Harrison S. P., Werner M., Rehfeld K., Scroxton N., Veiga-Pires C. and SISAL working group members (2019) Evaluating model outputs using integrated global speleothem records of climate change since the last glacial. Clim Past 15, 1557–1579.

Deininger M., Fohlmeister J., Scholz D. and Mangini A. (2012) The influence of evaporation effects on the carbon and oxygen isotope composition of speleothems — a model approach. Geochim. Cosmochim. Acta 96, 57–79.

Deininger M. and Scholz D. (2019) ISOLUTION 1.0: an ISOtope evoLUTION model describing the stable oxygen ($\delta^{18}O$) and carbon ($\delta^{13}C$) isotope values of speleothems. Int. J. Speleology 48,3.

Demény A., Kern Z., Czuppon G., Németh A., Leél- Össy S., Siklosy Z., Lin K., Hu H.-M., Shen C.-C., Vennemann T. W. and Haszpra L. (2017a) Stable isotope compositions of speleothems from the last interglacial – Spatial patterns of climate fluctuations in Europe. Quat. Sci. Rev. 161, 68–80.

Demény A., Németh A., Kern Z., Czuppon G., Molnar M., Leél- Össy S., Ovari M. and Stieber J. (2017b) Recently forming stalagmites from the Baradla Cave and their suitability assessment for climate–proxy relationships. Central Eur. Geol. 60, 1–34.

Dragusin V., Staubwasser M., Hoffmann D. L., Ersek V., Onac B. P. and Veres D. (2014) Constraining Holocene hydrological changes in the Carpathian-Balkan region using speleothem $\delta^{18}O$ and pollen-based temperature reconstructions. Clim. Past 10, 1363–1380.

Day C. C. and Henderson G. M. (2011) Oxygen isotopes in calcite grown under cave-analogue conditions. Geochim. Cosmochim. Acta 75, 3956–3972.

Dreybrodt W. (1980) Deposition of calcite from thin films of natural calcareous solutions and the growth of speleothems. Chem. Geol. 29, 89–105.

Dreybrodt W. (1988) Processes in Karst Systems. Springer, Berlin, p. 288.

Dreybrodt W. (2008) Evolution of the isotopic composition of carbon and oxygen in a calcite precipitating H2O– CO_2– $CaCO_3$ solution and the related isotopic composition of calcite in stalagmites. Geochim. Cosmochim. Acta 72, 4712–4724.

Dreybrodt W., Eisenlohr L., Madry B. and Ringer S. (1997) Precipitation kinetics of calcite in the system $CaCO_3$ -H_2O- CO_2: The conversion to CO_2 by the slow process H^+ + HCO^{3-} -> CO_2 +H_2O as a rate limiting step. Geochim. Cosmochim. Acta 61, 3897–3904.

Dreybrodt W., Hansen M. and Scholz D. (2016) Processes affecting the stable isotope composition of calcite during precipitation on the surface of stalagmites: Laboratory experiments investigating the isotope exchange between DIC in the solution layer on top of a speleothem and the CO_2 of the cave atmosphere. Geochim. Cosmochim. Acta 174, 247–262.

Dreybrodt W. and Scholz D. (2011) Climatic dependence of stable carbon and oxygen isotope signals recorded in speleothems: From soil water to speleothem calcite. Geochim. Cosmochim. Acta 75, 734–752.

Drysdale R. N., Hellstrom J. C., Zanchetta G., Fallick A. E., Sanchez Goni M. F., Couchoud I., McDonald J., Maas R., Lohmann G. and Isola I. (2009) Evidence for obliquity forcing of glacial termination II. Science 325, 1527–1531.

Ester M., Kriegel H. P., Sander J. and Xu X. (1996) A density based algorithm for discovering clusters in large spatial databases with noise. Kdd-Proceedings 96, 226–231.

Fairchild I. J., Borsato A., Tooth A. F., Frisia S., Hawkesworth C. J., Huang Y., McDermott F. and Spiro B. (2000) Controls on trace element (Sr–Mg) compositions of carbonate cave waters: implications for speleothem climatic records. Chem. Geol. 166, 255–269.

Fleitmann D., Cheng H., Badertscher S., Edwards R. L., Mudelsee M., Gokturk O. M., Fankhauser A., Pickering R., Raible C. C., Matter A., Kramers J. and Tuysuz O. (2009) Timing and climatic impact of Greenland interstadials recorded in stalagmites from northern Turkey. Geophys. Res. Lett., 36.

Fohlmeister J., Arps J., Spötl C., Schröder-Ritzrau A., Plessen B., Günter C., Frank N. and Trüssel M. (2018) Carbon and oxygen isotope fractionation in the water-calcite-aragonite system. Geochim. Cosmochim. Acta 235, 127–139.

Fohlmeister J., Plessen B., Dudashvili A. S., Tjallingii R., Wolff C., Gafurov A. and Cheng H. (2017) Winter precipitation changes during the medieval climate anomaly and the little ice age in arid Central Asia. Quaternary Sci. Rev. 178, 24–36.

Fohlmeister J., Scholz D., Kromer B. and Mangini A. (2011) Modelling carbon isotopes of carbonates in cave drip water. Geochim. Cosmochim. Acta 75, 5219–5228.

Fohlmeister J., Schröder-Ritzrau A., Scholz D., Spötl C., Riechelmann D. F. C., Mudelsee M., Wackerbarth A., Gerdes A., Riechelmann S., Immenhauser A., Richter D. K. and Mangini A. (2012) Bunker Cave stalagmites: an archive for central European Holocene climate variability. Climate of the Past 8, 1751–1764.

Fohlmeister J., Schro¨der-Ritzrau A., Spötl C., Frisia S., Miorandi R., Kromer B. and Mangini A. (2010) The influences of hydrology on the radiogenic and stable carbon isotope composition of cave drip water, Grotta die Ernesto (Italy). Radiocarbon 52, 1529–1544.

Frisia S., Fairchild I., Fohlmeister J., Miorandi R., Spo¨ tl C. and Borsato A. (2011) Carbon mass balance modelling and carbon isotope exchange processes in dynamic caves. Geochim. Cosmochim. Acta 75, 380–400.

Genty D., Blamart D., Ghaleb B., Plagnes V., Causse C., Bakalowicz M., Zouari K., Chkir N., Hellstrom J. and Wainer K. (2006) Timing and dynamics of the last deglaciation from European and North African $\delta^{13}C$ stalagmite profiles—comparison with Chinese and South Hemisphere stalagmites. Quat. Sci. Rev. 25, 2118–2142.

Genty D., Blamart D., Ouahdi R., Gilmour M., Baker A., Jouzel J. and Van-Exter S. (2003) Precise dating of Dansgaard-Oeschger climate oscillations in western Europe from stalagmite data. Nature 421, 833–837.

Genty D., Combourieu-Nebout N., Peyron O., Blamart D., Wainer K., Mansuri F., Ghaleb B., Isabello L., Dormoy I. and von Grafenstein U. (2010) Isotopic characterization of rapid climatic events during OIS3 and OIS4 in Villars Cave stalagmites (SW-France) and correlation with Atlantic and Mediterranean pollen records. Quat. Sci. Rev. 29, 2799–2820.

Genty D., Vokal B., Obelic B. and Massault M. (1998) Bomb 14C time history recorded in two modern stalagmites — importance for soil organic matter dynamics and bomb 14C distribution over continents, Earth Planet. Sci. Lett. 160, 795–809.

Grant K. M., Rohling E. J., Bar-Matthews M., Ayalon A., Medina-Elizalde M., Ramsey C. B., Satow C. and Roberts A. P. (2012) Rapid coupling between ice volume and polar temperature over the past 150,000 years. Nature 491, 744–747.

Griffiths M. L., Drysdale R. N., Gagan M. K., Hellstrom J. C., Couchoud I., Ayliffe L. K., Vonhof H. B. and Hantoro W. S. (2013) Australasian monsoon response to Dansgaard-Oeschger event 21 and teleconnections to higher latitudes. Earth Planet. Sci. Lett. 369–370, 294–304.

Griffiths M. L., Fohlmeister J., Drysdale R. N., Hua Q., Johnson K. R., Hellstrom J. C., Gagan M. K. and Zhao J.-X. (2012) Hydrological control on the dead-carbon content of a Holocene tropical speleothem. Quaternary Geochronology 14, 81–93.

Griffiths M. L., Kimbrough A. K., Gagan M. K., Drysdale R. N., Cole J. E., Johnson K. R., Zhao J.-X., Cook B. I., Hellstrom J. C. and Hantoro W. S. (2016) Western Pacific hydroclimate linked to global climate variability over the past two millennia. Nat. Commun. 7, 11719.

Hansen M., Scholz D., Froeschmann M.-L., Schöne B. R. and Spötl C. (2017) Carbon isotope exchange between gaseous CO_2 and thin solution films: Artificial cave experiments and a complete diffusion-reaction model. Geochim. Cosmochim. Acta 211, 28–47.

Hansen M., Scholz D., Schöne B. R. and Spötl C. (2019) Simulating speleothem growth in the laboratory: Determination of the stable isotope fractionation ($\delta^{13}C$ and $\delta^{18}O$) between H_2O, DIC and $CaCO_3$. Chem. Geol. 509, 20–44.

Hartman G. and Danin A. (2010) Isotopic values of plants in relation to water availability in the Eastern Mediterranean region. Oecologia 162, 837–852.

Hartmann A., Eiche E., Neumann T., Fohlmeister J., Schröder-Ritzrau A., Mangini A. and Haryono E. (2013) Multi-proxy evidence for human-induced deforestation and cultivation from a Late-Holocene stalagmite from middle Java, Indonesia. Chem. Geol. 357, 8–17.

Hendy C. H. (1971) The isotopic geochemistry of speleothems – I. the calculation of the effects of different modes of formation on the isotopic composition of speleothems and their applicability as palaeoclimatic indicators. Geochim. Cosmochim. Acta 35, 801–824.

Holmgren K., Lee-Thorp J. A., Cooper G. R. J., Lundblad K., Partridge T. C., Scott L., Sithaldeen R., Talma A. S. and Tyson P. D. (2003) Persistent millennial-scale climatic variability over the past 25,000 years in Southern Africa. Quaternary Sci. Rev. 22, 2311–2326.

Hu C., Henderson G. M., Huang J., Xie S., Sun Y. and Johnson K. R. (2008) Quantification of Holocene Asian monsoon rainfall from spatially separated cave records. Earth Planet Sci. Lett. 266, 221–232.

Huang W., Wang Y., Cheng H., Edwards R. L., Shen C.-C., Liu D., Shao Q., Deng C., Zhang Z. and Wang Q. (2016) Multiscale Holocene Asian monsoon variability deduced from a twin-stalagmite record in southwestern China. Quat. Res. 86, 34–44.

Johnson K. R., Hu C., Belshaw N. S. and Henderson G. M. (2006) Seasonal trace-element and stable-isotope variations in a Chinese speleothem: The potential for high-resolution paleomonsoon reconstruction. Earth Planetary Sci. Lett. 244, 394– 407.

Johnston V. E., Borsato A., Spo¨ tl C., Frisia S. and Miorandi R. (2013) Stable isotopes in caves over altitudinal gradients: fractionation behaviour and inferences for speleothem sensitivity to climate change. Climate of the Past 9, 99–118.

Kacanski A., Carmi I., Shemesh A., Kronfeld J., Yam R. and Flexer A. (2001) Late holocene climatic change in the balkans: speleothem isotopic data from serbia. Radiocarbon 43, 647–658.

Kathayat G., Cheng H., Sinha A., Spötl C., Edwards R. L., Zhang H., Li X., Yi L., Ning Y., Cai Y., Lui W. L. and Breitenbach S. F. M. (2016) Indian monsoon variability on millennial-orbital timescales. Sci. Rep. 6, 24374.

Kätterer T., Reichstein M., Andre´n O. and Lomander A. (1998) Temperature dependence of organic matter decomposition: a critical review using literature data analyzed with different models. Biol. Fertility Soils 27, 258–262.

Kaufmann G. (2003) Stalagmite growth and palaeo-climate: the numerical perspective. Earth Planetary Sci. Lett. 214, 251–266.

Kennett D. J., Breitenbach S. F. M., Aquino V. V., Asmerom Y., Awe J., Baldini J. U. L., Bartlein P., Culleton B. J., Ebert C., Jazwa C., Macri M. J., Marwan N., Polyak V., Prufer K. M., Ridley, Sodemann H., Winterhalder B. and Haug G. H. (2012) Development and disintegration of maya political systems in response to climate change. Science 338, 788–791.

Koltai G., Spötl C., Shen C.-C., Wu C.-C., Rao Z., Palcsu L., Kele S., Suranyi G. and Barany-Kevei I. (2017) A penultimate glacial climate record from southern Hungary. J. Quat. Sci. 32, 946– 956.

Kucera C. L. and Kirkham D. L. (1971) Soil respiration studies in tallgrass prairie in Missouri. Ecology 52, 912–915.

Labuhn I., Genty D., Vonhof H., Bourdin C., Blamart D., Douville E., Ruan J., Cheng H., Edwards R. L., Pons-Branchu E. and Pierre M. (2015) A high-resolution fluid inclusion $\delta^{18}O$ record from a stalagmite in SW France: modern calibration and comparison with multiple proxies. Quat. Sci. Rev. 110, 152–165.

Lachniet M. S., Denniston R. F., Asmerom Y. and Polyak V. J. (2014) Orbital control of western North America atmospheric circulation and climate over two glacial cycles. Nat. Commun., 5.

Lechleitner F. A., Amirnezhad-Mozhdehi S., Columbu A., Comas-Bru L., Labuhn I., Pe´rez-Mejı´as C. and Rehfeld K. (2018) The potential of speleothems from Western Europe as recorders of regional climate: a critical assessment of the SISAL database. Quaternary 1, 30.

Lechleitner F. A., Baldini J. U. L., Breitenbach S. F. M., Fohlmeister J., McIntyre C., Goswami B., Jamieson R. A., van der Voort T. S., Prufer K., Marwan N., Culleton B. J., Kennett D. J., Asmerom Y., Polyak V. and Eglinton T. I. (2016) Hydrological and climatological controls on radiocarbon concentrations in a tropical stalagmite. Geochim. Cosmochim. Acta 194, 233–252.

Li H.-C., Lee Z.-H., Wan N.-J., Shen C.-C., Li T.-Y., Yuan D.-X. and Chen Y.-H. (2011) The $\delta^{18}O$ and $\delta^{13}C$ records in an aragonite stalagmite from Furong Cave, Chongqing, China: A2000-year record of monsoonal climate. J. Asian Earth Sci. 40, 1121–1130.

Li J.-Y., Li H.-C., Li T.-Y., Mii H.-S., Yu T.-L., Shen C.-C. and Xu X. (2017) High-resolution $\delta^{18}O$ and $\delta^{13}C$ records of an AMS 14C and 230Th/U dated stalagmite from Xinya Cave in Chongqing: Climate and vegetation change during the late Holocene. Quat. Int. 447, 75–88.

Linge H., Lauritzen S.-E., Andersson C., Hansen J. K., Skoglund R. Ø. and Sundqvist H. S. (2009) Stable isotope records for the last 10 000 years from Okshola cave (Fauske, northern Norway) and regional comparisons. Clim. Past 5, 667–682.

Linge H., Lauritzen S.-E., Lundberg J. and Berstad I. M. (2001) Stable isotope stratigraphy of Holocene speleothems: examples from a cave system in Rana, northern Norway. Palaeogeogr. Palaeoclimatol. Palaeoecol. 167, 209–224.

Luetscher M., Hoffmann D. L., Frisia S. and Spötl C. (2011) Holocene glacier history from alpine speleothems, Milchbach cave, Switzerland, Earth Planet. Sci. Lett. 302, 95–106. Markowska M., Fohlmeister J., Treble P., Baker A., Andersen M. S. and Hua Q. (2019) Modelling the 14C bomb-pulse in young speleothems using a soil carbon continuum model. Geochim. Cosmochem. Acta 261, 342–367.

Mattey D. P., Atkinson T. C., Barker J. A., Fisher R., Latin J. P., Durrell R. and Ainsworth M. (2016) Carbon dioxide, ground air and carbon cycling in Gibraltar karst. Geochim. Cosmochim. Acta 184, 88–113.

Mattey, D., Fairchild, I. J., Atkinson, T. (2010) Seasonal microclimate control on calcite fabrics, stable isotopes and trace elements in modern speleothem from St. Michaels Cave, Gibraltar: Geological Society, London, Special Publications 336, 323–344.

Mattey D., Lowry D., Duffet J., Fisher R., Hodge E. and Frisia S. (2008) A 53~year seasonally resolved oxygen and carbon isotope record from a modern Gibraltar speleothem: Reconstructed drip water and relationship to local precipitation. Earth Planet. Sci. Lett. 269, 80–95.

McDermott F. (2004) Palaeo-climate reconstruction from stable isotope variations in speleothems: a review. Quaternary Sci. Rev. 23, 901–918.

McDermott F., Frisia S., Huang Y., Longinelli A., Spiro B., Heaton T. H. E., Hawkesworth C. J., Borsato A., Keppens E., Fairchild I. J., van der Borg K., Verheyden S. and Selmo E. (1999) Holocene climate variability in Europe: Evidence from $\delta^{18}O$, textural and extension-rate variations in three speleothems. Quat. Sci. Rev. 18, 1021–1038.

Meyer K. W., Feng W., Breecker D. O., Banner J. L. and Guilfoyle A. (2014) Interpretation of speleothem calcite $\delta^{13}C$ variations: Evidence from monitoring soil CO_2, drip water, and modern speleothem calcite in central Texas. Geochim. Cosmochim. Acta 142, 281–298.

Minami M., Kato T., Horikawa K. and Nakamura T. (2015) Seasonal variations of 14C and $\delta^{13}C$ for cave drip waters in Ryugashi Cave, Shizuoka Prefecture, central Japan. Nucl. Instrum. Methods Phys. Res. Section B: Beam Interactions Mater. Atoms 362, 202–209.

Mischel S. A., Scholz D., Spötl C., Jochum K. P., Schro¨der-Ritzrau A. and Fiedler S. (2017) Holocene climate variability in Central Germany and a potential link to the polar North Atlantic: A replicated record from three coeval speleothems. The Holocene 27, 509–525.

Moreno A., Perez-Mejıas C., Bartolome M., Sancho C., Cacho I., Stoll H., Delgado-Huertas A., Hellstrom J., Edwards R. L. and Cheng H. (2017) New speleothem data from Molinos and Ejulve caves reveal Holocene hydrological variability in northeast Iberia. Quat. Res. 88, 223–233.

Moseley G. E., Edwards R. L., Wendt K. A., Cheng H., Dublyansky Y., Lu Y., Boch R. and Spötl C. (2016) Reconciliation of the Devils Hole climate record with orbital forcing. Science 351, 165–168.

Mühlinghaus C., Scholz D. and Mangini A. (2007) Modelling stalagmite growth and $\delta^{13}C$ as a function of drip interval and temperature. Geochim. Cosmochim. Acta 71, 2780–2790.

Mühlinghaus C., Scholz D. and Mangini A. (2009) Modelling fractionation of stable isotopes in stalagmites. Geochim. Cosmochim. Acta 73, 7275–7289.

Onac B. P., Constantin S., Lundberg J. and Lauritzen S.-E. (2002) Isotopic climate record in a Holocene stalagmite from Ursilor Cave (Romania). J. Quat. Sci. 17, 319–327.

Oster J. L., Montanez I. P., Guilderson T. P., Sharp W. D. and Banner J. L. (2010) Modeling speleothem $\delta^{13}C$ variability in a central Sierra Nevada cave using 14C and 87Sr/86Sr. Geochim. Cosmochim. Acta 74, 5228–5242.

Oster J. L., Warken S. F., Sekhon N., Arienzo M. M. and Lachniet M. (2019) Speleothem paleoclimatology for the Caribbean, Central America, and North America. Quaternary 2,5.

Owen R., Day C. C. and Henderson G. M. (2018) CaveCalc: A new model for speleothem chemistry & isotopes. Comput. Geosci. 119, 115–122.

Parker L. W., Miller J., Steinberger Y. and Whitford W. G. (1983) Soil respiration in a Chihuahuan desert rangeland. Soil Biol. Biochem. 15, 303–309.

Polag D., Scholz D., Mühlinghaus C., Spötl C., Schröder-Ritzrau A., Segl M. and Mangini A. (2010) Stable isotope fractionation in speleothems: Laboratory experiments. Chem. Geol. 279, 31– 39.

Partin J. W., Quinn T. M., Shen C.-C., Emile-Geay J., Taylor F. W., Maupin C. R., Lin K., Jackson C. S., Banner J. L., Sinclair D. J. and Huh C.-A. (2013) Multidecadal rainfall variability in South Pacific Convergence Zone as revealed by stalagmite geochemistry. Geology 41, 1143–1146.

Raich J. W. and Potter C. S. (1995) Global patterns of carbon dioxide emissions from soils. Global Biogeochem. Cycles 9, 23– 36.

Raich J. W. and Schlesinger W. H. (1992) The global carbon dioxide flux in soil respiration and its relationship to vegetation and climate. Tellus B 44, 81–99.

Ridley H. E., Asmerom Y., Baldini J. U. L., Breitenbach S. F. M., Aquino V. V., Prufer K. M., Culleton B. J., Polyak V., Lechleitner F. A., Kennett D. J., Zhang M., Marwan N., Macpherson C. G., Baldini L. M., Xiao T., Peterkin J. L., Awe J. and Haug G. H. (2015) Aerosol forcing of the position of the intertropical convergence zone since ad 1550. Nat. Geosci. 8, 195–200.

Riechelmann D. F., Fohlmeister J., Kluge T., Jochum K. P., Richter D. K., Deininger M., Friedrich R., Frank N. and Scholz D. (2019) Evaluating the potential of tree-ring methodology for cross-dating of three annually laminated stalagmites from Zoolithencave (SE Germany). Quaternary Geochronology 52, 37–50. Riechelmann D. F. C., Schröder-Ritzrau A., Scholz D., Fohlmeister J., Spötl C., Richter D. K. and Mangini A. (2011) Monitoring Bunker Cave (NW Germany): A prerequisite to interpret geochemical proxy data of speleothems from this site. J. Hydrology 409, 682–695.

Romanek C. S., Grossman E. L. and Morse J. W. (1992) Carbon isotopic fractionation in synthetic aragonite and calcite: effects of temperature and precipitation rate. Geochim. Cosmochim. Acta 56, 419–430.

Romanov D., Kaufmann G. and Dreybrodt W. (2008) $\delta^{13}C$ profiles along growth layers of stalagmites: Comparing theoretical and experimental results. Geochim. Cosmochim. Acta 72, 438–448.

Ruan J., Kherbouche F., Genty D., Blamart D., Cheng H., Dewilde F., Hachi S., Edwards R. L., Re´gnier E. and Michelot J.-L. (2016) Evidence of a prolonged drought ca. 4200 yr BP correlated with prehistoric settlement abandonment from the Gueldaman GLD1 Cave, Northern Algeria. Clim. Past 12, 1–14.

Rudzka D., McDermott F., Baldini L. M., Fleitmann D., Moreno A. and Stoll H. (2011) The coupled $\delta^{13}C$ - radiocarbon systematics of three Late Glacial/early Holocene speleothems; insights into soil and cave processes at climatic transitions. Geochim. Cosmochim. Acta 75, 4321–4339.

Rudzka D., McDermott F. and Suric M. (2012) A late Holocene climate record in stalagmites from Modric Cave (Croatia). J. Quat. Sci. 27, 585–596.

Schlesinger W. H. (1977) Carbon balance in terrestrial detritus. Annu. Rev. Ecol. Syst. 8, 51–81.

Scholz D., Frisia S., Borsato A., Spötl C., Fohlmeister J., Mudelsee M., Miorandi R. and Mangini A. (2012) Holocene climate variability in north-eastern Italy: potential influence of the NAO and solar activity recorded by speleothem data. Climate of the Past 8, 1367–1383.

Scholz D., Mühlinghaus C. and Mangini A. (2009) Modelling $\delta^{13}C$ and $\delta^{18}O$ in the solution layer on stalagmite surfaces. Geochim. Cosmochim. Acta 73, 2592–2602.

Scroxton N., Burns S. J., McGee D., Hardt B., Godfrey L. R., Ranivoharimanana L. and Faina P. (2017) Hemispherically in-phase precipitation variability over the last 1700 years in a Madagascar speleothem record. Quat. Sci. Rev. 164, 25–36.

Sherwin C. M. and Baldini J. U. L. (2011) Cave air and hydrological controls on prior calcite precipitation and stalagmite growth rates: Implications for palaeoclimate reconstructions using speleothems. Geochim. Cosmochim. Acta 75, 3915– 3929.

Singh J. S. and Gupta S. R. (1977) Plant decomposition and soil respiration in terrestrial ecosystems. Bot. Rev. 43, 449–528.

Sinha A., Berkelhammer M., Stott L., Mudelsee M., Cheng H. and Biswas J. (2011) The leading mode of Indian Summer Monsoon precipitation variability during the last millennium. Geophys. Res. Lett. 38, L15703.

Sinha A., Kathayat G., Cheng H., Breitenbach S. F. M., Berkelhammer M., Mudelsee M., Biswas J. and Edwards R. L. (2015) Trends and oscillations in the Indian summer monsoon rainfall over the last two millennia. Nat. Commun. 6, 6309.

Spötl C., Fairchild I. J. and Tooth A. F. (2005) Speleothem deposition in a dynamically ventilated cave, Obir Caves (Austrian Alps). Evidence from modern cave air and drip water monitoring. Geochim. Cosmochim. Acta 69, 2451–2468.

Spötl C., Fohlmeister J., Cheng H. and Boch R. (2016) Modern aragonite formation at near-freezing conditions in an alpine cave, Carnic Alps, Austria. Chem. Geol. 435, 60–70.

Springer G. S., Rowe H. D., Hardt B., Cheng H. and Edwards R. L. (2014) East central North America climates during marine isotope stages 3–5. Geophys. Res. Lett. 41, 3233–3237.

Sundqvist H. S., Holmgren K., Fohlmeister J., Zhang Q., Matthews M. B., Spötl C. and Körnich H. (2013) Evidence of a large cooling between 1690 and 1740 AD in southern Africa. Sci. Rep. 3, 1767.

Sundqvist H. S., Holmgren K., Moberg A., Spo¨ tl C. and Mangini A. (2010) Stable isotopes in a stalagmite from NW Sweden document environmental changes over the past 4000 years. Boreas 39, 77–86.

Talma A. S. and Vogel J. C. (1992) Late Quaternary Paleotemperatures Derived from a Speleothem from Cango Caves, Cape Province, South Africa. Quat. Res. 37, 203–213.

Treble P. C., Baker A., Ayliffe L. K., Cohen T. J., Hellstrom J. C., Gagan M. K., Frisia S., Drysdale R. N., Griffiths A. D. and Borsato A. (2017) Hydroclimate of the Last Glacial Maximum and deglaciation in southern Australia's arid margin interpreted from speleothem records (23–15 ka). Clim. Past 13, 667–687.

Tremaine D. M., Froelich P. N. and Wang Y. (2011) Speleothem calcite farmed in situ: modern calibration of $\delta^{18}O$ and $\delta^{13}C$ paleoclimate proxies in a continuously-monitored natural cave system. Geochim. Cosmochim. Acta 75, 4929–4950.

Unal-_Imer E., Shulmeister J., Zhao J.-X., Tonguc¸ Uysal I., Feng Y.-X., Duc Nguyen A. and Yuce G. (2015) An 80 kyr-long continuous speleothem record from Dim Cave, SW Turkey with paleoclimatic implications for the Eastern Mediterranean. Sci. Rep. 5, 13560.

Voarintsoa N. R. G., Brook G. A., Liang F., Marais E., Hardt B., Cheng H., Edwards R. L. and Railsback L. B. (2017a) Stalagmite multi-proxy evidence of wet and dry intervals in northeastern Namibia: Linkage to latitudinal shifts of the Inter-Tropical Convergence Zone and changing solar activity from AD 1400 to 1950. The Holocene 27, 384–396.

Voarintsoa N. R. G., Railsback L. B., Brook G. A., Wang L., Kathayat G., Cheng H., Li X., Edwards R. L., Rakotondrazafy A. F. M. and Madison Razanatseheno M. O. (2017b) Three distinct Holocene intervals of stalagmite deposition and non-deposition revealed in NW Madagascar, and their paleoclimate implications. Clim. Past 13, 1771–1790.

Voarintsoa N. R. G., Wang L., Railsback L. B., Brook G. A., Liang F., Cheng H. and Edwards R. L. (2017c) Multiple proxy analyses of a U/Th-dated stalagmite to reconstruct paleoenvironmental changes in northwestern Madagascar between 370CE and 1300CE. Palaeogeogr. Palaeoclimatol. Palaeoecol. 469, 138–155.

Wainer K., Genty D., Blamart D., Daeron M., Bar-Matthews M., Vonhof H., Dublyansky Y., Pons-Branchu E., Thomas L., van Calsteren P., Quinif Y. and Caillon N. (2011) Speleothem record of the last 180 ka in Villars cave (SW France): Investigation of a large $\delta^{18}O$ shift between MIS6 and MIS5. Quat. Sci. Rev. 30, 130–146.

Wang X., Edwards R. L., Auler A. S., Cheng H., Kong X., Wang Y., Cruz F. W., Dorale J. A. and Chiang H.-W. (2017) Hydroclimate changes across the Amazon lowlands over the past 45,000 years. Nature 541, 204–207.

Webster J. W., Brook G. A., Railsback L. B., Cheng H., Edwards R. L., Alexander C. and Reeder P. P. (2007) Stalagmite evidence from Belize indicating significant droughts at the time of Preclassic Abandonment, the Maya Hiatus, and the Classic Maya collapse. Palaeogeogr. Palaeoclimatol. Palaeoecol. 250, 1–17.

Whittaker T. E. (2008) High-resolution speleothem-based palaeoclimate records from. Zealand reveal robust teleconnection to North Atlantic during MIS 1–4, Ph.D. thesis, The. University of Waikato, New.

Wiedner E., Scholz D., Mangini A., Polag D., Mühlinghaus C. and Segl M. (2008) Investigation of the stable isotope fractionation in speleothems with laboratory experiments. Quaternary Int. 187, 15–24.

Winter A., Miller T., Kushnir Y., Sinha A., Timmermann A., Jury M. R., Gallup C., Cheng H. and Edwards R. L. (2011) Evidence for 800 years of North Atlantic multi-decadal variability from a Puerto Rican speleothem, Earth Planet. Sci. Lett. 308, 23–28.

Wong C. I., Banner J. L. and Musgrove M. (2015) Holocene climate variability in Texas, USA: An integration of existing paleoclimate data and modeling with a new, high-resolution speleothem record. Quat. Sci. Rev. 127, 155–173.

Wong C. I. and Breecker D. O. (2015) Advancements in the use of speleothems as climate archives. Quat. Sci. Rev. 127, 1–18.

Wortham B. E., Wong C. I., Silva L. C. R., McGee D., Montanez I. P., Troy Rasbury E., Cooper K. M., Sharp W. D., Glessner J. J. G. and Santos R. V. (2017) Assessing response of local moisture conditions in central Brazil to variability in regional monsoon intensity using speleothem 87Sr/86Sr values. Earth Planet. Sci. Lett. 463, 310–322.

Associate editor: Miryam Bar-Matthews

B.4. The stalagmite record of southern Arabia: climatic extremes, human evolution, and societal development

Nicholson, S.L., **Jacobson, M.J.**, Hosfield, R. & Fleitmann, D. 2021. The stalagmite record of southern Arabia: climatic extremes, human evolution, and societal development.

Submitted to: Frontiers in Earth Science. Extreme Events in Human Evolution: From the Pliocene to the Anthropocene

The stalagmite record of Southern Arabia: climatic extremes, human evolution, and societal development

Samuel Luke Nicholson[1], Matthew J. Jacobson[2], Rob Hosfield[2], Dominik Fleitmann[3]

[1]Ecology and Evolutionary Biology, University of Reading, Reading, United Kingdom

[2]School of Archaeology, Geography and Environmental Science, University of Reading, United Kingdom

[3]Quaternary Geology, Department of Environmental Sciences, University of Basel, Switzerland

*** Correspondence:** Samuel Luke Nicholson (sam.nicholson@reading.ac.uk)

Abstract

The fluctuating climatic conditions of the Saharo-Arabian deserts are increasingly linked to human evolutionary events and societal developments. On orbital timescales, the African and Indian Summer Monsoons were displaced northward and increased precipitation to the Arabian Peninsula which led to favourable periods for human occupation in the now arid interior. At least 4 periods of climatic optima occurred within the last 130,000 years, related to Marine Isotope Stages (MIS) 5e (128-121 ka BP), 5c (104-97 ka BP), 5a (81-74 ka BP) and 1 (10.5-6.2 ka BP), and potentially early MIS 3 (60-50 ka BP). Stalagmites from Southern Arabia have been key to understanding climatic fluctuations and human-environmental interactions; their precise and high-resolution chronologies can be linked to evidence for changes in human distribution and climate/environment induced societal developments. Here, we review the most recent advances in the Southern Arabian Late Pleistocene and Early Holocene stalagmite records. We compare and contrast MIS 5e and Early Holocene climates to understand how these differed, benchmark the extremes of climatic variability and summarise the impacts on human societal development. We suggest

that, while the extreme of MIS 5e was important for *H. sapiens* dispersal, subsequent, less intense, wet phases mitigate against a simplistic narrative. We highlight that while climate can be a limiting and important factor, there is also the potential of human adaptability and resilience. Further studies will be needed to understand spatio-temporal difference in human-environment interactions in a climatically variable region.

1. Introduction

The fluctuating palaeoclimate conditions of Southern Arabia are frequently related to broad changes in hominin distribution as well as regional societal developments. Intensifications and expansions of the monsoon domain increased precipitation across Southern Arabia during periods of increased solar insolation, following orbitally-paced cycles (Burns et al., 1998, 2001; Fleitmann et al., 2003b, 2011; Jennings et al., 2015; Parton et al., 2015b; Nicholson et al., 2020). During the last 130 kyrs, at least four prolonged periods of increased precipitation have been identified and dated to MIS 5e (128-121 ka BP), MIS 5c (104-97 ka BP), MIS 5a (81-74 ka BP) and the Early Holocene (10.5-6.2 ka BP), and perhaps early MIS 3 (60-50 ka BP), each lasting for a few millennia (Burns et al., 2001; Fleitmann et al., 2011; Parton et al., 2013; Nicholson et al., 2020). These extreme increases in rainfall permitted the formation of large, deep and perennial lakes and other waterbodies in the now arid interiors (Rosenberg et al., 2011, 2012, 2013; Petraglia et al., 2012; Parton et al., 2013, 2015a). As well as increased surface water availability and refilling of aquifers, increased rainfall led to 'greening' events of Arabia, in which grassland environments expanded into the now arid desert interiors and supported the spread of large mammals and human settlement (Rose et al., 2011; Petraglia et al., 2012; Groucutt et al., 2015, 2018, 2021; Stimpson et al., 2016; Stewart et al., 2020a, 2020b; Scerri et al., 2021).

Speleothems (stalagmites, stalactite and flowstones) have been key sources of terrestrial palaeoclimatic information in Southern Arabia. Unlike other terrestrial archives (e.g., lacustrine and alluvial records), their subterranean location protects them from desert weathering conditions (Burns et al., 1998; Vaks et al., 2010; El-Shenawy et al., 2018; Burstyn et al., 2019; Henselowsky et al., 2021). Additionally, speleothem growth requires a positive precipitation-evaporation balance, and can thus inform the timing of prolonged soil humidity

above the cave. Stalagmites are particularly useful for palaeoclimate reconstructions; their laminated growth permits the development of precise climatic records through U-Th dating and analyses of calcite oxygen ($\delta^{18}O_{ca}$) and carbon ($\delta^{13}C_{ca}$) stable-isotopes, which can be linked to archaeological (and historical) records. Since 1998, a series of publications have provided a unique insight into the palaeoclimate of Southern Arabia using stalagmites collected from Hoti (23.08 N, 57.35 E), Mukallah (14.91 N, 48.59 E), and Qunf (17.16 N, 54.3 E) caves (Fig. 1A). Specific site descriptions of the caves have been made available elsewhere (Burns et al., 1998; Fleitmann et al., 2003b, 2003a, 2007, 2011). Here, we summarise these works and provide a comparison between two of these climatically extreme periods: MIS 5e and the Early Holocene.

2. Timing of increased rainfall during the last 130 kyrs

At least four South Arabian Humid Periods (SAHPs) occurred during the Late Pleistocene and Early Holocene. At Mukallah Cave, stalagmite deposition was recorded during MIS 5e (~128-121 ka BP; SAHP 4), 5c (~104-97 ka BP; SAHP 3), and the Early Holocene (~10-6 ka BP; SAHP 1). At Hoti cave, stalagmite deposition occurred during MIS 5e, 5a (~85-74 ka BP; SAHP 2) and the Holocene (10 to 5.2 ka BP and 2.6 ka BP to present) (Fleitmann et al., 2007). Stalagmite growth is also recorded at Qunf Cave (Q5), Defore Cave (S3, S4, S6, S9) and Dimarshim (D1). An almost continuous climatic record (~10.6 ka to 0.3 ka) is provided by Q5, whereas S3 and S4 are only active before and after SAHP 1 and D1 grows from ~4.2 to 0 ka. Determination of stalagmite fluid inclusion water $\delta^{18}O$ and δD values from Mukallah and Hoti caves have shown that increased precipitation during MIS 5e and the Holocene were delivered by the African Summer Monsoon (ASM) and the Indian Summer Monsoon (ISM) (Fleitmann et al., 2003b; Nicholson et al., 2020). This is in good coherence with other records of ASM and ISM intensity, particularly sapropel layers S5 (128.3-121.5 ka), S4 (107.8-101.8 ka), S3 (85.8-80.8 ka) and S1 (10.5-6.1 ka) from Mediterranean Sea core ODP 967 (Rohling et al., 2015; Grant et al., 2017).

Stalagmite distribution, size and shape can reveal changes in precipitation amounts in arid environments. An estimated annual precipitation >300 mm/yr^{-1} for SAHPs was established using the distribution of active stalagmite growth in the Negev desert (Vaks et al.,

2006, 2010, 2013), suggesting palaeo-precipitation doubled current amounts at Mukallah and Hoti Caves (Fleitmann et al., 2011; Nicholson et al., 2020; Fig. 1A). MIS 5e stalagmites (Y99 and H13) are large (width >30 cm; and height >1 m), suggesting annual rainfall was considerably higher than 300 mm/yr^{-1}. This is supported by deposition of a large MIS 5e flowstone at Hoti Cave, which indicates flowing water on the cave floor, activation of large lakes (Rosenberg et al., 2011, 2012), the deposition of sapropel S5 caused by ~8 times higher Nile outflow (Amies et al., 2019) and modelled rainfall amounts of 300-600 mm/yr^{-1} during MIS 5e (Otto-Bliesner, 2006; Jennings et al., 2015; Fig. 1A). Stalagmites from later growth periods, such as Y97-4 and Y97-5 and H4, are comparatively smaller (Fleitmann et al., 2011), suggesting that annual rainfall was less than during SAHP 4. This is consistent with modelled Early Holocene rainfall of 200-300 mm/yr^{-1} over Mukallah Cave (Fordham et al., 2017; Brown et al., 2018).

Differing rainfall amounts between SAHPs are confirmed by stalagmite $\delta^{18}O_{ca}$ values, which are influenced by the intensity of ASM (Mukallah) and ISM (Hoti) rainfall (Fleitmann et al., 2011; Nicholson et al., 2020). SAHP 4 (MIS 5e) has the most negative $\delta^{18}O_{ca}$ values (increased rainfall), whereas SAHP 1 (Holocene) has the most positive $\delta^{18}O_{ca}$ values (drier conditions) (Nicholson et al., 2020). The competing effects of high-latitude glacial-boundary conditions and low-latitude insolation are both considered to control the expansion, contraction and intensity of the monsoon domain (Burns et al., 2003; Cheng et al., 2009a; Beck et al., 2018) and are key differentiating factors of SAHPs (Nicholson et al., 2020). While precipitation intensities of SAHP 4, 3 and 2 follow the declining intensity of glacial-boundary minima, SAHP 1 contradicts this trend, as positive $\delta^{18}O$ occurred during an interglacial maximum. Instead, SAHP $\delta^{18}O$ values consistently follow the pattern of declining low-latitude summer Northern Hemisphere Insolation (NHI) maxima, which are regulated on orbital eccentricity (100 kyr) and precession (21 kyr) cycles (Fig. 1B). Low-latitude insolation is a key control on the interhemispheric pressure gradient, whereby greater solar heating of the Tibetan Plateau and northern Indian Ocean results in enhanced low pressure and intensification of northern hemisphere cyclones (Burns et al., 2003; Fleitmann et al., 2007; Parton et al., 2015b; Beck et al., 2018). Thus, comparatively low insolation values during SAHP 1 are matched by a weaker response of monsoon intensity compared to preceding SAHPs.

Importantly, SAHPs had differing climatic conditions and likely brought unique environmental responses and challenges for human populations.

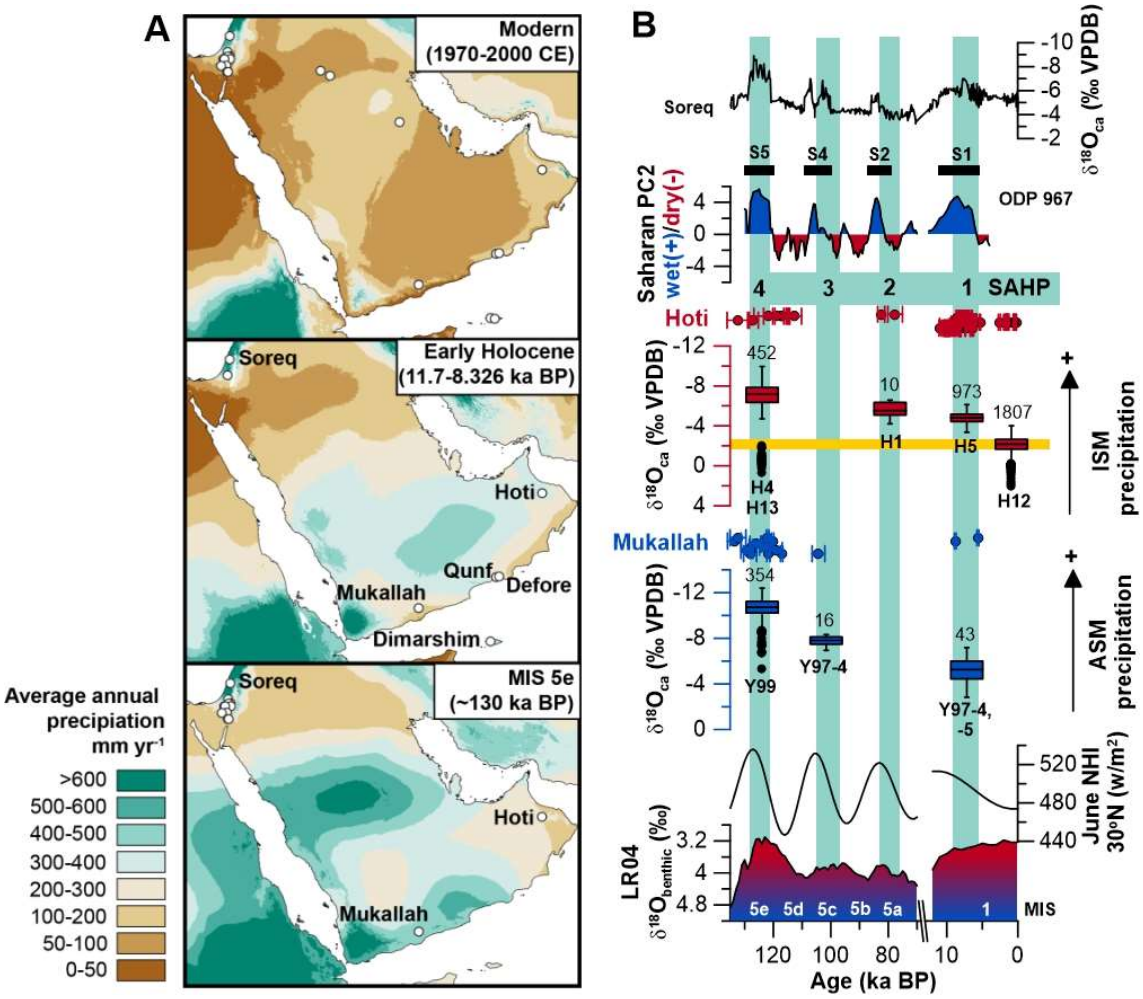

Fig. 1. A) simulated average annual precipitation maps of the Arabian Peninsula for modern (Fick and Hijmans, 2017), Early Holocene (Fick and Hijmans, 2017; Fordham et al., 2017; Brown et al., 2018) and MIS 5e (Otto-Bliesner, 2006; WorldClim, 2015) periods. Speleothem cave sites (white circles) show distribution of fossil stalagmites (modern) and their respective growth periods (Early Holocene and MIS 5e). B) box-whisker plots of stalagmite $\delta^{18}O_{ca}$ values from Hoti (top) and Mukallah (bottom) caves vs. the Soreq Cave $\delta^{18}O_{ca}$ curve (Bar-Matthews et al., 2003; Grant et al., 2012, 2016), ODP 967 PC2 wet/dry index and sapropel layers (Grant et al., 2017), low latitude (30oN; Berger and Loutre, 1991) and global ice-volume (LR04; Lisiecki and Raymo, 2005). Black circles denote statistically extreme values. Sample counts and stalagmite specimens are given above and below boxes, respectively. See supplementary files for results of ANOVA and Wilcoxon rank sum test. The yellow bar denotes the range of modern stalagmite $\delta^{18}O_{ca}$ values from Hoti Cave. ^{230}Th ages and age uncertainties for Mukallah (blue) and Hoti (red) cave speleothems are given above their respective boxplots. Relevant Marine Isotope Stages are provided using the taxonomy of Railsback et al. (2015).

3. Rainfall trends during MIS 5e and the Holocene

3.1. MIS 5e

Precise ^{230}Th ages of stalagmites combined with $\delta^{18}O_{ca}$ values have provided records of MIS 5e and Holocene climatic variability. The Y99 (Mukallah) $\delta^{18}O_{ca}$ and $\delta^{13}C_{ca}$ (Y99) covers SAHP 4 in Yemen, with onset and termination of stalagmite growth at 127.8 and 121.1 ka BP. There are four distinct features of the Y99 $\delta^{18}O_{ca}$ curve: 1) onset of enhanced rainfall is characterised by negative $\delta^{18}O_{ca}$ values, suggesting this was abrupt, perhaps within <500 years as suggested by other ASM records (e.g., Bar-Matthews et al., 2003). 2) There is a clear relationship to the July 30°N isolation curve, demonstrating rainfall intensity was modulated by low-latitude insolation (Fig. 1B and 2B). 3) While there is considerable variability, $\delta^{18}O_{ca}$ values are consistently more negative (wetter conditions) than succeeding wet phases. 4) There is an abrupt increase in $\delta^{18}O_{ca}$ and $\delta^{13}C_{ca}$ (drier conditions) at the termination of the wet period as the tropical rain-belt retreated southwards and annual rainfall fell below the threshold for large stalagmite formation (Nicholson et al., 2020). Additionally, sub-annually resolved H13 (Hoti) $\delta^{18}O_{ca}$ and $\delta^{13}C_{ca}$ records shows MIS 5e was characterised by increased seasonality (wetter summers and drier winters) dominated by a monsoon-driven precipitation regime (Nicholson et al., 2020). This was likely echoed by a seasonal vegetation response, as indicated by the presence of C4 plants (Bretzke et al., 2013; Nicholson et al., 2020), with potentially significant implications for animals and human hunter-gatherers.

3.2. The Holocene

The Early Holocene is characterised by another period of increased rainfall in Arabia, known as the Holocene Humid Period (HHP), or SAHP 1 in Southern Arabia (Burns et al., 1998, 2001; Fleitmann et al., 2003a, 2007; Fleitmann and Matter, 2009; Lézine, 2009; Rosenberg et al., 2011, 2013; Engel et al., 2012). Stalagmite records from Hoti (H5 and H12), Qunf (Q5) and Defore (S3 and S4) caves provide information of rainfall variability throughout the Holocene. At Hoti Cave $\delta^{18}O_{ca}$ values show shifting dominances of winter (derived from the Mediterranean Sea) vs. summer (derived from the Indian Ocean) precipitation, whereas Qunf Cave $\delta^{18}O_{ca}$ values record ISM precipitation intensity. Whereas Hoti Cave $\delta^{18}O_{ca}$ values indicate that winter precipitation has been dominant over the last ~6 ka, the Early Holocene

is marked by more negative $\delta^{18}O_{ca}$ values reflecting increased summer precipitation (Neff et al., 2001; Burns et al., 2003; Fleitmann et al., 2007; Shakun et al., 2007). This is coeval to more negative $\delta^{18}O_{ca}$ values at Qunf Cave which indicate an intensification of the ISM. At both caves $\delta^{18}O_{ca}$ values show:

1) Intensification of summer precipitation between 10.6 to 9.4 ka BP, which slightly lags low-latitude insolation due to comparatively high glacial-boundary forcing (Fleitmann et al., 2007).

2) Considerable multi-decadal variability within both H5 and Q5, displaying clear relationships with GRIP, NGRIP and DYE-3 ice-core $\delta^{18}O$ records (Johnsen et al., 2001; Neff et al., 2001; Fleitmann et al., 2003a, 2007; Fleitmann and Matter, 2009). More negative ice-core $\delta^{18}O$ (colder northern-hemisphere conditions) were reflected by more positive (drier conditions) stalagmite $\delta^{18}O_{ca}$ values.

3) A distinct increase of $\delta^{18}O_{ca}$ values (drier conditions) is observed between ~8.2-8.0 ka BP and is related to the so-called "8.2-kyr event"; a global climatic event caused by the collapse of Atlantic Overturning Meridional Circulation (AMOC) due to draining of Hudson Bay glacial lakes and freshwater influx into the Atlantic (Barber et al., 1999; Kobashi et al., 2007). $\delta^{18}O_{ca}$ values of H14 and H5 (Hoti Cave) show this period was characterised by a weakening of rainfall and led to a hiatus of H14 growth (Cheng et al., 2009b).

4) Summer precipitation declines at ~6.2 ka BP. At Qunf Cave, this decline is gradual and closely follows the 30°N isolation-curve (for an extended discussion, see Fleitmann et al., 2007). At Hoti Cave, this precipitation decline is more abrupt (identifiable by change point analysis; Fig. 2) and related to winter rainfall becoming the dominant source of precipitation in northern Oman (Fleitmann et al., 2007). As Hoti Cave provides solid timing on the shifting dominance of winter vs. summer precipitation, the H5 record has been used to define the duration of SAHP 1 and is consistent with the ^{230}Th ages of Holocene stalagmites from Mukallah Cave (Fleitmann et al., 2011; Nicholson et al., 2020). Whereas the Y99 record indicates SAHP 4 (during MIS 5e) persisted for ~6.5 kyrs, the Hoti Cave composite record indicates SAHP 1 lasted for a shorter period of ~4 kyrs.

These patterns follow established conditions during SAHP 1, which in Southern Arabia are also evidenced by vegetation expansion (Fuchs and Buerkert, 2008), vegetation that requires adequate precipitation (Parker et al., 2004), and palaeolake and river formation (Farraj and Harvey, 2004; Preston, 2011; Berger et al., 2012). Across Arabia, these changes are asynchronous (Preston and Parker, 2013; Preston et al., 2015), with northern Arabia experiencing a truncated period of increased rainfall compared to the south.

4. Discussion

4.1. MIS 5e

What do the varied conditions between SAHPs mean for discussions of human populations and climatic extremes? There is a growing body of evidence which relates Pleistocene human movements between Arabia and Africa to periods of enhanced precipitation. Archaeological remains at Jebel Faya were dated to MIS 5e and may evidence the earliest instance of *H. sapiens* in the region (Armitage et al., 2011). Outside of Arabia, MIS 5 *H. sapiens* fossils uncovered at Skhul, Qafzeh (Israel, Millard, 2008) and Fuyan Cave (≥80 ka BP, China; Liu et al., 2015) represent some of the earliest instances of Late Pleistocene humans outside of Africa. MIS 5e saw the most intense enhancement of precipitation, highlighting that this period may have been particularly favourable for hominin occupation and dispersal across the Saharo-Arabian deserts (Larrasoaña et al., 2013; Nicholson et al., 2021). Such a large increase of precipitation was likely echoed by a greater vegetation response than later SAHPs, as evidenced by Mukallah Cave $\delta^{13}C_{ca}$ values (Nicholson et al., 2020) and the Jebel Faya phytolith record (Bretzke et al., 2013). It is thus likely that the carrying capacity of the Arabian Peninsula was greater during SAHP 4 compared to subsequent SAHPs, meaning population expansions and/or dispersals could have been rapid (Nicholson et al., 2021). Additionally, the longer duration of SAHP 4 indicates that 'green' environments were longer-lived than in SAHP 1, offering potentially longer-term occupation of the now arid interior. In this sense, climatic conditions during MIS 5e were at one extreme of Southern Arabia climatic variability and should not be understated as an optimal period for human dispersal.

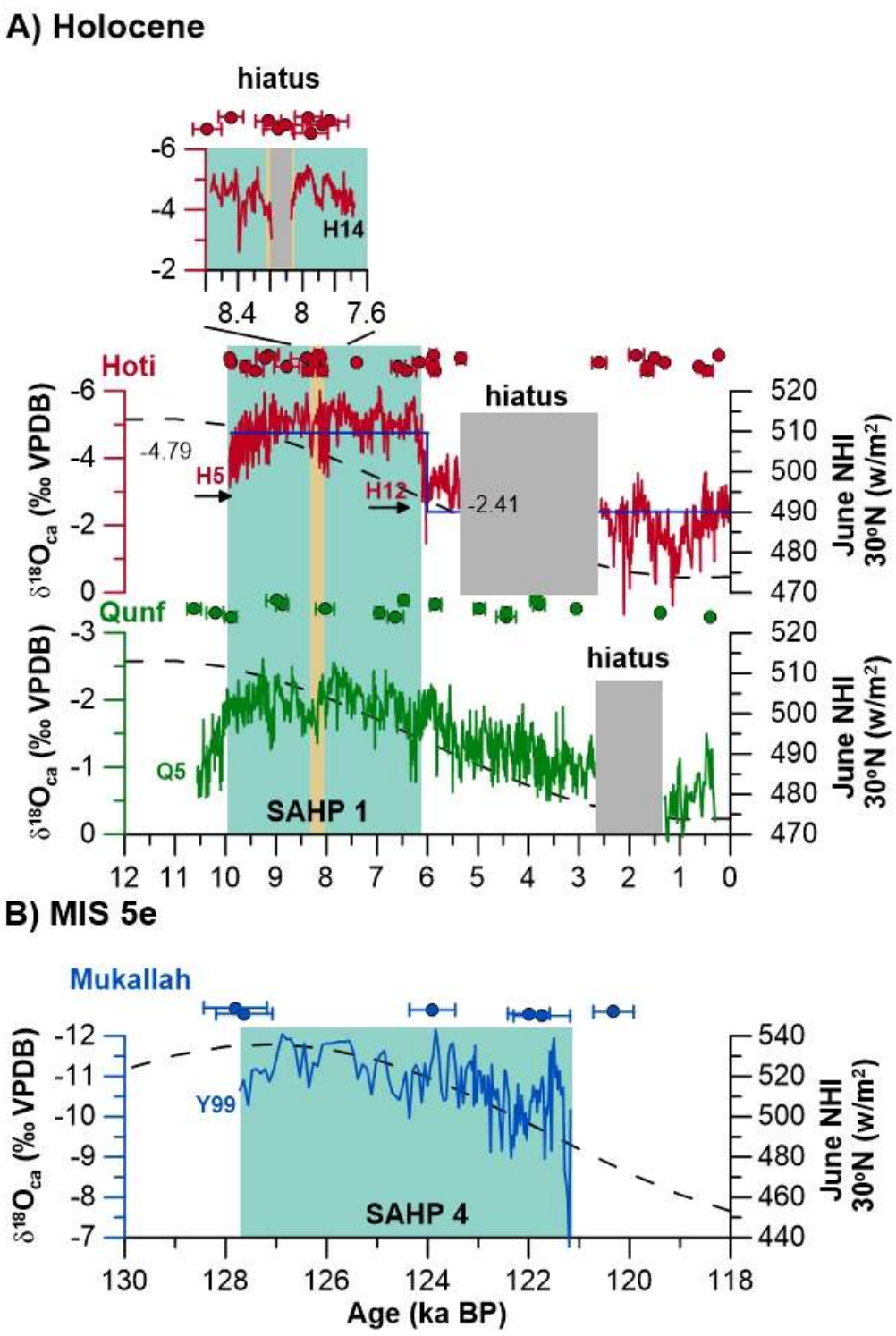

Fig. 2. A) High-resolution $\delta^{18}O_{ca}$ stalagmite values for the Holocene (H5, H12, H14 and Q5) Blue lines for H5 and H12 represent means before and after the change-point at ~6.2 ka BP. The change-point was identified using the changepoint package for R (Killick et al., 2016). ^{230}Th ages (circles) and uncertainty bars are given above their respective curves. B) High-resolution $\delta^{18}O_{ca}$ stalagmite values for MIS 5e (Y99). ^{230}Th ages from Fleitmann et al. (2011) are represented by triangles; these been superseded by measurements from Nicholson et al. (2020) (circles) used to create the StalAge (Scholz and Hoffmann, 2011) age-depth model.

However, it must be noted that archaeological finds are also dated to MIS 5c, 5a and 3 (Petraglia et al., 2011; Rose et al., 2011; Delagnes et al., 2012; Groucutt et al., 2018). While MIS 5e may therefore be the most extreme period of increased rainfall, other periods were still able to support human populations despite being 'less favourable'. Do these climatic differences suggest that strategies of survival differed between SAHPs (e.g., Bretzke and Conard, 2017)? Were subsequent dispersals more limited in terms of numbers of people and other animals? What do statistically significant differences in $\delta^{18}O_{ca}$ values translate to in terms of annual rainfall differences, as well as spatio-temporal variance on long (e.g., millennial) and short (e.g., annual) timescales? Or were the additional benefits of SAHP 4 compared to other SAHPs simply not that important for human occupation (i.e., humans could make do with less)? Additionally, the presence of *H. sapiens* in Arabia within MIS 3 suggests either occupation throughout the MIS 4 glacial or re-entry despite a 'drier' climate (Armitage et al., 2011; Delagnes et al., 2012; Nicholson et al., 2020). One message we may take from this is resilience/adaptation despite climatic differences, and that while the stalagmite record provides useful information on the timing of major climatic changes and major *H. sapiens* biogeographic shifts, providing a climatic 'bench-mark' for Late Pleistocene occupations from the stalagmite record is too deterministic and overlooks uncertainties within the archaeological record.

One thing that is perhaps clearer is that the termination of these wet periods saw a substantial change in environmental conditions. The termination of SAHP 4 likely meant annual rainfall declined to <300 mm/yr^{-1} and was echoed by a decline in vegetation resources. In terms of the "lived" experiences of humans, such a decline would have likely required a shift in survival strategies. This may have included increased home-range foraging size and mobility patterns, retraction to high-resource retaining areas (such as the Yemeni Highlands; Delagnes et al., 2012, 2013) or in some cases dispersal out of Arabia (Nicholson et al., 2021). Such responses to declining precipitation were also likely variable and not simplistic. Recent archaeological finds in Northern Arabia hint at techno-cultural continuity between Mid-Pleistocene wetter phases (Scerri et al., 2021), perhaps suggesting human resilience in spite of declining climatic conditions.

4.2. Early Holocene

The key precipitation changes during the HHP/SAHP 1 of gradual intensification of summer precipitation (~10.6-9.4 ka BP) that only declines following ~6.2 ka BP, and temporarily during the 9.2 and 8.2ka events (Fleitmann et al., 2008), influenced humans and communities living in Arabia (for full summaries, see Parker et al., 2006; Goudie and Parker, 2010; Groucutt et al., 2020; Petraglia et al., 2020).

When compared to MIS 5e however, precipitation increases and associated vegetation response were less intense (Fleitmann et al., 2011; Bretzke et al., 2013; Nicholson et al., 2020). Despite this, and similar to MIS 5c, 5a and 3 (see above), there remains archaeological evidence for human occupation. Mustatils appear in northern Arabia from 9.2 ka BP (Kennedy, 2017; Guagnin et al., 2020; Thomas et al., 2021), and desert kites are evidenced in Jordan from 10 ka BP (al Khasawneh et al., 2019). In southern Arabia, occupation of the Jebel Qara took place ~10.5-9.5 ka BP (Cremaschi et al., 2015), pastoralism is evidenced by 8.0 ka BP (Drechsler, 2007, 2009; Martin et al., 2009), graves are attested 7.2-6.0 ka BP (Kiesewetter, 2006) and monumental stone platforms are evidenced 6.4 ka BP (McCorriston et al., 2012; Magee, 2014).

Reduced rainfall following ~6.2 ka BP led to a temporary end of Neolithic herding in the desert interiors, shrinking population numbers, and migration to areas with greater ecological diversity, perhaps suggesting a minimum amount of precipitation is required for human occupation in these marginal environments (Uerpmann, 1992, 2002; Vogt, 1994; Potts et al., 2003; Goudie and Parker, 2010). However, human communities returned to the interior of Southern Arabia from ~5.2 ka BP without amelioration of climate, which even aridified further; varied occupation continues until the modern day (Magee, 2014; Petraglia et al., 2020).Therefore, it seems likely that drier climates create challenges for human populations, but these can be overcome by technological (e.g. mustatils, pottery, water management; camels domestication) and strategic (e.g. mobility, pastoralism) adaptations (Petraglia et al., 2020).

Finally, stability and variance of precipitation (which can be hard to detect in palaeoclimate records) may have been more influential to humans than long-term changes in amounts (Thornton et al., 2014). A temporary transition to herding practices occurred in

some parts of Arabia during the 8.2ka BP event (Drechsler, 2009; Crassard and Drechsler, 2013) whilst more positive $\delta^{18}O_{ca}$ values are observed at Hoti cave, indicating drier conditions (Fig. 2A). Conversely, (Cremaschi et al., 2015) suggested that overly 'wet' landscapes at Jebel Qara led to a preference for ameliorated coastal settings during the HHP, hinting at the varied human responses to fluctuating climatic conditions during the Holocene.

5. Conclusion

Overall, when compared to other periods, stalagmite climate records indicate that the African and Indian Summer Monsoons were most intense during MIS 5e and was one extreme of climatic variability in the last 130 kyrs. This was likely an important period for the dispersal of *H. sapiens* from Africa, as well as the occupation in the now desert interiors of Arabia, and the subsequent decline back to more arid conditions likely impacted survival strategies in Southern Arabia. We emphasise that evidence for human occupation during all periods of insolation maxima, and the varying climates of these drier periods, highlights human resilience/adaptation despite climatic differences and mitigates against a simplistic narrative. Future research will benefit from the addition of climate/environmental proxies (trace-element, n-alkanes, biomarkers and perhaps aDNA), increased surveys to advance the spatial-temporal coverage of the speleothem record and development of continuous climate records for SAHP 3 and 2. Understanding the shifting survival strategies in context of declining rainfall and aridification, as Arabia transitioned from one extreme to another, will be of key importance to future debates of *H. sapiens* biogeography, behavioural flexibility, and both past and future climate-induced socio-political change.

Acknowledgements

This work was supported by the AHRC South, West and Wales Doctoral Training Partnership (Grant AH/L503939/1) the Swiss National Science Foundation (Grant PP002-110554/1 to DF).

References

al Khasawneh, S., Murray, A., Thomsen, K., AbuAzizeh, W., Tarawneh, M., 2019. Dating a near eastern desert hunting trap (kite) using rock surface luminescence dating. Archaeological and Anthropological Sciences. 11, 2109–2119.

Amies, J.D., Rohling, E.J., Grant, K.M., Rodríguez-Sanz, L., Marino, G., 2019. Quantification of African Monsoon Runoff During Last Interglacial Sapropel S5. Paleoceanography and Paleoclimatology. 34, 1487–1516.

Armitage, S.J., Jasim, S.A., Marks, A.E., Parker, A.G., Usik, V.I., Uerpmann, H.P., 2011. The southern route "out of Africa": Evidence for an early expansion of modern humans into Arabia. Science. 331, 453–456.

Bar-Matthews, M., Ayalon, A., Gilmour, M., Matthews, A., Hawkesworth, C.J., 2003. Sea - land oxygen isotopic relationships from planktonic foraminifera and speleothems in the Eastern Mediterranean region and their implication for paleorainfall during interglacial intervals. Geochimica et Cosmochimica Acta. 67, 3181–3199.

Barber, D.C., Dyke, A., Hillaire-Marcel, C., Jennings, A.E., Andrews, J.T., Kerwin, M.W., Bilodeau, G., McNeely, R., Southon, J., Morehead, M.D., Gagnon, J.-M., 1999. Forcing of the cold event of 8,200 years ago by catastrophic drainage of Laurentide lakes. Nature. 400, 344–348.

Beck, J.W., Zhou, W., Li, C., Wu, Z., White, L., Xian, F., Kong, X., An, Z., 2018. A 550,000-year record of East Asian monsoon rainfall from 10Be in loess. Science. 360, 877–881.

Berger, A., Loutre, M.F., 1991. Insolation values for the climate of the last 10 million years. Quaternary Science Reviews. 10, 297–317.

Berger, J.-F., Bravard, J.-P., Purdue, L., Benoist, A., Mouton, M., Braemer, F., 2012. Rivers of the Hadramawt watershed (Yemen) during the Holocene: Clues of late functioning. Quaternary International. 266, 142–161.

Bretzke, K., Armitage, S.J., Parker, A.G., Walkington, H., Uerpmann, H.P., 2013. The environmental context of Paleolithic settlement at Jebel Faya, Emirate Sharjah, UAE. Quaternary International. 300, 83–93.

Bretzke, K., Conard, N.J., 2017. Not just a crossroad population dynamics and changing material culture in southwestern asia during the late pleistocene. Current Anthropology. 58, S449–S462.

Brown, J.L., Hill, D.J., Dolan, A.M., Carnaval, A.C., Haywood, A.M., 2018. Paleoclim, high spatial resolution paleoclimate surfaces for global land areas. Scientific Data.

Burns, S.J., Fleitmann, D., Matter, A., Kramers, J., Al-Subbary, A.A., 2003. Indian Ocean Climate and an Absolute Chronology over Dansgaard/Oeschger Events 9 to 13. Science. 301, 1365 LP – 1367.

Burns, S.J., Fleitmann, D., Matter, A., Neff, U., Mangini, A., 2001. Speleothem evidence from Oman for continental pluvial events during interglacial periods. Geology. 29, 623–626.

Burns, S.J., Matter, A., Frank, N., Mangini, A., 1998. Speleothem-based paleoclimate record from northern Oman. Geology. 26, 499–502.

Burstyn, Y., Martrat, B., Lopez, J.F., Iriarte, E., Jacobson, M.J., Lone, M.A., Deininger, M., 2019. Speleothems from the Middle East: An Example of Water Limited Environments in the SISAL Database. Quaternary. 2, 16.

Cheng, H., Edwards, R.L., Broecker, W.S., Denton, G.H., Kong, X., Wang, Y., Zhang, R., Wang, X., 2009a. Ice age terminations. Science. 326, 248–252.

Cheng, H., Fleitmann, D., Edwards, R.L., Wang, X., Cruz, F.W., Auler, A.S., Mangini, A., Wang, Y., Kong, X., Burns, S.J., Matter, A., 2009b. Timing and structure of the 8.2. kyr B.P. event inferred from $\delta^{18}O$

records of stalagmites from China, Oman, and Brazil. Geology. 37, 1007–1010.

Crassard, R., Drechsler, P., 2013. Towards new paradigms: multiple pathways for the Arabian Neolithic. Arabian Archaeology and Epigraphy. 24, 3–8.

Cremaschi, M., Zerboni, A., Charpentier, V., Crassard, R., Isola, I., Regattieri, E., Zanchetta, G., 2015. Early–Middle Holocene environmental changes and pre-Neolithic human occupations as recorded in the cavities of Jebel Qara (Dhofar, southern Sultanate of Oman). Quaternary International. 382, 264–276.

Delagnes, A., Crassard, R., Bertran, P., Sitzia, L., 2013. Cultural and human dynamics in southern Arabia at the end of the Middle Paleolithic. Quaternary International.

Delagnes, A., Tribolo, C., Bertran, P., Brenet, M., Crassard, R., Jaubert, J., Khalidi, L., Mercier, N., Nomade, S., Peigné, S., Sitzia, L., Tournepiche, J.F., Al-Halibi, M., Al-Mosabi, A., MacChiarelli, R., 2012. Inland human settlement in southern Arabia 55,000 years ago. New evidence from the Wadi Surdud Middle Paleolithic site complex, western Yemen. Journal of Human Evolution. 63, 452–474.

Drechsler, P., 2007. The Neolithic dispersal into Arabia. Proceedings of the Seminar for Arabian Studies. 37, 93–109.

Drechsler, P., 2009. The dispersal of the Neolithic over the Arabian Peninsula, BAR International Series 1969. Archaeopress, Oxford.

El-Shenawy, M.I., Kim, S.-T., Schwarcz, H.P., Asmerom, Y., Polyak, V.J., 2018. Speleothem evidence for the greening of the Sahara and its implications for the early human dispersal out of sub-Saharan Africa. Quaternary Science Reviews. 188, 67–76.

Engel, M., Brückner, H., Pint, A., Wellbrock, K., Ginau, A., Voss, P., Grottker, M., Klasen, N., Frenzel, P., 2012. The early Holocene humid period in NW Saudi Arabia – Sediments, microfossils and palaeo-hydrological modelling. Quaternary International. 266, 131–141.

Farraj, A. Al, Harvey, A.M., 2004. Late Quaternary interactions between aeolian and fluvial processes: a case study in the northern UAE. Journal of Arid Environments. 56, 235–248.

Fick, S.E., Hijmans, R.J., 2017. WorldClim 2: new 1-km spatial resolution climate surfaces for global land areas. International Journal of Climatology. 37, 4302–4315.

Fleitmann, D., Burns, S.J., Mangini, A., Mudelsee, M., Kramers, J., Villa, I., Neff, U., Al-Subbary, A.A., Buettner, A., Hippler, D., Matter, A., 2007. Holocene ITCZ and Indian monsoon dynamics recorded in stalagmites from Oman and Yemen (Socotra). Quaternary Science Reviews. 26, 170–188.

Fleitmann, D., Burns, S.J., Mudelsee, M., Neff, U., Kramers, J., Mangini, A., Matter, A., 2003a. Holocene forcing of the Indian monsoon recorded in a stalagmite from Southern Oman. Science. 300, 1737–1739.

Fleitmann, D., Burns, S.J., Neff, U., Mangini, A., Matter, A., 2003b. Changing moisture sources over the last 330,000 years in Northern Oman from fluid-inclusion evidence in speleothems. Quaternary Research. 60, 223–232.

Fleitmann, D., Burns, S.J., Pekala, M., Mangini, A., Al-Subbary, A., Al-Aowah, M., Kramers, J., Matter, A., 2011. Holocene and Pleistocene pluvial periods in Yemen, southern Arabia. Quaternary Science Reviews. 30, 783–787.

Fleitmann, D., Matter, A., 2009. The speleothem record of climate variability in Southern Arabia. Comptes Rendus - Geoscience. 341, 633–642.

Fleitmann, D., Mudelsee, M., Burns, S.J., Bradley, R.S., Kramers, J., Matter, A., 2008. Evidence for a widespread climatic anomaly at around 9.2 ka before present. Paleoceanography. 23.

Fordham, D.A., Saltré, F., Haythorne, S., Wigley, T.M.L., Otto-Bliesner, B.L., Chan, K.C., Brook, B.W., 2017. PaleoView: a tool for generating continuous climate projections spanning the last 21 000 years at regional and global scales. Ecography. 40, 1348–1358.

Fuchs, M., Buerkert, A., 2008. A 20 ka sediment record from the Hajar Mountain range in N-Oman, and its implication for detecting arid–humid periods on the southeastern Arabian Peninsula. Earth and Planetary Science Letters. 265, 546–558.

Goudie, A.S., Parker, A.G., 2010. Paleoenvironments and Prehistory in the Holocene of SE Arabia. In: Martini, I.P., Chesworth, W. (Eds.), Landscapes and Societies: Selected Cases. Springer Netherlands, Dordrecht, pp. 109–120.

Grant, K.M., Grimm, R., Mikolajewicz, U., Marino, G., Ziegler, M., Rohling, E.J., 2016. The timing of Mediterranean sapropel deposition relative to insolation, sea-level and African monsoon changes. Quaternary Science Reviews. 140, 125–141.

Grant, K.M., Rohling, E.J., Bar-Matthews, M., Ayalon, A., Medina-Elizalde, M., Ramsey, C.B., Satow, C., Roberts, A.P., 2012. Rapid coupling between ice volume and polar temperature over the past 50,000 years. Nature. 491, 744–747.

Grant, K.M., Rohling, E.J., Westerhold, T., Zabel, M., Heslop, D., Konijnendijk, T., Lourens, L., 2017. A 3 million year index for North African humidity/aridity and the implication of potential pan-African Humid periods. Quaternary Science Reviews. 171, 100–118.

Groucutt, H.S., Breeze, P.S., Guagnin, M., Stewart, M., Drake, N., Shipton, C., Zahrani, B., Omarfi, A. Al, Alsharekh, A.M., Petraglia, M.D., 2020. Monumental landscapes of the Holocene humid period in Northern Arabia: The mustatil phenomenon. The Holocene. 30, 1767–1779.

Groucutt, H.S., Grün, R., Zalmout, I.A.S., Drake, N.A., Armitage, S.J., Candy, I., Clark-Wilson, R., Louys, J., Breeze, P.S., Duval, M., Buck, L.T., Kivell, T.L., Pomeroy, E., Stephens, N.B., Stock, J.T., Stewart, M., Price, G.J., Kinsley, L., Sung, W.W., Alsharekh, A., Al-Omari, A., Zahir, M., Memesh, A.M., Abdulshakoor, A.J., Al-Masari, A.M., Bahameem, A.A., Al Murayyi, K.M.S., Zahrani, B., Scerri, E.M.L., Petraglia, M.D., 2018. Homo sapiens in Arabia by 85,000 years ago. Nature Ecology & Evolution. 2, 800–809.

Groucutt, H.S., White, T.S., Clark-Balzan, L., Parton, A., Crassard, R., Shipton, C., Jennings, R.P., Parker, A.G., Breeze, P.S., Scerri, E.M.L., Alsharekh, A., Petraglia, M.D., 2015. Human occupation of the Arabian Empty Quarter during MIS 5: Evidence from Mundafan Al-Buhayrah, Saudi Arabia. Quaternary Science Reviews. 119, 116–135.

Groucutt, H.S., White, T.S., Scerri, E.M.L., Andrieux, E., Clark-Wilson, R., Breeze, P.S., Armitage, S.J., Stewart, M., Drake, N., Louys, J., Price, G.J., Duval, M., Parton, A., Candy, I., Carleton, W.C., Shipton, C., Jennings, R.P., Zahir, M., Blinkhorn, J., Blockley, S., Al-Omari, A., Alsharekh, A.M., Petraglia, M.D., 2021. Multiple hominin dispersals into Southwest Asia over the past 400,000 years. Nature. 597, 376–380.

Guagnin, M., Breeze, P., Shipton, C., Ott, F., Stewart, M., Bateman, M., Martin, L., Graham, L., El-Dossary, S., Kingwell-Banham, E., Zahrani, B., Al-Omari, A., Alsharekh, A.M., Petraglia, M., 2020. The Holocene humid period in the Nefud Desert: Hunters and herders in the Jebel Oraf palaeolake basin, Saudi Arabia. Journal of Arid Environments. 178, 104146.

Henselowsky, F., Eichstädter, R., Schröder-Ritzrau, A., Herwartz, D., Almoazamy, A., Frank, N., Kindermann, K., Bubenzer, O., 2021. Speleothem growth phases in the central Eastern Desert of Egypt reveal enhanced humidity throughout MIS 5. Quaternary International.

Jennings, R.P., Singarayer, J., Stone, E.J., Krebs-Kanzow, U., Khon, V., Nisancioglu, K.H., Pfeiffer, M., Zhang, X., Parker, A., Parton, A., Groucutt, H.S., White, T.S., Drake, N.A., Petraglia, M.D., 2015. The greening of Arabia: Multiple opportunities for human occupation of the Arabian Peninsula during the Late Pleistocene inferred from an ensemble of climate model simulations.

Quaternary International. 382, 181–199.

Johnsen, S.J., Dahl-Jensen, D., Gundestrup, N., Steffensen, J.P., Clausen, H.B., Miller, H., Masson-Delmotte, V., Sveinbjörnsdottir, A.E., White, J., 2001. Oxygen isotope and palaeotemperature records from six Greenland ice-core stations: Camp Century, Dye-3, GRIP, GISP2, Renland and NorthGRIP. Journal of Quaternary Science. 16, 299–307.

Kennedy, D., 2017. 'Gates': a new archaeological site type in Saudi Arabia. Arabian Archaeology and Epigraphy. 28, 153–174.

Kiesewetter, H., 2006. Analyses of the Human Remains from the Neolithic Cemetary at al-Buhais 18. In: Funeral Monuments and Human Remains from Jebel Al-Buhais. Tübingen, pp. 103–380.

Killick, R., Haynes, K., Eckley, I., Fearnhead, P., Lee, J., 2016. Methods for Changepoint Detection.

Kobashi, T., Severinghaus, J.P., Brook, E.J., Barnola, J.-M., Grachev, A.M., 2007. Precise timing and characterization of abrupt climate change 8200 years ago from air trapped in polar ice. Quaternary Science Reviews. 26, 1212–1222.

Larrasoaña, J.C., Roberts, A.P., Rohling, E.J., 2013. Dynamics of Green Sahara Periods and Their Role in Hominin Evolution. PLoS ONE. 8, e76514.

Lézine, A.-M., 2009. Timing of vegetation changes at the end of the Holocene Humid Period in desert areas at the northern edge of the Atlantic and Indian monsoon systems. Comptes Rendus Geoscience. 341, 750–759.

Lisiecki, L.E., Raymo, M.E., 2005. A Pliocene-Pleistocene stack of 57 globally distributed benthic δ 18O records. Paleoceanography. 20, 1–17.

Liu, W., Martinón-Torres, M., Cai, Y.J., Xing, S., Tong, H.W., Pei, S.W., Sier, M.J., Wu, X.H.X.J., Edwards, R.L., Cheng, H., Li, Y.Y., Yang, X.X., De Castro, J.M.B., Wu, X.H.X.J., 2015. The earliest unequivocally modern humans in southern China. Nature. 526, 696–699.

Magee, P., 2014. The Archaeology of Prehistoric Arabia. Adaptation and Social Formation From the Neolithic to the Iron Age. Cambridge University Press, New York.

Martin, L., McCorriston, J., Crassard, R., 2009. Early Arabian pastoralism at Manayzah in Wadi Sana, Hadramawt. Proceedings of the Seminar for Arabian Studies. 39, 285–296.

McCorriston, J., Harrower, M., Martin, L., Oches, E., 2012. Cattle Cults of the Arabian Neolithic and Early Territorial Societies. American Anthropologist. 114, 45–63.

Millard, A.R., 2008. A critique of the chronometric evidence for hominid fossils: I. Africa and the Near East 500-50 ka. Journal of Human Evolution. 54, 848–847.

Neff, U., Burns, S.J., Mangini, A., Mudelsee, M., Fleitmann, D., Matter, A., 2001. Strong coherence between solar variability and the monsoon in Oman between 9 and 6 kyr ago. Nature. 411, 290–293.

Nicholson, S.L., Hosfield, R., Groucutt, H.S., Pike, A.W.G., Fleitmann, D., 2021. Beyond arrows on a map: The dynamics of Homo sapiens dispersal and occupation of Arabia during Marine Isotope Stage 5. Journal of Anthropological Archaeology. 62, 101269.

Nicholson, S.L., Pike, A.W.G., Hosfield, R., Roberts, N., Sahy, D., Woodhead, J., Cheng, H., Edwards, R.L., Affolter, S., Leuenberger, M., Burns, S.J., Matter, A., Fleitmann, D., 2020. Pluvial periods in Southern Arabia over the last 1.1 million-years. Quaternary Science Reviews. 229, 106112.

Otto-Bliesner, B.L., 2006. Simulating Arctic Climate Warmth and Icefield Retreat in the Last Interglaciation. Science. 311, 1751–1753.

Parker, A.G., Eckersley, L., Smith, M.M., Goudie, A.S., Stokes, S., Ward, S., White, K., Hodson, M.J., 2004. Holocene vegetation dynamics in the northeastern Rub' al-Khali desert, Arabian Peninsula: a

phytolith, pollen and carbon isotope study. Journal of Quaternary Science. 19, 665–676.

Parker, A.G., Manning, M., Goudie, A.S., Kennet, D., Stokes, S., White, K., Hodson, M.J., 2006. A Record of Holocene Climate Change from Lake Geochemical Analyses in Southeastern Arabia. Quaternary Research. 66, 465–476.

Parton, A., Farrant, A.R., Leng, M.J., Schwenninger, J.L., Rose, J.I., Uerpmann, H.P., Parker, A.G., 2013. An early MIS 3 pluvial phase in Southeast Arabia: Climatic and archaeological implications. Quaternary International. 300, 62–74.

Parton, A., Farrant, A.R., Leng, M.J., Telfer, M.W., Groucutt, H.S., Petraglia, M.D., Parker, A.G., 2015a. Alluvial fan records from southeast Arabia reveal multiple windows for human dispersal. Geology. 43, 295–298.

Parton, A., White, T.S., Parker, A.G., Breeze, P.S., Jennings, R., Groucutt, H.S., Petraglia, M.D., 2015b. Orbital-scale climate variability in Arabia as a potential motor for human dispersals. Quaternary International. 382, 82–97.

Petraglia, M.D., Alsharekh, A., Breeze, P., Clarkson, C., Crassard, R., Drake, N.A., Groucutt, H.S., Jennings, R.P., Parker, A.G., Parton, A., Roberts, R.G., Shipton, C., Matheson, C., Al-Omari, A., Veall, M.A., 2012. Hominin Dispersal into the Nefud Desert and Middle Palaeolithic Settlement along the Jubbah Palaeolake, Northern Arabia. PLoS ONE. 7, e49840.

Petraglia, M.D., Alsharekh, A.M., Crassard, R., Drake, N.A., Groucutt, H., Parker, A.G., Roberts, R.G., 2011. Middle Paleolithic occupation on a Marine Isotope Stage 5 lakeshore in the Nefud Desert, Saudi Arabia. Quaternary Science Reviews. 30, 1555–1559.

Petraglia, M.D., Groucutt, H.S., Guagnin, M., Breeze, P.S., Boivin, N., 2020. Human responses to climate and ecosystem change in ancient Arabia. Proceedings of the National Academy of Sciences. 117, 8263–8270.

Potts, D., Al Naboodah, H., Hellyer, P., 2003. Archaeology of the United Arab Emirates: Proceedings of the First International Conference. Trident Press, London.

Preston, G.W., 2011. From Nomadic Herder-hunters to Sedentary Famers: the Relationship Between Climate, Environment and Human Societies in the United Arab Emirates from the Neolithic to the Iron Age. Oxford Brookes University.

Preston, G.W., Parker, A.G., 2013. Understanding the evolution of the Holocene Pluvial Phase and its impact on Neolithic populations in south-east Arabia. Arabian Archaeology and Epigraphy. 24, 87–94.

Preston, G.W., Thomas, D.S.G., Goudie, A.S., Atkinson, O.A.C., Leng, M.J., Hodson, M.J., Walkington, H., Charpentier, V., Méry, S., Borgi, F., Parker, A.G., 2015. A multi-proxy analysis of the Holocene humid phase from the United Arab Emirates and its implications for southeast Arabia's Neolithic populations. Quaternary International. 382, 277–292.

Railsback, L.B., Gibbard, P.L., Head, M.J., Voarintsoa, N.R.G., Toucanne, S., 2015. An optimized scheme of lettered marine isotope substages for the last 1.0 million years, and the climatostratigraphic nature of isotope stages and substages. Quaternary Science Reviews. 111, 94–106.

Rohling, E.J., Marino, G., Grant, K.M., 2015. Mediterranean climate and oceanography, and the periodic development of anoxic events (sapropels). Earth-Science Reviews. 143, 62–97.

Rose, J.I., Usik, V.I., Marks, A.E., Hilbert, Y.H., Galletti, C.S., Parton, A., Geiling, J.M., Černý, V., Morley, M.W., Roberts, R.G., 2011. The Nubian complex of Dhofar, Oman: An African Middle Stone Age industry in Southern Arabia. PLoS ONE. 6, e28239.

Rosenberg, T.M., Preusser, F., Blechschmidt, I., Fleitmann, D., Jagher, R., Matter, A., 2012. Late Pleistocene palaeolake in the interior of Oman: A potential key area for the dispersal of anatomically modern humans out-of-Africa? Journal of Quaternary Science. 27, 13–16.

Rosenberg, T.M., Preusser, F., Fleitmann, D., Schwalb, A., Penkman, K.E.H., Schmid, T.W., Al-Shanti, M.A., Kadi, K.A., Matter, A., 2011. Humid periods in southern Arabia: Windows of opportunity for modern human dispersal. Geology. 39, 1115–1118.

Rosenberg, T.M., Preusser, F., Risberg, J., Plikk, A., Kadi, K.A., Matter, A., Fleitmann, D., 2013. Middle and Late Pleistocene humid periods recorded in palaeolake deposits of the Nafud desert, Saudi Arabia. Quaternary Science Reviews. 70, 109–123.

Scerri, E.M.L., Frouin, M., Breeze, P.S., Armitage, S.J., Candy, I., Groucutt, H.S., Drake, N., Parton, A., White, T.S., Alsharekh, A.M., Petraglia, M.D., 2021. The expansion of Acheulean hominins into the Nefud Desert of Arabia. Scientific Reports. 11, 10111.

Scholz, D., Hoffmann, D.L., 2011. StalAge - An algorithm designed for construction of speleothem age models. Quaternary Geochronology. 6, 369–382.

Shakun, J.D., Burns, S.J., Fleitmann, D., Kramers, J., Matter, A., Al-Subary, A., 2007. A high-resolution, absolute-dated deglacial speleothem record of Indian Ocean climate from Socotra Island, Yemen. Earth and Planetary Science Letters. 259, 442–456.

Stewart, M., Clark-Wilson, R., Breeze, P.S., Janulis, K., Candy, I., Armitage, S.J., Ryves, D.B., Louys, J., Duval, M., Price, G.J., Cuthbertson, P., Bernal, M.A., Drake, N.A., Alsharekh, A.M., Zahrani, B., Al-Omari, A., Roberts, P., Groucutt, H.S., Petraglia, M.D., 2020a. Human footprints provide snapshot of last interglacial ecology in the Arabian interior. Science Advances. 6, eaba8940.

Stewart, M., Louys, J., Breeze, P.S., Clark-Wilson, R., Drake, N.A., Scerri, E.M.L., Zalmout, I.S., Al-Mufarreh, Y.S.A., Soubhi, S.A., Haptari, M.A., Alsharekh, A.M., Groucutt, H.S., Petraglia, M.D., 2020b. A taxonomic and taphonomic study of Pleistocene fossil deposits from the western Nefud Desert, Saudi Arabia. Quaternary Research. 95, 1–22.

Stimpson, C.M., Lister, A., Parton, A., Clark-Balzan, L., Breeze, P.S., Drake, N.A., Groucutt, H.S., Jennings, R.P., Scerri, E.M.L., White, T.S., Zahir, M., Duval, M., Grün, R., Al-Omari, A., Al Murayyi, K.S.M., Zalmout, I.S., Mufarreh, Y.A., Memesh, A.M., Petraglia, M.D., 2016. Middle Pleistocene vertebrate fossils from the Nefud Desert, Saudi Arabia: Implications for biogeography and palaeoecology. Quaternary Science Reviews. 143, 13–36.

Thomas, H., Kennedy, M.A., Dalton, M., McMahon, J., Boyer, D., Repper, R., 2021. The mustatils: cult and monumentality in Neolithic north-western Arabia. Antiquity. 95, 605–626.

Thornton, P.K., Ericksen, P.J., Herrero, M., Challinor, A.J., 2014. Climate variability and vulnerability to climate change: a review. Global Change Biology. 20, 3313–3328.

Uerpmann, M., 1992. Structuring the Late Stone Age of Southeastern Arabia. Arabian Archaeology and Epigraphy. 3, 65–109.

Uerpmann, M., 2002. The Dark Millennium - Remarks on the final Stone Age in the Emirates and Oman. In: Potts, D., Al Naboodah, H., Hellyer, P. (Eds.), Archaeology of the United Arab Emirates: Proceedings of the First International Conference on the Archaeology of the U.A.E. Trident Press, London.

Vaks, A., Bar-Matthews, M., Ayalon, A., Matthews, A., Frumkin, A., Dayan, U., Halicz, L., Almogi-Labin, A., Schilman, B., 2006. Paleoclimate and location of the border between Mediterranean climate region and the Saharo-Arabian Desert as revealed by speleothems from the northern Negev Desert, Israel. Earth and Planetary Science Letters. 249, 384–399.

Vaks, A., Bar-Matthews, M., Matthews, A., Ayalon, A., Frumkin, A., 2010. Middle-Late Quaternary paleoclimate of northern margins of the Saharan-Arabian Desert: Reconstruction from speleothems of Negev Desert, Israel. Quaternary Science Reviews. 29, 2647–2662.

Vaks, A., Woodhead, J., Bar-Matthews, M., Ayalon, A., Cliff, R.A., Zilberman, T., Matthews, A., Frumkin, A., 2013. Pliocene-Pleistocene climate of the northern margin of Saharan-Arabian Desert

recorded in speleothems from the Negev Desert, Israel. Earth and Planetary Science Letters. 368, 88–100.

Vogt, B., 1994. In search for coastal sites in Pre-Historic Makkan: mid-Holocene 'shell-eaters' in the coastal desert of Ras al-Khaimah, U.A.E. In: Kenoyer, J.M. (Ed.), From Sumer to Meluhha: Contributions to the Archaeology of South and West Asia in Memory of George F. Dales, Jr. Wisconsin Arhcaeological Reports, Volume 3.

WorldClim, 2015. WorldClim - Global Climate Data: Free climate data for ecological modeling and GIS. Very high resolution interpolated climate surfaces for global land areas.

Appendix C – List of Conference Presentations

Apr 2019

Department of Geology and Department of Classics, University of Georgia, USA

"Archaeology and Climate in Roman and Byzantine Lycia"

(With Dr Jordan Pickett)

Jan 2019

Science & Humanities Interdisciplinary Dialogues (SAHID) conference, University of Reading, UK

"The Late Holocene record of climatic variability at Kocain Cave, southwest Anatolia, and links to local settlements"

Nov 2018

Climate Science and Ancient History Colloquium: Decoding Archives, University of Basel, Switzerland

"Did droughts lead to the collapse of Himyar and pave-the-way for Islam?"

May 2018

Society, Environment and Change Colloquium, Princeton University, USA

"A collapse of Himyar? Correlative Causality and S Arabia in the 6th century"

(With Professor John Haldon)

Mar 2018

Asian School of the Environment, Nanyang Technological University, Singapore

"Did climate change assist the emergence and rapid expansion of Islam in the 7th century CE?"